frontiers | Research Topics

Animal emerging and reemerging diseases

Edited by
Qing Pan, Li Wang, Kuan Zhao, Zhenyu Zhang
and Haili Zhang

Published in
Frontiers in Microbiology

ISSN 1664-8714
ISBN 978-2-8325-3407-6
DOI 10.3389/978-2-8325-3407-6

About Frontiers

Frontiers is more than just an open access publisher of scholarly articles: it is a pioneering approach to the world of academia, radically improving the way scholarly research is managed. The grand vision of Frontiers is a world where all people have an equal opportunity to seek, share and generate knowledge. Frontiers provides immediate and permanent online open access to all its publications, but this alone is not enough to realize our grand goals.

Frontiers journal series

The Frontiers journal series is a multi-tier and interdisciplinary set of open-access, online journals, promising a paradigm shift from the current review, selection and dissemination processes in academic publishing. All Frontiers journals are driven by researchers for researchers; therefore, they constitute a service to the scholarly community. At the same time, the *Frontiers journal series* operates on a revolutionary invention, the tiered publishing system, initially addressing specific communities of scholars, and gradually climbing up to broader public understanding, thus serving the interests of the lay society, too.

Dedication to quality

Each Frontiers article is a landmark of the highest quality, thanks to genuinely collaborative interactions between authors and review editors, who include some of the world's best academicians. Research must be certified by peers before entering a stream of knowledge that may eventually reach the public - and shape society; therefore, Frontiers only applies the most rigorous and unbiased reviews. Frontiers revolutionizes research publishing by freely delivering the most outstanding research, evaluated with no bias from both the academic and social point of view. By applying the most advanced information technologies, Frontiers is catapulting scholarly publishing into a new generation.

What are Frontiers Research Topics?

Frontiers Research Topics are very popular trademarks of the *Frontiers journals series*: they are collections of at least ten articles, all centered on a particular subject. With their unique mix of varied contributions from Original Research to Review Articles, Frontiers Research Topics unify the most influential researchers, the latest key findings and historical advances in a hot research area.

Find out more on how to host your own Frontiers Research Topic or contribute to one as an author by contacting the Frontiers editorial office: frontiersin.org/about/contact

Animal emerging and reemerging diseases

Topic editors

Qing Pan — Qingdao Agricultural University, China
Li Wang — Northeast Agricultural University, China
Kuan Zhao — Hebei Agricultural University, China
Zhenyu Zhang — University of Wisconsin-Madison, United States
Haili Zhang — Jilin University, China

Citation

Pan, Q., Wang, L., Zhao, K., Zhang, Z., Zhang, H., eds. (2023). *Animal emerging and reemerging diseases*. Lausanne: Frontiers Media SA.
doi: 10.3389/978-2-8325-3407-6

Table of contents

frontiers | Frontiers in Microbiology

TYPE Original Research
PUBLISHED 05 October 2022
DOI 10.3389/fmicb.2022.1029426

OPEN ACCESS

EDITED BY
Qing Pan,
Qingdao Agricultural University,
China

REVIEWED BY
Yuexiu Zhang,
The Ohio State University, United States
Victor H. Bustamante,
National Autonomous University of Mexico, Mexico
Jorge Antonio Yañez,
Meritorious Autonomous University of Puebla, Mexico
Abraham Loera Muro,
Centro de Investigación Biológica del Noroeste (CIBNOR), Mexico

*CORRESPONDENCE
Weicheng Bei
beiwc@mail.hzau.edu.cn
Liancheng Lei
leiliancheng@163.com

†These authors have contributed equally to this work

SPECIALTY SECTION
This article was submitted to Infectious Agents and Disease, a section of the journal Frontiers in Microbiology

RECEIVED 27 August 2022
ACCEPTED 21 September 2022
PUBLISHED 05 October 2022

CITATION
Liu F, Yao Q, Huang J, Wan J, Xie T, Gao X, Sun D, Zhang F, Bei W and Lei L (2022) The two-component system CpxA/CpxR is critical for full virulence in *Actinobacillus pleuropneumoniae*. *Front. Microbiol.* 13:1029426. doi: 10.3389/fmicb.2022.1029426

The two-component system CpxA/CpxR is critical for full virulence in *Actinobacillus pleuropneumoniae*

Feng Liu[1†], Qing Yao[1†], Jing Huang[2], Jiajia Wan[1], Tingting Xie[1], Xuejun Gao[1], Diangang Sun[1], Fuxian Zhang[1], Weicheng Bei[3*] and Liancheng Lei[1,4*]

[1]College of Animal Sciences, Yangtze University, Jingzhou, Hubei, China, [2]School of Foreign Languages, Zhejiang Gongshang University, Hangzhou, Zhejiang, China, [3]State Key Laboratory of Agricultural Microbiology, College of Veterinary Medicine, Huazhong Agricultural University, Wuhan, Hubei, China, [4]College of Veterinary Medicine, Jilin University, Changchun, China

Actinobacillus pleuropneumoniae, a major bacterial porcine respiratory tract pathogen causing pig pleuropneumonia, has resulted in high economic losses worldwide. The mutation of the two-component system CpxAR strongly impacted the virulence of *A. pleuropneumoniae*, but the underlying regulatory mechanism remained unclear. Here, we found that CpxAR positively regulated the *cpxDCBA* gene cluster involved in polysaccharide capsule export. A capsular layer was confirmed in wild-type cells by transmission electron microscopy, whereas *cpxAR* and *cpxD* mutants were non-capsulated. The mutants for polysaccharide capsule export gene *cpxD* exhibited non-capsulated and were strongly impaired in virulence for mice, indicating a major role of CPS export system in virulence. We then demonstrated that CpxR directly regulated the transcription of the CPS export gene cluster *cpxDCBA*. Taken together, our data suggested that CpxAR is a key modulator of capsule export that facilitates *A. pleuropneumoniae* survival in the host.

KEYWORDS

Actinobacillus pleuropneumoniae*, two-component system, CpxAR, polysaccharide capsule export, *cpxDCBA

Introduction

Actinobacillus pleuropneumoniae is a Gram-negative facultative anaerobic bacterium belonging to the *Pasteurellaceae* family (Sassu et al., 2018). This pathogen is the aetiological agent of porcine pleuropneumonia in pigs of all ages, which is a highly contagious and often deadly respiratory disease causing substantial economic losses in the swine industry worldwide (Cohen et al., 2021). *A. pleuropneumoniae* colonizes the tonsils and nasal cavities of infected pigs, and transmission from pig to pig occurs mainly by respiratory droplets or direct contact (Bosse et al., 2002). It is currently classified into 19 serovars based on the antigenic properties of their capsular polysaccharides and lipopolysaccharides

(Stringer et al., 2021). Previous studies have reported that many virulence factors play an important role in the pathogenicity of *A. pleuropneumoniae*, such as lipopolysaccharide, Apx toxins, polysaccharide capsule, and iron acquisition proteins (Loera-Muro et al., 2021).

Capsule polysaccharide (CPS) is encoded by the genes of the CPS biosynthetic locus *cpsABCD* and the CPS export locus *cpxDCBA* in *A. pleuropneumoniae* (Hathroubi et al., 2016). Unlike the former, the CPS export genes, *cpxDCBA*, are conserved in different *A. pleuropneumoniae* serovars (Bandara et al., 2003). The four genes encode an outer membrane lipoprotein (CpxD), a cytoplasmic membrane protein (CpxC), an integral membrane protein (CpxB), and an ATP-binding protein (CpxA) (Ward and Inzana, 1997).

Two-component signaling systems (TCSs), usually comprising a sensor histidine kinase (HK) and a cytoplasmic response regulator (RR), are involved in bacterial colonization and virulence through sensing environmental stimulus and responding accordingly (West and Stock, 2001; Li et al., 2018). Once it senses a physical or chemical signal, the histidine kinase will lead to autophosphorylation. The phosphoryl group is then transferred to the response regulator, which subsequently binds the target DNA promoters to alter gene expression (Gu et al., 2020). The genome of *A. pleuropneumoniae* encodes 5 paired of two-component systems, such as CpxAR, QseBC, ArcAB, PhoBR, and NarPQ (Xu et al., 2008).

The well-known TCS CpxAR, including the sensor histidine kinase CpxA, the cytopalsmic response regulator CpxR and the accessory protein CpxP, is required for sensing and coordinating the response to the envelope stress in *E. coli* (Raivio and Silhavy, 1997; Xu et al., 2014). In *A. pleuropneumoniae*, the Cpx system is composed of the histidine kinase CpxA and response regulator CpxR, and their genes constitute the *cpxRA* gene cluster (Li et al., 2018). Previous studies showed that the CpxAR system is a pleiotropic TCS in *A. pleuropneumoniae*, and involved in biofilm formation, oxidative stress, osmotic stress, heat stress, and virulence (Li et al., 2018; Yan et al., 2020). Li et al. found that CpxAR affects biofilm formation by regulating the expression of the *pgaABCD* operon through *rpoE* in *A. pleuropneumoniae* (Li et al., 2018). CpxAR has been reported to contribute to the virulence of *A. pleuropneumoniae* by altering O-antigen repeating unit biosynthesis (Yan et al., 2020). However, more underlying mechanisms of the CpxAR-mediated pathogensis of *A. pleuropneumoniae* remain to be elucidated. Here, the principal objective of this study is to reveal that the regulatory mechanism employed by CpxAR contributes to *A. pleuropneumoniae* virulence.

Materials and methods

Bacterial strains, culture conditions, plasmids, and primers

For this study, we used *A. pleuropneumoniae* strain S4074 as a representative strain. *A. pleuropneumoniae* strain was routinely grown at 37°C with shaking (180 rpm) in tryptic soy broth (TSB) medium (Solarbio, Beijing, China) supplemented with 10 μg/ml Nicotinamide Adenine Dinucleotide (NAD; Biofroxx, Einhausen, Germany) and 10% (vol/vol) newborn bovine serum (FBS; EVERY GREEN, Hangzhou, China). *Escherichia coli* strain BL21 was grown at 37°C with shaking (180 rpm) in Luria-Bertani (LB) medium. *E. coli* β2155 was grown in LB medium supplemented with 50 μg/ml diaminopimelic acid (Sigma-Aldrich, St. Louis, United States). We added 5 μg/ml chloramphenicol, or 50 μg/ml kanamycin as required. All strains and plasmids used in this study are listed in Table 1, and primers (Sangon Biotech Co., Ltd., Shanghai, China) are shown in Table 2.

The pEMOC2 suicide plasmid was used to construct the mutant strain Δ*cpxD* following an allelic exchange methodology, as described earlier (Liu et al., 2018). The complementation strain CΔ*cpxD* was generated using the shuttle plasmid pJFF224-XN as previously described (Liu et al., 2018). The Δ*cpxD* mutant and complementation strain CΔ*cpxD* were verified by PCR (Supplementary Figure 1) and sequencing.

RNA extraction, qRT-PCR, and RT-PCR

RNA extraction and qRT-PCR assays were performed as described earlier, with some modifications (Huang et al., 2018). The wild-type and Δ*cpxAR* mutant strains were grown in 5 ml of TSB overnight, normalized to an optical density of 600 nm (OD600) of 0.05, and incubated at 37°C with shaking (180 rpm) to an OD600 of 0.6. After the cells have grown to an OD600 of 0.6, cells were centrifuged at 4°C for 5 min at 10, 000 *g*, treated with the Bacteria Total RNA Isolation Kit (Sangon Biotech, Shanghai, China), and stored at −80°C until analysis. Reverse transcription was performed using the HiScript II first-strand cDNA synthesis kit (Vazyme, Nanjing, China). qRT-PCR was performed using the ViiA-7 Real-Time PCR System (Applied Biosystems, Waltham, United States) and SYBR qPCR Mix (Vazyme, Nanjing, China). Fold change data were normalized according to the housekeeping gene 16S rRNA, and analyzed using the $2^{-\Delta\Delta Ct}$ method (Livak and Schmittgen, 2001). RT-PCR acrossing the *cps2A-cpxD*, *cpxD-cpxC*, *cpxC-cpxB*, and *cpxB-cpxA* junctions was conducted as described previously (Xiong et al., 2019; Cheng et al., 2021). Amplified RT-*PCR products were* electrophoresed and photographed using a Gel Image Analyzing JS-1800 system (Peiqing, China).

Protein expression and purification

The PCR-amplified *cpxR* gene from *A. pleuropneumoniae* strain S4074 was cloned into the pET30a vector by digesting with Nde I and Xho I. Then, the CpxR expression plasmid was transformed into *E. coli* BL21(DE3), and their expression was induced by the addition of 0.5 mM IPTG and incubated at 16°C

TABLE 1 Bacterial strains and plasmids used in this study.

Strains/plasmids	Characteristics	Source/reference
A. pleuropneumoniae		
S4074	*A. pleuropneumoniae* reference strain of serovar 1; WT strain	From Prof. Weicheng Bei
Δ*cpxAR*	*A. pleuropneumoniae* 4,074 *cpxAR*-deletion mutant	From Prof. Weicheng Bei
Δ*cpxD*	*A. pleuropneumoniae* 4,074 *cpxD*-deletion mutant	This study
CΔcpxAR	Complemented strain of Δ*cpxAR*; Cm^r	From Prof. Weicheng Bei
CΔcpxD	Complemented strain of Δ*cpxD*; Cm^r	This study
E. coli		
DH5a	Cloning host for recombinant vector	Takara
β2155	Transconjugation donor for constructing mutant strain	From Prof. Weicheng Bei
Plasmid		
pEMOC2	Transconjugation vector: ColE1 ori mob RP4 sacB, Amp^rCm^r	From Prof. Weicheng Bei
pEΔ*cpxD*	Up- and down-stream arms of *cpxD* were ligated sequentially into pEMOC2, and used as the transconjugation vector for *cpxD* gene deletion	This study
pJFF224-XN	*E. coli*-APP shuttle vector: RSF1010 replicon; mob oriV, Cm^r	From Prof. Weicheng Bei
pCΔ*cpxD*	pJFF224-XN carrying the intact *cpxD*	This study
pET-30a	Expression vector; Kan^r	Novagen
pET30a-*cpxR*	pET-30a carrying cpxR gene	This study

Cm^r, Chloramphenicol resistance; Amp^r, Ampicillin resistance; Kan^r, Kanamycin resistance.

overnight. The cells were disrupted using a Ultrasonic Homogenizer (SCIENTZ, Ningbo, China), and centrifuged at 12,000 *g* for 20 min to remove cellular debris. The supernatant was extracted with Ni-nitrilotriacetic acid (Ni-NTA) resin affinity chromatography following the manufacturer's instructions. The purified protein concentration was determined by a BCA protein assay kit (Beyotime, Shanghai, China), and the purity was checked by 12% SDS-PAGE.

Electrophoretic mobility shift assay

To study the binding of CpxR to the DNA probes, the electrophoretic mobility shift assays (EMSAs) were performed using a Chemiluminescent EMSA Kit (Beyotime, Shanghai, China) as previously described (Cheng et al., 2021). The DNA probes were generated by PCR amplification from 1 to 196 bp upstream of the start codon of *cpxD* gene, purified using a Gel Extraction Kit (Omega, Norcross, United States), and labeled using a EMSA Probe Biotin Labeling Kit (Beyotime, Shanghai, China). The recombinant protein CpxR was phosphorylated *in vitro* by 50 mM acetyl phosphate (Sigma, St. Louis, United States) (Pogliano et al., 1997). Increasing amounts of phosphorylated CpxR protein (0 to 4 pmol) were incubated with the labeled probe (1 μM) in binding buffer (50 mM Tris (pH 8.0), 100 mM KCl, 2.5 mM MgCl2, 0.2 mM dithiothreitol (DTT), 2 μg salmon sperm DNA, 10% glycerol) for 20 min at room temperature. The reaction mixtures were directly subjected to 4% non-denaturing polyacrylamide electrophoresis. The gel was transferred to a nylon membrane (Beyotime, Shanghai, China), and imaging was performed using JS-1070 fluorescent chemiluminescence gel imaging system (Peiqing, Shanghai, China).

DNase I footprinting assay

For preparation of fluorescent 6-carboxyfluorescein (FAM) labeled probe, the *cpxD* promoter was amplified from 1 to 196 bp upstream of the start codon by PCR using the plasmid pEASY-cpxD as a template and primers of M13F (FAM) and M13R. For each assay, the 6-FAM-labeled probe (400 ng) was mixed with different amounts of phosphorylated CpxR protein in a 40 μl reaction volume for 30 min at 25°C. Subsequently, the mixture was incubated with 0.015 unit DNase I (Promega, Madison, United States) at 37°C for 1 min. The reaction was terminated by adding 140 μl DNase I stop solution (200 mM unbuffered sodium acetate, 30 mM EDTA and 0.15% SDS). The samples were extracted by phenol/chloroform, and the pellets containing DNA were dissolved in 30 μl water. The results were analyzed using 3130xl DNA analyzer and Peak Scanner software v1.0 (Applied Biosystems, Waltham, United States).

Transmission electron microscope

For transmission electron microscope (TEM), *A. pleuropneumoniae* strain was grown on TSA plates overnight at 37°C, harvested by centrifugation (5,000 *g*, 4°C, 5 min), and then incubated in FBS (EVERY GREEN, Hangzhou, China) for 30 min at 37°C. The samples were fixed

TABLE 2 Primers used in this study.

Primer	Sequence (5′–3′) a	Use
cpxD-S-F	CTGTCGACTCTTGTCTCGTCTCATCCAGCCACT	Amplification of *cpxD* upstream homology arms
cpxD-S-R	ATTCAGACAACGGCGCATTTATCCGAACTTTGTGAATTAGCCTCT	
cpxD-X-F	AGAGGCTAATTCACAAAGTTCGGATAAATGCGCCGTTGTCTGAAT	Amplification of *cpxD* downstream homology
cpxD-X-R	ATGCGGCCGCCGGTTTGCTTGGCTGACTGA	arms
cpxD-W-F	GCTAGTTTGGCTGCCTGCTC	Detection exterior of *cpxD* mutants
cpxD-W-R	TGTTCCGCAAATGAAATGGT	
cpxD-N-F	TTACCGTGCCGTTCGTGG	Detection interior of *cpxD* mutants
cpxD-N-R	GCAGCAACCGCATCTAATACAC	
cpxD-C-F	CCGCTCGAGTAATGCTTATCTGTTGAACCCTCCT	Amplification of *cpxD*
cpxD-C-R	AAGGAAAAAAGCGGCCGCTTAATAGGCACGAACGGCATTGGTC	
cpxD-F	GTATTCCGTCACGTGCCTTT	Detection the transcription of *cpxD*
cpxD-R	GCATTGGGAAACGCTGTAAT	
cpxC-F	ATTTCATTTGCGGAACAAGC	Detection the transcription of *cpxC*
cpxC-R	CGCATAAGCAATGCATCAAC	
cpxB-F	GCTACCAAGCCAAGCTCAAC	Detection the transcription of *cpxB*
cpxB-R	TTGCGGTTCGATTCCTTTAC	
cpxA-F	GGCAGTTTAACCGGTATGGA	Detection the transcription of *cpxA*
cpxA-R	CGAGAGTCACCTACCGCAAT	
16SrRNA-F	CCATGCCGCGTGAATGA	Detection the transcription of 16SrRNA
16SrRNA-R	TTCCTCGCTACCGAAAGAACTT	
cpxD-EMSA-F	TAATGCTTATCTGTTGAACCCTCCT	Amplification of *cpxD* promoter region for EMSA
cpxD-EMSA-R	CCCCAAAGAAAGGAGTAATCTAAGT	
rpoE-EMSA-F	TAAAAAGATAAGATAAGCGGTC	Amplification of *rpoE* promoter region for EMSA
rpoE-EMSA-R	AGTGTGTAACAAAAATGAAAAGT	
rpoD-EMSA-F	GCGGAAGAAAAGCAAGAGTTGGTCA	Amplification of *rpoD* promoter region for EMSA
rpoD-EMSA-R	TCCATAATTGTATCCGTTTTGTGTG	

for 2 h with 2.5% glutaraldehyde and placed onto 200 mesh copper grids. Subsequently, the copper grids were air-dried and observed with a 120KV biological transmission electron microscope (HITACHI, Tokyo, Japan).

Animal test

In all experiments, Kunming (KM) mice (female, 6 weeks old) purchased from CTGU University Laboratory Animal Center (Quality Certificate No. 42010200007283) were used. All animal experiments were approved by the Animal Ethics Committee of the Yangtze University. To investigate the survival curves of the mice, 1×10^7 CFUs of WT S4074, Δ*cpxAR*, Δ*cpxD*, CΔ*cpxAR* or CΔ*cpxD* was injected *via* the abdominal cavity of each mouse (8 mice per group). The survival rates were recorded daily in 1 week after challenge.

In addition, to evaluate the colonization ability, another 5 groups (8 mice/group) were given intraperitoneal injections with 1×10^7 CFUs of WT S4074, Δ*cpxAR*, Δ*cpxD*, CΔ*cpxAR* or CΔ*cpxD*. At 8 h after injection, one half of the lung and liver from each mice was collected aseptically, weighed, homogenized, diluted serially, and plated to determine bacterial counts. The remaining lungs were fixed in tissuse's fixative (Biosharp, Beijing, China) at 4°C for histo pathological analysis as described earlier (Guo et al., 2018).

Bioinformatic and statistical analysis

The promoter and the transcriptional start site of the *cpxD* gene were, respectively, predicated by using BPROM[1] and BDGP.[2] Two-tailed Student's *t* tests were used to analyze the significance between various mutants and WT strain using GraphPad Prism version 7.0 (GraphPad, La Jolla, United States). Values of $p < 0.05$ was considered statistically significant.

1 http://linux1.softberry.com/berry.phtml?topic=bprom&group=programs&subgroup=gfindb

2 https://www.fruitfly.org/seq_tools/promoter.html

Results

CpxAR is required for capsule synthesis in *Actinobacillus pleuropneumoniae*

The growth traits of the WT S4074, Δ*cpxAR*, CΔ*cpxAR*, Δ*cpxD,* and CΔ*cpxD* strains were investigated. As shown in Figure 1A, only the Δ*cpxAR* mutant exhibited growth defects, which was consistent with previous studies (Li et al., 2018). To elucidate the mechanism by which CpxAR impacts the pathogenicity of *A. pleuropneumoniae*, qRT-PCR was performed to identify the genes regulated by CpxAR. The qRT-PCR analysis showed that the relative transcript levels of the four CPS export genes, *cpxD*, *cpxC*, *cpxB,* and *cpxA* (capsular polysaccharide export gene), were significantly decreased in the Δ*cpxAR* mutant strain (Figure 1B). These data indicated that CpxAR regulate the expression of the four CPS export genes in *A. pleuropneumoniae.*

Previous work on *A. pleuropneumoniae* found that the WT S4074 strain forms a extensive layer of capsular material covering the cells (Jacques et al., 1988). Here, we observed an extensive layer of capsular material covering the WT S4074 as expected, whereas Δ*cpxAR* and Δ*cpxD* mutant strains were not found layer of capsular material (Figure 1C). These data indicated that CpxAR contributes to capsule synthesis in *A. pleuropneumoniae.*

Characterization of the *cpxDCBA* operon in *Actinobacillus pleuropneumoniae*

These four capsule export genes, including *cpxD*, *cpxC*, *cpxB,* and *cpxA* (capsular polysaccharide export gene), are in the chromosome, and such cluster is adjacent to the gene *cps2A* (Figures 2A,B). To verify whether these four genes are controlled by one promoter, we performed RT-PCR across the *cps2A-cpxD*, *cpxD-cpxC*, *cpxC-cpxB*, and *cpxB-cpxA* junctions. The RT-PCR analysis indicated that the *cpxDCBA* gene cluster is a single operon (Figure 2C).

CpxR binds specifically to the *cpxD* promoter region

To investigate the mechanism of CpxAR-mediated transcriptional regulation of the *cpxDCBA* operon, we analyzed

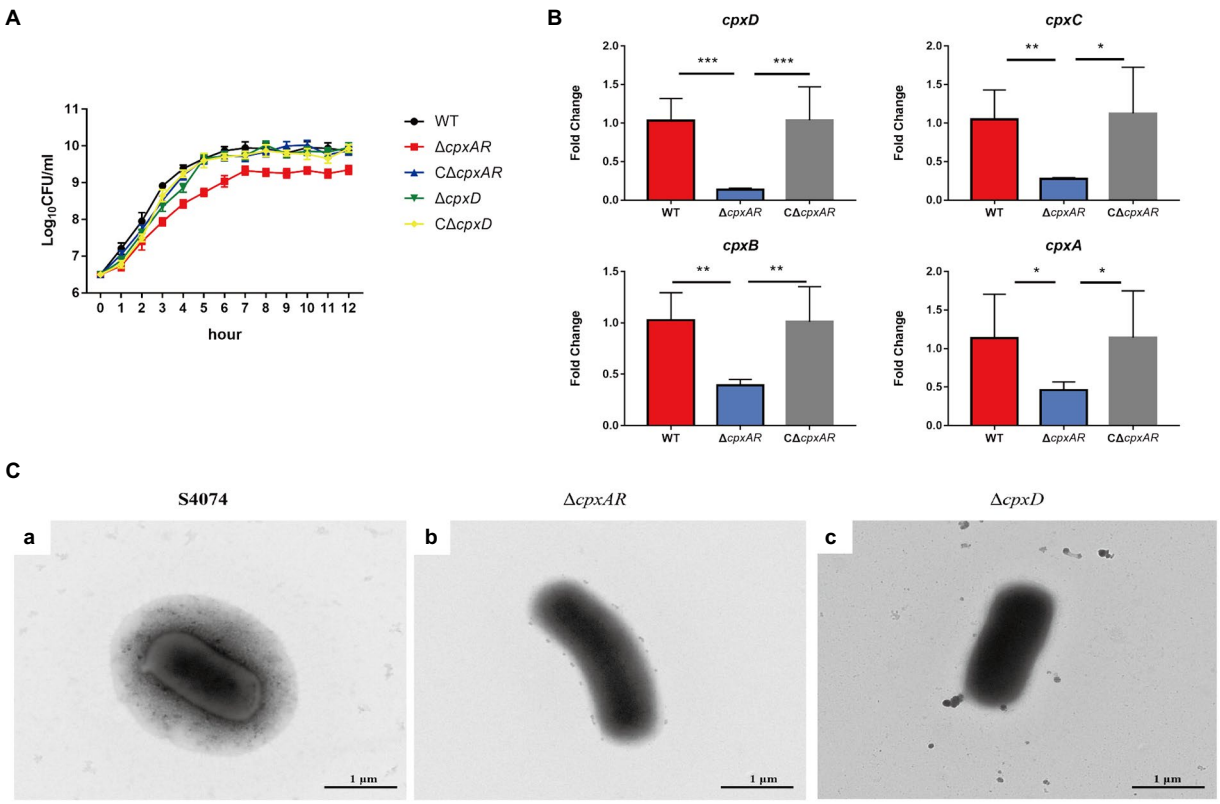

FIGURE 1
CpxAR impacts the capsule production. **(A)** The growth analysis of the WT S4074, Δ*cpxAR*, CΔ*cpxAR*, Δ*cpxD*, and CΔ*cpxD* strains. **(B)** The relative mRNA levels of *cpxD, cpxC, cpxB, and cpxA (capsular polysaccharide export gene) in* the Δ*cpxAR* mutant compared to the parent strain *determined by* RT-qPCR. **p*<0.05, ***p*<0.01, ****p*<0.001. **(C)** Observation of the capsule layer of the WT S4074 **(A)**, Δ*cpxAR* **(B)**, Δ*cpxD* **(C)**, strains by TEM.

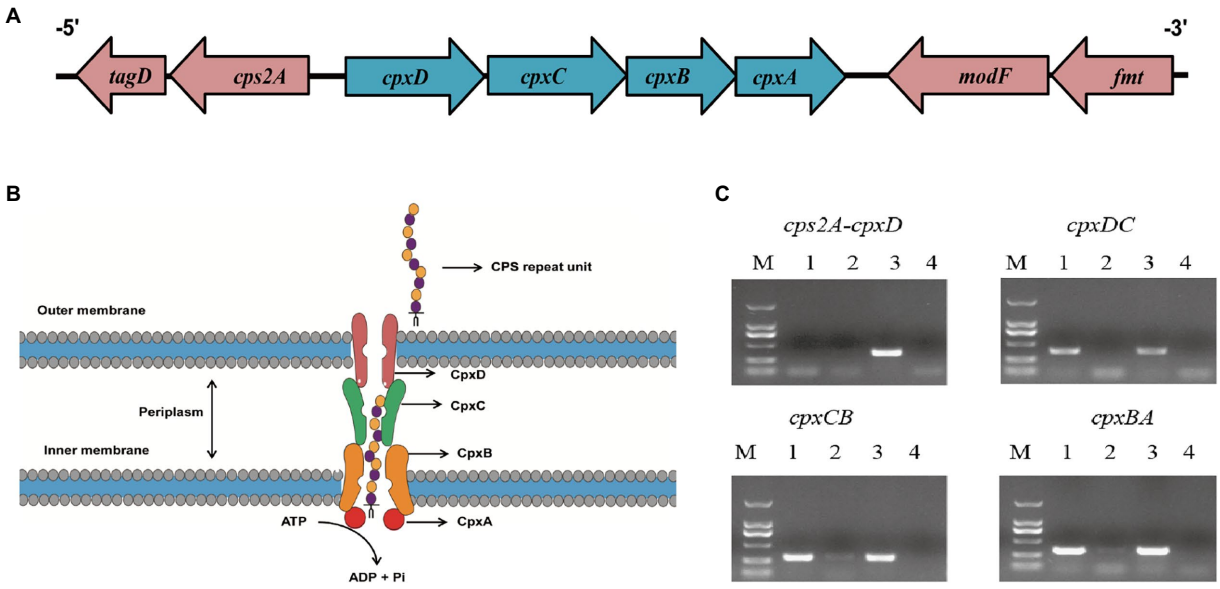

FIGURE 2
The *cpxD*, *cpxC*, *cpxB*, and *cpxA* genes form a single operon. **(A)** Schematic presentation of the capsule export locus. **(B)** Diagram showing the role of CpxD, CpxC, CpxB, and CpxA (capsular polysaccharide export protein) in CPS synthesis. **(C)** RT-PCR analysis confirmed that the *cpxD*, *cpxC*, *cpxB*, and *cpxA* (capsular polysaccharide export gene) genes form an operon. The Lane 1–4 were cDNA, total RNA, genomic DNA, and no-template control, respectively.

the binding site for CpxR in the upstream region of *cpxDCBA* operon using EMSA. EMSAs showed that the CpxR protein could bind to the promoter region of the *cpxDCBA* operon (Figure 3A). To further analyze the CpxR-*cpxD* interaction, DNase I footprinting was used to map the precise binding site. Two CpxR-binding sites were found 92 to 121 bp and 146 to 170 bp upstream of the start codon, and the sequences were 5'-TCTATTTACTTTCTTTACAAATGAT-3' and 5'-TTTTGTA AATTTTTTATATTTAATTTCTCT-3' respectively (Figure 3B). Collectively, these findings indicated that CpxR directly regulates the expression of *cpxDCBA* operon.

To obtain a more detailed picture of the CpxR binding site, the promoter and the transcription start site of the *cpxD* gene were, respectively, predicted by BPROM and BDGP. The *cpxD* transcriptional start site, designated as TSS, was detected 21-bp upstream of the start codon, and determined as A (Figure 3C). In addition, we performed a bioinformatic search in the promoter region of *cpxD* and identified a putative -10 CTATATAGT box and a putative -35 TTTAAG box, respectively, located 33 bp and 48 bp upstream of the start codon (Figure 3C).

CpxAR and *cpxD* are involved in virulence for mice

To verify whether the CpxAR-*cpxDCBA* pathway plays an important role in the virulence of *A. pleuropneumoniae*, the WT S4074, Δ*cpxAR*, CΔ*cpxAR*, Δ*cpxD*, and CΔ*cpxD* strains were further compared through survival and colonization assays *in vivo* in KM mice. As shown in Figure 4A, the mice infected by the Δ*cpxAR* and Δ*cpxD* strain showed significantly higher survival rate of 83 and 100% respectively; whereas, the mice infected by the WT, CΔ*cpxAR* and CΔ*cpxD* strains showed the survival rate of 0, 17 and 0%, respectively. As shown in Figure 4B, the bacterial loads in the lungs and livers of Δ*cpxAR*- and Δ*cpxD*-infected mice were significantly lower than that of WT-, CΔ*cpxAR*- and CΔ*cpxD*-infected mice.

Histologic examination of the lung tissue sections from all of the mice infected with WT, CΔ*cpxAR* and CΔ*cpxD* strains showed the classic features of pneumonia, such as hyperemia, swelling, hemorrhage, edema, consolidation, but this was not evident in Δ*cpxAR*- and Δ*cpxD*-infected mice (Figure 4C). Taken together, these observations indicated that the CpxAR-*cpxDCBA* pathway contributs to the pathogenesis of *A. pleuropneumoniae*.

Discussion

Two-component system is one of the key bacterial mechanisms that enables bacteria to sense and respond to host stimulation, which is critical for the pathogenic process (Matanza et al., 2021). The CpxAR system is the principal determinant of many biological processes in *A. pleuropneumoniae*, such as biofilm formation, heat stress and O-antigen repeating unit biosynthesis (Li et al., 2018; Yan et al., 2020). Previous studies have found that CpxAR is required for virulence in *A. pleuropneumoniae* (Li et al., 2018; Yan et al., 2020). However, the crucial role of CpxAR in the pathogenesis

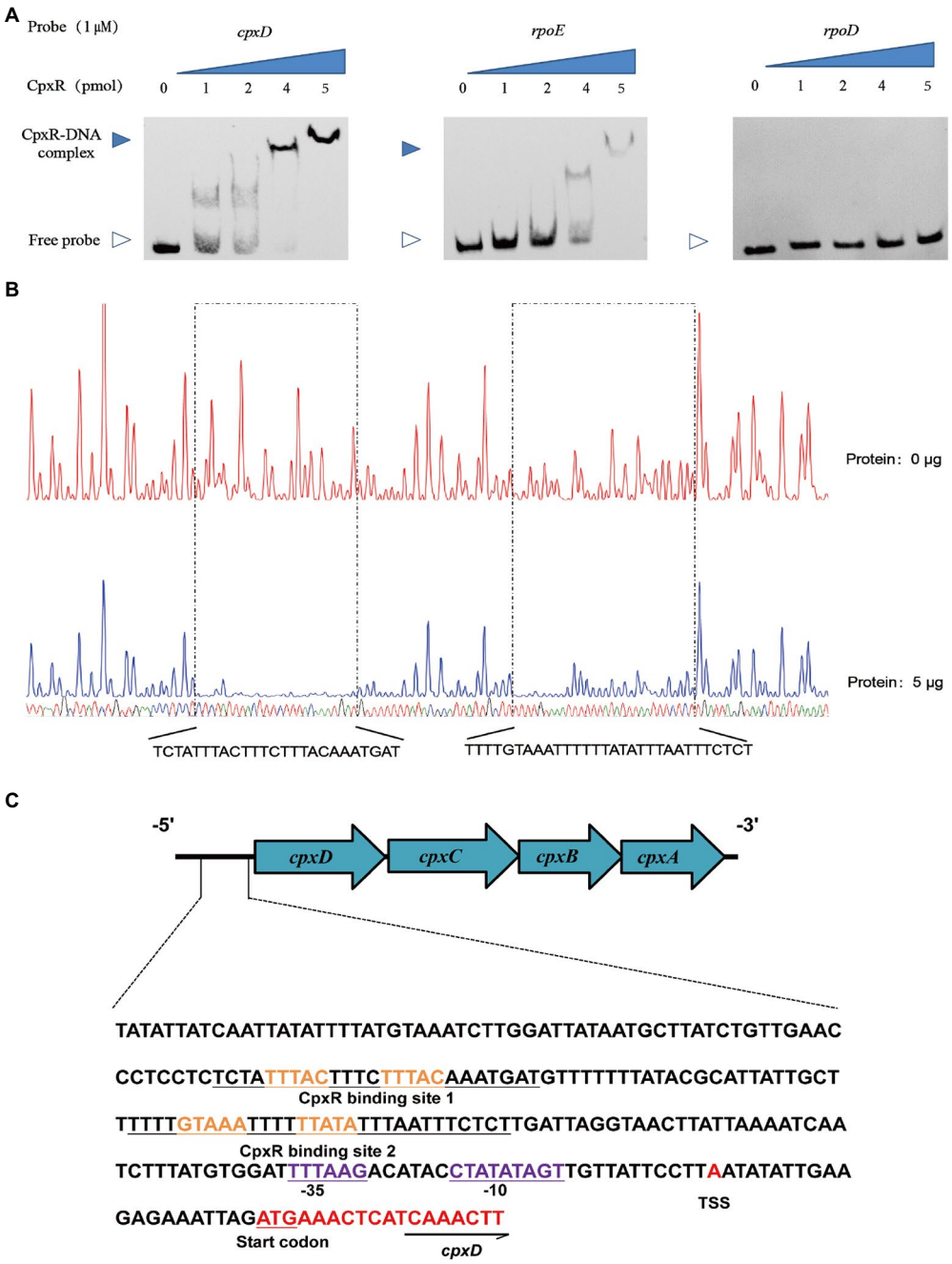

FIGURE 3
CpxR binds to the *cpxD* promoter region. **(A)** EMSAs performed with various concentrations of phosphorylated CpxR (0–4pmol) and the promoter regions of *cpxD*, *rpoE* (positive control) and *rpoD* (negative control). **(B)** Mapping the CpxR binding sites in the *cpxD* promoter by DNase I footprinting. Protected regions were shown below the footprinting results. **(C)** Nucleotide sequences of *cpxD* promoter. CpxR-binding site was shown in blue nucleotides boxed in black, and–35 box, –10 box were underlined and shown in green. Start codon of *cpxD* was underlined and shown in red, and the TSS was shown in red.

of *A. pleuropneumoniae* requires further investigation. In this study, we explored whether CpxAR-regulated genes are critical to the successful infection of *A. pleuropneumoniae*.

CPS is one of the major virulence factors of *A. pleuropneumoniae*, which can protect the bacteria from the host's immune response, such as phagocytic uptake and complement-mediated bacteriolysis (Budde et al., 2020). The thickness of the capsule is related to the virulence of *A. pleuropneumoniae*, and generally, the thicker the capsule, the more virulent the strain (Dubreuil et al., 2000). However, the regulation of capsule production in *A. pleuropneumoniae* is still unknown. In this study, TEM confirmed that the capsule layer of

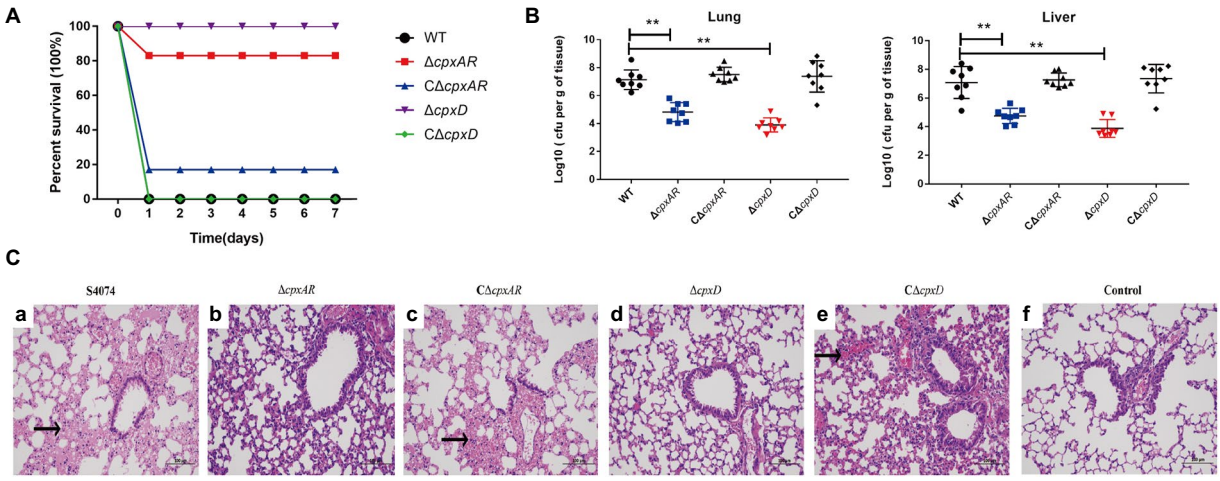

FIGURE 4
CpxAR and CpxD contribute to the virulence and colonization of *A. pleuropneumoniae*. The survival rates **(A)**, bacterial loads in the lungs and livers **(B)**, and histopathology of the lung tissues **(C)** of Kunming mice challenged with the WT S4074 (a), Δ*cpxAR* (b), Δ*cpxD* (c), CΔ*cpxAR* (d), and CΔ*cpxD* (e) strains at a dose of 1x10^{7}CFU/mouse. The control group (f) was only injected with 100 μl of PBS $^{**}p<0.01$.

the Δ*cpxAR* strain was difficult to observe. These observations identified that CpxAR is a capsule regulator, which has been implicated in controlling the gene expression and production of CPS in *A. pleuropneumoniae*.

Previous studies showed that the sequence GTAAA-$(N)_{4-8}$-GTAAA, or TTTAC-$(N)_{4-8}$-TTTAC is the binding consensus sequence of CpxR (Keilwagen et al., 2009; Srinivasan et al., 2012; Feldheim et al., 2016; Tian et al., 2016). Here, two putative CpxR-binding sequence (TTTAC-N_4-TTTAC and GTAAA-N_4-TTATA) were, respectively, located 39–68 bp and 94–118 bp upstream of the promoter −35 region of the *cpxD* gene. Furthermore, we found that CpxR could directly bind to the *cpxD* promoter region by EMSA, and identified two CpxR-binding sites by DNase I footprinting which were consistent with the two putative sequences. In general, the CpxR-binding site is located upstream of the promoter region and activates their transcription (Raffa and Raivio, 2002). Previous work identified only one CpxR-binding site, but we found two in this study. The reason and the function of the two sites is worthy of further investigation.

In the present study, we showed that CpxAR positively regulates the CPS export operon *cpxDCBA* using qRT-PCR. Furthermore, EMSA and DNase I footprinting demonstrated that CpxR directly regulated the *cpx* operon by binding to the *cpxD* promoter region. In addition, these animal challenge tests showed that CpxD plays an important role in the virulence of *A. pleuropneumoniae*. Previous studies have shown that an insertion mutant in *cpxC*, encoding a cytoplasmic membrane protein which is essential for polysaccharide transport, caused less mortality in pigs compared to the parent strain (Rioux et al., 2000). These findings indicated that CpxAR contributes to the virulence of *A. pleuropneumoniae* by directly regulating the CPS export locus, *cpxDCBA* (Figure 5).

Our results showed that CpxAR plays a contributing role in virulence by affecting capsule synthesis through directly regulating the expression of the *cpxDCBA* operon. The CpxAR and CPS are present in many bacteria (Vogt and Raivio, 2012; Whitfield et al., 2020). Therefore, our findings may not only contribute to the understanding of the pathogenesis of *A. pleuropneumoniae*, but also to other bacteria. Future studies will focus on identifying more virulence factors regulated by CpxAR in *A. pleuropneumoniae*.

Data availability statement

The original contributions presented in the study are included in the article/Supplementary material, further inquiries can be directed to the corresponding authors.

Ethics statement

The animal study was reviewed and approved by the Animal Ethics Committee of the Yangtze University.

Author contributions

FL, WB, and LL: conceived and designed the experiments. QY, JW, and TX: performed the experiments. FL and QY: analyzed the data. XG, DS, and FZ: contributed reagents, materials, and analysis

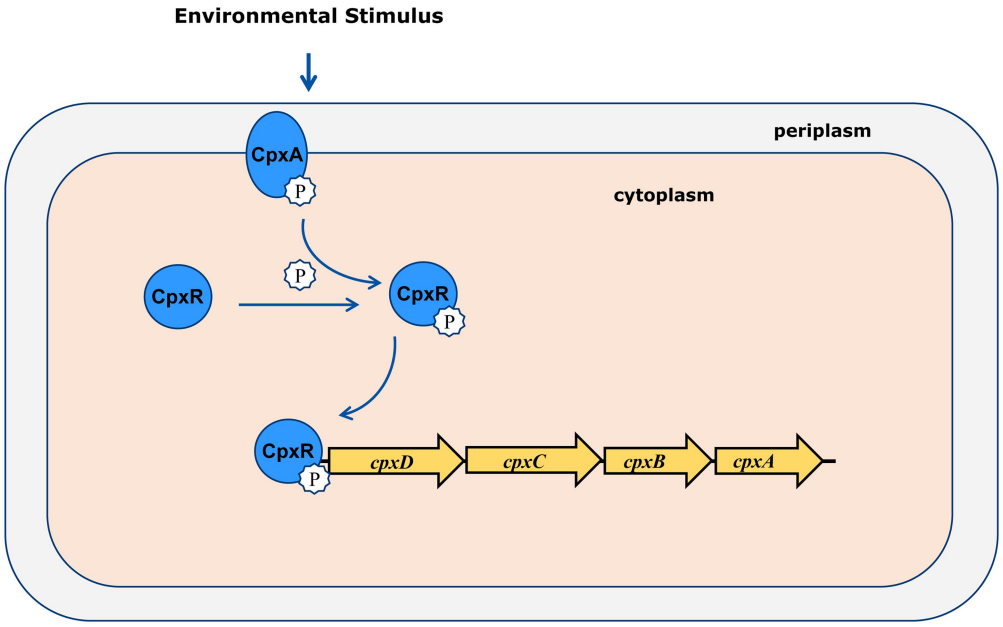

FIGURE 5
Molecular model of virulence regulation by CpxAR. *CpxDCBA* transcription is activated by CpxR-P, which contributes to the virulence in *A. pleuropneumoniae*.

tools. JH: polished the language. All authors contributed to the article and approved the submitted version.

Funding

This research was supported by the National Natural Science Foundation of China (32002252).

Conflict of interest

The authors declare that the research was conducted in the absence of any commercial or financial relationships that could be construed as a potential conflict of interest.

Publisher's note

Supplementary material

The Supplementary material for this article can be found online at: https://www.frontiersin.org/articles/10.3389/fmicb.2022.1029426/full#supplementary-material

References

Bandara, A. B., Lawrence, M. L., Veit, H. P., and Inzana, T. J. (2003). Association of *Actinobacillus pleuropneumoniae* capsular polysaccharide with virulence in pigs. *Infect. Immun.* 71, 3320–3328. doi: 10.1128/IAI.71.6.3320-3328.2003

Bosse, J. T., Janson, H., Sheehan, B. J., Beddek, A. J., Rycroft, A. N., Kroll, J. S., et al. (2002). *Actinobacillus pleuropneumoniae*: pathobiology and pathogenesis of infection. *Microbes Infect.* 4, 225–235. doi: 10.1016/s1286-4579(01)01534-9

Budde, I., Litschko, C., Fuhring, J. I., Gerardy-Schahn, R., Schubert, M., and Fiebig, T. (2020). An enzyme-based protocol for cell-free synthesis of nature-identical capsular oligosaccharides from *Actinobacillus pleuropneumoniae* serotype 1. *J. Biol. Chem.* 295, 5771–5784. doi: 10.1074/jbc.RA120.012961

Cheng, C., Liu, F., Jin, H., Xu, X., Xu, J., Deng, S., et al. (2021). The DegU orphan response regulator contributes to heat stress resistance in *listeria monocytogenes*. *Front. Cell. Infect. Microbiol.* 11:761335. doi: 10.3389/fcimb.2021.761335

Cohen, L. M., Bosse, J. T., Stegger, M., Li, Y., Langford, P. R., Kielland, C., et al. (2021). Comparative genome sequence analysis of *Actinobacillus pleuropneumoniae* Serovar 8 isolates from Norway, Denmark, and the United Kingdom indicates distinct phylogenetic lineages and differences in distribution of antimicrobial resistance genes. *Front. Microbiol.* 12:729637. doi: 10.3389/fmicb.2021.729637

Dubreuil, J. D., Jacques, M., Mittal, K. R., and Gottschalk, M. (2000). *Actinobacillus pleuropneumoniae* surface polysaccharides: their role in diagnosis and immunogenicity. *Anim. Health Res. Rev.* 1, 73–93. doi: 10.1017/s1466252300000074

Feldheim, Y. S., Zusman, T., Speiser, Y., and Segal, G. (2016). The *legionella pneumophila* CpxRA two-component regulatory system: new insights into CpxR's function as a dual regulator and its connection to the effectors regulatory network. *Mol. Microbiol.* 99, 1059–1079. doi: 10.1111/mmi.13290

Gu, D., Zhang, Y., Wang, Q., and Zhou, X. (2020). S-nitrosylation-mediated activation of a histidine kinase represses the type 3 secretion system and promotes

virulence of an enteric pathogen. *Nat. Commun.* 11:5777. doi: 10.1038/s41467-020-19506-1

Guo, Y., Xiao, Z., Wang, Y., Yao, W., Liao, S., Yu, B., et al. (2018). Sodium butyrate ameliorates Streptozotocin-induced type 1 diabetes in mice by inhibiting the HMGB1 expression. *Front. Endocrinol.* 9:630. doi: 10.3389/fendo.2018.00630

Hathroubi, S., Hancock, M. A., Bosse, J. T., Langford, P. R., Tremblay, Y. D., Labrie, J., et al. (2016). Surface polysaccharide mutants reveal that absence of O antigen reduces biofilm formation of *Actinobacillus pleuropneumoniae*. *Infect. Immun.* 84, 127–137. doi: 10.1128/IAI.00912-15

Huang, Y., Wang, H., and Yang, Y. (2018). Expression of fibroblast growth factor 5 (FGF5) and its influence on survival of breast cancer patients. *Med. Sci. Monit.* 24, 3524–3530. doi: 10.12659/MSM.907798

Jacques, M., Foiry, B., Higgins, R., and Mittal, K. R. (1988). Electron microscopic examination of capsular material from various serotypes of *Actinobacillus pleuropneumoniae*. *J. Bacteriol.* 170, 3314–3318. doi: 10.1128/jb.170.7.3314-3318.1988

Keilwagen, J., Baumbach, J., Kohl, T. A., and Grosse, I. (2009). MotifAdjuster: a tool for computational reassessment of transcription factor binding site annotations. *Genome Biol.* 10:R46. doi: 10.1186/gb-2009-10-5-r46

Li, H., Liu, F., Peng, W., Yan, K., Zhao, H., Liu, T., et al. (2018). The CpxA/CpxR two-component system affects biofilm formation and virulence in *Actinobacillus pleuropneumoniae*. *Front. Cell. Infect. Microbiol.* 8:72. doi: 10.3389/fcimb.2018.00072

Liu, F., Peng, W., Liu, T., Zhao, H., Yan, K., Yuan, F., et al. (2018). Biological role of *Actinobacillus pleuropneumoniae* type IV pilus proteins encoded by the apf and pil operons. *Vet. Microbiol.* 224, 17–22. doi: 10.1016/j.vetmic.2018.08.006

Livak, K. J., and Schmittgen, T. D. (2001). Analysis of relative gene expression data using real-time quantitative PCR and the 2(-Delta Delta C(T)) method. *Methods* 25, 402–408. doi: 10.1006/meth.2001.1262

Loera-Muro, A., Ramirez-Castillo, F. Y., Moreno-Flores, A. C., Martin, E. M., Avelar-Gonzalez, F. J., and Guerrero-Barrera, A. L. (2021). *Actinobacillus pleuropneumoniae* surviving on environmental multi-species biofilms in swine farms. *Front Vet Sci* 8:722683. doi: 10.3389/fvets.2021.722683

Matanza, X. M., Lopez-Suarez, L., do Vale, A., and Osorio, C. R. (2021). The two-component system RstAB regulates production of a polysaccharide capsule with a role in virulence in the marine pathogen *Photobacterium damselae* subsp. damselae. *Environ. Microbiol.* 23, 4859–4880. doi: 10.1111/1462-2920.15731

Pogliano, J., Lynch, A. S., Belin, D., Lin, E. C., and Beckwith, J. (1997). Regulation of *Escherichia coli* cell envelope proteins involved in protein folding and degradation by the Cpx two-component system. *Genes Dev.* 11, 1169–1182. doi: 10.1101/gad.11.9.1169

Raffa, R. G., and Raivio, T. L. (2002). A third envelope stress signal transduction pathway in *Escherichia coli*. *Mol. Microbiol.* 45, 1599–1611. doi: 10.1046/j.1365-2958.2002.03112.x

Raivio, T. L., and Silhavy, T. J. (1997). Transduction of envelope stress in *Escherichia coli* by the Cpx two-component system. *J. Bacteriol.* 179, 7724–7733. doi: 10.1128/jb.179.24.7724-7733.1997

Rioux, S., Galarneau, C., Harel, J., Kobisch, M., Frey, J., Gottschalk, M., et al. (2000). Isolation and characterization of a capsule-deficient mutant of *Actinobacillus pleuropneumoniae* serotype 1. *Microb. Pathog.* 28, 279–289. doi: 10.1006/mpat.1999.0347

Sassu, E. L., Bosse, J. T., Tobias, T. J., Gottschalk, M., Langford, P. R., and Hennig-Pauka, I. (2018). Update on Actinobacillus pleuropneumoniae-knowledge, gaps and challenges. *Transbound. Emerg. Dis.* 65, 72–90. doi: 10.1111/tbed.12739

Srinivasan, V. B., Vaidyanathan, V., Mondal, A., and Rajamohan, G. (2012). Role of the two component signal transduction system CpxAR in conferring cefepime and chloramphenicol resistance in *Klebsiella pneumoniae* NTUH-K2044. *PLoS One* 7:e33777. doi: 10.1371/journal.pone.0033777

Stringer, O. W., Bosse, J. T., Lacouture, S., Gottschalk, M., Fodor, L., Angen, O., et al. (2021). Proposal of *Actinobacillus pleuropneumoniae* serovar 19, and reformulation of previous multiplex PCRs for capsule-specific typing of all known serovars. *Vet. Microbiol.* 255:109021. doi: 10.1016/j.vetmic.2021.109021

Tian, Z. X., Yi, X. X., Cho, A., O'Gara, F., and Wang, Y. P. (2016). CpxR activates MexAB-OprM efflux pump expression and enhances antibiotic resistance in both laboratory and clinical nalB-type isolates of Pseudomonas aeruginosa. *PLoS Pathog.* 12:e1005932. doi: 10.1371/journal.ppat.1005932

Vogt, S. L., and Raivio, T. L. (2012). Just scratching the surface: an expanding view of the Cpx envelope stress response. *FEMS Microbiol. Lett.* 326, 2–11. doi: 10.1111/j.1574-6968.2011.02406.x

Ward, C. K., and Inzana, T. J. (1997). Identification and characterization of a DNA region involved in the export of capsular polysaccharide by *Actinobacillus pleuropneumoniae* serotype 5a. *Infect. Immun.* 65, 2491–2496. doi: 10.1128/iai.65.6.2491-2496.1997

West, A. H., and Stock, A. M. (2001). Histidine kinases and response regulator proteins in two-component signaling systems. *Trends Biochem. Sci.* 26, 369–376. doi: 10.1016/s0968-0004(01)01852-7

Whitfield, C., Wear, S. S., and Sande, C. (2020). Assembly of bacterial capsular polysaccharides and exopolysaccharides. *Annu. Rev. Microbiol.* 74, 521–543. doi: 10.1146/annurev-micro-011420-075607

Xiong, Y., Huang, H., Chen, S., Dai, H., and Zhang, L. (2019). ERK5regulated RERG expression promotes cancer progression in prostatic carcinoma. *Oncol. Rep.* 41, 1160–1168. doi: 10.3892/or.2018.6852

Xu, L., Zhou, X., and He, X. (2014). Cpx two-component regulatory system in gram-negative bacteria--a review. *Wei Sheng Wu Xue Bao* 54, 269–275.

Xu, Z., Zhou, Y., Li, L., Zhou, R., Xiao, S., Wan, Y., et al. (2008). Genome biology of *Actinobacillus pleuropneumoniae* JL03, an isolate of serotype 3 prevalent in China. *PLoS One* 3:e1450. doi: 10.1371/journal.pone.0001450

Yan, K., Liu, T., Duan, B., Liu, F., Cao, M., Peng, W., et al. (2020). The CpxAR two-component system contributes to growth, stress resistance, and virulence of *Actinobacillus pleuropneumoniae* by upregulating wecA transcription. *Front. Microbiol.* 11:1026. doi: 10.3389/fmicb.2020.01026

frontiers | Frontiers in Microbiology

TYPE Original Research
PUBLISHED 13 October 2022
DOI 10.3389/fmicb.2022.1017792

OPEN ACCESS

EDITED BY
Qing Pan,
Qingdao Agricultural University,
China

REVIEWED BY
Vlad Petrovan,
The Pirbright Institute,
United Kingdom
Fernando Costa Ferreira,
University of Lisbon,
Portugal
Su Li,
Harbin Veterinary Research Institute (CAAS),
China

*CORRESPONDENCE
Zhijie Liu
liuzhijie@caas.cn

†These authors have contributed equally to this work

SPECIALTY SECTION
This article was submitted to Infectious Agents and Disease, a section of the journal Frontiers in Microbiology

RECEIVED 12 August 2022
ACCEPTED 20 September 2022
PUBLISHED 13 October 2022

CITATION
Yang J, Jing M, Niu Q, Wang J, Zhao Y, Liu M, Guan G, Luo J, Yin H and Liu Z (2022) Identification and characterization of nanobodies specifically against African swine fever virus major capsid protein p72.
Front. Microbiol. 13:1017792.
doi: 10.3389/fmicb.2022.1017792

Identification and characterization of nanobodies specifically against African swine fever virus major capsid protein p72

Jifei Yang[1†], Mengyao Jing[1†], Qingli Niu[1], Jinming Wang[1], Yaru Zhao[1,2], Meng Liu[3], Guiquan Guan[1], Jianxun Luo[1], Hong Yin[1,4] and Zhijie Liu[1,5*]

[1]African Swine Fever Regional Laboratory of China (Lanzhou), State Key Laboratory of Veterinary Etiological Biology, Lanzhou Veterinary Research Institute, Chinese Academy of Agricultural Sciences, Lanzhou, Gansu, China, [2]China Agricultural VET. BIO. Science and Technology Co, Ltd, Lanzhou, China, [3]Animal Husbandry and Veterinary Bureau of Dingxi City, Dingxi, Gansu, China, [4]Jiangsu Co-Innovation Center for the Prevention and Control of Important Animal Infectious Disease and Zoonosis, Yangzhou University, Yangzhou, China, [5]Institute of Special Animal and Plant Sciences, Chinese Academy of Agricultural Sciences, Changchun, China

African swine fever virus (ASFV) is a large and very complex DNA virus. The major capsid protein p72 is the most predominant structural protein and constitutes the outmost icosahedral capsid of the virion. In the present study, the nanobodies against ASFV p72 protein were screened from a camelid immune VHH library by phage display technique. Nine distinct nanobodies were identified according to the amino acid sequences of the complementary determining regions (CDRs), and contain typical amino acid substitutions in the framework region 2 (FR2). Six nanobodies were successfully expressed in *E. coli*, and their specificity and affinity to p72 protein were further evaluated. The results showed that nanobodies Nb25 had the best affinity to both recombinant and native p72 protein of ASFV. The Nb25 possesses an extremely long CDR3 with 23 amino acids compared with other nanobodies, which may allow this nanobody to access the hidden epitopes of target antigen. Furthermore, the Nb25 can specifically recognize the virus particles captured by polyclonal antibody against ASFV in a sandwich immunoassay, and its application as a biosensor to target virus in PAM cells was verified by an immunofluorescence assay. Nanobodies have been proven to possess many favorable properties with small size, high affinity and specificity, easier to produce, low costs and deep tissue penetration that make them suitable for various biotechnological applications. These findings suggest that nanobody Nb25 identified herein could be a valuable alternative tool and has potential applications in diagnostic and basic research on ASFV.

KEYWORDS

African swine fever, major capsid protein p72, phage display, nanobody, biosensor

Introduction

African swine fever (ASF) is one of the most devastating infectious diseases of domestic pigs and wild boar caused by African swine fever virus (ASFV) (Dixon et al., 2020). The disease is characterized by highly contagious, acute, hemorrhagic fever and exceptionally high lethality (Gallardo et al., 2019). Although the causative agent is very host specific and without zoonotic potential, the frequent outbreaks and the continue spread of the disease have caused serious socio-economic consequences globally (Ata et al., 2022). Since its identification in Georgia in 2007, the dispersal of ASF was accelerated and the situation worsened deeply after the outbreaks occurred in China in 2018 (Zhou et al., 2018; Dixon et al., 2020). Nowadays, continual outbreaks and spread of ASF are taking place in Europe and Asia. More recently, the disease was reintroduced into the Dominican Republic in July 2021 and later Haiti after its initial emergence in the Western hemisphere over 40 years (Gonzales et al., 2021; Urbano and Ferreira, 2022). In the last decade, great efforts and notable advances have been made on the vaccine development of ASF, especially for the live attenuated vaccines (LAVs) (Urbano and Ferreira, 2022). Previous attempts on the inactivated vaccines against ASFV have failed to induce protection (Dixon et al., 2020). Some viral antigens of ASFV have been evaluated and applied in the development of subunit, DNA and virus-vectored vaccines, which provide a variable degree of protection against challenge with ASFV (Urbano and Ferreira, 2022). Currently, several LAVs containing one or more deletion of virulence-associated genes in the genome have been reported and showed to confer fully protection during challenge, such as ASFV-G-Δ9GL/ΔUK, HLj/18-7GD and ASFV-G-ΔI177L (O'Donnell et al., 2017; Borca et al., 2020; Chen et al., 2020). Although LAVs seem to be the promising vaccine candidates against ASFV so far (Urbano and Ferreira, 2022); their safety, genetic stability and side effects in animals should be fully considered and evaluated prior to large-scale field application.

ASFV is the only known DNA arbovirus, the soft ticks of the genus *Ornithodoros* could serve as reservoirs and biological vectors, and the vector competences of *Ornithodoros moubata* in the sylvatic transmission cycle in Africa and *Ornithodoros erraticus* in Europe have been well documented (Plowright et al., 1974; Boinas et al., 2011). As the solely member of the *Asfivirus* genus of *Asfarviridae* family, ASFV is a large enveloped virus with 170 to 190 kb double stranded DNA genome, which contains more than 150 open reading frames (ORFs) and encodes 150 ~ 200 viral proteins, depending on virus isolates (de Villiers et al., 2010; Dixon et al., 2013; Alejo et al., 2018). Currently, 24 genotypes of ASFV have been identified based on the *B646L* gene, and the highly virulent genotype II is the major one circulating outside of Africa since its introduction into Caucasus in 2007 (Quembo et al., 2018; Ata et al., 2022).

Despite great efforts and decades of research, the functions of many ASFV-encoded proteins have not been disclosed yet (Gaudreault et al., 2020). The basic research relevant to virus invasion, replication and pathogenesis mechanisms is vital for the development of effective vaccine and other control measures of ASF. To date, 68 structural proteins of ASFV have been identified by mass spectrometry (Alejo et al., 2018). Among them, p72 is the most predominant structural protein and comprises 31 ~ 33% of the total protein of the virion (Carrascosa et al., 1984). It constitutes the outmost icosahedral capsid and is a high immunogenic viral protein, which has been efficiently used as an antigen for diagnostic purpose (Yu et al., 1996). Moreover, the p72 major capsid protein has also been proven to be involved in the virus attachment to target cells (Gomez Puertas et al., 1996). Recently, the high-resolution cryo-EM structure of the p72 protein has been reported and the results revealed that three p72 molecules form a thermostable trimer with the assistance of B602L (Liu et al., 2019).

Nanobodies, also referred to single-domain antibodies, are derived from heavy-chain antibodies (HCAbs) that naturally occurring in sera of camelids and lacking light chains. As a novel type of antibody fragment, nanobody has attracted extensive interest and is expected to be applied as a potential tool in the research and biomedical fields in the past two decades (Hamers-Casterman et al., 1993). Compared with conventional antibodies, nanobodies have been shown to possess many striking properties, including high affinity and specificity, small molecular size, economical and easy production, deep tissue penetration and recognition of hidden epitopes (Muyldermans, 2013; Salvador et al., 2019). Due to the beneficial properties, an increasing number of nanobodies have been explored and used in a wide range of routine and innovative applications for diagnostics and therapeutics (Salvador et al., 2019).

In this study, specific nanobodies against ASFV p72 protein were screened from a camelid VHH library by phage display technique. The identified nanobodies could be used as valuable alternative tools in diagnostic and research purposes on ASFV.

Materials and methods

Biosafety and ethics statements

All experiments involving ASFV were conducted under biosafety level 3 (BSL-3) facilities in Lanzhou Veterinary Research Institute (LVRI) of Chinese Academy of Agricultural Sciences (CAAS), and were accredited by China National Accreditation Service for Conformity Assessment (CNAS) and the Ministry of Agriculture and Rural Affairs of China. The animal treatments and sample collection were performed in accordance with the Animal Ethics Procedures and Guidelines and have been approved by the Animal Ethics Committee of LVRI, CAAS.

Cells, virus, and samples

The primary porcine alveolar macrophages (PAMs) were isolated by lung lavage from 2 months old healthy pig tested negative

for ASFV, classical swine fever virus (CSFV), porcine reproductive and respiratory syndrome virus (PRRSV), pseudorabies virus (PRV), porcine parvovirus (PPV) and porcine circovirus type 2 (PCV2). PAM cells were cultured in RPMI 1640 medium (Gibco, United States) containing 10% (*v*/*v*) fetal bovine serum (FBS; Gibco, United States) and antibiotics (100 units/ml penicillin and 100 mg/ml streptomycin) at 37°C in a 5% CO_2 incubator, as described previously (Malmquist and Hay, 1960). ASFV genotype II strain CN/SC/2019 and the positive sera collected from surviving pigs naturally infected by virus were provided by African Swine Fever Regional Laboratory of China (Lanzhou).

Phage display VHH library and bio-panning

The phage display library containing VHHs raised against ASFV p72 protein (GenBank: FR682468) was previously constructed from peripheral blood lymphocytes of immunized Bactrian camels (*Camelus bactrianus*) in our laboratory, with a library capacity of 2.2×10^8 cfu/ml. The generated VHH library exhibited high capacity with a correct insert rate of 91.2% and rich sequence diversity of complementary determining regions (CDRs) determined by colony PCR and sequencing (Zhao, 2019). The nanobodies specifically against ASFV p72 protein were screened from the generated phage display library by bio-panning as described previously (Sheng et al., 2019). After rescued by helper phage M13K07, three consecutive rounds of bio-panning were carried out on solid phase coated p72 antigen. Briefly, the recombinant p72 protein was coated onto a microtiter plate at a concentration of 10 μg/ml and blocked with 5% skim milk in PBST (PBST containing 0.05% Tween 20). Antigen free wells were set up for the blank control. In order to eliminate no specific binding, the recombinant phage particles were primary incubated with 2% skim milk for 30 min, and then added to the blocked wells and incubated with coated antigen for 1 h. After washing nine time with 0.1% PBST (PBS containing 0.1% Tween), the bound phages were eluted from the plate and used to infect exponential *E. coli* TG1 cells for amplification and titration. The amplified phages were used in the following round of bio-panning. Decreased antigen on coated plate (5 μg/ml and 2 μg/ml) and intensive washing buffer with increased concentrations of Tween 20 in PBST (0.2 and 0.3% PBST) were used in the second and third round of bio-panning to remove the off-target and weak binders, respectively. The enrichments for antigen-specific phages of each round of bio-panning were assessed according to the number of output and input phages.

Phage ELISA

After three rounds of bio-panning, 40 individual colonies were randomly selected and subjected to monoclonal phage ELISA to identify the binders with p72 protein as previous described (Yang et al., 2014). Briefly, clones were cultured in 2×YT-AG medium (supplemented with 100 μg/ml ampicillin and 1% glucose) to OD_{600} reached 0.4 ~ 0.5 and infected with M13K07 helper phage. A microliter plate was coated with 2.5 μg/ml recombinant p72 protein overnight at 4°C, and PBS was used as a negative control. After washing three times with PBST, the plate was blocked with 2.5% (w/v) skim milk in PBS for 2 h at room temperature (RT). Then, recombinant phages were incubated in the antigen coated microliter plate for 2 h at RT. The plate was washed six times, and the rabbit anti-M13 IgG was added to each well and incubated for 1 h at 37°C. The plate was washed again, and the goat anti-rabbit IgG conjugated to HRP was added and incubated for 1 h at 37°C. After another washing step, the colorimetric reaction was developed by adding of o-phenylenediamine dihydrochloride (OPD) substrate solution and incubated for 30 min at RT. The reaction was stopped by 3 M H_2SO_4 and the absorbance at 490 nm was measured by a microtiter plate reader (Thermofisher, United States). Colonies were considered to be positive when their absorbance was 3-fold more than that of negative control. The plasmids from positive colonies were sequenced (Sangon Biotech Co. Ltd., Shanghai, China) to identify different nanobodies.

Expression and purification of nanobodies

The identified VHH genes of positive clones were amplified by PCR with primers VHH-F (5′-CGGAATTCGATGTGCAGCTG GTGGAGTCT-3′) and VHH-R (5′- TGCTCGAGTGAGGAGAC AGTGACCTGGGTCC-3′). They were subcloned into the expression vector pET-28a by *EcoR* I and *Xho* I restriction enzyme sites. After confirmed by PCR and sequencing, the recombinant plasmids were transformed into the *E. coli* BL21 (DE3) competent cells. Then, the *E. coli* cells were cultured in terrific broth medium (containing 50 μg/ml kanamycin) and incubated at 37°C with shaking at 200 rpm/min. Once the optical density reached 0.6 ~ 0.8, the cultures were induced using *isopropy β-D-thiogalactopyranoside* (IPTG) at a final concentration of 0.4 mM and incubated for 7 ~ 9 h at 37°C with shaking at 220 rpm. The cells were harvested by 8,000 × g centrifugation for 10 min. Cell pellet was resuspended in PBS and disrupted by ultrasonication on ice bath. The expressed nanobodies were purified using affinity chromatography on nickel column (GE Healthcare, United States). The purified nanobodies were further identified by sodium dodecyl sulfate polyacrylamide gel electrophoresis (SDS-PAGE) and quantified by Qubit 2.0 fluorometer using Qubit Protein Assay Kit (Qubit, Thermo Fisher Scientific) according to the protocols.

The reactivity of isolated nanobodies

The reactivity of nanobodies was analyzed by an indirect ELISA. The microtiter plate was coated with 100 μl (1 μg/ml) nanobodies diluted in carbonate buffer and incubated at 4°C

overnight. After washing three times with PBST, 100 µl (5 µg/ml) of ASFV p72 protein was added to each well and incubated for 1 h at 37°C. The plate was washed and blocked with 1% BSA in PBST for 1 h at 37°C. Then, the ASFV positive and negative swine sera (diluted 1:100 in PBST) were added and incubated for 1 h at 37°C. The plate was washed and 100 µl of HRP-conjugated rabbit anti-pig antibody (diluted 1:20,000 in PBST, sigma, United States) was added and incubated for 1 h at 37°C. After another washing step, 100 µl of TMB substrate was added to develop the color reactions. Afterward, the reaction was terminated with 0.3 M H_2SO_4 and the absorbance at 450 nm was measured by a microtiter plate reader (Thermofisher, United States). All assays were carried out in duplicate.

The specificity of isolated nanobodies

Primary PAMs were inoculated with ASFV at a multiplicity of infection (MOI) of 1.0. The cells and supernatants were collected at 96 h post-infection and then lysed by freeze–thaw cycles. Cell debris was removed by centrifugation at 4°C and 12,000 × g for 15 min and cell-free supernatant containing viral particles was collected for further analysis. The IgG purified from ASFV-positive swine sera using Protein A-immunomagnetic beads (Sangon Biotech Co. Ltd., Shanghai, China) was coated (1:1000 diluted in carbonate buffer) on the microtiter plate and incubated at 4°C overnight. The plate was washed three time with PBST, and the diluted virus stock (1:20 in PBS) was added and incubated for 1 h at 37°C. The plate was washed and blocked with 1% BSA in PBST for 1 h at 37°C. Then, nanobodies was added and incubated for 1 h at 37°C, and PBS was used as a negative control. The plate was washed again and incubated with HRP-conjugated rabbit anti-His IgG (diluted 1:15,000 in PBST, Abcam, United Kingdom) for 1 h at 37°C. After another washing step, the colorimetric reaction was developed and measured as aforementioned. All assays were carried out in duplicate.

Western blot analysis

Primary PAMs infected with ASFV at an MOI of 1.0 were collected at 96 h post-infection. The cell lysates were separated by SDS-PAGE and transferred to a polyvinylidene fluoride (PVDF) membrane. The membrane was blocked with 5% skim milk in TBST (Tris-buffered saline containing 0.05% Tween 20) at 4°C overnight. The membrane was washed three times and incubated with nanobodies for 1 h at RT. Then, the membrane was washed and incubated with HRP-conjugated rabbit anti-His IgG (diluted 1:2,000, Abcam, United Kingdom) for 1 h at RT. After washed again, the immunoreactive bands were visualized with a chemiluminescent substrate (ECL; Thermo-Fisher, United States).

Immunofluorescence assay

Nanobodies were conjugated with fluorescein isothiocyanate (FITC) using a FITC Conjugation Kit (Bioss, China) according to the manufacturer's instructions. Primary PAMs were seeded in glass bottom cell culture dishes (NEST, China) at a density of 4.0×10^6 cells and infected with ASFV at an MOI of 1.0. At 48 h post-infection, ASFV-infected or negative control cells were fixed with 4% paraformaldehyde for 10 min, permeabilized in 0.1% Triton-X 100 for 10 min, and blocked with 5% BSA for 1 h at RT. The fixed ASFV-free and -infected PAMs were washed three times with PBS and incubated with FITC-conjugated nanobodies for 1 h at 37°C. Moreover, ASFV-infected PAMs were also incubated with ASFV-positive and -negative serum for 1 h at 37°C, respectively. After washing three times with PBS, the FITC-conjugated rabbit anti-pig IgG (Sigma, United States) was added and incubated for 1 h at 37°C. Then, cells were incubated with DAPI (Invitrogen, United States) for 2 min at RT and rinsed with PBS. The cells were visualized for immunofluorescence with a fluorescence microscope (Leica, Germany).

Results

Bio-panning and phage ELISA analysis

In the present study, three consecutive rounds of bio-panning were performed to isolate the nanobodies specific for ASFV p72 protein from a phage display VHH library. The enrichment of phages of each round of bio-panning was evaluated and the results showed that the recombinant phage particles were significantly enriched during the bio-panning (Table 1). In order to verify whether the enriched phages contained specific VHHs against ASFV-p72 protein, 40 clones were selected from the final round of bio-panning and subjected to single-phage ELISA for further identification of specific binders. The results revealed that all selected clones were positive and showed a good target recognition with binding ratios in contrast to blank control of greater than 3.0 (Figure 1).

Alignment of VHH amino acid sequences

All 40 clones were subsequently sequenced and showed to contain the correct framework regions of VHH fragments.

TABLE 1 The enrichment of the nanobodies in the phage display library as detected through three rounds of bio-panning.

Round	Input	Output	Enriching factor (input / output)
1st	3.80×10^{11}	1.66×10^{5}	2.29×10^{6}
2nd	1.93×10^{12}	1.40×10^{8}	1.38×10^{4}
3rd	2.49×10^{11}	3.59×10^{8}	6.94×10^{2}

Sequence analysis revealed that nine distinct nanobodies were obtained based on the amino acid sequence classification of the complementary determining regions (CDRs). These nanobodies were designated as Nb6, Nb8, Nb10, Nb11, Nb13, Nb16, Nb23, Nb25 and Nb29, respectively (Figure 2). Among them, typical amino acid substitutions were observed in the framework region 2 (FR2), including G/E and L/R substitutions at positions 44 and 45 of all nanobodies, V/Y and W/L substitutions at positions 37 and 47 of seven nanobodies (Nb6, Nb8, Nb13, Nb16, Nb23, Nb25, and Nb29), and V/F and W/G substitutions at positions 37 and 47 of two nanobodies (Nb10 and Nb11), respectively (Figure 2). These results indicated that they are camelid-derived heavy-chain-only antibodies. Moreover, these nanobodies possess especially long CDR3, which contain 17–23 amino acids and exhibit high sequence variability (Figure 2).

Expression and purification of nanobodies

The VHH sequences identified from the positive clones were inserted into the expression vector pET-28a, and transformed into *E. coli*. After IPTG induction, six nanobodies (Nb6, Nb8, Nb10, Nb13, Nb23 and Nb25) possess hypervariable CDR3 were successfully expressed with a His-tag. The purification of nanobodies were performed using Ni-NTA affinity column and analyzed by SDS-PAGE. The results showed that the nanobodies were isolated with high purity and exhibited specific band with approximately 20 kDa, which is consistent with the expected molecular size (Figure 3).

The reactivity of isolated nanobodies

The affinities of the six nanobodies bind with ASFV-p72 protein were assessed by ELISA. ASFV-p72 protein was incubated with solid phase coated nanobodies as capture reagents, and the immunoreaction was further determined by ASFV-positive swine sera and HRP-conjugated rabbit anti-pig antibody. The results revealed that all six nanobodies could capture ASFV-p72 protein, and high ratios of the absorbance values at $OD_{450\,nm}$ between positive and negative sera were observed (Figure 4A). These results suggest that six nanobodies had relatively high affinities to ASFV-p72 protein.

The specificity of isolated nanobodies

In order to determine whether the nanobodies could bind with native p72 protein of ASFV, a sandwich ELISA was performed. The polyclonal antibody against ASFV was coated on the microtiter plate and applied to capture ASFV particles, and the nanobodies were subsequently allowed to react with viral antigen. In contrast to other nanobodies, Nb25 showed highest binding capacity to native ASFV p72 protein (Figure 4B). The interaction between Nb25 and native ASFV p72 protein was further validated by Western blot. The results showed that Nb25 can specifically recognize the p72 protein of ASFV particles, and excluded the possibility that Nb25 react with His tag of recombinant protein (Figure 4C).

ASFV imaging in PAM cells with Nb25 probe

The PAM cells infected with ASFV were fixed and the presence of virus particles was detected by direct immunofluorescence

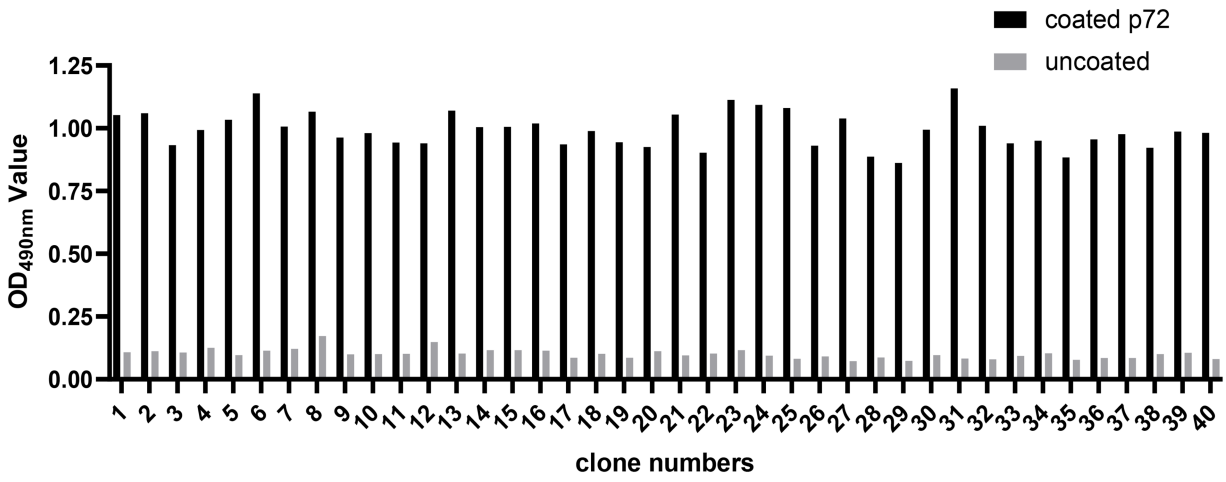

FIGURE 1
Identification of ASFV p72 protein binding phages by monoclonal phage ELISA. Forty clones selected from final round bio-panning were detected, and all of them were identified as positive. The clone was regarded as positive if the absorbance in the antigen-coated well was at least threefold greater than that in uncoated well.

10.3389/fmicb.2022.1017792

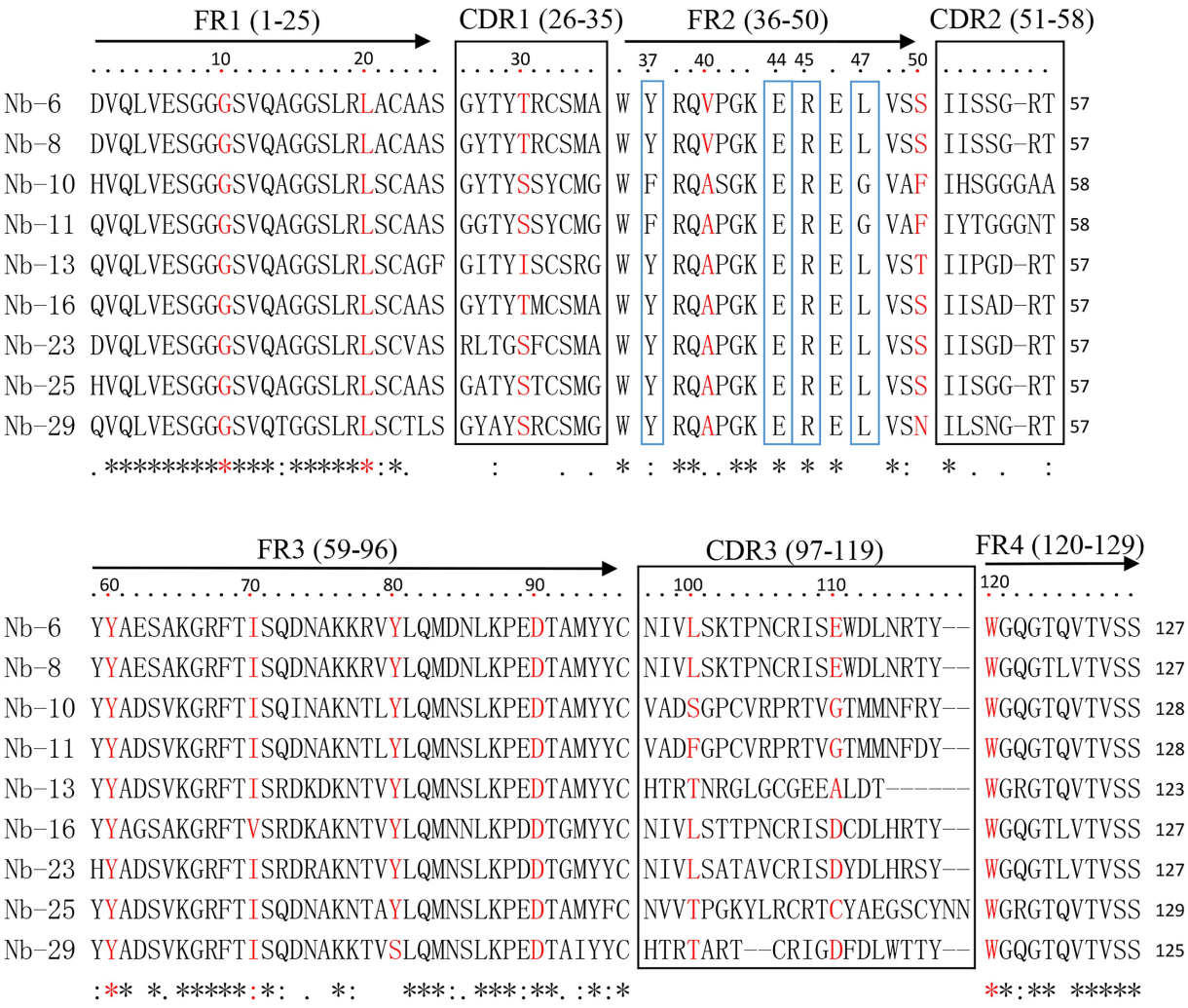

FIGURE 2
Alignment of amino acid sequence of nanobodies against ASFV p72 protein. The sequences are grouped according to their CDRs. The residues at positions 37, 44, 45, and 47 in FR2 are indicated by blue boxes.

assay. As shown in Figure 5, ASFV was localized in the cytoplasm after cells were probed with Nb25 conjugated with FITC, and no fluorescence was observed as expected in negative control. The indirect immunofluorescence assay also showed that ASFV can be detected in PAM cells by ASFV-positive serum and the FITC-conjugated rabbit anti-pig IgG (Figure 5). These results suggested that Nb25 can bind with ASFV specifically. As a consequence, Nb25 is a desirable probe to target and visualize ASFV *in vitro* and has potential applications in basic research on ASFV.

Discussion

Antibodies are very important biological macromolecules that have been widely used for detection, targeting and basic research purposes due to their high affinity and specificity (Salvador et al., 2019). However, the performance of traditional antibodies is still confined in terms of big size, poor penetration and problems in large-scale preparation. As aforementioned, nanobodies exhibit many advantages that could overcome these drawbacks, and make them suitable for various biological applications (Salvador et al., 2019). In the present study, nanobodies against ASFV p72 were screened from the camelid immune VHH library. After three rounds of bio-panning, the recombinant phage particles were enriched obviously, and all selected clones were positive to target protein. These results suggested that the panning process conducted herein is highly efficient and three rounds of panning could sufficiently enrich the recombinant clones containing specific VHHs (Muyldermans, 2013). Ultimately, nine distinct nanobodies specific for p72 protein were retrieved and identified according to their diverse amino acid sequences of CDRs, which are responsible for the antigen binding specificity. Furthermore, these nanobodies possess the hallmark amino acid substitutions

at specific sites in the FR2 that involved in the VH/VL interaction of conventional antibodies (Gonzalez-Sapienza et al., 2017).

The molecule of nanobody is 10-fold smaller than conventional antibody (Hamers-Casterman et al., 1993). Owing to its small size, the engineering and recombinant expression of nanobody *in vitro* are readily achieved using prokaryotic and eukaryotic expression systems. In this study, six nanobodies specific to ASFV p72 were expressed in *E. coli*, and their affinities bind with target were subsequently verified by ELISA. Although all six nanobodies could bind with recombinant p72 protein with high affinities, their binding affinities to native p72 protein of ASFV varied significantly. This is probably due to the recombinant p72 protein was applied in the bio-panning and screen processes.

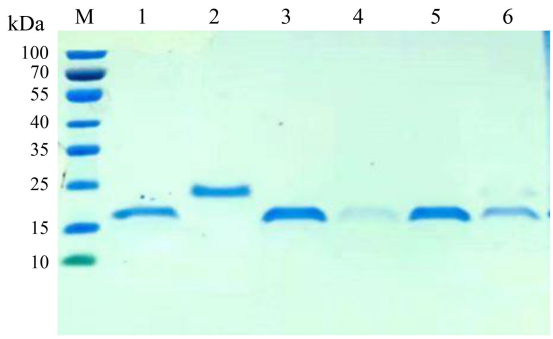

FIGURE 3
SDS-PAGE analysis of the purification of nanobodies. M: protein molecular marker; lane 1: The purified Nb6; lane 2: Nb8; lane 3: Nb10; lane 4: Nb13; lane 5: Nb23; lane 6: Nb25.

Among those nanobodies, Nb25 had the best affinity to native p72 protein determined by ELISA and Western blot. According to the sequence analysis, the Nb25 possess an extremely long CDR3 with 23 amino acids compared with other nanobodies. The long CDR3s are more frequently observed in camelid nanobodies, which can enhance the affinity of nanobodies to target antigens (Nguyen et al., 2000). In addition, the CDR1 and CDR3 of Nb25 contains cysteine residues, the stability of this nanobody might be reinforced by the intermolecular disulfide bridge formed between Cys residues of CDR1 and CDR3. Its small size, extremely long CDR3 and high stability allow Nb25 to better access the concave or hidden epitopes of p72 protein, which may not be accessed by conventional antibodies (Lutje Hulsik et al., 2013; Gonzalez-Sapienza et al., 2017).

Owing to their intrinsic and unique properties, nanobodies have been widely used in the detection of specific causative agents in laboratory tests (Salvador et al., 2019). More recently, several nanobodies against the p54 and K205R protein of ASFV have been isolated from the camelid immune library, they were subsequently applied in the development of nanobody-based cELISA for detection of ASFV antibodies (Zhang et al., 2022; Zhao et al., 2022). In the present study, the nanobodies specific for native p72 protein were selected by a sandwich ELISA, and the Nb25 can specifically recognize the virus particles captured by polyclonal antibody against ASFV. Therefore, the nanobody Nb25 might be served as a potential new diagnostic reagent for detection of ASFV.

The nanobodies exhibit high target specificity and have better tissue penetration than conventional antibodies because of their smaller molecular size, which are suitable for the imaging and investigation of target proteins at the cellular level

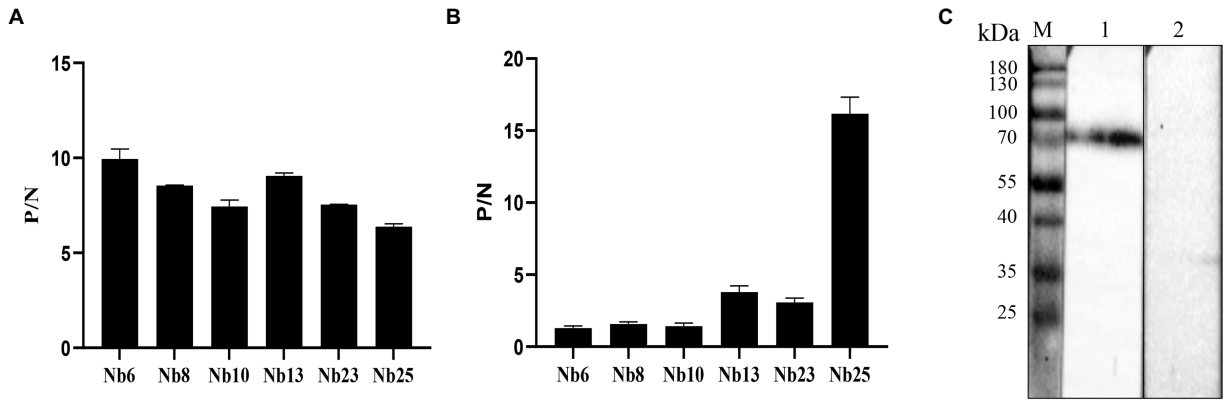

FIGURE 4
Specificity and affinity of nanobodies with ASFV p72 protein. **(A)** The affinity of nanobodies with recombinant p72 protein analyzed by an indirect ELISA. ASFV-p72 protein was incubated with solid phase coated nanobodies. The ASFV-positive serum and HRP-conjugated rabbit anti-pig antibody were then added. The ASFV-negative serum was used as negative control. The P/N value is the average of two wells. Error bars represent ±SD. **(B)** The affinity of nanobodies with native p72 protein of ASFV analyzed by a sandwich ELISA. The polyclonal antibody against ASFV was coated on the microtiter plate. The diluted virus stock was added to each well. The nanobody was then added, and PBS was used as negative control. The P/N value is the average of two wells. Error bars represent ±SD. **(C)** The specificity of Nb25 analyzed by Western blot. The p72 protein in PVDF membrane was detected by Nb25 and HRP-conjugated rabbit anti-His IgG. M: protein molecular marker; lane 1: PAM cells inoculated with ASFV; lane 2: Negative control.

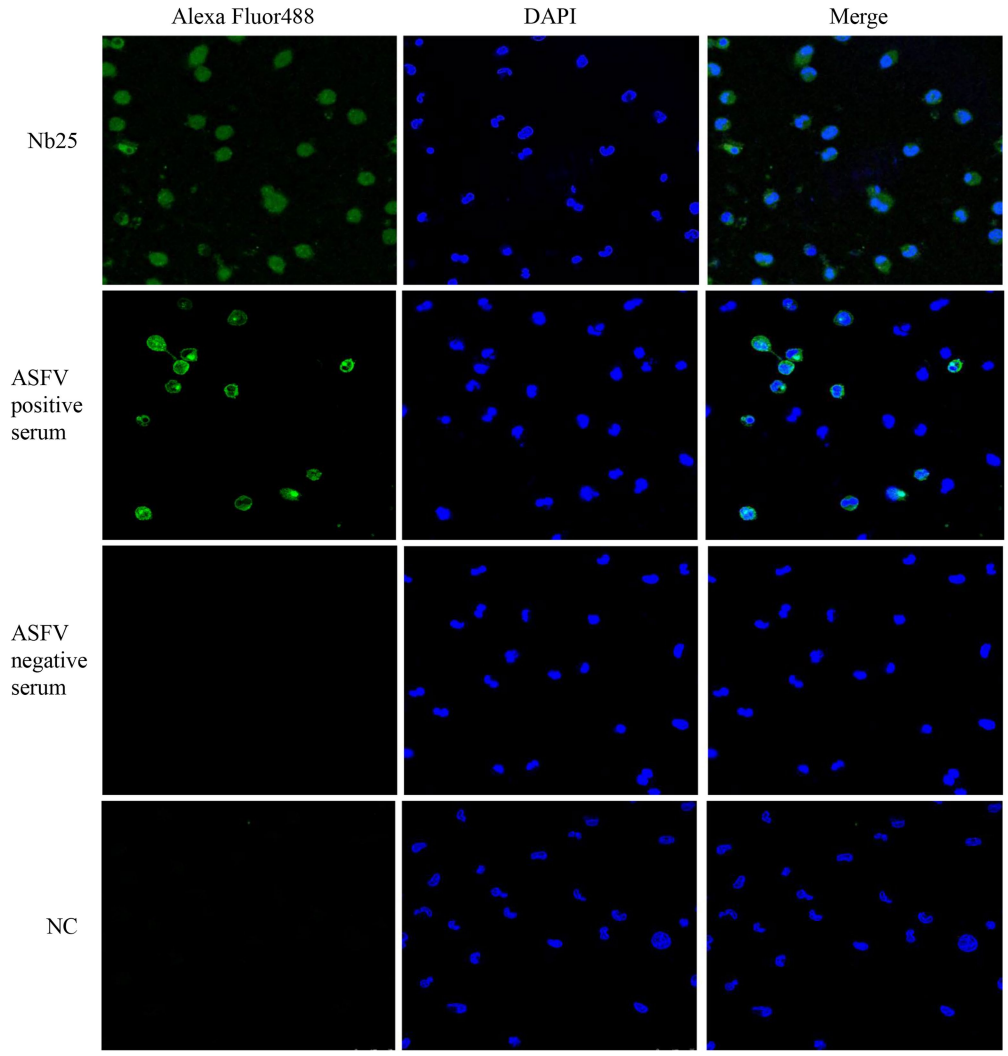

FIGURE 5
Nb25 as biosensor in imaging ASFV in PAM cells. The PAM cells were immobilized at 48h post ASFV infection, virus free PAM cells were used as a negative control (NC). ASFV in PAM cells was detected by immunofluorescence assay based on FITC-Nb25, ASFV-positive and -negative serum. ASFV free PAM cells were used as negative control (NC). Nucleus were stained with DAPI.

(Salvador et al., 2019; Bao et al., 2021). As a good tracer, nanobody has been considered to be an attractive alternative for cancer imaging by target tumor specific biomarker (Vaneycken et al., 2011); and it has also been developed as biosensors to target and trace virus in cells, such as foot and mouth disease virus (FMDV) (Wang et al., 2015) and PEDV (Yang et al., 2018). In this study, the immunofluorescence assay revealed that ASFV can be targeted by Nb25 in PAM cells. Therefore, this nanobody could be used as a biosensor for the dynamic tracing of ASFV in living cells, which may be desired to be a promising tool and applied in the basic research related to virus-host interaction in the future.

In conclusion, ASFV p72 specific nanobodies were screened from a camelid immune VHH library by the phage display technique. The nanobody Nb25 was identified and showed high specificity and affinity to both recombinant and native p72 protein of ASFV. Furthermore, the p72-specific Nb25 could be used as a biosensor in tracing, diagnostic applications and basic research on ASFV.

Data availability statement

The raw data supporting the conclusions of this article will be made available by the authors, without undue reservation.

Author contributions

JY and ZL: conceptualization, data curation, formal analysis, and funding acquisition. JY and MJ: investigation, methodology, and writing-original draft. JW, QN, and YZ: methodology, formal analysis, clinical sample detection. ML, GG, JL, and HY: formal

analysis, review, and editing. All authors contributed to the article and approved the submitted version.

Funding

This study was financially supported by the National Natural Science Foundation of China (31941012 and 32072830), the Longyuan Youth Innovation and Entrepreneurship Talent Project (2021LQGR24), the Natural Science Foundation of Gansu (21JR7RA018), Gansu Provincial Major Project for science and technology development (20ZD7NA006), ASTIP (CAAS-ASTIP-2016-LVRI), the Jiangsu Co-innovation Center program for Prevention and Control of Important Animal Infectious Diseases and Zoonoses.

Acknowledgments

We thank the staff for their assistance and work at the Core Facility and ABSL-3 Facility, Lanzhou Veterinary Research Institute, Chinese Academy of Agricultural Sciences. We also thank Associate Professor Yin Shuanghui and Wu Jinyan for their support and assistance for this study.

Conflict of interest

YZ was employed by China Agricultural VET. BIO. Science and Technology Co, Ltd.

The remaining authors declare that the research was conducted in the absence of any commercial or financial relationships that could be construed as a potential conflict of interest.

Publisher's note

References

Alejo, A., Matamoros, T., Guerra, M., and Andres, G. (2018). A proteomic atlas of the African swine fever virus particle. *J. Virol.* 92:e01293. doi: 10.1128/JVI.01293-18

Ata, E. B., Li, Z. J., Shi, C. W., Yang, G. L., Yang, W. T., and Wang, C. F. (2022). African swine fever virus: a raised global upsurge and a continuous threaten to pig husbandry. *Microb. Pathog.* 167:105561. doi: 10.1016/j.micpath.2022.105561

Bao, G., Tang, M., Zhao, J., and Zhu, X. (2021). Nanobody: a promising toolkit for molecular imaging and disease therapy. *EJNMMI Res.* 11:6. doi: 10.1186/s13550-021-00750-5

Boinas, F. S., Wilson, A. J., Hutchings, G. H., Martins, C., and Dixon, L. J. (2011). The persistence of African swine fever virus in field-infected Ornithodoros erraticus during the ASF endemic period in Portugal. *PLoS One* 6:e20383. doi: 10.1371/journal.pone.0020383

Borca, M. V., Ramirez-Medina, E., Silva, E., Vuono, E., Rai, A., Pruitt, S., et al. (2020). Development of a highly effective African swine fever virus vaccine by deletion of the I177L gene results in sterile immunity against the current epidemic Eurasia strain. *J. Virol.* 94:e02017. doi: 10.1128/JVI.02017-19

Carrascosa, J. L., Carazo, J. M., Carrascosa, A. L., Garcia, N., Santisteban, A., and Vinuela, E. (1984). General morphology and capsid fine structure of African swine fever virus particles. *Virology* 132, 160–172. doi: 10.1016/0042-6822(84)90100-4

Chen, W., Zhao, D., He, X., Liu, R., Wang, Z., Zhang, X., et al. (2020). A seven-gene-deleted African swine fever virus is safe and effective as a live attenuated vaccine in pigs. *Sci. China Life Sci.* 63, 623–634. doi: 10.1007/s11427-020-1657-9

de Villiers, E. P., Gallardo, C., Arias, M., da Silva, M., Upton, C., Martin, R., et al. (2010). Phylogenomic analysis of 11 complete African swine fever virus genome sequences. *Virology* 400, 128–136. doi: 10.1016/j.virol.2010.01.019

Dixon, L. K., Chapman, D. A., Netherton, C. L., and Upton, C. (2013). African swine fever virus replication and genomics. *Virus Res.* 173, 3–14. doi: 10.1016/j.virusres.2012.10.020

Dixon, L. K., Stahl, K., Jori, F., Vial, L., and Pfeiffer, D. U. (2020). African swine fever epidemiology and control. *Annu. Rev. Anim. Biosci.* 8, 221–246. doi: 10.1146/annurev-animal-021419-083741

Gallardo, C., Fernandez-Pinero, J., and Arias, M. (2019). African swine fever (ASF) diagnosis, an essential tool in the epidemiological investigation. *Virus Res.* 271:197676. doi: 10.1016/j.virusres.2019.197676

Gaudreault, N. N., Madden, D. W., Wilson, W. C., Trujillo, J. D., and Richt, J. A. (2020). African swine fever virus: an emerging DNA Arbovirus. *Front. Vet. Sci.* 7:215. doi: 10.3389/fvets.2020.00215

Gomez Puertas, P., Rodriguez, F., Oviedo, J. M., Ramiro Ibanez, F., Ruiz Gonzalvo, F., Alonso, C., et al. (1996). Neutralizing antibodies to different proteins of African swine fever virus inhibit both virus attachment and internalization. *J. Virol.* 70, 5689–5694. doi: 10.1128/jvi.70.8.5689-5694.1996

Gonzales, W., Moreno, C., Duran, U., Henao, N., Bencosme, M., Lora, P., et al. (2021). African swine fever in the Dominican Republic. *Transbound. Emerg. Dis.* 68, 3018–3019. doi: 10.1111/tbed.14341

Gonzalez-Sapienza, G., Rossotti, M. A., and Tabares-da Rosa, S. (2017). Single-domain antibodies as versatile affinity reagents for analytical and diagnostic applications. *Front. Immunol.* 8:977. doi: 10.3389/fimmu.2017.00977

Hamers-Casterman, C., Atarhouch, T., Muyldermans, S., Robinson, G., Hamers, C., Songa, E. B., et al. (1993). Naturally occurring antibodies devoid of light chains. *Nature* 363, 446–448. doi: 10.1038/363446a0

Liu, Q., Ma, B., Qian, N., Zhang, F., Tan, X., Lei, J., et al. (2019). Structure of the African swine fever virus major capsid protein p72. *Cell Res.* 29, 953–955. doi: 10.1038/s41422-019-0232-x

Lutje Hulsik, D., Liu, Y. Y., Strokappe, N. M., Battella, S., El Khattabi, M., McCoy, L. E., et al. (2013). A gp41 MPER-specific llama VHH requires a hydrophobic CDR3 for neutralization but not for antigen recognition. *PLoS Pathog.* 9:e1003202. doi: 10.1371/journal.ppat.1003202

Malmquist, W. A., and Hay, D. (1960). Hemadsorption and cytopathic effect produced by African swine fever virus in swine bone marrow and buffy coat cultures. *Am. J. Vet. Res.* 21, 104–108. PMID: 14420403

Muyldermans, S. (2013). Nanobodies: natural single-domain antibodies. *Annu. Rev. Biochem.* 82, 775–797. doi: 10.1146/annurev-biochem-063011-092449

Nguyen, V. K., Hamers, R., Wyns, L., and Muyldermans, S. (2000). Camel heavy-chain antibodies: diverse germline V(H)H and specific mechanisms enlarge the antigen-binding repertoire. *EMBO J.* 19, 921–930. doi: 10.1093/emboj/19.5.921

O'Donnell, V., Risatti, G. R., Holinka, L. G., Krug, P. W., Carlson, J., Velazquez-Salinas, L., et al. (2017). Simultaneous deletion of the 9GL and UK genes from the African swine fever virus Georgia 2007 isolate offers increased safety and protection against homologous challenge. *J. Virol.* 91:e01760. doi: 10.1128/JVI.01760-16

Plowright, W., Perry, C. T., and Greig, A. (1974). Sexual transmission of African swine fever virus in the tick, Ornithodoros moubata porcinus, Walton. *Res. Vet. Sci.* 17, 106–113. doi: 10.1016/S0034-5288(18)33716-0

Quembo, C. J., Jori, F., Vosloo, W., and Heath, L. (2018). Genetic characterization of African swine fever virus isolates from soft ticks at the wildlife/domestic interface

in Mozambique and identification of a novel genotype. *Transbound. Emerg. Dis.* 65, 420–431. doi: 10.1111/tbed.12700

Salvador, J. P., Vilaplana, L., and Marco, M. P. (2019). Nanobody: outstanding features for diagnostic and therapeutic applications. *Anal. Bioanal. Chem.* 411, 1703–1713. doi: 10.1007/s00216-019-01633-4

Sheng, Y. M., Wang, K., Lu, Q. Z., Ji, P. P., Liu, B. Y., Zhu, J. H., et al. (2019). Nanobody-horseradish peroxidase fusion protein as an ultrasensitive probe to detect antibodies against Newcastle disease virus in the immunoassay. *J. Nanobiotechnol.* 17:35. doi: 10.1186/s12951-019-0468-0

Urbano, A. C., and Ferreira, F. (2022). African swine fever control and prevention: an update on vaccine development. *Emerg. Microbes Infect.* 11, 2021–2033. doi: 10.1080/22221751.2022.2108342

Vaneycken, I., Devoogdt, N., Van Gassen, N., Vincke, C., Xavier, C., Wernery, U., et al. (2011). Preclinical screening of anti-HER2 nanobodies for molecular imaging of breast cancer. *FASEB J.* 25, 2433–2446. doi: 10.1096/fj.10-180331

Wang, D., Yang, S., Yin, S., Shang, Y., Du, P., Guo, J., et al. (2015). Characterization of single-domain antibodies against foot and mouth disease virus (FMDV) serotype O from a camelid and imaging of FMDV in baby hamster kidney-21 cells with single-domain antibody-quantum dots probes. *BMC Vet. Res.* 11:120. doi: 10.1186/s12917-015-0437-2

Yang, S., Li, L., Yin, S., Shang, Y., Khan, M. U. Z., He, X., et al. (2018). Single-domain antibodies as promising experimental tools in imaging and isolation of porcine epidemic diarrhea virus. *Appl. Microbiol. Biotechnol.* 102, 8931–8942. doi: 10.1007/s00253-018-9324-7

Yang, S., Shang, Y., Yin, S., Tian, H., Chen, Y., Sun, S., et al. (2014). Selection and identification of single-domain antibody fragment against capsid protein of porcine circovirus type 2 (PCV2) from C. bactrianus. *Vet. Immunol. Immunopathol.* 160, 12–19. doi: 10.1016/j.vetimm.2014.03.004

Yu, M., Morrissy, C. J., and Westbury, H. A. (1996). Strong sequence conservation of African swine fever virus p72 protein provides the molecular basis for its antigenic stability. *Arch. Virol.* 141, 1795–1802. doi: 10.1007/BF01718302

Zhang, A., Wu, S., Duan, X., Zhao, H., Dong, H., Ren, J., et al. (2022). K205R specific nanobody-horseradish peroxidase fusions as reagents of competitive ELISA to detect African swine fever virus serum antibodies. *BMC Vet. Res.* 18:321. doi: 10.1186/s12917-022-03423-0

Zhao, Y. (2019). Establishment of Sandwich ELISA based on the single domain antibodies against the structural protein of African swine fever virus. [dissertation/master's thesis]. [China]: Chinese Academy of Agricultural Sciences.

Zhao, H., Ren, J., Wu, S., Guo, H., Du, Y., Wan, B., et al. (2022). HRP-conjugated-nanobody-based cELISA for rapid and sensitive clinical detection of ASFV antibodies. *Appl. Microbiol. Biotechnol.* 106, 4269–4285. doi: 10.1007/s00253-022-11981-4

Zhou, X., Li, N., Luo, Y., Liu, Y., Miao, F., Chen, T., et al. (2018). Emergence of African swine fever in China, 2018. *Transbound. Emerg. Dis.* 65, 1482–1484. doi: 10.1111/tbed.12989

frontiers | Frontiers in Microbiology

TYPE Original Research
PUBLISHED 19 October 2022
DOI 10.3389/fmicb.2022.1022481

OPEN ACCESS

EDITED BY
Kuan Zhao,
Hebei Agricultural University,
China

REVIEWED BY
Nanhua Chen,
Yangzhou University,
China
Ján Matiašovic,
Veterinary Research Institute (VRI), Czechia

*CORRESPONDENCE
Yefei Zhou
yfzhou@njxzc.edu.cn
Xinglong Wang
wxlong@nwsuaf.edu.cn

SPECIALTY SECTION
This article was submitted to Infectious Agents and Disease, a section of the journal Frontiers in Microbiology

RECEIVED 21 August 2022
ACCEPTED 15 September 2022
PUBLISHED 19 October 2022

CITATION
Wang P, Ma X, Zhang R, Zhao Y, Hu R, Luo C, Zeshan B, Yang Z, Qiu L, Wang J, Liu H, Zhou Y and Wang X (2022) The transcriptional characteristics of NADC34-like PRRSV in porcine alveolar macrophages.
Front. Microbiol. 13:1022481.
doi: 10.3389/fmicb.2022.1022481

The transcriptional characteristics of NADC34-like PRRSV in porcine alveolar macrophages

Peixin Wang[1], Xin Ma[1], Riteng Zhang[1], Yongxin Zhao[1], Ruochen Hu[1], Chen Luo[1], Basit Zeshan[2], Zengqi Yang[1], Li Qiu[1], Juan Wang[1], Haijin Liu[1], Yefei Zhou[3]* and Xinglong Wang[1]*

[1]College of Veterinary Medicine, Northwest A&F University, Yangling, Shaanxi, China, [2]Faculty of Sustainable Agriculture, Universiti Malaysia Sabah, Sandakan, Sabah, Malaysia, [3]Department of Life Science, Nanjing Xiaozhuang University, Nanjing, Jiangsu, China

The widespread and endemic circulation of porcine reproductive and respiratory syndrome virus (PRRSV) cause persistent financial losses to the swine industry worldwide. In 2017, NADC34-like PRRSV-2 emerged in northeastern China and spread rapidly. The dynamics analysis of immune perturbations associated with novel PRRSV lineage is still incomplete. This study performed a time-course transcriptome sequencing of NADC34-like PRRSV strain YC-2020-infected porcine alveolar macrophages (PAMs) and compared them with JXA1-infected PAMs. The results illustrated dramatic changes in the host's differentially expressed genes (DEGs) presented at different timepoints after PRRSV infection, and the expression profile of YC-2020 group is distinct from that of JXA1 group. Functional enrichment analysis showed that the expression of many inflammatory cytokines was up-regulated following YC-2020 infection but at a significantly lower magnitude than JXA1 group, in line with the trends for most interferon-stimulated genes (ISGs) and their regulators. Meanwhile, numerous components of histocompatibility complex (MHC) class II and phagosome presented a stronger transcription suppression after the YC-2020 infection. All results imply that YC-2020 may induce milder inflammatory responses, weaker antiviral processes, and more severe disturbance of antigen processing and presentation compared with HP-PRRSV. Additionally, *LAPTM4A*, *GLMP*, and *LITAF,* which were selected from weighted gene co-expression network analysis (WGCNA), could significantly inhibit PRRSV proliferation. This study provides fundamental data for understanding the biological characteristics of NADC34-like PRRSV and new insights into PRRSV evolution and prevention.

KEYWORDS

PRRSV, NADC34-like, comparative transcriptome, time-course transcriptome, WGCNA

Introduction

Porcine reproductive and respiratory syndrome (PRRS) is an economically devastating pandemic of swine, which mainly causes respiratory failure, decreased boar semen quality, sow abortion, and stillbirth (Terpstra et al., 1991; Wensvoort et al., 1991; Benfield et al., 1992; Collins et al., 1992). The causative agent, porcine reproductive and respiratory virus (PRRSV), which belongs to the genus *Betaarterivirus* under the family *Arteriviridae* and can be divided into two major genotypes, PRRSV-1 (represented by Lelystad strain) and PRRSV-2 (represented by VR-2332 strain), according to The International Committee on Taxonomy of Viruses (ICTV) classification standards (Chen et al., 2006; Kuhn et al., 2016). PRRSV-2 was further classified into nine monophyletic lineages with several sub-lineages each (Shi et al., 2010); among them, the lineage 1.5 PRRSV-2 NADC34 became prevalent in the United States (in 2014), causing dramatic abortion storms in sow herds and high mortality among piglets (van Geelen et al., 2018). Recently, NADC34-like PRRSV has been detected in several Chinese provinces, including Liaoning, Henan, Fujian, and Jiangsu (Xu et al., 2022). These PRRSV-2 strains are also classified as lineage 1.5, with shared genomic features such as a 1–7-4 restriction fragment polymorphism (RFLP; *Mlu* I = 0, *Hinc* II = nt 88, 219, 360; *Sac* II = nt 24, 555) in the ORF5 sequence and a 100 amino acid continuum deletion in the NSP2 region compared to VR-2332 PRRSV (Bao and Li, 2021). Different NADC34-like PRRSV isolates exhibit distinct pathogenicity among themselves (Song et al., 2020; Yuan et al., 2022). Moreover, recombination events have been reported in NADC34-like PRRSVs in China (Xu et al., 2022); whether these phenomena will become the trigger of the next PRRS outbreak is still a concern.

Transcriptomics, an essential bioinformatics method in the post-genomic era, has been used widely in gene transcriptional structure identification, gene expression level quantification, and functional genomic investigation (Stark et al., 2019). It is also frequently applied in PRRSV infection assays to determine the gene expression changes in host cells under pathological conditions, thus further refining the virus-host interaction network (Miller et al., 2017; Sun et al., 2022). Research has focused on transcriptional characteristics under different organs/duration of infection and host/virus species. Several time-series studies showed that differentially expressed genes (DEGs) in PRRSV-infected PAMs were concentrated in innate immunity-related biological processes and pathways such as "pattern recognition receptors," "cytokines," and "antigen processing and presentation," the level of enrichment showed dynamic changes throughout of the infection (Zeng et al., 2018). Moreover, an *in vivo* experiment showed that pigs could release characteristic signals of innate immunity in multiple tissues 3 days post-infection (dpi), with a host response summit at around 10 dpi (Lim et al., 2020). In addition, comparative transcriptome between three PRRSV strains showed that the host biological process stimulated by PRRSV infection was similar regardless of genotype differences. However, the response intensity triggered by PRRSV-2 was more prominent (Yang et al., 2018). The virulent PRRSV-1 strain, Lena, has a higher immune co-inhibitory receptor expression level than the avirulent 3294 strain (Sánchez-Carvajal et al., 2021). Besides, PRRSV-2 XJ17-5 induces innate immune-related genes such as cytokines and ISGs more strongly than the homologous JSTZ1712-12 (Li et al., 2021), which may indicate that the host immune system can respond more intensively to virulent PRRSV strains.

In the present study, host transcriptional characteristics of PAMs during NADC34-like PRRSV isolate YC-2020 infection were analyzed and compared with that of JXA1-infected PAMs. The results could provide essential data for the basic study of the emerging NADC34-like PRRSV and new insights into the prevention and control of PRRS.

Materials and methods

Cells and viruses

Porcine alveolar macrophages (PAMs) obtained from bronchoalveolar lavage of 12 4-week-old piglets (PRRSV-, PCV-, and PRV-negative) were cultured in Roswell Park Memorial Institute (RPMI) 1640 medium (Gibco, United States), while Monkey Embryonic Kidney Epithelial cells (MARC-145) were cultured in Dulbecco's modified eagle medium (DMEM) both supplemented with 10% fetal bovine serum (FBS, Gibco), and 1% antibiotic/antimycotic solution (100 U/ml penicillin, 100 μg/ml streptomycin) in a humidified chamber at 37°C under 5% CO_2 conditions; The PRRSV-2 strain JXA1 (GenBank No. EF112445) and YC-2020 (GenBank No. ON180781) propagated in PAMs were used in this study. The virus titer in PAMs was assessed through an indirect fluorescent antibody assay (IFA) conducted as previously described (Ma et al., 2021), with PRRSV-N mAb (monoclonal antibody, gifted by Professor Shuqi Xiao from NWAFU) and Goat Anti-Mouse IgG H&L (Alexa Fluor® 488) (Abcam, Cambridge, United Kingdom) as primary and secondary antibody, respectively. The 50% tissue culture infective dose (TCID50) was calculated using the Reed-Muench method.

RNA preparation and sequencing

PAMs from every four piglets were equally mixed; the mixtures were then divided and designed as the negative control group (NC, without PRRSV infection) and two experimental groups [infected with one of PRRSVs described above at a multiplicity of infection (MOI) of 0.1]. All groups were incubated (NC with RPMI-1640) for 18, 28, and 38 h. All the samples were sent to Gene Denovo Biotechnology Co. (Guangzhou, China) for transcriptome sequencing (Supplementary Figure 1).

Total RNA was extracted using TRIzol reagent (Takara, Japan) following the manufacturer's protocol. RNA quality was assessed on Agilent 2100 Bioanalyzer (Agilent Technologies, Palo Alto, CA, United States). mRNA with ployA tail was enriched by Oligo(dT) beads. Then the enriched mRNA was broken into short segments using fragmentation buffer and reverse-transcribed into

cDNA using NEBNext Ultra RNA Library Prep Kit (NEB #7530, New England Biolabs, Ipswich, MA, United States). The purified double-stranded cDNA fragments were ligated to Illumina sequencing adapters after end repair & A base adding. Ligated fragments were further subjected to size selection by agarose gel electrophoresis and polymerase chain reaction (PCR) amplification. The resulting cDNA library was sequenced using Illumina NovaSeq 6000, and 150 bp paired-end reads were generated. All raw data generated in this study were deposited in the NCBI Sequence Read Archive (SRA) database under the accession number PRJNA857481.

Data processing and DEGs analysis

High-quality and adapter-trimming reads were filtered by Fastp (v0.22.0) (Chen et al., 2018) from the raw data (FASTQ format) and then aligned to the ribosomal RNA (rRNA) database of Sus scrofa by Bowtie2 (v2.4.4) to remove rRNA-derived reads. HISAT2 aligner (version 2.2.1) (Kim et al., 2015) was used for mapping clean reads to the Ensembl Sscrofa11.1 reference genome (release 104). Gene-wise abundances of each sample were calculated based on the exons annotated in the Ensembl Sscrofa11.1 GTF file (release 104), using the FeatureCounts software (v2.0.1) (Liao et al., 2014). Moreover, the fragments per kilobase per million mapped reads (FPKM) measurement for each gene in each sample was also calculated as auxiliary data for downstream analysis.

Differentially expressed genes analyses were performed with R package DESeq2 (v1.34.0) (Love et al., 2014). To reduce statistical bias caused by compositional and size differences between the libraries, we conducted the raw counts' normalization using the Relative Log Expression (RLE) method first. Then estimated the log2 fold change (LFC) of gene expression between each comparison group based on the above-mentioned experimental variables [treatment, hours post infection (hpi)] and "shrank" them through *apeglm* and *ashr* algorithms. The false discovery rate (FDR) was applied for multiple testing corrections of raw *p*-values (using the *Benjamini–Hochberg* (BH) method). A $|LFC| > 1$, an FDR-adjusted *p*-value (padj) < 0.05 and FPKM subtraction >2 were set as the threshold for determining statistically significant DEGs.

Functional annotation analysis

To identify relevant biological processes and pathways involved in each comparison group, functional gene set enrichment analysis (GSEA) of gene ontology (GO) and Kyoto encyclopedia of genes and genomes (KEGG) pathway annotations were conducted with the R package ClusterProfiler (v4.2.1) (Wu et al., 2021). Signal-to-noise ratio (SNR) was selected as the gene-ranking method, and the result of gene set enrichment with a |normalized enrichment score (NES)| >= 1.5 and *Q* value <0.1 was considered to be statistically significant. Enriched GO terms were visualized in Cytoscape (v3.9.0) (Shannon et al., 2003). The EnrichmentMap plugin (Merico et al., 2010) was used to construct a similarity-based network, in which GO terms were represented as nodes and edges were drawn based on a combined similarity coefficient (Jaccard + Overlap score > 0.4). The titles of term clusters were annotated by the AutoAnnotate plugin (Kucera et al., 2016), using the Markov cluster algorithm (MCL).

Construction of weighted gene co-expression network

To explore the potential relationship between genes more comprehensively from the perspective of overall expression trend, we constructed the mRNA co-expression network by using the R package WGCNA (v1.7) (Langfelder and Horvath, 2008) with entire samples. The specific process can be roughly divided into the following steps: (1) import gene expression data from all samples and obtain a similarity matrix from genes' correlations calculated by the Pearson method; (2) select an optimal soft thresholding power that can bring the target network closer to a scale-free network (scale-free fit R^2 > 0.9), and transform the similarity matrix into an adjacency matrix; (3) furthermore, transform the adjacency matrix into a topological overlap matrix (TOM) and perform gene clustering on TOM-based dissimilarity matrix (dissTOM); (4) utilize the dynamic tree cut algorithm to determine the co-expression gene sets, namely modules; (5) the module eigengene (ME) of each module is calculated, based on which the correlations between all modules are obtained, and then modules with a dissimilarity <0.2 are merged into a new one.

Identification of key modules and functional enrichment analysis

The Pearson correlation coefficients between the MEs of each module and each sample trait were calculated to estimate the module-trait associations, and relationships with a *t*-test *p*-value <0.01 were considered statistically significant. Meanwhile, to explore the biological processes in which members within the module may be involved, we performed GO and KEGG functional enrichment analyses for each module using the R package ClusterProfiler (v4.2.1) with the over-representation analysis (ORA) method. Gene sets were significantly over-represented with an adjusted *p*-value less than 0.05.

Identification and functional validation of hub genes

Hub genes exhibit high interconnection with other genes in a module and are generally considered to play important roles in a scale-free gene expression network. Intra-modular Connectivity function within the WGCNA R package was used to calculate gene connectivity, and the hub candidates were recognized as the

top 5% of genes with the highest connectivity in each module. In addition, we also determine module membership (MM, measurement of gene-module correlation) and gene significance (GS, measurement representing the correlation between the gene and a given trait) for each gene to assist the identification process.

The full-length of selected hub genes' coding sequences (CDSs) were amplified from the RNA extraction of infected PAMs and cloned into the vector pCDNA-KHA (Miaoling biology, Hubei, China) to generate three recombinant plasmids pCDNA-LITAF, pCDNA-LAPTM4A, and pCDNA-GLMP, respectively. MARC-145 cells transfected with specific plasmid were then infected with PRRSV strain JXA1, cell lysates were collected for RT-qPCR assay and Western blot assay at both 24- and 48 hpi.

RT-qPCR and Western Blot

Total extracted RNA was reversely transcribed to cDNA using M-MLV Reverse Transcriptase (Genstar, China). RT-qPCR was carried out with a real-time thermocycler (Four-channel, Tianlong, China) using the 2× Fast qPCR Master Mixture (DiNing, Beijing, China), following the instruction manual. All reactions were performed in triplicate. The previously described method of $2^{-\Delta\Delta CT}$ was used to calculate the relative expression level of target mRNAs (Livak and Schmittgen, 2001). The β-actin gene was used to normalize the fold changes in expression. Supplementary Table 1 shows the respective primer sequences of the reference gene (β-actin) and selected mRNA transcripts.

Cell lysates were denatured in 1 × protein loading buffer (10 mM Tris–HCl, pH 8.5, 50 mM DTT, 1% SDS, 10% glycerol, and 0.008% bromophenol blue) by heating for 5 min at 100°C. Protein samples in cell lysates were separated by SDS-PAGE and transferred to nitrocellulose membranes (Millipore, United States) as described previously (Lv et al., 2018). Membranes were then blocked with 5% skimmed milk in TBST (YaMei, Shanghai, China), followed by incubation with the primary antibody (PRRSV-N mAb, SLA-DRA mAb (gifted by Professor Qin Zhao from NWAFU), β-actin (Sungene Biotech, Tianjin, China), HA (Sungene)) and secondary antibody (HRP-labelled goat anti-mouse IgG (Sangon Biotech, Shanghai, China)), both diluted in TBST containing 2% BSA. The resulting signals were visualized by ECL ENhanced Kit (DiNing) with an Odyssey infrared imaging system (LI-COR, Nebraska, United States), and the protein band intensity was measured using ImageJ quantification software (available online at: https://imagej.net). All washes were using TBST, six times every 6 min.

Results

NADC34-like PRRSV YC-2020 has more viral transcripts

After trimming, filtering & rRNA removal, 1,136 million 150 bp pair-end high-quality reads were obtained from all 27 objects. Each sample was mapped to the pig reference genome, the YC-2020 genome, and the JXA1 genome, respectively, with an overall reads mapping rate of 96% or more (Supplementary Table 2). No virus reads mapping occurred in the NC group. No cross-infection was noticed between JXA1 and YC-2020 groups as only corresponding virus reads were detected, indicating that all the data are suitable for further analysis.

Notably, the YC-2020 PRRSV-derived reads reached a quarter of the total sequencing data at 18 hpi and rose above 60% at 28 hpi, while JXA1-derived reads hovered around 1% throughout the observation (Figure 1A). This phenomenon was further confirmed at the transcription, protein, and virus titer levels by RT-qPCR (Figure 1B), Western Blot (Figure 1C), and TCID50 (Figure 1D) assays, respectively.

Gene expression profiles in NADC34-like PRRSV-infected PAMs

The principal component analysis (PCA) (Figure 2A) showed no significant segregation of replicates; moreover, the first principal component explained the differences in host gene expression caused by virus type, suggesting that YC-2020 may have different infection characteristics from JXA1. Time-course DEGs analysis based on the YC-2020 and NC groups revealed dynamic changes in gene expression. DEGs with the threshold described in section "Methods" were identified as 59 at 18 hpi but significantly increased to 708 at 28 hpi and maintained the trend at 38 hpi. Up-regulated DEGs accounted for a more significant proportion (Figure 2B; Supplementary Table 3). The top 20 up-and down-regulated genes (sorted by LFCs) at each hpi were listed in Figure 2C, where the presence of *TNF*, *IL-1A*, *IL-1B*, *CCL2*, *SLA-DRB1*, *SLA-DMA*, and *GVIN1* suggested that the DEGs were possibly involved in the inflammatory response, antigen presentation, and antiviral process.

Gene set enrichment analysis based on GO and KEGG databases indicated that many biological processes and gene pathways were significantly enriched during YC-2020 PRRSV infection. The immune-related GO terms, such as "immune response," "defense response to virus," "chemokine-mediated signaling pathway" were positively enriched (NES > 0); interestingly, most of these enriched states further pointed to the negative regulation (e.g., "negative regulation of innate immune response," "negative regulation of inflammatory response," "negative regulation of defense response," "negative regulation of cytokine production"); a few genes sets that presented as a negative enrichment state (NES < 0) were also focused on associative processes adverse to viral invasion (e.g., "activation of immune response," "negative regulation of viral transcription"). The enrichment number of general immune-related terms diminished along with the duration of infection. Meanwhile, GO terms related to antigen processing and presentation, such as "antigen presentation and processing," "MHC protein complex," "lysosome," and "proteasome" were

10.3389/fmicb.2022.1022481

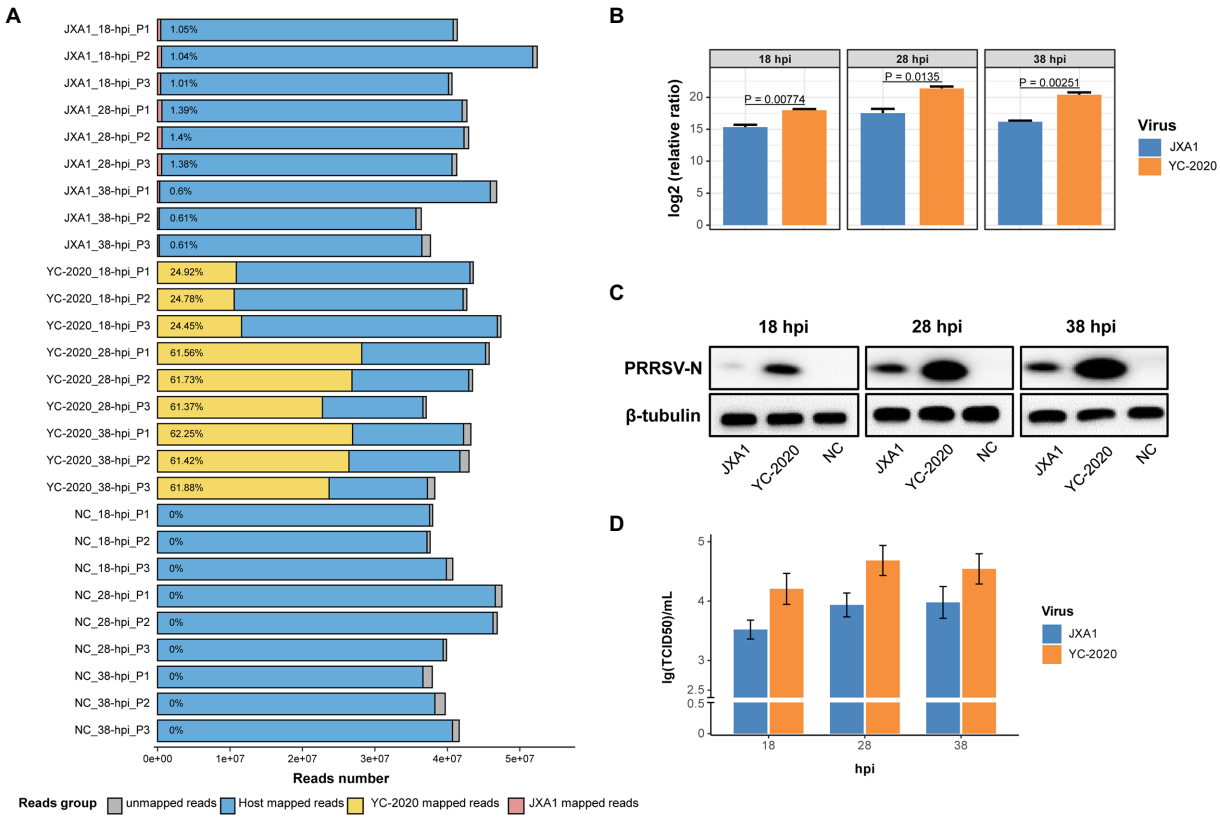

FIGURE 1
RNA-seq mapping statistic and virus transcripts validation assays. **(A)** Bar plot of RNA-seq mapping statistic. Y-axis represents 27 samples that were generated by treatment (YC-2020, JXA1, and NC), time (18-, 28-, and 38-hpi), and three replicates (P1, P2, and P3); numbers within the bars represent the percentage of virus-derived reads in each sample. **(B)** The viral loads of two PRRSV strains at different hpi were validated by RT-qPCR. Data are mean±SD from three independent experiments, and *p*-values are calculated by unpaired two-tailed Student's *t*-test. **(C)** Detection of PRRSV-N protein expression at different hpi by Western Blot assay. **(D)** Determination of virus titer at different hpi by TCID50 assay.

in a negative enrichment state at all three timepoints (Figure 3A). Results of KEGG pathways were similar to that of GO terms (Figure 3B). Furthermore, the expression profiles of innate immune-related marker genes also elucidated that the majority of cytokines, including type I interferons (IFNs, *IFN-ALPHAOMEGA*, and *IFNB1*), inflammatory chemokines (*CCL4, CCL2, CCL3L1, CCL5, CCL20, CXCL8*, and *AMCF-II*), interleukin (IL) family (*IL-1A, IL-1B*, and *IL-11*) and NF-κB pathway inhibitory proteins (*NFKBIA, NFKBIZ*, and *TNFAIP3*) showed significantly high expression level under all observation points. In contrast, the expression of some inflammation-inducing factors (*PPBP, MARCO*) was consistently down-regulated in the middle and late stages of infection. Most interferon-stimulated genes (ISGs, such as *GVIN1, RTP4, IFIH1, IFIT1, IFIT5, MX1, MX2, RSAD2*, and *BST2*) exhibited an increase in transcript amount at 18 and 28 hpi but a decrease at 38 hpi. The expression level of MHC class II molecules associated with antigen presentation (*SLA-DMA1, SLA-DQB1, SLA-DMB, SLA-DRB1, SLA-DQA1*, and *SLA-DRA1*) was down-regulated at all observed timepoints (Figure 3C; Supplementary Table 4).

NADC34-like PRRSV YC-2020 infection induced more significant gene transcriptional regulation

DEGs analysis between YC-2020 and JXA1 groups was performed to explore the distinctions in transcriptional characteristics of NADC34-like- and HP-PRRSV-infected PAMs. Similar to YC-2020 vs. NC group, DEGs between YC-2020 and JXA1 group also displayed a considerable increase at 28 hpi and did not overlap well with those at 38 hpi (Figure 4A; Supplementary Table 3). The significantly up-regulated genes (such as *DNAJB1*, *FOS*, *ATF3*, and *NR4A3*) were focused on the transcriptional regulation process, whereas the significantly down-regulated genes (*CXCL10, CCL2, CCL8, AMCF-II, BST2, RSAD2*, and *GVIN1*) were annotated to the immune response (Figure 4B). GO terms and KEGG pathways involved in the viral immune response and its positive regulation (including "positive regulation of pattern recognition receptors," "positive regulation of immune response," "Cytokine-cytokine receptor interaction," "influenza A") were found to be negatively enriched

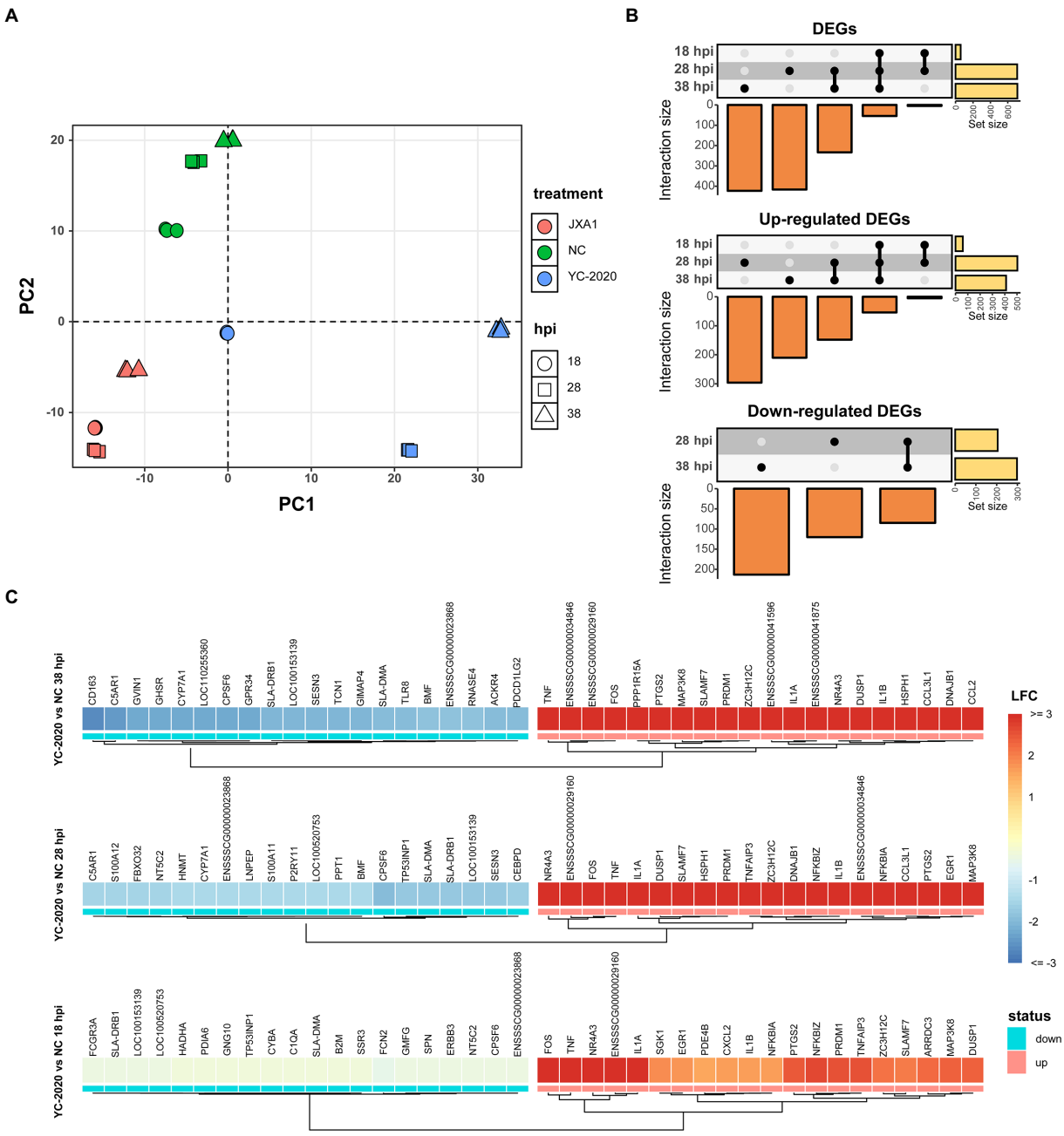

FIGURE 2
DEGs analysis between YC-2020 and NC group. **(A)** Principal component analysis of 27 samples based on gene expression. The eigenvalues from the first two principal components (PC1 and PC2) are plotted. The characteristics of each sample are marked by both color and shape aesthetics. **(B)** UpSet plot shows the dynamic distribution of DEGs under each comparison. Each vertical bar represents the number of DEGs in one distribution set, and the horizontal bars represent DEGs' total number at different hpi. **(C)** Heat map of the expression of the top 20 up- and down-regulated DEGs (sorted by LFCs) at three timepoints.

throughout the observation phase. Negative enrichment terms related to the negative regulation of viral replication ("negative regulation of viral process," "negative regulation of viral genome replication") also suggested that PAMs infected with YC-2020 PRRSV exhibited weaker restraint against the virus (Figures 5A,B). Part of ILs (*IL-1A*, *IL-11*) and chemokines (*CCL4*, *CCL20*) showed higher expression in the YC-2020 group instead of JXA1 group. However, toll-like receptors (TLRs, *TLR3*, and *TLR8*), interferon regulator factors (IRFs, *IRF3*, and *IRF7*), most of the cytokines (*CXCL10*, *CCR5*, *CCL2*, *CCL8*, *AMCF-II*), ISGs (such as *ISG15*, *ISG20*, *GBP1*, *GVIN1*, *RTP4*, *NMI*, *PARP9*, *IFIT1*,

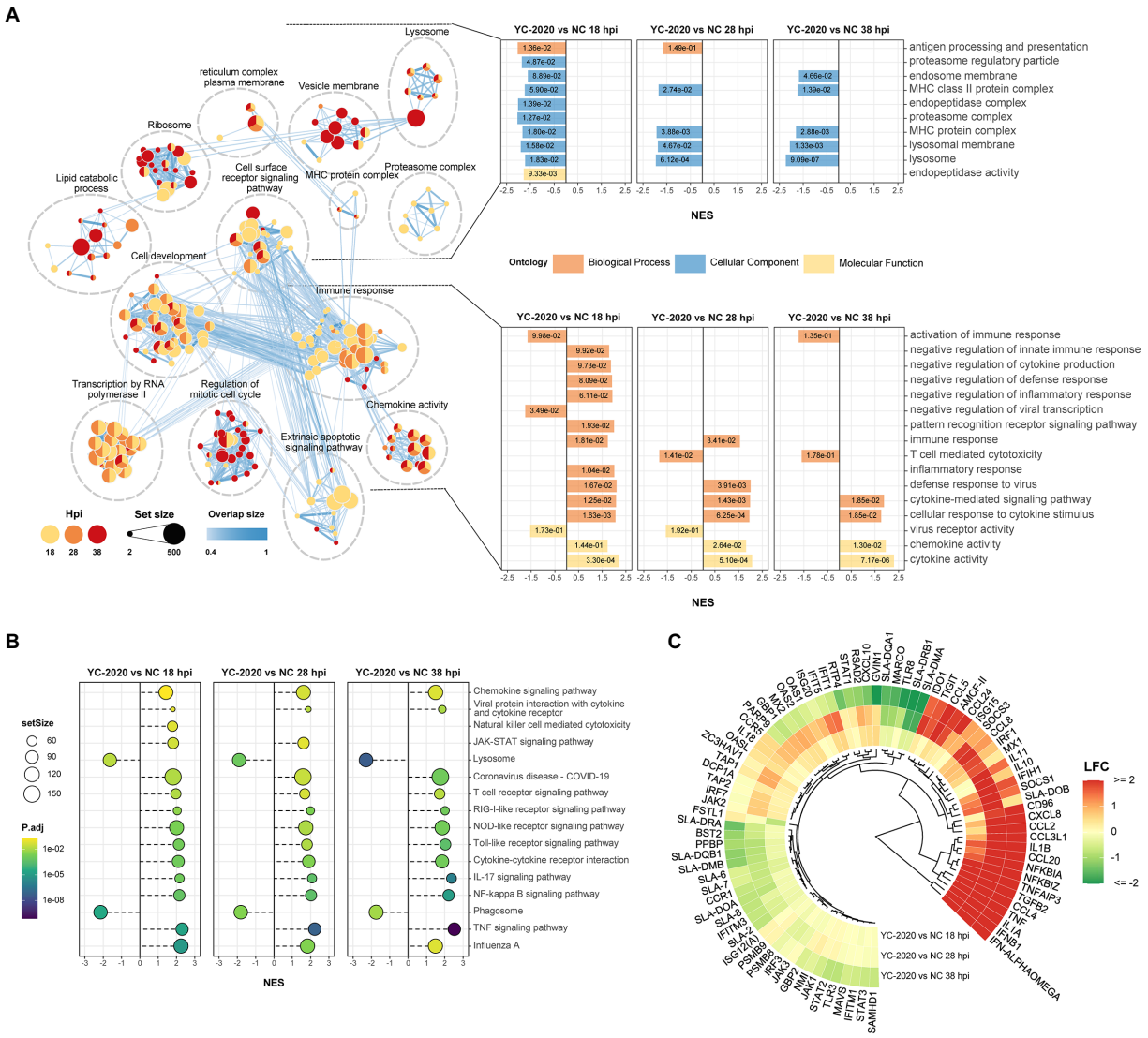

FIGURE 3
Functional annotation analysis of DEGs determined from the YC-2020 and NC group. **(A)** GO enrichment at different hpi. The left side of the panel shows the significantly enriched GO terms (|NES|≥1.5, padj <0.1) obtained at all three hpi. Gene sets are represented by nodes, which color corresponds to hpi; node size corresponds to the number of gene members within them; the size and color of the edges correspond to the similarity score between terms. All GO terms are clustered according to their gene members' overlap size, and each cluster's subject is written on top. GO terms associated with immune response, antigen processing and presentation are shown in the panel's lower and upper bar plots on the right side. Each bar contains a padj of the permutation test. **(B)** Lollipop plot of the significantly enriched KEGG pathway at different hpi. **(C)** Heat map of the expression profiles of hotspot genes associated with innate immunity. Each layer of circles represents a comparison group, and the selected genes include common cytokines, ISGs, MHCs, and critical regulators in associated pathways.

IFITM3, OAS1, RSAD2, and *BST2*), antigen processing and presentation associated genes (including *SLA-DMA1, SLA-DRB1, TAP1, TAP2, PSMB8, PSMB9*) presented lower transcription levels in the comparison of the YC-2020 and JXA1 groups, and fold change of the above genes expanded along with the infection duration (Figure 5C; Supplementary Table 4). The results of DEGs and functional enrichment analysis between JXA1 and NC groups were presented in Supplementary Figures 2, 3 to understand the transcriptional differences between the two strains more sufficiently.

Eighteen DEGs selected from different comparison groups were validated by RT-qPCR. Despite slight variations in the magnitude of changes in a few genes, the RT-qPCR results exhibited superior consistency with RNA-Seq, indicating the sequencing data's reliability (Figure 6A). *SLA-DRA* was chosen as the representation protein to confirm that YC-2020 PRRSV possessed a stronger inhibitory capacity for antigen presentation than JXA1 PRRSV through the Western Blotting assay. As the gray intensity analysis showed, the expression level of *SLA-DRA* was lower in both virus groups than that in the NC group at all observation points, and

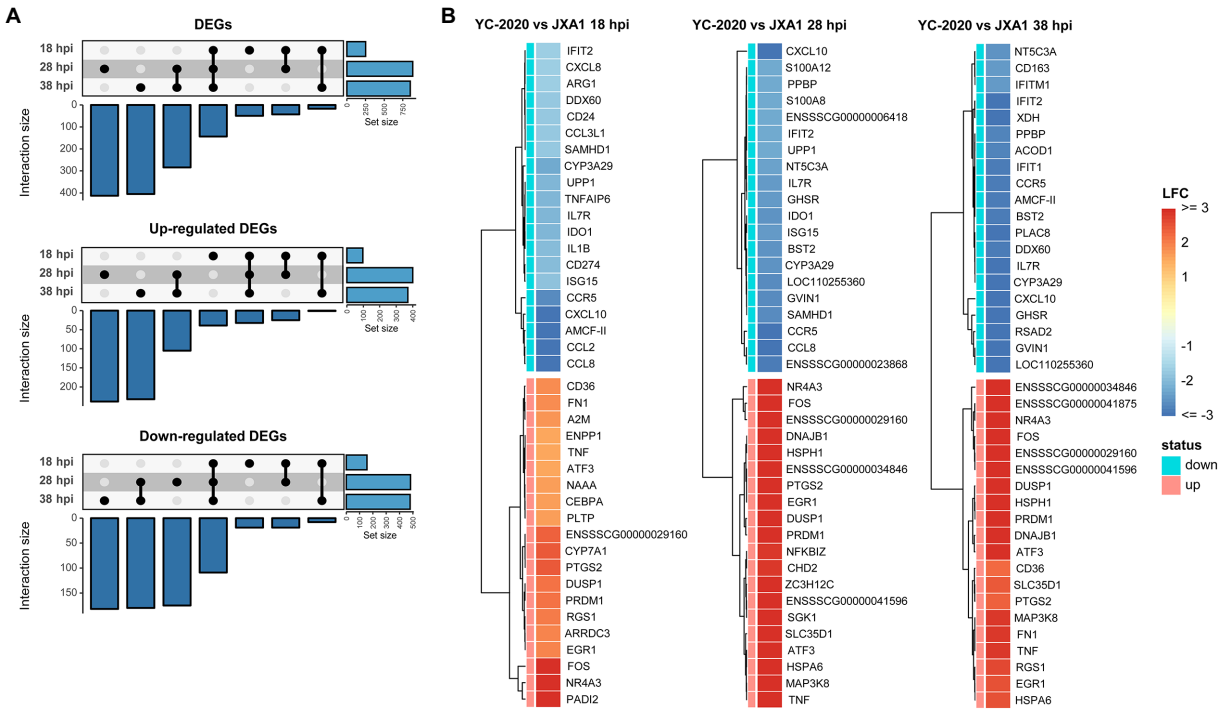

FIGURE 4
DEGs analysis between YC-2020 and JXA1 group. **(A)** UpSet plot shows the dynamic distribution of DEGs under each comparison. **(B)** Heat map of the expression of the top 20 up- and down-regulated DEGs (sorted by LFCs) at three timepoints.

YC-2020 showed a more significant down-regulation trend than JXA1 from 28 hpi (Figure 6B).

The identification of key modules and hub genes through WGCNA

To discover some novel possible intergenic linkages from the overall expression trends, a gene co-expression network was constructed by WGCNA. The hierarchical clustering results obtained using the gene FPKM values in each sample detected no significant outlier. 14 was set to be the optimal power to construct a scale-free, unsigned gene expression network after multiple testing (Figure 7A). Afterward, the expression profiles of 7,597 genes were converted into a TOM-based gene-wise clustering tree, and 22 modules were finally identified (Figure 7B; Supplementary Table 5).

The relationship between each module and sample information (Supplementary Table 6), and biological processes involved in modules, were determined by correlation calculations and ORA-based functional enrichment analysis before the identification, respectively. The greenyellow and darkgrey were considered key modules because both of them contained terms or pathways associated with antigen processing and presentation (Figures 8B,C); meanwhile, these two modules were highly negatively correlated with the "YC-2020 PRRSV infection" trait ($r^{greenyellow} = -0.77$, $P^{greenyellow} = 2.73e\text{-}06$, $r^{darkgrey} = -0.75$, $P^{darkgrey} = 7.45e\text{-}06$, Figure 8C). The overall expression profiles of all genes in key modules are shown in Figure 8A. Based on the threshold (top 5% of kIM) and auxiliary selection criteria ($|MM| > 0.85$, $|GS| > 0.4$, mean expression counts >4,000, and max $|LFCs| > 1$), *LAPTM4A*, *GLMP*, *LITAF* in key modules were finally selected as hub genes for further study (Supplementary Table 7). MARC-145 cells were transfected with pCDNA-LITAF, pCDNA-LAPTM4A, and pCDNA-GLMP, respectively. And then infected with JXA1 at 12 h post transfection. Cell lysates were collected at 24 h and 48 h after virus infection, followed with RT-qPCR and Western Blot. Three hub genes could significantly inhibit PRRSV propagation at mRNA-expression and protein levels compared to mock; among them, *LITAF* showed a stronger inhibitory effect (Figure 9).

Discussion

Porcine reproductive and respiratory syndrome virus infection triggers a series of cellular responses in PAMs, forming a complex viral-host gene expression regulation network. Considering the differences in pathogenicity caused by rapidly recombinant events in PRRSV and the limitation of traditional molecular biology techniques, high-throughput transcriptome sequencing was conducted to analyze the host transcriptional characteristics of NADC34-like PRRSV YC-2020 infection to obtain important data on the organismal response induced by this emerging strain. At the same time, a comparative analysis with JXA1 (one of the representative strains of HP-PRRSV, often

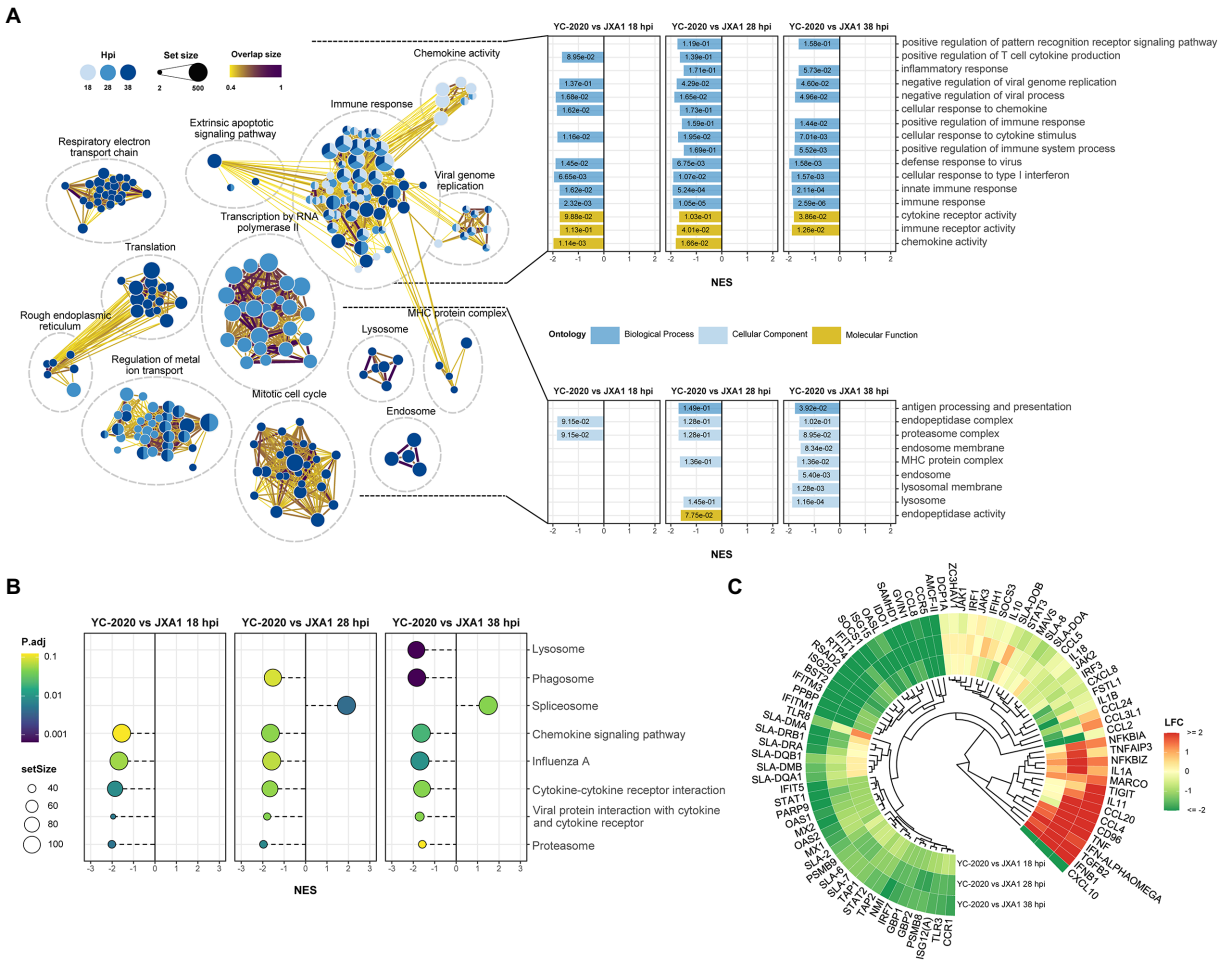

FIGURE 5
Functional annotation analysis of DEGs determined from the YC-2020 and JXA1 group. **(A)** GO enrichment at different timepoints post-infection. The left side of the panel shows the significantly enriched GO terms (|NES|≥1.5, padj <0.1) obtained at all three timepoints. Gene sets are represented by nodes, in which color corresponds to hpi; node size corresponds to the number of gene members within them; the size and color of the edges correspond to the similarity score between terms. All GO terms are clustered according to their gene members' overlap size, and each cluster's subject is written on top. GO terms associated with immune response, antigen processing and presentation are shown in the panel's upper and lower bar plots on the right side. Each bar contains a padj of the permutation test. **(B)** Lollipop plot of the significantly enriched KEGG pathway at different hpi. **(C)** Heat map of the expression profiles of hotspot genes associated with innate immunity. Each layer of circles represents a comparison group, and the selected genes include common cytokines, ISGs, MHCs, and critical regulators in associated pathways.

compared with other novel strains) was also carried out to explore the host transcriptional differences between NADC34-like and highly pathogenic strains infection. The results of each specific comparison group demonstrated a substantial increase in the number of DEGs at 28 h after YC-2020 infection and a large proportion of up-regulated genes, implying that the response of PAMs was significantly activated between 18 and 28 h. From the comparison between the YC-2020 and JXA1 group, down-regulated DEGs at 28 and 38 h showed a relatively high overlap degree, suggesting that PAMs infected with NADC34-like PRRSV may possess sustained suppressive effects in some aspects relative to those infected with HP-PRRSV.

In this study, functional enrichment analysis was performed by GSEA instead of ORA method to reveal the pathways annotated by differential genes since the former can show the enrichment status of the target gene set in the whole gene list. More importantly, GSEA can effectively avoid the information loss caused by the hard threshold. The classified enrichment results are mainly related to immune response, lipid metabolism, cell cycle, translation, and other processes. Immune response was chosen as the key focus of this study. Innate immunity, the first line of host defense to limit virus transmission and regulate acquired immunity, activates a series of related signaling pathways in cells with pattern recognition receptor binding as a trigger (Zeng et al., 2018). The gene sets "immune response," "defense response to the virus," "pattern recognition receptor signaling pathway" were positively enriched after YC-2020 infection, but negatively enriched in comparison with JXA1; positive enrichment was also observed in the anti-immune regulatory gene sets at 18 hpi, indicating that the activation and suppression of innate immunity

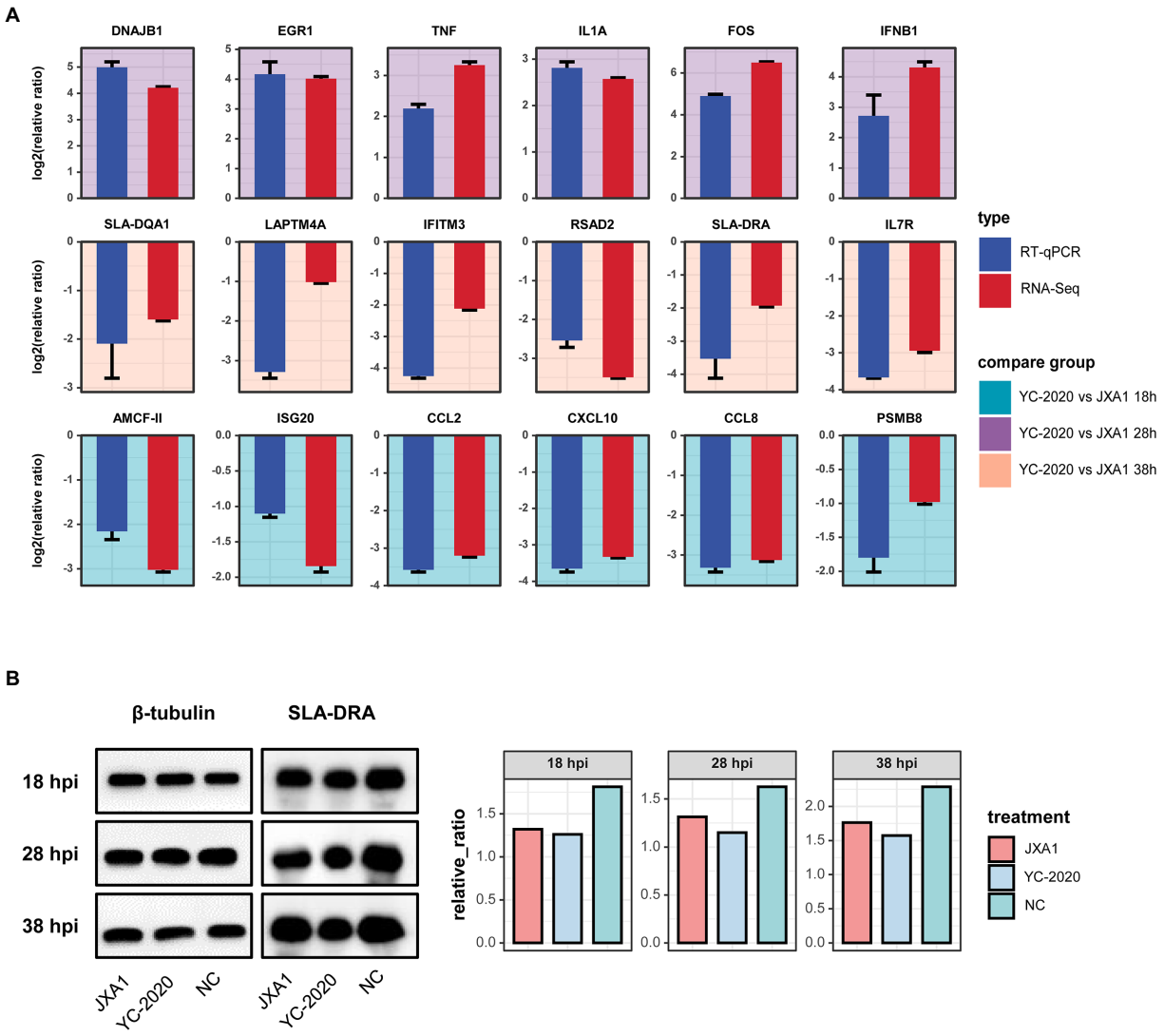

FIGURE 6
Validation of RNA-Seq data. **(A)** Comparative bar plot between RT-qPCR validation of the 18 selected DEGs and their RNA-seq data. Each subplot corresponds to a gene, and the background color represents the comparison group. All results are shown as means ± SE. **(B)** Detection of SLA-DRA protein expression at different hpi by Western Blot assay. Tubulin was used as an internal reference. **(C)** Proteins were quantified with gray intensity analysis software.

coexisted after the YC-2020 infection, however, the activation level was lower than that of JXA1.

Inflammation is one of the essential features of the immune response, and it can be induced after PRRSV infection, which promotes immune cell infiltration (Xiao et al., 2010). Various inflammatory cytokines such as TNF (*TNF*), some ILs (*IL1α*, *IL1β*), and chemokines (including *CCL2*, *CCL4*, *CCL5*, *CXCL8*) were significantly up-regulated under all observation points after YC-2020 infection. Meanwhile, anti-inflammatory factors such as *TNFAIP3, NFKBIA, NFKBIZ, SOCS1, SOCS3,* and *IL-10* were elevated, with the reverse trends for the inflammation-inducing genes *PPBP* and *MARCO* at 38 hpi, suggesting that the pro- and anti-inflammatory responses might coexist in PAMs during YC-2020 infection. These phenomena were also captured in a recent study (Chaudhari et al., 2021), where the author thought that the production of pro-inflammatory factors originates from the body's immune defenses, while anti-inflammatory factors are attributed to PRRSV-induced negative regulation of immunity. The majority of inflammatory cytokines presented lower expression levels except for *TNF*, *IL1α*, and some chemokines (*CCL4, CCL20*) in the YC-2020 vs. JXA1 groups, but expression of the anti-inflammatory gene markers (*NFKBIA, NFKBIZ,* and *TNFAIP3*) was higher, indicating that YC-2020 PRRSV may cause a weaker inflammatory response than HP-PRRSV through stronger inhibition of the NF-κB signaling pathway (Oeckinghaus and Ghosh, 2009; Das et al., 2018). Previous

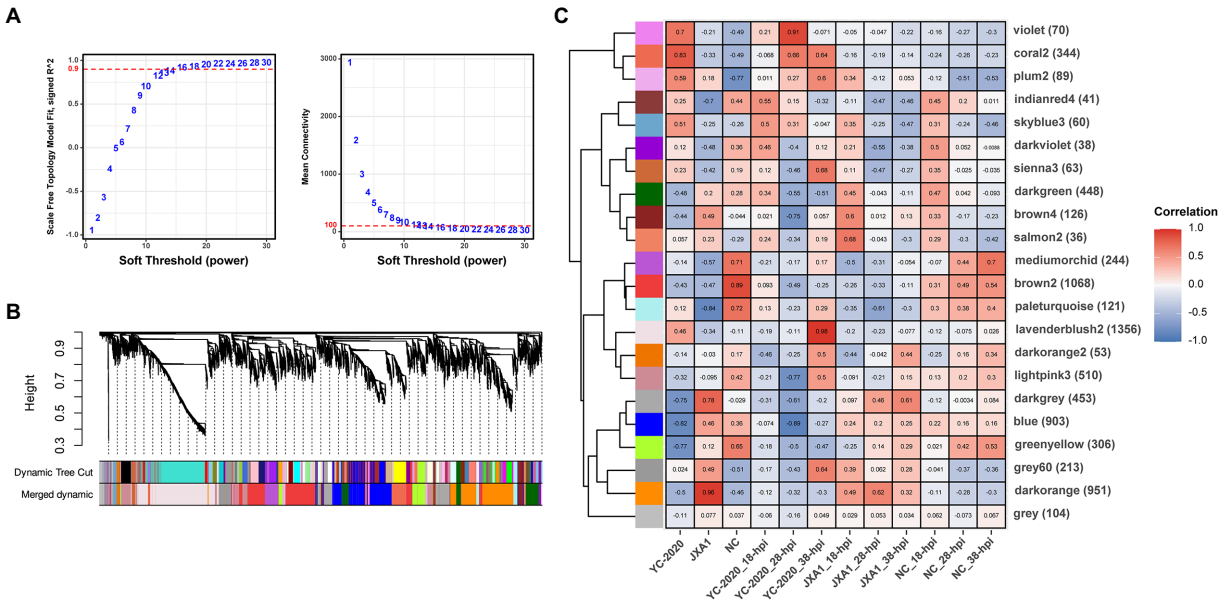

FIGURE 7
Gene co-expression network construction and module identification. **(A)** Determination of soft-thresholding power in WGCNA. The numbers in the panel are the power candidates. **(B)** Hierarchical clustering dendrograms of identified DEGs. Modules correspond to branches and are labeled by colors as indicated by the first color band underneath. After the ME-based hierarchical clustering, the original modules are merged and presented in the second color band. **(C)** Heatmap of module-trait associations. Correlation is written into each cell with fill color as an indicator.

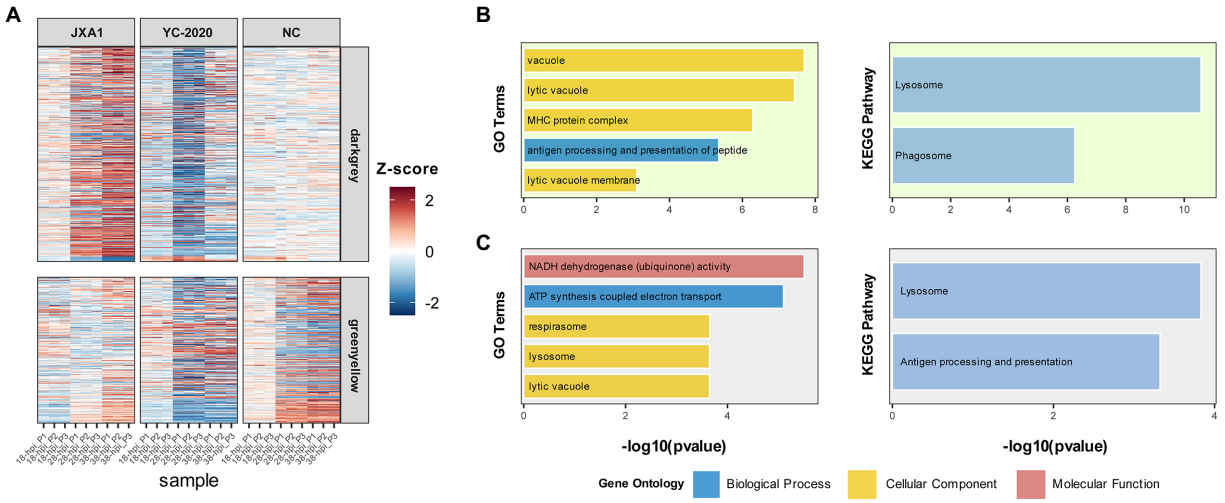

FIGURE 8
Information on modules of interest. **(A)** The expression profile of gene members in the darkgray and greenyellow modules in all samples. Each row corresponds to a gene, while each column corresponds to a sample. FPKM of each gene across samples is centralized and normalized for more precise visualization. GO and KEGG-based functional enrichment analysis of greenyellow and darkgrey modules are presented in **(B,C)**, respectively.

studies have demonstrated a similar theory both *in vitro* and *vivo*, where HP-PRRSV tended to generate more severe lung damage by leading to excessive inflammation but could be eliminated quickly from the organism (Weesendorp et al., 2014). Therefore, we consider that a milder inflammatory response is also a strategy for YC-2020 to evade the host's immune response.

As a critical pathway in the anti-PRRSV process, cytokines, especially the IFN-mediated JAK–STAT pathway, have been extensively studied (Huang et al., 2015). IFN-I activated by

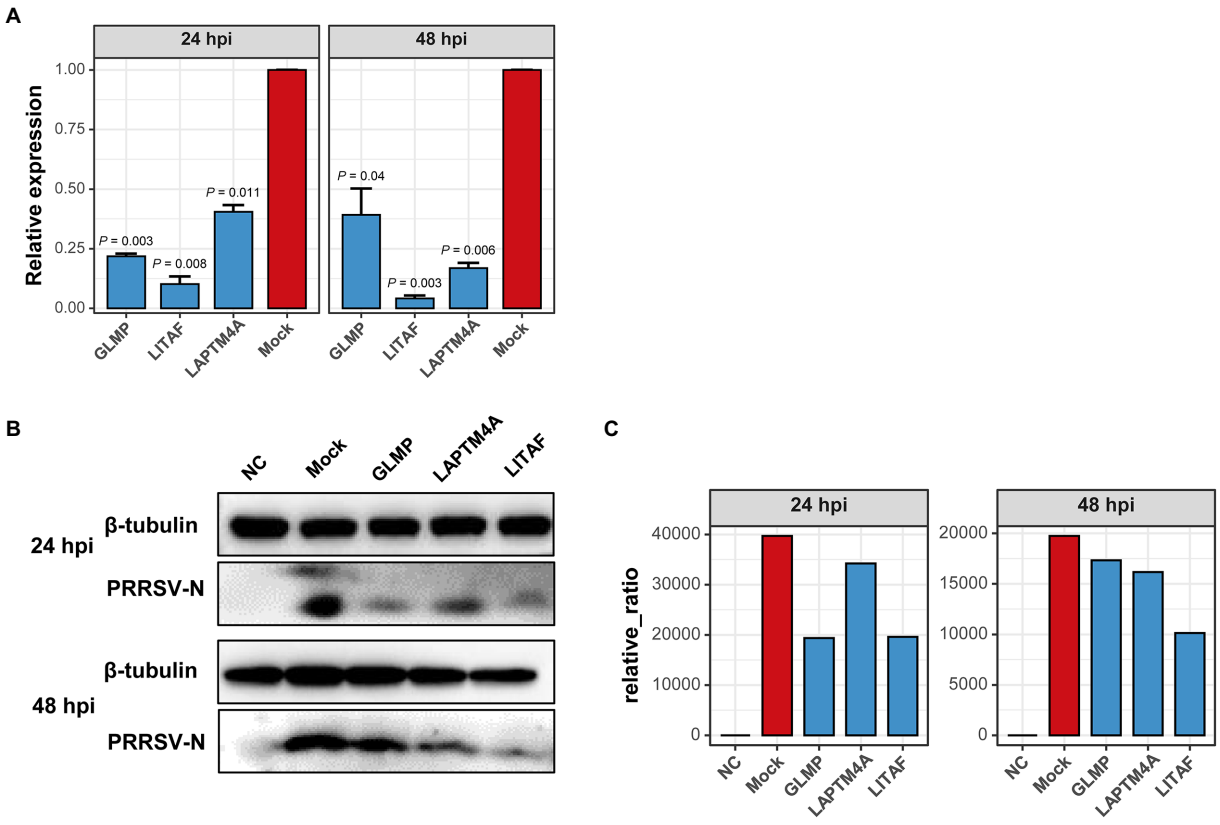

FIGURE 9
Over-expression of three hub-genes down-regulates PRRSV replication *in vitro*, respectively. **(A)** PRRSV proliferation was quantified by detecting mRNA transcription of protein N in Marc-145 cells overexpressing hub genes or not. Overexpressing hub genes downregulated virus-derived N expression significantly at both 24- and 48 hpi relative to that in mock cells. Data are mean±SD from three independent experiments, and *p*-values are calculated by unpaired one-tailed Student's *t*-test. **(B)** PRRSV-derived N expression decreased significantly in cells transfected with hub genes detected by Western Blot using anti-PRRSV-N pAb. Tubulin was used as an internal reference. **(C)** Proteins were quantified with gray intensity analysis software.

several transcription factors such as NF-κB and IRFs triggers the production of numerous ISGs through this pathway, yet PRRSV can counteract it through viral proteins (Schoggins and Rice, 2011; Wang et al., 2021). In the present study, both *IFN-ALPHAOMEGA* and *IFNB1* were extremely significantly up-regulated (LFCs >5) at three timepoints after YC-2020 infection, which has been detected in some previous RNA-Seqs toward PRRSV-2 infection (Lim et al., 2020; Chaudhari et al., 2021). Intriguingly, most of the downstream ISGs' up-regulation levels were much lower in the comparison between YC-2020 and NC, with some even exhibiting a reversal at 38 hpi. Except for *DCP1A* and *ZAP* (*ZC3HAV1*), most ISGs in the YC-2020 group showed a significantly lower expression than the JXA1 group, and gaps widened with the continuance of infection, which imply that YC-2020 may possess a more powerful capacity to weaken the host's antiviral responses. Considering the remarkably lower transcription of *STAT1* and *STAT2* was also founded in the comparison between YC-2020 and JXA1 groups; whether viruses would primarily rely on transcriptional repression of these two genes to limit the production of ISGs under the circumstance of highly expressed IFNs remains to be explored in depth.

Recently, antigen processing and presentation has become a hot spot because of its role as a "bridge" between innate and adaptive immunity. The impairment of this process is considered one of the main tactics of PRRSV-induced immunosuppression (Chaudhuri et al., 2016; Liang et al., 2017; Zeng et al., 2018). GO and KEGG terms such as "antigen processing and presentation," "lysosome" and "proteasome" were enriched negatively both in the comparison of YC-2020 vs. NC and YC-2020 vs. JXA1 groups throughout the experiment. Besides, the transporter associated with antigen processing (TAP, *TAP1, TAP2*) and most MHCs showed a decrease in expression at 28, 38 h post-YC-2020 infection, with a stronger downtrend than the JXA1 group. The results indicate that YC-2020 may cause a more severe antigen-presentation disturbance than HP-PRRSV by inhibiting the transcription of genes associated with phagosome and MHC complexes.

We also discovered that the YC-2020-derived viral reads accounted for a significantly higher percentage than JXA1, once reaching more than 60% of the belonging sample's total data volume. The proportion of viral-derived reads in existing PRRSV-associated transcriptome studies typically ranges from 1 to 20%

(Liang et al., 2017; Wu et al., 2020; Chaudhari et al., 2021); however, a recent analysis of SARS-CoV-2 transcriptome exhibited that the percentage of viral data approached 70% (Kim et al., 2020). Therefore, without exogenous contamination, the dramatically transcriptional differences between the two PRRSV strains may be attributed to the discrepancy in the viral transcriptional capacity. In addition, three hub genes were selected from the mRNA co-expression network constructed by WGCNA. Among them, *GLMP* is required to protect lysosomal transporter *MFSD1* from lysosomal proteolysis and is often involved in protein localization to the lysosome (López et al., 2019). Research has found that *LAPTM4A* functions to regulate the compartmentalization of amphiphilic solutes within lysosomes and late endosomes (Vergarajauregui et al., 2011). *LITAF*, as the small integral membrane protein of lysosome/endosome, plays a part in proteins' lysosomal degradation and the expression regulation of various cytokines (such as *TNF, CCL2, CCL5, IL1A*) (Myokai et al., 1999; Tang et al., 2005). In this study, PRRSV propagation was significantly inhibited in both mRNA and protein levels after overexpressing three genes. As discussed above, we speculate that the inhibition may cause by disruption of lysosome structure/function, but the mechanism still needs further exploration.

Data availability statement

The datasets presented in this study can be found in online repositories. The names of the repository/repositories and accession number(s) can be found at: https://www.ncbi.nlm.nih.gov/, PRJNA857481.

Ethics statement

All the animal-related experiments were handled according to the Ethics Committee at Northwest A&F University (approval number DY2022009). Experiments were carried out following the approved guidelines.

Author contributions

XLW and PXW designed the experiments, and PXW conducted the bioinformatics analyses; XM, YXZ, and RCH performed the data validation; XLW, PXW, RTZ, CL, and BZ wrote the manuscript; ZQY, JW, HJL and LQ guided the research. All authors read and approved the final manuscript.

Funding

This research was supported by grants from the National Natural Science Foundation of China awarded to XW (grant no. 31672581) and the grants from the General Projects of Key R&D Program in Shaanxi Province (2022SF-421).

Acknowledgments

Sincerely appreciate Prof. Shuqi Xiao and Prof. Qin Zhao from Northwest A&F University for providing the antibody against PRRSV and SLA-DRA.

Conflict of interest

The authors declare that the research was conducted in the absence of any commercial or financial relationships that could be construed as a potential conflict of interest.

Publisher's note

Supplementary material

The Supplementary material for this article can be found online at: https://www.frontiersin.org/articles/10.3389/fmicb.2022.1022481/full#supplementary-material

SUPPLEMENTARY FIGURE 1
Diagram of the experimental design. The sample preparation process used for RNA-Seq in this study;

SUPPLEMENTARY FIGURE 2
DEGs analysis between JXA1 and NC group. **(A)** Volcano plots show the dynamic change of DEGs under each comparison. Each gene's change state is mapped by color, and the horizontal and vertical dash lines represent the DEGs cutoff (LFC = ±1, padj = 0.05). **(B)** Heat map of the expression of the top 20 up- and down-regulated DEGs (sorted by LFCs) at three timepoints.

SUPPLEMENTARY FIGURE 3
Functional annotation analysis of DEGs determined from the JXA1 and NC group. **(A)** GO enrichment at different hpi. The left side of the panel shows the significantly enriched GO terms ($|NES| \geq 1.5$, padj < 0.1) obtained at all three hpi. Gene sets are represented by nodes, which color corresponds to hpi; node size corresponds to the number of gene members within them; the size and color of the edges correspond to the similarity score between terms. All GO terms are clustered according to their gene members' overlap size, and each cluster's subject is written on top. GO terms associated with immune response, antigen processing and presentation are shown in the panel's lower and upper bar plots on the right side. Each bar contains a padj of the permutation test. **(B)** Lollipop plot of the significantly enriched KEGG pathway at different hpi. **(C)** Heat map of the expression profiles of hotspot genes associated with innate immunity. Each layer of circles represents a comparison group, and the selected genes include common cytokines, ISGs, MHCs, and critical regulators in associated pathways.

References

Bao, H., and Li, X. (2021). Emergence and spread of NADC34-like PRRSV in China. *Transbound. Emerg. Dis.* 68, 3005–3008. doi: 10.1111/tbed.14316

Benfield, D. A., Nelson, E., Collins, J. E., Harris, L., Goyal, S. M., Robison, D., et al. (1992). Characterization of swine infertility and respiratory syndrome (SIRS) virus (isolate ATCC VR-2332). *J. Vet. Diagn. Investig.* 4, 127–133. doi: 10.1177/104063879200400202

Chaudhari, J., Liew, C. S., Riethoven, J. M., Sillman, S., and Vu, H. L. X. (2021). Porcine reproductive and respiratory syndrome virus infection Upregulates negative immune regulators and T-cell exhaustion markers. *J. Virol.* 95:e0105221. doi: 10.1128/JVI.01052-21

Chaudhuri, S., McKenna, N., Balce, D. R., and Yates, R. M. (2016). Infection of porcine bone marrow-derived macrophages by porcine respiratory and reproductive syndrome virus impairs phagosomal maturation. *J. Gen. Virol.* 97, 669–679. doi: 10.1099/jgv.0.000384

Chen, J., Liu, T., Zhu, C.-G., Jin, Y.-F., and Zhang, Y.-Z. (2006). Genetic variation of Chinese PRRSV strains based on ORF5 sequence. *Biochem. Genet.* 44, 421–431. doi: 10.1007/s10528-006-9039-9

Chen, S., Zhou, Y., Chen, Y., and Gu, J. (2018). Fastp: an ultra-fast all-in-one FASTQ preprocessor. *Bioinformatics* 34, i884–i890. doi: 10.1093/bioinformatics/bty560

Collins, J. E., Benfield, D. A., Christianson, W. T., Harris, L., Hennings, J. C., Shaw, D. P., et al. (1992). Isolation of swine infertility and respiratory syndrome virus (isolate ATCC VR-2332) in North America and experimental reproduction of the disease in gnotobiotic pigs. *J. Vet. Diagn. Investig.* 4, 117–126. doi: 10.1177/104063879200400201

Das, T., Chen, Z., Hendriks, R. W., and Kool, M. (2018). A20/tumor necrosis factor α-induced protein 3 in immune cells controls development of autoinflammation and autoimmunity: lessons from mouse models. *Front. Immunol.* 9:104. doi: 10.3389/fimmu.2018.00104

Huang, C., Zhang, Q., and Feng, W.-H. (2015). Regulation and evasion of antiviral immune responses by porcine reproductive and respiratory syndrome virus. *Virus Res.* 202, 101–111. doi: 10.1016/j.virusres.2014.12.014

Kim, D., Langmead, B., and Salzberg, S. L. (2015). HISAT: a fast spliced aligner with low memory requirements. *Nat. Methods* 12, 357–360. doi: 10.1038/nmeth.3317

Kim, D., Lee, J.-Y., Yang, J.-S., Kim, J. W., Kim, V. N., and Chang, H. (2020). The architecture of SARS-CoV-2 transcriptome. *Cells* 181, 914–921. doi: 10.1016/j.cell.2020.04.011

Kucera, M., Isserlin, R., Arkhangorodsky, A., and Bader, G. D. (2016). AutoAnnotate: a Cytoscape app for summarizing networks with semantic annotations. *F1000Research* 5. doi: 10.12688/f1000research.9090.1

Kuhn, J. H., Lauck, M., Bailey, A. L., Shchetinin, A. M., Vishnevskaya, T. V., Bào, Y., et al. (2016). Reorganization and expansion of the nidoviral family Arteriviridae. *Arch. Virol.* 161, 755–768. doi: 10.1007/s00705-015-2672-z

Langfelder, P., and Horvath, S. (2008). WGCNA: an R package for weighted correlation network analysis. *BMC Bioinformatics* 9, 1–13. doi: 10.1186/1471-2105-9-559

Li, S., Li, X., Qiu, M., Li, J., Xiao, Y., Lin, H., et al. (2021). Transcriptomic profiling reveals different innate immune responses in primary alveolar macrophages infected by two highly homologous porcine reproductive and respiratory syndrome viruses with distinct virulence. *Microb. Pathog.* 158:105102. doi: 10.1016/j.micpath.2021.105102

Liang, W., Ji, L., Zhang, Y., Zhen, Y., Zhang, Q., Xu, X., et al. (2017). Transcriptome differences in porcine alveolar macrophages from Tongcheng and large white pigs in response to highly pathogenic porcine reproductive and respiratory syndrome virus (PRRSV) infection. *Int. J. Mol. Sci.* 18:1475. doi: 10.3390/ijms18071475

Liao, Y., Smyth, G. K., and Shi, W. (2014). Feature counts: an efficient general purpose program for assigning sequence reads to genomic features. *Bioinformatics* 30, 923–930. doi: 10.1093/bioinformatics/btt656

Lim, B., Kim, S., Lim, K. S., Jeong, C. G., Kim, S. C., Lee, S. M., et al. (2020). Integrated time-serial transcriptome networks reveal common innate and tissue-specific adaptive immune responses to PRRSV infection. *Vet. Res.* 51:128. doi: 10.1186/s13567-020-00850-5

Livak, K. J., and Schmittgen, T. D. (2001). Analysis of relative gene expression data using real-time quantitative PCR and the $2^{-\Delta\Delta C_T}$ method. *Methods* 25, 402–408. doi: 10.1006/meth.2001.1262

López, D. M., Thelen, M., Stahl, F., Thiel, C., Linhorst, A., Sylvester, M., et al. (2019). The lysosomal transporter MFSD1 is essential for liver homeostasis and critically depends on its accessory subunit GLMP. *elife* 8:e50025. doi: 10.7554/eLife.50025

Love, M. I., Huber, W., and Anders, S. (2014). Moderated estimation of fold change and dispersion for RNA-seq data with DESeq2. *Genome Biol.* 15, 1–21. doi: 10.1186/s13059-014-0550-8

Lv, C., Liu, W., Wang, B., Dang, R., Qiu, L., Ren, J., et al. (2018). Ivermectin inhibits DNA polymerase UL42 of pseudorabies virus entrance into the nucleus and proliferation of the virus in vitro and vivo. *Antivir. Res.* 159, 55–62. doi: 10.1016/j.antiviral.2018.09.010

Ma, X., Lv, C., Wang, Q., Li, C., Wang, P., Luo, C., et al. (2021). C1QBP inhibits proliferation of porcine circovirus type 2 by restricting nuclear import of the capsid protein. *Arch. Virol.* 166, 767–778. doi: 10.1007/s00705-020-04950-7

Merico, D., Isserlin, R., Stueker, O., Emili, A., and Bader, G. D. (2010). Enrichment map: a network-based method for gene-set enrichment visualization and interpretation. *PLoS One* 5:e13984. doi: 10.1371/journal.pone.0013984

Miller, L. C., Fleming, D. S., Li, X., Bayles, D. O., Blecha, F., and Sang, Y. (2017). Comparative analysis of signature genes in PRRSV-infected porcine monocyte-derived cells to different stimuli. *PLoS One* 12:e0181256. doi: 10.1371/journal.pone.0181256

Myokai, F., Takashiba, S., Lebo, R., and Amar, S. (1999). A novel lipopolysaccharide-induced transcription factor regulating tumor necrosis factor α gene expression: molecular cloning, sequencing, characterization, and chromosomal assignment. *Proc. Natl. Acad. Sci.* 96, 4518–4523. doi: 10.1073/pnas.96.8.4518

Oeckinghaus, A., and Ghosh, S. (2009). The NF-κB family of transcription factors and its regulation. *Cold Spring Harb. Perspect. Biol.* 1:a000034. doi: 10.1101/cshperspect.a000034

Sánchez-Carvajal, J., Rodríguez-Gómez, I., Ruedas-Torres, I., Zaldívar-López, S., Larenas-Muñoz, F., Bautista-Moreno, R., et al. (2021). Time-series transcriptomic analysis of bronchoalveolar lavage cells from virulent and low virulent PRRSV-1-infected piglets. *J. Virol.* 96, e01140–21. doi: 10.1128/JVI.01140-21

Schoggins, J. W., and Rice, C. M. (2011). Interferon-stimulated genes and their antiviral effector functions. *Curr. Opin. Virol.* 1, 519–525. doi: 10.1016/j.coviro.2011.10.008

Shannon, P., Markiel, A., Ozier, O., Baliga, N. S., Wang, J. T., Ramage, D., et al. (2003). Cytoscape: a software environment for integrated models of biomolecular interaction networks. *Genome Res.* 13, 2498–2504. doi: 10.1101/gr.1239303

Shi, M., Lam, T. T.-Y., Hon, C.-C., Murtaugh, M. P., Davies, P. R., Hui, R. K.-H., et al. (2010). Phylogeny-based evolutionary, demographical, and geographical dissection of north American type 2 porcine reproductive and respiratory syndrome viruses. *J. Virol.* 84, 8700–8711. doi: 10.1128/JVI.02551-09

Song, S., Xu, H., Zhao, J., Leng, C., Xiang, L., Li, C., et al. (2020). Pathogenicity of NADC34-like PRRSV HLJDZD32-1901 isolated in China. *Vet. Microbiol.* 246:108727. doi: 10.1016/j.vetmic.2020.108727

Stark, R., Grzelak, M., and Hadfield, J. (2019). RNA sequencing: the teenage years. *Nat. Rev. Genet.* 20, 631–656. doi: 10.1038/s41576-019-0150-2

Sun, W., Wu, W., Jiang, N., Ge, X., Zhang, Y., Han, J., et al. (2022). Highly pathogenic PRRSV-infected alveolar macrophages impair the function of pulmonary microvascular endothelial cells. *Viruses* 14:452. doi: 10.3390/v14030452

Tang, X., Marciano, D. L., Leeman, S. E., and Amar, S. (2005). LPS induces the interaction of a transcription factor, LPS-induced TNF-α factor, and STAT6 (B) with effects on multiple cytokines. *Proc. Natl. Acad. Sci.* 102, 5132–5137. doi: 10.1073/pnas.0501159102

Terpstra, C., Wensvoort, G., and Pol, J. (1991). Experimental reproduction of porcine epidemic abortion and respiratory syndrome (mystery swine disease) by infection with Lelystad vims: Koch's postulates fulfilled. *Vet. Q.* 13, 131–136. doi: 10.1080/01652176.1991.9694297

van Geelen, A. G., Anderson, T. K., Lager, K. M., Das, P. B., Otis, N. J., Montiel, N. A., et al. (2018). Porcine reproductive and respiratory disease virus: evolution and recombination yields distinct ORF5 RFLP 1-7-4 viruses with individual pathogenicity. *Virology* 513, 168–179. doi: 10.1016/j.virol.2017.10.002

Vergarajauregui, S., Martina, J. A., and Puertollano, R. (2011). LAPTMs regulate lysosomal function and interact with mucolipin 1: new clues for understanding mucolipidosis type IV. *J. Cell Sci.* 124, 459–468. doi: 10.1242/jcs.076240

Wang, T. Y., Sun, M. X., Zhang, H. L., Wang, G., Zhan, G., Tian, Z. J., et al. (2021). Evasion of antiviral innate immunity by porcine reproductive and respiratory syndrome virus. *Front. Microbiol.* 12:693799. doi: 10.3389/fmicb.2021.693799

Weesendorp, E., Rebel, J. M., Popma-De Graaf, D. J., Fijten, H. P., and Stockhofe-Zurwieden, N. (2014). Lung pathogenicity of European genotype 3 strain porcine reproductive and respiratory syndrome virus (PRRSV) differs from that of subtype 1 strains. *Vet. Microbiol.* 174, 127–138. doi: 10.1016/j.vetmic.2014.09.010

Wensvoort, G., Terpstra, C., Pol, J., Ter Laak, E., Bloemraad, M., De Kluyver, E., et al. (1991). Mystery swine disease in the Netherlands: the isolation of Lelystad virus. *Vet. Q.* 13, 121–130. doi: 10.1080/01652176.1991.9694296

Wu, T., Hu, E., Xu, S., Chen, M., Guo, P., Dai, Z., et al. (2021). clusterProfiler 4.0: a universal enrichment tool for interpreting omics data. *Innovation* 2:100141. doi: 10.1016/j.xinn.2021.100141

Wu, J., Peng, X., Qiao, M., Zhao, H., Li, M., Liu, G., et al. (2020). Genome-wide analysis of long noncoding RNA and mRNA profiles in PRRSV-infected porcine alveolar macrophages. *Genomics* 112, 1879–1888. doi: 10.1016/j.ygeno.2019.10.024

Xiao, S., Mo, D., Wang, Q., Jia, J., Qin, L., Yu, X., et al. (2010). Aberrant host immune response induced by highly virulent PRRSV identified by digital gene expression tag profiling. *BMC Genomics* 11, 1–18. doi: 10.1186/1471-2164-11-544

Xu, H., Li, C., Li, W., Zhao, J., Gong, B., Sun, Q., et al. (2022). Novel characteristics of Chinese NADC34-like PRRSV during 2020-2021. *Transbound. Emerg. Dis.* 69:e3215–e3224. doi: 10.1111/tbed.14485

Yang, T., Zhang, F., Zhai, L., He, W., Tan, Z., Sun, Y., et al. (2018). Transcriptome of porcine PBMCs over two generations reveals key genes and pathways associated with variable antibody responses post PRRSV vaccination. *Sci. Rep.* 8:2460. doi: 10.1038/s41598-018-20701-w

Yuan, L., Zhu, Z., Fan, J., Liu, P., Li, Y., Li, Q., et al. (2022). High pathogenicity of a Chinese NADC34-like PRRSV on pigs. *Microbiol. Spect.* 10:e01541–e01522. doi: 10.1128/spectrum.01541-22

Zeng, N., Wang, C., Liu, S., Miao, Q., Zhou, L., Ge, X., et al. (2018). Transcriptome analysis reveals dynamic gene expression profiles in porcine alveolar macrophages in response to the Chinese highly pathogenic porcine reproductive and respiratory syndrome virus. *Biomed. Res. Int.* 2018:1538127, –1538123. doi: 10.1155/2018/1538127

frontiers | Frontiers in Microbiology

TYPE Original Research
PUBLISHED 28 October 2022
DOI 10.3389/fmicb.2022.1054651

OPEN ACCESS

EDITED BY
Zhenyu Zhang,
University of Wisconsin-Madison,
United States

REVIEWED BY
Da Shi,
Harbin Veterinary Research Institute
(CAAS), China
Yang Li,
China Animal Health and Epidemiology
Center, China

*CORRESPONDENCE
Zhi Cao
201901252@qau.edu.cn

SPECIALTY SECTION
This article was submitted to
Infectious Agents and Disease,
a section of the journal
Frontiers in Microbiology

RECEIVED 27 September 2022
ACCEPTED 13 October 2022
PUBLISHED 28 October 2022

CITATION
Zhang H, Yin D, Qin H, Zhang K, Li Z, Cui G, Ma G, Sun P and Cao Z (2022) Immunogenicity of the recombinant adenovirus fusion-expressing E0-E2 gene of the classical swine fever virus. *Front. Microbiol.* 13:1054651. doi: 10.3389/fmicb.2022.1054651

Immunogenicity of the recombinant adenovirus fusion-expressing E0-E2 gene of the classical swine fever virus

Heng Zhang[1], Dehua Yin[2], Huairui Qin[2], Ke Zhang[2], Zhaoyang Li[1], Guangchao Cui[1], Guangbin Ma[1], Peng Sun[3] and Zhi Cao[2]*

[1]Swine Disease R&D Center, Shandong SINDER Technology Co., Ltd., Qingdao, China, [2]College of Animal Medicine, Qingdao Agricultural University, Qingdao, China, [3]YEBIO Bioengineering Co., Ltd of Qingdao, Qingdao, China

Adenovirus vector vaccines have been the mainstream research direction of CSF vaccines, due to the replication deficiency of adenovirus vectors, achieving double effects with the safety of inactivated vaccines and the efficacy of live vaccines. Therefore, the E0 and E2 genes were expressed by an adenovirus vector, a recombinant adenovirus E0-E2 (rAd-E0-E2) vaccine was constructed, and the minimum immunization dose and immune duration period were determined in this study. Forty healthy piglets were randomly divided into 8 groups (n=5). Groups 1~5 were used to determine the minimum immunization dose, and 5 groups were inoculated with rAd-E0-E2 at different immune doses. Serum was collected at 7 d and 14 d after immunization to detect CSFV antibodies by ELISA, and piglets were challenged at 7 d post immunization. Groups 6~8 were immunized with 1 dose of rAd-E0-E2, the CSFV live attenuated vaccine C strain and saline to identify the immune duration period. Serum was collected at different time points after immunization, CSFV antibodies were detected by ELISA, and piglets were challenged at 8months post immunization. Meanwhile, temperature, clinical symptoms and pathology were observed. The results of groups 1~5 showed that 1 piglet was protected after challenge, and 4 piglets exhibited high fever retention, typical CSFV symptoms and tissue lesions in the 1/50 dose group, whereas no clinical symptoms were observed in the 1/10 dose, 1/5 dose or 1 dose groups with 5/5 protection after challenge. The minimum dose was determined as 1/10 dose. The results of groups 6~8 showed that all piglets survived after challenge, but the antibody level of the rAd-E0-E2 strain was higher than that of the C strain at 8months post immunization, and all piglets in the negative group developed the disease process after challenge. Overall, the minimum immunization dose of rAd-E0-E2 was 1/10 dose ($3.16\times10^{6.0}$ IFU) and the minimum immune dose was determined to be 1 dose ($3.16\times10^{7.0}$ IFU) to achieve the expected effects. The immune duration period of piglets immunized with 1 dose of rAd-E0-E2 was at least 8months.

KEYWORDS

classical swine fever virus, E0-E2 gene, recombinant adenovirus vaccine, minimum immunization dose, immune duration

Introduction

Classical swine fever (CSF) is a highly contagious, economically significant, multisystemic viral disease in swine, that is notifiable to the World Organization for Animal Health (WOAH; Blome et al., 2017; Ganges et al., 2020). The causative agent, CSF virus (CSFV), is an enveloped, positive-sense, single-stranded RNA virus. It belongs to the Pestivirus genus within the *Flaviviridae* family (Becher et al., 2003). At present, vaccination is still one of the effective ways to prevent CSF, but the symptoms of pigs infected by CSFV gradually trend towards chronic, insidious, and other atypical epidemic forms, thus making it imperative to develop a safe and effective vaccine to control the epidemic of CSF (Dong and Chen, 2007; Popescu et al., 2019).

At present, five structural proteins of CSFV have been identified, named N^{pro}, C, E0 (E^{rns}), E1 and E2. E0 and E2 are two main protective antigens for the viral-induced production of neutralizing antibodies in the organism, and are essential for virus adsorption and entry into host cells (Sun et al., 2013a). The host tropism of CSFV is related to E0, and the E0 protein can effectively neutralize E0 specific monoclonal antibodies and protect susceptible animals from infection (Xu et al., 2008). The E2 protein induces the production of neutralizing antibodies to the virus *in vitro*, and stimulates protective immunity against CSFV *in vivo*, protecting pigs from lethal CSFV infection (Huang et al., 2014; Henke et al., 2018; Tran et al., 2020). In addition, E0 and E2 chimeric antigens significantly improved the sensitivity of serological diagnosis and detected CSFV infection 7 days earlier than using E2 antigen alone (Lin et al., 2005; Sun et al., 2010, 2013a).

With the continuous development of molecular biology technology, more innovative vaccines for CSF have been developed and approved for use. The most widely used CSF vaccine in China is the live attenuated CSF vaccine (CSFV C strain, China), which is one of the most effective vaccines for CSF control. Moreover, with the cooperation of several companies, the CSFV E2 subunit vaccine (WH-09 strain) was developed using BEVS, whose production permit and new veterinary drug certificate were issued in 2020, and used in the swine industry. The inactivated CSFV E2 protein recombinant baculovirus vaccine (strain WH-09), jointly developed by Huazhong Agricultural University and Wuhan Keqian Biological Co., Ltd. and other companies, received a new veterinary drug certificate and production licence in 2020. Another subunit vaccine expressing CSFV E2 protein in HEK 293 T cells was developed by YEBIO Bioengineering Co., Ltd. of Qingdao, and is currently in the process of applying for a new veterinary drug certificate. In addition, human replication-deficient adenovirus type 5 live vector CSF vaccine and chimeric CSFV vaccine can induce complete immune protection. Adenovirus vector vaccines have been the mainstream research direction of CSF vaccines, due to the replication deficiency of adenovirus vectors, providing double effects with the safety of inactivated vaccines and the efficacy of live vaccines (Yan et al., 2020).

In our study, considering the deficiency of live vaccines and the high-safety of adenovirus vector vaccines, we examined a novel adenovirus live vector vaccine (rAd-E0-E2 strain) targeting to CSFV E0 and E2 genes. To verify the immune efficacy of the rAd-E0-E2 vaccine, the minimum immune dose and immune duration period were determined, with the hope of offering enough practical data for clinical application and provide a reference for subsequent application studies of this vaccine.

Materials and methods

Vaccines and viruses

A recombinant adenovirus vaccine (rAd-E0-E2 strain) expressing the E0-E2 gene of CSFV (live vector vaccine, $3.16 \times 10^{7.0}$ IFU per dose) was lyophilized and preserved at the Swine Diseases R&D Center of SINDER. Live CSF vaccine (splenic lymphogen source, C strain), was produced by the lyophilized vaccine workshop of SINDER. CSFV Shimen strain (CVCC AV1411) blood virus (F115 generation, $\geq 10^{5.0}$ MLD), was purchased from the China Veterinary Culture Collection Center (CVCC).

Animals

Six-to eight-week-old healthy and susceptible weaned piglets ($n = 60$), which were free of CSFV, porcine circovirus 2 (PCV2), and porcine reproduction and respiratory syndrome virus (PRRSV) infection. All piglet experiments were performed at YEBIO Bioengineering Co., Ltd. of Qingdao and in accordance with the protocols approved by the Animal Care and Ethics Committee of the China Animal Health and Epidemiology Center under number CNASL1005.

Package and identification of recombinant adenovirus

The primers for the CSFV E0 and E2 genes were designed by Oligo 5.0 according to the CSFV genome sequence (Table 1)

TABLE 1 Primers for CSFV E0 and E2 proteins.

Genes	Primer sequences (5′-3′)	Restriction sites
CSFV-E0	F:AAATCTAGAATGGAAAATATAACTCAAT	*Kpn* I, *Bgl* II
	R:CCCGGTACCGGCATAAGCGCCAAAC	
CSFV-E2	F:AAAGGTACCAGGGGACAGATCGTGCAT	*Not* I, *Bgl* II
	R:CCCGCGGCCGCGGCGAGTTGTTCTGTT AG	

and synthesized by Sangon Biotech (Shanghai) after codons were optimized. The E0 and E2 protein genes were amplified by PCR and cloned sequentially into the adenovirus shuttle vector pAdTrack-CMV. The positive recombinant shuttle plasmid was named pAdTrack-E0-E2. pAdTrack-E0-E2 and the skeleton plasmid were cotransfected into HEK293 cells, and recombinant adenovirus was harvested when typical CPEs were observed, such as those that were rounded and broken. Then, the specificity of the recombinant adenovirus rAd-E0-E2 strain was identified by indirect immunofluorescence (IFA).

Determination of virus content

HEK293 cells were cultured in DMEM containing 10% NBS, and cells were seeded in 24-well plates and incubated at 37°C in 5% CO_2 for 2 to 3 h. Then, 100 μl/well of 10-fold-diluted (from 10^{-3} to 10^{-7}) rAd-E0-E2 strain virus in DMEM was added to HEK293 cells in 24-well plates for three replicates of each dilution, accompanied by cell-negative control wells. After incubation for 48 h, indirect immunofluorescence (IFA) was used to detect cell infection and calculate the viral content.

$$\text{Virus content per well} = \frac{\text{Numbers of positive cells in vision field}}{\text{total number of fields of vision}} \times \frac{\text{standard well area}}{\text{visual field area}} \times \frac{\text{dilution ratio}}{0.1\text{mL}}$$

$$\text{Virus content} = \frac{\text{sum of virus content per well}}{\text{number of wells}}$$

Piglet vaccination and challenge

Forty healthy piglets were randomly divided into 8 groups ($n = 5$), groups 1 ~ 5 were used to determine the minimum immunization dose and groups 6 ~ 8 were used to determine the immune duration period. The detailed experimental design is provided in Table 2.

Detection of antibodies in serum samples

Blood was collected from the precaval vein of piglets at 7 d and 14 d post immunization in groups 1 ~ 5 and at 7 d, 14 d, 21 d, 30 d, 60 d, 90 d, 120 d, 150 d, 180 d, 210 d and 240 d post immunization in groups 6 ~ 8, and the serum was separated. CSFV-specific antibodies were tested with a classical swine fever virus antibody test kit (IDEXX, United States) following the manufacturer's instructions.

Examination of clinical signs and pathological changes

The temperatures of all experimental animals were measured from 2 days before the challenge to 16 days after the challenge. The spirit, food and water intake, faeces, and morbidity of pigs were observed daily, and all surviving pigs were dissected at 16 days post challenge. The tissue lesions were observed, and the survival rate was recorded.

Histopathology

The representative organs were collected and fixed in 10% neutral formalin at room temperature for 24 h. The fixed tissues were embedded in paraffin wax, stained with haematoxylin and eosin (H&E), and examined by light microscopy.

Statistical analysis

Data are presented as the mean ± standard deviation (SD) of five replicates using Origin software.

TABLE 2 Experiments design of determination of minimum immune dose and immune duration period.

Experimental content	Groups	Immune dose	Viral titer(IFU/dose)	Number	Challente time
Minimum immune	1	1/50 dose	6.32×10^5	5	Day 7 post vaccination
dose group	2	1/10 dose	3.16×10^6	5	
	3	1/5 dose	6.32×10^6	5	
	4	1 dose	3.16×10^7	5	
	5	Saline	0	5	
Immune duration group	6	rAd-E0-E2 strain	3.16×10^7	5	8th month post
	7	C strain	1 dose	5	vaccination
	8	Saline	0	5	

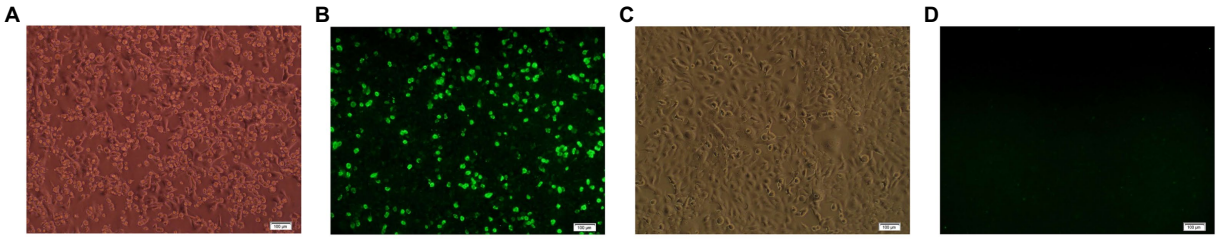

FIGURE 1
IFA identified with the recombinant adenovirus rAd-E0-E2. **(A)** Cytopathic effects (CPE) in HEK 293 cells transfected with pAdEasy-E0-E2. **(B)** Green fluorescence in HEK 293 cells transfected with pAdEasy-E0-E2. **(C)** No CPE in normal cell controls. **(D)** No fluorescence in normal control cells. Scale bar: 100μm.

Results

Identification and loads of recombinant adenovirus rAd-E0-E2 strain

After pAdEasy-E0-E2 and pAdTrack-CMV were transfected into HEK293 cells by lipidosomes, obvious CPE was found in HEK 293 cells on the 10th day post transfection (Figure 1A), and green fluorescence was observed in the cells transfected with pAdEasy-E0-E2 (Figure 1B), while there was no CPE or fluorescence in the control cells without plasmid transfection (Figures 1C,D). The results showed that the recombinant adenovirus rAd-E0-E2 strain was obtained. HEK293 cells were inoculated with10^5-diluted adenovirus, and the loads of recombinant adenovirus rAd-E0-E2 was $10^{8.5}$ IFU/ml.

Determination of the minimum immune dose of the rAd-E0-E2 live vector vaccine

Detection of specific antibodies

Groups 1 ~ 5 were used to determine the minimum immune dose (1/50 dose, 1/10 dose, 1/5 dose, 1 dose and control group) and serum was collected to detect CSFV-specific antibodies by ELSA. The Results showed that the antibody-positive rate of group 1 (1/50 dose) was 1/5 with a 26.3% antibody blocking rate, and the specific antibody of all piglets was positive in groups 2 ~ 4 (1/10 dose, 1/5 dose and 1 dose) with 45.6, 57.8 and 61.1% blocking rates, respectively. However, 0 piglets were positive in group 5 (control group), with a ≤ 12.0% blocking rate. These results indicated that specific antibodies of piglets vaccinated with 1/10 dose of live vector vaccine (rAd-E0-E2) were close to positive, and ≥ 1/5 dose were positive at 7 d post vaccination (Figure 2A).

Temperature monitoring

Compared to the normal temperature of 39.5°C, group 5 (control group) maintained a higher fever until death, and 4 piglets in group 1 (1/50 dose) had a higher fever than 40°C at 2 d post challenge and maintained a high fever until 16 d post challenge, exhibiting continued fever. Conversely, the temperatures of group 2 ~ 4 (1/10 dose, 1/5 dose, and 1 dose) piglets were normal, which indicated that the 1/10 dose of live vector vaccine (rAd-E0-E2) could protect piglets from CSFV infection (Figure 2B).

Mortality examination

Four pigs in group 1 died at 11 d ~ 12 d post challenge, but no deaths occurred in groups 2, 3, and 4. All piglets in group 5 died at 9 ~ 10d post challenge, showing typical CSF symptoms, which demonstrated that piglets immunized with 1/10 dose or above of the rAd-E0-E2 strain for 7 d were completely protected from lethal CSFV attack (Figure 2C).

Determination of the immune duration of the rAd-E0-E2 live vector vaccine

Detection of specific antibodies

Groups 6 ~ 8 were vaccinated with live vector vaccine (rAd-E0-E2, 1 dose), live vector vaccine (CSFV C strain, 1 dose) and saline, and were used to determine the immune duration period. The results showed that CSFV-specific antibodies of piglets were positive at 7 d post vaccination and sustained at least 8 months in group 6. The antibody-positive rate of group 7 was 4/5 at 7 d post vaccination and subsequently decreased to suspicious, while the antibody rate of 5/5 piglets was positive. However, the CSFV-specific antibody of group 8 was negative throughout the experiment (Figure 3A). These results showed that CSFV-specific antibody of piglets vaccinated with 1 dose of live vector vaccine (rAd-E0-E2) could be sustained for at least 8 months, which was superior to that of piglets vaccinated with live vaccine (CSFV C strain, 1 dose).

Temperature monitoring

In the immune duration experiment, the temperatures of groups 6 and 7 were normal while group 8 had a fever higher than 40°C and exhibited continued fever, suggesting that piglets vaccinated with the live vector vaccines rAd-E0-E2 strain and C strain did not exhibit typical fever symptoms (Figure 3B).

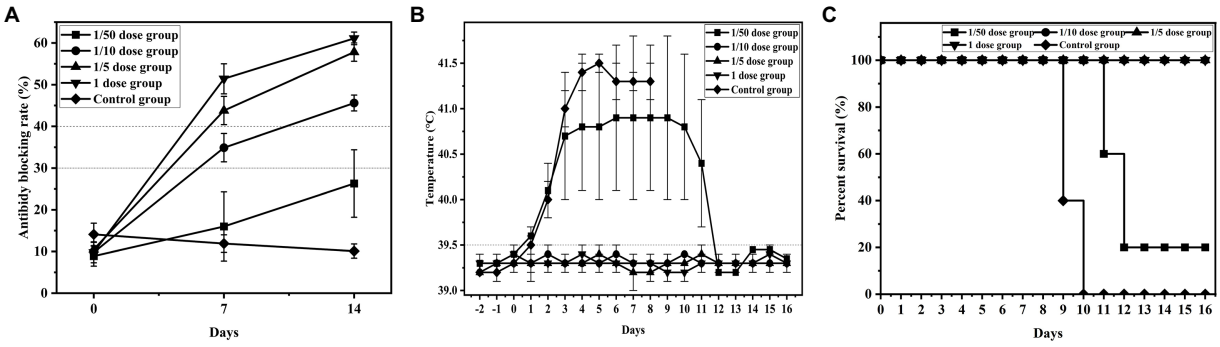

FIGURE 2
Detection results of minimum immune dose groups. Piglets were immunized with different doses of recombinant adenovirus live vector vaccine (1/20 dose, 1/10 dose, 1/2 dose, 1 dose), and control group were immunized with saline. All groups was challenged at 14 dpi post immunization. **(A)** Variation in the average blocking rate of antibodies in serum was measured at 7 dpi and 14 dpi. **(B)** Rectal temperature was measured during the 16-day observation period, and **(C)** the survival rate was recorded. Data are presented as the mean±standard deviation (SD).

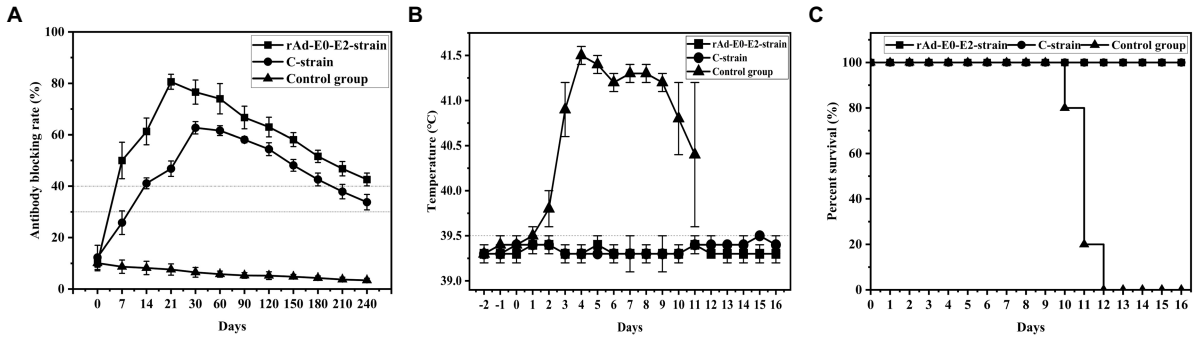

FIGURE 3
Determination of the immune duration of the rAd-E0-E2 live vector vaccine. Piglets were immunized with different types of live vector vaccines (rAd-E0-E2 strain and C strain), and the control group was immunized with saline. All groups were challenged at 8 months post immunization. **(A)** Variation in the average blocking rate of antibodies in serum was measured at 7 dpi and 14 dpi, in which a higher antibody-blocking rate indicated higher antibodies level. **(B)** Rectal temperature was measured during the 8-month observation period, and **(C)** the survival rate was recorded. Data are presented as the mean±standard deviation (SD).

Mortality examination

Groups 6 and 7 had no CSF clinical symptoms or pathological changes post challenge, and the survival rate was 100%. All piglets in group 8 died at 10 ~ 12 d post challenge, showing typical CSF symptoms such as continued high fever. The results showed that both the rAd-E0-E2 strain and C strain could also protect immunized pigs from CSFV for at least 8 months (Figure 3C).

Clinical symptoms post challenge

The challenged piglets of group 5 (5/5) and group 1 (4/5) showed CSF-related clinical symptoms including high body temperature, depression, conjunctivitis, diarrhoea and loss of appetite, and obvious pathological changes, such as marginal spleen infarction and haemorrhagia in the kidney and lymph gland (Figure 4A), which were observed in groups 5 and group 8. However, no clinical symptoms or pathological changes were observed in groups 2, 3 and 4, which suggested that a 1/10 dose of live vector vaccine (rAd-E0-E2) had a protective effect on pigs (Figure 4B).

No CSF-related symptoms or pathological changes in tissues were observed in groups 6 and 7 at 8th month post immunization, while all piglets exhibited high fever at 40°C from 2 ~ 3 days post challenge, and symptoms of CSF appeared in group 8 (Figures 4C–H). These data suggested that piglets vaccinated with the live vector vaccines rAd-E0-E2 and C strain can protect piglets from CSFV attack for at least 8 months.

Discussion

CSFV E0 protein is the only glycoprotein secreted into the culture supernatant of CSFV-infected cells. It can stimulate

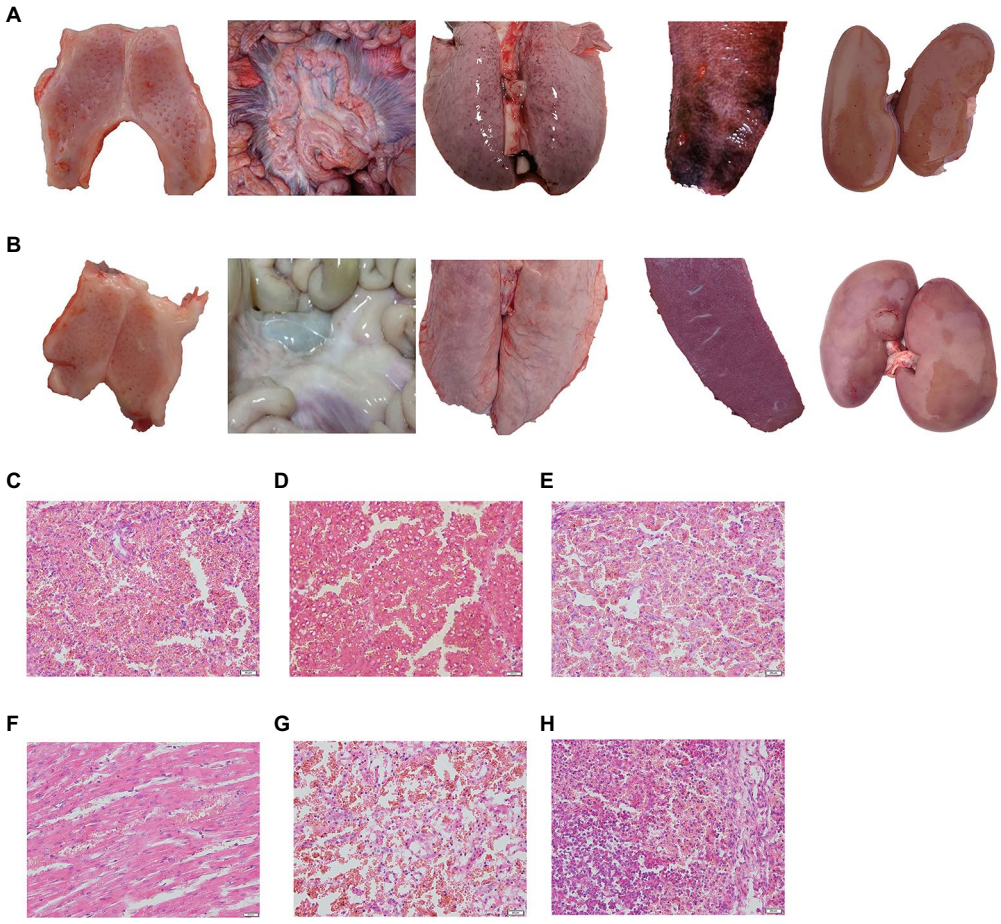

FIGURE 4
Typical pathological lesions of tonsil, intestinal lymph node, lung, spleen, and kidney in control group **(A)** and normal piglets **(B)**, and histopathological examination of the spleen **(C)**, liver **(D)**, lung **(E)**, heart **(F)**, kidney **(G)**, and lymph gland **(H)**. Scale bar: 200μm.

pigs to produce neutralizing antibodies against CSFV infection (Xu et al., 2020; Reuscher et al., 2021). The glycoprotein E2 has been proven to be the main structural protein of CSFV and can induce a protective response in pigs (Panyasing et al., 2018). As a research hotspot in recent years, the recombinant live vector recombinant vaccine of CSF is a novel vaccine prepared by recombining the virus antigen gene into a live vector that can express exogenous virus protein, which can stimulate the body to produce a specific immune response (Wei et al., 2021). At present, the structure and function of the adenovirus genome have been studied thoroughly; meanwhile, human type 5 nonreplicating adenovirus vectors have attracted researchers' attention because of their safety, wide host range and stability (Zhu et al., 2017; Yan et al., 2020). Previous studies have shown that adenovirus vectors can induce strong specific cellular and humoral immune responses, which are widely used in the construction of new vaccines against severe zoonotic diseases (Gabitzsch et al., 2011; Lapuente et al., 2018; Zhang et al., 2018).

In our study, the E0 and E2 genes were inserted into the human type 5 adenovirus vector, the complete virions were packaged into HEK 293 cells (Figure 1A), and high-titre adenoviruses were harvested. After 10 continuous passages, we constructed a recombinant adenovirus vaccine based on CSFV E0 and E2 proteins using an adenovirus vector (rAd-E0-E2), and conducted detailed experiments to determine the minimum immune dose and immune duration period in piglets. Overall, the recombinant adenovirus vector vaccine (rAd-E0-E2) showed no difference from the CSF splenic lymphoid vaccine (CSFV C strain) in protecting piglets.

To determine the minimum immune dose of the rAd-E0-E2 live vaccine, we designed four doses, including a 1/50 dose, 1/10 dose, 1/5 dose and 1 dose, and sera were collected at 7 dpi and 14 dpi. The CSFV-specific antibody was positive partly from 7 days post immunization, and all piglets were CSFV antibody-positive at 14 dpi with a blocking rate $\geq$ 40% (Figure 2A). Although piglets immunized with the 1/10 dose of live vector vaccine (rAd-E0-E2 strain) were not CSFV antibody-positive

completely, the piglets were protected completely from CSFV lethal attack without high-temperature symptoms (Figures 2B,C), which indicated that cellular immunity or mucosal immunity was enhanced, covering the shortage of lower humoral immunity. Therefore, a 1/10 dose of live vector vaccine can offer protection in a short time, reducing the probability of CSFV infection during the immune window period. On the other hand, the immune duration period of the rAd-E0-E2 vaccine lasted at least 8 months, which was comparable to that of the live vector vaccine C-strain, and all piglets survived without any CSF-related symptoms (Figures 3B,C). In terms of CSFV-specific antibodies, a higher blocking rate was observed in the rAd-E0-E2-immunized serum than in the serum-immunized live attenuated vaccine C-strain (Figure 3A).

Sun et al. constructed a recombinant adenovirus vector vaccine expressing E2 protein (rAdV-SFV-E2) and evaluated the vaccine performance in rabbits and pigs (Sun et al., 2013b). In a rabbit vaccination-challenge model, one dose of 10^6 $TCID_{50}$ rAdV-SFV-E2 induced early (as early as 9 days) and long-lasting (up to 189 days) immune responses, and the minimum dose was determined to be one dose of 2.5×10^5 $TCID_{50}$. Moreover, pigs were conferred immunity with two doses of 10^7 $TCID_{50}$. However, the rAd-E0-E2 live vector vaccine in our study elicited robust immune responses as early as 7 days, and the immune duration period lasted up to 8 months, which suggested that the rAd-E0-E2 vaccine can offer comprehensive protection compared to a recombinant adenovirus vector vaccine expressing a single protein. In addition, a long immune period can be achieved, which provides convenience for large-scale herds and sharply reduces costs.

In conclusion, a recombinant adenovirus live vector vaccine (rAd-E0-E2 strain) was successfully constructed. The minimum immunization dose of the rAd-E0-E2 vaccine was 1/10 dose ($3.16 \times 10^{6.0}$ IFU) to protect piglets from lethal CSFV challenge, and the duration of immunization in piglets immunized with 1 dose of rAd-E0-E2 was at least 8 months. These data provide scientific material for the clinical application of the vaccine.

Data availability statement

The raw data supporting the conclusions of this article will be made available by the authors, without undue reservation.

Ethics statement

The animal study was reviewed and approved by Animal Care and Ethics Committee of the China Animal Health and Epidemiology Center, under the number CNASL1005.

Author contributions

ZC, HQ, GM, and DY: data curation. HQ, KZ, and ZL: formal analysis. HZ, GC, and PS: methodology. ZC, ZL, and GC: project administration. ZC: supervision. HZ, DY, HQ, and KZ: writing–original draft. HZ and ZC: writing–review and editing. All authors contributed to the article and approved the submitted version.

Funding

This work was supported by the Post Expert of Disease Control in Shandong Technique System for Pig Industry (Project No. SDAIT-08-07) and the National Natural Science Foundation of China (32002269).

Conflict of interest

HZ, ZL, GC, and GM were employed by the company Shandong SINDER Technology Co., Ltd., and PS was employed by the company YEBIO Bioengineering Co., Ltd of Qingdao.

The remaining authors declare that the research was conducted in the absence of any commercial or financial relationships that could be construed as a potential conflict of interest.

Publisher's note

All claims expressed in this article are solely those of the authors and do not necessarily represent those of their affiliated organizations, or those of the publisher, the editors and the reviewers. Any product that may be evaluated in this article, or claim that may be made by its manufacturer, is not guaranteed or endorsed by the publisher.

References

Becher, P., Avalos Ramirez, R., Orlich, M., Cedillo Rosales, S., Konig, M., Schweizer, M., et al. (2003). Genetic and antigenic characterization of novel pestivirus genotypes: implications for classification. *Virology* 311, 96–104. doi: 10.1016/s0042-6822(03)00192-2

Blome, S., Staubach, C., Henke, J., Carlson, J., and Beer, M. (2017). Classical swine fever-an updated review. *Viruses* 9:086. doi: 10.3390/v9040086

Dong, X. N., and Chen, Y. H. (2007). Marker vaccine strategies and candidate CSFV marker vaccines. *Vaccine* 25, 205–230. doi: 10.1016/j.vaccine.2006.07.033

Gabitzsch, E. S., Xu, Y., Balint, J. P. Jr., Balcaitis, S., Sanders-Beer, B., and Jones, F. R. (2011). Induction and comparison of SIV immunity in Ad5 naive and Ad5 immune non-human primates using an Ad5 [E1-, E2b-] based vaccine. *Vaccine* 29, 8101–8107. doi: 10.1016/j.vaccine.2011.08.038

Ganges, L., Crooke, H. R., Bohorquez, J. A., Postel, A., Sakoda, Y., Becher, P., et al. (2020). Classical swine fever virus: the past, present and future. *Virus Res.* 289:198151. doi: 10.1016/j.virusres.2020.198151

Henke, J., Carlson, J., Zani, L., Leidenberger, S., Schwaiger, T., Schlottau, K., et al. (2018). Protection against transplacental transmission of moderately virulent

classical swine fever virus using live marker vaccine "CP7_E2alf". *Vaccine* 36, 4181–4187. doi: 10.1016/j. vaccine. 2018.06.014

Huang, Y. L., Deng, M. C., Wang, F. I., Huang, C. C., and Chang, C. Y. (2014). The challenges of classical swine fever control: modified live and E2 subunit vaccines. *Virus Res.* 179, 1–11. doi: 10.1016/j.virusres.2013.10.025

Lapuente, D., Ruzsics, Z., Thirion, C., and Tenbusch, M. (2018). Evaluation of adenovirus 19a as a novel vector for mucosal vaccination against influenza a viruses. *Vaccine* 36, 2712–2720. doi: 10.1016/j.vaccine.2018.02.075

Lin, M., Trottier, E., and Mallory, M. (2005). Enzyme-linked immunosorbent assay based on a chimeric antigen bearing antigenic regions of structural proteins erns and E2 for serodiagnosis of classical swine fever virus infection. *Clin. Diagn. Lab. Immunol.* 12, 877–881. doi: 10.1128/CDLI.12.7.877-881.2005

Panyasing, Y., Thanawongnuwech, R., Ji, J., Gimenez-Lirola, L., and Zimmerman, J. (2018). Detection of classical swine fever virus (CSFV) E2 and E (rns) antibody (IgG, IgA) in oral fluid specimens from inoculated (ALD strain) or vaccinated (LOM strain) pigs. *Vet. Microbiol.* 224, 70–77. doi: 10.1016/j.vetmic.2018.08.024

Popescu, L. N., Panyasing, Y., Gimenez-Lirola, L., Zimmerman, J., and Rowland, R. R. R. (2019). E2 and E (rns) isotype-specific antibody responses in serum and oral fluid after infection with classical swine fever virus (CSFV). *Vet. Microbiol.* 235, 265–269. doi: 10.1016/j.vetmic.2019.07.007

Reuscher, C. M., Schmidt, L., Netsch, A., and Lamp, B. (2021). Characterization of a cytopathogenic reporter CSFV. *Viruses* 13:1209. doi: 10.3390/v13071209

Sun, Y., Liu, D. F., Wang, Y. F., Liang, B. B., Cheng, D., Li, N., et al. (2010). Generation and efficacy evaluation of a recombinant adenovirus expressing the E2 protein of classical swine fever virus. *Res. Vet. Sci.* 88, 77–82. doi: 10.1016/j.rvsc.2009.06.005

Sun, Y., Tian, D. Y., Li, S., Meng, Q. L., Zhao, B. B., Li, Y., et al. (2013b). Comprehensive evaluation of the adenovirus/alphavirus-replicon chimeric vector-based vaccine rAdV-SFV-E2 against classical swine fever. *Vaccine* 31, 538–544. doi: 10.1016/j.vaccine.2012.11.013

Sun, Y., Yang, Y., Zheng, H., Xi, D., Lin, M., Zhang, X., et al. (2013a). Co-expression of erns and E2 genes of classical swine fever virus by replication-defective recombinant adenovirus completely protects pigs against virulent challenge with classical swine fever virus. *Res. Vet. Sci.* 94, 354–360. doi: 10.1016/j.rvsc.2012.09.012

Tran, H. T. T., Truong, D. A., Ly, V. D., Vu, H. T., Hoang, T. V., Nguyen, C. T., et al. (2020). The potential efficacy of the E2-subunit vaccine to protect pigs against different genotypes of classical swine fever virus circulating in Vietnam. *Clin Exp Vaccine Res* 9, 26–39. doi: 10.7774/cevr.2020.9.1.26

Wei, Q., Liu, Y., and Zhang, G. (2021). Research Progress and challenges in vaccine development against classical swine fever virus. *Viruses* 13:445. doi: 10.3390/v13030445

Xu, X. G., Chiou, M. T., Zhang, Y. M., Tong, D. W., Hu, J. H., Zhang, M. T., et al. (2008). Baculovirus surface display of E (rns) envelope glycoprotein of classical swine fever virus. *J. Virol. Methods* 153, 149–155. doi: 10.1016/j.jviromet.2008.07.019

Xu, H., Wang, Y., Han, G., Fang, W., and He, F. (2020). Identification of E2 with improved secretion and immunogenicity against CSFV in piglets. *BMC Microbiol.* 20:26. doi: 10.1186/s12866-020-1713-2

Yan, L., Zhao, Z., Xue, X., Zheng, W., Xu, T., Liu, L., et al. (2020). A bivalent human adenovirus type 5 vaccine expressing the rabies virus glycoprotein and canine distemper virus hemagglutinin protein confers protective immunity in mice and foxes. *Front. Microbiol.* 11:1070. doi: 10.3389/fmicb.2020.01070

Zhang, Y., Feng, Y., Li, L., Ye, X., Wang, J., Wang, Q., et al. (2018). Immunization with an adenovirus-vectored TB vaccine containing Ag85A-Mtb 32 effectively alleviates allergic asthma. *J. Mol. Med. (Berl)* 96, 249–263. doi: 10.1007/s00109-017-1614-5

Zhu, F.-C., Wurie, A. H., Hou, L.-H., Liang, Q., Li, Y.-H., Russell, J. B. W., et al. (2017). Safety and immunogenicity of a recombinant adenovirus type-5 vector-based Ebola vaccine in healthy adults in Sierra Leone: a single-Centre, randomised, double-blind, placebo-controlled, phase 2 trial. *Lancet* 389, 621–628. doi: 10.1016/s0140-6736(16)32617-4

frontiers | Frontiers in Microbiology

TYPE Original Research
PUBLISHED 28 October 2022
DOI 10.3389/fmicb.2022.1049287

OPEN ACCESS

EDITED BY
Peirong Jiao,
South China Agricultural University, China

REVIEWED BY
Matteo Legnardi,
University of Padua,
Italy
Anna Pikula,
National Veterinary Research Institute (NVRI), Poland

*CORRESPONDENCE
Xiaorong Zhang
zxr@yzu.edu.cn
Yantao Wu
ytwu@yzu.edu.cn

†These authors have contributed equally to this work

SPECIALTY SECTION
This article was submitted to Virology, a section of the journal Frontiers in Microbiology

RECEIVED 20 September 2022
ACCEPTED 11 October 2022
PUBLISHED 28 October 2022

CITATION
Bo Z, Chen S, Zhang C, Guo M, Cao Y, Zhang X and Wu Y (2022) Pathogenicity evaluation of GVI-1 lineage infectious bronchitis virus and its long-term effects on reproductive system development in SPF hens.
Front. Microbiol. 13:1049287.
doi: 10.3389/fmicb.2022.1049287

Pathogenicity evaluation of GVI-1 lineage infectious bronchitis virus and its long-term effects on reproductive system development in SPF hens

Zongyi Bo[1,2†], Shuqin Chen[1†], Chengcheng Zhang[1], Menjiao Guo[1], Yongzhong Cao[2], Xiaorong Zhang[1*] and Yantao Wu[1,2*]

[1]College of Veterinary Medicine, Jiangsu Co-Innovation Center for the Prevention and Control of Important Animal Infectious Disease and Zoonoses, Yangzhou University, Yangzhou, Jiangsu, China, [2]Joint International Research Laboratory of Agriculture and Agri-Product Safety, The Ministry of Education of China, Yangzhou University, Yangzhou, China

Infectious bronchitis virus (IBV) has gained increasing attention in the poultry industry due to its ability to cause tissue injuries not only in the respiratory system and kidney but also in the reproductive system of layers. Recently, the GVI-1 lineage IBVs have spread widely in China, whereas their pathogenicity in egg-laying chickens has rarely been studied, especially its long-term influence in egg production upon the early infection in chicks. In this study, 10-day-old SPF chicks were infected with the GVI-1 lineage JX181 strain and monitored over a 170-day period after infection. The pathogenicity evaluation of the JX181 strain included clinical observations, immunohistochemical assay, viral load, viral shedding, gross autopsy, and laying rate. The results showed that JX181 has a high pathogenicity, causing severe system lesions, and the decrease in egg production. In summary, this study describes the long-term damages caused by the early infection with the IBV GVI-1 lineage on the reproductive system of hens, providing a comprehensive understanding of the pathogenicity of the IBV GVI-1 lineage and emphasizing the importance of its early prevention.

KEYWORDS

infectious bronchitis virus, GVI-1 lineage, pathogenicity, early infection, reproductive system, egg production

Introduction

Infectious bronchitis virus (IBV), the causative agent of avian infectious bronchitis, has been widely prevalent worldwide since it was first reported in the 1930s (Beach and Schalm, 1936). IBV infects chickens of all ages and breeds, resulting in respiratory tract damage, nephritis, and reproductive problems, such as declines in egg production and

quality (Cavanagh, 2007). IBV belongs to the gamma-coronaviruses, and its genome is a single positive-strand RNA with a high mutation and recombination rate (Thor et al., 2011), which leads to the continuous emergence of new genotypes and serotypes (Jackwood, 2012). To date, eight genotypes (GI ~ GVII) and more than 30 distinct viral lineages of IBV have been defined worldwide based on the complete S1 gene sequences (Valastro et al., 2016; Chen et al., 2017; Ma et al., 2019; Domanska-Blicharz et al., 2020).

As the most effective method to prevent and control infectious bronchitis, vaccination is widely used in the poultry industry. Nonetheless, outbreaks of IBV continue to occur, and multiple IBV genotypes are cocirculating in China (Li et al., 2010; Zhang et al., 2021). The GI-19 (QX) genotype first appeared in the 1990s and was associated predominantly with proventriculitis, respiratory stress, nephritis, and false layer syndrome (Liu and Kong, 2004; Fan et al., 2019). The proportion of GI-19 isolates has increased continuously over the past two decades and has become the most frequently isolated IBV genotype in China at present (Zhao et al., 2016). In addition, the GI-7 (TWI) lineage has been the second most prevalent type since the first report in the Chinese mainland in 2009, which showed similar pathogenicity to strains of the QX genotype (Xu et al., 2018; Zhang et al., 2020). The GVI-1 lineage TC07-2 strain was first isolated in Guangdong, China, in 2007 and subsequently occurred in many other countries in Asia (Mase et al., 2010; Lim et al., 2012; Raja et al., 2020). Epidemiological surveillance data demonstrated that the detection rate of the GVI-1 strains has continually increased in recent years, especially in southern China (Fan et al., 2019; Chen et al., 2021). The existing results have revealed that GVI-1 strains show a high affinity for the respiratory tract rather than the kidney (Jang et al., 2018; Sun et al., 2021). However, there are few systematic studies on the pathogenicity of IBV GVI-1 strains, especially the effects of its early infection in chicks to the long-term performance of laying hens.

The objective of this study was to comprehensively evaluate the pathogenicity of the GVI-1 lineage IBV by examining clinical signs, gross lesions, histological lesions, viral shedding, and egg production in infected chickens. This research revealed that early infection with the GVI-1 lineage JX181 strain induced severe lesions in different organs, which finally resulted in reduced egg production.

Materials and methods

SPF chickens and embryonated chicken eggs

SPF white leghorn chickens were purchased from Jinan Sipai Furui Livestock Technology Co., Ltd. (Jinan, China). SPF embryonated chicken eggs were purchased from Beijing Boehringer Ingelheim Merial Vital Laboratory Animal Technology Co., Ltd. (Beijing, China).

Virus isolation and titration

The IBV GVI-1 lineage strain CK/CH/JX/2018/1 (abbreviation: JX181) was isolated from a 200-day-old parent egg breeder chicken flock that showed respiratory signs, diarrhea, and egg production dropping in 2018 in Jiangxi Province of China. The virus was propagated in embryonated SPF eggs. The allantoic fluid was harvested and titrated by inoculating serial 10-fold dilutions of the virus into 10-day-old SPF embryos. The 50% embryo infectious doses (EID_{50}) were determined as described by Reed and Muench (Reed and Muench, 1938).

Pathogenicity evaluation of the JX181 strain in SPF chickens

A total of 70 female SPF chicks were randomly divided into two groups of 35 chicks each. Ten-day-old chicks in the challenge group were inoculated with 100 µl of PBS containing $10^{6.5}$ EID_{50} of the JX181 strain *via* the ocular-nasal route, and those in the control group were inoculated with equal amounts of PBS. Throughout the study period of 170 days, the chickens in the two groups were raised in two separate negative-pressure isolators under uniform standard management conditions with feed and water provided *ad libitum*.

Clinical symptoms (dyspnea, tracheal rales, depression, anorexia, and diarrhea) were monitored daily after the virus challenge. Three chicks from each group were selected randomly and euthanized by cervical dislocation at 3, 6, 9, 12, and 15 dpi. Necropsies were performed to observe gross lesions, and tissue samples from the trachea, lung, spleen, kidney, and bursa of Fabricius were collected individually to determine viral load by quantitative reverse transcriptase PCR (RT–qPCR) or placed into 10% neutral-buffered formalin for histologic evaluation. Oral and cloacal swabs were collected from 10 chicks in the challenge and control groups at 3, 6, 9, 12, and 15 dpi and kept in separate tubes containing 500 µl of sterile PBS to detect viral shedding.

The remaining 20 hens from each group continued to be fed in negative pressure isolators, and their reproductive performance was observed. The number of eggs and the egg quality parameters, such as albumen height, egg shape index, and eggshell thickness, were recorded daily after egg laying as described previously (Wang et al., 2014). All hens were euthanized by cervical dislocation at 170 dpi and necropsied. The length of the oviducts was measured, and the number of ovarian follicles with a diameter larger than 10 mm was recorded to evaluate the development of the reproductive system (Robinson and Etches, 1986; Zhang et al., 2020).

Real-time quantitative PCR

Total RNA of the tissues (trachea, lung, spleen, kidney, and bursa of Fabricius) and oral/cloacal swabs were extracted with the Ultrapure RNA Kit (CoWin Biosciences, Beijing, China) according to the manufacturer's instructions. The cDNA was prepared by reverse transcription using the EasyScript® Reverse Transcriptase [M-MLV, RNaseH-] Kit (TransGen Biotech, Beijing, China). Previously described primers and probe (Callison et al., 2006) were used for RT–qPCR, which was performed using LineGene 9,600 Plus (FQD-96A, Bioer Technology, Hangzhou, China). The reaction mixture comprised 10 μl of AceQ qPCR Probe Master Mix (Vazyme Biotech Nanjing, China), 0.4 μl of forward primer, 0.4 μl of reverse primer, 0.2 μl of probe and 2 μl of cDNA (or nuclease-free water for the control). ddH_2O was added to a total volume of 20 μl. The thermal cycling parameters were as follows: 95°C for 5 min, followed by 40 cycles of 95°C for 10 s and 60°C for 30 s.

Histopathology

Tissue samples from the trachea, lung, spleen, kidney, and bursa of Fabricius were collected and fixed in 10% neutral-buffered formalin for 48 h and embedded in paraffin wax. Sections (5 μm thick) were cut and stained with hematoxylin and eosin (H&E) to examine pathological changes in tissues under a microscope.

Statistical analysis

All statistical analyses were performed using GraphPad Prism 8.0.2 (San Diego, CA, United States). Statistical differences between two groups were assessed by the Student's *t*-test Statistical significance was defined as follows: $^{*}p < 0.05$, $^{**}p < 0.01$, $^{***}p < 0.001$.

Results

Severe clinical signs and gross lesions were shown in JX181 challenged chicks

To explore the long-term pathogenicity of the GVI-1 lineage to chickens, 10-day-old chicks were challenged with $10^{6.5}$ EID_{50} of JX181 *via* the ocular–nasal route. The results demonstrate that the morbidity of the early infection of IBV GVI-1 lineage JX181 strain was 100%, the mortality was 0%, and early infection with JX181 strain could cause obvious clinical signs in chicks from 3 to 12 dpi, which primarily included the tracheal rales, dyspnea, depression, and ruffled feathers. Compared with the control group, necropsy revealed that the challenged chicks showed catarrhal exudate and severe punctate hemorrhage in the larynx and trachea (Figures 1A,B), pulmonary congestion (Figures 1C,D), hemorrhage in the bursa of Fabricius (Figures 1E,F), and cystic dilations in the oviduct (Figures 1G,H) from 3 to 12 dpi. No obvious renal lesions were found in challenged chicks.

FIGURE 1
Gross lesions in the different organs of chicks inoculated with strain JX181. 10-day-old chicks were challenged with $10^{6.5}$ EID_{50} of JX181 *via* the ocular–nasal route. The representative gross lesions of the chicks sacrificed at 6 dpi were shown in **(A,B)** Larynx and trachea, **(C,D)** Pulmonary congestion, **(E,F)** Bursa of Fabricius, **(G,H)** Oviduct.

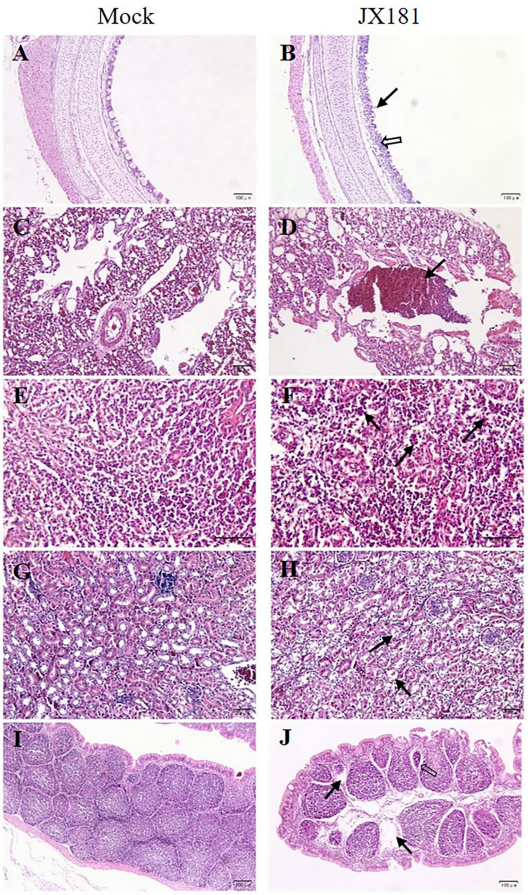

FIGURE 2
Histopathologic changes were observed in different tissues of chicks inoculated with strain JX181 at 6 dpi. **(A,B)** Trachea: the black arrow indicates the extensive loss and necrosis of ciliated epithelial cells, and the hollow arrow indicates the thickening of the lamina propria of the tracheal mucosa and lymphocyte infiltration. **(C,D)** Lung: the black arrow indicates erythrocyte infiltration in the bronchial lumen. **(E,F)** Spleen: black arrows indicate macrophages in the splenic sinus. **(G,H)** Kidney: black arrows indicate swelling and degeneration of tubular epithelial cells. **(I,J)** Bursa of Fabricius: the hollow arrow indicates the interstitial dilation of the lymphoid follicles, and black arrows indicate the lymphocyte loss.

Histopathological lesions were induced upon JX181 challenge

Histopathological examination was performed to check whether JX181 infection could induce histopathological lesions. The results showed noticeable pathological changes in the tissues of challenged chicks, which were predominant at 6 and 9 dpi. Compared with the control group, cilia loss, sloughing of epithelial cells, thickening of the lamina propria of the tracheal mucosa, and lymphocyte infiltration in the tracheas of chicks were observed in the challenge group (Figures 2A,B). Bronchial hemorrhage was seen in the lungs, and there was extensive erythrocyte infiltration in the lumen (Figures 2C,D). In the spleen, the number of macrophages in the splenic sinus was increased (Figures 2E,F). In the kidney, the tubular epithelial cells exhibited swelling and vacuolar degeneration (Figures 2G,H). In the bursa of Fabricius, interstitial dilation of the lymphoid follicles, atrophy of lymph follicles, and lymphocyte loss were observed (Figures 2I,J).

The viral loads and viral shedding remained positive early after incubation

Viral loads and shedding were detected to measure the dynamics of the virus in the challenged chicks. First, RT–qPCR was used to detect the dynamics of viral loads in different tissues of the sacrificed challenged chicks, including the trachea, lung, spleen, kidney, and bursa of Fabricius. The results demonstrated that the dynamics of virus copies in different kinds of collected tissues showed similar trends, which increased from 3 dpi to 6 dpi, peaked at 6 dpi, and then subsequently declined after 6 dpi (Figure 3). At 12 dpi, IBV could only be detected in the trachea, and it could not be further detected at 15 dpi (Figure 3). No viral RNA in tissues was detected at any time in the control group. Second, oral and cloacal swabs were collected from 10 chicks in the challenge group and control group at 3, 6, 9, 12, and 15 dpi. Similar to the viral load results, IBV viral shedding peaked at 6 dpi and then decreased in both oral and cloacal swabs. No viral shedding was detected in cloacal swabs, while 40% (4/10) of oral swabs were positive at 12 dpi (Figure 4). No viral shedding was detected in oral and cloacal swabs at 15 dpi. The results demonstrated that viral shedding in the oral swabs was slightly higher than that in the cloacal swabs. Taken together, these data demonstrate that the viral load and shedding could be detected for the first 12 days after the challenge.

Early infection with IBV JX181 resulted in a lower laying rate

The hen laying rate was measured to check whether early IBV infection in chicks could affect later egg production. The number of eggs in each group was counted, and the laying rate was measured. The results showed that the egg production of the challenge group was obviously lower than that of the control group from 21 to 25 weeks (Figure 5). However, there were no significant differences between the two groups in the egg shape indices and eggshell thickness. These data demonstrated that although viral loads and shedding of JX181 were positive for no more than 15 days, the performance of egg laying was severely affected by JX181 infection.

Reproductive system lesions were the causative factor of the decreased laying rate

As the above data showed that the laying rate was decreased after early infection with JX181, we proposed that reproductive

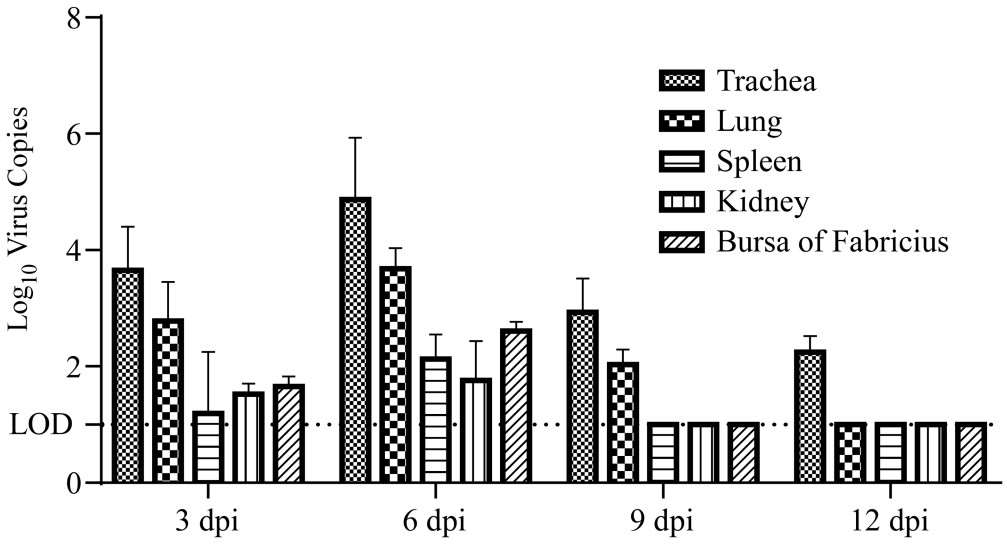

FIGURE 3
Viral load in different tissues of chickens at 3, 6, 9, and 12days post infection. The trachea, lung, spleen, kidney, and bursa of Fabricius samples were collected at 3, 6, 9, and 12 dpi, total RNA was extracted and reverse transcribed into cDNA, and RT–qPCR was used to measure the viral load in different tissues. LOD: limit of detection.

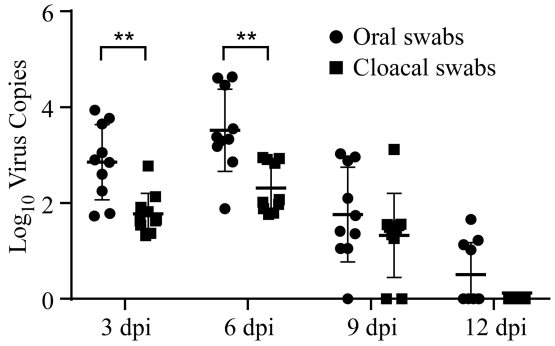

FIGURE 4
Viral shedding was detected in both oral and cloacal swab samples. Oral and cloacal swab samples were collected at 3, 6, 9, and 12 dpi, and RT-qPCR was used to measure the level of viral shedding in these samples. Statistical differences between two groups were assessed by the Student's *t*-test Statistical significance was defined as follows: $^{**}p < 0.01$.

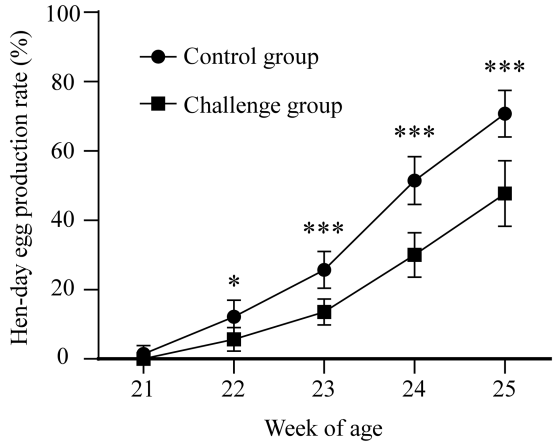

FIGURE 5
Decreased egg production was observed in the challenge group. The number of eggs in each group was counted from 21 to 25weeks. Statistical differences between two groups were assessed by the Student's *t*-test Statistical significance was defined as follows: $^{*}p < 0.05$, $^{***}p < 0.001$.

system lesions might contribute to this influence. All hens were euthanized by cervical dislocation at 170 dpi, and the necropsy results showed that the reproductive system of hens in the control group was well developed without any lesions (Figure 6A), while various types of lesions were observed in oviducts and ovaries in the challenge group. Specifically, 2/20 of the hens showed degenerated ovarian follicles (Figure 6B). Free yolk or fibrin clots were observed in the abdomen in 6/20 of the hens (Figures 6C,D). Sixteen hens in the challenge group had varied in size cystic dilatations with a watery content in the oviduct (Figure 6E). The development of oviducts and ovaries was also assessed, and 5/20 of hens showed moderately to severely retarded development of oviducts and ovaries (Figure 6F). Moreover, the statistical analysis of the lengths of the oviducts (Figures 7A–C) and the number of hierarchal ovarian follicles with diameters larger than 10 mm (Figures 7D–F) were decreased upon JX181 infection. Collectively, these data demonstrated that early infection of chicks with the IBV GVI-1 lineage JX181 strain has a long-term effect on the development of the layer reproductive system.

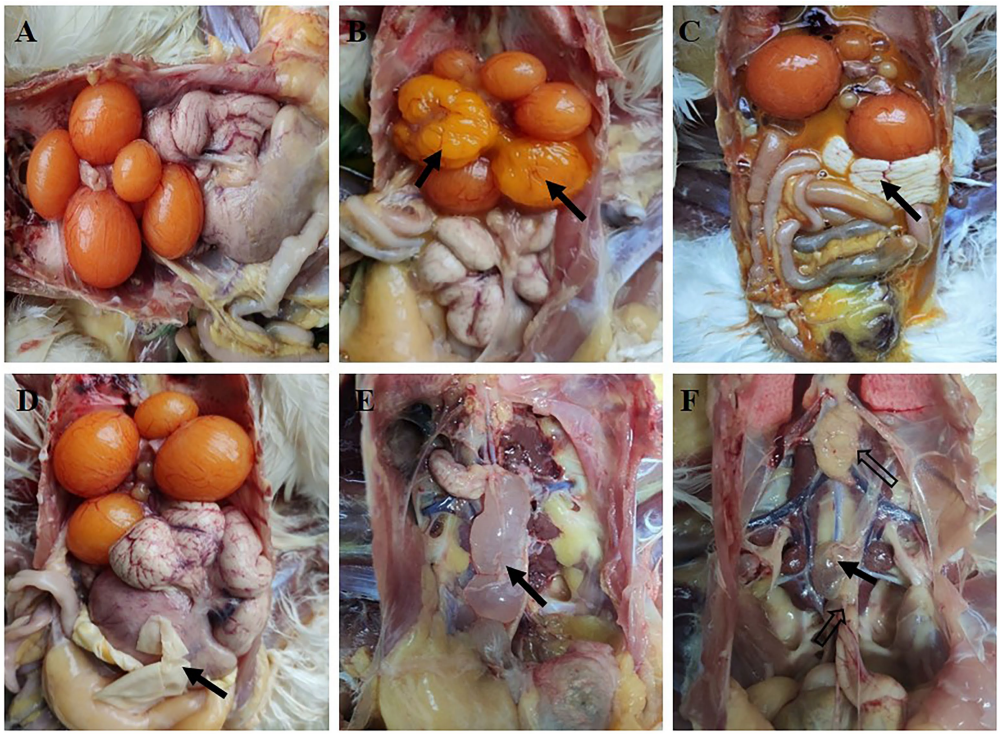

FIGURE 6
Gross lesions were observed in the ovary and oviduct of the hens at 170 dpi. **(A)** Well-developed organs from the control group. **(B)** Flaccid ovary. **(C,D)** The fluid yolk material and fibrin clots in the coelome. **(E)** Cystic dilation in the oviduct. **(F)** Oviduct and ovary with retarded development.

Discussion

IBV replicates in various organs, including the respiratory and intestinal tract, kidney, oviduct, and testes (Bande et al., 2016). Different genotypes of IBV exhibit varying virulence and tropism and cause different clinical symptoms. In recent years, the frequency of isolation of the GVI-1 lineage from vaccinated flocks has increased. Several previous studies have proven that GVI-1 viruses have strong respiratory tropism, but there are few studies on the pathogenicity of those strains in the reproductive system (Fan et al., 2019; Ma et al., 2019; Ren et al., 2019; Sun et al., 2021).

IBV infection may lead to two different forms of hen reproductive system disease (Hoerr, 2021). If the infection occurs during laying, it may lead to transiently decreased egg production accompanied by eggshell deformities and deterioration of egg quality. If the infection occurs in naïve pullets, it can lead to false layer syndrome, which is characterized as a mature hen with active ovaries but severe cystic dilation of the oviduct. The JX181 strain was first isolated from layers with decreased egg production. Therefore, we speculate that if infection occurs in early stages after hatching, the virus may also cause false layer syndrome. If this is the case, prevention and control of the loss caused by GVI-1 strains will be extremely difficult due to the large antigenicity difference between the GVI lineage strains and the currently commonly used vaccine strains, such as H120, Ma5, and 4/91 (Ma et al., 2019).

In the present study, we modeled GVI-1 JX181 infection in 10-day-old SPF chicks with long-term monitoring and explored its pathogenic characteristics. This result revealed that the GVI-1 lineage JX181 strain had a short incubation period and induced severe respiratory symptoms in the initial stage of infection. The autopsy results also indicated that JX181 could cause serious hemorrhage in the trachea and pulmonary congestion. These results were consistent with other studies on the pathogenicity of the GVI strain, which reflected the nature of the pathogenicity of GVI virus to the chicken respiratory system (Wang et al., 2022). However, in this study, the JX181 strain showed only moderate renal pathogenicity. Although the infected chickens showed some histological changes in the kidney at 6 and 9 dpi, there were no obvious gross lesions in it. We also noticed that although the incidence of the JX181 strain in the challenge group reached 100%, no chicken deaths occurred, indicating that JX181 was relatively mild compared with the other two genotypes (QX and TWI) that are currently widely circulating in China. Our analysis suggests that this low mortality may be related to the low renal pathogenicity of this strain because some studies have shown that the renal pathogenicity of IBV is one of the important reasons for the increased mortality due to kidney failure in susceptible birds

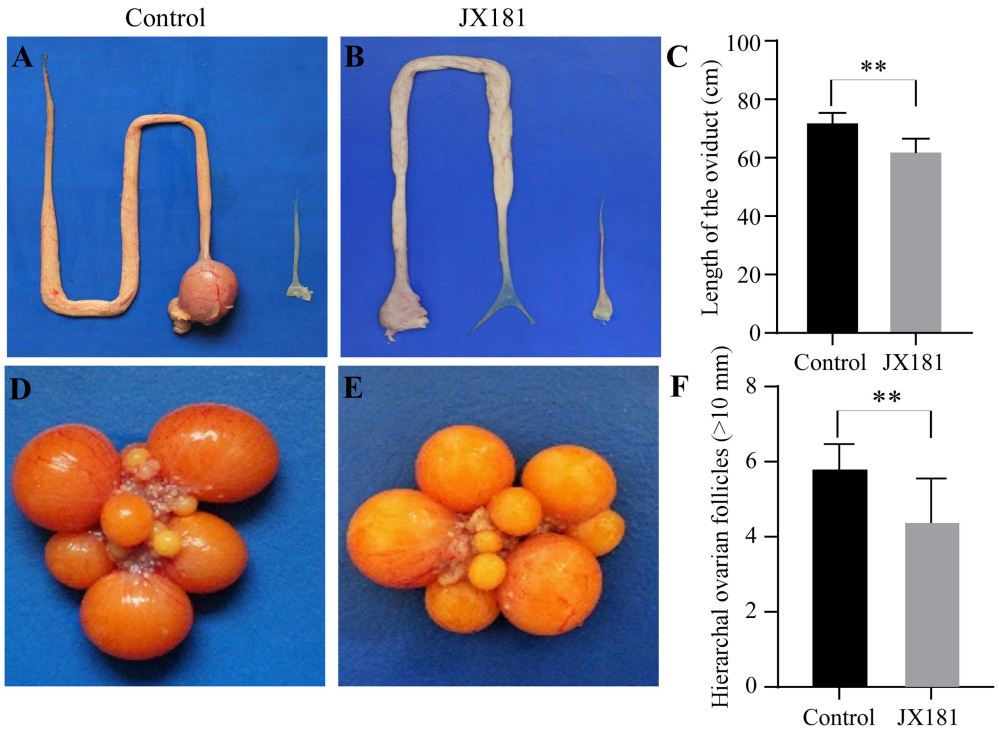

FIGURE 7
The lengths of the oviducts and the number of hierarchal ovarian follicles were impaired upon challenge with JX181 at 170 dpi. **(A,B)** The lengths of the oviducts were measured after the euthanasia of the chickens. **(C)** Statistical representation of the mean lengths of the oviducts. **(D,E)** The hierarchal ovarian follicles in mock and JX181 infected groups. **(F)** Statistical representation of the number of hierarchal ovarian follicles with diameters larger than 10mm.

(Chong and Apostolov, 1982; Butcher et al., 1990). Moreover, the JX181 strain also showed tropism for immune organs, including the spleen and bursa of Fabricius. Whether the ability of viruses to infect the immune system will lead to host immunosuppression still needs further study.

The incidence rate of oviduct damage has been reported to decrease with increasing age of exposure (Broadfoot et al., 1956). The pathogenic role of IBV on the oviduct differed strongly across strains. Five QX-like IBV strains can cause dilatation and serous fluid accumulation in the oviduct in different proportions but not in the 793/B strain (Benyeda et al., 2009). In our previous study, the second most prevalent genotype, TW I (also designated the GI-7 lineage), was demonstrated to also induce severe cystic oviduct in challenged chickens (Zhang et al., 2020). In the present study, cysts in the oviduct could be observed in approximately 80% of hens after infection with the JX181 strain, and this lesion was first found as early as 6 dpi and could still be observed at the end of the experiment at 170 dpi. These results indicate that GVI-1 IBV can cause irreversible damage to the oviducts of hens. The liquid-like yolk material and fibrin clots in the body cavity of hens are likely the result of oviduct damage resulting in dysfunction of actively capturing ova. A Korean study showed that K-I genotype virus infection inhibited the formation of hierarchal ovarian follicles in 80% and oviduct maturation in 50% (Hong et al., 2012). Likewise, we also observed a decrease in the number of hierarchal ovarian follicles, and the reproductive system of hens had stunted growth after infection with GVI-1 JX181 strain. Additionally, the length of the oviduct and the number of ovarian follicles in the challenge group decreased compared with those in the control group. All of these lesions in the reproductive system induced by early infection with the JX181 strain resulted in an obvious decrease in egg production.

In conclusion, this study showed that early infection with the IBV GVI-1 lineage JX181 strain is highly pathogenic to chickens and induces serious respiratory injuries, permanent damage to the oviduct, and reproductive system growth retardation, which ultimately results in a decrease in egg production. Our study comprehensively revealed the long-term influence of IBV infection, which proved that the early infection of IBV could lead to a decreased laying rate.

Data availability statement

The original contributions presented in the study are included in the article/supplementary material, further inquiries can be directed to the corresponding authors.

Ethics statement

This study was approved by the Experimental Animal Ethics Committee of Yangzhou University (approval ID: YZUDWLL-201906-008). The experimental design met the requirements of ethical principles related to animal experiments.

Author contributions

XZ, ZB, and SC conceived and designed the experiments. SC performed the experiments. XZ, SC, MG, CZ, and YC analyzed the data. SC and ZB wrote the paper. XZ and YW read and approved the manuscript. All authors contributed to the article and approved the submitted version.

Funding

This study was supported by the National Natural Science Foundation of China (31872496), the China Agriculture Research System of MOF and MARA (CARS-40), the Key Special Project "Science and Technology Promote Economy of 2020" of the National Key Research and Development Program (SQ2020YFF0426460), and the Priority Academic Program Development of Jiangsu Higher Education Institutions (PAPD).

Conflict of interest

The authors declare that the research was conducted in the absence of any commercial or financial relationships that could be construed as a potential conflict of interest.

Publisher's note

All claims expressed in this article are solely those of the authors and do not necessarily represent those of their affiliated organizations, or those of the publisher, the editors and the reviewers. Any product that may be evaluated in this article, or claim that may be made by its manufacturer, is not guaranteed or endorsed by the publisher.

References

Bande, F., Arshad, S. S., Omar, A. R., Bejo, M. H., Abubakar, M. S., and Abba, Y. (2016). Pathogenesis and diagnostic approaches of avian infectious bronchitis. *Adv. Virol.* 2016, 1–11. doi: 10.1155/2016/4621659

Beach, J. R., and Schalm, O. W. (1936). A filterable virus, distinct from that of laryngotracheitis, the cause of a respiratory disease of chicks[1]. *Poult. Sci.* 15, 199–206. doi: 10.3382/ps.0150199

Benyeda, Z., Mató, T., Süveges, T., Szabó, E., Kardi, V., Abonyi-Tóth, Z., et al. (2009). Comparison of the pathogenicity of QX-like, M41 and 793/B infectious bronchitis strains from different pathological conditions. *Avian Pathol.* 38, 449–456. doi: 10.1080/03079450903349196

Broadfoot, D. I., Pomeroy, B. S., and Smith, W. M. J. P. S. (1956). Effects of infectious bronchitis in baby chicks. *Poult. Sci.* 35, 757–762. doi: 10.3382/ps.0350757

Butcher, G. D., Winterfield, R. W., and Shapiro, D. P. (1990). Pathogenesis of H13 nephropathogenic infectious bronchitis virus. *Avian Dis.* 34, 916–921. doi: 10.2307/1591383

Callison, S. A., Hilt, D. A., Boynton, T. O., Sample, B. F., Robison, R., Swayne, D. E., et al. (2006). Development and evaluation of a real-time Taqman RT-PCR assay for the detection of infectious bronchitis virus from infected chickens. *J. Virol. Methods* 138, 60–65. doi: 10.1016/j.jviromet.2006.07.018

Cavanagh, D. (2007). Coronavirus avian infectious bronchitis virus. *Vet. Res.* 38, 281–297. doi: 10.1051/vetres:2006055

Chen, Y., Jiang, L., Zhao, W., Liu, L., Zhao, Y., Shao, Y., et al. (2017). Identification and molecular characterization of a novel serotype infectious bronchitis virus (GI-28) in China. *Vet. Microbiol.* 198, 108–115. doi: 10.1016/j.vetmic.2016.12.017

Chen, L., Xiang, B., Hong, Y., Li, Q., Du, H., Lin, Q., et al. (2021). Phylogenetic analysis of infectious bronchitis virus circulating in southern China in 2016-2017 and evaluation of an attenuated strain as a vaccine candidate. *Arch. Virol.* 166, 73–81. doi: 10.1007/s00705-020-04851-9

Chong, K. T., and Apostolov, K. (1982). The pathogenesis of nephritis in chickens induced by infectious bronchitis virus. *J. Comp. Pathol.* 92, 199–211. doi: 10.1016/0021-9975(82)90078-0

Domanska-Blicharz, K., Sajewicz-Krukowska, J., and Lisowska, A. (2020). New PA/1220/98-like variant of infectious bronchitis virus in Poland. *Avian Pathol.* 49, 380–388. doi: 10.1080/03079457.2020.1754332

Fan, W., Tang, N., Dong, Z., Chen, J., Zhang, W., Zhao, C., et al. (2019). Genetic analysis of avian coronavirus infectious bronchitis virus in yellow chickens in southern China over the past decade: revealing the changes of genetic diversity, dominant genotypes, and selection pressure. *Viruses* 11:898. doi: 10.3390/v11100898 10.3390/v11100898

Hoerr, F. J. (2021). The pathology of infectious bronchitis. *Avian Dis.* 65, 600–611. doi: 10.1637/aviandiseases-D-21-00096

Hong, S. M., Kwon, H. J., Kim, I. H., Mo, M. L., and Kim, J. H. (2012). Comparative genomics of Korean infectious bronchitis viruses (IBVs) and an animal model to evaluate pathogenicity of IBVs to the reproductive organs. *Viruses* 4, 2670–2683. doi: 10.3390/v4112670

Jackwood, M. W. (2012). Review of infectious bronchitis virus around the world. *Avian Dis.* 56, 634–641. doi: 10.1637/10227-043012-Review.1

Jang, I., Lee, H. J., Bae, Y. C., Park, S. C., Lee, H. S., and Choi, K. S. (2018). Genetic and pathologic characterization of a novel recombinant TC07-2-type avian infectious bronchitis virus. *Avian Dis.* 62, 109–113. doi: 10.1637/11764-103017-ResNote.1

Li, L., Xue, C., Chen, F., Qin, J., Xie, Q., Bi, Y., et al. (2010). Isolation and genetic analysis revealed no predominant new strains of avian infectious bronchitis virus circulating in South China during 2004-2008. *Vet. Microbiol.* 143, 145–154. doi: 10.1016/j.vetmic.2009.11.022

Lim, T. H., Kim, M. S., Jang, J. H., Lee, D. H., Park, J. K., Youn, H. N., et al. (2012). Live attenuated nephropathogenic infectious bronchitis virus vaccine provides broad cross protection against new variant strains. *Poult. Sci.* 91, 89–94. doi: 10.3382/ps.2011-01739

Liu, S., and Kong, X. (2004). A new genotype of nephropathogenic infectious bronchitis virus circulating in vaccinated and non-vaccinated flocks in China. *Avian Pathol.* 33, 321–327. doi: 10.1080/0307945042000220697

Ma, T., Xu, L., Ren, M., Shen, J., Han, Z., Sun, J., et al. (2019). Novel genotype of infectious bronchitis virus isolated in China. *Vet. Microbiol.* 230, 178–186. doi: 10.1016/j.vetmic.2019.01.020

Mase, M., Kawanishi, N., Ootani, Y., Murayama, K., Karino, A., Inoue, T., et al. (2010). A novel genotype of avian infectious bronchitis virus isolated in Japan in 2009. *J. Vet. Med. Sci.* 72, 1265–1268. doi: 10.1292/jvms.10-0080

Raja, A., Dhinakar Raj, G., and Kumanan, K. (2020). Emergence of variant avian infectious bronchitis virus in India. *Iran J. Vet. Res.* 21, 33–39.

Reed, L. J., and Muench, H. (1938). A simple method of estimating fifty per cent endpoints. *Am. J. Epidemiol.* 27, 493–497. doi: 10.1093/oxfordjournals.aje.a118408

Ren, M., Sheng, J., Ma, T., Xu, L., Han, Z., Li, H., et al. (2019). Molecular and biological characteristics of the infectious bronchitis virus TC07-2/GVI-1 lineage isolated in China. *Infect. Genet. Evol.* 75:103942. doi: 10.1016/j.meegid.2019.103942

Robinson, F. E., and Etches, R. J. (1986). Ovarian steroidogenesis during follicular maturation in the domestic fowl (*Gallus domesticus*). *Biol. Reprod.* 35, 1096–1105. doi: 10.1095/biolreprod35.5.1096

Sun, L., Tang, X., Qi, J., Zhang, C., Zhao, J., Zhang, G., et al. (2021). Two newly isolated GVI lineage infectious bronchitis viruses in China show unique molecular and pathogenicity characteristics. *Infect. Genet. Evol.* 94:105006. doi: 10.1016/j.meegid.2021.105006

Thor, S., Hilt, D., Kissinger, J., Paterson, A., and Jackwood, M. (2011). Recombination in avian gamma-coronavirus infectious bronchitis virus. *Viruses* 3, 1777–1799. doi: 10.3390/v3091777

Valastro, V., Holmes, E. C., Britton, P., Fusaro, A., Jackwood, M. W., Cattoli, G., et al. (2016). S1 gene-based phylogeny of infectious bronchitis virus: an attempt to harmonize virus classification. *Infect. Genet. Evol.* 39, 349–364. doi: 10.1016/j.meegid.2016.02.015

Wang, C. Y., Luo, Z. B., Shao, G. Q., and Hou, B. (2022). Genetic and pathogenic characteristics of a novel infectious bronchitis virus strain in genogroup VI (CK/CH/FJ/202005). *Vet. Microbiol.* 266:109352. doi: 10.1016/j.vetmic.2022.109352

Wang, Y., Xiao, L. H., Zhao, X. L., Liu, Y. P., and Zhu, Q. (2014). Identification of SNPs in cellular retinol binding protein 1 and cellular retinol binding protein 3 genes and their associations with laying performance traits in erlang mountainous chicken. *Asian Australas J. Anim. Sci.* 27, 1075–1081. doi: 10.5713/ajas.2013.13587

Xu, L., Han, Z., Jiang, L., Sun, J., Zhao, Y., and Liu, S. (2018). Genetic diversity of avian infectious bronchitis virus in China in recent years. *Infect. Genet. Evol.* 66, 82–94. doi: 10.1016/j.meegid.2018.09.018

Zhang, X., Guo, M., Zhao, J., and Wu, Y. (2021). Avian infectious bronchitis in China: epidemiology, vaccination, and control. *Avian Dis.* 65, 652–656. doi: 10.1637/aviandiseases-21-00098

Zhang, X., Liao, K., Chen, S., Yan, K., Du, X., Zhang, C., et al. (2020). Evaluation of the reproductive system development and egg-laying performance of hens infected with TW I-type infectious bronchitis virus. *Vet. Res.* 51:95. doi: 10.1186/s13567-020-00819-4

Zhao, Y., Zhang, H., Zhao, J., Zhong, Q., Jin, J. H., and Zhang, G. Z. (2016). Evolution of infectious bronchitis virus in China over the past two decades. *J. Gen. Virol.* 97, 1566–1574. doi: 10.1099/jgv.0.000464

frontiers | Frontiers in Microbiology

TYPE Original Research
PUBLISHED 08 November 2022
DOI 10.3389/fmicb.2022.1048648

OPEN ACCESS

EDITED BY
Bernat Pérez de Val, IRTA-CReSA, Centre for Research on Animal Health, Spain

REVIEWED BY
Joseph Cassidy,
University College Dublin, Ireland
Maria Emilia Eirin,
Consejo Nacional de Investigaciones Científicas y Técnicas (CONICET), Argentina
Mariano Domingo,
Universitat Autònoma de Barcelona, Spain

*CORRESPONDENCE
C. Kanipe
carly.kanipe@usda.gov

SPECIALTY SECTION
This article was submitted to Infectious Agents and Disease, a section of the journal Frontiers in Microbiology

RECEIVED 19 September 2022
ACCEPTED 24 October 2022
PUBLISHED 08 November 2022

CITATION
Kanipe C, Boggiatto PM, Putz EJ and Palmer MV (2022) Histopathologic differences in granulomas of *Mycobacterium bovis* bacille Calmette Guérin (BCG) vaccinated and non-vaccinated cattle with bovine tuberculosis.
Front. Microbiol. 13:1048648.
doi: 10.3389/fmicb.2022.1048648

Histopathologic differences in granulomas of *Mycobacterium bovis* bacille Calmette Guérin (BCG) vaccinated and non-vaccinated cattle with bovine tuberculosis

C. Kanipe[1,2]*, P. M. Boggiatto[1], E. J. Putz[1] and M. V. Palmer[1]

[1]Infectious Bacterial Diseases Research Unit, National Animal Disease Center, Agricultural Research Service (USDA), Ames, IA, United States, [2]Immunobiology Graduate Program, Iowa State University, Ames, IA, United States

Mycobacterium bovis (*M. bovis*) is the zoonotic bacterium responsible for bovine tuberculosis. An attenuated form of *M. bovis*, Bacillus Calmette-Guerin (BCG), is a modified live vaccine known to provide variable protection in cattle and other species. Protection for this vaccine is defined as a reduction in disease severity rather than prevention of infection and is determined by evaluation of the characteristic lesion of tuberculosis: the granuloma. Despite its recognized ability to decrease disease severity, the mechanism by which BCG imparts protection remains poorly understood. Understanding the histopathologic differences between granulomas which form in BCG vaccinates compared to non-vaccinates may help identify how BCG imparts protection and lead to an improved vaccine. Utilizing special stains and image analysis software, we examined 88 lymph nodes obtained from BGC-vaccinated and non-vaccinated animals experimentally infected with *M. bovis*. We evaluated the number of granulomas, their size, severity (grade), density of multinucleated giant cells (MNGC), and the amounts of necrosis, mineralization, and fibrosis. BCG vaccinates had fewer granulomas overall and smaller high-grade granulomas with less necrosis than non-vaccinates. The relative numbers of high- and low- grade lesions were similar as were the amounts of mineralization and the density of MNGC. The amount of fibrosis was higher in low-grade granulomas from vaccinates compared to non-vaccinates. Collectively, these findings suggest that BCG vaccination reduces bacterial establishment, resulting in the formation of fewer granulomas. In granulomas that form, BCG has a protective effect by containing their size, reducing the relative amount of necrosis, and increasing fibrosis in low-grade lesions. Vaccination did not affect the amount of mineralization or density of MNGC.

KEYWORDS

granuloma, *Mycobacterium bovis*, BCG, bovine tuberculosis, tuberculosis vaccine

Introduction

Mycobacterium bovis (*M. bovis*) is the most host-promiscuous member of the *Mycobacterium tuberculosis* complex (MTBC), capable of causing tuberculous disease in over 85 species of animals, including some endangered wildlife species (Kanipe and Palmer, 2020). It is the primary cause of bovine tuberculosis (bTB) worldwide. It is a scourge to farmers, livestock, and conservationists by exacting economic tolls, as well as causing disease in both animals and humans.

Bacillus Calmette-Guérin (BCG) is an attenuated strain of *Mycobacterium bovis* which has been used as a vaccine for protection against *Mycobacterium tuberculosis* (Mtb) in humans for over 100 years. It has long been accepted as providing variable protection against virulent *M. bovis* in livestock and wildlife (Buddle et al., 2018; Roy et al., 2019). Importantly however, protection is often defined as a decrease in disease severity rather than protection from infection. Additionally, currently utilized diagnostic techniques based on purified protein derivative (PPD), also known as tuberculin, fail to differentiate BCG-vaccinates from *M. bovis* infected animals, further complicating both its use, and role in disease eradication and control efforts. Reports of protection range widely from 0 to 100% depending on age, route of vaccination, vaccine dose and uncontrollable variables such as genetics and environment (Canto Alarcon et al., 2013; Buddle et al., 2018; Bayissa et al., 2021). In naturally infected cattle results vary, but BCG vaccinates have been shown to have lower bTB prevalence (based on isolation of *M. bovis*), lower numbers of cattle with gross lesions, and less severe disease than non-vaccinates (Nugent et al., 2018; Bayissa et al., 2021). Because of its cross reactivity with the primary herd diagnostic, the tuberculin skin test, and the success of eradication programs in decreasing overall prevalence of bTB, interest in BCG vaccination in most countries decreased during the mid to late 20th century. Unfortunately, complete eradication has been unsuccessful in most countries for various reasons including, lack of sensitivity and specificity in current diagnostic assays, increases in the size of concentrated feeding operations (CAFOs), importation of infected animals from other countries and the presence of wildlife reservoirs of *M. bovis* with persistent wildlife-to-cattle transmission (de la Rua-Domenech et al., 2006; Fitzgerald and Kaneene, 2013; Ciaravino et al., 2021). Thus, there is a renewed interest in vaccines. Even with the shortcomings of BCG, thus far, no experimental bTB vaccine has consistently outperformed BCG in vaccine efficacy studies. Until a vaccine which consistently improves protection against disease is found, it is prudent to continue research on BCG's properties and how it imparts protection. Numerous studies have explored the differences in peripheral responses between vaccinates and non-vaccinates, but this provides an incomplete picture of pathogenesis, as it is distant from the site of active host-pathogen interaction in the tissue. In order to fully elucidate how BCG works, we therefore need intralesional examination (Jones et al., 2017; Steinbach et al., 2021; Khalid et al., 2022).

The characteristic lesion of tuberculosis is the granuloma. Granulomas are collections of macrophages with multiple modifiers such as the presence or absence of varying amounts of neutrophils, lymphocytes, multinucleated giant cells (MNGC), fibrosis, necrosis, and mineralization. These are dynamic structures, with cell trafficking resulting from host- and bacterially-originating signals. Until recently, it was believed that the tuberculous granuloma was a structure which benefited both host and pathogen at different points in infection, early on by promoting dissemination of the bacteria as a result of migrating macrophages, and later by "walling off" the offending intruder through fibrosis. Although this paradigm remains popular, new advances in research create challenges for its defense (Ramakrishnan, 2012). Understanding the differences between granulomas that form in BCG vaccinates compared to non-vaccinates may not only help identify how BCG imparts protection but may also more aptly help define how it benefits pathogen as well as host. While tuberculous granulomas have been documented in numerous organs, the principal sites in cattle are the thoracic lymph nodes (tracheobronchial and mediastinal) and within the lung parenchyma. Interestingly, cattle and humans share histologic similarities in their granuloma structure only surpassed by non-human primates. Due to the financial and ethical implications with using non-human primates, this elevates the importance of work performed in cattle, which could yield valuable insight into human disease.

Previous pioneering works by Johnson, *et. al* have demonstrated reduced granuloma numbers, size, necrosis, peripheral fibrosis, and MNGC numbers in lymph nodes of BCG vaccinated animals compared to non-vaccinated controls when experimentally infected with virulent *M. bovis* (Johnson et al., 2006). The reduction in granuloma number and size, as well as decreased tissue destruction suggest improved host control over the bacteria and decreased MNGC numbers suggests a reduction in antigen persistence(Pagan and Ramakrishnan, 2018; Trout and Holian, 2020; Palmer et al., 2022). Decreased peripheral fibrosis is likely associated with decreased bacterial burden compared to non-vaccinates as demonstrated in non-human primates (Gideon et al., 2022). The aim of this study is to build, confirm and expand upon Johnson's work in several key areas. Using histopathologic examination combined with advanced imaging software, we examine a total of 88 pulmonary lymph nodes from 22 BCG-vaccinated and 22 non-vaccinated cattle, all of which were experimentally infected with virulent *M. bovis.* The result of this study is a comprehensive look of the pathology that forms in the pulmonary lymph nodes of BCG-vaccinates and non-vaccinates.

Materials and methods

Samples

Banked tissue samples from two previous studies were utilized. In both studies cattle were obtained from bTB-free

herds from Iowa, United States. Briefly, in Experiment 1, 23 castrated Holstein steers of 4–5 months of age were divided into two groups: non-vaccinates ($n = 11$) and BCG vaccinates ($n = 12$). Animals were kept on pasture prior to the start of the study. As environmental bacteria are present in our area, and in order to prevent possible confounding responses to BCG vaccination, animals were confirmed non-reactive to *Mycobacterium avium* (*M. avium*) *via* interferon gamma release assay (IGRA) immediately before the start of the study. Animals in the vaccinated group received a subcutaneous injection 1 ml of 5×10^5 CFU of BCG Danish. Three months following vaccination, both vaccinates and non-vaccinates received 5.5×10^2 CFU of *M. bovis* strain 1,315 *via* aerosolization as described elsewhere (Palmer et al., 2002). Strain 1,315 is a virulent field strain obtained from a white-tailed deer in Michigan, United States. Animals were euthanized 13–17 weeks post-challenge. In Experiment 2, 21 newborn Holstein steers were divided into two groups: non-vaccinates ($n = 11$) and BCG vaccinates ($n = 10$). Animals were bottle-raised on a pasteurized milk product and kept in clean pens to reduce exposure to environmental mycobacteria. Due to the cleanliness of the housing situation the risk of exposure to environmental mycobacteria was considered low and IGRA testing for *M. avium* was not performed. Animals in the vaccinated group received a subcutaneous injection 1 ml of 1×10^6 CFU of BCG Danish at 2 weeks of age. Three months following vaccination, both vaccinates and non-vaccinates received 1×10^3 CFU of *M. bovis* strain 1,315 *via* aerosolization. Approximately 18 weeks post-challenge animals were euthanized. In both studies animals were humanely euthanized by intravenous administration of sodium pentobarbital. All animal procedures were approved prior to the experiments by the Institutional Animal Care and Use Committee (IACUC) at the National Animal Disease Center. At necropsy, both experimental groups demonstrated a significant reduction in gross lesions in the lungs of BCG-vaccinates compared to non-vaccinates and a significant decrease in CFU/gram of lymph node tissue between vaccinates and non-vaccinates (Waters et al., 2009). An approximately $2.5 \times 2 \times 0.4$ cm randomly selected sample of both the tracheobronchial and mediastinal lymph nodes were collected from each animal resulting in a total of 88 lymph node samples, 44 from each group. Samples were fixed in 10% neutral buffered formalin, paraffin embedded following standard techniques, and sectioned 4–5 µm thick prior to staining with Harris hematoxylin and eosin (H&E). The two groups used in this study varied in age at the time of vaccination, 2 weeks vs. 4–5 mos. It was previously reported that neonatally vaccinated animals had at least as robust an immune response as adults (Hope et al., 2005). Nevertheless, to account for differences between experimental groups we evaluated the effect of group within all statistical analyses and found significance only for fibrosis metrics where group was included as a fixed effect (see stats section).

Stains and scanning into HALO

Paraffin-embedded sections were stained with H&E using a Leica 5,020 multistainer (Leica/Surgipath). Von Kossa Calcium and Masson's Trichrome staining were performed following manufacturer's instructions (Newcomer Supply) for calcium and collagen fiber analysis, respectively. Following staining, slides were digitally scanned using the Aperio AT2 whole slide imager, to generate bright-field whole- slide images at 20X (0.5 µm/pixel) and 40X (0.25 µm/pixel) magnification in a 24-bit color pyramid TIFF (.SVS file). The. SVS files were transferred into HALO software (HALO v3.1.1076.291, Indica labs) for annotation and analysis.

The mediastinal and tracheobronchial lymph node values for each metric were initially evaluated separately to ensure differences were not a result of anatomic location. No significant differences were noted, therefore values from the tracheobronchial and mediastinal lymph nodes were combined and averaged to yield a single value per animal.

Evaluation of granuloma number, grade, total size, necrosis area, cellular area, and number of MNGCs

Digitally scanned images were evaluated at 10X magnification. Using HALO annotation tools, granulomas were outlined in different colors based on grade, and the total granuloma area calculated using HALO's annotation software. A granuloma was defined as a focus consisting of increased accumulations of macrophages admixed with varying numbers of lymphocytes, neutrophils and MNGCs. If a tissue section lacked granulomas, it was excluded from the remaining histopathologic examinations. Granulomas were separated into two grades: low and high.

Low-grade granulomas were defined as singular, with approximately ≤10% necrosis. High-grade granulomas were defined as having greater than 10% of its total area as necrosis, being multicentric, or coalescent with other granulomas. Necrosis was defined as an area of tissue destruction characterized by degenerating, fragmented cells, and structural debris with or without mineralization. When present, fibrous encapsulation was included in the total granuloma area calculated. Care was made to closely follow the directional flow of the collagen fibers when numerous, closely associated but independent granulomas were present. When fibrous bands incompletely separated granulomas or had no identifiable pattern of separation, these were counted as a single, coalescing lesion and considered high grade.

High grade granulomas were outlined in green while low grade granulomas were outlined in yellow (Figure 1). The absolute number and the number of each type of granuloma were enumerated and totaled for each animal. For high- and low-grade granulomas, the average granuloma size was calculated by dividing the total granuloma area within an animal by the number of granulomas of that grade. Necrosis was outlined using a dotted line of the corresponding grade color, and its area

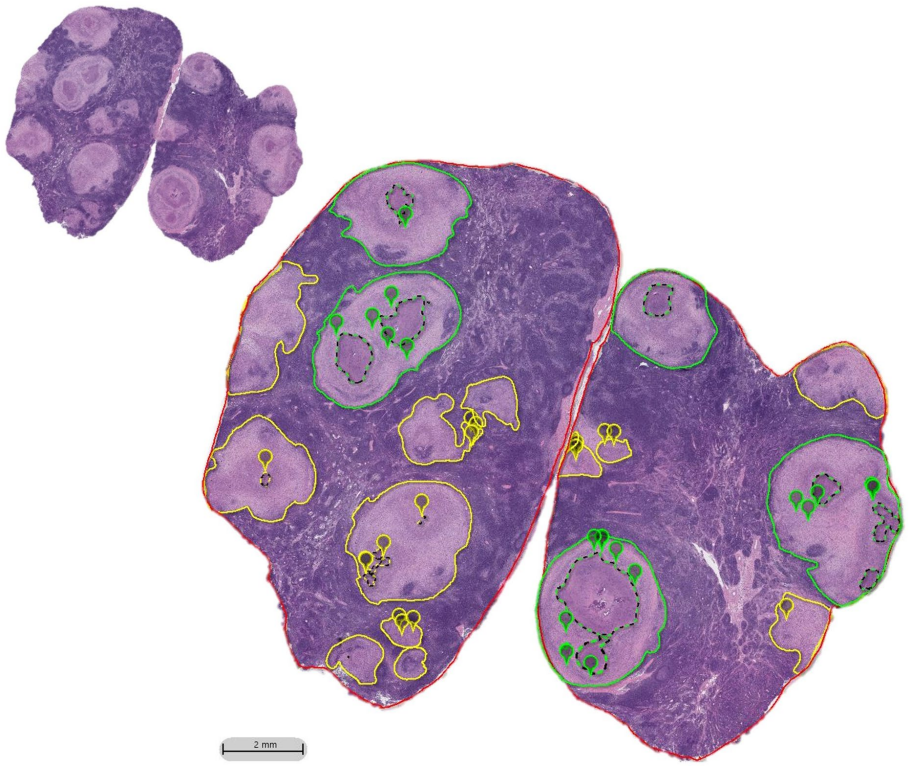

FIGURE 1
HALO imaging annotations performed on H&E tracehobronchial lymph node sections of BCG-vaccinated and non-vaccinated cattle challenged with aerosolized *M. bovis*. Granulomas were outlined in either green or yellow based on the amount of necrosis and/or if their boundaries were indistinguishable from the neighboring granuloma (coalescing). If there was ≤10% necrosis, it was classified as a low-grade granuloma and outlined in yellow. If there was >10% necrosis or if it was a collection of coalescing granulomas, it was outlined in green and categorized as high-grade. Necrosis, when present, was outlined by a dotted line of a matching color. MNGCs identified at 10X were marked with a pin of the same color as the grade designation. H&E section prior to annotation shown in inset.

summated to provide the total area of necrosis. The percent necrosis was calculated, and if a low-grade granuloma was found to contain ≥10% necrosis, it was redefined as a high-grade granuloma. Enumeration of MNGCs was performed by placement of digital pins which were summated (see Figure 1). Multinucleated giant cells were defined as macrophages containing three or more nuclei within a continuous cytoplasm, identifiable at 10X magnification, in accordance with other published studies(Trout and Holian, 2020; Losslein et al., 2021). The density of MNGCs was calculated as the number of MNGC present per 100μm² of non-necrotic area.

Numerous previous studies utilized a four-stage scoring system developed by Wangoo et al to describe granuloma histopathology (Wangoo et al., 2005; Johnson et al., 2006; Waters et al., 2007; Salguero et al., 2017; Palmer et al., 2021). Granulomas staged as I and II by the Wangoo system would be categorized as low-grade in this study while those granulomas classified as stage III, and IV by Wangoo et al. would be considered high-grade. Occasionally, a Wangoo stage III granuloma would fall under the low-grade designation when small foci of mineral were present with ≤10% necrosis. The Wangoo system categorizes any granuloma containing mineral as either a III or IV depending on the other characteristics present.

Evaluation of amount of mineralization

Utilizing Von Kossa-stained slides, high- and low-grade granulomas were identified in two independent layers, at 10X magnification. Samples without identifiable lesions were excluded. High- and low-grade designations used for the H&E stains were followed to classify the lesions into their respective groups. These outlines served as the boundaries for tissue to be analyzed. A digital filter was formulated to identify calcium-containing areas representative of mineralization. Starting with algorithm Indica labs-Area quantification v2.1.7, a stain color was selected and optimized to identify mineralization. The percent area of mineralization for both high- and low-grade granulomas was calculated using the area of staining identified by the filter divided by the total area analyzed for each high- and low-grade granuloma.

Evaluation of amount of fibrosis

Utilizing Masson's trichrome-stained slides, high- and low-grade granulomas were outlined in two independent layers, at 10X magnification to ensure all granulomas were identified.

Samples without identifiable lesions were excluded. High- and low-grade designations used for the H&E stains were followed to classify the lesions into their respective groups. A digital filter was formulated to identify collagenous areas highlighted by the trichrome stain and applied to the entire granuloma. Starting with algorithm Indica labs-Area quantification v2.1.7, a stain color was selected and optimized to identify fibrosis based on the color of collagen found in dense collagenous bundles. The filter was applied to each annotated layer. The percent fibrosis for high- and low-grade granulomas was calculated using the area of staining identified by the filter divided by the total area analyzed for each high- and low-grade granuloma.

Statistical analysis

For all scored granuloma metrics (count, average area, percent necrosis, MNGC frequency, percent mineralization, and percent fibrosis) data were analyzed with a simple linear regression model (lm) in R (version 4.2.1). Each scored metric was evaluated independently, fitting grade, vaccination status, and their interaction as fixed effects. A fixed effect of 'group', denoting the two separate experimental cohorts, was evaluated for model fit for each metric and only deemed appropriate to include for analysis of percent fibrosis. A pairwise comparison of Least Squares means (lsmeans package) was utilized to determine significant differences between specific grade and vaccination group contrasts. For all, significance was determined when p-value ≤ 0.05. Error bars represent standard errors.

Graph construction was performed using GraphPad Prism 9 (GraphPad Software Inc., San Diego, CA). Values for the mediastinal and tracheobronchial lymph nodes for each animal were combined to yield a single data point per animal. For all analyses performed except in the evaluation of the total number of granulomas, animals without granulomas in either lymph node were excluded. In cases where an animal lacked either high- or low-grade granulomas (and therefore their calculated values were 0), these data points were excluded with exception of granuloma count.

Results

Granuloma number and breakdown

BCG vaccinates had fewer granulomas compared to non-vaccinates. The ratios of high- and low-grade granulomas were similar between vaccinates and non-vaccinates.

Non-vaccinated animals had higher numbers of granulomas compared to BCG-vaccinates ($p < 0.0001$; Figure 2A). The mean number of individual granulomas per animal in BCG-vaccinates was 18.95 (range 0–51) while the mean number of granulomas per animal in non-vaccinates was 61.5 (range 17–178). In total, 1770 granulomas were evaluated. BCG vaccinates accounted for 417 (23.6%) of these granulomas while 1,353 (76.4%) granulomas were in lymph nodes of non-vaccinates. Eight lymph node samples from BCG-vaccinates lacked identifiable granulomas, and these samples were excluded for the remainder of the study.

While the number of granulomas varied markedly between BCG-vaccinates and non-vaccinates, the relative percentages of each grade of granuloma were similar (Figure 2B). There were approximately equal numbers of high- and low-grade granulomas, within each vaccinate group. Of the total granulomas present in BCG vaccinates, 58.52% of them were low grade while 43.14% were high grade. In non-vaccinates these percentages were 57.56 and 42.44%, respectively. Overall, these data indicate that there is a trend for fewer high-grade granulomas compared to low grade granulomas independent of vaccination status ($p = 0.551$ and $p = 0.0627$ for non-vaccinates and vaccinates, respectively).

Average granuloma size and amount of necrosis

BCG vaccinates had smaller high-grade granulomas and lesions with less necrosis.

The average size (area) of granulomas was compared between vaccinates and non-vaccinates. There was no significant difference ($p = 0.0675$) in the average size of granulomas between vaccinates and non-vaccinates, however lesions from non-vaccinated animals tended to be smaller (Figure 3A). Additionally, low-grade granulomas did not significantly vary in size between vaccinates and non-vaccinates however high-grade granulomas were larger in non-vaccinates than vaccinates ($p = 0.0434$; Figure 3B). Within vaccination groups, BCG vaccinates had similarly sized low- and high-grade granulomas ($p = 0.6296$) while non-vaccinates had larger high-grade granulomas compared to low-grade granulomas ($p = 0.0064$).

In this study, to be considered low-grade, the amount of necrosis had to be $\leq 10\%$ the total area. However, high grade granulomas may have $\leq 10\%$ of necrosis if they were multicentric or coalescing. BCG vaccinates had lesions containing significantly ($p = 0.0029$) less tissue destruction as evidenced by a lower percentage of necrosis than non-vaccinates (Figure 4A). As a result of the categorization method, necrosis was expected to be substantially higher in high grade granulomas compared to low grade and this was true for both vaccinates and non-vaccinates ($p < 0.001$ for both). There was no significant difference in the percentage of necrosis within low-grade granulomas of vaccinates compared to non-vaccinates with values being nearly identical ($p = 0.9766$; Figure 4B). High-grade granulomas of non-vaccinates contained a significantly ($p = 0.0080$) higher percentage of necrosis than high-grade granulomas from BCG-vaccinates.

Multinucleated giant cell numbers

MNGC numbers were not dependent on vaccination status or lesion severity.

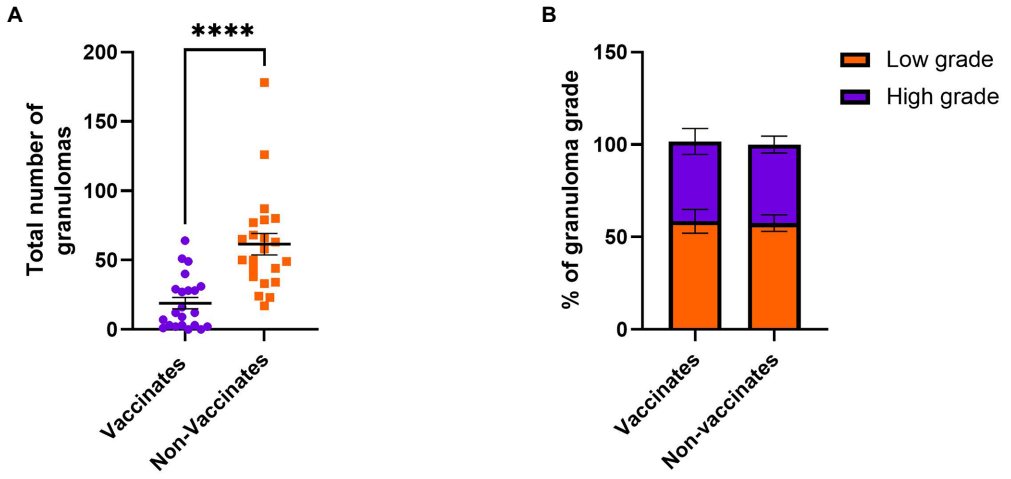

FIGURE 2
Absolute numbers of granulomas in BCG-vaccinated and non-vaccinated cattle infected with *M. bovis* and percentage of each granuloma grade. **(A)** The total number of granulomas present in vaccinates and non-vaccinates, respectively. Each dot represents one animal and the combined total of granulomas in its mediastinal and tracheobronchial lymph nodes. **(B)** the relative percentages of high- and low-grade granulomas. Values are presented as means ± SEM (****value of $p < 0.0001$).

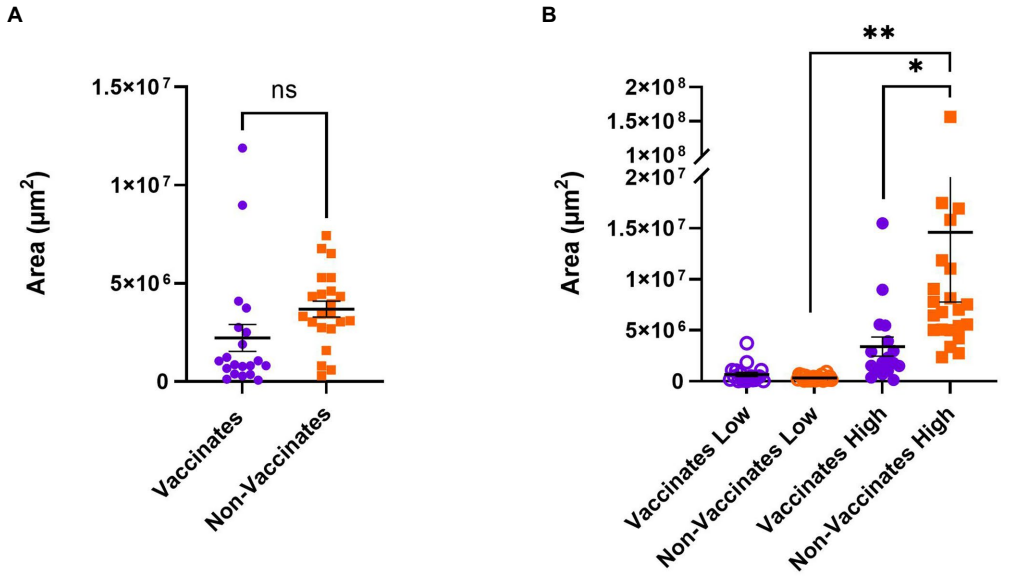

FIGURE 3
Average area of granulomas by both vaccination group and granuloma grade in BCG-vaccinated and non-vaccinated cattle infected with *M. bovis*. **(A)** Granuloma size by area (µm²) based on vaccination status. Each dot represents one animal. The average area of a granuloma was tabulated by dividing the total area occupied by all granulomas in the mediastinal and tracheobronchial lymph nodes of an animal by the total number of granulomas present. **(B)** Granuloma size by area (µm²) when broken down by grade (high or low). Values are presented as means ± SEM. (*=p value 0.0434, **=p value 0.0064, ns=not significant).

The density of MNGC was calculated as the number of MNGCs per 100 µm² of granuloma area. No significant differences were found in the density of MNGC between vaccination groups (Figure 5A). When separated by grade, there were no significant differences in the number of MNGC between high- and low-grade granulomas, however there was a trend ($p = 0.0632$) for low grade granulomas of non-vaccinates to contain a higher number of MNGC than high grade granulomas of the same group (Figure 5B).

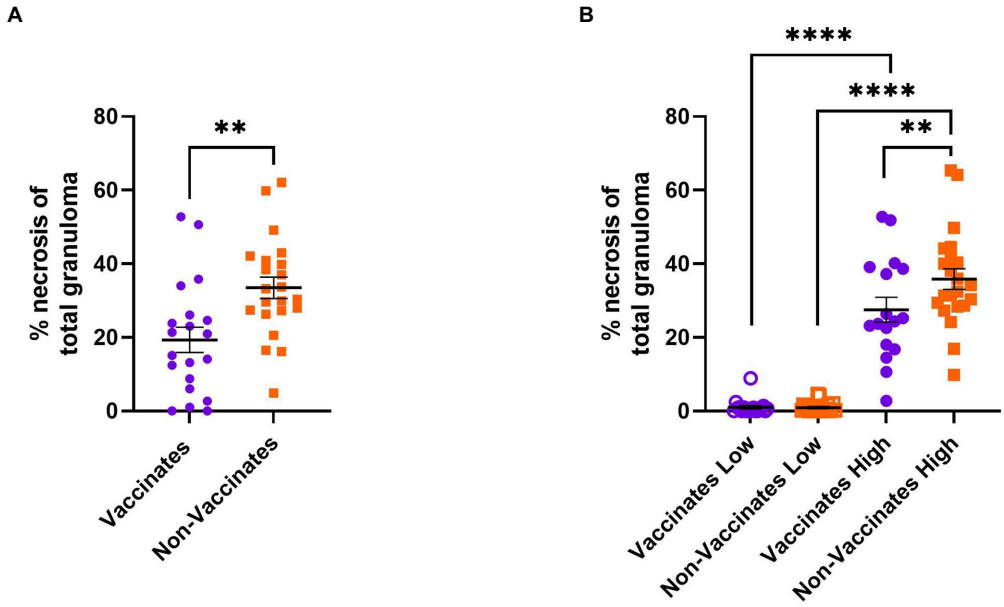

FIGURE 4
Percentage of granuloma area comprised of necrosis in BCG-vaccinated and non-vaccinated cattle infected with *M. bovis*. Values are broken down by vaccination group **(A)** and by vaccination group and grade **(B)**. Each dot represents one animal and its mediastinal and tracheobronchial lymph nodes. Values are presented as means ± SEM. (**=*p* value 0.0029 for A, **=*p* value 0.0080 for B, ****=*p* value <0.0001).

Fibrosis and mineralization

BCG vaccination increased the amount of fibrosis in low grade granulomas. BCG vaccination did not influence the amount of mineralization. Mineralization increased with the severity of the lesion.

Fibrosis was the only metric in which experimental group had a significant effect. The primary difference between the two groups of animals used for this study is age, where the older cohort (from Experiment 1) had higher average fibrosis than the younger animals (from Experiment 2; data not shown). That being said, there were no significant differences in the percentage of fibrosis per granuloma between vaccinates and non-vaccinates for either experimental group (Figure 6A). Collectively, when evaluated by grade, low grade granulomas of vaccinates had a significantly ($p = 0.0344$) higher percentage of fibrosis than low-grade granulomas of non-vaccinates (Figure 6B). When mineralization was evaluated, no significant differences were observed in the percentage of mineralization between vaccinates and non-vaccinates (Figure 7A). Additionally, mineralization was similar within grades of granuloma, despite different vaccination groups (Figure 7B). Significant differences existed between low grade granulomas and their corresponding high-grade granulomas with a $p = 0.0009$ in vaccinates and $p < 0.0001$ in non-vaccinates.

Discussion

This study utilized 88 pulmonary lymph nodes from 44 animals (22 BCG vaccinates, 22 non-vaccinates), resulting in the evaluation of a total of 1,770 granulomas. Of these, 417 granulomas were in BCG vaccinates while 1,353 were in non-vaccinates.

Previous studies which have focused on granuloma histopathology have utilized a 4-stage scoring system created by Wangoo et al (Wangoo et al., 2005; Johnson et al., 2006). While originally created to be a consistent, easy way to describe the severity of granulomas, we found it subjective in some regards, ([ex] "minimal necrotic areas") and inappropriately absolute in others, ([ex] mineralization not mentioned until stage III or above). These aspects could make it difficult to accurately compare results from different vaccine studies from different labs. As it pertains to vaccine efficacy in tuberculosis research, the primary concern is if disease severity is reduced. While the 4-stage system is more descriptive, in this study histopathologic lesion staging was streamlined and simplified into high- and low grades based primarily on amount of necrosis. Here, lesions were categorized into either low grade, with ≤10% necrosis and high grade, with >10% necrosis and/or coalescing lesions. This binary approach allowed for pertinent, precise evaluation while eliminating some of the subjective aspects of 4 stage scoring. While any amount of necrosis could have been selected for the high and low cutoff values, we found this new scoring system to align most closely to the Wangoo system while removing subjectivity. In this study, stage I and II lesions would be considered low grade while stage III and stage IV lesions would have been classified as high grade. Granulomas designated as low grade represent those in which cellular destruction is minimal, therefore they may still be considered under host control. In contrast, granulomas

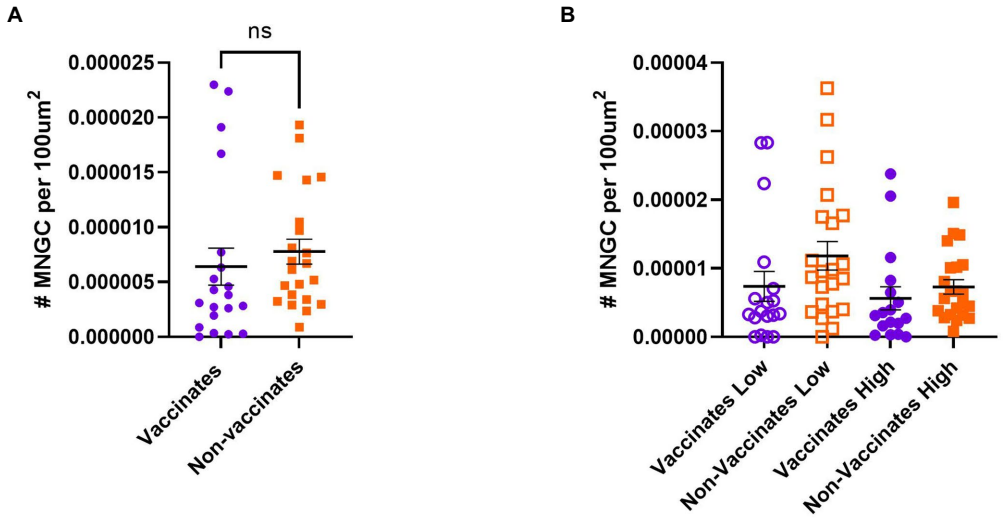

FIGURE 5
The density of multinucleated giant cells by vaccination group and granuloma grade in BCG-vaccinated and non-vaccinated cattle infected with *M. bovis*. Values represent the number per 100μm^2 and are broken down by vaccination group **(A)** and by vaccination group and grade **(B)**. Each dot represents one animal and its mediastinal and tracheobronchial lymph nodes. Values are presented as means ± SEM. (ns=not significant).

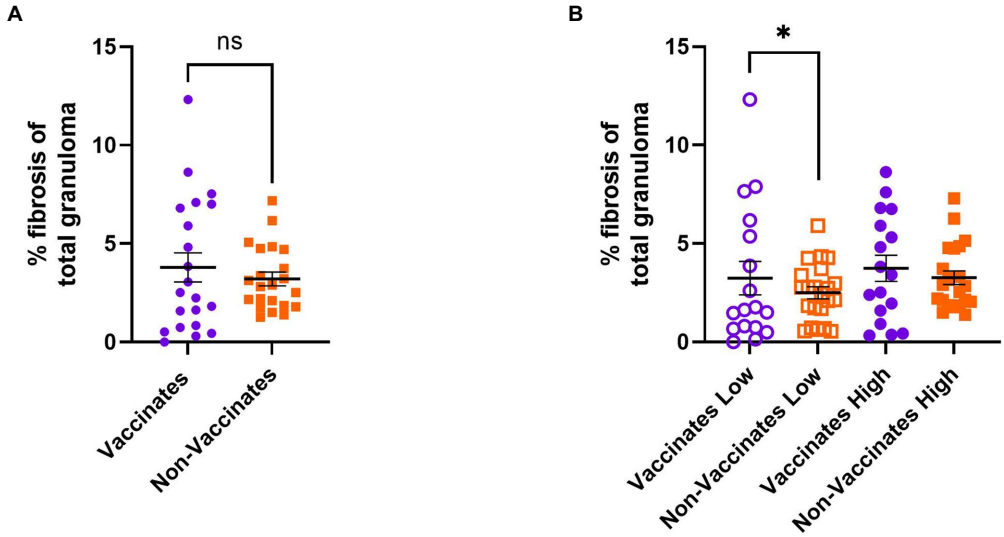

FIGURE 6
Percentage of granuloma area comprised of fibrosis as measured using Masson's trichrome staining in BCG-vaccinated and non-vaccinated cattle infected with *M. bovis*. Values are broken down by vaccination group **(A)** and by vaccination group and grade **(B)**. Each dot represents one animal and its mediastinal and tracheobronchial lymph nodes. Values are presented as means ± SEM. (*=*p* value 0.0344, ns=not significant).

designated as high grade may be interpreted as a loss of host control as necrotic cellular accumulations and/or multicentricity are features which likely benefit the bacterium and represent irreversible tissue damage (Basaraba, 2008; Basaraba and Orme, 2011). In human tuberculosis, reactivation of latent disease is associated with increased necrosis within granulomas (Russell et al., 2010). This binary microscopic scoring system is user-friendly and can be combined with gross lesion scoring if the purpose of a given study is to evaluate vaccine efficacy. The speed at which it can be applied additionally lends itself to studies utilizing large numbers of animals.

As expected, and in accordance with previous studies, BCG decreased the lesion burden (Buddle et al., 1995; Johnson et al., 2006; Canto Alarcon et al., 2013; Dean et al., 2014; Salguero et al.,

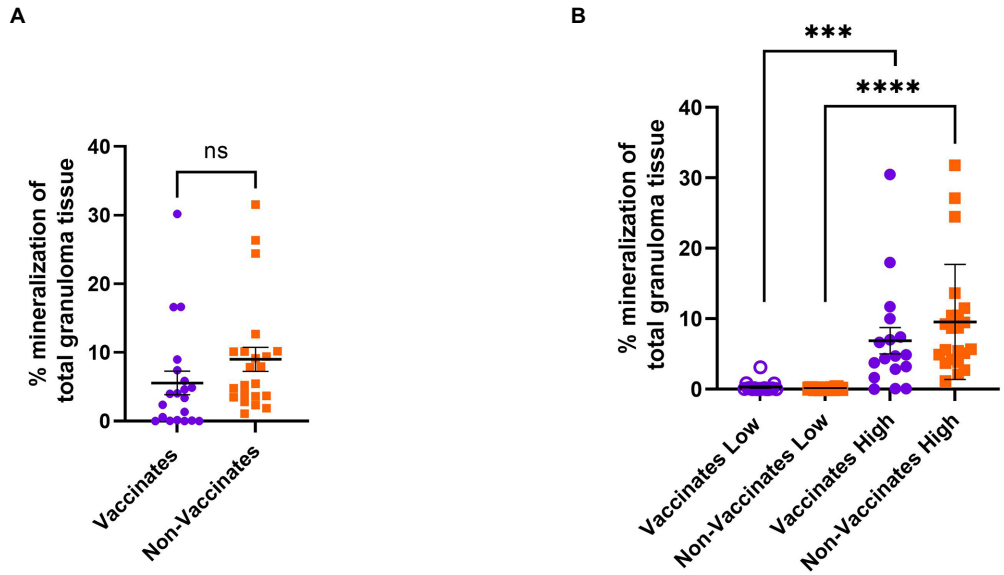

FIGURE 7
Percentage of granuloma area comprised of mineralization as measured using Von Kossa staining in BCG-vaccinated and non-vaccinated cattle infected with *M. bovis*. Values are broken down by vaccination group **(A)** and by vaccination group and grade **(B)**. Each dot represents one animal and its mediastinal and tracheobronchial lymph nodes. Values are presented as means ± SEM. (***=*p* value 0.0009, ****=*p* value <0.0001, ns=not significant).

2017; Palmer et al., 2022). Vaccinated animals had an average of 19 granulomas per tissue section while non-vaccinated animals averaged 62 granulomas. Interestingly, despite this contrast, the relative breakdown of high- and low-grade granulomas did not significantly vary, with vaccinates and non-vaccinates having similar percentages of each. This suggests that the protective nature of BCG is, in part, by preventing the establishment of granulomas as opposed to necessarily preventing their progression to a higher grade. These findings are consistent with Johnson et al. and studies performed in white-tailed deer which report all stages of granulomas in lymph nodes of BCG vaccinates (Johnson et al., 2006; Nol et al., 2008; Palmer et al., 2009). Although BCG did not prevent high grade granulomas from being formed, it maintained smaller lesions on average with less necrosis. This finding is reasonable, as BCG primes the immune system for a strong cell-mediated immune response, which is believed to reduce the growth of lesions (Watanabe et al., 2006; Domingo et al., 2014). Although not quantified, "satellite" granulomas, lesions closely associated with another granuloma, were present in both vaccinates and non-vaccinates. In this study, "satellite" lesions were of both high- and low-grades, a finding in contrast to previous studies which identified only low-grade granulomas (Palmer et al., 2007; Canal et al., 2017). While differences in study design between the previous studies and the current could potentially account for the disparity in satellite granuloma grades, it does raise a curious topic to scientifically explore. It is generally believed that satellite lesions represent dissemination from the nearby "primary granuloma." Quantifying and histologically characterizing the differences between "satellite" granulomas between vaccinates and non-vaccinates may provide insight on if a vaccine reduces dissemination of bTB within the host, and provide another metric in which to measure efficacy.

Fibrosis was the single metric in which there were statistical differences between experimental cohorts, of which the primary difference between the groups is age; older animals of Experiment 1 and the younger animals of Experiment 2. Older animals from Experiment 1 averaged more fibrosis in granulomas compared to younger animals of Experiment 2 (data not shown). This was unexpected and warrants further investigation, as it has not been reported previously. A possible explanation for the difference in fibrosis found between the two age groups could be levels of tumor growth factor beta (TGF-β), the cytokine most responsible for stimulating fibrosis. However, according to a study performed in sheep, TGF-β is lower in older animals vs. neonates (Sow et al., 2012). This would suggest other cytokines and/or immunological mechanisms are contributing to these differences. It has been demonstrated that calves vaccinated at birth with BCG produce similar levels of interferon gamma (IFN-γ) as calves 5–8 months old, however unlike the older calves, the neonatal vaccinates had a gradual decline in IFN-γ levels(Buddle et al., 2003). This might be relevant as IFN-γ can suppress TGF-β secretion by macrophages and could ultimately be responsible for the differences in fibrosis seen between age groups (Warsinske et al., 2017b). It is also possible that the older animals, being exposed for a longer period to the outdoors, may have come into contact with environmental mycobacteria, which altered their fibrotic response when exposed to virulent *M. bovis* (Buddle et al., 2003). Regardless, when taken as a collective group, vaccinates and non-vaccinates had similar

overall percentages of fibrosis, a finding in contrast to previous studies (Johnson et al., 2006; Salguero et al., 2017). A possible explanation for this difference is that previous studies evaluated only the collagen peripherally encircling granulomas. Central fibrosis has been noted in other studies and associated with healing and containment in non-human primates, therefore it was included in our evaluation and was found to frequently be prominent (Figure 8; Flynn, 2011; Warsinske et al., 2017a; Martinot, 2018). When broken down by vaccinate group, the amount of fibrosis was significantly higher in low grade granulomas of vaccinates than non-vaccinates. By the time lesions progressed to high-grade, this significance was lost. While fibrosis has previously been considered a sign of an advanced or progressing lesion, our findings support data derived from simulated non-human primate granulomas which demonstrated fibrosis onset in lesions as early as ~10 days post infection or as late as after 200 days (Wangoo et al., 2005; Russell et al., 2009; Warsinske et al., 2017a; Palmer et al., 2021). In humans and non-human primate models, organized peripheral and central fibrosis has been associated with healing (Basaraba, 2008; Flynn, 2011; Palmer et al., 2022). These studies frequently involve post-chemotherapeutic treatment which is not routinely performed in cattle due to cost and risk of antibiotic residues in meat and milk, and the histopathologic composition of a healing bovine granuloma is therefore definitively unknown. However, in light of those studies, the finding of increased fibrosis in the low-grade lesions of vaccinates is intriguing and may represent a rapid immunological response as a result of BCG-induced memory, and an attempt at early containment of the infection.

Dystrophic mineralization is a common sequela to necrosis and therefore it is not surprising to see levels of mineralization increased in high grade granulomas. Nevertheless, it is interesting to note that the percentage of mineralization between high-grade granulomas were similar between vaccination groups and that small amounts of mineralization were present in the low-grade granulomas. While the Wangoo categorization system attributes mineralization with increased lesion score, and therefore, increased disease severity, studies in humans and non-human primates associate mineralization with healing, similar to fibrosis (Wangoo et al., 2005; Basaraba, 2008; Gideon et al., 2022). Indeed calcification is preferable over necrosis as necrosis can harbor viable bacteria while mineralization does not (Basaraba, 2008). Our findings of small amounts of mineral in low-grade granulomas and similar overall amounts between vaccinates and non-vaccinates, puts into question how disease severity should be defined in BCG vaccination studies in cattle.

Multinucleated giant cells are associated with persistent antigen in multiple diseases (Gupta et al., 2014; Gharun et al., 2017; Pagan and Ramakrishnan, 2018; Trout and Holian, 2020; Palmer et al., 2022). We hypothesized that MNGCs would be lower in BCG vaccinates as vaccination is typically associated with lower bacterial burden and antigen persistence(Buddle et al., 2003; Hope et al., 2005; Canto Alarcon et al., 2013; Sirak et al., 2021). Additionally, we expected to see higher numbers in high-grade granulomas as severe lesions have previously been associated with higher MNGC numbers (Menin et al., 2013). In this study we found no significant differences between groups or grade, however there was a trend for non-vaccinates to have more MNGC in their high-grade granulomas compared to their low-grade granulomas, suggesting increased bacterial burden may have played a role. Our findings differ from those of Johnson et al, which reported a significant reduction in the numbers of MNGCs in BCG vaccinated animals (Johnson et al., 2006). This difference could be due to the fact that Johnson et al, included only Langhan's type giant cells. Although not explicitly quantified, and without a defined description of MNGC requirements, Salguero et al additionally reported a decrease in the number of MNGCs in BGC-vaccinated cattle (Salguero et al., 2017). Frequently the Langhan's-type MNGC, with its nuclei arranged in a horseshoe shape, is considered the hallmark of tuberculosis, but in-fact, multiple other types are present and transformation from one morphology to another has been documented in cell culture (Singhal et al., 2011; Palmer et al., 2016; Pagan and Ramakrishnan, 2018). In the current study, we identified any cell containing three nuclei within a continuous cytoplasm as a multinucleated giant cell, regardless of morphology. These findings in contrast to other studies suggests this is a metric which warrants further investigation into type, function and to whom (host or microbe) this unique cell type benefits.

One limitation of this study was in interpreting coalescing lesions which had effaced the majority of the lymph node parenchyma. These cases arose occasionally in both vaccinates and non-vaccinates. This phenomenon is well document in lymph nodes of chronically infected cattle, where it may completely erase any semblance of a normal lymph node (Domingo et al., 2014). BCG provides variable protection, and animals with such severely affected lymph nodes may represent animals which failed to respond appropriately to the vaccine. It would be interesting to investigate differences present in these vaccine-non-responders and compare granuloma level cytokine and chemokine differences. As it was difficult to determine exactly how many granulomas coalesced, these lesions were counted as single, large granulomas. While minimally decreasing total granuloma numbers, these cases could dramatically alter average granulomas sizes.

Using banked samples from two previous experiments meant that treatments between the two experiments were not identical. The vaccination dose and challenge dose varied slightly between experimental groups, however as these were < 1 log, we felt it was an acceptable range. Enumeration of *Mycobacterium bovis* in liquid culture is difficult due to the propensity of the bacilli to clump (Gautam et al., 2022). As a result, simple optical density (OD) readings are not reliable, and due to the lengthy culture time, exact dosages are often determined retrospectively. Although the dosages between groups were not exactly the same, they were well within the range of numerous other BCG efficacy studies conducted by us and other investigators (Hope et al., 2005; Waters et al., 2007; Vordermeier et al., 2009).

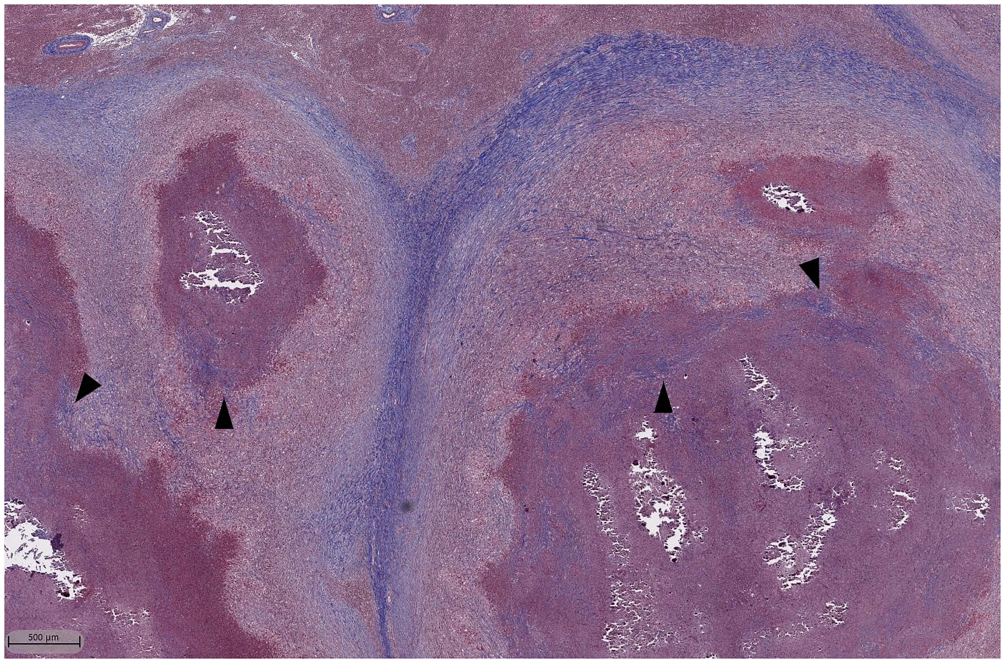

FIGURE 8
Masson's Trichrome stain of lymph node granulomas of cattle infected with *M. bovis*. Dark blue staining represents collagen which is found prominently surrounding the granulomas. Additionally, there are areas of centralized fibrosis throughout and immediately next to areas of necrosis (arrowheads).

Though not investigated in this study, it would be interesting to measure bacterial load between high- and low-grade granulomas between vaccination groups and how this may correlate with the metrics measured. While Ziehl-Neelson (ZN) staining for mycobacteria has historically been performed in histopathologic examinations of bTB it was not performed in this study due to limitations of the software and the relative insensitivity of ZN staining in formalin-fixed, paraffin-embedded tissues (Fukunaga et al., 2002). As quantitative culture would be impossible due to the small size of some of the lesions, techniques such as RNA *in-situ* hybridization, which would allow on-slide examination should be considered.

Our study provides further support to show that BCG vaccination reduced granuloma formation within the pulmonary lymph nodes of cattle following aerosol challenge with virulent *M. bovis*. Once established, BCG does not prevent the development of severe lesions, and the relative breakdown of high- and low- grade granulomas is similar to that of non-vaccinates. Despite this fact, BCG vaccinates have smaller granulomas with less tissue destruction than non-vaccinates. Fibrosis was higher in low-grade granulomas of vaccinates compared to non-vaccinates but this significance was lost when grade was excluded. Mineralization and MNGC density were similar between vaccinates and non-vaccinates, suggesting these may be vaccine-independent events.

Data availability statement

The original contributions presented in the study are included in the article, further inquiries can be directed to the corresponding author.

Ethics statement

The animal study was reviewed and approved by Institutional Animal Care and Use Committee at National Animal Disease Center.

Author contributions

CK, PB, and MP: experiment design. CK and MP: sample collection and experiments. CK and EP: data analysis. CK: manuscript preparation. CK, PB, EP, and MP: manuscript editing. All authors contributed to the article and approved the submitted version.

Funding

Financial support for these studies were provided by the United States Department of Agriculture, Agricultural

Research Service Project (CRIS #5030–32000-222). This research did not receive any specific grant from funding agencies in the public, commercial, or not-for-profit sectors.

Acknowledgments

We would like to thank Judith Stasko and Adrienne Shircliff of the Agricultural Research Service's Histology department for excellent and consistent slide handling and Adam Byersdorfer for HALO program support.

Authors disclaimer

USDA is an equal opportunity provider and employer. Mention of trade names or commercial products in this publication is solely for the purpose of providing specific information and does not imply recommendation or endorsement by the U.S. Department of Agriculture.

Conflict of interest

The authors declare that the research was conducted in the absence of any commercial or financial relationships that could be construed as a potential conflict of interest.

Publisher's note

All claims expressed in this article are solely those of the authors and do not necessarily represent those of their affiliated organizations, or those of the publisher, the editors and the reviewers. Any product that may be evaluated in this article, or claim that may be made by its manufacturer, is not guaranteed or endorsed by the publisher.

References

Basaraba, R. J. (2008). Experimental tuberculosis: the role of comparative pathology in the discovery of improved tuberculosis treatment strategies. *Tuberculosis (Edinb.)* 88, S35–S47. doi: 10.1016/S1472-9792(08)70035-0

Basaraba, R. J., and Orme, I. M. (2011). "Pulmonary tuberculosis in the Guinea pig" in *A Color atlas of Comparative Pathology of Pulmonary Tuberculosis*. eds. F. J. Leong, V. Dartois and T. Dick (Boca Raton, FL, USA: CRC Press), 137–141.

Bayissa, B., Sirak, A., Worku, A., Zewude, A., Zeleke, Y., Chanyalew, M., et al. (2021). Evaluation of the efficacy of BCG in protecting against contact challenge with bovine tuberculosis in Holstein-Friesian and zebu crossbred calves in Ethiopia. *Front. Vet. Sci.* 8:702402. doi: 10.3389/fvets.2021.702402

Buddle, B. M., Keen, D., Thomson, A., Jowett, G., Mccarthy, A. R., Heslop, J., et al. (1995). Protection of cattle from bovine tuberculosis by vaccination with BCG by the respiratory or subcutaneous route, but not by vaccination with killed mycobacterium vaccae. *Res. Vet. Sci.* 59, 10–16. doi: 10.1016/0034-5288(95)90023-3

Buddle, B. M., Vordermeier, H. M., Chambers, M. A., and De Klerk-Lorist, L. M. (2018). Efficacy and safety of BCG vaccine for control of tuberculosis in domestic livestock and wildlife. *Front. Vet. Sci.* 5:259. doi: 10.3389/fvets.2018.00259

Buddle, B. M., Wedlock, D. N., Parlane, N. A., Corner, L. A., De Lisle, G. W., and Skinner, M. A. (2003). Revaccination of neonatal calves with Mycobacterium bovis BCG reduces the level of protection against bovine tuberculosis induced by a single vaccination. *Infect. Immun.* 71, 6411–6419. doi: 10.1128/IAI.71.11.6411-6419.2003

Canal, A. M., Pezzone, N., Cataldi, A., Zumarraga, M., Larzabal, M., Garbaccio, S., et al. (2017). Immunohistochemical detection of pro-inflammatory and anti-inflammatory cytokines in granulomas in cattle with natural Mycobacterium bovis infection. *Res. Vet. Sci.* 110, 34–39. doi: 10.1016/j.rvsc.2016.10.006

Canto Alarcon, G. J., Rubio Venegas, Y., Bojorquez Narvaez, L., Pizano Martinez, O. E., Garcia Casanova, L., Sosa Gallegos, S., et al. (2013). Efficacy of a vaccine formula against tuberculosis in cattle. *PLoS One* 8:e76418. doi: 10.1371/journal.pone.0076418

Ciaravino, G., Laranjo-Gonzalez, M., Casal, J., Saez-Llorente, J. L., and Allepuz, A. (2021). Most likely causes of infection and risk factors for tuberculosis in Spanish cattle herds. *Vet. Rec.* 189:e140. doi: 10.1002/vetr.140

De La Rua-Domenech, R., Goodchild, A. T., Vordermeier, H. M., Hewinson, R. G., Christiansen, K. H., and Clifton-Hadley, R. S. (2006). Ante mortem diagnosis of tuberculosis in cattle: a review of the tuberculin tests, gamma-interferon assay and other ancillary diagnostic techniques. *Res. Vet. Sci.* 81, 190–210. doi: 10.1016/j.rvsc.2005.11.005

Dean, G., Whelan, A., Clifford, D., Salguero, F. J., Xing, Z., Gilbert, S., et al. (2014). Comparison of the immunogenicity and protection against bovine tuberculosis following immunization by BCG-priming and boosting with adenovirus or protein based vaccines. *Vaccine* 32, 1304–1310. doi: 10.1016/j.vaccine.2013.11.045

Domingo, M., Vidal, E., and Marco, A. (2014). Pathology of bovine tuberculosis. *Res. Vet. Sci.* 97, S20–S29. doi: 10.1016/j.rvsc.2014.03.017

Fitzgerald, S. D., and Kaneene, J. B. (2013). Wildlife reservoirs of bovine tuberculosis worldwide: hosts, pathology, surveillance, and control. *Vet. Pathol.* 50, 488–499. doi: 10.1177/0300985812467472

Flynn, J. L. K. E. (2011). "Pulmonary tuberculosis in monkeys" in *A color atlas of comparative pathology of pulmonary tuberculosis*. eds. F. J. Leong, V. Dartois and T. Dick (Boca Raton, FL, USA: CRC Press), 83–105.

Fukunaga, H., Murakami, T., Gondo, T., Sugi, K., and Ishihara, T. (2002). Sensitivity of acid-fast staining for mycobacterium tuberculosis in formalin-fixed tissue. *Am. J. Respir. Crit. Care Med.* 166, 994–997. doi: 10.1164/rccm.2111028

Gautam, U. S., Asrican, R., and Sempowski, G. D. (2022). Targeted dose delivery of mycobacterium tuberculosis in mice using silicon antifoaming agent via aerosol exposure system. *PLoS One* 17:e0276130. doi: 10.1371/journal.pone.0276130

Gharun, K., Senges, J., Seidl, M., Losslein, A., Kolter, J., Lohrmann, F., et al. (2017). Mycobacteria exploit nitric oxide-induced transformation of macrophages into permissive giant cells. *EMBO Rep.* 18, 2144–2159. doi: 10.15252/embr.201744121

Gideon, H. P., Hughes, T. K., Tzouanas, C. N., Wadsworth, M. H. 2nd, Tu, A. A., Gierahn, T. M., et al. (2022). Multimodal profiling of lung granulomas in macaques reveals cellular correlates of tuberculosis control. *Immunity* 55:e810, 827–846. doi: 10.1016/j.immuni.2022.04.004

Gupta, G., Athanikar, S. B., Pai, V. V., and Naveen, K. N. (2014). Giant cells in dermatology. *Indian J. Dermatol.* 59, 481–484. doi: 10.4103/0019-5154.139887

Hope, J. C., Thom, M. L., Villarreal-Ramos, B., Vordermeier, H. M., Hewinson, R. G., and Howard, C. J. (2005). Vaccination of neonatal calves with Mycobacterium bovis BCG induces protection against intranasal challenge with virulent M. bovis. *Clin. Exp. Immunol.* 139, 48–56. doi: 10.1111/j.1365-2249.2005.02668.x

Johnson, L., Gough, J., Spencer, Y., Hewinson, G., Vordermeier, M., and Wangoo, A. (2006). Immunohistochemical markers augment evaluation of vaccine efficacy and disease severity in bacillus Calmette-Guerin (BCG) vaccinated cattle challenged with Mycobacterium bovis. *Vet. Immunol. Immunopathol.* 111, 219–229. doi: 10.1016/j.vetimm.2006.01.016

Jones, G. J., Coad, M., Khatri, B., Bezos, J., Parlane, N. A., Buddle, B. M., et al. (2017). Tuberculin skin testing boosts interferon gamma responses to DIVA reagents in Mycobacterium bovis-infected cattle. *Clin. Vaccine Immunol.* 24:24. doi: 10.1128/CVI.00551-16

Kanipe, C., and Palmer, M. V. (2020). Mycobacterium bovis and you: a comprehensive look at the bacteria, its similarities to mycobacterium tuberculosis, and its relationship with human disease. *Tuberculosis (Edinb.)* 125:102006. doi: 10.1016/j.tube.2020.102006

Khalid, H., Van Hooij, A., Connelley, T. K., Geluk, A., and Hope, J. C. (2022). Protein levels of pro-inflammatory cytokines and chemokines as biomarkers of Mycobacterium bovis infection and BCG vaccination in cattle. *Pathogens* 11:738. doi: 10.3390/pathogens11070738

Losslein, A. K., Lohrmann, F., Scheuermann, L., Gharun, K., Neuber, J., Kolter, J., et al. (2021). Monocyte progenitors give rise to multinucleated giant cells. *Nat. Commun.* 12:2027. doi: 10.1038/s41467-021-22103-5

Martinot, A. J. (2018). Microbial offense vs host defense: who controls the TB granuloma? *Vet. Pathol.* 55, 14–26. doi: 10.1177/0300985817705177

Menin, A., Fleith, R., Reck, C., Marlow, M., Fernandes, P., Pilati, C., et al. (2013). Asymptomatic cattle naturally infected with Mycobacterium bovis present exacerbated tissue pathology and bacterial dissemination. *PLoS One* 8:e53884. doi: 10.1371/journal.pone.0053884

Nol, P., Palmer, M. V., Waters, W. R., Aldwell, F. E., Buddle, B. M., Triantis, J. M., et al. (2008). Efficacy of oral and parenteral routes of Mycobacterium bovis bacille Calmette-Guerin vaccination against experimental bovine tuberculosis in white-tailed deer (Odocoileus virginianus): a feasibility study. *J. Wildl. Dis.* 44, 247–259. doi: 10.7589/0090-3558-44.2.247

Nugent, G., Yockney, I. J., Cross, M. L., and Buddle, B. M. (2018). Low-dose BCG vaccination protects free-ranging cattle against naturally-acquired bovine tuberculosis. *Vaccine* 36, 7338–7344. doi: 10.1016/j.vaccine.2018.10.025

Pagan, A. J., and Ramakrishnan, L. (2018). The formation and function of granulomas. *Annu. Rev. Immunol.* 36, 639–665. doi: 10.1146/annurev-immunol-032712-100022

Palmer, M. V., Kanipe, C., and Boggiatto, P. M. (2022). The bovine Tuberculoid granuloma. *Pathogens* 11:061. doi: 10.3390/pathogens11010061

Palmer, M. V., Thacker, T. C., Kanipe, C., and Boggiatto, P. M. (2021). Heterogeneity of pulmonary granulomas in cattle experimentally infected with Mycobacterium bovis. *Front. Vet. Sci.* 8:671460. doi: 10.3389/fvets.2021.671460

Palmer, M. V., Thacker, T. C., and Waters, W. R. (2009). Vaccination with Mycobacterium bovis BCG strains Danish and Pasteur in white-tailed deer (Odocoileus virginianus) experimentally challenged with Mycobacterium bovis. *Zoonoses Public Health* 56, 243–251. doi: 10.1111/j.1863-2378.2008.01198.x

Palmer, M. V., Thacker, T. C., and Waters, W. R. (2016). Multinucleated giant cell cytokine expression in pulmonary granulomas of cattle experimentally infected with Mycobacterium bovis. *Vet. Immunol. Immunopathol.* 180, 34–39. doi: 10.1016/j.vetimm.2016.08.015

Palmer, M. V., Waters, W. R., and Thacker, T. C. (2007). Lesion development and immunohistochemical changes in granulomas from cattle experimentally infected with Mycobacterium bovis. *Vet. Pathol.* 44, 863–874. doi: 10.1354/vp.44-6-863

Palmer, M. V., Waters, W. R., and Whipple, D. L. (2002). Aerosol delivery of virulent Mycobacterium bovis to cattle. *Tuberculosis (Edinb.)* 82, 275–282. doi: 10.1054/tube.2002.0341

Ramakrishnan, L. (2012). Revisiting the role of the granuloma in tuberculosis. *Nat. Rev. Immunol.* 12, 352–366. doi: 10.1038/nri3211

Roy, A., Tome, I., Romero, B., Lorente-Leal, V., Infantes-Lorenzo, J. A., Dominguez, M., et al. (2019). Evaluation of the immunogenicity and efficacy of BCG and MTBVAC vaccines using a natural transmission model of tuberculosis. *Vet. Res.* 50:82. doi: 10.1186/s13567-019-0702-7

Russell, D. G., Barry, C. E. 3rd, and Flynn, J. L. (2010). Tuberculosis: what we don't know can, and does, hurt us. *Science* 328, 852–856. doi: 10.1126/science.1184784

Russell, D. G., Cardona, P. J., Kim, M. J., Allain, S., and Altare, F. (2009). Foamy macrophages and the progression of the human tuberculosis granuloma. *Nat. Immunol.* 10, 943–948. doi: 10.1038/ni.1781

Salguero, F. J., Gibson, S., Garcia-Jimenez, W., Gough, J., Strickland, T. S., Vordermeier, H. M., et al. (2017). Differential cell composition and cytokine expression within lymph node granulomas from BCG-vaccinated and non-vaccinated cattle experimentally infected with *Mycobacterium bovis*. *Transbound. Emerg. Dis.* 64, 1734–1749. doi: 10.1111/tbed.12561

Singhal, A. A. E. M., Creusy, C., Kaplan, G., and Bifani, P. (2011). "Pulmonary tuberculosis in the rat" in *A color atlas of comparative pathology of pulmonary tuberculosis*. eds. D. F. J. Leongv and T. Dick (Boca Raton, FL, USA: CRC Press), 166.

Sirak, A., Tulu, B., Bayissa, B., Gumi, B., Berg, S., Salguero, F. J., et al. (2021). Cellular and cytokine responses in lymph node granulomas of bacillus Calmette Guerin (BCG)-vaccinated and non-vaccinated Cross-breed calves naturally infected with Mycobacterium bovis. *Front. Vet. Sci.* 8:698800. doi: 10.3389/fvets.2021.698800

Sow, F. B., Gallup, J. M., Derscheid, R., Krishnan, S., and Ackermann, M. R. (2012). Ontogeny of the immune response in the ovine lung. *Immunol. Investig.* 41, 304–316. doi: 10.3109/08820139.2011.631657

Steinbach, S., Jalili-Firoozinezhad, S., Srinivasan, S., Melo, M. B., Middleton, S., Konold, T., et al. (2021). Temporal dynamics of intradermal cytokine response to tuberculin in Mycobacterium bovis BCG-vaccinated cattle using sampling microneedles. *Sci. Rep.* 11:7074. doi: 10.1038/s41598-021-86398-6

Trout, K. L., and Holian, A. (2020). Multinucleated giant cell phenotype in response to stimulation. *Immunobiology* 225:151952. doi: 10.1016/j.imbio.2020.151952

Vordermeier, H. M., Villarreal-Ramos, B., Cockle, P. J., Mcaulay, M., Rhodes, S. G., Thacker, T., et al. (2009). Viral booster vaccines improve Mycobacterium bovis BCG-induced protection against bovine tuberculosis. *Infect. Immun.* 77, 3364–3373. doi: 10.1128/IAI.00287-09

Wangoo, A., Johnson, L., Gough, J., Ackbar, R., Inglut, S., Hicks, D., et al. (2005). Advanced granulomatous lesions in Mycobacterium bovis-infected cattle are associated with increased expression of type I procollagen, gammadelta (WC1+) T cells and CD 68+ cells. *J. Comp. Pathol.* 133, 223–234. doi: 10.1016/j.jcpa.2005.05.001

Warsinske, H. C., Difazio, R. M., Linderman, J. J., Flynn, J. L., and Kirschner, D. E. (2017a). Identifying mechanisms driving formation of granuloma-associated fibrosis during mycobacterium tuberculosis infection. *J. Theor. Biol.* 429, 1–17. doi: 10.1016/j.jtbi.2017.06.017

Warsinske, H. C., Pienaar, E., Linderman, J. J., Mattila, J. T., and Kirschner, D. E. (2017b). Deletion of TGF-beta1 increases bacterial clearance by cytotoxic T cells in a tuberculosis granuloma model. *Front. Immunol.* 8:1843. doi: 10.3389/fimmu.2017.01843

Watanabe, Y., Watari, E., Matsunaga, I., Hiromatsu, K., Dascher, C. C., Kawashima, T., et al. (2006). BCG vaccine elicits both T-cell mediated and humoral immune responses directed against mycobacterial lipid components. *Vaccine* 24, 5700–5707. doi: 10.1016/j.vaccine.2006.04.049

Waters, W. R., Palmer, M. V., Nonnecke, B. J., Thacker, T. C., Scherer, C. F., Estes, D. M., et al. (2009). Efficacy and immunogenicity of Mycobacterium bovis DeltaRD1 against aerosol M. bovis infection in neonatal calves. *Vaccine* 27, 1201–1209. doi: 10.1016/j.vaccine.2008.12.018

Waters, W. R., Palmer, M. V., Nonnecke, B. J., Thacker, T. C., Scherer, C. F., Estes, D. M., et al. (2007). Failure of a mycobacterium tuberculosis DeltaRD1 DeltapanCD double deletion mutant in a neonatal calf aerosol M. bovis challenge model: comparisons to responses elicited by M. bovis bacille Calmette Guerin. *Vaccine* 25, 7832–7840. doi: 10.1016/j.vaccine.2007.08.029

frontiers | Frontiers in Microbiology

TYPE Original Research
PUBLISHED 01 December 2022
DOI 10.3389/fmicb.2022.1063578

OPEN ACCESS

EDITED BY
Qing Pan,
Qingdao Agricultural University, China

REVIEWED BY
Mangesh Vasant Suryavanshi,
Lerner Research Institute - Cleveland Clinic, United States
Mingmin Lu,
Nanjing Agricultural University, China

*CORRESPONDENCE
Huihua Zhang
hhzhang2@163.com

†These authors have contributed equally to this work

SPECIALTY SECTION
This article was submitted to Infectious Agents and Disease, a section of the journal Frontiers in Microbiology

RECEIVED 07 October 2022
ACCEPTED 17 November 2022
PUBLISHED 01 December 2022

CITATION
Feng X, Li T, Zhu H, Liu L, Bi S, Chen X and Zhang H (2022) Effects of challenge with *Clostridium perfringens*, *Eimeria* and both on ileal microbiota of yellow feather broilers. *Front. Microbiol.* 13:1063578. doi: 10.3389/fmicb.2022.1063578

Effects of challenge with *Clostridium perfringens*, *Eimeria* and both on ileal microbiota of yellow feather broilers

Xin Feng[1†], Tonghao Li[1†], Hui Zhu[1†], Lidan Liu[2], Shengqun Bi[1], Xiaolin Chen[1] and Huihua Zhang[1*]

[1]School of Life Sciences and Engineering, Foshan University, Foshan, China, [2]Foshan Zhengdian Biology Technology Co., Ltd., Foshan, China

In the poultry industry worldwide, *Clostridium perfringens* has been causing major economic loss as it can cause necrotic enteritis (NE). The coccidial infection has been considered as the most important predisposing factor of NE caused by *C. perfringens*. In this study, we aimed to advance our knowledge on ileal microbiota of yellow feather broilers under *C. perfringens* and/or *Eimeria* challenge. Total of 80 healthy day old yellow feather broilers were randomly assigned to four groups including: Control, *C. perfringens* challenge group (C. Per), *Eimeria* challenge group (Cocc), and *C. perfringens* plus *Eimeria* challenge group (Comb). On day 14, the Cocc and Comb group broilers were orally gavaged 1 ml PBS solution containing 25,000 oocysts of *Eimeria brunetti* and 25,000 oocysts of *Eimeria maxima*. Starting on day 17, the C. Per and Comb group broilers were orally gavaged 10 mL of *C. perfringens* per bird (4×10^7 CFU/mL, ATCC® 13124™ Strain) every day for 6 days. 16S rRNA gene sequencing was performed on extracted DNA of ileal digesta samples. The results showed that *C. perfringens* alone did not affect the alpha diversity of ileal microbiome in yellow feather broilers but co-infection with *Eimeria* significantly decreased the diversity of ileal microbiota. *C. perfringens* and *Eimeria* challenge also decreased the relative abundance of beneficial bacteria including *Bacteroidetes* at the phylum level and *Faecalibacterium* at the genus level. At the species level, the relative abundance of *Candidatus Arthromitus* was significantly decreased in the *Eimeria* challenged groups. This microbial shift information of ileal microbiota under *C. Perfringens* and *Eimeria* challenge provide important reference data for the development of therapeutic approaches to necrotic enteritis in yellow-feather broiler chickens.

KEYWORDS

challenge, *C. perfringens*, *Eimeria*, microbiota, yellow feather broiler

Introduction

Clostridium perfringens (*C. perfringens*) is a constituent of normal flora in the digestive tract of animals and humans (Miller et al., 2010). In the poultry industry worldwide, *C. perfringens* has been causing major economic loss as it can cause necrotic enteritis (NE). Clinical or subclinical NE usually occurs in broiler chickens between the ages of 2–6 weeks (Skinner et al., 2010). In healthy chickens, *C. perfringens* almost always exist at levels less than 10^5 CFU/g intestinal content (Caly et al., 2015). Predisposing factors including high levels of dietary non-starch polysaccharide grains or fish meal proteins, physiological stress, *Fusarium* mycotoxins in feed as well as coccidial infection normally exist to induce the outbreak of NE (Timbermont et al., 2011; Moore, 2016; Zaytsoff et al., 2020).

The coccidial infection has been considered the most important predisposing factor of NE caused by *C. perfringens*. The species of obligate intracellular parasites of the genus *Eimeria* can cause potentially severe enteritis (Attree et al., 2021), resulting significantly economic loss to the poultry industry. Four species of *Eimeria*, including *E. acervulina*, *E. maxima*, *E. necatrix*, and *E. tenella*, are considered most important due to their pathogenicity, global prevalence, and overall economic impact (Attree et al., 2021). When co-infected with *Eimeria*, the NE incidence and the mortality rate of chickens are higher (Baba et al., 1992). *Eimeria* can cause damage to the epithelium or induce mucogenesis, thus providing a niche for *C. perfringens* colonization and proliferation (Collier et al., 2008; Van Immerseel et al., 2009). Infectious dose, age, and immune status of the host could all affect the response of the chicken to coccidial infection, ranging from few clinical signs or reduction in weight gain, feed conversion, or egg production to severe enteritis and death (Attree et al., 2021). Coccidiosis prevention would be one way to reduce the incidence of NE caused by *C. perfringens*.

Due to the significant economic loss and compromised animal welfare caused by *C. perfringens* and *Eimeria*, effective control of NE necessitates explorations of alternative strategies due to chemoprophylaxis resistance and limited cost-effective vaccines (Giannenas et al., 2012; Ritzi et al., 2014). In 2020, the ban of antibiotic growth promoters in China has resulted in re-emergence of NE in poultry industry. Gut microbial shift plays a role in the progress of disease development. It was reported that NE development in chickens is associated with microbial shift within the GI tract (Kim et al., 2015). It has not been clear if microbial shift is a predisposing factor or more of a consequence of NE. To prevent *C. perfringens* and *Eimeria* infection and improve the gut health of broilers, the gut microbial information of infected chickens is important to know. In this study, we aimed to advance our knowledge on ileal microbiome of yellow feather broilers under *C. perfringens* and/or *Eimeria* challenge and provide reference data for future therapeutic strategies for disease control.

Materials and methods

Ethics statement

This experimental protocol was approved by the Ethical Committee and conducted under the supervision of the Institutional Animal Care and Use Committee of Foshan University (Foshan, China).

Experimental design and sampling

Total of 80 healthy day old yellow feather broilers were randomly assigned to four groups including: Control, *C. perfringens* challenge group (C. Per), *Eimeria* challenge group (Cocc), and *C. perfringens* plus *Eimeria* challenge group (Comb). Birds under different treatments were raised in different pens. On day 14, the Cocc and Comb groups broilers were orally gavaged 1 mL mixed-species *Eimeria* oocysts solution. The mixed-species *Eimeria* spp. PBS-based solution contained 25,000 oocysts of *Eimeria brunetti* and 25,000 oocysts *E. maxima*. Starting on day 17, the C. Per and Comb groups broilers were orally gavaged 10 mL of *C. perfringens*/bird (4×10^7 CFU/mL; *Clostridium perfringens* ATCC® 13124™ Strain; cultured in Reinforced Clostridium Medium) everyday for 6 days. Fot the control groups birds, 1 ml of sterile PBS solution was orally gavaged. On day 24, six broilers randomly selected from each group were sacrificed by cervical dislocation and exsanguinated. The ileal digesta was collected from each broiler and immediately placed into a 2 mL Eppendorf tube. The digesta samples were stored at −80°C for later analysis.

The facility was thoroughly cleaned and disinfected before the bird placement. Temperature was maintained at 33–34°C initially and gradually decreased until 22–24°C by the third week. During the study, all the birds had free access to the same feed and clean water.

Ileal digesta DNA extraction and microbiota data analysis

The DNA extraction and high-throughput sequencing analysis for this study were the same as our previous study (Feng et al., 2020). Briefly, total genome DNA from ileal digesta was extracted using the Cetyltrimethyl Ammonium Bromide method. Extracted DNA was monitored on 1% agarose gels before being diluted to 1 ng/μL to prepare amplicons for high-throughput sequencing. Conventional PCR was used to amplify the V3-V4 regions of the 16S rRNA genes using primers 515F (5′- GTGYCAGCMGCCGCGGTAA-3′) and 806R (5′-GGACTACNNGGGTATCTAAT-3′). The PCR reaction mix consisted of 15 μL of Phusion® High-Fidelity PCR Master Mix (New England Biolabs, MA, USA), 0.2 μM of forward and reverse primers, and about 10 ng template DNA. Sequencing

libraries were generated using TruSeq® DNA PCR-Free sample preparation kit (Illumina, San Diego, CA, USA). The library quality was assessed on a Qubit @ 2.0 Fluorometer (Thermo Fisher Scientific, MA, USA) and Agilent Bioanalyzer 2100 system (Agilent Technologies, Inc., Santa Clara, CA, USA). The bar-coded amplicons were sequenced on an Illumina NovaSeq system and 250 bp paired-end reads were generated.

Paired-end reads were merged using Fast Length Adjustment of Short reads software (FLASH; V1.2.11) to obtain raw tags. Then quality control was conducted using fastp software to obtain high-quality clean tags. Finally, the Vsearch software was used to compare the clean tags with the database to detect and remove chimeras to obtain the effective tags (Haas et al., 2011). The obtained effective tags were denoised using the DADA2 module in QIIME2. Sequences with an abundance less than five were filtered out to obtain the final amplicon sequence variants (ASVs). Subsequently, the obtained ASVs were compared with the database (Silva138.1) using the classify-sklearn module in QIIME2 to obtain the species information of each ASV. Alpha diversity analysis (shannon, simpson, chao1, goods coverage, dominance, and pielou) and Beta diversity analysis were conducted in QIIME2. Principal component analysis (PCA) plot was generated using the "ade4" and "ggplot2" packages of the R software (v. 3.5.3).[1] Differentially abundant genera among groups were identified using linear discriminant analysis (LDA) effect size (LEfSe) analysis (Segata et al., 2011). Phylogenetic Investigation of Communities by Reconstruction of Unobserved States (PICRUSt2) was performed to make inferences about the metabolic functions of the microbial community and metagenome metabolic functions were assessed using the KEGG orthology database (Douglas et al., 2020).

Statistical analysis

Alpha diversity index and taxonomic data were analyzed using the PROC GLIMMIX procedure of SAS (SAS Institute, Inc., Cary, NC, USA) including treatment as fixed effect in the model. The significance was declared at $P < 0.05$ and trends at $P < 0.1$. Tukey multiple comparison method was used to detect difference between two groups when treatment effect was significant.

Results

Similarity analysis and alpha diversity

To evaluate how infection of *C. perfringens* and *Eimeria* shift the microbial composition of chickens, 16S rRNA gene sequencing was performed on extracted DNA of ileal digesta samples. Total number of Amplicon Sequence Variants (ASVs) in all four groups was 1,185 and 58 ASVs were shared by all groups (**Figure 1A**). Compared to the control group, all the other three groups had lower number of group specific ASVs (control 373 vs. C. Per 183, Cocc 148, and Comb 111) indicating lower diversity of bacterial species. Rarefaction curve of observed otus revealed that there was sufficient sequence coverage to describe the bacterial composition of each group (**Figure 1B**). Principal component analysis revealed that the first and second principal components explained 11.48 and 10.55% of the variation among samples, respectively (**Figure 2**). Samples from different groups could not be clearly separated from each other. However, it can be seen from the PCA plot that the three groups under challenge clustered together. Effects of *C. Perfringens* and *Eimeria* challenge on alpha diversity of ileal microbiota in yellow feather broilers are present in **Table 1**. Compared to the control group, challenge with *C. perfringens* alone did not affect alpha indices including Shannon, and Chao1. But *Eimeria* challenge alone or combined infection with *C. perfringens* all significantly decreased the values of these indices ($P < 0.05$). The indices of Simpson, Pielou, and Dominance were not different among four groups ($P > 0.05$).

Taxonomic composition of ileal microbiota

The main phyla present in the ileal digesta microbiota of the birds are shown in **Table 2** and **Figure 3**. It was observed that *Firmicutes* and *Bacteroidetes* were the most frequent phyla, regardless of the treatment. Among the top 10 phyla, only the relative abundance of *Bacteroidetes* and *Desulfobacterota* were different among four groups. The *C. perfringens* and/or *Eimeria* challenge significantly decreased the relative abundance of *Bacteroidetes* compared to the control group ($P < 0.05$). In the ileal microbiota of yellow feather broilers, *Bacteroidetes* has the third highest abundance. At the genus level, among the top 15 genera analyzed, the relative abundance of *Faecalibacterium* was lower in the C. Per and Comb group in comparison with the control group. No difference between the control group and Cocc group was observed regarding the relative abundance of *Faecalibacterium* (**Table 3**). The relative abundance of the top 15 species in the ileal digesta microbiota of the broilers is shown in **Table 4**. The *Lactobacillus aviarius* was the most abundant species and its relative abundance was not different among the four groups ($P = 0.90$). Compared to the control group, the C. Per group had higher relative abundance of *Motilimonas eburnea* ($P = 0.04$). Its relative abundance in Cocc and Comb groups were not different from the control group. The control and C. Per groups had significantly higher abundance of *Candidatus Arthromitus* than the Cocc and Comb groups ($P = 0.018$).

1 https://www.r-project.org/

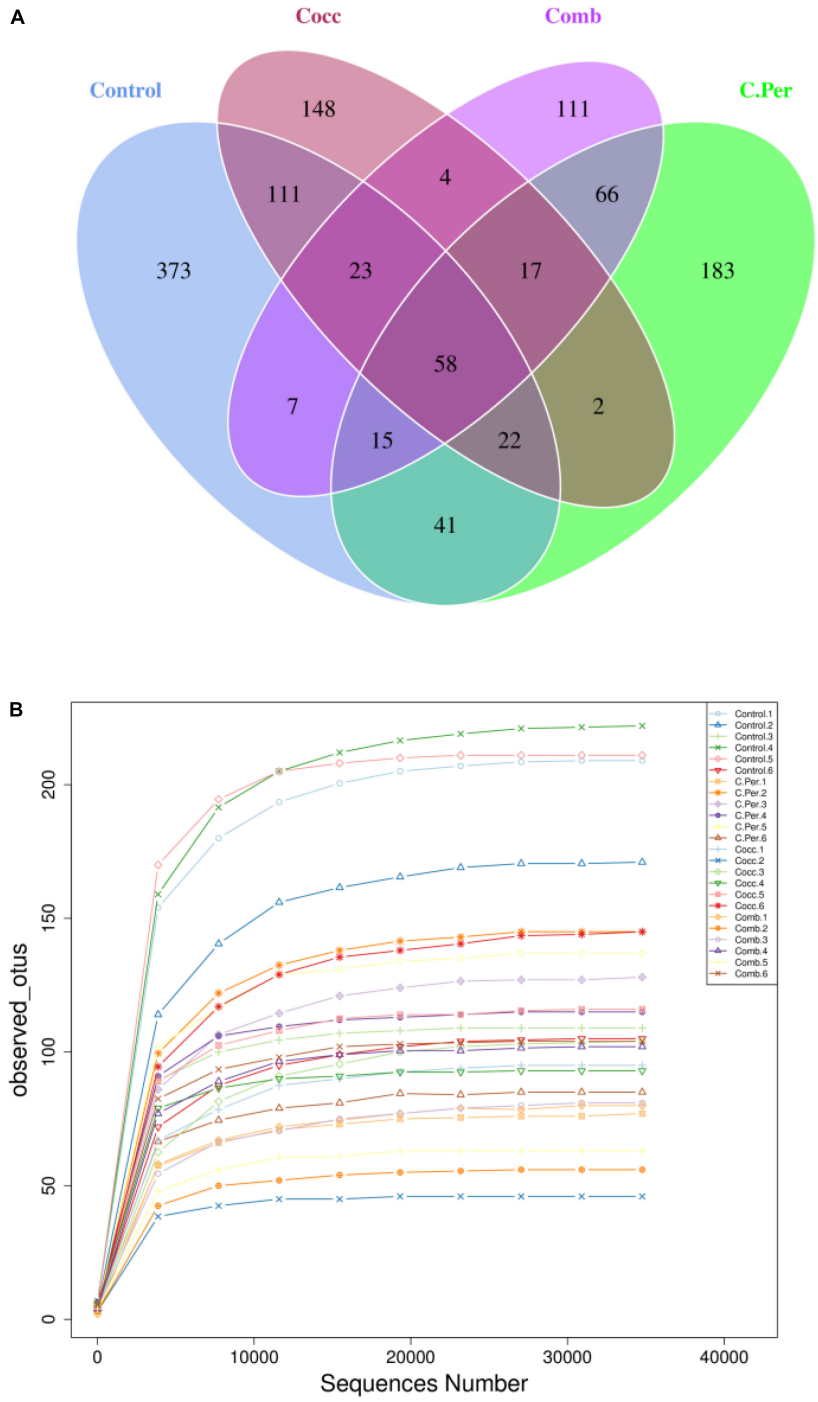

FIGURE 1
Number of Amplicon Sequence Variants (ASVs) in each group. **(A)** Venn diagram of shared and specific ASVs in the four groups. **(B)** Rarefaction curve of observed otus in all samples. C. Per, *C. perfringens* challenge; Cocc, *Eimeria* challenge; Comb, *C. perfringens* and *Eimeria* challenge.

Linear discriminant analysis (LDA) effect size analysis (LDA > 3.5) was performed to discriminate the differences on the community composition between groups. A total of 25 biomarkers bacterial genera were identified in the four groups (Figure 4). *Bacteroidales*, *Muribaculaceae* (both at the family and genus level), *Oscillospirales*, *Cyanobacteria*, *Cyanobacteria*, *Chloroplast* (at the order, family, and genus levels), *Lachnospirales*, *Lachnospiraceae*, *Ruminococcaceae* were enriched in the control group. The C. Per group was enriched with *Clostridiales*, *Clostridiaceae*, *Candidatus Arthromitus*,

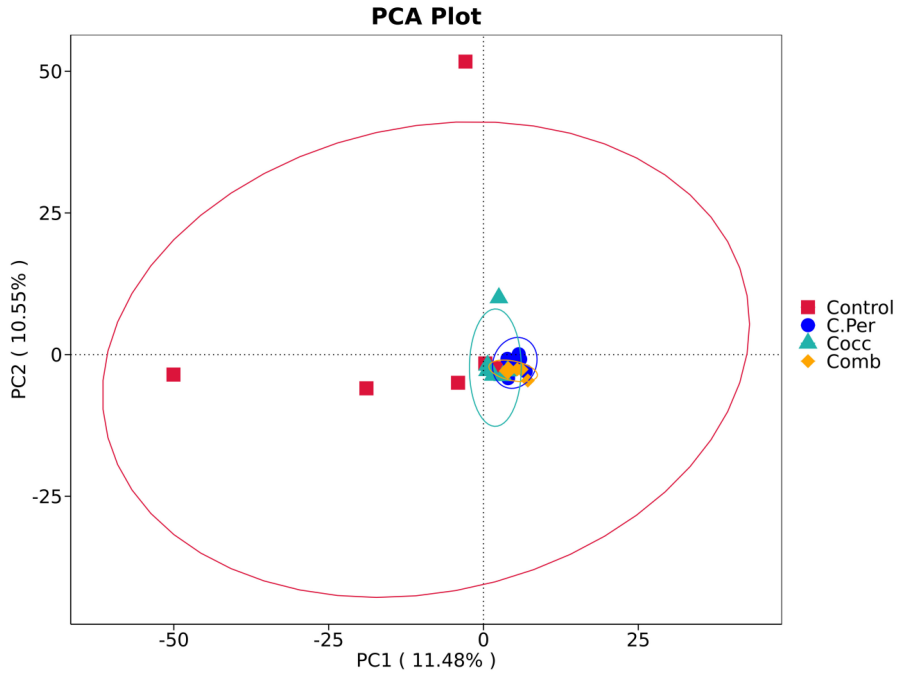

FIGURE 2
Principle component analysis of the ileal microbiota in different groups. C. Per, *C. perfringens* challenge; Cocc, *Eimeria* challenge; Comb, *C. perfringens* and *Eimeria* challenge.

TABLE 1 Effects of *Clostridium perfringens* and/or *Eimeria* challenge on alpha diversity indices of ileal microbiota in yellow-feather broilers.

Items	Control	C. Per	Cocc	Comb	SEM	*P*
Shannon	3.56^{a}	2.98^{ab}	2.41^{b}	2.39^{b}	0.293	0.026
Simpson	0.79	0.72	0.64	0.65	0.059	0.28
Chao1	171.9^{a}	115.1^{ab}	100.2^{b}	81.6^{b}	14.52	0.0018
Pielou	0.48	0.44	0.37	0.38	0.039	0.16
Dominance	0.21	0.27	0.36	0.35	0.059	0.28

C. Per, *C. perfringens* challenge; Cocc, *Eimeria* challenge; Comb, *C. perfringens* and *Eimeria* challenge. Within a row, means without a common superscript (a, b) differ ($P < 0.05$).

Clostridia, *Gallibacterium*, *Gallibacterium anatis*, *Pasteurellales*, and *Pasteurellaceae*. In addition, *Bacilli* was enriched in Cocc group and *Weissella* and *Leuconostocaceae* were enriched in the Comb group. Consistent with results from Table 2, the control group had the highest abundance of *Cyanobacteria*, but not statistically different compared with other groups. This also applies to *Candidatus Arthromitus*, *Muribaculaceae*, *Gallibacterium*, and *Chloroplast* meaning that the groups in which they were enriched had the highest abundance but not significantly different from other groups. Based on the LEfSe analysis, *Faecalibacterium* was enriched in the control group. The control group did have significantly higher abundance of *Faecalibacterium* compared to the C. Per and Comb group ($P < 0.05$), but not different from the Cocc group.

TABLE 2 Effects of *Clostridium perfringens* and/or *Eimeria* challenge on taxonomic composition of ileal microbiota at phylum level in yellow-feather broilers.

Items,%	Control	C. Per	Cocc	Comb	SEM	*P*
Firmicutes	91.77	96.26	98.70	90.79	4.014	0.47
Proteobacteria	2.74	2.67	0.62	8.43	3.867	0.53
Bacteroidetes	3.07^{a}	0.16^{b}	0.37^{b}	0.18^{b}	0.760	0.03
Cyanobacteria	1.25	0.27	0.02	0.0008	0.478	0.24
Actinobacteriota	0.52	0.57	0.22	0.55	0.248	0.72
Verrucomicrobiota	0.24	0.02	0.05	0.01	0.117	0.49
Campilobacterota	0.21	0.015	0.007	9.58E-6	0.080	0.21
Fusobacteriota	0.06	0.013	0.013	0.012	0.033	0.65
Desulfobacterota	0.07^{a}	0.001^{ab}	0.002^{ab}	0^{b}	0.017	0.03
Synergistota	0.016	0	0.004	0	0.008	0.49
Others	0.06	0.02	1.11E-16	0.05	0.016	0.09

C. Per, *C. perfringens* challenge; Cocc, *Eimeria* challenge; Comb, *C. perfringens* and *Eimeria* challenge. Within a row, means without a common superscript (a, b) differ ($P < 0.05$).

Function prediction using phylogenetic investigation of communities by reconstruction of unobserved states

The predicted functions against the KEGG orthology database are presented in Figure 5. Total of 6,378 KOs were predicted among four groups and 5,215 were shared by all groups (Figure 5A). Compared to the control group, the other

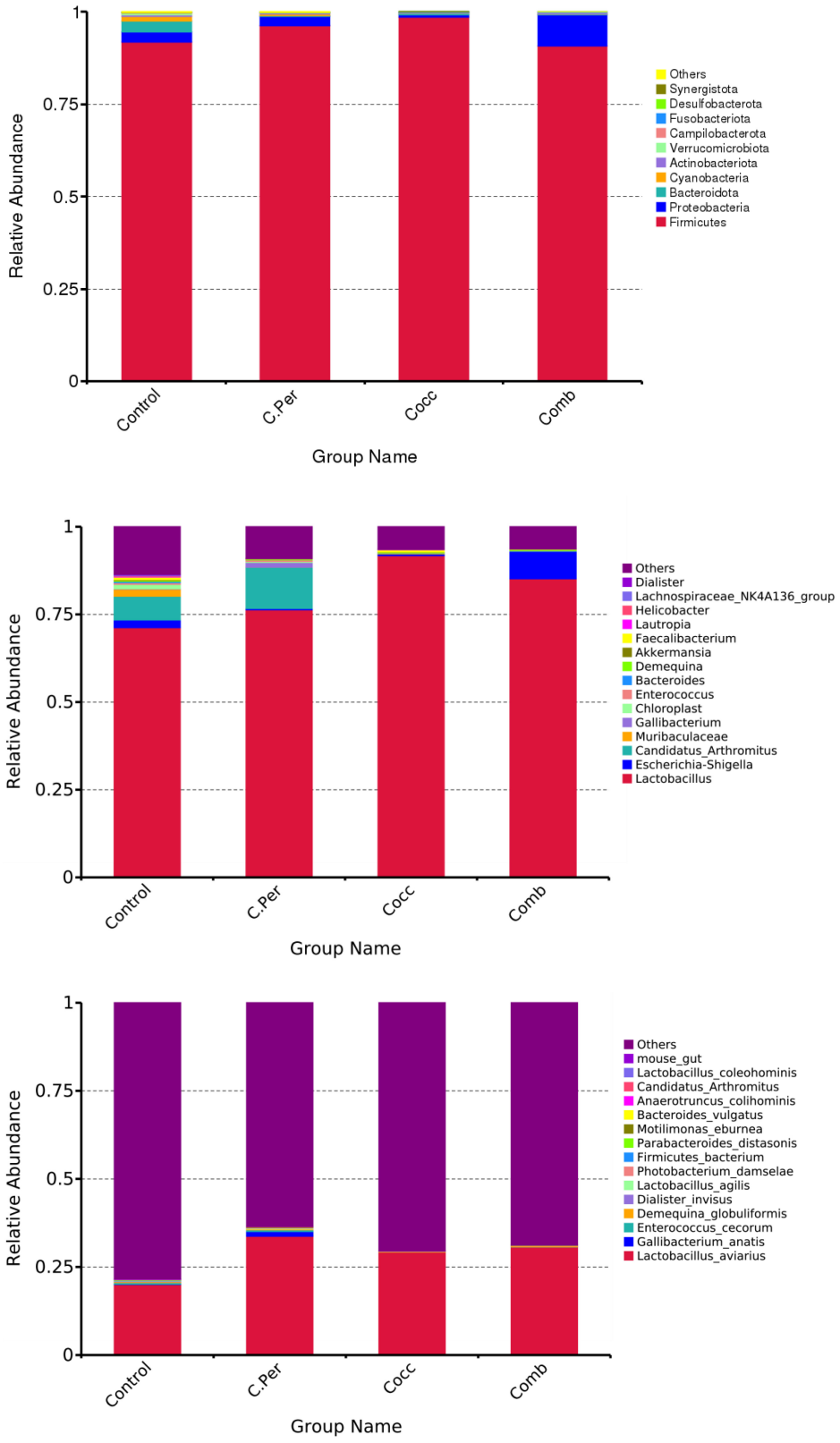

FIGURE 3
Phylum-level, genus-level, and species level taxonomic composition of the ileal bacterial communities in four groups. C. Per, *C. perfringens* challenge; Cocc, *Eimeria* challenge; Comb, *C. perfringens* and *Eimeria* challenge.

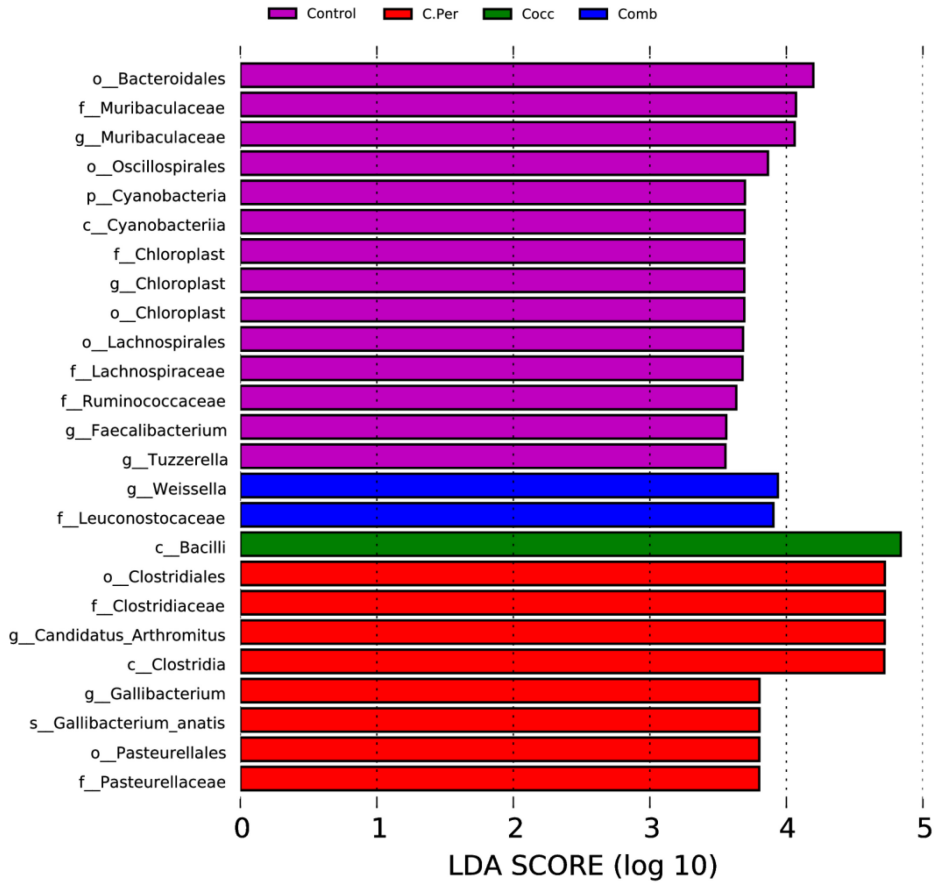

FIGURE 4
linear discriminant analysis (LDA) effect size (LEfSe) Analysis of differential species among all groups shown in the LDA value distribution histogram. The presented species are biomarkers with statistical differences between groups (LDA > 3.5). The length of the histogram (LDA score) represents the impact of the different species.

three groups had lower number of group specific microbial functions (330 for control vs. 61 for C. Per, 20 for Cocc, and 68 for Comb). The relative abundance of the top 10 microbial functions (**Figure 5B**) are most involved in the metabolism (K07024, K02761, K15634, and K01223), Cellular Processes (K02035 and K15508); genetic information processing (K02529 and K07496), and Environmental Information Processing (K01990 and K02004). All these functions were not statistically different among the four groups. The principal component analysis plot showed clusters of samples based on their microbial function similarity. It can be seen that samples from four groups could not be separated completely. The first and second components explained 36.37 and 22.67% of the variation, respectively (**Figure 5C**).

Discussion

Necrotic enteritis (NE) is a disease of the small intestine of chickens caused by *C. perfringens* (Zaytsoff et al., 2020). When *C. Perfringens* colonizes and proliferates in the small intestine, extracellular toxins produced can damage the intestinal wall thus cause necrotic enteritis. Modulation of *C. perfringens* on intestinal tight junctions and host immune response was reported earlier (Mitchell and Koval, 2010; Daneshmand et al., 2022). Predisposing factors such as high dietary protein or *Eimeria* infection have been utilized in the experimental reproduction of NE to investigate its pathogenesis or prevention (Shojadoost et al., 2012). Physiological stress as predisposing factor to NE has also been shown to increase densities of *C. perfringens* in the small intestine and weight gain impairment in chickens (Zaytsoff et al., 2020).

We used coccidia to facilitate an optimal NE reproduction in yellow feather broilers. During coccidiosis, *Eimeria* colonize the intestine and destroy intestinal epithelium cells which create an optimal environment for *C. perfringens* proliferation (Williams, 2005). In our study, lesions were not observed in the small intestine of the broilers inoculated with *C. perfringens* and/or *Eimeria*. Similarly, Wu et al. (2014) reported no observed lesions in the jejunum and ileum of *Eimeria* challenged birds.

TABLE 3 Effects of *Clostridium perfringens* and/or *Eimeria* challenge on taxonomic composition of ileal microbiota at genus level in yellow-feather broilers.

Items,%	Control	C. Per	Cocc	Comb	SEM	*P*
Lactobacillus	71.25	76.33	91.79	85.19	6.498	0.15
Candidatus_Arthromitus	6.77	11.79	0.08	0.17	4.242	0.18
Muribaculaceae	2.03	0.02	0.19	0	0.679	0.13
Escherichia_Shigella	2.18	0.36	0.48	7.83	3.762	0.47
Gallibacterium	0.11	1.36	$1.95E-18$	0.01	0.573	0.30
Chloroplast	1.24	0.27	0.018	0.008	0.478	0.25
Enterococcus	0.45	0.48	0.008	0.06	0.198	0.23
Bacteroides	0.37	0.002	0.06	0.01	0.129	0.19
Demequina	0.29	0.27	0.18	0.30	0.152	0.94
Akkermansia	0.22	$4.8E-6$	0.04	0	0.109	0.45
Faecalibacterium	0.76^{a}	0.04^{b}	0.59^{a}	0.07^{b}	0.077	< 0.0001
Lautropia	0.19	0.007	0.06	0.003	0.097	0.51
Helicobacter	0.21	0.006	0.003	0	0.081	0.22
Lachnospiraceae_NK4A136_group	0.21	0	0.004	0	0.080	0.19
Dialister	0.16	0.03	0.04	0.02	0.085	0.59
Others	13.55	9.05	6.44	6.31	3.093	0.33

C. Per, *C. perfringens* challenge; Cocc, *Eimeria* challenge; Comb, *C. perfringens* and *Eimeria* challenge. Within a row, means without a common superscript (a, b) differ ($P < 0.05$).

TABLE 4 Effects of *Clostridium perfringens* and/or *Eimeria* challenge on taxonomic composition of ileal microbiota at species level in yellow-feather broilers.

Items,%	Control	C. Per	Cocc	Comb	SEM	*P*
Lactobacillus_aviarius	20.05	33.74	29.30	30.66	13.65	0.90
Gallibacterium_anatis	0.11	1.36	$2.17E-17$	0.01	0.572	0.29
Enterococcus_cecorum	0.45	0.46	0.007	0.056	0.199	0.23
Demequina_globuliformis	0.27	0.24	0.16	0.27	0.137	0.94
Dialister_invisus	0.16	$9.58E-4$	0.04	$4.34E-17$	0.084	0.48
Photobacterium_damselae	0.004	0.20	0	0.14	0.074	0.18
Lactobacillus_agilis	0.08	0.23	$1.08E-17$	0.01	0.069	0.09
Firmicutes_bacterium	0.11	0	0.006	$2.17E-17$	0.057	0.43
Parabacteroides_distasonis	0.10	0	0.01	0	0.051	0.44
Motilimonas_eburnea	0.006^{a}	0.15^{b}	0.005^{a}	0.084^{ab}	0.040	0.04
Bacteroides_vulgatus	0.07	0	0.01	0	0.033	0.38
Anaerotruncus_colihominis	0.07	0.002	0.03	0	0.023	0.17
Candidatus_Arthromitus	6.76^{a}	11.79^{a}	0.078^{b}	0.17^{b}	4.242	0.018
Lactobacillus_coleohominis	0.06	0.03	0.02	0.03	0.021	0.43
mouse_gut	0.03	0	0.007	0	0.013	0.49
Others	78.43	63.51	70.40	68.74	13.79	0.89

C. Per, *C. perfringens* challenge; Cocc, *Eimeria* challenge; Comb, *C. perfringens* and *Eimeria* challenge. Within a row, means without a common superscript (a, b) differ ($P < 0.05$).

Daneshmand et al. (2022) observed that birds challenged with both *Eimeria* and *C. Perfringens* either on control diet or wheat-based diet had reduced performance coupled with enteric gross lesions and epithelial damage. The inconsistent findings might be related to the dose amount and *Eimeria* species used.

It has been shown that gut microbial community can alter the susceptibility of poultry to necrotic enteritis as they can affect gene expression in the ileum of the host (Tang et al., 2020). Six indices were often used to measure alpha diversity including Shannon, Simpson, Chao1, Good's coverage, dominance, and Pielou. The greater the Chao1 and dominance indices, the higher the expected species richness of the microbiome. The greater the Shannon or the smaller the Simpson indices, the higher the diversity of the microbiome (Forbes et al., 2018). Pielou's evenness index measures diversity along with species richness. A calculated value of Pielou's evenness ranges from 0 (no evenness) to 1 (complete evenness). Compared to the control group, *C. perfringens* alone did not affect the

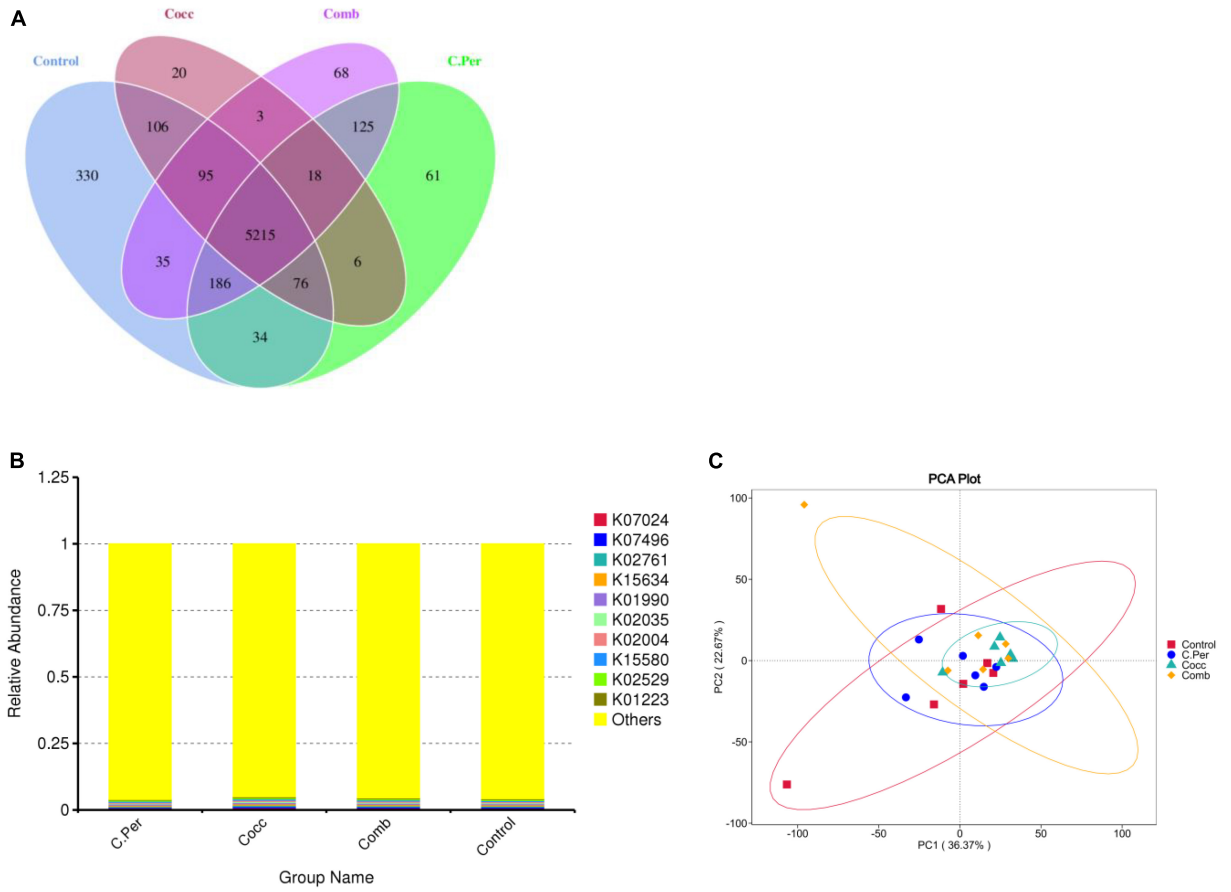

FIGURE 5
Function predictions using phylogenetic investigation of communities by reconstruction of unobserved states (PICRUSt2). **(A)** Venn diagram of shared and specific functions predicted in the four groups. **(B)** Barplot of the top functions predicted against KEGG orthology (KO) database. **(C)** Principle component analysis (PCA) of the functions predicted in different groups; C. Per, *C. perfringens* challenge; Cocc, *Eimeria* challenge; Comb, *C. perfringens and Eimeria challenge.*

richness or diversity of ileal microbiota. *Eimeria* challenge with or without *C. perfringens* all significantly decreased the Shannon and Chao1 indices indicating lower richness and diversity of intestinal microbiota in yellow feather broilers. Inconsistent to our results, increased chao1 index was observed in challenged birds (Bortoluzzi et al., 2019). *Eimeria* infection can significantly reduce the gut microbial diversity, most through reducing low abundance of operational taxonomic units (OTUs) and increasing dominance in the community (Perez et al., 2011). This was also observed in our study as groups challenged with *Eimeria* all had lower microbial diversity compared to the control group. Yang et al. (2021) investigated the link between ileal microbiota and disease severity in a chicken model of clinical NE. The authors reported that NE can significantly reduce the richness and Shannon index of ileal microbiota. Yang et al. (2019) reported that co-infection of *C. perfringens* and *Eimeria* significantly reduced species diversity in jejunal microbiota of broiler chicks but not cecal microbiota. Gastrointestinal tract is highly complex with numerous bacterial species, which would all contribute the development of NE. As shown in our results, changes in gut microbiota diversity induced by *Eimeria* may play an important role in predisposing the *C. Perfringens* infected birds to NE.

Healthy intestinal microbiota can enhance the host immune system and protection against intestinal pathogens (Ritzi et al., 2014). The dominance of beneficial microorganisms is essential to maintain gut homeostasis. Reduction of beneficial probiotic bacteria can predispose chickens to the onset of NE (Wu et al., 2014). LEfSe (Linear discriminant analysis Effect Size) determines the features most likely to explain differences between groups (Segata et al., 2011). Based on the LEfSe analysis, *Faecalibacterium* was enriched in the control group. Statistical analysis showed that the control group had significantly higher relative abundance of *Faecalibacterium* compared to the C. Per and Comb group. Surprisingly, no difference between the control group and Cocc group was observed. The sole known species of *Faecalibacterium*, *Faecalibacterium prausnitzii*, is a

probiotic and its decline is associated with the development of chronic inflammation (Maioli et al., 2021). The decreased relative abundance of *Faecalibacterium* in the C. Per and Comb group indicated possible intestinal inflammation after challenge with *C. perfringens*. In chickens with severe NE, *Firmicutes* was significantly decreased whereas *Proteobacteria* was increased (Yang et al., 2021). The increase in the relative abundance of pathogenic group indicates that the birds are carriers of pathogenic bacteria, which might lead to future health issues (Akerele et al., 2022). As stated previously, in our study no lesions are observed in our study and the relative abundance of *Firmicutes* and *Proteobacteria* were not affected either. Bortoluzzi et al. (2019) observed no difference on the relative abundance of the most abundant phyla (*Firmicutes*, *Bacteroidetes*, and *Proteobacteria*) between the challenged and unchallenged birds. But in our study, the challenge groups had lower abundance of *Bacteroidetes* which was inconsistent to Bortoluzzi et al. (2019). The *Bacteroidetes* phylum has the ability to degrade a wide range of complex carbohydrates, making its dominance in many diverse environments (McKee et al., 2021). Decreased abundance of *Bacteroidetes* indicates lower ability of the ileal microbes on degradation of complex carbohydrates. Coccidial infection can dramatically decrease the resident microbiota and increase conditionally pathogenic bacteria such as *Clostridiales* (Ramanan et al., 2016; Lu et al., 2021). It can lead to more severe clinical manifestations by providing an environment which is conducive for pathogenic bacteria, such as *Campylobacter jejuni*, *C. perfringens*, *Salmonella*, and other bacteria (Kogut et al., 1994; Ficko-Blean et al., 2012; Macdonald et al., 2019). Major perturbations in lactic acid-producing and butyrate-producing families of bacteria in chickens with NE were observed (Antonissen et al., 2016). However, the results have been inconsistent among studies due to the varying severity degree of NE. *Lactobacillus* is known as beneficial bacteria by competition with pathogens and produce lactic acid which can inhibit pathogenic bacteria (Belenguer et al., 2007). *Lactobacillus* was more abundant in the upper GI tract compared with the lower tract. *C. Perfringens* challenge could decrease the *Lactobacillus* population in ileum (Antonissen et al., 2016; Akerele et al., 2022). But this was not observed in our study. *Lactobacillus reuteri*, *L. johnsonii*, *L. acidophilus*, *L. crispatus*, *L. salivarius*, and *L. aviarius* were the predominant *Lactobacillus* species and present throughout the GI tract of chickens (Wang et al., 2014). Our results showed that at the species level, *L. aviarius* had the highest relative abundance which is similar to Gong et al. (2007)'s findings. *Lactobacillus aviarius* was first isolated from the intestine of chickens in Fujisawa et al. (1984) and is very useful enhancing immunity systems of the organisms (Al-Shaer et al., 2019). It has been reported that probiotics supplementation shifted bacterial community in broiler digestive tract, with *Lactobacillus salivarius* and *Lactobacillus aviarius* as dominant species in the treatment group. Some researchers reported suppressed *Lactobacillus* at the early stage of *C. perfringens* challenge (Fasina et al., 2016) whereas opposite findings were also reported by others (Liu et al., 2010). *C. perfringens* infection could suppress *L. aviarius* in the ileum of broilers (Du et al., 2015). In our study, the relative abundance of *Lactobacillus aviaries* was not different among all four groups. However, it should be noted that the variation of *Lactobacillus aviaries* abundance within groups was fairly high. *Lactobacillaceae* shift in broilers with NE induced by dual *E. maxima* and *C. perfringens* are dependent on breed whereas relative abundance of *Lactobacillus* was increasing in the ileal content of Cobb 500 broilers but decreasing in Ross 308 (Kim et al., 2015). In addition, the time of challenge may also play a role. In Yang et al. (2021)'s study, the chickens were inoculated with *E. maxima* on day 10 and 4×10^8 CFU of *C. perfringens* on day 14. In our Comb group, we did this on day 14 and day 17. Rearing conditions could also affect the gut microbial compositions for NE challenged birds. Bortoluzzi et al. (2019) found that the cecal microbiota composition and function was more affected than the ileal microbiota for NE challenged bird raised in floor pens with reused litter compared to birds raised in cages. *Motilimonas eburnea* in the order *Alteromonadales*, was first isolated from coastal sediment and this novel species was named by the authors (Ling et al., 2017). The reason that the C. Per and Comb groups had higher abundance is not clear as limited research was reported on this species. *Candidatus Arthromitus*, also known as *Candidatus Savagella*, may provide a protective role in preventing the onset of the enteric condition in Turkeys (Hedblom et al., 2018). It has the potential to serve as an immune-stimulatory probiotic making it an organism of great interest to poultry researchers. Stanley et al. (2012) reported decreased abundance of *Candidatus Arthromitus* in the cecal digesta of broiler chickens challenged with oocysts of *E. acervulina*, *E. maxima*, and *E. brunette*. This was similar to our study as that the Cocc and Comb groups with *Eimeria* challenge had significantly lower abundance than the control and the C. Per groups.

Studying the composition of the gut microbiota not only can reflect the relationship between microorganisms and the host but also provide information of the microbial functions on the gut (Bortoluzzi et al., 2019). To further understand the functions performed by the gut microbes, we used PICRUSt2 to make inferences about the metabolic functions of the gut microbes against the KEGG orthology database. We found that the top 10 microbial functions are most involved in the metabolism (starch and sucrose metabolism), Cellular Processes (Quorum sensing), genetic information processing (transcription factors), and Environmental Information Processing (ABC transporters). All these predicted functions were not affected by treatments. Bortoluzzi et al. (2019) reported that NE mainly affected microbial functions of cecal microorganisms not ileal microorganism. They observed NE challenge enriched pathways related to DNA replication,

proteins, amino acids related enzymes and metabolism, and transcription factors (Bortoluzzi et al., 2019). In that study, the challenged birds groups had enriched "ion channel" function compared to the control groups. We did not observe any difference regarding specific functions among the four groups and this might be because we analyzed the ileal digesta samples. Enriched pathways related to amino acid metabolism was observed in the challenged birds (Zhang et al., 2018; Yang et al., 2021). The possible reasons could be due to pathogens such as *Helicobacter pylori* and *Salmonella Typhimurium* which use amino acids as energy source (Zhang et al., 2018) or activated amino acid synthetic pathways in the remaining bacterial population to compensate for an inability of *C. perfringens* to synthesize amino acids (Yang et al., 2021). Yang et al. (2021) also suggested that metabolism of cofactors and vitamins may be enhanced in severe NE cases. In our study, the microbial functions were all predicted based on 16S rRNA sequencing data and follow-up metagenomics of the microbiota warrants further investigation.

Yellow-feather broiler, also known as three-yellow chicken (yellow feather, yellow skin, and yellow shank.) are high-quality chicken with excellent meat quality and flavor. They are mainly raised in south China. Researches on the inter relationship of NE and gut microbiota of yellow feather broilers were limited. An better understanding of the importance of gut microbiota in disease onset, progression, and treatment is utmost. The disease model would lay foundation for microbial manipulation of NE in yellow feather broilers. Further studies are needed to determine and improve the robustness and reproducibility of NE disease model.

Conclusion

The present study used *Eimeria* for NE reproduction to evaluate the effects of *C. perfringens* on ileal microbiota of yellow feather broilers. In summary, *C. perfringens* alone did not affect the alpha diversity of ileal microbiota in yellow feather broilers but co-infection with *Eimeria* significantly decreased the Shannon and Chao1 indices. *Eimeria* or *C. perfringens* challenge also decreased the relative abundance of beneficial bacteria including *Bacteroidetes* at the phylum level, *Faecalibacterium* at the genus level and *Candidatus Arthromitus* at the species level.

Data availability statement

The datasets presented in this study can be found in online repositories. The names of the repository/repositories and accession number(s) can be found below: Bioproject accession number: PRJNA892261.

Ethics statement

The animal study was reviewed and approved by the Institutional Animal Care and Use Committee of Foshan University.

Author contributions

XF, TL, and HZ conducted the experiment and wrote the manuscript together. LL and SB analyzed the samples. XC analyzed the data. HHZ provided critical feedback and helped shape the research. All authors contributed to the article and approved the submitted version.

Funding

This work received financial support from the Discipline Construction Program of Foshan University (CGZ0400162), the Scientific Research Foundation in the Higher Education Institutions of Educational Commission of Guangdong Province (2017GCZX006), the Guangdong Basic and Applied Basic Research Foundation (2019A1515110780), the Guangdong Province Modern Agriculture Poultry Industry Technology System Innovation Team Construction Project (2022KJ128), Special Projects in Key Fields of Guangdong Provincial Department of Education (2019KZDZX2006), the Guangdong Science and Technology Innovation Strategy Special Fund (DZX20192520309), the Research Start-Up Fund for Postdoctoral Fellows from Foshan City (BKS209059), and the Scientific Research Start-Up Fund for High-Level Talents of Foshan University (Gg07145).

Conflict of interest

Author LL was employed by Foshan Zhengdian Biology Technology Co., Ltd.

The remaining authors declare that the research was conducted in the absence of any commercial or financial relationships that could be construed as a potential conflict of interest.

Publisher's note

References

Akerele, G., Al Hakeem, W. G., Lourenco, J., and Selvaraj, R. K. (2022). The effect of necrotic enteritis challenge on production performance, cecal microbiome, and cecal tonsil transcriptome in broilers. *Pathogens* 11:839. doi: 10.3390/pathogens11080839

Al-Shaer, B. M., Al-Batshan, H. A., and Al-Atiyat, R. M. (2019). Effect of probiotics on diversity of bacterial community in the gastrointestinal tract of chickens. *Singapore J. Sci. Res.* 9, 86–94.

Antonissen, G., Eeckhaut, V., Van Driessche, K., Onrust, L., Haesebrouck, F., Ducatelle, R., et al. (2016). Microbial shifts associated with necrotic enteritis. *Avian Pathol.* 45, 308–312. doi: 10.1080/03079457.2016.1152625

Attree, E., Sanchez-Arsuaga, G., Jones, M., Xia, D., Marugan-Hernandez, V., Blake, D., et al. (2021). Controlling the causative agents of coccidiosis in domestic chickens; an eye on the past and considerations for the future. *CABI Agric. Biosci.* 2:37. doi: 10.1186/s43170-021-00056-5

Baba, E., Wakeshima, H., Fukui, K., Fukata, T., and Arakawa, A. (1992). Adhesion of bacteria to the cecal mucosal surface of conventional and germ-free chickens infected with *Eimeria tenella*. *Am. J. Vet. Res.* 53, 194–197.

Belenguer, A., Duncan, S. H., Holtrop, G., Anderson, S. E., Lobley, G. E., and Flint, H. J. (2007). Impact of pH on lactate formation and utilization by human fecal microbial communities. *Appl. Environ. Microbiol.* 73, 6526–6533. doi: 10.1128/AEM.00508-07

Bortoluzzi, C., Vieira, B. S., Hofacre, C., and Applegate, T. J. (2019). Effect of different challenge models to induce necrotic enteritis on the growth performance and intestinal microbiota of broiler chickens. *Poult. Sci.* 98, 2800–2812. doi: 10.3382/ps/pez084

Caly, D. L., D'Inca, R., Auclair, E., and Drider, D. (2015). Alternatives to antibiotics to prevent necrotic enteritis in broiler chickens: A microbiologist's perspective. *Front. Microbiol.* 6:1336. doi: 10.3389/fmicb.2015.01336

Collier, C. T., Hofacre, C. L., Payne, A. M., Anderson, D. B., Kaiser, P., Mackie, R. I., et al. (2008). Coccidia-induced mucogenesis promotes the onset of necrotic enteritis by supporting *Clostridium perfringens* growth. *Vet. Immunol. Immunopathol.* 122, 104–115. doi: 10.1016/j.vetimm.2007.10.014

Daneshmand, A., Kermanshahi, H., Mohammed, J., Sekhavati, M. H., Javadmanesh, A., Ahmadian, M., et al. (2022). Intestinal changes and immune responses during *Clostridium perfringens*-induced necrotic enteritis in broiler chickens. *Poult. Sci.* 101:101652. doi: 10.1016/j.psj.2021.101652

Douglas, G. M., Maffei, V. J., Zaneveld, J. R., Yurgel, S. N., Brown, J. R., Taylor, C. M., et al. (2020). PICRUSt2 for prediction of metagenome functions. *Nat. Biotechnol.* 38, 685–688. doi: 10.1038/s41587-020-0548-6

Du, E., Gan, L., Li, Z., Wang, W., Liu, D., and Guo, Y. (2015). In vitro antibacterial activity of thymol and carvacrol and their effects on broiler chickens challenged with *Clostridium perfringens*. *J. Anim. Sci. Biotechnol.* 6:58. doi: 10.1186/s40104-015-0055-7

Fasina, Y. O., Newman, M. M., Stough, J. M., and Liles, M. R. (2016). Effect of *Clostridium perfringens* infection and antibiotic administration on microbiota in the small intestine of broiler chickens. *Poult. Sci.* 95, 247–260. doi: 10.3382/ps/pev329

Feng, X., Zhu, H., Chen, B., Zhu, C., Gong, L., Hu, Z., et al. (2020). Effects of phytosterols supplementation on growth performance and intestinal microflora of yellow-feather broilers. *Poult. Sci.* 99, 6022–6030. doi: 10.1016/j.psj.2020.07.036

Ficko-Blean, E., Stuart, C. P., Suits, M. D., Cid, M., Tessier, M., Woods, R. J., et al. (2012). Carbohydrate recognition by an architecturally complex alpha-N-acetylglucosaminidase from *Clostridium perfringens*. *PLoS One* 7:e33524. doi: 10.1371/journal.pone.0033524

Forbes, J. D., Chen, C. Y., Knox, N. C., Marrie, R. A., El-Gabalawy, H., de Kievit, T., et al. (2018). A comparative study of the gut microbiota in immune-mediated inflammatory diseases-does a common dysbiosis exist? *Microbiome* 6:221. doi: 10.1186/s40168-018-0603-4

Fujisawa, T., Shirasaka, S., Watabe, J., and Mitsuoka, T. (1984). *Lactobacillus aviarius* sp. nov.: A new species isolated from the intestine of chickens. *Syst. Appl. Microbiol.* 5, 414–420. doi: 10.1016/S0723-2020(84)80042-9

Giannenas, I., Papadopoulos, E., Tsalie, E., Triantafillou, E., Henikl, S., Teichmann, K., et al. (2012). Assessment of dietary supplementation with probiotics on performance, intestinal morphology and microflora of chickens infected with *Eimeria tenella*. *Vet. Parasitol.* 188, 31–40. doi: 10.1016/j.vetpar.2012.02.017

Gong, J., Si, W., Forster, R. J., Huang, R., Yu, H., Yin, Y., et al. (2007). 16S rRNA gene-based analysis of mucosa-associated bacterial community and phylogeny in the chicken gastrointestinal tracts: From crops to ceca. *FEMS Microbiol. Ecol.* 59, 147–157. doi: 10.1111/j.1574-6941.2006.00193.x

Haas, B. J., Gevers, D., Earl, A. M., Feldgarden, M., Ward, D. V., Giannoukos, G., et al. (2011). Chimeric 16S rRNA sequence formation and detection in Sanger and 454-pyrosequenced PCR amplicons. *Genome Res.* 21, 494–504. doi: 10.1101/gr.112730.110

Hedblom, G. A., Reiland, H. A., Sylte, M. J., Johnson, T. J., and Baumler, D. J. (2018). Segmented filamentous bacteria - metabolism meets immunity. *Front. Microbiol.* 9:1991. doi: 10.3389/fmicb.2018.01991

Kim, J. E., Lillehoj, H. S., Hong, Y. H., Kim, G. B., Lee, S. H., Lillehoj, E. P., et al. (2015). Dietary *Capsicum* and *Curcuma longa* oleoresins increase intestinal microbiome and necrotic enteritis in three commercial broiler breeds. *Res. Vet. Sci.* 102, 150–158. doi: 10.1016/j.rvsc.2015.07.022

Kogut, M. H., Fukata, T., Tellez, G., Hargis, B. M., Corrier, D. E., and DeLoach, J. R. (1994). Effect of *Eimeria tenella* infection on resistance to *Salmonella* typhimurium colonization in broiler chicks inoculated with anaerobic cecal flora and fed dietary lactose. *Avian Dis.* 38, 59–64. doi: 10.2307/1591837

Ling, S. K., Guo, L. Y., Chen, G. J., and Du, Z. J. (2017). *Motilimonas eburnea* gen. nov., sp. nov., isolated from coastal sediment. *Int. J. Syst. Evol. Microbiol.* 67, 306–310. doi: 10.1099/ijsem.0.001621

Liu, D., Guo, Y., Wang, Z., and Yuan, J. (2010). Exogenous lysozyme influences *Clostridium perfringens* colonization and intestinal barrier function in broiler chickens. *Avian Pathol.* 39, 17–24. doi: 10.1080/03079450903447404

Lu, C., Yan, Y., Jian, F., and Ning, C. (2021). Coccidia-microbiota interactions and their effects on the host. *Front. Cell. Infect. Microbiol.* 11:751481. doi: 10.3389/fcimb.2021.751481

Macdonald, S. E., van Diemen, P. M., Martineau, H., Stevens, M. P., Tomley, F. M., Stabler, R. A., et al. (2019). Impact of *Eimeria tenella* Coinfection on *Campylobacter jejuni* Colonization of the Chicken. *Infect. Immun.* 87:e00772-18. doi: 10.1128/IAI.00772-18

Maioli, T. U., Borras-Nogues, E., Torres, L., Barbosa, S. C., Martins, V. D., Langella, P., et al. (2021). Possible benefits of *Faecalibacterium prausnitzii* for obesity-associated gut disorders. *Front. Pharmacol.* 12:740636. doi: 10.3389/fphar.2021.740636

McKee, L. S., La Rosa, S. L., Westereng, B., Eijsink, V. G., Pope, P. B., and Larsbrink, J. (2021). Polysaccharide degradation by the Bacteroidetes: Mechanisms and nomenclature. *Environ. Microbiol. Rep.* 13, 559–581. doi: 10.1111/1758-2229.12980

Miller, R. W., Skinner, E. J., Sulakvelidze, A., Mathis, G. F., and Hofacre, C. L. (2010). Bacteriophage therapy for control of necrotic enteritis of broiler chickens experimentally infected with *Clostridium perfringens*. *Avian Dis.* 54, 33–40. doi: 10.1637/8953-060509-Reg.1

Mitchell, L. A., and Koval, M. (2010). Specificity of interaction between *Clostridium perfringens* Enterotoxin and Claudin-Family tight junction proteins. *Toxins* 2, 1595–1611. doi: 10.3390/toxins2071595

Moore, R. J. (2016). Necrotic enteritis predisposing factors in broiler chickens. *Avian Pathol.* 45, 275–281. doi: 10.1080/03079457.2016.1150587

Perez, V. G., Jacobs, C. M., Barnes, J., Jenkins, M. C., Kuhlenschmidt, M. S., Fahey, G. C. Jr., et al. (2011). Effect of corn distillers dried grains with solubles and *Eimeria acervulina* infection on growth performance and the intestinal microbiota of young chicks. *Poult. Sci.* 90, 958–964. doi: 10.3382/ps.2010-01066

Ramanan, D., Bowcutt, R., Lee, S. C., Tang, M. S., Kurtz, Z. D., Ding, Y., et al. (2016). Helminth infection promotes colonization resistance via type 2 immunity. *Science* 352, 608–612. doi: 10.1126/science.aaf3229

Ritzi, M. M., Abdelrahman, W., Mohnl, M., and Dalloul, R. A. (2014). Effects of probiotics and application methods on performance and response of broiler chickens to an *Eimeria* challenge. *Poult. Sci.* 93, 2772–2778. doi: 10.3382/ps.2014-04207

Segata, N., Izard, J., Waldron, L., Gevers, D., Miropolsky, L., Garrett, W. S., et al. (2011). Metagenomic biomarker discovery and explanation. *Genome Biol.* 12:R60. doi: 10.1186/gb-2011-12-6-r60

Shojadoost, B., Vince, A. R., and Prescott, J. F. (2012). The successful experimental induction of necrotic enteritis in chickens by *Clostridium perfringens*: A critical review. *Vet. Res.* 43:74. doi: 10.1186/1297-9716-43-74

Skinner, J. T., Bauer, S., Young, V., Pauling, G., and Wilson, J. (2010). An economic analysis of the impact of subclinical (mild) necrotic enteritis in broiler chickens. *Avian Dis.* 54, 1237–1240. doi: 10.1637/9399-052110-Reg.1

Stanley, D., Keyburn, A. L., Denman, S. E., and Moore, R. J. (2012). Changes in the caecal microflora of chickens following *Clostridium perfringens* challenge to

induce necrotic enteritis. *Vet. Microbiol.* 159, 155–162. doi: 10.1016/j.vetmic.2012.03.032

Tang, D., Li, Z., Mahmood, T., Liu, D., Hu, Y., and Guo, Y. (2020). The association between microbial community and ileal gene expression on intestinal wall thickness alterations in chickens. *Poult. Sci.* 99, 1847–1861. doi: 10.1016/j.psj.2019.10.029

Timbermont, L., Haesebrouck, F., Ducatelle, R., and Van Immerseel, F. (2011). Necrotic enteritis in broilers: An updated review on the pathogenesis. *Avian Pathol.* 40, 341–347. doi: 10.1080/03079457.2011.590967

Van Immerseel, F., Rood, J. I., Moore, R. J., and Titball, R. W. (2009). Rethinking our understanding of the pathogenesis of necrotic enteritis in chickens. *Trends Microbiol.* 17, 32–36. doi: 10.1016/j.tim.2008.09.005

Wang, L., Fang, M., Hu, Y., Yang, Y., Yang, M., and Chen, Y. (2014). Characterization of the most abundant Lactobacillus species in chicken gastrointestinal tract and potential use as probiotics for genetic engineering. *Acta Biochim. Biophys. Sin. (Shanghai)* 42, 612–619. doi: 10.1093/abbs/gmu037

Williams, R. B. (2005). Intercurrent coccidiosis and necrotic enteritis of chickens: Rational, integrated disease management by maintenance of gut integrity. *Avian Pathol.* 34, 159–180. doi: 10.1080/03079450500112195

Wu, S. B., Stanley, D., Rodgers, N., Swick, R. A., and Moore, R. J. (2014). Two necrotic enteritis predisposing factors, dietary fishmeal and *Eimeria* infection, induce large changes in the caecal microbiota of broiler chickens. *Vet. Microbiol.* 169, 188–197. doi: 10.1016/j.vetmic.2014.01.007

Yang, Q., Liu, J., Wang, X., Robinson, K., Whitmore, M. A., Stewart, S. N., et al. (2021). Identification of an intestinal microbiota signature associated with the severity of necrotic enteritis. *Front. Microbiol.* 12:703693. doi: 10.3389/fmicb.2021.703693

Yang, W.-Y., Lee, Y., Lu, H., Chou, C. H., and Wang, C. (2019). Analysis of gut microbiota and the effect of lauric acid against necrotic enteritis in *Clostridium perfringens* and *Eimeria* side-by-side challenge model. *PLoS One* 14:e0205784. doi: 10.1371/journal.pone.0205784

Zaytsoff, S. J. M., Lyons, S. M., Garner, A. M., Uwiera, R. R. E., Zandberg, W. F., Abbott, D. W., et al. (2020). Host responses to *Clostridium perfringens* challenge in a chicken model of chronic stress. *Gut Pathog.* 12:24. doi: 10.1186/s13099-020-00362-9

Zhang, B., Lv, Z., Li, Z., Wang, W., Li, G., and Guo, Y. (2018). Dietary l-arginine supplementation alleviates the intestinal injury and modulates the gut microbiota in broiler chickens challenged by *Clostridium perfringens*. *Front. Microbiol.* 9:1716. doi: 10.3389/fmicb.2018.01716

frontiers | Frontiers in Microbiology

TYPE Original Research
PUBLISHED 01 December 2022
DOI 10.3389/fmicb.2022.1067173

OPEN ACCESS

EDITED BY
Kuan Zhao,
Hebei Agricultural University,
China

REVIEWED BY
Yankuo Sun,
South China Agricultural University, China
Zhendong Zhang,
Jiangsu University of Science and Technology, China

*CORRESPONDENCE
Guohui Zhou
zhouguohui@caas.cn
Hongliang Zhang
zhanghongliang01@caas.cn

†These authors have contributed equally to this work

SPECIALTY SECTION
This article was submitted to Infectious Agents and Disease, a section of the journal Frontiers in Microbiology

RECEIVED 11 October 2022
ACCEPTED 17 November 2022
PUBLISHED 01 December 2022

CITATION
Li C, Xu H, Zhao J, Gong B, Sun Q, Xiang L, Li W, Guo Z, Li J, Tang Y-d, Leng C, Peng J, Wang Q, An T, Cai X, Tian Z-J, Zhou G and Zhang H (2022) Epidemiological investigation and genetic evolutionary analysis of PRRSV-1 on a pig farm in China. *Front. Microbiol.* 13:1067173. doi: 10.3389/fmicb.2022.1067173

Epidemiological investigation and genetic evolutionary analysis of PRRSV-1 on a pig farm in China

Chao Li[1†], Hu Xu[1†], Jing Zhao[1†], Bangjun Gong[1], Qi Sun[1], Lirun Xiang[1], Wansheng Li[1], Zhenyang Guo[1], Jinhao Li[1], Yan-dong Tang[1], Chaoliang Leng[2], Jinmei Peng[1], Qian Wang[1], Tongqing An[1], Xuehui Cai[1], Zhi-Jun Tian[1], Guohui Zhou[1*] and Hongliang Zhang[1*]

[1]State Key Laboratory of Veterinary Biotechnology, Harbin Veterinary Research Institute, Chinese Academy of Agricultural Sciences, Harbin, China, [2]Henan Key Laboratory of Insect Biology in Funiu Mountain, Henan Provincial Engineering Laboratory of Insects Bio-Reactor, China-UK-NYNU-RRes Joint Laboratory of Insect Biology, Nanyang Normal University, Nanyang, China

Porcine reproductive and respiratory syndrome virus (PRRSV) has brought serious economic losses to pig industry. PRRSV-1 have existed in China for more than 25years. The prevalence and features of PRRSV-1 on Chinese farms are unclear. We continuously monitored PRRSV in a pig farm with strict biosafety measures in Henan Province, China, in 2020. The results showed that multiple types of PRRSV coexisted on this single pig farm. PRRSV-1 was one of the main circulating strains on the farm and was responsible for infections throughout nearly the entire epidemic cycle. Phylogenetic analysis showed that PRRSV-1 isolates from this pig farm formed an independent branch, with all isolates belonging to BJEU06-1-like PRRSV. The analysis of selection pressure on ORF5 on this branch identified 5 amino acids as positive selection sites, indicating that PRRSV-1 had undergone adaptive evolution on this farm. According to the analysis of ORF5 of PRRSV-1 on this farm, the evolutionary rate of the BJEU06-1-like branch was estimated to be 1.01×10^{-2} substitutions/site/year. To further understand the genome-wide characteristics of PRRSV-1 on this pig farm, two full-length PRRSV-1 genomes representative of pig farms were obtained. The results of amino acid alignment revealed that although one NSP2 deletion was consistent with BJEU06-1, different new features were found in ORF3 and ORF4. According to the above results, PRRSV-1 has undergone considerable evolution in China. This study is the first to report the prevalence and characteristics of PRRSV-1 on a large farm in mainland China, which will provide a reference for the identification and further prevention and control of PRRSV-1.

KEYWORDS

PRRSV-1, first detection, main epidemic strain, Chinese pig farm, evolution and genetic diversity

Introduction

Porcine reproductive and respiratory syndrome (PRRS) is among the most devastating diseases affecting the pig industry and mainly caused reproductive failure of sows and respiratory symptoms in pigs of all ages (An et al., 2011; Yuzhakov et al., 2017; VanderWaal and Deen, 2018). PRRSV has caused serious economic losses to commercial pig farms in China (Zhang et al., 2022). According to antigenicity, PRRSV isolates can be classified into two separate species, *Betaarterivirus suid 1* (PRRSV-1) and *Betaarterivirus suid 2* (PRRSV-2) which share 60% nucleotide identity at the whole-genome level (Brinton et al., 2021).

Similar to other RNA viruses, PRRSV shows a high evolutionary rate, generating a plethora of variants (Franzo et al., 2022). These mutations accumulate mainly in the NSP2 protein encoded by ORF1a and the GP3, GP4 and GP5 envelope proteins encoded by ORF3-5 (Le Gall et al., 1997; Allende et al., 2000; Chang et al., 2002). The GP5 protein plays an important role in inducing cross protection between virus neutralizing antibody and PRRSV mutation (Kim et al., 2013). Determining the selection pressure for genetic variation of PRRSV by ORF5 is an important part of many molecular evolution studies (Paploski et al., 2021). Moreover, gene recombination events can promote the diversity of PRRSV (Forsberg et al., 2002). Therefore, the long-term investigation of PRRSV infection on a single farm can be helpful for understanding and controlling PRRSV on swine farms (Kim et al., 2011; Li et al., 2021; Xiang et al., 2022).

PRRSV-1 first appeared in Europe and was subsequently reported in Asia, America and other places (Wensvoort et al., 1991; Chen et al., 2011). PRRSV-1 was further classified into four subtypes [subtype 1 (Global), subtype 1 (Russia), and subtypes 2 and 3] based on ORF5 sequences (Stadejek et al., 2006; Shi et al., 2010). Currently, only subtype 1 (Global) has been reported in countries spanning the globe, whereas other subtypes are mainly prevalent in Europe. In Asia, PRRSV-1 has been reported to exist in several countries, including China (Chen et al., 2011). In China, PRRSV-1 was first detected in 1997(Zhang et al., 2020b). Later, PRRSV-1 was sporadically reported around the country, and PRRSV-1 subtype 1 (Global) has been reported in more than 20 provinces in China to date (Zhou et al., 2015; Liu et al., 2017; Chen et al., 2020; Lin et al., 2020; Flay et al., 2022). At present, there are four main clusters of subtype 1 (Global) strains in China: Amervac-like, BJEU06-1-like, HKEU16-like and NMEU09-like (Chen et al., 2017). Recent studies have reported outbreaks of strains of this subtype on Russian pig farms, causing huge economic losses (Havas et al., 2022). Since the emergence of the BJEU06-1-like strain in China in 2006, there have been an increasing number of reports of PRRSV-1 (Chen et al., 2011; Wang et al., 2019; Chen et al., 2020). However, the prevalence and molecular characteristics of PRRSV-1 on Chinese pig farms are unknown. In this study, PRRSV was monitored on a pig-fattening farm, and we studied the epidemic process and molecular characteristics of PRRSV-1 isolates from this pig farm in detail.

Materials and methods

Farm information

A pig-finishing farm (500 head) that has been monitored for PRRSV was investigated in the study. The farm is located in Henan Province, China, and there are no neighboring pig farms within 3 km. The 500 piglets (42–49 days old) entered the farm at the same time. Since no cases of PRRSV had been found on this farm, PRRSV-related vaccines had not been administered. A total of 50 serum samples were collected at a ratio of 1:10 from piglets before they were transported to the farm to identify PRRSV antigens by RT-PCR and antibodies by ELISA, and the results were negative for PRRSV antigens, with an 85% antibody-positive rate.

Sample collection

During the study period, samples were randomly collected in each breeding unit by resident professional veterinarians, and samples (lung, jaw lymph, and blood) were submitted for laboratory testing every 15 days. A total of 132 samples were collected and tested (Supplementary Table S1).

RNA extraction, PCR screening and sequencing

Tissue sample disposal, RNA extraction, PCR screening and sequencing were conducted as previously described(Xiang et al., 2022). The primers designed to detect PRRSV and to amplify the whole genome are shown in Supplementary Table S2.

Phylogenetic analysis

Representative PRRSV-1 strains were used as reference strains (Stadejek et al., 2008; Shi et al., 2010; Chen et al., 2017). All data on the reference strains shown in Supplementary Table S3 were downloaded from the NCBI database. All sequences were aligned using MAFFT version 7 in BioAider V1.423 (Katoh and Standley, 2013; Zhou et al., 2020) with the default parameters and were manually adjusted in MEGA6 (Tamura et al., 2013). Phylogenetic trees were constructed as previously described (Jin and Nei, 1990; Ripplinger and Sullivan, 2008; Li et al., 2021).

Estimation of evolutionary rates

Maximum-likelihood (ML) phylogeny was constructed by IQ-TREE (Nguyen et al., 2015). To ensure sufficient time structures in alignment for reliable rate estimates, we first regressed root-to-tip genetic distances in ML trees using TempEst to determine accurate sampling dates (Rambaut et al., 2016). The

collected PRRSV-1 ORF5 sequences were analyzed using the BEAST 1.10.4 package (Kalyaanamoorthy et al., 2017; Zhang et al., 2020a). All analyses were conducted as previously described (Li et al., 2021; Xiang et al., 2022).

Positive selection pressure analysis

An analysis of the selection pressure acting on the ORF5 codons of PRRSV-1, including 12 new isolates and 129 PRRSV-1 reference strains (Supplementary Table S3), was conducted using the Datamonkey webserver[1] (Delport et al., 2010).

Recombinant analysis

The preliminary identification of possible recombination events in our sample sequences was performed using RDP4 (Sharma et al., 2013).

Results and discussion

Dynamics of PRRSV on the farm

A total of 132 samples were collected over 150 days, and samples were sent for testing every 15 days, which was recorded as one time period. Sample details are shown in Supplementary Table S1. After RT–PCR analysis, 38 samples were identified as PRRSV antigen-positive samples, and the positive rate was approximately 28.79%. The presence of PRRSV was detected in eight of the ten time periods, and the highest positivity rate was 57.14% on days 106 to 120 (Figure 1A). To explore the distribution of PRRSV subtypes on this farm, a total of 13 partial NSP2 sequences, 27 ORF5 sequences and 24 partial ORF7 sequences were obtained, and a phylogenetic tree was constructed based on ORF5 and ORF7 (Supplementary Figure S1; Table 1); 14 of these samples were identified as PRRSV-1 (36.94%), 14 as HP-PRRSV-like (36.94%), 10 as NADC30-like PRRSV (26.32%), and 1 as ATCC-VR2332-like PRRSV (2.63%). Therefore, PRRSV-1, HP-PRRSV-like, and NADC30-like PRRSV strains were the main epidemic strains on this farm, which presented multiple types of PRRSV coinfection. The results showed that PRRSV was detected in eight of the ten evaluated time periods, and the presence of PRRSV-1 was detected in seven of these, with the highest percentage of PRRSV-1 positivity consistently found from days 0–75 (Figure 1). The identification of PRRSV-1 as a dominant strain on a Chinese pig-fattening farm is reported for the first time in this study.

Since the first PRRSV strain was reported in China in 1996, PRRSV has been a major threat to Chinese pig farms. Considering the increasing reports of PRRSV-1 across China since 2011 (Chen et al., 2017, 2020), we speculate that coinfection with PRRSV-1 and PRRSV-2 may have profound effects on pig farms. During the course of this study, we discovered an interesting phenomenon: we detected the presence of PRRSV in the first time period (0–15 days) even though the pigs on this farm had never been infected with PRRSV before, and the PRRSV antigen results obtained during the entry of the pigs at this time were negative. Nevertheless, latent PRRSV infection has always been a very troublesome problem, and results similar to those obtained in this study have appeared in previous studies (Kick et al., 2019), in which PRRSV could not be detected in certain time periods. Therefore, we speculate that the piglets were latently infected with PRRSV before they entered the farm.

Sequence analysis of ORF5 of PRRSV-1

A total of 12 complete ORF5 sequences of PRRSV-1 were identified. The ORF5 nucleotide homology of the 12 strains was between 97.9–100%. Previous studies have reported that PRRSV-1 can be divided into 4 subtypes, among which only subtype 1 has been found in China, and four groups have ultimately been formed: Amervac-like, BJEU06-1-like, HKEU16-like and NMEU09-like (Chen et al., 2017). To understand the origin and evolution of PRRSV-1 on this farm, the available data on all PRRSV-1 from China and some other representative strains of PRRSV-1 were downloaded from NCBI and compared (Supplementary Table S3). A phylogenetic tree of the PRRSV-1 isolates analyzed in this study was constructed according to a previously reported typing method (Chen et al., 2017), and the results showed that the PRRSV-1 strains on this pig-finishing farm were BJEU06-1-like strains (Figure 2A). BJEU06-1-like strains first appeared in mainland China in 2006, and the spread of these strains in China has been reported several times since then (Chen et al., 2011; Liu et al., 2017; Zhang et al., 2020b). By comparing the homology of ORF5 nucleotide sequences from this branch, it was found that the identity of PRRSV-1 strains from this pig farm with other strains of this branch was between 85.0–88.8% (Supplementary Table S4), representing a reduction in homology compared to the previous results for this branch (87.5–94.2%, Supplementary Table S5). Therefore, the BJEU06-1-like group has been circulating since its emergence in China and has continued to evolve. While early studies suggested that a lower degree of variability might exist in PRRSV-1 (Suarez et al., 1996; Drew et al., 1997), later studies in some countries, such as Denmark and Italy, reported high divergence of PRRSV-1 isolates (Oleksiewicz et al., 2000; Forsberg et al., 2001, 2002). To understand the genetic evolution of PRRSV-1 isolated from this pig farm in China, the ORF5 sequences of PRRSV-1 isolated on this farm were compared with those of PRRSV-1 isolates previously reported in China, and the results showed that the consistency was between 79.9 and 88.8% (Supplementary Table S5). Additionally, the nucleotide sequence identity of BJEU06-1 strains on this pig farm was as high

1 http://www.datamonkey.org/

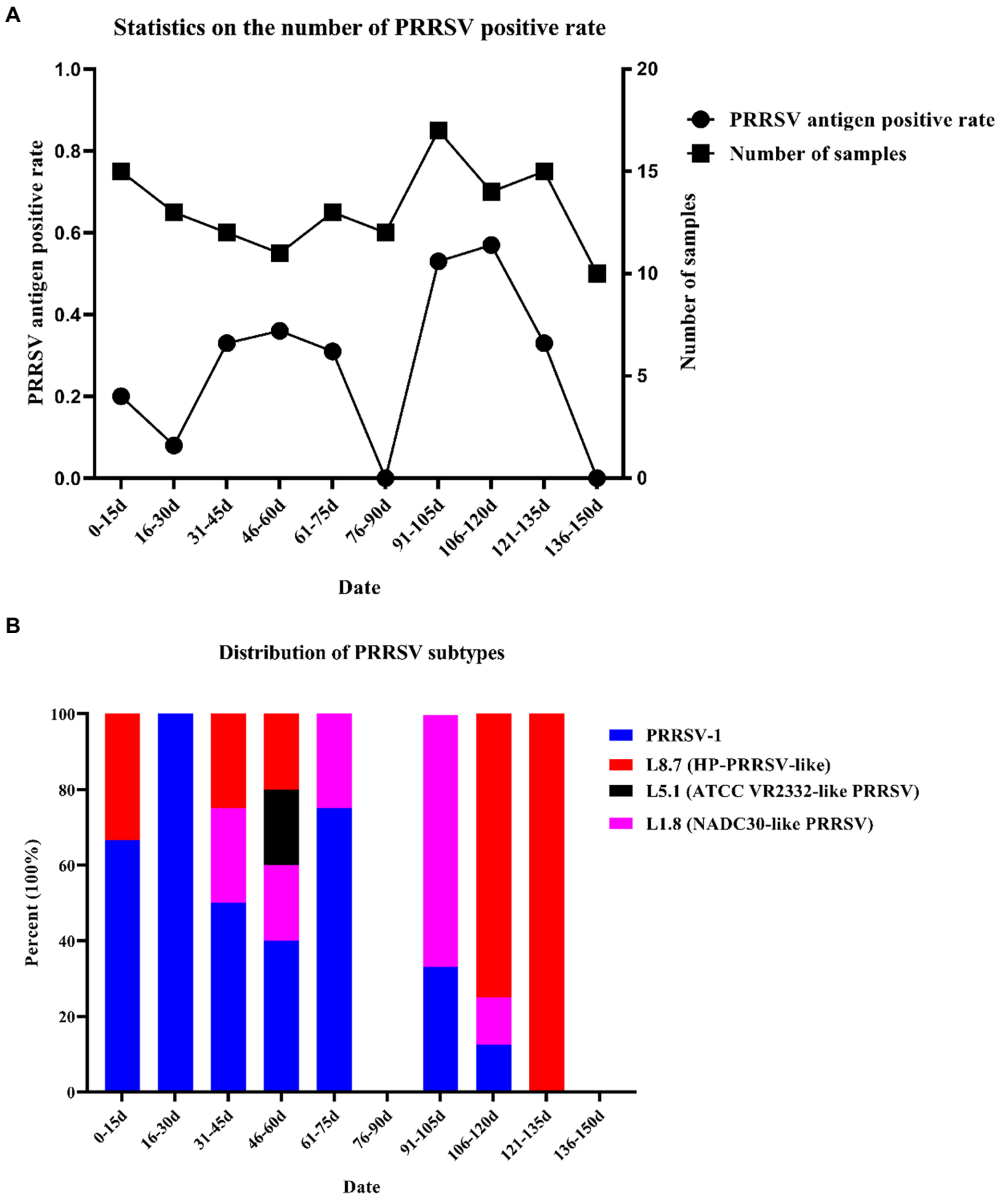

FIGURE 1
Number of samples collected and statistics of virus subtypes. **(A)** Number of samples tested and number of PRRSV stains detected. **(B)** Distribution of PRRSV subtypes.

as 97.9–100%, so we speculate that the PRRSV-1 isolates identified on this farm evolved from a single strain.

Evolution of ORF5 of PRRSV-1 on the farm during the study

The evolution of a single strain on the farm created favorable conditions for estimating the evolutionary time of this type of strain (Li et al., 2021). The PRRSV-1 strains from this farm showed a strong time signal [the correlation (r^2) between the genetic difference and sampling time was 0.28] and were thus suitable for molecular clock-based phylogenetic analysis. The PRRSV-1 isolates showed a lower mutation rate [1.01×10^{-2} substitutions/site/year, 95% highest posterior density (3.18×10^{-3}/ ~ 1.66×10^{-2})] than PRRSV-1 isolates from other countries (1.47×10^{-2} substitutions/site/year) but a higher mutation rate than PRRSV-2 (9.6×10^{-3} substitutions/site/year; Kim et al., 2011; Li et al., 2021; Xiang et al., 2022). The higher evolutionary rate provides a theoretical basis for the differentiation of the BJEU06-1-like branch, and this result suggests that this branch may accumulate many mutations in

TABLE 1 PRRSV identification information.

Number	Sample serial number	PRRSV		
		NSP2	ORF5	ORF7
1	TZJ220	\[a]	\	L8.7 (HP-PRRSV-like)
2	TZJ226	\	PRRSV-1	PRRSV-1
3	TZJ227	\	PRRSV-1	PRRSV-1
4	TZJ234	\	PRRSV-1	PRRSV-1
5	TZJ242	\	L8.7 (HP-PRRSV-like)	\
6	TZJ609	\	PRRSV-1	PRRSV-1
7	TZJ612	\	\	L1.8 (NADC30-like PRRSV)
8	TZJ613	\	PRRSV-1	PRRSV-1
9	TZJ620	L1.8 (NADC30-like PRRSV)	ATCC-VR2332	\
10	TZJ622	\	PRRSV-1	PRRSV-1
11	TZJ623	\	L8.7 (HP-PRRSV-like)	\
12	TZJ624	\	PRRSV-1	PRRSV-1
13	TZJ636	\	L1.8 (NADC30-like PRRSV)	L1.8 (NADC30-like PRRSV)
14	TZJ637	\	PRRSV-1	PRRSV-1
15	TZJ641	\	\	PRRSV-1
16	TZJ642	\	PRRSV-1	PRRSV-1
17	TZJ643			
18	TZJ657	\	PRRSV-1	PRRSV-1
19	TZJ658	\	\	L1.8 (NADC30-like PRRSV)
20	TZJ659	\	PRRSV-1	PRRSV-1
21	TZJ660	\	PRRSV-1	PRRSV-1
22	TZJ661	\	\	L1.8 (NADC30-like PRRSV)
23	TZJ663	\	\	L1.8 (NADC30-like PRRSV)
24	TZJ664	\	\	L1.8 (NADC30-like PRRSV)
25	TZJ669	\	\	L1.8 (NADC30-like PRRSV)
26	TZJ670	\	\	L1.8 (NADC30-like PRRSV)
27	TZJ672	\	\	L1.8 (NADC30-like PRRSV)
28	TZJ675	\	\	PRRSV-1
29	TZJ679	L8.7 (HP-PRRSV-like)	L8.7 (HP-PRRSV-like)	\
30	TZJ680	L8.7 (HP-PRRSV-like)	L8.7 (HP-PRRSV-like)	\
31	TZJ681	L8.7 (HP-PRRSV-like)	L8.7 (HP-PRRSV-like)	\
32	TZJ683	L8.7 (HP-PRRSV-like)	L8.7 (HP-PRRSV-like)	\
33	TZJ684	L8.7 (HP-PRRSV-like)	L8.7 (HP-PRRSV-like)	\
34	TZJ685	L8.7 (HP-PRRSV-like)	L8.7 (HP-PRRSV-like)	\
35	TZJ686	L8.7 (HP-PRRSV-like)	L8.7 (HP-PRRSV-like)	\
36	TZJ687	L8.7 (HP-PRRSV-like)	L8.7 (HP-PRRSV-like)	\
37	TZJ688		L8.7 (HP-PRRSV-like)	\
38	TZJ690	L8.7 (HP-PRRSV-like)	L8.7 (HP-PRRSV-like)	\
39	TZJ692	L8.7 (HP-PRRSV-like)	L8.7 (HP-PRRSV-like)	\

\[a]: Sequence not detected.

the next short time period. During the rapid evolution of the virus, natural selection is generally imposed episodically. A growing number of studies have reported the emergence of virulent strains during PRRSV evolution (An et al., 2010; Havas et al., 2022; Yuan et al., 2022), associated with significant economic losses. Therefore, for PRRSV-1 monitoring, more data should be obtained to prevent the occurrence of tragic outcomes.

Positive selection pressure analysis of ORF5 of PRRSV-1 on this pig farm

The GP5 protein of PRRSV is one of the most important structural proteins exposed on the surface of the virion and contains epitopes involved in virus neutralization and protection (Music and Gagnon, 2010). The identification of point mutations under positive selection pressure is often interpreted as evidence

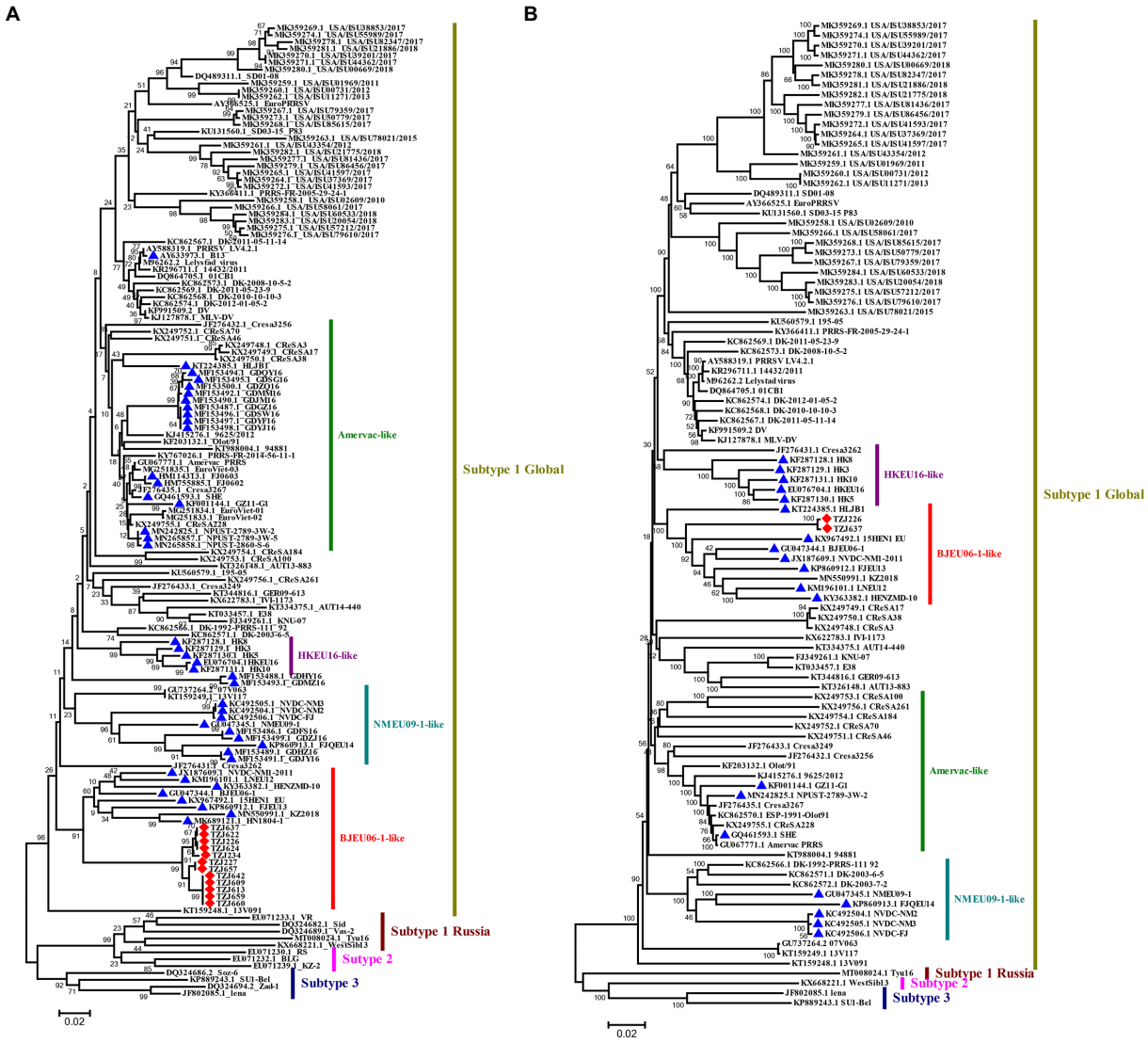

FIGURE 2
Phylogenetic analysis of PRRSV-1. **(A)** Phylogenetic tree constructed based on the ORF5 gene of PRRSV-1 isolates and reference PRRSV strains from each subtype. **(B)** Phylogenetic tree constructed based on full-length genomes of 2 PRRSV-1 isolates and reference PRRSV strains from each subtype. In the NCBI library, the PRRSV-1 strains from China and the PRRSV-1 strains from the pig farm are marked with ▲ and ◆, respectively. Chinese PRRSV 1 isolates all belong to subtype 1 and can be divided into four subgroups (Amervac-like, BJEU06-1-like, HKEU16-like, and NMEU09-1-like isolates). The scale bars indicate the number of nucleotide substitutions per site.

of increased evolutionary fitness (Kryazhimskiy and Plotkin, 2008). Selection pressure analysis of the ORF5 gene revealed four positively selected sites (amino acids 2, 8, 10 and 106) based on at least three methods (Table 2). The identified positively selected sites were diverse, and most of the sites were hydrophilic (Table 3). There were no regular changes in the polarity of the positively selected amino acids, but a change from a nonpolar amino acid (F) at position 10 to a polar amino acid (S) was observed (Table 3). Selection pressure analysis revealed that the ORF5 gene had experienced positive selection, and several positively selected sites were identified, which could help to identify the molecular determinants of virulence or pathogenesis and to clarify the driving force of PRRSV-1 evolution in China.

Whole-genome analysis of TZJ226 and TZJ637

To explore the genomic characteristics of PRRSV-1 on this pig farm, the full-length genomes of TZJ226 (the first PRRSV-1 isolate from this farm) and TZJ637 (PRRSV-1 from the fifth of the ten time periods, to analyze whether the full-length PRRSV-1 genome showed variation over a shorter time period) were evaluated in this study. The complete genomes of TZJ226 and TZJ637 were 15,068 nucleotides (nt) in length, excluding the poly (A) tail (Supplementary Table S6). The nucleotide homology between the two strains was approximately 99.7%, and combined with ORF5 nucleotide

TABLE 2 Selection pressure analysis of the GP5 protein of PRRSV.

Protein	Codon	SLAC		FEL		MEME		FUBAR	
		dN-dS	*p*	alpha = beta	*p*	*β*+	*p*	*β*-α	Post.pr.
GP5	2	1.07	0.0362	0.111	0.005	0.45	1	0.656	0.973
	8	1.91	0.00182	\	0.7368	1.03	1	1.61	0.995
	10	0.895	0.102	10,268	0.0469	4.45	0.17	0.557	0.938
	106	1.87	0.0718	1.731	0.0301	4.74	0.51	3.853	0.881

The sites found to be under positive selection (significance value) by at least three methods are shown. Codons with $p < 0.1$ by the SLAC method, $p < 0.1$ by the FEL method, $p < 0.1$ by the MEME method, or Post.pr. A value ≥0.9 by the FUBAR method was considered to be under positive selection.

TABLE 3 Positions and polarities of the positively selected amino acids.

Sites	2		8			10	106		
Majority	T^0		E^-			S^0	N^0		
Substitution	R^+	K^+	G^0	$V^\times$	$A^\times$	$F^\times$	G^0	R^+	K^+

The polarities of positively selected aa are indicated at the top-right corner of each amino acids. ×: Nonpolar amino acids (hydrophobic). +: Positively charged amino acids (hydrophilic). −: Negatively charged amino acids (hydrophilic). 0: Uncharged amino acids (hydrophilic).

homology, these results genetically indicated that the different PRRSV-1 isolates from this pig farm evolved from the same strain. To determine the phylogenetic relationship of the isolates from this farm with other PRRSV-1 isolates, a whole-genome-based phylogenetic tree was constructed based on all 98 available PRRSV-1 genomes (Figure 2B). The phylogenetic tree showed that the farm PRRSV-1 strain still belonged to BJEU06-1-like according to genome-wide typing. BLAST searches of TZJ226 and TZJ637 in the NCBI database showed the highest consistency with BJEU06-1 (GU047344.1). Compared with the BJEU06-1 strain, their nucleotide identities were 88.4 and 88.5%, representing reductions in homology compared to the previous results for this branch (89.5–93.8%). These results indicated that the BJEU06-1-like breach in China experienced a great deal of variation at the whole-genome level. Combined with the above ORF5 analysis, the homology of the BJEU06-1-like branch was observed to be further reduced, and the results showed that PRRSV-1 is undergoing rapid evolution in China.

Each fragment of the TZJ226 and TZJ637 genomes was compared with eight representative strains, and characteristic changes were identified in NSP2, GP3 and GP4 (Figure 3). TZJ226 and TZJ637 are similar to the BJEU06-1-like branch, with a 4 amino acids deletion between aa 356 and 359 and a 1 amino acids deletion at position 411 of NSP2 (Figure 3A). The highly variable PRRSV protein NSP2 is the least conserved viral protein (Allende et al., 1999). Previous molecular epidemiological studies of PRRSV have shown that NSP2 sequences with specific amino acid deletions can easily become characteristic sequences of dominant strains or local epidemic strains, as found in HP-PRRSV, NADC30-like PRRSV and NADC34-like PRRSV (Tong et al., 2007; Zhao et al., 2015; Xu et al., 2020). Hence, our findings are useful for understanding the epidemiological changes in PRRSV-1.

Among the structural proteins of PRRSV-1, ORF3 and ORF4 contain hypervariable regions similar to those of NSP2 (Supplementary Table S6); these hypervariable regions include aa237 to 252 of ORF3 and aa57 to 72 of ORF4. The structural protein encoded by ORF3 in these two strains showed premature termination (Figure 3B): ORF3 was found to be terminated 25 aa early in the TZJ226 and TZJ637 strains in this study. This study is the first to report the 25-aa premature termination of ORF3 of PRRSV-1. The consecutive deletion of 5 aa from positions 59 to 63 of ORF4 was found in TZJ226 and TZJ637 (Figure 3C). In regard to amino acid sequence analysis, the hypervariable region of GP4 extended from 49 to 72 aa; in particular, the 57–68-aa region was revealed to represent the core site of the neutralizing antibody in earlier studies (Vanhee et al., 2010, 2011). Importantly, PRRSV GP4 is a major determinant of viral cellular tropism (Tian et al., 2012). Previous studies have shown that GP4 interacts with CD163, an indispensable receptor for PRRSV infection (Das et al., 2010; Tian et al., 2012). Here, we provide more data to facilitate the study of its biological function. A previous report indicated that ORF3/4 deletion mutants probably evolved from deletion mutant progenitors originating in the Danish epidemic (Chen et al., 2017). It has been reported that PRRSV-1 reported in China may be the product of ancestral isolates introduced from continental Europe that spread to different regions of China and independently experienced mutational accumulation (Chen et al., 2017).

Recombination analysis

To determine whether recombination events played a role in the generation of the TZJ226 and TZJ637 isolates, RDP4 analysis was performed based on the multiple alignment of 98 PRRSV-1 genomes, and no obvious recombination was found.

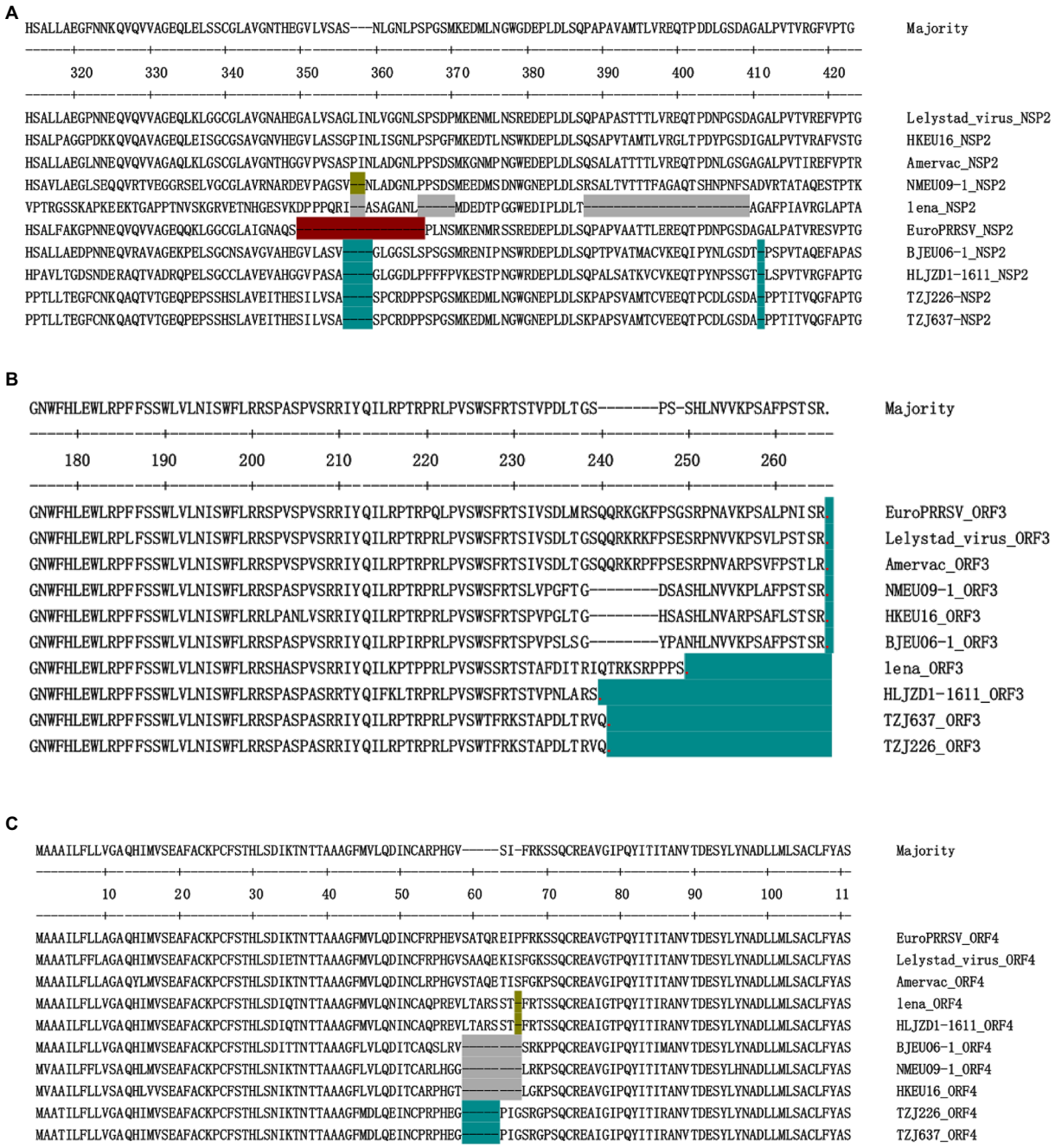

FIGURE 3
Identification of PRRSV strains with amino acid deletions in NSP2, ORF3 and ORF4. **(A)** Sequence alignment of NSP2 proteins, different aa deletion patterns are indicated by different colors. Similar to the BJEU06-1 strain, TZJ226 and TZJ637 PRRSV show deletions of 4 amino acids and 1 amino acid, respectively, corresponding to positions 356–359 and 411 of the Lelystad NSP2 protein. **(B)** Sequence alignment of ORF3 proteins. Stop codons are represented by red dots, and the number of amino acids lacking due to premature termination relative to Lelystad is indicated by an azure background. **(C)** Sequence alignment of ORF4 proteins, different aa deletion patterns are indicated by different colors. TZJ226 and TZJ637 shared the same 5-aa deletion, labeled with an azure background, corresponding to positions 59–63 of the Lelystad NSP2 protein. The positions marked in the figure represent the positions of the amino acid sequences and refer to the positions in Lelystad.

Conclusion

In summary, PRRSV-1 was first reported as one of the main endemic strains on a pig farm where multiple PRRSV subtypes coexist. The PRRSV-1 strains of this farm belong to the BJEU06-1-like branch of subtype 1, and this clade presents high strain diversity. Whole-genome analysis revealed that the same 4 + 1 aa deletion signature found in BJEU06-1-like is present in NSP2 and

identified two novel signatures, a 25-aa premature termination in ORF3 and the consecutive deletion of 5 aa in ORF4. Therefore, we should prioritize the continuous monitoring of PRRSV-1 and the strengthening of PRRSV prevention and control measures.

Data availability statement

The datasets presented in this study can be found in online repositories. The names of the repository/repositories and accession number(s) can be found at: https://www.ncbi.nlm.nih.gov/genbank/, OP566682; https://www.ncbi.nlm.nih.gov/genbank/, OP566683.

Funding

This study was supported by grants from the National Natural Science Foundation of China (grant nos. 32002315 and 32172890), the China Postdoctoral Fund (grant no. 2020M680788), the Key Programme Foundation of Higher Education of Educational Commission of Henan Province (22A230016) and the National Center of Technology Innovation for Pigs.

Author contributions

GZ, HZ, LX, and Z-JT: conceptualization. CLi, HX, QS, and JZ: data curation. WL, JL, ZG, QW, CLe, JP, Y-dT, GZ, and JZ: sample collection. CLi and HX: writing—original draft preparation. CLi and JZ: writing—review and editing. Z-JT, BG, TA, and XC: supervision. GZ, HZ, and Z-JT: project administration. All authors have read and agreed to the published version of the manuscript.

Conflict of interest

The authors declare that the research was conducted in the absence of any commercial or financial relationships that could be construed as a potential conflict of interest.

Publisher's note

All claims expressed in this article are solely those of the authors and do not necessarily represent those of their affiliated organizations, or those of the publisher, the editors and the reviewers. Any product that may be evaluated in this article, or claim that may be made by its manufacturer, is not guaranteed or endorsed by the publisher.

Supplementary material

The Supplementary material for this article can be found online at: https://www.frontiersin.org/articles/10.3389/fmicb.2022.1067173/full#supplementary-material

References

Allende, R., Laegreid, W. W., Kutish, G. F., Galeota, J. A., Wills, R. W., and Osorio, F. A. (2000). Porcine reproductive and respiratory syndrome virus: description of persistence in individual pigs upon experimental infection. *J. Virol.* 74, 10834–10837. doi: 10.1128/jvi.74.22.10834-10837.2000

Allende, R., Lewis, T. L., Lu, Z., Rock, D. L., Kutish, G. F., Ali, A., et al. (1999). North American and European porcine reproductive and respiratory syndrome viruses differ in non-structural protein coding regions. *J. Gen. Virol.* 80, 307–315. doi: 10.1099/0022-1317-80-2-307

An, T. Q., Tian, Z. J., Leng, C. L., Peng, J. M., and Tong, G. Z. (2011). Highly pathogenic porcine reproductive and respiratory syndrome virus, Asia. *Emerg. Infect. Dis.* 17, 1782–1784. doi: 10.3201/eid1709.110411

An, T. Q., Tian, Z. J., Xiao, Y., Li, R., Peng, J. M., Wei, T. C., et al. (2010). Origin of highly pathogenic porcine reproductive and respiratory syndrome virus, China. *Emerg. Infect. Dis.* 16, 365–367. doi: 10.3201/eid1602.090005

Brinton, M. A., Gulyaeva, A. A., Balasuriya, U. B. R., Dunowska, M., Faaberg, K. S., Goldberg, T., et al. (2021). ICTV virus taxonomy profile: Arteriviridae 2021. *J. Gen. Virol.* 102:001632. doi: 10.1099/jgv.0.001632

Chang, C. C., Yoon, K. J., Zimmerman, J. J., Harmon, K. M., Dixon, P. M., Dvorak, C. M., et al. (2002). Evolution of porcine reproductive and respiratory syndrome virus during sequential passages in pigs. *J. Virol.* 76, 4750–4763. doi: 10.1128/jvi.76.10.4750-4763.2002

Chen, N., Cao, Z., Yu, X., Deng, X., Zhao, T., Wang, L., et al. (2011). Emergence of novel European genotype porcine reproductive and respiratory syndrome virus in mainland China. *J. Gen. Virol.* 92, 880–892. doi: 10.1099/vir.0.027995-0

Chen, N., Liu, Q., Qiao, M., Deng, X., Chen, X., and Sun, M. (2017). Whole genome characterization of a novel porcine reproductive and respiratory syndrome virus 1 isolate: genetic evidence for recombination between Amervac vaccine and circulating strains in mainland China. *Infect. Genet. Evol.* 54, 308–313. doi: 10.1016/j.meegid.2017.07.024

Chen, N., Xiao, Y., Ye, M., Li, X., Li, S., Xie, N., et al. (2020). High genetic diversity of Chinese porcine reproductive and respiratory syndrome viruses from 2016 to 2019. *Res. Vet. Sci.* 131, 38–42. doi: 10.1016/j.rvsc.2020.04.004

Das, P. B., Dinh, P. X., Ansari, I. H., de Lima, M., Osorio, F. A., and Pattnaik, A. K. (2010). The minor envelope glycoproteins GP2a and GP4 of porcine reproductive and respiratory syndrome virus interact with the receptor CD163. *J. Virol.* 84, 1731–1740. doi: 10.1128/JVI.01774-09

Delport, W., Poon, A. F., Frost, S. D., and Kosakovsky Pond, S. L. (2010). Datamonkey 2010: a suite of phylogenetic analysis tools for evolutionary biology. *Bioinformatics* 26, 2455–2457. doi: 10.1093/bioinformatics/btq429

Drew, T. W., Lowings, J. P., and Yapp, F. (1997). Variation in open reading frames 3, 4 and 7 among porcine reproductive and respiratory syndrome virus isolates in the UK. *Vet. Microbiol.* 55, 209–221. doi: 10.1016/s0378-1135(96)01328-4

Flay, K. J., Yang, D. A., Choi, S. C., Ip, J., Lee, S. H., and Pfeiffer, D. U. (2022). First study to describe the prevalence of porcine reproductive and respiratory syndrome virus and porcine Circovirus type 2 among the farmed pig population in the Hong Kong special administrative region. *Vet. Sci.* 9:80. doi: 10.3390/vetsci9020080

Forsberg, R., Oleksiewicz, M. B., Petersen, A. M., Hein, J., Botner, A., and Storgaard, T. (2001). A molecular clock dates the common ancestor of European-type porcine reproductive and respiratory syndrome virus at more than 10 years before the emergence of disease. *Virology* 289, 174–179. doi: 10.1006/viro.2001.1102

Forsberg, R., Storgaard, T., Nielsen, H. S., Oleksiewicz, M. B., Cordioli, P., Sala, G., et al. (2002). The genetic diversity of European type PRRSV is similar to that of the north American type but is geographically skewed within Europe. *Virology* 299, 38–47. doi: 10.1006/viro.2002.1450

Franzo, G., Faustini, G., Legnardi, M., Cecchinato, M., Drigo, M., and Tucciarone, C. M. (2022). Phylodynamic and phylogeographic reconstruction of porcine reproductive and respiratory syndrome virus (PRRSV) in Europe: patterns and determinants. *Transbound. Emerg. Dis.* 69, e2175–e2184. doi: 10.1111/tbed.14556

Havas, K. A., Makau, D. N., Shapovalov, S., Tolkova, E., VanderWaal, K., Tkachyk, T., et al. (2022). A molecular and epidemiological description of a severe

porcine reproductive and respiratory syndrome outbreak in a commercial swine production system in Russia. *Viruses* 14:375. doi: 10.3390/v14020375

Jin, L., and Nei, M. (1990). Limitations of the evolutionary parsimony method of phylogenetic analysis. *Mol. Biol. Evol.* 7, 82–102. doi: 10.1093/oxfordjournals.molbev.a040588

Kalyaanamoorthy, S., Minh, B. Q., Wong, T. K. F., von Haeseler, A., and Jermiin, L. S. (2017). ModelFinder: fast model selection for accurate phylogenetic estimates. *Nat. Methods* 14, 587–589. doi: 10.1038/nmeth.4285

Katoh, K., and Standley, D. M. (2013). MAFFT multiple sequence alignment software version 7: improvements in performance and usability. *Mol. Biol. Evol.* 30, 772–780. doi: 10.1093/molbev/mst010

Kick, A. R., Amaral, A. F., Cortes, L. M., Fogle, J. E., Crisci, E., Almond, G. W., et al. (2019). The T-cell response to type 2 porcine reproductive and respiratory syndrome virus (PRRSV). *Viruses* 11:796. doi: 10.3390/v11090796

Kim, W. I., Kim, J. J., Cha, S. H., Wu, W. H., Cooper, V., Evans, R., et al. (2013). Significance of genetic variation of PRRSV ORF5 in virus neutralization and molecular determinants corresponding to cross neutralization among PRRS viruses. *Vet. Microbiol.* 162, 10–22. doi: 10.1016/j.vetmic.2012.08.005

Kim, H. K., Park, S. J., Rho, S. M., Han, J. Y., Nguyen, V. G., and Park, B. K. (2011). One year's study of dynamic and evolution of types I and II PRRSV in a swine farm. *Vet. Microbiol.* 150, 230–238. doi: 10.1016/j.vetmic.2011.01.025

Kryazhimskiy, S., and Plotkin, J. B. (2008). The population genetics of dN/dS. *PLoS Genet.* 4:e1000304. doi: 10.1371/journal.pgen.1000304

Le Gall, A., Albina, E., Magar, R., and Gauthier, J. P. (1997). Antigenic variability of porcine reproductive and respiratory syndrome (PRRS) virus isolates. Influence of virus passage in pig. *Vet. Res.* 28, 247–257. PMID: 9208445

Li, C., Gong, B., Sun, Q., Xu, H., Zhao, J., Xiang, L., et al. (2021). First detection of NADC34-like PRRSV as a Main epidemic strain on a large farm in China. *Pathogens* 11:32. doi: 10.3390/pathogens11010032

Lin, W. H., Kaewprom, K., Wang, S. Y., Lin, C. F., Yang, C. Y., Chiou, M. T., et al. (2020). Outbreak of porcine reproductive and respiratory syndrome virus 1 in Taiwan. *Viruses* 12:316. doi: 10.3390/v12030316

Liu, J. K., Wei, C. H., Dai, A. L., Fan, K. W., Yang, B. H., Huang, C. F., et al. (2017). Complete genomic characterization of two European-genotype porcine reproductive and respiratory syndrome virus isolates in Fujian province of China. *Arch. Virol.* 162, 823–833. doi: 10.1007/s00705-016-3136-9

Music, N., and Gagnon, C. A. (2010). The role of porcine reproductive and respiratory syndrome (PRRS) virus structural and non-structural proteins in virus pathogenesis. *Anim. Health Res. Rev.* 11, 135–163. doi: 10.1017/S1466252310000034

Nguyen, L. T., Schmidt, H. A., von Haeseler, A., and Minh, B. Q. (2015). IQ-TREE: a fast and effective stochastic algorithm for estimating maximum-likelihood phylogenies. *Mol. Biol. Evol.* 32, 268–274. doi: 10.1093/molbev/msu300

Oleksiewicz, M. B., Botner, A., Toft, P., Grubbe, T., Nielsen, J., Kamstrup, S., et al. (2000). Emergence of porcine reproductive and respiratory syndrome virus deletion mutants: correlation with the porcine antibody response to a hypervariable site in the ORF 3 structural glycoprotein. *Virology* 267, 135–140. doi: 10.1006/viro.1999.0103

Paploski, I. A. D., Pamornchainavakul, N., Makau, D. N., Rovira, A., Corzo, C. A., Schroeder, D. C., et al. (2021). Phylogenetic structure and sequential dominance of sub-lineages of PRRSV Type-2 lineage 1 in the United States. *Vaccines (Basel)* 9:608. doi: 10.3390/vaccines9060608

Rambaut, A., Lam, T. T., Max Carvalho, L., and Pybus, O. G. (2016). Exploring the temporal structure of heterochronous sequences using TempEst (formerly path-O-gen). *Virus Evol* 2:vew007. doi: 10.1093/ve/vew007

Ripplinger, J., and Sullivan, J. (2008). Does choice in model selection affect maximum likelihood analysis? *Syst. Biol.* 57, 76–85. doi: 10.1080/10635150801898920

Sharma, S., Joshi, G., Dash, P. K., Thomas, M., Athmaram, T. N., Kumar, J. S., et al. (2013). Molecular epidemiology and complete genome characterization of H1N1pdm virus from India. *PLoS One* 8:e56364. doi: 10.1371/journal.pone.0056364

Shi, M., Lam, T. T., Hon, C. C., Hui, R. K., Faaberg, K. S., Wennblom, T., et al. (2010). Molecular epidemiology of PRRSV: a phylogenetic perspective. *Virus Res.* 154, 7–17. doi: 10.1016/j.virusres.2010.08.014

Stadejek, T., Oleksiewicz, M. B., Potapchuk, D., and Podgorska, K. (2006). Porcine reproductive and respiratory syndrome virus strains of exceptional diversity in eastern Europe support the definition of new genetic subtypes. *J. Gen. Virol.* 87, 1835–1841. doi: 10.1099/vir.0.81782-0

Stadejek, T., Oleksiewicz, M. B., Scherbakov, A. V., Timina, A. M., Krabbe, J. S., Chabros, K., et al. (2008). Definition of subtypes in the European genotype of porcine reproductive and respiratory syndrome virus: nucleocapsid characteristics and geographical distribution in Europe. *Arch. Virol.* 153, 1479–1488. doi: 10.1007/s00705-008-0146-2

Suarez, P., Zardoya, R., Martin, M. J., Prieto, C., Dopazo, J., Solana, A., et al. (1996). Phylogenetic relationships of European strains of porcine reproductive and respiratory syndrome virus (PRRSV) inferred from DNA sequences of putative ORF-5 and ORF-7 genes. *Virus Res.* 42, 159–165. doi: 10.1016/0168-1702(95)01305-9

Tamura, K., Stecher, G., Peterson, D., Filipski, A., and Kumar, S. (2013). MEGA6: molecular evolutionary genetics analysis version 6.0. *Mol. Biol. Evol.* 30, 2725–2729. doi: 10.1093/molbev/mst197

Tian, D., Wei, Z., Zevenhoven-Dobbe, J. C., Liu, R., Tong, G., Snijder, E. J., et al. (2012). Arterivirus minor envelope proteins are a major determinant of viral tropism in cell culture. *J. Virol.* 86, 3701–3712. doi: 10.1128/JVI.06836-11

Tong, G. Z., Zhou, Y. J., Hao, X. F., Tian, Z. J., An, T. Q., and Qiu, H. J. (2007). Highly pathogenic porcine reproductive and respiratory syndrome, China. *Emerg. Infect. Dis.* 13, 1434–1436. doi: 10.3201/eid1309.070399

VanderWaal, K., and Deen, J. (2018). Global trends in infectious diseases of swine. *Proc. Natl. Acad. Sci. U. S. A.* 115, 11495–11500. doi: 10.1073/pnas.1806068115

Vanhee, M., Costers, S., Van Breedam, W., Geldhof, M. F., Van Doorsselaere, J., and Nauwynck, H. J. (2010). A variable region in GP4 of European-type porcine reproductive and respiratory syndrome virus induces neutralizing antibodies against homologous but not heterologous virus strains. *Viral Immunol.* 23, 403–413. doi: 10.1089/vim.2010.0025

Vanhee, M., Van Breedam, W., Costers, S., Geldhof, M., Noppe, Y., and Nauwynck, H. (2011). Characterization of antigenic regions in the porcine reproductive and respiratory syndrome virus by the use of peptide-specific serum antibodies. *Vaccine* 29, 4794–4804. doi: 10.1016/j.vaccine.2011.04.071

Wang, A., Zhang, J., Shen, H., Zheng, Y., Feng, Q., Yim-Im, W., et al. (2019). Genetic diversity of porcine reproductive and respiratory syndrome virus 1 in the United States of America from 2010 to 2018. *Vet. Microbiol.* 239:108486. doi: 10.1016/j.vetmic.2019.108486

Wensvoort, G., Terpstra, C., Pol, J. M., ter Laak, E. A., Bloemraad, M., de Kluyver, E. P., et al. (1991). Mystery swine disease in the Netherlands: the isolation of Lelystad virus. *Vet. Q.* 13, 121–130. doi: 10.1080/01652176.1991.9694296

Xiang, L., Xu, H., Li, C., Tang, Y. D., An, T. Q., Li, Z., et al. (2022). Long-term genome monitoring retraces the evolution of novel emerging porcine reproductive and respiratory syndrome viruses. *Front. Microbiol.* 13:885015. doi: 10.3389/fmicb.2022.885015

Xu, H., Song, S., Zhao, J., Leng, C., Fu, J., Li, C., et al. (2020). A potential endemic strain in China: NADC34-like porcine reproductive and respiratory syndrome virus. *Transbound. Emerg. Dis.* 67, 1730–1738. doi: 10.1111/tbed.13508

Yuan, L., Zhu, Z., Fan, J., Liu, P., Li, Y., Li, Q., et al. (2022). High pathogenicity of a Chinese NADC34-like PRRSV on pigs. *Microbiol. Spectr.* 10:e0154122. doi: 10.1128/spectrum.01541-22

Yuzhakov, A. G., Raev, S. A., Skrylev, A. N., Mishin, A. M., Grebennikova, T. V., Verkhovsky, O. A., et al. (2017). Genetic and pathogenic characterization of a Russian subtype 2 PRRSV-1 isolate. *Vet. Microbiol.* 211, 22–28. doi: 10.1016/j.vetmic.2017.09.017

Zhang, D., Gao, F., Jakovlic, I., Zou, H., Zhang, J., Li, W. X., et al. (2020a). PhyloSuite: an integrated and scalable desktop platform for streamlined molecular sequence data management and evolutionary phylogenetics studies. *Mol. Ecol. Resour.* 20, 348–355. doi: 10.1111/1755-0998.13096

Zhang, Z., Li, Z., Li, H., Yang, S., Ren, F., Bian, T., et al. (2022). The economic impact of porcine reproductive and respiratory syndrome outbreak in four Chinese farms: based on cost and revenue analysis. *Front. Vet. Sci.* 9:1024720. doi: 10.3389/fvets.2022.1024720

Zhang, Q., Song, Z., Yu, Y., Huang, J., Jiang, P., and Shan, H. (2020b). Genetic analysis of a porcine reproductive and respiratory syndrome virus 1 strain in China with new patterns of amino acid deletions in nsp2, GP3 and GP4. *Microb. Pathog.* 149:104531. doi: 10.1016/j.micpath.2020.104531

Zhao, K., Ye, C., Chang, X. B., Jiang, C. G., Wang, S. J., Cai, X. H., et al. (2015). Importation and recombination are responsible for the latest emergence of highly pathogenic porcine reproductive and respiratory syndrome virus in China. *J. Virol.* 89, 10712–10716. doi: 10.1128/JVI.01446-15

Zhou, Z., Liu, Q., Hu, D., Zhang, Q., Han, T., Ma, Y., et al. (2015). Complete genomic characterization and genetic diversity of four European genotype porcine reproductive and respiratory syndrome virus isolates from China in 2011. *Virus Genes* 51, 375–384. doi: 10.1007/s11262-015-1256-z

Zhou, Z. J., Qiu, Y., Pu, Y., Huang, X., and Ge, X. Y. (2020). BioAider: An efficient tool for viral genome analysis and its application in tracing SARS-CoV-2 transmission. *Sustain. Cities Soc.* 63:102466. doi: 10.1016/j.scs.2020.102466

frontiers | Frontiers in Microbiology

TYPE Original Research
PUBLISHED 05 December 2022
DOI 10.3389/fmicb.2022.1062544

OPEN ACCESS

EDITED BY
Zhenyu Zhang,
University of Wisconsin-Madison,
United States

REVIEWED BY
Gloria Sánchez Moragas,
Spanish National Research Council (CSIC),
Spain
Xinglong Wang,
Northwest University,
China
Martin Ashby,
The Pirbright Institute,
United Kingdom

*CORRESPONDENCE
Junping Yu
yujp@wh.iov.cn
Hongping Wei
hpwei@wh.iov.cn

†These authors have contributed equally to this work

SPECIALTY SECTION
This article was submitted to Infectious Agents and Disease, a section of the journal Frontiers in Microbiology

RECEIVED 06 October 2022
ACCEPTED 09 November 2022
PUBLISHED 05 December 2022

CITATION
Liu H, Meng F, Nyaruaba R, He P, Hong W, Jiang M, Liu D, Zhou W, Bai D, Yu J and Wei H (2022) A triton X-100 assisted PMAxx-qPCR assay for rapid assessment of infectious African swine fever virus. *Front. Microbiol.* 13:1062544. doi: 10.3389/fmicb.2022.1062544

A triton X-100 assisted PMAxx-qPCR assay for rapid assessment of infectious African swine fever virus

Huan Liu[1,2†], Fei Meng[1,3†], Raphael Nyaruaba[1,2], Ping He[1,2], Wei Hong[1,2], Mengwei Jiang[1,3], Dongqing Liu[4], Wenhao Zhou[1,2], Dan Bai[1,2], Junping Yu[1,2,3*] and Hongping Wei[1,2,3*]

[1]CAS Key Laboratory of Special Pathogens and Biosafety, Center for Biosafety Mega-Science, Wuhan Institute of Virology, Chinese Academy of Sciences, Wuhan, China, [2]College of Life Sciences, University of Chinese Academy of Sciences, Beijing, China, [3]African Swine Fever Regional Laboratory of China (Wuhan), Wuhan, China, [4]Comprehensive Agricultural Law Enforcement Bureau, Wuhan, China

Introduction: African Swine Fever (ASF) is a highly infectious disease of pigs, caused by *African swine fever virus* (ASFV). The lack of vaccines and drugs makes strict disinfection practices to be one of the main measurements to curb the transmission of ASF. Therefore, it is important to assess if all viruses are inactivated after disinfection or after long time exposure in their natural conditions. Currently, the infectivity of ASFV is determined by virus isolation and culture in a biosafety level 3 (BSL-3) laboratory. However, BSL-3 laboratories are not readily available, need skilled expertise and may be time consuming.

Methods: In this study, a Triton X-100 assisted PMAxx-qPCR method was developed for rapid assessment of infectious ASFV in samples. PMAxx, an improved version of propidium monoazide (PMA), can covalently cross-link with naked ASFV-DNA or DNA inside inactivated ASFV virions under assistance of 0.1% (v/v) TritonX-100, but not with ASFV-DNA inside live virions. Formation of PMAxx-DNA conjugates prevents PCR amplification, leaving only infectious virions to be detected. Under optimum conditions, the limit of detection of the PMAxx-qPCR assay was 2.32$\log_{10}$HAD$_{50}$/mL of infectious ASFV. Testing different samples showed that the PMAxx-qPCR assay was effective to evaluate intact ASFV virions after treatment by heat or chemical disinfectants and in simulated samples such as swine tissue homogenate, swine saliva swabs, and environmental swabs. However, whole-blood and saliva need to be diluted before testing because they may inhibit the PCR reaction or the cross-linking of PMAxx with DNA.

Conclusion: The Triton X-100 assisted PMAxx-qPCR assay took less than 3 h from sample to result, offering an easier and faster way for assessing infectious ASFV in samples from places like pig farms and pork markets.

KEYWORDS

African swine fever virus, infection, disinfectant, propidium monoazide, TritonX-100, quantitative PCR

Introduction

African Swine Fever (ASF) is a highly contagious and epidemic disease of pigs caused by a large, icosahedral, enveloped, double-stranded DNA virus named *African swine fever virus* (ASFV), which is the sole member of the family *Asfarviridae* (Galindo and Alonso, 2017; Dixon et al., 2019). Different isolates of ASFV exhibit variable virulence (Portugal et al., 2015). ASFV in blood (Plowright and Parker, 1967), feces (Fischer et al., 2020a), urine (Davies et al., 2017) and tissues (Mazur-Panasiuk and Wozniakowski, 2020) can survive in different environments for long time periods. Contaminated animal feed, pork, clothing, footwear, farming tools, equipment and vehicles etc. will increase the risk of ASFV transmission. Therefore, in the absence of commercial vaccines and therapeutic agents against ASFV (Teklue et al., 2020), culling infected pigs and strict disinfections are the main measurements for protecting the pig industry. It is therefore important to assess whether there exists infectious ASFV after disinfection.

The gold standard for evaluating the infectivity of ASFV after disinfection is virus isolation and culture. However, this method has some shortcomings: (1) A biosafety level 3 (BSL-3) laboratory and porcine primary macrophage cells are needed for ASFV isolation and culture, which are expensive and not available to standard microbiology labs; (2) It takes at least 5 days to determine infectivity; (3) Different sample pretreatments are needed to remove cell toxicity of the chemical disinfectants before virus culture; and (4) well-trained personnel are needed to perform infectivity tests. Due to these strict and unfavorable conditions, rapid and regular monitoring of infectious ASFV is limited, especially for low resource settings.

Real time or conventional PCR assays are recommended by the World Organization for Animal Health (WOAH) for rapid screening and diagnosis of ASFV (Wang et al., 2020). However, these assays cannot determine viral infectivity of ASFV. Some viability dyes such as ethidium monoazide (EMA; Elizaquivel et al., 2014), propidium monoazide (PMA; Sarmento et al., 2020), and an advanced version of PMA dye, PMAxx (Shirasaki et al., 2020), can penetrate damaged or destroyed viral capsids but not intact capsid (Lee et al., 2018) and intercalate covalently into the chains of the nucleic acid after photoactivation to prevent the PCR amplification of these nucleic acids (Li et al., 2015; Nyaruaba et al., 2022). These viability dyes combined with real time PCR (qPCR), have been successfully applied to discriminate infectious viruses from inactivated ones in various studies involving Hepatitis A virus (HAV; Randazzo et al., 2018), Hepatitis E virus (HEV; Schielke et al., 2011), Human rotaviruses (HuRV; Coudray-Meunier et al., 2013), Human Norovirus (HuNoV; Razafimahefa et al., 2021), Porcine epidemic diarrhea coronavirus (PEDV; Puente et al., 2020), and the severe acute respiratory syndrome coronavirus 2 (SARS-CoV-2; Canh et al., 2021). Compared to virus culture, the qPCR-based viability assays overcome the requirements of a BSL-3 laboratory and cell culture for assessing viral infectivity. Additionally, the qPCR technology is widely and readily available even to low resource settings, making it an attractive option to the conventional culture technique.

In this study, we aimed to develop a qPCR assay combined with PMAxx pretreatment for rapid assessment of infectious ASFV in different bio-matrixes after chemical inactivation or heat-treatment. The technique is simple, fast, and can be easily adapted by normal molecular diagnostic laboratories to monitor infectious ASFV.

Materials and methods

Virus stocks and cell culture

Porcine alveolar macrophages (PAMs) were prepared from bronchoalveolar lavage and maintained in Roswell Park Memorial Institute (RPMI) 1640 medium (Gibco, United States) supplemented with 10% fetal bovine serum (FBS, Sigma, United States), 100 U/ml penicillin, 100 μg/ml streptomycin and 250 ng/ml amphotericin B (Beyotime Biotechnology, China) at 37°C with 5% CO_2. ASFV (CSTR: 16533.06. IVCAS 6.7494, genotype II) was stored at −80°C in the biosafety level 3 (BSL-3) facility of Wuhan Institute of Virology, Chinese Academy of Sciences (WIV-CAS). All the experiments involving infectious ASFV were performed in the BSL-3 laboratory. The titer of ASFV stocks were determined by the hemadsorbing (HAD) test. Briefly, 4×10^4 cells/well of PAMs were seeded into 96-well plates and infected with 10-fold diluted ASFVs. After 1-day infection, 1% porcine erythrocyte cell suspensions stored in PBS (Gibco, United States) were added into each well. The phenomena of hemadsorption were observed over 7 days by a microscope. The 50% hemadsorbing dose (HAD_{50}) was calculated by the Reed and Muench method (Zhao et al., 2019).

Reagents used and sources

Reagents used to develop the assays and perform viability experiments were purchased from different companies. In summary, the PMAxx (40,069, 20 mM in H_2O) was purchased from Biotium (United States), TritonX-100 from Sigma-Aldrich (United States), Virkon™ S from DuPont (United States), and Disinfectant Basi containing 4.0–4.99% (w/v) chlorine from Yiheng (Dezhou, China). Primers and probes were synthesized by Sangon Biotech (Shanghai, China). All other chemical reagents used in the experiments were purchased from Sinopharm (Shanghai, China) except otherwise stated. Double distilled water was used in all experiments.

Virus inactivation and sample preparation

Heat inactivation of ASFV

A series of 10-fold gradient dilutions of ASFV suspensions were prepared by diluting the ASFV stock solution with

phosphate buffer solution (PBS, pH 7.4). Parts of the dilution series were aliquoted and inactivated at different temperatures (60°C, 70°C, and 95°C) for 20 min, respectively. After heat treatment, all the aliquots were centrifuged at 10,000 × g (4°C) for 5 min to obtain the supernatants which were then collected and stored on ice until use. Each step was performed in triplicate.

ASFV disinfection by chemicals

The chemical disinfectants and reaction conditions used in this study are summarized in Table 1. These chemicals were verified as ASFV disinfectants in previous studies (Krug et al., 2018; Juszkiewicz et al., 2019, 2020; McCleary et al., 2021). Briefly, aliquots of 180 µl ASFV suspensions with 4.3$\log_{10}HAD_{50}$/mL were mixed with either 20 µl of commercially purchased 84 surfactant [composed of sodium hypochlorite (NaClO) with the chloride concentration between 4 and 4.99% (w/v)], 25% (w/v) glutaraldehyde (GA), acetic acid (HAc), 8% (w/v) sodium hydroxide (NaOH), or 10% (w/v) Virkon (VK), respectively. After incubation at room temperature for 30 min, the disinfection was stopped by immediately adding the corresponding neutralizer and PBS to a total volume of 1 ml. NaOH and HAc were neutralized by 0.2 M hydrogen chloride (HCl) and 0.2 M NaOH, respectively. 7% (w/v) glycine was used to stop the reaction of glutaraldehyde (Cheung and Brown, 1982). The neutralizer used for the NaClO and VK was 0.5% (w/v) sodium thiosulphate ($Na_2S_2O_3$; Olmez-Hanci et al., 2014; Sahebi et al., 2020). Finally, all the disinfected samples were centrifuged at 10,000 × g (4°C) for 5 min to get the supernatants prior to storage on ice until use. All the treatments were performed in triplicate.

TABLE 1 Chemicals and corresponding neutralizers used for ASFV disinfection.

Chemicals	Disinfection conditions			Neutralizer
	Method	Time (min)	Temperature (°C)	
0.4–0.499% (w/v) NaClO	Immersion	30	22–25	0.5% (w/v) $Na_2S_2O_3$
2.5%(w/v) GA	Immersion	30	22–25	7% (w/v) glycine
10% (v/v) HAc	Immersion	30	22–25	0.2 M NaOH
0.8% (w/v) NaOH	Immersion	30	22–25	0.2 M HCl
1% (w/v) VK	Immersion	30	22–25	0.5% (w/v) $Na_2S_2O_3$

Optimization of PMAxx and triton X-100 pretreatment

Extracted ASFV DNA using the Blood viral DNA extraction kit (Qiagen, catalog 51104) and virus suspensions before and after inactivation at different conditions were used to optimize the conditions of the PMAxx-qPCR assay. As shown in Figure 1, PMAxx (0, 5, 10, 25, 50, and 100 µM) together with Triton X-100 (5, 1, 0.1, 0.01%, and 0) were added into the samples. The mixtures were then incubated in the dark at room temperature (22–26°C) for 10 min. Subsequently, the mixtures were exposed to photolysis at different times (5, 10, 15, or 20 min) using a PMA-Lite™ LED photolysis device (Biotium, United States). The photolyzed samples were heat treated at 95°C for 5 min prior to DNA extraction. Extracted DNA samples were finally detected by qPCR to determine the cycle threshold (Ct) values of the mixtures. Samples without PMAxx treatment served as positive controls. Each condition was performed in triplicate.

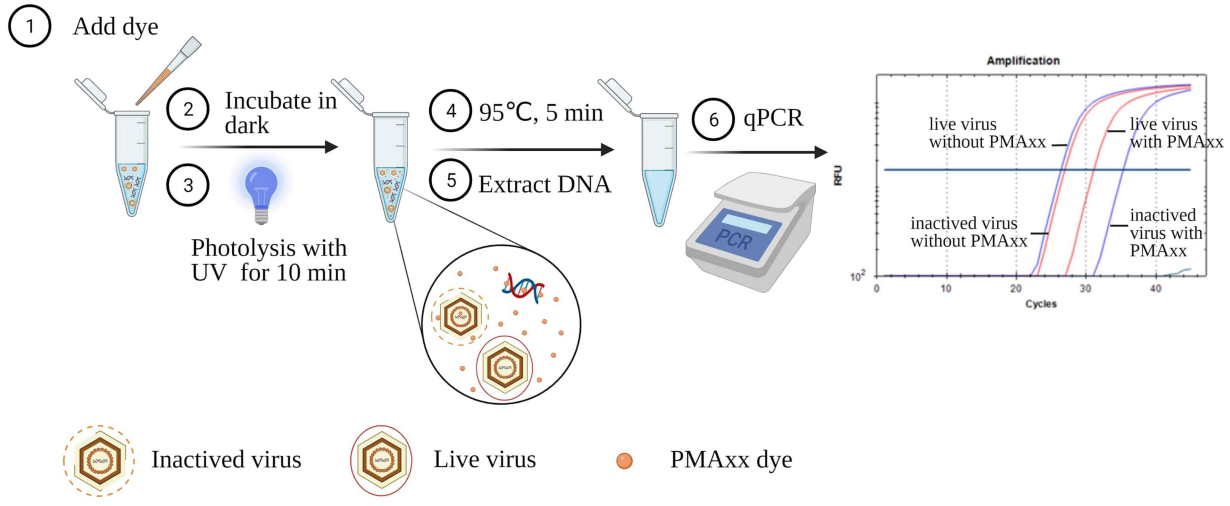

FIGURE 1
Schematic diagram of the PMAxx-qPCR assay for discriminating infectious and inactivated ASFV. The schematic was produced on https://biorender.com.

Quantitative real-time PCR assay

Nucleic acids of the samples were extracted using the Blood viral DNA extraction kit. The primer pairs and probes targeting the ASFV-P72 gene are listed in Table 2. The qPCR reaction system (total 20 μl) consisted of 5 μl template DNA, 10 μl 2 × reaction mix (Luna® Universal Probe qPCR Master Mix, M3004S, NEB, United States), 0.4 μM forward primer, 0.4 μM reverse primer, 0.2 μM probe, and DNase free water. The qPCR reaction was performed on a Biorad CFX96 Real-Time PCR System (Bio-Rad, United States) with a denaturation step at 95°C for 1 min, followed by 45 cycles of denaturation at 95°C for 15 s and annealing/extension at 60°C for 30 s.

Statistical analysis

The ΔCt value was used to estimate the risk and presence of infectious ASFV in tested samples. To obtain the ΔCt value, the average Ct value of a sample after PMAxx pretreatment was subtracted from the average Ct value of the same sample without PMAxx pretreatment. Resultant data was graphically presented and statistically analyzed by GraphPad Prism version 8 (GraphPad software, United States) software. A t-test was used to test the impact of variables and determine the significant differences. Ordinary one-way ANOVA test was used to analyze the significant differences of the data among different groups. A *P*-Value of $p < 0.05$ was deemed significant.

Results

Optimization of the PMAxx-qPCR assay

Three main factors that may affect the ΔCt of the PMAxx-qPCR assay include the PCR amplicon size, PMAxx concentration, and photolysis time. As shown in Figure 2A, ΔCt values of the free ASFV DNA amplified using the primer/probe set #3 (amplicon size 189) were higher than those of primer/probe sets #1 (amplicon size 75) or #2 (amplicon size 163), indicating that longer amplicons were better for discrimination. Therefore, the primer/probe set #3 was used in further optimization experiments. Further tests on two types of samples (free DNA and PBS-diluted ASFV positive swine plasma) showed that PMAxx concentrations ranging from

TABLE 2 Primers and probes used in the PMAxx-qPCR assay for detecting the P72 gene of ASFV.

Gene	Name	Sequence (5′-3′)	Amplicon size (bp)
P72	#1-Forward	TCCTGAAAGCTTATCTCTGCG	75
	#1-Reverse	AGATTGGCACAAGTTCGGAC	
	#1-Probe	FAM-TGAGTGGGCTGCATAATGGCGTT-BHQ	
P72	#2-Forward	AAGGTAATCATCATCGCACC	163
	#2-Reverse	ATCCGATCACATTACCTATTAT	
	#2-Probe	FAM-TCCGTAACTGCTCATGGTATCAATCTT-BHQ	
P72	#3-Forward	TTGATACCATGAGCAGTTACGG	189
	#3-Reverse	AGATTGGCACAAGTTCGGAC	
	#3-Probe	FAM-TGAGTGGGCTGCATAATGGCGTT-BHQ	

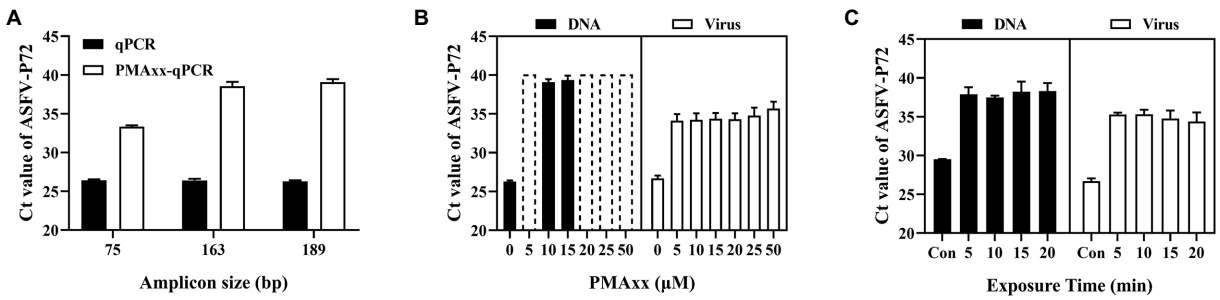

FIGURE 2
Optimization conditions of the PMAxx-qPCR assay targeting the ASFV-P72 gene for discriminating inactivated ASFV and free DNA. **(A)** Effects of different amplicon sizes on Ct values of free ASFV DNA (samples treated with 10 μM PMAxx and 15 min photolysis time). **(B)** Effects of different PMAxx concentrations on Ct values of free ASFV DNA and ASFV in 100 times PBS-diluted swine plasma inactivated at 95°C for 20 min (each concentration was exposed to a photolysis time of 15 min). **(C)** Effects of photolysis time on Ct of free ASFV DNA and ASFV in 100 times PBS-diluted swine plasma inactivated at 95°Cfor 20 min (each sample was treated with a PMAxx concentration of 25 μM). Data were shown as mean±SD of three independent repeats. Dotted plots represent no amplification after 40cycles and the Ct is assigned to 40 in order to calculate ΔCt.

5 μM to 100 μM (Figure 2B) and the photolysis time ranging from 5 min to 20 min (Figure 2C) had no significant difference in the ΔCt values. However, considering the fact that large amounts of nucleic acids of other organisms may be present in real life samples, a relatively high PMAxx concentration of 25 μM and longer photolysis time of 15 min was chosen for the following experiments. These conditions were also found not to have any significant interference with infectious virions when determined by cell culture as seen in Supplementary Table S1.

Determination of heat-inactivated ASFV by the triton X-100 assisted PMAxx-qPCR assay

Heat treatment is an important method of inactivating ASFV, and it has been reported that ASFV can be inactivated after heating at temperatures higher than 60°C for 20 min (Mazur-Panasiuk et al., 2019). Using this analogy, infectious ASFV samples were heat inactivated at temperatures ≥60°C, subjected to PMAxx, and results compared to their respective control samples (without heat treatment). Compared to the control, the ΔCt values were 1.6, 2.19, 3 and 11.43 for the infectious sample and samples subjected to 60°C, 70°C and 95°C temperatures, respectively (Figure 3A). These results indicated that the PMAxx-qPCR assay could optimally determine inactivated viruses heated at higher temperatures of ≥95°C, but not at mild temperatures (60°C or 70°C). The probable reason for this dismal performance at mild temperatures was thought to be related to the existence of intact ASFV capsid structures not easily broken by mild temperatures.

It has been reported that surfactants such as Triton X-100 (Coudray-Meunier et al., 2013) and SDS (Hong et al., 2021) can increase the permeability of monoazide dyes to pathogenic viruses with intact viral capsids. Therefore, we attempted to add Triton

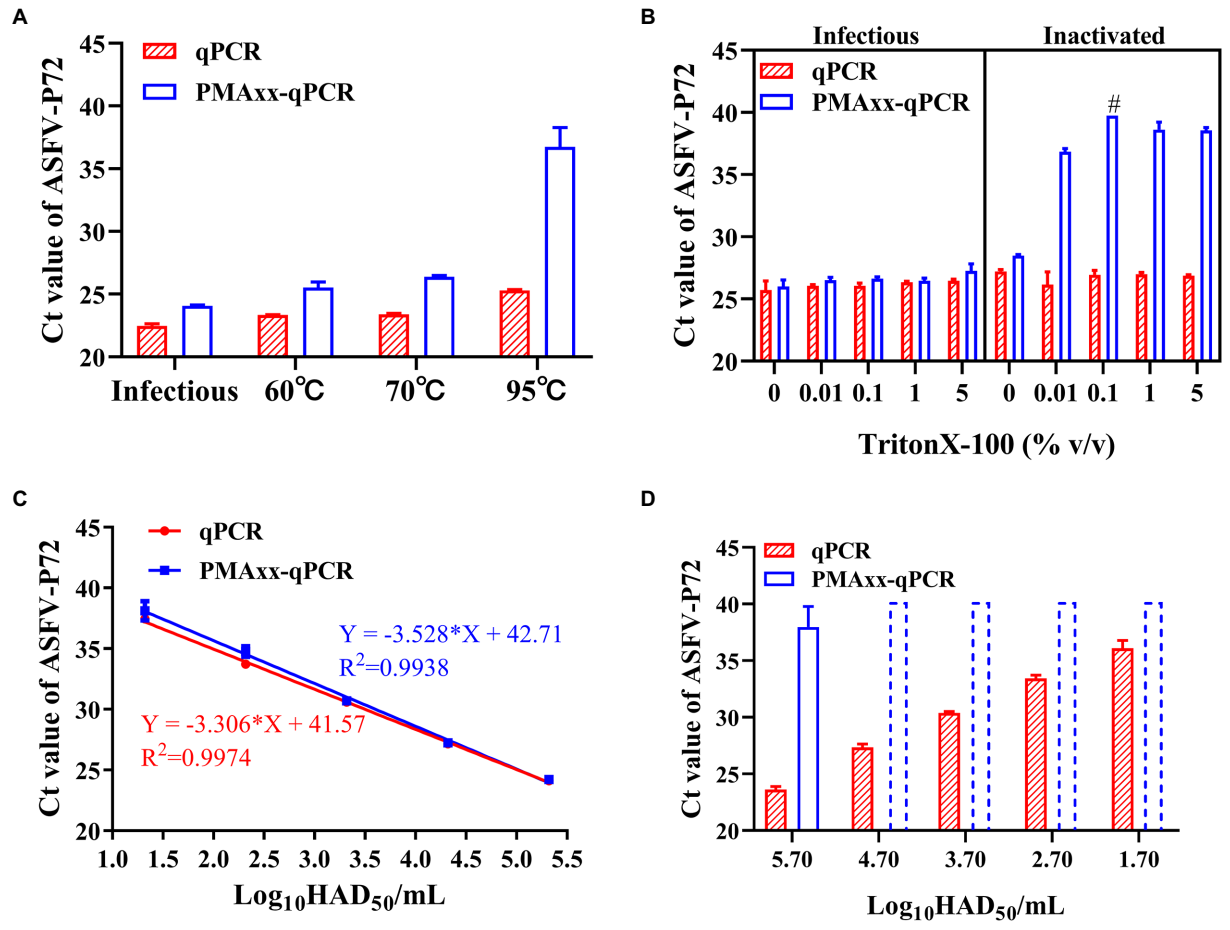

FIGURE 3
Performance of the PMAxx-qPCR assay and the Triton X-100 assisted PMAxx-qPCR assay in detecting infectious ASFV and thermo-inactivated ASFV. **(A)** Ct values of infectious ASFV and their inactivated counterparts treated at three temperatures (60°C, 70°C, or 95°C) for 20 min and determined by qPCR (without PMAxx) and PMAxx-qPCR. **(B)** Effects of the Triton X-100 assisted PMAxx-PCR assay in detecting infectious or live ASFV (left) and their counterpart inactivated ASFV at 60°C for 20 min (right). **(C)** Linear curve fitting of the qPCR and the Triton X-100 assisted PMAxx-qPCR assay using serial dilutions of infectious ASFV with 0.1% Triton X-100. **(D)** Ct values of ASFV samples inactivated at 60°C for 20 min and detected using qPCR (without PMAxx) and Triton X-100 assisted PMAxx-qPCR. Dotted plots represent no amplification after 40cycles and the Ct is assigned to 40 in order to calculate ΔCt. Data were shown as mean±SD of three independent repeats. #, two of the three repeats were found to have no amplification after 40 cycles.

X-100 to enhance the penetration of PMAxx into the intact ASFV virions inactivated at 60°C. As shown in Figure 3B (left), Triton X-100 (5, 1, 0.1, 0.01% (v/v)) did not promote PMAxx penetration into the control (infectious ASFV viruses without heat treatment), but it increased the PMAxx penetration into ASFV samples inactivated at 60°C (Figure 3B, right). Further analysis of the ΔCt values of inactivated samples showed that 0.1% Triton X-100 had the largest ΔCt value (Figure 3B, right) and was hence chosen as an assistant to the PMAxx-qPCR assay in the following tests.

Using this concentration, further testing on serial dilutions of infectious ASFV suspensions (Figure 3C) showed that there was no significant difference between the Triton X-100-qPCR alone (without PMAxx treatment) and the Triton X-100 assisted PMAxx-qPCR. These results indicated that the Triton X-100 assisted PMAxx treatment had no effects on infectious ASFV. However, after heat treatment at 60°C for 20 min (Figure 3D), the Ct values of the qPCR did not change, but the Ct values of the Triton X-100 assisted PMAxx-qPCR increased significantly ($p < 0.001$ for all groups), showing no amplification after 40 cycles except for the highest concentration of $5.7\log_{10}HAD_{50}$/mL (Ct value: 37.96 ± 1.83).

Application of the triton X-100 assisted PMAxx-qPCR assay

In order to verify if the Triton X-100 assisted PMAxx-qPCR assay could discriminate infectious ASFV in partially inactivated samples, a series of samples were prepared by mixing the infectious $5.32\log_{10}HAD_{50}$/mL ASFV and heat-inactivated $5.7\log_{10}HAD_{50}$/mL ASFV at different ratios. As shown in Table 3, an increase in the percentage of infectious ASFV in the samples led to a decrease in ΔCt values. Even at 1% infectious ASFV in the samples, the ΔCt values were significantly lower than those of the ΔCt values of 100% inactivated ASFV. The same trends were observed even with lower titers of ASFV mixtures. These results demonstrated the possibility of using the Triton X-100 assisted PMAxx-qPCR assay to determine small percentages of infectious ASFV in samples by comparing the difference between the ΔCt value of the sample before inactivation and that of the same sample inactivated at 60°C for 20 min.

Effects of different matrices on the triton X-100 assisted PMAxx-qPCR assay

The detection of ASFV varies in different bio-matrices, this may possibly affect the performance of Triton X-100 assisted PMAxx-qPCR assays. To determine this, samples with inactivated ASFV suspended in five bio-matrices [PBS, swine blood, swine tissue homogenate, pig saliva swab (SS), and environmental swabs (ES)] were tested using both qPCR (without PMAxx treatment) and Triton X-100 assisted PMAxx-qPCR. Compared to PBS at 1× concentration, late Ct values were observed in blood and saliva matrices when detected by qPCR (Table 4). However, after adding the inactivated ASFV into 4 × or 8 × PBS-diluted matrices, early Ct values were observed. These results indicated that these two matrices would affect either the efficacy of the DNA extraction kits or contain some inhibitors that might inhibit the qPCR reaction. Additionally, blood may also affect the PMAxx treatment process since a late Ct value was observed in the undiluted blood when detected by the Triton X-100 assisted PMAxx-qPCR assay. Therefore, blood and saliva samples need to be diluted with PBS at least 4× or 8× times before detection, while tissue homogenates and the environmental swabs do not need any dilutions.

Evaluating the efficacy of chemical disinfectants using the triton X-100 assisted PMAxx-qPCR assay

In order to evaluate whether the Triton X-100 assisted PMAxx-qPCR assay is suitable for detecting viable ASFV after chemical disinfection, ASFV inactivated by five types of chemical disinfectants (NaClO, GA, HAc, NaOH, and VK) at different

TABLE 3 Determining ΔCt values from mixtures of infectious and inactivated ASFV under different titers using qPCR ($Ct_{(-PMAxx)}$) and Triton X-100 assisted PMAxx-qPCR ($Ct_{(+PMAxx)}$) assays. A decrease in ΔCt values positively correlated to an increase in the percentage of infectious virions across all titers tested. The assay could detect as low as 1% infectious virion in the samples tested with a significantly lower ΔCt value compared to 100% inactivated ASFV (i.e., 0% infectious ASFV).

Percentage of infectious ASFV%	High titer ($5.32\log_{10}HAD_{50}$/ml infectious virus mixed with $5.7\log_{10}HAD_{50}$/ml dead virus)			Middle titer (10 × dilution of high titer)			Low titer (100 × dilution of high titer)		
	$Ct_{(-PMAxx)}$	$Ct_{(+PMAxx)}$	ΔCt	$Ct_{(-PMAxx)}$	$Ct_{(+PMAxx)}$	ΔCt	$Ct_{(-PMAxx)}$	$Ct_{(+PMAxx)}$	ΔCt
0	23.37 ± 0.80	38.43 ± 0.76	15.06	26.50 ± 0.77	39.65†	>13.15	29.60 ± 0.88	NA	>10.40
1	23.12 ± 0.06	33.64 ± 0.37	10.52	27.07 ± 0.11	37.26 ± 0.91	10.19	29.95 ± 0.34	37.82†	>7.87
10	22.49 ± 1.26	30.30 ± 0.74	7.81	27.53 ± 0.28	34.15 ± 0.11	6.62	29.99 ± 0.30	37.42 ± 0.27	7.43
25	23.46 ± 0.21	28.75 ± 0.76	5.29	26.53 ± 1.09	32.14 ± 0.95	5.61	30.15 ± 0.11	35.54 ± 0.76	5.39
50	24.17 ± 0.23	27.85 ± 0.06	3.68	27.59 ± 0.57	31.15 ± 0.20	3.56	31.47 ± 0.85	35.43 ± 0.05	3.96
90	25.39 ± 0.21	27.27 ± 0.16	1.88	28.68 ± 0.37	30.25 ± 0.31	1.57	31.81 ± 0.37	34.43 ± 1.07	2.62
100	25.35 ± 0.27	26.31 ± 0.94	0.96	29.54 ± 0.49	30.43 ± 0.08	0.89	32.41 ± 0.27	33.85 ± 0.12	1.44

†two of the three repeats were found to have no amplification after 40 cycles. NA represents no amplification after 40 cycles and the Ct is assigned to 40 in order to calculate ΔCt.

TABLE 4 Detection of inactivated ASFV suspended in different matrices by qPCR ($Ct_{(-PMAxx)}$) and Triton X-100-PMAxx-qPCR ($Ct_{(+PMAxx)}$) assays. Undiluted blood and saliva had later Ct values compared to PBS indicative of qPCR inhibition. These values improved after 4× and 8× dilution in PBS. Undiluted blood (1×) could also interfere with the Triton X-100-PMAxx-qPCR assay as an earlier Ct value was observed. Tissue homogenate and environmental swab had no effects on both assays.

Matrices	PBS	Dilution times of swine blood with PBS			Dilution times of pig saliva swab with PBS			Tissue homogenate	Environmental swab
Dilution	1	1	4	8	1	4	8	1	1
$Ct_{(-PMAxx)}$	25.35 ± 0.38	27.42 ± 0.49	25.96 ± 0.62	25.64 ± 0.19	35.81 ± 0.09	29.93 ± 0.50	27.28 ± 0.25	24.01 ± 0.03	23.90 ± 0.01
$Ct_{(+PMAxx)}$	NA	31.83 ± 0.09	NA	NA	NA	NA	NA	37.14 ± 0.83	NA

Data was shown as mean ± SD of three independent repeats. NA represents no amplification after 40 cycles.

concentrations was tested, with ddH_2O treatment serving as a positive control. Cell culture was also used to determine if there remained infectious ASFV after the disinfections. As shown in Figure 4A, the cell culture revealed that only the H_2O-treatment group contained the infectious ASFV and no growth of ASFV could be detected after the chemical disinfections. The Triton X-100 assisted PMAxx-qPCR assay also revealed that there existed infectious ASFV in the H_2O-treatment group because the ΔCt value was only 0.37 ($p < 0.05$). However, for the chemical disinfection groups, the Ct values of qPCR (without PMAxx treatment) alone were significantly increased except for the NaOH-treated group (Figure 4B). The increase in Ct value may be a result of the four chemical disinfectants degrading or covalently cross-linking with ASFV DNA, especially GA. After the Triton X-100 assisted PMAxx treatment, the Ct values of these chemical groups increased further to above 37 or no amplification after 40 cycles (Figure 4B). This signified that the chemicals were indeed active against ASFV.

Discussion

It has been shown that ASFV can remain viable in natural conditions for long time periods (Arzumanyan et al., 2021) and be directly transmitted by complex transmission routes such as contact between infected and susceptible pigs (Gaudreault et al., 2020), consumption of infected pig meat (Ito et al., 2020), and bites from infected acari (*Ornithodoros* spp.; Pereira De Oliveira et al., 2020). In addition to the above primary routes, there are some potential routes for indirect transmission of ASFV through contact with virus contaminated objects and fluids such as blood, feces, urine, or saliva from infected pigs (Guinat et al., 2014; Fischer et al., 2020b; Olesen et al., 2020; Health et al., 2021). Due to there being no drugs and vaccines against ASFV, strict disinfections are the main measurements to curb the transmission of ASFV. The gold standard cell culture method is not suitable for regular monitoring of the presence of infectious ASFV in natural environments and after disinfections.

The Triton X-100 assisted PMAxx-qPCR assay developed in this study may provide some advantages over cell culture. Firstly, it could not only be used to detect ASFV DNA, but also to assess the presence of infectious ASFV in samples within 3 h. By exploring the property of PMAxx which could not penetrate the capsid of infectious virions, the PMAxx-qPCR could discriminate live virus as low as 1% from dead virus (Table 3). Secondly, it is biologically safe to perform the test without the need of a BSL-3 laboratory. By obviating the need for virus culture, the PMAxx treatment and DNA extraction can be performed within a biosafety cabinet. This makes the assay scalable with a possibility of deployment to places with limited resources, such as pig farms. Additionally, PMA assays are said to be capable of detecting live but unculturable pathogens [according to the manufacturer's instructions, and other literature (Zhong and Zhao, 2018; Ou et al., 2021; Zhao et al., 2022)]. Lastly, considering time, and labor costs of cell culture, it is more convenient to include the PMAxx-qPCR in routine diagnosis to detect infectious ASFV.

However, validation tests need to be performed before application of the Triton X-100 assisted PMAxx-qPCR assay for real-life samples. Similar to other PMA assays (Banihashemi et al., 2012; Kragh et al., 2020; Van Holm et al., 2021), in this study, primers amplifying longer amplicons (>100 bp) for ASFV-P72 performed optimally compared to shorter amplicons. Hence chosen for further tests. Despite the advantage of using longer amplicons, no clear guideline exists towards selecting and designing amplicon lengths for optimal PMA results (Van Holm et al., 2021). As shown in Table 4, sample matrices may affect the Ct values of the qPCR assay, as well as the Triton X-100 assisted PMAxx-qPCR assay. Not only should the effects of the matrices on the DNA extraction and amplification be checked, but also on the PMAxx-DNA crosslinking. Where applicable, measures such as dilution should be used to minimize the adverse effects of the matrices. Furthermore, chemical disinfectants may affect the Ct values of the qPCR and the Triton X-100 assisted PMAxx-qPCR assay. Disinfectants recommended by the WOAH against ASFV consist of detergents, oxidizing agents, alkalis, organic acids and glutaraldehyde (Juszkiewicz et al., 2020). Among them, NaClO, GA, HAc, NaOH, and VK are widely used to sanitize contaminated agricultural and veterinary facilities, especially in the farm settings (Turner and Williams, 1999; Kalmar et al., 2018). However, different disinfectants may degrade DNA or covalently cross-link with ASFV DNA during disinfection, resulting in increased Ct values (Figure 4B). All these factors should be validated first to make sure that the PMAxx-qPCR assay can accurately discriminate infectious ASFV in samples.

In summary, a Triton X-100 assisted PMAxx-qPCR assay was developed to discriminate infectious ASFV from inactivated ASFV based on changes in Ct value (ΔCt). Under optimum conditions, the limit of detection of the PMAxx-qPCR assay was

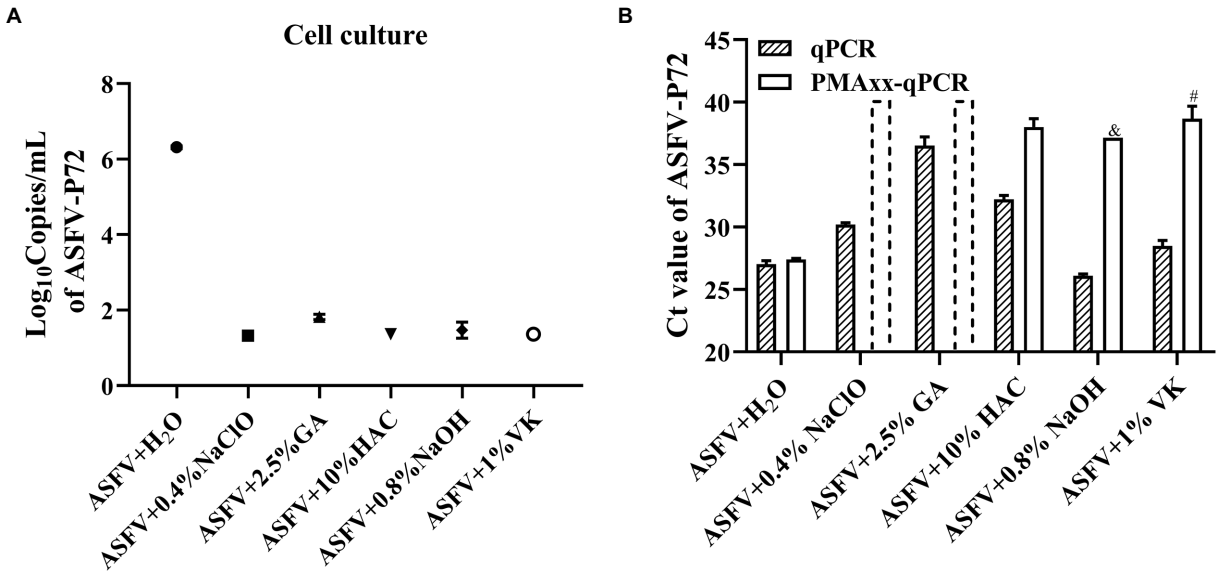

FIGURE 4
Evaluating the efficacy of the chemical disinfectants by cell culture **(A)** and the Triton X-100 assisted PMAxx-qPCR assay **(B)**. Data were shown as mean±SD of three independent repeats. The dotted columns represent the assigned Ct value of the result of no DNA amplification after 40 cycles. &, represents two of three repeats with no amplification after 40 cycles. #, represents one of three repeats with no DNA amplification after 40 cycles.

$2.32\log_{10}HAD_{50}$/mL of infectious ASFV. Testing different samples showed that the PMAxx-qPCR assay was effective in evaluating intact ASFV virions after treatment by heat or chemical disinfectants within 3 h. However, validation should be performed first to determine the ΔCt cutoff value for assessing the presence of infectious ASFV in different types of samples.

Data availability statement

The original contributions presented in the study are included in the article/Supplementary material, further inquiries can be directed to the corresponding authors.

Author contributions

HW and JY conceived and designed the project and revised the manuscript. HL and FM performed the experiments and wrote the original manuscript. RN made suggestions in this study and revised the manuscript. MJ and FM provided the ASFV viruses. DL was responsible for sample collection. RN, WH, PH, WZ, and DB performed data analyses. All authors contributed to the article and approved the submitted version.

Funding

This work was supported by Key technologies for ASFV control from Department of Science and Technology of Hubei province, China (Grant No: 2019ABA08) and the National Key Research and Development Program of China from the Ministry of Science and Technology of China (No. 2018YFC0840402).

Acknowledgments

We would like to acknowledge all the staff members at the BSL-3 laboratory of Wuhan Institute of Virology, CAS, for providing technical support for this project.

Conflict of interest

The authors declare that the research was conducted in the absence of any commercial or financial relationships that could be construed as a potential conflict of interest.

Publisher's note

Supplementary material

The Supplementary material for this article can be found online at: https://www.frontiersin.org/articles/10.3389/fmicb.2022.1062544/full#supplementary-material

References

Arzumanyan, H., Hakobyan, S., Avagyan, H., Izmailyan, R., Nersisyan, N., and Karalyan, Z. (2021). Possibility of long-term survival of African swine fever virus in natural conditions. *Vet World* 14, 854–859. doi: 10.14202/vetworld.2021.854-859

Banihashemi, A., Van Dyke, M. I., and Huck, P. M. (2012). Long-amplicon propidium monoazide-PCR enumeration assay to detect viable campylobacter and salmonella. *J. Appl. Microbiol.* 113, 863–873. doi: 10.1111/j.1365-2672.2012.05382.x

Canh, V. D., Torii, S., Yasui, M., Kyuwa, S., and Katayama, H. (2021). Capsid integrity RT-qPCR for the selective detection of intact SARS-CoV-2 in wastewater. *Sci. Total Environ.* 791:148342. doi: 10.1016/j.scitotenv.2021.148342

Cheung, H. Y., and Brown, M. R. (1982). Evaluation of glycine as an inactivator of glutaraldehyde. *J. Pharm. Pharmacol.* 34, 211–214. doi: 10.1111/j.2042-7158.1982.tb04230.x

Coudray-Meunier, C., Fraisse, A., Martin-Latil, S., Guillier, L., and Perelle, S. (2013). Discrimination of infectious hepatitis a virus and rotavirus by combining dyes and surfactants with RT-qPCR. *BMC Microbiol.* 13:216. doi: 10.1186/1471-2180-13-216

Davies, K., Goatley, L. C., Guinat, C., Netherton, C. L., Gubbins, S., Dixon, L. K., et al. (2017). Survival of African swine fever virus in excretions from pigs experimentally infected with the Georgia 2007/1 isolate. *Transbound. Emerg. Dis.* 64, 425–431. doi: 10.1111/tbed.12381

Dixon, L. K., Sun, H., and Roberts, H. (2019). African swine fever. *Antivir. Res.* 165, 34–41. doi: 10.1016/j.antiviral.2019.02.018

Elizaquivel, P., Aznar, R., and Sanchez, G. (2014). Recent developments in the use of viability dyes and quantitative PCR in the food microbiology field. *J. Appl. Microbiol.* 116, 1–13. doi: 10.1111/jam.12365

Fischer, M., Huhr, J., Blome, S., Conraths, F. J., and Probst, C. (2020a). Stability of African swine fever virus in carcasses of domestic pigs and wild boar experimentally infected with the ASFV "Estonia 2014". *Isolate. Viruses* 12:1118. doi: 10.3390/v12101118

Fischer, M., Mohnke, M., Probst, C., Pikalo, J., Conraths, F. J., Beer, M., et al. (2020b). Stability of African swine fever virus on heat-treated field crops. *Transbound. Emerg. Dis.* 67, 2318–2323. doi: 10.1111/tbed.13650

Galindo, I., and Alonso, C. (2017). African swine fever virus: a review. *Viruses* 9:103. doi: 10.3390/v9050103

Gaudreault, N. N., Madden, D. W., Wilson, W. C., Trujillo, J. D., and Richt, J. A. (2020). African swine fever virus: an emerging DNA arbovirus. *Front Vet Sci* 7:215. doi: 10.3389/fvets.2020.00215

Guinat, C., Reis, A. L., Netherton, C. L., Goatley, L., Pfeiffer, D. U., and Dixon, L. (2014). Dynamics of African swine fever virus shedding and excretion in domestic pigs infected by intramuscular inoculation and contact transmission. *Vet. Res.* 45:93. doi: 10.1186/s13567-014-0093-8

Health, E. P. O. A., Welfare Nielsen, S. S., Alvarez, J., Bicout, D. J., Calistri, P., Canali, E., et al. (2021). Ability of different matrices to transmit African swine fever virus. *EFSA J.* 19:e06558. doi: 10.2903/j.efsa.2021.6558

Hong, W., Xiong, J., Nyaruaba, R., Li, J., Muturi, E., Liu, H., et al. (2021). Rapid determination of infectious SARS-CoV-2 in PCR-positive samples by SDS-PMA assisted RT-qPCR. *Sci. Total Environ.* 797:149085. doi: 10.1016/j.scitotenv.2021.149085

Ito, S., Jurado, C., Sanchez-Vizcaino, J. M., and Isoda, N. (2020). Quantitative risk assessment of African swine fever virus introduction to Japan via pork products brought in air passengers' luggage. *Transbound. Emerg. Dis.* 67, 894–905. doi: 10.1111/tbed.13414

Juszkiewicz, M., Walczak, M., Mazur-Panasiuk, N., and Wozniakowski, G. (2019). Virucidal effect of chosen disinfectants against African swine fever virus (ASFV) - preliminary studies. *Pol. J. Vet. Sci.* 22, 777–780. doi: 10.24425/pjvs.2019.131407

Juszkiewicz, M., Walczak, M., Mazur-Panasiuk, N., and Wozniakowski, G. (2020). Effectiveness of chemical compounds used against African swine fever virus in commercial available disinfectants. *Pathogens* 9:878. doi: 10.3390/pathogens9110878

Kalmar, I. D., Cay, A. B., and Tignon, M. (2018). Sensitivity of African swine fever virus (ASFV) to heat, alkalinity and peroxide treatment in presence or absence of porcine plasma. *Vet. Microbiol.* 219, 144–149. doi: 10.1016/j.vetmic.2018.04.025

Kragh, M. L., Thykier, M., and Truelstrup Hansen, L. (2020). A long-amplicon quantitative PCR assay with propidium monoazide to enumerate viable listeria monocytogenes after heat and desiccation treatments. *Food Microbiol.* 86:103310. doi: 10.1016/j.fm.2019.103310

Krug, P. W., Davis, T., O'Brien, C., LaRocco, M., and Rodriguez, L. L. (2018). Disinfection of transboundary animal disease viruses on surfaces used in pork packing plants. *Vet. Microbiol.* 219, 219–225. doi: 10.1016/j.vetmic.2018.04.029

Lee, H. W., Lee, H. M., Yoon, S. R., Kim, S. H., and Ha, J. H. (2018). Pretreatment with propidium monoazide/sodium lauroyl sarcosinate improves discrimination of infectious waterborne virus by RT-qPCR combined with magnetic separation. *Environ. Pollut.* 233, 306–314. doi: 10.1016/j.envpol.2017.10.081

Li, H., Xin, H., and Li, S. F. (2015). Multiplex PMA-qPCR assay with internal amplification control for simultaneous detection of viable legionella pneumophila, salmonella typhimurium, and Staphylococcus aureus in environmental waters. *Environ. Sci. Technol.* 49, 14249–14256. doi: 10.1021/acs.est.5b03583

Mazur-Panasiuk, N., and Wozniakowski, G. (2020). Natural inactivation of African swine fever virus in tissues: influence of temperature and environmental conditions on virus survival. *Vet. Microbiol.* 242:108609. doi: 10.1016/j.vetmic.2020.108609

Mazur-Panasiuk, N., Zmudzki, J., and Wozniakowski, G. (2019). African swine fever virus - persistence in different environmental conditions and the possibility of its indirect transmission. *J Vet Res* 63, 303–310. doi: 10.2478/jvetres-2019-0058

McCleary, S., McCarthy, R. R., Strong, R., Edwards, J., and Crooke, H. (2021). Inactivation of African swine fever virus by reagents commonly used in containment laboratories. *J. Virol. Methods* 295:114203. doi: 10.1016/j.jviromet.2021.114203

Nyaruaba, R., Mwaliko, C., Dobnik, D., Neužil, P., Amoth, P., Mwau, M., et al. (2022). Digital PCR applications in the SARS-CoV-2/COVID-19 era: a roadmap for future outbreaks. *Clin. Microbiol. Rev.* 35:e0016821. doi: 10.1128/cmr.00168-21

Olesen, A. S., Belsham, G. J., Bruun Rasmussen, T., Lohse, L., Bodker, R., Halasa, T., et al. (2020). Potential routes for indirect transmission of African swine fever virus into domestic pig herds. *Transbound. Emerg. Dis.* 67, 1472–1484. doi: 10.1111/tbed.13538

Olmez-Hanci, T., Arslan-Alaton, I., and Dursun, D. (2014). Investigation of the toxicity of common oxidants used in advanced oxidation processes and their quenching agents. *J. Hazard. Mater.* 278, 330–335. doi: 10.1016/j.jhazmat.2014.06.021

Ou, A., Wang, K., Ye, Y., Chen, L., Gong, X., Qian, L., et al. (2021). Direct detection of viable but non-culturable (VBNC) salmonella in real food system by a rapid and accurate PMA-CPA technique. *Front. Microbiol.* 12:634555. doi: 10.3389/fmicb.2021.634555

Pereira De Oliveira, R., Hutet, E., Lancelot, R., Paboeuf, F., Duhayon, M., Boinas, F., et al. (2020). Differential vector competence of Ornithodoros soft ticks for African swine fever virus: what if it involves more than just crossing organic barriers in ticks? *Parasit. Vectors* 13:618. doi: 10.1186/s13071-020-04497-1

Plowright, W., and Parker, J. (1967). The stability of African swine fever virus with particular reference to heat and pH inactivation. *Arch. Gesamte Virusforsch.* 21, 383–402. doi: 10.1007/BF01241738

Portugal, R., Coelho, J., Hoper, D., Little, N. S., Smithson, C., Upton, C., et al. (2015). Related strains of African swine fever virus with different virulence: genome comparison and analysis. *J. Gen. Virol.* 96, 408–419. doi: 10.1099/vir.0.070508-0

Puente, H., Randazzo, W., Falco, I., Carvajal, A., and Sanchez, G. (2020). Rapid selective detection of potentially infectious porcine epidemic diarrhea coronavirus exposed to heat treatments using viability RT-qPCR. *Front. Microbiol.* 11:1911. doi: 10.3389/fmicb.2020.01911

Randazzo, W., Vasquez-Garcia, A., Aznar, R., and Sanchez, G. (2018). Viability RT-qPCR to distinguish between HEV and HAV with intact and altered capsids. *Front. Microbiol.* 9:1973. doi: 10.3389/fmicb.2018.01973

Razafimahefa, R. M., Ludwig-Begall, L. F., Le Guyader, F. S., Farnir, F., Mauroy, A., and Thiry, E. (2021). Optimisation of a PMAxx-RT-qPCR assay and the preceding extraction method to selectively detect infectious murine norovirus particles in mussels. *Food Environ Virol* 13, 93–106. doi: 10.1007/s12560-020-09454-w

Sahebi, S., Sobhnamayan, F., Moazami, F., and Naseri, M. (2020). Assessment of sodium thiosulfate neutralizing effect on micro-hardness of dentin treated with sodium hypochlorite. *BMC Oral Health* 20:326. doi: 10.1186/s12903-020-01320-2

Sarmento, S. K., Guerra, C. R., Malta, F. C., Coutinho, R., Miagostovich, M. P., and Fumian, T. M. (2020). Human norovirus detection in bivalve shellfish in Brazil and evaluation of viral infectivity using PMA treatment. *Mar. Pollut. Bull.* 157:111315. doi: 10.1016/j.marpolbul.2020.111315

Schielke, A., Filter, M., Appel, B., and Johne, R. (2011). Thermal stability of hepatitis E virus assessed by a molecular biological approach. *Virol. J.* 8:487. doi: 10.1186/1743-422X-8-487

Shirasaki, N., Matsushita, T., Matsui, Y., and Koriki, S. (2020). Suitability of pepper mild mottle virus as a human enteric virus surrogate for assessing the efficacy of thermal or free-chlorine disinfection processes by using infectivity assays and enhanced viability PCR. *Water Res.* 186:116409. doi: 10.1016/j.watres.2020.116409

Teklue, T., Sun, Y., Abid, M., Luo, Y., and Qiu, H. J. (2020). Current status and evolving approaches to African swine fever vaccine development. *Transbound. Emerg. Dis.* 67, 529–542. doi: 10.1111/tbed.13364

Turner, C., and Williams, S. M. (1999). Laboratory-scale inactivation of African swine fever virus and swine vesicular disease virus in pig slurry. *J. Appl. Microbiol.* 87, 148–157. doi: 10.1046/j.1365-2672.1999.00802.x

Van Holm, W., Ghesquière, J., Boon, N., Verspecht, T., Bernaerts, K., Zayed, N., et al. (2021). A viability quantitative PCR dilemma: are longer amplicons better? *Appl. Environ. Microbiol.* 87:e0265320. doi: 10.1128/AEM.02653-20

Wang, A., Jia, R., Liu, Y., Zhou, J., Qi, Y., Chen, Y., et al. (2020). Development of a novel quantitative real-time PCR assay with lyophilized powder reagent to detect African swine fever virus in blood samples of domestic pigs in China. *Transbound. Emerg. Dis.* 67, 284–297. doi: 10.1111/tbed.13350

Zhao, D., Liu, R., Zhang, X., Li, F., Wang, J., Zhang, J., et al. (2019). Replication and virulence in pigs of the first African swine fever virus isolated in China. *Emerg Microbes Infect* 8, 438–447. doi: 10.1080/22221751.2019.1590128

Zhao, S., Lu, X., Zhang, J., and Kan, B. (2022). Absolute quantification of viable but Nonculturable vibrio cholerae using droplet digital PCR with oil-enveloped bacterial cells. *Microbiol Spectr* 10:e0070422. doi: 10.1128/spectrum.00704-22

Zhong, J., and Zhao, X. (2018). Detection of viable but non-culturable Escherichia coli O157:H7 by PCR in combination with propidium monoazide. *3 Biotech* 8:28. doi: 10.1007/s13205-017-1052-7

frontiers | Frontiers in Microbiology

TYPE Original Research
PUBLISHED 09 December 2022
DOI 10.3389/fmicb.2022.1059118

OPEN ACCESS

EDITED BY
Axel Cloeckaert,
Institut National de recherche pour l'Agriculture, l'Alimentation et l'Environnement (INRAE), France

REVIEWED BY
Dongming Zhao,
Harbin Veterinary Research Institute (CAAS), China
Laura Constance,
Agricultural Research Service (USDA), United States
Helen Roberts,
Food and Rural Affairs, United Kingdom

*CORRESPONDENCE
Gerald C. Shurson
shurs001@umn.edu
Declan C. Schroeder
dcschroe@umn.edu

SPECIALTY SECTION
This article was submitted to Infectious Agents and Disease, a section of the journal Frontiers in Microbiology

RECEIVED 30 September 2022
ACCEPTED 11 November 2022
PUBLISHED 09 December 2022

CITATION
Palowski A, Balestreri C, Urriola PE, van de Ligt JLG, Sampedro F, Dee S, Shah A, Yancy HF, Shurson GC and Schroeder DC (2022) Survival of a surrogate African swine fever virus-like algal virus in feed matrices using a 23-day commercial United States truck transport model.
Front. Microbiol. 13:1059118.
doi: 10.3389/fmicb.2022.1059118

Survival of a surrogate African swine fever virus-like algal virus in feed matrices using a 23-day commercial United States truck transport model

Amanda Palowski[1], Cecilia Balestreri[1], Pedro E. Urriola[2], Jennifer L. G. van de Ligt[1], Fernando Sampedro[3], Scott Dee[4], Apoorva Shah[5], Haile F. Yancy[6], Gerald C. Shurson[2]* and Declan C. Schroeder[1,7]*

[1]Department of Veterinary Population Medicine, College of Veterinary Medicine, University of Minnesota, St. Paul, MN, United States, [2]Department of Animal Science, College of Food Agricultural and Natural Resource Sciences, University of Minnesota, St. Paul, MN, United States, [3]Environmental Health Sciences Division, School of Public Health, University of Minnesota, Minneapolis, MN, United States, [4]Pipestone Applied Research, Pipestone Veterinary Services, Pipestone, MN, United States, [5]SAM Nutrition, Eden Prairie, MN, United States, [6]U.S. Food and Drug Administration, Center for Veterinary Medicine, Office of Research, Laurel, MD, United States, [7]School of Biological Sciences, University of Reading, Reading, United Kingdom

African swine fever virus (ASFV) is a member of the nucleocytoplasmic large DNA viruses (NCLDVs) and is stable in a variety of environments, including animal feed ingredients as shown in previous laboratory experiments and simulations. *Emiliania huxleyi* virus (EhV) is another member of the NCLDVs, which has a restricted host range limited to a species of marine algae called *Emiliania huxleyi*. This algal NCLDV has many similar morphological and physical characteristics to ASFV thereby making it a safe surrogate, with results that are applicable to ASFV and suitable for use in real-world experiments. Here we inoculated conventional soybean meal (SBMC), organic soybean meal (SBMO), and swine complete feed (*CF*) matrices with EhV strain 86 (EhV-86) at a concentration of 6.6×10^7 virus g^{-1}, and then transported these samples in the trailer of a commercial transport vehicle for 23 days across 10,183 km covering 29 states in various regions of the United States. Upon return, samples were evaluated for virus presence and viability using a previously validated viability qPCR (V-qPCR) method. Results showed that EhV-86 was detected in all matrices and no degradation in EhV-86 viability was observed after the 23-day transportation event. Additionally, sampling sensitivity (we recorded unexpected increases, as high as 49% in one matrix, when virus was recovered at the end of the sampling period) rather than virus degradation best explains the variation of virus quantity observed after the 23-day transport simulation. These results demonstrate for the first time that ASFV-like NCLDVs can retain viability in swine feed matrices during long-term transport across the continental United States.

KEYWORDS

African swine fever virus, *Emiliania huxleyi* virus, NCLDVs, feed, transport, viability PCR

Introduction

Foreign animal diseases, such as African swine fever virus (ASFV), pose a significant threat to the United States pork industry because contaminated feed ingredients, pork products, and humans can all be potential sources of disease introduction (Dee et al., 2014; Álvarez et al., 2019; Niederwerder et al., 2019; Dee et al., 2020a). Some RNA viruses such as Seneca virus A (SVA), Porcine reproductive and respiratory syndrome virus (PRRSV), and Porcine epidemic diarrhea virus (PEDV), have been shown to survive in feed ingredients and infect pigs under experimental conditions (Dee et al., 2014; Niederwerder et al., 2019; Dee et al., 2020b). Laboratory-based studies using experimentally inoculated ASFV in conventional and organic soybean meal, choline chloride, and complete feed have shown that the virus can survive for extended periods of time under simulated transoceanic shipping model conditions (Dee et al., 2018; Stoian et al., 2019; Dee et al., 2022). However, because ASFV is a highly contagious virus (Penrith, 2009; Costard et al., 2013; Oura, 2019), and countries such as those in the Americas, Australia and New Zealand where the disease is still absent,[1] research with ASFV can only be conducted in a highly restricted biosecurity level 3 facility. Consequently, this has resulted in only a few laboratories in the world that have regulatory approval to work with this virus (Shurson et al., 2021). These biosecurity restrictions also limit the capability of evaluating ASFV survival and inactivation in various feed ingredients under real world feed supply chain demonstrations because unlike many RNA viruses (Dee et al., 2018), no suitable surrogate has been available for ASFV.

African swine fever virus is a member of the *Asfarviridae* family which is part of a larger group of virus families that are classified as nucleocytoplasmic large DNA viruses (NCLDVs) and evolved from a common ancestor. These NCLDVs are found in a variety of environments, and can infect humans (*Poxviridae*), fish (*Iridoviridae*), insects (*Ascoviridae*), swine (*Asfarviridae*), amoeba (*Marseilleviridae* and *Mimiviridae*) and algae (*Phycodnaviridae*) (Iyer et al., 2001, 2006; Yutin et al., 2009; Colson et al., 2013). Until now, no surrogate NCLDV with similar features to that of ASFV, nor any other virus with suitable surrogate properties, have been proposed for use in studies to evaluate ASFV survival and inactivation in feed ingredients and complete feeds. *Emiliania huxleyi* virus strain 86 (EhV-86) is an ecologically important NCLDV which controls blooms of the marine unicellular phytoplankton *Emiliania huxleyi* (Schroeder et al., 2002; Allen et al., 2006) and shares many important features with ASFV (Balestreri et al., 2022). Both ASFV and EhV-86 share many physical characteristics, such as complex virion ultrastructure and sensitivity profile to time and temperature exposure (Balestreri et al., 2022). In fact, EhV-86 has recently been shown to be one of the most thermally stable viruses known, with temperatures up to 100°C damaging most of the virus particles yet leaving a subset of intact and potentially viable particles for future re-infections. Given the similarities shared between ASFV and EhV-86, Balestreri et al. (2022) proposed the use of EhV-86 as a surrogate for ASFV.

There are many challenges involving various analytical methods and data interpretation when determining virus inactivation kinetics or survival in various types of feed matrices (Shurson et al., 2021). A common method used to measure virus inactivation is quantitative PCR or qPCR (De León et al., 2013; Shurson et al., 2021). The qPCR method is useful for quantifying the amount of virus nucleic acids in a sample, but it fails to distinguish nucleic acids from viable versus non-viable viruses. Viability PCR (V-PCR) is a relatively quick, new technique used to evaluate infectivity of a virus with the use of viable dyes, such as ethidium monoazide (EMA) or propidium monoazide (PMA) prior to nucleic acid extraction and PCR or RT-PCR evaluation (Moreno et al., 2015). Balestreri et al. (2022) developed a viability qPCR (V-qPCR) version of the technique that can be used to quantify the viable EhV-86 NCLDV from the background damaged viruses.

Considering the challenges of determining ASFV survival in feed ingredients under commercial conditions, we chose to use EhV-86 as a suitable and safe surrogate for ASFV and employ the use of a new V-qPCR assay to quantify EhV-86 infectivity when recovered from selected feeds after an extended transport time period. This data can then be compared with the lab-based quantitative data on the half-life of ASFV Georgia 2007 in animal feed ingredients exposed to moderate temperature and humidity conditions simulating transoceanic shipment (Stoian et al., 2019). The main conclusion of this study was that longer virus half-lives in feed compared with half-lives in media support the concept that the feed matrix provides an environment that increases ASFV stability. We hypothesized that EhV-86 would survive in conventional and organic soybean meal and complete feed in real-world conditions similar to ASFV in simulated conditions. Specifically, we applied the V-qPCR method on three commonly used feed matrices inoculated with EhV-86 to determine whether this ASFV surrogate virus remains viable when exposed to the conditions of a 23-d transcontinental truck transport across the United States.

Materials and methods

Cell culture and EhV-86 stock

A culture of *Emiliania huxleyi* CCMP374 (courtesy of Dr. Martinez-Martinez laboratory, Bigelow – Laboratory for Ocean Sciences, East Boothbay, Maine) was grown in Alga-Gro® Seawater Medium (Carolina Biological Supply Company, Burlington, North Carolina) at 15°C with 18 h/6 h light/dark cycle (*ca.* 2400 lux) until the concentration of 2×10^5 cells mL^{-1} was reached. Isolate EhV-86 (also courtesy of Dr. Martinez-Martinez laboratory) was added to *E. huxleyi* at a multiplicity of infection (MOI) of 1 and grown in a 15°C incubator until lysis was observed, which was usually after 4 d (Schroeder et al., 2002). The lysate was filtered through a 0.45 µm filter (Nalgene™

1 https://empres-i.apps.fao.org/

Rapid-Flow™ Bottle Top Filters, ThermoFisher Scientific, Waltham, Massachusetts) to remove cell debris. This filtration and infection procedure was repeated several times. The filtered lysate was divided into aliquots and kept in the dark at 4°C until use.

Feed matrices

Previous research results have shown that swine viruses, such as ASFV, can survive in various experimentally-inoculated feed matrices including conventional and organic soybean meal (Dee et al., 2016, 2018). Therefore, feed ingredients used in this study included conventional solvent extracted, dehulled soybean meal (SBMC: containing 1–2% oil and 46–47% crude protein), organic mechanically extracted soybean meal (SBMO: containing 6–7% oil and 44–45% crude protein), and a complete grower-finisher swine feed (*CF*: corn and soybean meal-based). For each feed matrix, four subsamples (30 g each) were weighed and placed into individual 50 ml mini-bioreactor tubes with vented caps. A total of three allotments per feed matrix were spiked with 2 ml EhV-86 (1×10^9 viruses mL^{-1} as calculated by qPCR and flow cytometry (Balestreri et al., 2022) *via* injection using a 3 ml syringe with an 18-gauge needle. The remaining three samples served as negative controls with no virus added to the feed matrix.

Transport model

All feed samples were placed in a box on the trailer floor of a commercial semi-truck with a 15.8 m trailer (Csp Delivery, Fridley, Minnesota, USA). The truck carrying the inoculated feed samples departed from Minneapolis, Minnesota on November 30, 2020 and returned on December 22, 2020 (23 days). The route covered various regions of the United States including 29 states in the Midwest, Rocky Mountains, Southwest, Gulf Coast, Eastern Seaboard, New England region, and the Great Lakes region (Figure 1). The temperature and humidity were recorded every 15 min during transport and were reported by Dee et al. (2021). The commercial truck did not encounter any unexpected stops or accidents. The goal of this route was to cover several regions of the United States and expose the feed ingredients and viruses to a wide variety of environmental conditions. The temperature ranged for 1–17.5°C within the feed with the relative humidity ranging from 20 to 68% (Dee et al., 2021). Upon completion of the journey, samples were removed from the truck and stored at −20°C until analysis.

Testing of protocol for EhV-86 elution from soybean meal

Two hundred µL of EhV-86 filtrate (1×10^9 viruses mL^{-1}) was added to 1 g of SBMC in a 50 ml Falcon tube (Corning™ Falcon 50 ml Conical Centrifuge Tubes, ThermoFisher Scientific, Waltham, Massachusetts), and held at room temperature for 5 min before eluting the virus from the soybean meal by adding 10 ml of Alga-Gro® Seawater Medium (Carolina Biological Supply Company, Burlington, North Carolina). The tube was vortexed repeatedly for 1 min before incubating in a water bath (Isotemp 205 Digital Water Bath, ThermoFisher Scientific, Waltham, Massachusetts) set at 40°C for a total time of 30 min. The tube was removed and vortexed every 5 min for 30 s. At the end of the temperature exposure, the tube was centrifuged at 4700 rpm for 5 min to collect the soybean meal at the bottom of the tube. The supernatant (virus eluant) was removed and filtered through 0.22 µm syringe filter (Millex™-GP Sterile Syringe Filters with PES Membrane, MilliporeSigma™, Waltham, Massachusetts) into an Amicon centrifugal tube (Millipore Amicon Ultra 15 ml, MilliporeSigma™, Waltham, Massachusetts). The virus eluant was washed 3 times with 1X phosphate buffered saline (1 × PBS, ThermoFisher Scientific, Waltham, Massachusetts) *via* centrifugation as per manufacturer's instructions, and the final 200 µl volume obtained was split into two aliquots of 100 µl each. This process was repeated to create biologically independent replicate samples.

Standard (S-qPCR) and viability (V-qPCR) assays

All assays were conducted in triplicate. To one set of 100 µl virus eluants previously mentioned, PMAxx dye (Biotium Inc., Fremont, California; 25 µM final concentration) was added according to methods optimized by Balestreri et al. (2022) and represented the viability qPCR (V-qPCR) treatments. An untreated duplicate set (i.e., no addition of PMAxx dye) of samples served as a control template for standard qPCR (S-qPCR). All samples were incubated in the dark at room temperature for 10 min on a rocker for optimal mixing. The treated V-qPCR samples were then exposed for 30 min to light using PMA-Lite device (Biotium Inc., Fremont, California) to cross-link PMAxx dye to the DNA (free or within broken viruses). The duplicate S-qPCR samples were kept in the dark at room temperature for the same length of time. All samples were then used for DNA extraction (QIAamp® MinElute® Virus Spin, Qiagen, Valencia, California). The final 30 µl elution volumes were stored at 4°C until qPCR analysis was conducted.

One µL from all the samples (virus eluants and DNA extractions) served as the DNA template in the subsequent 20 µl qPCR mix (QuantiNova SYBR Green PCR kit, Qiagen, Valencia, California): 10 µl Master Mix, 0.1 µl QN ROX Reference Dye, 1.4 µl reverse primer (GACCTTTAGGCCAGGGAG, 0.7 µM final concentration), 1.4 µl forward primer (TTCGCGCTCGAG TCGATC, 0.7 µM final concentration), and 6.1 µl molecular grade water. The primers amplify part of the single copy major capsid protein (MCP) gene of EhV as described by Schroeder et al. (2003). The qPCR analysis was conducted using a QuantStudio™ 3 Real Time PCR machine (ThermoFisher Scientific, Waltham, Massachusetts) run on the following qPCR conditions: 2 min at 95°C followed by 40 cycles of 5 s at 95°C and 10 s at 60°C.

FIGURE 1
Map of the route traveled by a commercial truck carrying test feed ingredients inoculated with *Emiliania huxleyi* virus strain 86. Cities and towns indicated by letters of the alphabet show the journey start (A) and end points (N), with overnight stays labelled from B to M (adapted from Dee et al., 2021).

Standards for the qPCR assays were created using EhV-86 as the template, with the MCP amplificon purity confirmed using E-Gel electrophoresis system (ThermoFisher Scientific, Waltham, Massachusetts) and extracted using Zymoclean™ Gel DNA Recovery Kit (Zymo Research, Irvine, California). The number of EhV-86 genomic copies that equate to MCP copies in our extracted MCP amplicon product was calculated using the following formula:

$$\text{No of copies} = \frac{(\text{ng} \times 6.022 \times 10^{23})}{83454.93\ \text{Da} \times 1 \times 10^{9}}$$

where ng is the amount of the MCP amplicon as measured by Qubit4 (Invitrogen, ThermoFisher Scientific, Waltham, Massachusetts), 6.022×10^{23} is Avogadro's number, 83454.93 Da is the molecular weight of our MCP amplicon as calculated using the Sequence Manipulation Suite (Stothard, 2000), and 1×10^{9} is used to convert the molecular weight of the amplicon to nanograms. A dilution series of the MCP amplicon was used to create a EhV-86 genomic equivalent standard curve. Fresh dilutions for the standard curve were made for every qPCR run.

Protocol for EhV-86 elution from feed matrices used in transport study

One gram of each 30 g of feed matrix was sampled on d 23 and was used in the virus elution protocol as previously described. The qPCRs were carried out on DNA extracted from the eluant. The percentage of virus recovered was calculated as follows:

$$\frac{\text{Amount of virus per gram recovered after treatment and analysis}}{\text{Starting amount of virus per gram}} \times 100\%$$

Statistical analysis

Visualization of data was performed using the ggplot2 package of RStudio environment (Version 1.1.456, RStudio, Inc., Boston, Massachusetts) using R programming language [Version 4.0.5 (2021-03-31), R Core Team, R Foundation for Statistical Computing, Vienna, Austria]. Viral quantity averages (virus μL^{-1}) were normally distributed and compared using two-sample t-test assuming unequal variances in Excel.

Results

qPCR standards

A 10-fold serial dilution of the EhV-86 MCP qPCR amplicon was used to create a standard curve ($y = 3.5926x + 7.0205$) to convert the Ct values from the qPCR assay to EhV-86 genomic equivalents (Figure 2). The standard curve had an R^2 value of 0.9996 indicating high accuracy of prediction (Bustin and

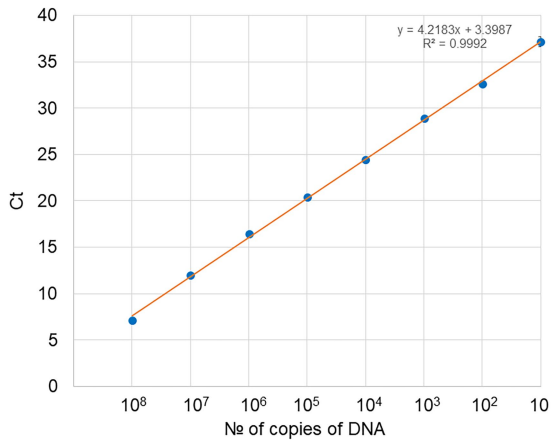

FIGURE 2
Standard curve obtained for EhV-86 PCR assays. Number of copies of DNA in the dilution series (1 μl used per dilution) against Ct (cycle threshold) values as obtained by real time PCR, with each dot representing three replicates. For 10^8 copies of target DNA stock, the Ct was 7.16 and gradually increased to a final value of 37.16 with only 10 copies of DNA present.

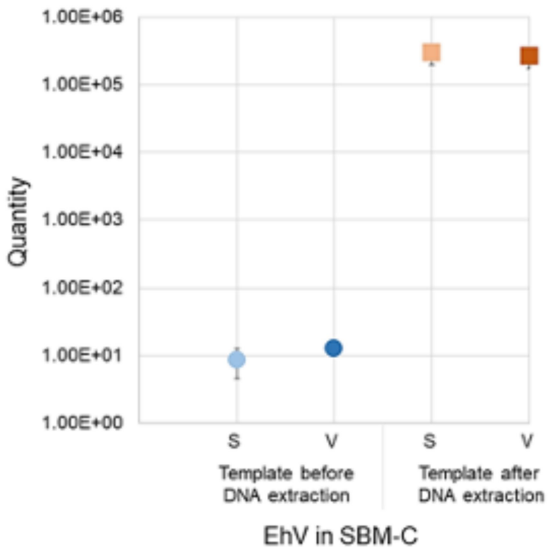

FIGURE 3
Emiliania huxleyi virus (EhV-86) quantity in conventional soybean meal (SBMC) as detected by S-qPCR and V-qPCR using EhV-86 eluant before (blue) and after extracting DNA (red). Bar=standard deviation from the mean.

Huggett, 2017). The EhV-86 MCP qPCR assay had a quantifiable range of 10–10 million EhV-86 genomes per reaction.

Virus extraction efficiency of conventional soybean meal

Before performing multiple extractions from feed samples, we first evaluated the EhV-86 elution protocol using a SBMC sample. We also determined if the eluants could be used directly as templates in the qPCR or if EhV-86 DNA needed to be extracted from the final eluant. Concentrations of 8.53×10^0 (± 4.0 SD, Ct 40.4) and 1.26×10^1 (± 0 SD, Ct 38.2) EhV-86 μl^{-1} from the eluant in both standard (S) and viability (V) qPCRs, respectively, were obtained (Figure 3), which were equivalent to 4.26×10^2 and 6.28×10^2 EhV-86 g^{-1}, or 0.01 and 0.01% recovery, respectively. In contrast, performing DNA extraction on the eluant significantly increased ($p = 0.012$) the amount of virus that was detected *via* standard (22.8%, ± 1.8 SD, Ct 19.2) and V-qPCR (19.9%; ± 1.6 SD, Ct 19.3) (Figure 3). Comparing the detection rates of both qPCR assays, we observed similar or identical recovery percentages ($p = 0.81$), suggesting that EhV-86 is stable in SBMC over the 5 min assay incubation period. Moreover, the elution efficiency of EhV-86 from SBMC was about 20% indicating that about 80% of the virus remained attached or associated to the feed matrix in some way.

Virus DNA concentrations of feed matrices transported across the United States

On d 0, 30 g of each type of feed sample was inoculated with 2 ml of EhV-86 at a concentration of 1×10^9 viruses mL^{-1}, which resulted in an initial virus load of 6.6×10^7 viruses g^{-1} of feed matrix. For the inoculated *CF* samples, an average of 2.36×10^3 EhV-86 μl^{-1} of eluant (Ct 24.9) or 1.18×10^5 EhV-86 g^{-1} of *CF* was recovered on d 0, which represented only a 0.2% average recovery rate. In inoculated SBMC and SBMO samples, 6.83×10^3 EhV-86 μl^{-1} (Ct 23.3) or 3.41×10^5 EhV-86 g^{-1}, and 8.61×10^3 EhV-86 μl^{-1} (Ct 23.2) or 4.31×10^5 EhV-86 g^{-1}, respectively, were recovered. The average recovery rates for SBMC and SBMO were 0.52 and 0.65%, respectively (Figure 4). In addition, of the three feed matrices evaluated, the least variation of EhV-86 content from the mean was in *CF* (2.10×10^3 and 2.82×10^3 for the 1st and 3rd quartiles, respectively). There was also greater EhV-86 deviation from the mean in SBMC (5.39×10^3 and 1.17×10^4 for the 1st and 3rd quartiles, respectively) than in SBMO (5.48×10^3 and 2.82×10^3 for the 1st and 3rd quartiles, respectively; Figure 4). These results suggest that sampling sensitivity is greatest in *CF* followed by SBMO and lastly SBMC and should be considered when evaluating results to determine the most effective virus inactivation methods.

After the 23-days commercial trucking journey across the United States, an average of 6.81×10^3 EhV-86 μl^{-1} (Ct 22.2) or 3.41×10^5 EhV-86 g^{-1} was recovered from the *CF* matrix. This represents an average recovery rate of 0.52%, with a 289% increase in virus concentration compared to d 0 (Figure 4). Similarly, an average of 1.87×10^3 EhV-86 μl^{-1} (Ct 25.3) or 9.37×10^4 EhV-86 g^{-1} was detected in SBMC (0.14% recovery or 28% more viruses) on d 23. For SMBO, an average of 6.25×10^3 EhV-86 μl^{-1} (Ct 24.0) or 3.13×10^5 EhV-86 g^{-1} was recovered, which equates to 0.47% recovery and a 73% increase in virus concentration compared to EhV-86 concentrations on d 0 (Figure 4). As previously described, the deviation from the mean was greater in the SBM matrices

(SMBC = 1.96×10^2 and 2.14×10^3 for the 1st and 3rd quartiles, respectively, and SBMO = 5.76×10^2 and 6.40×10^3 for the 1st and 3rd quartiles, respectively) compared to the *CF* (3.90×10^3 and 9.40×10^3 for the 1st and 3rd quartiles, respectively; Figure 4). These results indicate that there is greater variation of virus quantity recovered in the SBM matrices compared with *CF* which implies that sampling sensitivity is greatest in *CF* followed by the SBM matrices.

Viable virus concentrations of feed matrices transported across the United States

On d 0, an average of 2.19×10^2 EhV-86 μl^{-1} (Ct 29.0) or 1.10×10^4 EhV-86 g^{-1} viable virus was detected with the V-qPCR assay from the *CF* matrix. These concentrations represent an average of 0.02% recovery rate and 9% viability at the start of the study when compared with the eluted virus counts on d 0. On d 23, an average of 7.46×10^2 EhV-86 μl^{-1} (Ct 25.5) or 3.73×10^4 EhV-86 g^{-1} was recovered representing an average recovery rate of 0.06%. This resulted in a range from 11 to 32% in virus viability depending on whether the d 23 or d 0 standard qPCR results were used as baselines, respectively. These results indicate that EhV-86 viability increased by 2 to 22%, and no loss in viability due to the 23-d transport event.

Similarly, an average of 2.08×10^3 EhV-86 μl^{-1} (Ct 25.1) or 1.04×10^5 EhV-86 g^{-1} viable virus was detected on d 0 from SBMC. This represents an average 0.16% recovery rate and 31% viability at the beginning of the study. On d 23, 9.10×10^2 EhV-86 μl^{-1} (Ct 26.2) or 4.55×10^4 EhV-86 g^{-1} was measured, which equates to 0.07% recovery rate and a range in viability from 13 to 49%, depending on whether the d 0 or d 23 standard qPCR results were used as baselines, respectively (Figure 4). These results indicate a range in virus viability from a 17% loss to a gain of 18% compared with standard qPCR results. Given the large deviation from the mean for the 1st and 3rd quartiles observed for both the standard and viability qPCR data (Figure 4), no significant loss of virus was also observed in SBMC matrix over the 23-days transport period. Therefore, sampling methods are extremely important when evaluating the accuracy of virus survival results.

Finally, an average of 4.52×10^2 EhV-86 μl^{-1} (Ct 27.7) or 2.26×10^2 EhV-86 g^{-1} viable virus was detected on d 0 from SBMO, which represents an average 0.003% recovery rate and 0.05% viability at the start of the study. On d 23, 8.31×10^2 EhV-86 μl^{-1} (Ct 27.1) or 4.15×10^4 EhV-86 g^{-1} concentrations were obtained, which equate to a 0.06% recovery rate and a 10 to 13% range in viability depending on whether the d 0 or d 23 standard qPCR results were used as baselines, respectively. These results indicate that there was a gain of 10 to 13% in virus viability compared to standard qPCR results. As for the SBMC matrix, the large deviation from the mean for 1st and 3rd quartiles observed for both the standard and viability qPCR data (Figure 4), indicates that no significant loss of virus occurred in the SBMO matrix over the 23-days transport period.

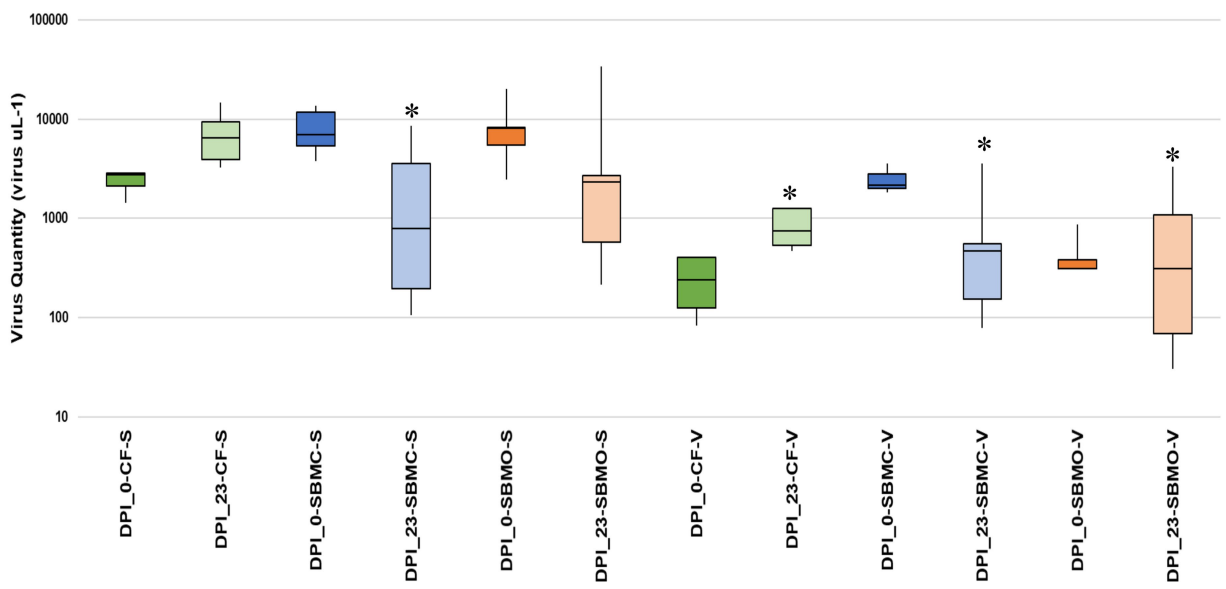

FIGURE 4
Boxplot showing the interquartile range of EhV-86 quantity (virus μL^{-1}) in complete feed (*CF*_ green), conventional soybean meal (SBMC_blue), and organic soybean meal (SBMO_orange) with V-qPCR and S-qPCR. DNA presence on d 0 post infection (DPI_0) and after 23-d commercial truck journey (DPI_23). Asterisks represent the significant difference in average virus recovered between day 23 samples when comparing *CF*-S to SBMC-S, SBMC-V, SBMO-V and *CF*-V, p=0.006, 0.001, 0.002 and 0.001, respectively, as determined by ANOVA (Tukey's test) at 95% confidence level. The line extending from the top and the bottom of the boxes are the upper (maximum) and lower (minimum) limits, respectively. The middle line in the box in the median. The upper box is Q3, the upper quartile or 75th percentile. The lower box is Q1, the lower quartile or 25th percentile.

Variation in EhV-86 concentrations among feed matrices

There was a large range in EhV-86 concentrations in the SBM matrices compared with the *CF* matrix (Figure 4). The average virus quantity for *CF* (standard qPCR) was significantly greater than in SBMC based on using both standard and viable qPCR methods, SBMO based on viable qPCR, and *CF* based on viable qPCR, with $p = 0.006$, 0.001, 0.002, and 0.001, respectively). The uninoculated negative control matrices had negative PCR results (no amplification observed after 40 cycles, data not shown) as expected.

Assessment if PCR bias was associated with feed matrices

A standard curve ($y = -1.528\ln(x) + 42.55$) was created by plotting virus quantity (virus g^{-1}) against Ct values in the various feed matrices using both viable or standard qPCR (Figure 5). The standard curve had an R^2 value of 0.8009 which suggests that there were no inhibitors due to type of matrix in the qPCR assay, and was suitable for use in accurately quantifying amounts of virus for all of these feed matrices. The EhV-86 qPCR assay in feed matrices had a quantifiable range of 6,800 to 340,567 EhV-86 genomes per reaction (Figure 5).

Discussion

In this study, the algal NCLDV EhV-86 was used as a surrogate for ASFV to study virus survival in selected feed matrices subjected to environmental conditions during a 23-days commercial trucking journey across the United States. Overall, viral load (virus μL^{-1}) in samples was successfully quantified using the novel technology of the V-qPCR assay.

Current methods used to measure ASFV inactivation include hemadsorption (HAD_{50}) tests, plaque assays, an EGFP-fluorescent technique, swine bioassays, median tissue culture infectious dose ($TCID_{50}$) or cytopathic effect (CPE) assays, real-time RT-PCR and quantitative PCR (qPCR) (De León et al., 2013; Shurson et al., 2021). Although the quantification of the amount of virus nucleic acids using the qPCR method is useful, it fails to distinguish nucleic acids from viable versus non-viable viruses. Viability PCR utilizes viability dyes, such as ethidium monoazide (EMA) or propidium monoazide (PMA), prior to nucleic acid extraction and PCR or RT-PCR evaluation to evaluate infectivity of a virus (Moreno et al., 2015). Propidium monoazide (PMA) is a photoreactive, membrane-impermeant dye that will selectively penetrate cells which have compromised cell membranes, and thereby considered dead (Nocker et al., 2007; Elizaquível et al., 2014; Zhang et al., 2020). These dyes bind to the nucleic acids which then inhibits DNA from amplifying during PCR amplification (Nocker et al., 2007; Elizaquível et al., 2014; Zhang et al., 2020). Recently, viability RT-qPCR was used to evaluate the viability of PEDV exposed to heat treatments, with the goal of using this method to monitor PEDV contamination in feed and feed ingredients (Puente et al., 2022).

In this transcontinental United States transport scenario, EhV-86 viral DNA was present in the complete feed (average Ct value of 22.2 or 3.4×10^5 virus g^{-1}), conventional soybean meal (average Ct value of 25.3 or 9.37×10^4 EhV-86 g^{-1}), and organic soybean meal (average Ct value of 24.0 or 3.13×10^5 EhV-86 g^{-1}) after 23-days transport, which implies that NCLDVs like ASFV, are relatively stable in certain feed matrices (Dee et al., 2016, 2018, 2020b). In addition to detecting viral genome in these three types of feed matrices, viable EhV-86 was quantified in complete feed (average Ct value of 25.5 or 3.13×10^5 EhV-86 g^{-1}), conventional soybean meal (average Ct value of 26.2 or 4.55×10^4 EhV-86 g^{-1}), and organic soybean meal (average Ct value of 27.1 or 4.15×10^4 EhV-86 g^{-1}) after the 23-days transport period *via* viability qPCR. These results provide empirical evidence that the NCLDV ASFV-like *E. huxleyi* virus can remain viable in these three types of swine feed matrices for more than 3-wks. Among the three different feed matrices, the variation in the quantity of standard and viable DNA was greatest in the organic soybean meal and least in the complete feed. We also observed an increase in amount of virus detected in complete feed after the 23-days of transport time period compared with the amount on d 0 using the S-qPCR analysis, and an increase in the amount of viable virus detected in complete feed and organic soybean meal using the V-qPCR analysis. The factors contributing to these differences between feed matrices is unclear, but the likely reasons involve differences in their complexity and physiochemical properties (i.e., complex mixture of ingredients in complete feed compared with a single ingredient of soybean meal). Limited evidence suggests that moisture content and water activity of feed matrices may play a role in survival of some viruses in some feed matrices (Trudeau et al., 2016) but no studies have been conducted to evaluate this possibility with NCLDVs (Shurson et al., 2021). Understanding the amount and variation of viable virus in feed matrices is important because ASFV is extremely resilient and remains viable in a variety of environments and porcine tissues for many months (Mazur-Panasiuk et al., 2019). The minimum infectious dose of 10^4 $TCID_{50}$ that has been determined for ASFV demonstrates that ASFV can be transmitted orally through contaminated feed, and that repeated exposures exponentially increase the likelihood of infection (Niederwerder et al., 2019), which emphasizes the significance of our results regarding recovery of high concentrations of viable virus in these feed matrices under the environmental conditions of a 23-days transcontinental United States transport time period.

In their recent 23-days bulk transport study, Dee et al. (2021) found that RNA viruses (PEDV, SVA, and PRRSV) were present in one tonne totes of conventional soybean meal (average Ct values of 34.6, 35.7, and 34.9, respectively) and organic soybean meal (average Ct values of 37.6, 35.3 and 34.1, respectively) using real time RT-PCR. When evaluating totes with complete feed, SVA was recovered in only one tote (Ct value of 35.5), with no detectable PEDV or PRRSV found in inoculated totes using the same real time RT-PCR methodology. However, when pigs were fed contaminated

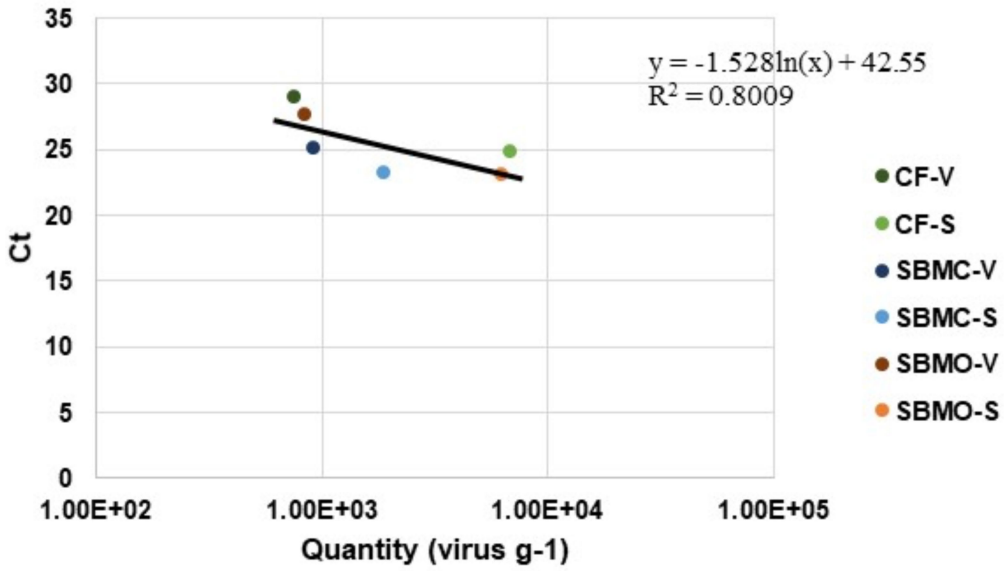

FIGURE 5
Emiliania huxleyi virus-86 quantity (virus g^{-1}) relative to C_t values in complete feed (CF), conventional soybean meal (SBMC), and organic soybean meal (SBMO) with viable (V) and non-viable or standard (S) DNA presence after a 23-d commercial truck journey.

complete feed, they developed a positive PEDV infection, but were negative for PRRSV, suggesting that PEDV remained infectious in a feed matrix after a trans-continental journey, while PRRSV did not (Dee et al., 2021). These observations are not surprising because of the lack of adequate sensitivity of commonly used diagnostic assays to characterize the quantity of viable virus capable of causing infection (Shurson et al., 2021). Furthermore, uneven virus distribution in bulk quantities of feed ingredients can easily occur due to localized contamination events, and depending on the sampling protocol used, could erroneously infer absence or presence of viruses when subsamples are taken. Although a sampling protocol has been developed for the detection of PEDV in soybean meal (Jones et al., 2019), it has not been validated for other viruses and feed ingredients (Shurson et al., 2021). Unfortunately, Dee et al. (2021) only reported mean Ct values for SVA, PEDV, and PRRSV which makes it impossible to determine if inadequate sampling or uneven virus distribution within the bulk feed mass contributed to this contradictory result. It must also be noted that the limitations with animal-based experiments and the consequent subsampling of animal products are overcome by using the V-qPCR method. Viable virus numbers can be accurately quantified down to 10 copies per PCR assay, before and after exposure using the identical methodology. This method is not reliant on whether symptoms are observed or whether the correct sample was collected from the animal at the correct time to confirm presence or absence of virus infection.

In our study, a minimum of 1,500 viable EhV-86 per gram of organic soybean meal was detected at the end of a 23-days transport period, which indicates that a pig consuming 1.4 kg of feed a day would be exposed to 9.26×10^5 EhV-86 daily. If these values are representative for ASFV, then an ASFV infection would most likely be observed based on current estimates of the minimum infective dose (Niederwerder et al., 2019). However, it is important to note that these calculations are based on the methodological bias of EhV-86 being eluted from the feed. Results obtained in the current study showed that >80% of the NCDLV remained in the feed matrix, either in a potentially viable or degraded form, because we were only able to elute 20% of the added virus from the whole SBMC sample, which were all viable. Therefore, the remaining 80% of virus was not in the eluent. Only subsamples of infected feed (1 g from 30 g or 3.3% of the sample) could be analyzed at any one time. We observed mean virus recovery rates much less than 20%, with up to 99.9% of virus still retained in the solid matrix, indicating a potential subsampling effect, and thus detection sensitivity problem due to the non-homogenous distribution of virus across the sample. Consequently, accurate determination of the final exposure to the animal, herd, or farm based on subsampling data is difficult especially in low contamination scenarios. Further research is also required to address whether a similar virus retention rate is observed in other matrices and constituents used by the swine industry. With the help of the surrogate, *in situ* tests can be run in all real-world scenarios. Such experiments will provide invaluable information on the risk ASFV poses in current practices used in feed mills, refineries, processing plants and farm settings.

Currently, chemical mitigation strategies involving formaldehyde, medium chain fatty acids, and glycerol monolaurate have been shown to reduce ASFV infectivity in feed matrices in laboratory settings (Jackman et al., 2020; Niederwerder et al., 2020). These mitigation strategies need to be evaluated in full scale commercial feed mills and supply chains, which now appears to be possible by using a suitable surrogate for ASFV, such as EhV-86. The results of this study demonstrate the benefit of using a safe (non-infectious for animals, humans, or plants) ASFV-like

NCLDV to make direct comparisons of ASFV survival and inactivation in various types of feed ingredients and complete feeds.

Conclusion

Use of the NCLDV EhV-86 as a surrogate for ASFV in experimentally inoculated conventional and organic soybean meal and complete feed based on corn and soybean meal was present in a viable form after a 23-days transcontinental truck transport journey. However, sampling sensitivity rather than virus inactivation best explains the variation of in EhV-86 quantity detected in feed matrices after the 23-days transport period. These results demonstrate for the first time that ASFV-like NCLDVs can retain viability in swine feed matrices during long-term transport across the continental United States, thereby providing evidence for the use of EhV as a surrogate for ASFV for evaluating virus survival and inactivation under real-world demonstrations.

Data availability statement

The original contributions presented in the study are included in the article/supplementary material, further inquiries can be directed to the corresponding authors.

Author contributions

DS, Jv, PU, and GS designed the use of EhV-86 as a surrogate for ASFV. AP maintained the *Emiliania huxleyi* and EhV-86 stocks, performed the bioassays, ran the virus lysates on the flow cytometer, performed the viability qPCRs and wrote the manuscript. DS and HY designed the viability qPCR experiments. CB created the PCR EhV standards, optimized the viability qPCR, and prepared EhV-86 stock for the 23-day transport study. SD and AS designed and ran the 23-day transport study. DS supervised writing of the manuscript. All authors contributed to the article and approved the submitted version.

Funding

This project was funded by SAM Nutrition.

Conflict of interest

The authors declare that the research was conducted in the absence of any commercial or financial relationships that could be construed as a potential conflict of interest.

Publisher's note

All claims expressed in this article are solely those of the authors and do not necessarily represent those of their affiliated organizations, or those of the publisher, the editors and the reviewers. Any product that may be evaluated in this article, or claim that may be made by its manufacturer, is not guaranteed or endorsed by the publisher.

References

Allen, M. J., Schroeder, D. C., and Wilson, W. H. (2006). Preliminary characterisation of repeat families in the genome of EhV-86, a giant algal virus that infects the marine microalga *Emiliania huxleyi*. *Arch. Virol.* 151, 525–535. doi: 10.1007/s00705-005-0647-1

Álvarez, J., Bicout, D., Boklund, A., Bøtner, A., Depner, K., More, S. J., et al. (2019). Research gap analysis on African swine fever. *EFSA J.* 17:e05811. doi: 10.2903/j.efsa.2019.5811

Balestreri, C., Schroeder, D. C., Sampedro, F., Marques, F., Palowski, A., van de Ligt, J. L. G., et al. (2022). Unexpected thermal stability of two enveloped megaviruses, *Emiliania huxleyi* virus and African swine fever virus, as measured by viability PCR. In review.

Bustin, S., and Huggett, J. (2017). qPCR primer design revisited. *Biomol. Detect. Quantif.* 14, 19–28. doi: 10.1016/j.bdq.2017.11.001

Colson, P., De Lamballerie, X., Yutin, N., Asgari, S., Bigot, Y., Bideshi, D. K., et al. (2013). "Megavirales", a proposed new order for eukaryotic nucleocytoplasmic large DNA viruses. *Arch. Virol.* 158, 2517–2521. doi: 10.1007/s00705-013-1768-6

Costard, S., Mur, L., Lubroth, J., Sanchez-Vizcaino, J. M., and Pfeiffer, D. U. (2013). Epidemiology of African swine fever virus. *Virus Res.* 173, 191–197. doi: 10.1016/j.virusres.2012.10.030

De León, P., Bustos, M. J., and Carrascosa, A. L. (2013). Laboratory methods to study African swine fever virus. *Virus Res.* 173, 168–179. doi: 10.1016/j.virusres.2012.09.013

Dee, S. A., Bauermann, F. V., Niederwerder, M. C., Singrey, A., Clement, T., De Lima, M., et al. (2018). Survival of viral pathogens in animal feed ingredients under transboundary shipping models. *PLoS One* 13:e0194509. doi: 10.1371/journal.pone.0194509

Dee, S., Clement, T., Schelkopf, A., Nerem, J., Knudsen, D., Christopher-Hennings, J., et al. (2014). An evaluation of contaminated complete feed as a vehicle for porcine epidemic diarrhea virus infection of naïve pigs following consumption via natural feeding behavior: proof of concept. *BMC Vet. Res.* 10, 1–9. doi: 10.1186/s12917-014-0176-9

Dee, S., Havas, K., and Spronk, G. (2022). Detection of Senecavirus A in pig from a historically negative national swine herd and associated with feed imports from endemically infected countries. *Transbound. Emerg. Dis.* 1–3. doi: 10.1111/tbed.14684

Dee, S., Neill, C., Singrey, A., Clement, T., Cochrane, R., Jones, C., et al. (2016). Modeling the transboundary risk of feed ingredients contaminated with porcine epidemic diarrhea virus. *BMC Vet. Res.* 12:51. doi: 10.1186/s12917-016-0674-z

Dee, S. A., Niederwerder, M. C., Patterson, G., Cochrane, R., Jones, C., Diel, D., et al. (2020b). The risk of viral transmission in feed: what do we know, what do we do? *Transbound. Emerg. Dis.* 67, 2365–2371. doi: 10.1111/tbed.13606

Dee, S., Shah, A., Cochrane, R., Clement, T., Singrey, A., Edler, R., et al. (2020a). Use of a demonstration project to evaluate viral survival in feed: proof of concept. *Transbound. Emerg. Dis.* 68, 248–252. doi: 10.1111/tbed.13682

Dee, S., Shah, A., Jones, C., Singrey, A., Hanson, D., Edler, R., et al. (2021). Evidence of viral survival in representative volumes of feed and feed ingredients during long-distance commercial transport across the continental United States. *Transbound. Emerg. Dis.* 69, 149–156. doi: 10.1111/tbed.14057

Elizaquível, P., Aznar, R., and Sánchez, G. (2014). Recent developments in the use of viability dyes and quantitative PCR in the food microbiology field. *J. Appl. Microbiol.* 116, 1–13. doi: 10.1111/jam.12365

Iyer, L. M., Aravind, L., and Koonin, E. V. (2001). Common origin of four diverse families of large eukaryotic DNA viruses. *J. Virol.* 75, 11720–11734. doi: 10.1128/jvi.75.23.11720-11734.2001

Iyer, L. M., Balaji, S., Koonin, E. V., and Aravind, L. (2006). Evolutionary genomics of nucleo-cytoplasmic large DNA viruses. *Virus Res.* 117, 156–184. doi: 10.1016/j.virusres.2006.01.009

Jackman, J. A., Hakobyan, A., Zakaryan, H., and Elrod, C. C. (2020). Inhibition of African swine fever virus in liquid and feed by medium-chain fatty acids and glycerol monolaurate. *J. Anim. Sci. Biotechnol.* 11:114. doi: 10.1186/s40104-020-00517-3

Jones, C., Stewart, S., Woodworth, J., Dritz, S., and Paulk, C. (2019). Validation of sampling methods in bulk feed ingredients for detection of swine viruses. *Transbound. Emerg. Dis.* 67, 1–5. doi: 10.1111/tbed.13326

Mazur-Panasiuk, N., Żmudzki, J., and Woźniakowski, G. (2019). African swine fever virus – persistence in different environmental conditions and the possibility of its indirect transmission. *J. Vet. Res.* 63, 303–310. doi: 10.2478/jvetres-2019-0058

Moreno, L., Aznar, R., and Sánchez, G. (2015). Application of viability PCR to discriminate the infectivity of hepatitis a virus in food samples. *Int. J. Food Microbiol.* 201, 1–6. doi: 10.1016/j.ijfoodmicro.2015.02.012

Niederwerder, M. C., Dee, S., Diel, D. G., Stoian, A. M. M., Constance, L. A., Olcha, M., et al. (2020). Mitigating the risk of African swine fever virus in feed with anti-viral chemical additives. *Transbound. Emerg. Dis.* 68, 477–486. doi: 10.1111/tbed.13699

Niederwerder, M. C., Stoian, A. M. M., Rowland, R. R. R., Dritz, S. S., Petrovan, V., Constance, L. A., et al. (2019). Infectious dose of African swine fever virus when consumed naturally in liquid or feed. *Emerg. Infect. Dis.* 25, 891–897. doi: 10.3201/eid2505.181495

Nocker, A., Sossa-Fernandez, P., Burr, M. D., and Camper, A. K. (2007). Use of propidium monoazide for live/dead distinction in microbial ecology. *Appl. Environ. Microbiol.* 73, 5111–5117. doi: 10.1128/AEM.02987-06

Oura, C. (2019). *Overview of African swine fever-generalized conditions-Merck veterinary manual [online]* Available at https://www.merckvetmanual.com/generalized-conditions/african-swine-fever/overview-of-african-swine-fever.

Penrith, M.-L. (2009). African swine fever. *Ondersteport J. Vet. Res.* 76, 91–95. doi: 10.4102/ojvr.v76i1.70

Puente, H., Randazzo, W., Falcó, I., Carvajal, A., and Sánchez, G. (2022). Rapid selective detection of potentially infectious porcine epidemic diarrhea coronavirus exposed to heat treatments using viability RT-qPCR. *Front. Microbiol.* 11:1911. doi: 10.3389/FMICB.2020.01911

Schroeder, D. C., Oke, J., Hall, M., Malin, G., and Wilson, W. H. (2003). Virus succession observed during an *Emiliania huxleyi* bloom. *Appl. Environ. Microbiol.* 69, 2484–2490. doi: 10.1128/AEM.69.5.2484-2490.2003

Schroeder, D. C. J., Oke, G. M., and Wilson, W. H. (2002). Coccolithovirus (Phycodnaviridae): characterisation of a new large dsDNA algal virus that infects *Emiliania huxleyi*. *Arch. Virol.* 147, 1685–1698. doi: 10.1007/s00705-002-0841-3

Shurson, G. C., Palowski, A., Ligt, J. L. G., Schroeder, D. C., Balestreri, C., Urriola, P. E., et al. (2021). New perspectives for evaluating relative risks of African swine fever virus contamination in global feed ingredient supply chains. *Transbound. Emerg. Dis.* 69, 31–56. doi: 10.1111/tbed.14174

Stoian, A. M. M., Zimmerman, J., Ji, J., Hefley, T. J., Dee, S., Diel, D. G., et al. (2019). Half-life of African swine fever virus in shipped feed. *Emerg. Infect. Dis.* 25, 2261–2263. doi: 10.3201/eid2512.191002

Stothard, P. (2000). The sequence manipulation suite: JavaScript programs for analyzing and formatting protein and DNA sequences. *BioTechniques* 28, 1102–1104. doi: 10.2144/00286ir01

Trudeau, M. P., Verma, H., Sampedro, F., Urriola, P. E., Shurson, G. C., McKelvey, J., et al. (2016). Comparison of thermal and non-thermal processing of swine feed and the use of selected feed additives on inactivation of porcine epidemic diarrhea virus (PEDV). *PLoS One* 11:e0158128. doi: 10.1371/journal.pone.0158128

Yutin, N., Wolf, Y. I., Raoult, D., and Koonin, E. V. (2009). Eukaryotic large nucleo-cytoplasmic DNA viruses: clusters of orthologous genes and reconstruction of viral genome evolution. *Virol.* 6, 1–13. doi: 10.1186/1743-422X-6-223

Zhang, J., Khan, S., and Chousalkar, K. K. (2020). Development of PMAxxTM-based qPCR for the quantification of viable and non-viable load of salmonella from poultry environment. *Front. Microbiol.* 11:2323. doi: 10.3389/fmicb.2020.581201

frontiers | Frontiers in Microbiology

TYPE Original Research
PUBLISHED 23 December 2022
DOI 10.3389/fmicb.2022.1079390

OPEN ACCESS

EDITED BY
Qing Pan,
Qingdao Agricultural University,
China

REVIEWED BY
Santosh Kumar,
University of Wisconsin-Madison,
United States
Miguel A. De la Cruz,
Mexican Social Security Institute (IMSS),
Mexico

*CORRESPONDENCE
Feng Liu
✉ liufeng68431@163.com
Liancheng Lei
✉ leiliancheng@163.com

SPECIALTY SECTION
This article was submitted to Infectious Agents and Disease, a section of the journal Frontiers in Microbiology

RECEIVED 25 October 2022
ACCEPTED 09 December 2022
PUBLISHED 23 December 2022

CITATION
Yao Q, Xie T, Fu Y, Wan J, Zhang W, Gao X, Huang J, Sun D, Zhang F, Bei W, Lei L and Liu F (2022) The CpxA/CpxR two-component system mediates regulation of *Actinobacillus pleuropneumoniae* cold growth. *Front. Microbiol.* 13:1079390. doi: 10.3389/fmicb.2022.1079390

The CpxA/CpxR two-component system mediates regulation of *Actinobacillus pleuropneumoniae* cold growth

Qing Yao[1], Tingting Xie[1], Yu Fu[1], Jiajia Wan[1], Wendie Zhang[1], Xuejun Gao[1], Jing Huang[2], Diangang Sun[1], Fuxian Zhang[1], Weicheng Bei[3], Liancheng Lei[1,4]* and Feng Liu[1]*

[1]College of Animal Sciences, Yangtze University, Jingzhou, Hubei, China, [2]School of Foreign Languages, Zhejiang Gongshang University, Hangzhou, Zhejiang, China, [3]State Key Laboratory of Agricultural Microbiology, College of Veterinary Medicine, Huazhong Agricultural University, Wuhan, Hubei, China, [4]College of Veterinary Medicine, Jilin University, Changchun, China

Introduction: To survive in various hostile environments, two-component system is an adaptive mechanism for diverse bacteria. Activity of the CpxA/CpxR two-component system contributes to coping with different stimuli, such as pH, osmotic and heat stress.

Methods: However, the role of the CpxA/CpxR system in cold resistance is little-known. In this study, we showed that CpxA/CpxRwas critical for *A. pleuropneumoniae* growth under cold stress.

Results: β-Galactosidaseanalysis showed that CpxA/CpxR positively regulated the predicted cold stress gene *cspC*. The mutant for cold stress gene *cspC* was impaired in the optimal growth of *A. pleuropneumoniae* under cold stress. Furthermore, electrophoretic mobility shift assays demonstrated that CpxR-P could directly regulate the transcription of the cold stress gene *cspC*.

Discussion: These results presented in this study illustrated that the CpxA/CpxR system plays an important role in cold resistance by upregulating expression of *CspC*. The data give new insights into how *A. pleuropneumoniae* survives in cold stress.

KEYWORDS

Actinobacillus pleuropneumoniae*, two-component system, CpxA/CpxR, cold stress, *cspC

Introduction

Actinobacillus pleuropneumoniae is an important swine pathogen responsible for respiratory infectious disease, porcine contagious pleuropneumonia (PCP). PCP is characterized by fibrinous, hemorrhagic, and necrotic lung lesions, and causes substantial losses in the swine industry worldwide (Guitart-Matas et al., 2022; Zhang et al., 2022). To date, 19 reference serovars have been identified based on the composition of the capsular polysaccharide (CPS; Stringer et al., 2021; Scherrer et al., 2022). Previous studies have

reported that five putative two-component systems (TCS) were found in the genome of *A. pleuropneumoniae*, such as CpxR/CpxA, ArcA/ArcB, QseB/QseC, NarP/NarQ, and PhoB/PhoR (Xu et al., 2008).

The CpxR/CpxA system is commonly used by Gram-negative bacteria to regulate many bacterial processes, mainly triggered by a wide range of environmental conditions, such as pH, osmolarity and temperature (Nakayama and Watanabe, 1995; Tschauner et al., 2014; Liu et al., 2022a). The CpxR/CpxA system is composed of the transmembrane sensor kinase CpxA and the cytoplasmic response regulator CpxR (Danese et al., 1995; Raivio and Silhavy, 1997). When bacteria are exposed to extracytoplasmic stresses, the histidine kinase CpxA autophoshorylates and then transfers a phosphoryl group to the response regulator CpxR (Price and Raivio, 2009; Raivio, 2014). Phosphorylation enables CpxR to bind to the promoter region of multiple genes, and alters the transcription of these genes (Raivio et al., 2013).

Bacteria have evolved various complicated networks to cope with different stress factors, such as temperature, pH and mosmotic (Telhig et al., 2020). When subjected to a sudden drop in temperatures, microbes undergo severe unfavorable disturbances such as decreased membrane fluidity and ribosome efficiency, and increase formation of stable secondary structures in nucleic acids (Goto et al., 2015). To adapt to the extreme environments, bacteria activate the expression of cold shock proteins (Csp) that function as general RNA or DNA chaperones to eliminate their secondary structures (Kloska et al., 2020). Csp protein are ubiquitous in a broad variety of bacteria, and multiple variants of this protein have been found, such as CspA, CspB, CspC, CspD, CspE, CspF, CspG, CspH and CspI in *E. coli* (Derzelle et al., 2000).

Porcine pleuropneumonia caused by *A. pleuropneumoniae* leads to economic losses to affected pig farmers. Before causing infection in the host, *A. pleuropneumoniae* must well cope with different environmental cues *in vitro*. However, the cold adaptation mechanism of *A. pleuropneumoniae* is poorly understood. In the present study, we found that the CpxA/CpxR system plays an important role in APP resistance to cold stress. Furthermore, we investigated the mechanism of the Cpx-mediated cold resistance, and showed that the CpxA/CpxR-CspC pathway contribute to the cold stress response in *A. pleuropneumoniae*.

Materials and methods

Bacterial strains, culture conditions, and plasmids and primers

The bacterial strains and plasmids, as well as primers used in this study, are listed in Tables 1,2. *A. pleuropneumoniae*

TABLE 1 Bacterial strains and plasmids used in this study.

Strains/plasmids	Characteristics	Source/reference
Actinobacillus pleuropneumoniae		
S4074	*A. pleuropneumoniae* reference strain of serovar 1; WT strain	From Prof. Weicheng Bei
Δ*cpxAR*	*A. pleuropneumoniae* 4,074 *cpxAR*-deletion mutant	From Prof. Weicheng Bei
Δ*cspC*	*A. pleuropneumoniae* 4,074 *cspC*-deletion mutant	This study
Δ*cspD*	*A. pleuropneumoniae* 4,074 *cspD*-deletion mutant	This study
CΔ*cpxAR*	Complemented strain of Δ*cpxAR*; Cm^r	From Prof. Weicheng Bei
CΔ*cspC*	Complemented strain of Δ*cspC*; Cm^r	This study
Escherichia coli		
DH5a	Cloning host for recombinant vector	Takara
β2155	Transconjugation donor for constructing mutant strain	From Prof. Weicheng Bei
Plasmid		
pEMOC2	Transconjugation vector: ColE1 ori mob RP4 sacB, Amp^rCm^r	From Prof. Weicheng Bei
pEΔ*cspC*	Up- and down-stream arms of *cspC* were ligated sequentially into pEMOC2, and used as the transconjugation vector for *cspC* gene deletion	This study
pEΔ*cspD*	Up- and down-stream arms of *cspD* were ligated sequentially into pEMOC2, and used as the transconjugation vector for *cspD* gene deletion	This study
pJFF224-XN	E. coli-APP shuttle vector: RSF1010 replicon; mob oriV, Cm^r	From Prof. Weicheng Bei
pCΔ*cspC*	pJFF224-XN carrying the intact *cspC*	This study
pET-30a	Expression vector; Kan^r	Novagen
pET30a-*cpxR*	pET-30a carrying *cpxR* gene	Our Laboratory

Cm^r, Chloramphenicol resistance; Amp^r, Ampicillin resistance; Kan^r, Kanamycin resistance.

TABLE 2 Primers used in this study.

Primer	Sequence (5′–3′) a	Use
cspC-S-F	CTGTCGACAAGACGGGATGGCGGAAGAT	amplification of *cspC* upstream homology arms
cspC-S-R	CAACAGGTATCGTTAAATGGTTCAACTTCAGCGGTAAACGTAAAAACACT	amplification of *cspC* upstream homology arms
cspC-X-F	AGTGTTTTTACGTTTACCGCTGAAGTTGAACCATTTAACGATACCTGTTG	amplification of *cspC* downstream homology arms
cspC-X-R	ATGCGGCCGCTCTTTGCGTTGCTCTTTTCGCTGTT	amplification of *cspC* downstream homology arms
cspC-W-F	TTGTATCCGCTGGCGTATGA	detection exterior of *cspC* mutants
cspC-W-R	TAGCGTTCTTGAGTACGATTGCTT	detection exterior of *cspC* mutants
cspC-N-F	GGACCGCGCTCTGAATCTTGAACTT	detection interior of *cspC* mutants
cspC-N-R	GGAAAATCCTATGTCTAAAGCAACA	detection interior of *cspC* mutants
cspC-C-F	CCGCTCGAGAAGTCCAAATAGATGCCGACCCAAT	amplification of *cspC*
cspC-C-R	AAGGAAAAAAGCGGCCGCTTAAAGTGTTTTTACGTTTACCGCT	amplification of *cspC*
cspD-S-F	ACGCGTCGACAGACAAAGTCGGTATCCCAGG	amplification of *cspD* upstream homology arms
cspD-S-R	GATGCACCGCGTTCACCGTTAAACCATTTCACGATGCCAACTTCCA	amplification of *cspD* upstream homology arms
cspD-X-F	TGGAAGTTGGCATCGTGAAATGGTTTAACGGTGAACGCGGTGCATC	amplification of *cspD* downstream homology arms
cspD-X-R	AAGGAAAAAAGCGGCCGCAGCGGCGGTAACAATAGAACT	amplification of *cspD* downstream homology arms
cspD-W-F	CCGCCACTCCAGCAAAATACC	detection exterior of *cspD* mutants
cspD-W-R	TGTACCTTTTGACCTACTTTAAGCG	detection exterior of *cspD* mutants
cspD-N-F	CAATAGTGCGAAAGGATTCGGATTT	detection interior of *cspD* mutants
cspD-N-R	TGTACCTTTTGACCTACTTTAAGCG	detection interior of *cspD* mutants
CpxR-F	CGCCCATATGATGCCTAGAATTTTACTCGTTG	amplification of *cpxR*
CpxR-R	CGCCCTCGAGTTTTTCAGTAACGAGTAAATAACCTCGACCGC	amplification of *cpxR*
16SrRNA-F	CCATGCCGCGTGAATGA	detection the transcription of 16SrRNA
16SrRNA-R	TTCCTCGCTACCGAAAGAACTT	detection the transcription of 16SrRNA
cspC-EMSA-F	TTGATGAAAAGAATTGCTGCACGTT	amplification of *cspC* promoter region for EMSA
cspC-EMSA-R	ATTTAAGTCCAAATAGATGCCGACC	amplification of *cspC* promoter region for EMSA
cspD-EMSA-F	AACCTCCGTATTTTAAAAAATTTTG	amplification of *cspD* promoter region for EMSA
cspD-EMSA-R	CCGAATCCTTTCGCACTATTGAACC	amplification of *cspD* promoter region for EMSA
rpoE-EMSA-F	TAAAAAGATAAGATAAGCGGTC	amplification of *rpoE* promoter region for EMSA
rpoE-EMSA-R	AGTGTGTAACAAAAATGAAAAGT	amplification of *rpoE* promoter region for EMSA
rpoD-EMSA-F	GCGGAAGAAAAGCAAGAGTTGGTCA	amplification of *rpoD* promoter region for EMSA
rpoD-EMSA-R	TCCATAATTGTATCCGTTTTGTGTG	amplification of *rpoD* promoter region for EMSA

cells were grown in tryptic soy broth (TSB; Solarbio, China) or on TSB agar plates supplemented with 10 μg/ml NAD (Sigma-Aldrich, United States) and 10% fetal bovine serum (FBS; Every Green, China). *E. coli* cells were grown in LB medium supplemented with 50 μg/ml diaminopimelic acid (Sigma-Aldrich, United States) or relevant antibiotics (chloramphenicol, 5 μg/ml; kanamycin, 50 μg/ml). The Δ*cspC*, Δ*cspD* and CΔ*cspC* strains were generated using the suicide plasmid pEMOC2 and the shuttle plasmid pJFF224-XN as described earlier (Liu et al., 2022a). In order to induce gene expression, plasmid pJFF224-P*cspC* which expressed the *cspC* gene under the control of IPTG-inducible promoter was constructed, and electrically transferred to the mutant strain Δ*cpxAR*.

RNA extraction, transcriptome analysis and qRT-PCR

Bacterial cells grown overnight in TSB medium at 37°C were subcultured 1:1000 in fresh TSB broth. Cells grown up to the exponential phase (OD600; 0.6) were exposed to 4°C for a series of times. Total RNA was extracted from bacterial cultures using the Bacteria Total RNA Isolation Kit (Sangon Biotech, China). The synthesis of complementary DNA (cDNA) was achieved using the HiScript II Q RT SuperMix for qRT-PCR (Vazyme, China). For quantitative RT-PCR, the reactions were performed using SYBR qPCR Mix (Vazyme, China) and run in the CFX96 Real-Time System (Bio-Red, United States). Data were normalized using the 16S rRNA as internal control, and calculated using the $2^{-\Delta\Delta Ct}$ method.

β-Galactosidase assay

A *cspC/cspD*-lacZ fusions containing the promoter region of *cspC/cspD* and the *lacZ* gene, and cloned into the Xho I and Not I sites of the plasmid pJFF224-XN. Then, the recombinant plasmid was introduced into the wild-type and the Δ*cpxAR* mutant strain. All strains were grown overnight in TSB broth at 37°C, diluted 1:1,000 in fresh TSB broth, and grown at 20°C for a series of times. The collected culture was assayed for β-Galactosidase activity by using a β-galactosidase (β-GAL) Activity Assay Kit (Micromethod; Sangon Biotech) according to the manufacturer's specification.

Electrophoretic mobility shift assay

The His6-CpxR protein was expressed using *E. coli* BL21 (DE3)-containing pET30a-CpxR and purified by using a Ni-nitrilotriacetic acid (Ni-NTA) resin affinity chromatography (Qiagen, Germany). The purified protein was phosphorylated by acetyl phosphate (Sigma, United States) according to previously described procedures (Li et al., 2018). DNA probes were amplified and purified and then labeled using a Biotin Labeling Kit (Beyotime, China). Then, the phosphorylated CpxR and labeled probes were used for protein-DNA EMSAs as described previously (Cheng et al., 2021). Labeled DNA probe (1 μM) and various concentrations of phosphorylated CpxR protein (0–4 pmol) were incubated at 24°C for 20 min in reaction buffer (50 mM Tris–HCl, pH 8.0, 2.5 mM $MgCl_2$, 100 mM KCl, 0.2 mM DTT, 10% glycerol, 2 μg salmon sperm DNA). For competition experiments with unlabeled DNA probes, a 100-fold molar excess was preincubated with phosphorylated CpxR protein. The reaction mixtures were loaded on a 4% non-denaturing polyacrylamide electrophoresis in 0.5 × Tris-borate-EDTA (TBE) buffer. The bands of labeled probes were subsequently transferred to nylon membrane (Beyotime, China), and detected using the Chemiluminescent EMSA Kit (Beyotime, China).

Growth assays under cold stress

To measure cold growth, the *A. pleuropneumoniae* strain S4074 and its mutant derivatives were cultured in TSB medium overnight at 37°C, then diluted 1:100 (~1×10^7 CFU/ml) into fresh TSB broth and incubated at 20°C for 48 h. Every 4 h for 48 h, samples were serially diluted and plated on TSB agar, and the OD600 was measured.

Bioinformatic and statistical analysis

The −10 and −35 promoter regions, and transcriptional atart site (TSS) of the cold shock gene *cspC* were, respectively, predicated by BPROM (Prediction of bacterial promoters)[1] and Berkeley Drosophila Genome Project (BDGP).[2] All data were analyzed using two-tailed Student's *t*-tests (GraphPad Prism version 7.0, GraphPad Software, inc., San Diego, United States), and presented as mean ± standard deviation (SD). $p < 0.05$ was considered statistically significant.

Results

Cpxa/CpxR is required for cold growth in *Actinobacillus pleuropneumoniae*

To investigate whether CpxAR is involved in the cold adaptation of *A. pleuropneumoniae*, we tested the growth rates of the WT, Δ*cpxAR* and CΔ*cpxAR* strains when exposed to cold stress (20°C). Under cold stress, the growth rate of the mutant strain Δ*cpxAR* was significantly lower than that of the WT and CΔ*cpxAR* strains (Figures 1A,B). Our previous study found that the growth rate of Δ*cpxAR* was also lower than that of the WT at 37°C, and the difference was obviously much smaller than that at 20°C (Li et al., 2018). The qRT-PCR analysis showed that the mRNA level of the *cpxA* and *cpxR* genes were upregulated under cold stress in the WT strain (Figures 1C,D). These results suggest that CpxA/CpxR plays an important role in cold adaptation of *A. pleuropneumoniae*.

Cpxa/CpxR transcriptionally regulates the expression of *cspC* under cold stress

Analysis of the *A. pleuropneumoniae* genome revealed that it contains two Csp proteins (CspC and CspD) which have a high amino acid identity with *E.coli* CspA (Figure 2A). Each protein possesses a conserved cold shock domain (CSD) that harbors two nucleic acid-binding motifs RNAP1 and RNAP2.

To elucidate the mechanism of CpxA/CpxR affecting APP cold adaptability, β-Galactosidase assay was performed to examine the link between CpxR and the cold shock genes *cspC* and *cspD*. As shown in Figures 2B,C, the promoter activity of *cspC*-lacZ under cold stress were significantly elevated in the WT strain, and decreased in the Δ*cpxAR* mutant compared with the former, but the the *cspD* gene was not. These findings indicated that CpxA/CpxR regulates the expression of the cold shock gene *cspC* which is cold inducible in *A. pleuropneumoniae*.

The cold shock gene *cspC* is adjacent to the gene *bioB* and *proQ* in the *A. pleuropneumoniae* chromosome (Figure 2D). In order to describe the *cspC* gene, we performed RT-PCR across the

1 http://linux1.softberry.com/berry.phtml?topic=bprom&group=programs&subgroup=gfindb

2 https://www.fruitfly.org/seq_tools/promoter.html

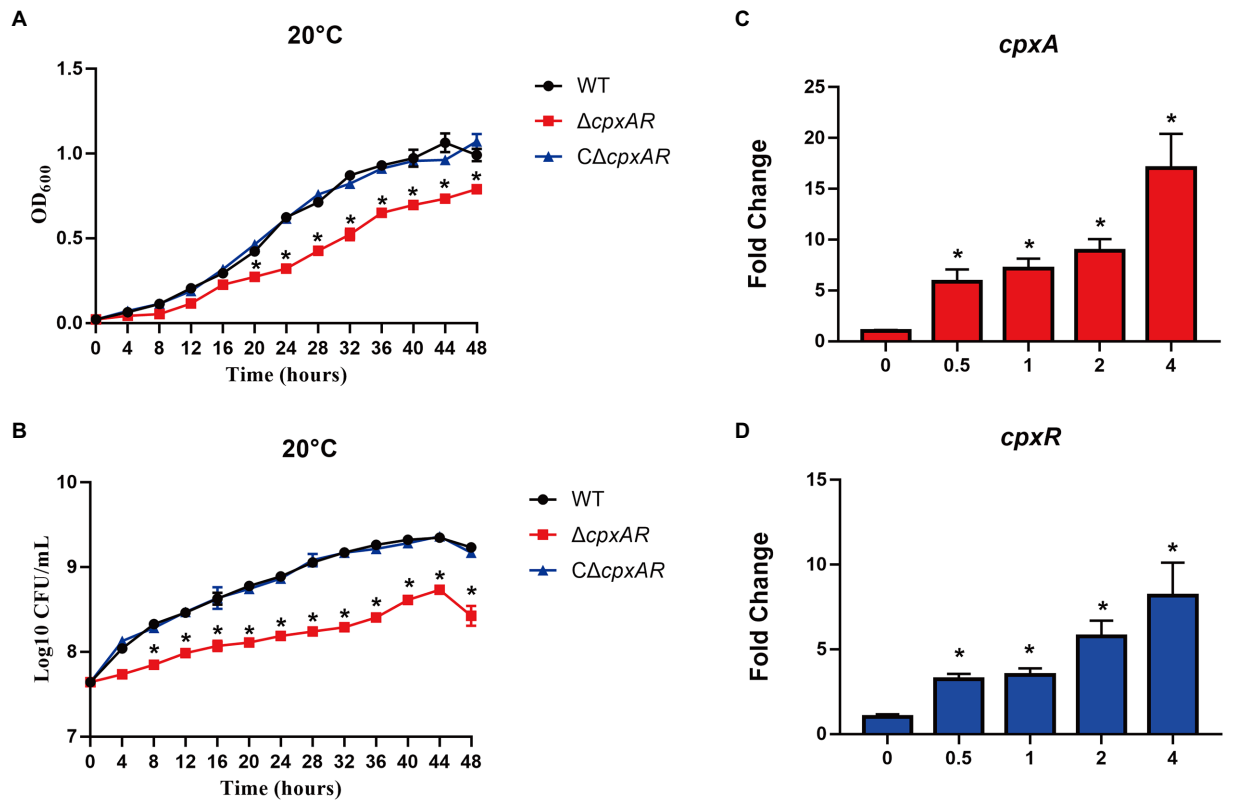

FIGURE 1
CpxA/CpxR is required for APP cold growth. The growth rates of the WT, Δ*cpxAR* and CΔ*cpxAR* strains at 20°C were monitored by measurement of OD600 **(A)** and viable cell counts **(B)**. qRT-PCR analysis of *cpxA* **(C)** and *cpxR* **(D)** genes in *A. pleuropneumoniae* S4074 under 20°C. *$p < 0.05$.

bioB-cspC and *cspC-proQ* junctions. The RT-PCR analysis indicated that the *cspC* gene is transcribed separately from the *proQ* gene.

Cspc is essential for cold growth in *Actinobacillus pleuropneumoniae*

To investigate whether CspC and CspD are involved in cold stress, we generated the Δ*cspC* and Δ*cspD* mutant strains, and the CΔ*cspC* complemented strain, and tested the growth rates of the WT, Δ*cspC*, Δ*cspD* and CΔ*cspC* strains at 20°C and 37°C. Under cold stress (20°C), the Δ*cspC* mutant exhibited growth defects, whereas the WT, Δ*cspD* and CΔ*cspC* strains displayed normal growth (Figures 3A,B). When the bacteria were cultured at 37°C, the growth property of Δ*cspC* mutant was similar to those of the WT and CΔ*cspC* strains (Figures 3C,D). The growth of Δ*cpxAR*/P*cspC* in liquid media was then assayed. Clearly, when CspC was produced with IPTG at 0.1 mM and above, the growth defect of the Δ*cpxAR* mutant strain was significantly rescued (Figures 3E,F). These results suggested that CspC is essential for cold growth in *A. pleuropneumoniae*.

Cpxr binds specifically to the *cspC* promoter region

Since CpxR is a response regulator, we examined the interaction between the recombinant CpxR protein and the putative *cspC* promoter region using EMSA. As shown in Figure 4A, incubation of biotin-labeled *cspC* with CpxR protein led to the formation of DNA-protein complexes in a protein concentration-dependent manner. Meanwhile, no CpxR-DNA complex was observed with adding excess amounts of unlabeled probes, suggesting that the CpxR could bind specifically to the *cspC* promoter region (Figure 4B).

Previous studies found that the CpxR binding site has a conserved sequence GTAAA-$(N)_{4-8}$-GTAAA (Bruna et al., 2018; Jia et al., 2022). In this study, we found that a 16-nt region (5'-GGAAAACATCGATAAA-3′) was relatively consistent with the characteristics of conserved sequence. As shown in Figure 4C, CpxR-P was unable to bind to a mutant *cspC* putative promoter region in which the 16-nt region was deleted from the putative CpxR-P binding box. In order to describe the CpxR binding site in detail, the *cspC* promoter region and transcription start site were, respectively, analyzed by BPROM and BDGP. As shown in Figure 4D, a putative −10 AGAATTGC box, −35 TGGAGA box

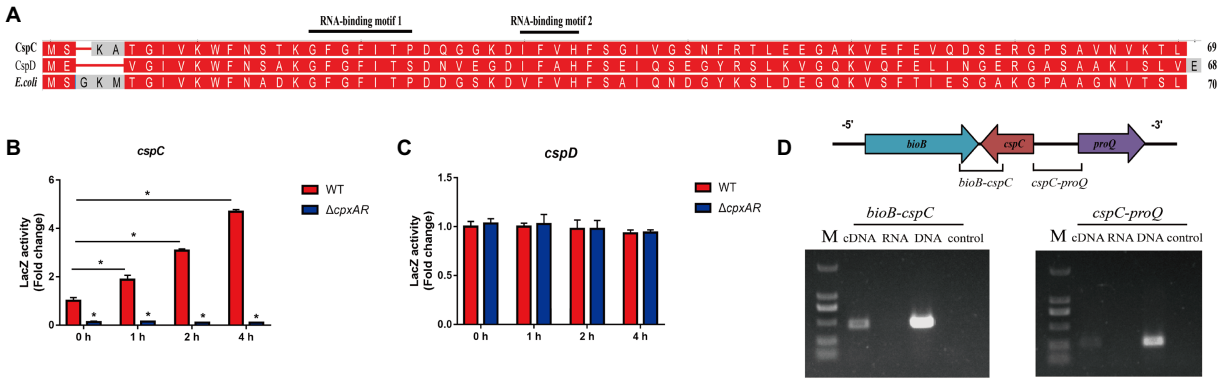

FIGURE 2
cspC transcription is activated by CpxR. **(A)** Alignment of cold shock proteins homologs showing the conserved cold shock domain (CSD), which harbors two nucleic acid-binding motifs RNAP1 and RNAP2. The *A. pleuropneumoniae* CspC and CspD, and *E. coli* CspA are included for comparison. Promoter activity of *cspC* **(B)** and *cspD* **(C)** genes in the WT, Δ*cpxAR* and CΔ*cpxAR* strains under 20°C. *$p < 0.05$. **(D)** Transcriptional characteristics of *cspC* gene as determined by RT-PCR at 20°C.

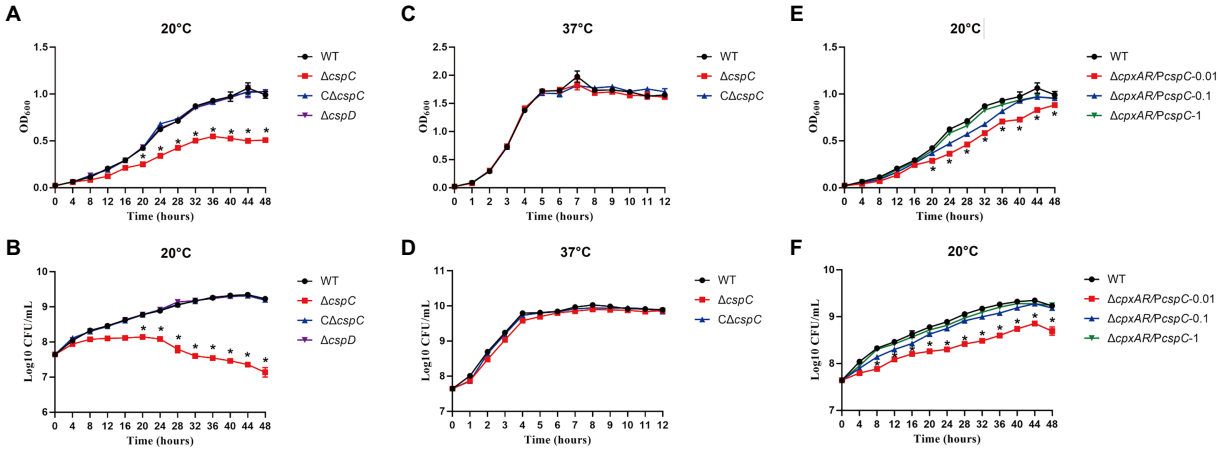

FIGURE 3
CspC is critical for APP cold growth. The growth rates of the WT, Δ*cspC*, CΔ*cspC* and Δ*cspD* strains at 20°C were monitored by measurement of OD600 **(A)** and viable cell counts **(B)**. The growth rates of the WT, Δ*cspC* and CΔ*cspC* strains at 37°C were monitored by measurement of OD600 **(C)** and viable cell counts **(D)**. The growth rates of strains expressing *cspC* with IPTG at indicated concentrations were monitored by measurement of OD600 **(E)** and viable cell counts **(F)**. *$p < 0.05$.

and TSS were detected, and, respectively, located 30 bp, 50 bp and 12 bp upstream of the start codon.

Discussion

Two-component system (TCS) is a key signal transduction mechanism that controls many aspects of bacterial physiology, sense a broad range of stimuli and make an appropriate response to adapt and survive in changing environmental conditions. The CpxA/CpxR system identified as a pleiotropic TCS in many Gram-negative bacteria, regulates many virulence factors, such as lipopolysaccharide, polysaccharide capsule, and type IV pilus and responds to a variety of extracellular stimuli including salt, heat, metals, and pH (Jubelin et al., 2005; Hunke et al., 2012; Yan et al., 2020; Liu et al., 2022a,b). However, the link between CpxA/CpxR and cold stress is still unknown. In this study, in-frame mutation of the *cpxA* and *cpxR* genes exhibited growth defects, and the mRNA level of the *cpxA* and *cpxR* genes elevated under cold stress, suggesting that CpxA/CpxR plays a crucial role in cold adaptation of *A. pleuropneumoniae*. Furthermore, we provided the first insights into how CpxA/CpxR contributes to cold growth in *A. pleuropneumoniae*.

Cold is an adverse environment for bacteria, altering secondary structures of nucleic acids that render cells nonviable (Balhesteros et al., 2010). To stabilize secondary structures of the RNA, bacteria activate the expression of multiple variants of Csp proteins under cold stress, such as the nine Csp proteins (CspA to CspI) in *E. coli*

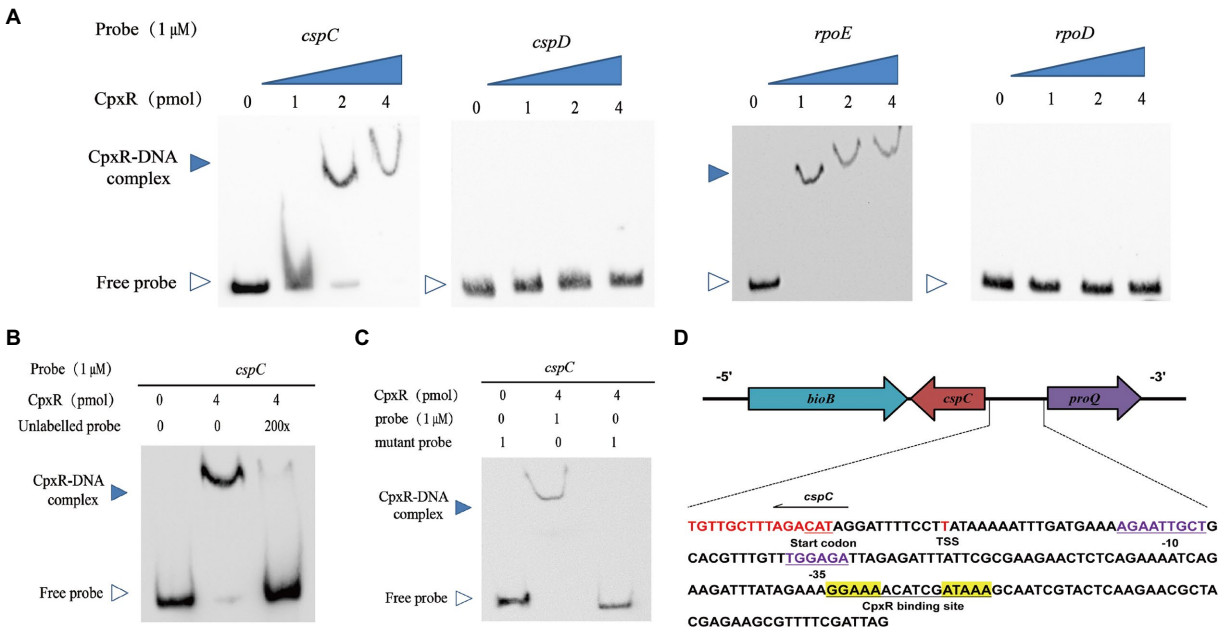

FIGURE 4
CpxR binds promoter of *cspC* but not that of *cspD*. **(A)** EMSAs analysis of the binding affinity of various amounts of CpxR-P with the *cspC*, *cspD*, *rpoE* (positive control), *rpoD* (negative control) promoter regions. **(B)** EMSAs analysis of the binding of CpxR-P with the *cspC* promoter region under adding excess amounts of unlabeled probes. **(C)** Labeled mutant *cspC* promoter region were incubated with various concentrations of CpxR-P. **(D)** Characterizing the CpxR binding site. The putative CpxR binding site is underlined and shown in yellow background. The −35 and −10 box are underlined and shown in purple nucleotides. The transcription start site (TSS) is shown in red.

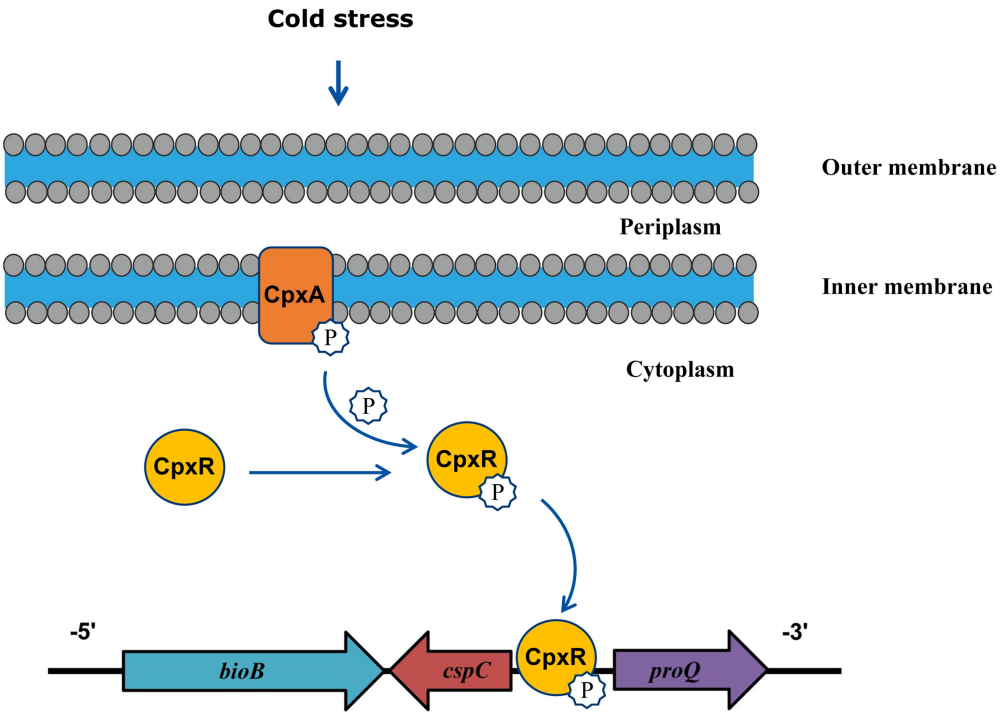

FIGURE 5
Model illustrating that CpxA/CpxR mediates cold stress in *A. pleuropneumoniae*. Under cold stress, phosphorylated form of CpxA transfers the phosphate group to CpxR, then the active CpxR binds the promoter of the *cspC* gene to upregulate its transcription.

(Graumann and Marahiel, 1999; Li et al., 2021). In the present study, we found that the genome of *A. pleuropneumoniae* encodes two Csp proteins (CspC and CspD), which are constituted of a single cold shock domain (CSD). Here, β-Galactosidase analysis showed that CspC is cold inducible, and positively regulated by CpxA/CpxR. In addition, these cold growth tests revealed that CspC was vital for APP cold adaptability. These results indicated that CspC is involved in the mechanism of CpxA/CpxR-mediated cold stress.

To response to the adverse condition, activated CpxR binds to the promoter region of target genes, and regulates these genes expression. Previous studies showed that the CpxR binding consensus sequence is identified as GTAAA-$(N)_{4\text{-}8}$-GTAAA, or TTTAC-$(N)_{4\text{-}8}$-TTTAC in many other bacteria (De Wulf et al., 2002; Srinivasan et al., 2012; Feldheim et al., 2016). According to the consensus sequence, we found a potential CpxR binding site (GGAAA-N_6-ATAAA) located 52 bp upstream of the promoter −35 region, and 95 bp upstream of the transcription start site. Previous studies showed that the CpxR-binding site is generally located upstream of the promoter region and within 100 bp upstream of the transcription start site, primarily functions as a class I factor and activates their transcription (De Wulf and Lin, 2000; Raffa and Raivio, 2002; Yamamoto and Ishihama, 2006). In addition, we verified that CpxR could directly bind to the promoter region of the *cspC* gene, and the CpxR-*cspC* interaction was specific by EMSA. These results revealed that CpxR positively regulates the *cspC* gene transcription.

In conclusion, this study illuminates the mechanism of *A. pleuropneumoniae* cold stress and demonstrate the involvement of CpxA/CpxR for the first time. These findings indicated that CpxA/CpxR contributes to cold growth by positively regulating the expression of *cspC* gene (Figure 5). Since the CpxA/CpxR and CspC are conserved in many bacteria, the revelation of the CpxA/CpxR-CspC pathway will provide important implications for elucidating cold stress in other bacteria.

Data availability statement

The datasets presented in this study can be found in online repositories. The names of the repository/repositories and accession number(s) can be found in the article/Supplementary material.

Author contributions

FL and LL conceived and designed the experiments. QY, YF, JW, WZ and TX performed the experiments. FL and QY analyzed the data. XG,WB, DS, and FZ contributed reagents, materials, and analysis tools. JH polished the language. All authors contributed to the article and approved the submitted version.

Funding

This research was supported by the National Natural Science Foundation of China (32002252).

Conflict of interest

The authors declare that the research was conducted in the absence of any commercial or financial relationships that could be construed as a potential conflict of interest.

Publisher's note

All claims expressed in this article are solely those of the authors and do not necessarily represent those of their affiliated organizations, or those of the publisher, the editors and the reviewers. Any product that may be evaluated in this article, or claim that may be made by its manufacturer, is not guaranteed or endorsed by the publisher.

Supplementary material

The Supplementary material for this article can be found online at: https://www.frontiersin.org/articles/10.3389/fmicb.2022.1079390/full#supplementary-material

References

Balhesteros, H., Mazzon, R. R., da Silva, C. A., Lang, E. A., and Marques, M. V. (2010). CspC and CspD are essential for Caulobacter crescentus stationary phase survival. *Arch. Microbiol.* 192, 747–758. doi: 10.1007/s00203-010-0602-8

Bruna, R. E., Molino, M. V., Lazzaro, M., Mariscotti, J. F., and Garcia Vescovi, E. (2018). CpxR-dependent thermoregulation of Serratia marcescens PrtA metalloprotease expression and its contribution to bacterial biofilm formation. *J. Bacteriol.* 200, e00006–18. doi: 10.1128/JB.00006-18

Cheng, C., Liu, F., Jin, H., Xu, X., Xu, J., Deng, S., et al. (2021). The DegU orphan response regulator contributes to heat stress resistance in *listeria monocytogenes*. *Front. Cell. Infect. Microbiol.* 11:761335. doi: 10.3389/fcimb.2021.761335

Danese, P. N., Snyder, W. B., Cosma, C. L., Davis, L. J., and Silhavy, T. J. (1995). The Cpx two-component signal transduction pathway of *Escherichia coli* regulates transcription of the gene specifying the stress-inducible periplasmic protease. *DegP. Genes Dev* 9, 387–398. doi: 10.1101/gad.9.4.387

De Wulf, P., and Lin, E. C. (2000). Cpx two-component signal transduction in *Escherichia coli*: excessive CpxR-P levels underlie CpxA* phenotypes. *J. Bacteriol.* 182, 1423–1426. doi: 10.1128/JB.182.5.1423-1426.2000

De Wulf, P., McGuire, A. M., Liu, X., and Lin, E. C. (2002). Genome-wide profiling of promoter recognition by the two-component response regulator CpxR-P in *Escherichia coli*. *J. Biol. Chem.* 277, 26652–26661. doi: 10.1074/jbc.M203487200

Derzelle, S., Hallet, B., Francis, K. P., Ferain, T., Delcour, J., and Hols, P. (2000). Changes in *cspL*, *cspP*, and *cspC* mRNA abundance as a function of cold shock and growth phase in lactobacillus plantarum. *J. Bacteriol.* 182, 5105–5113. doi: 10.1128/JB.182.18.5105-5113.2000

Feldheim, Y. S., Zusman, T., Speiser, Y., and Segal, G. (2016). The *legionella pneumophila* CpxRA two-component regulatory system: new insights into CpxR's function as a dual regulator and its connection to the effectors regulatory network. *Mol. Microbiol.* 99, 1059–1079. doi: 10.1111/mmi.13290

Goto, S., Kawamoto, J., Sato, S. B., Iki, T., Watanabe, I., Kudo, K., et al. (2015). Alkyl hydroperoxide reductase enhances the growth of *Leuconostoc mesenteroides* lactic acid bacteria at low temperatures. *AMB Express* 5:11. doi: 10.1186/s13568-015-0098-3

Graumann, P. L., and Marahiel, M. A. (1999). Cold shock proteins CspB and CspC are major stationary-phase-induced proteins in *Bacillus subtilis*. *Arch. Microbiol.* 171, 135–138. doi: 10.1007/s002030050690

Guitart-Matas, J., Gonzalez-Escalona, N., Maguire, M., Vilaro, A., Martinez-Urtaza, J., Fraile, L., et al. (2022). Revealing genomic insights of the unexplored porcine pathogen *Actinobacillus pleuropneumoniae* using whole genome sequencing. *Microbiol Spectr* 10:e0118522. doi: 10.1128/spectrum.01185-22

Hunke, S., Keller, R., and Muller, V. S. (2012). Signal integration by the Cpx-envelope stress system. *FEMS Microbiol. Lett.* 326, 12–22. doi: 10.1111/j.1574-6968.2011.02436.x

Jia, Y., Hu, H., Zhai, Y., Zhao, B., Sun, H., Hu, G., et al. (2022). CpxR negatively regulates IncFII-replicon plasmid pEC011 conjugation by directly binding to multi-promoter regions. *Res. Vet. Sci.* 150, 98–106. doi: 10.1016/j.rvsc.2022.05.016

Jubelin, G., Vianney, A., Beloin, C., Ghigo, J. M., Lazzaroni, J. C., Lejeune, P., et al. (2005). CpxR/OmpR interplay regulates curli gene expression in response to osmolarity in *Escherichia coli*. *J. Bacteriol.* 187, 2038–2049. doi: 10.1128/JB.187.6.2038-2049.2005

Kloska, A., Cech, G. M., Sadowska, M., Krause, K., Szalewska-Palasz, A., and Olszewski, P. (2020). Adaptation of the marine bacterium *Shewanella baltica* to low temperature stress. *Int. J. Mol. Sci.* 21:338. doi: 10.3390/ijms21124338

Li, H., Liu, F., Peng, W., Yan, K., Zhao, H., Liu, T., et al. (2018). The CpxA/CpxR two-component system affects biofilm formation and virulence in *Actinobacillus pleuropneumoniae*. *Front. Cell. Infect. Microbiol.* 8:72. doi: 10.3389/fcimb.2018.00072

Li, H., Yang, R., Hao, L., Wang, C., and Li, M. (2021). CspB and CspC are induced upon cold shock in *Bacillus cereus* strain D2. *Can. J. Microbiol.* 67, 703–712. doi: 10.1139/cjm-2021-0025

Liu, F., Peng, W., Yan, K., Huang, J., Yuan, F., He, Q., et al. (2022a). CpxAR of *Actinobacillus pleuropneumoniae* contributes to heat stress response by repressing expression of type IV pilus gene apfA. *Microbiol. Spectr*. e02523–22. doi: 10.1128/spectrum.02523-22

Liu, F., Yao, Q., Huang, J., Wan, J., Xie, T., Gao, X., et al. (2022b). The two-component system CpxA/CpxR is critical for full virulence in *Actinobacillus pleuropneumoniae*. *Front. Microbiol.* 13:1029426. doi: 10.3389/fmicb.2022.1029426

Nakayama, S., and Watanabe, H. (1995). Involvement of *cpxA*, a sensor of a two-component regulatory system, in the pH-dependent regulation of expression of *Shigella sonnei virF* gene. *J. Bacteriol.* 177, 5062–5069. doi: 10.1128/jb.177.17.5062-5069.1995

Price, N. L., and Raivio, T. L. (2009). Characterization of the Cpx regulon in *Escherichia coli* strain MC4100. *J. Bacteriol.* 191, 1798–1815. doi: 10.1128/JB.00798-08

Raffa, R. G., and Raivio, T. L. (2002). A third envelope stress signal transduction pathway in *Escherichia coli*. *Mol. Microbiol.* 45, 1599–1611. doi: 10.1046/j.1365-2958.2002.03112.x

Raivio, T. L. (2014). Everything old is new again: an update on current research on the Cpx envelope stress response. *Biochim. Biophys. Acta* 1843, 1529–1541. doi: 10.1016/j.bbamcr.2013.10.018

Raivio, T. L., Leblanc, S. K., and Price, N. L. (2013). The *Escherichia coli* Cpx envelope stress response regulates genes of diverse function that impact antibiotic resistance and membrane integrity. *J. Bacteriol.* 195, 2755–2767. doi: 10.1128/JB.00105-13

Raivio, T. L., and Silhavy, T. J. (1997). Transduction of envelope stress in *Escherichia coli* by the Cpx two-component system. *J. Bacteriol.* 179, 7724–7733. doi: 10.1128/jb.179.24.7724-7733.1997

Scherrer, S., Peterhans, S., Neupert, C., Rademacher, F., Bartolomei, G., Sidler, X., et al. (2022). Development of a novel high resolution melting assay for identification and differentiation of all known 19 serovars of *Actinobacillus pleuropneumoniae*. *Microbiology* 11:e1272. doi: 10.1002/mbo3.1272

Srinivasan, V. B., Vaidyanathan, V., Mondal, A., and Rajamohan, G. (2012). Role of the two component signal transduction system CpxAR in conferring cefepime and chloramphenicol resistance in *Klebsiella pneumoniae* NTUH-K2044. *PLoS One* 7:e33777. doi: 10.1371/journal.pone.0033777

Stringer, O. W., Bosse, J. T., Lacouture, S., Gottschalk, M., Fodor, L., Angen, O., et al. (2021). Proposal of *Actinobacillus pleuropneumoniae* serovar 19, and reformulation of previous multiplex PCRs for capsule-specific typing of all known serovars. *Vet. Microbiol.* 255:109021. doi: 10.1016/j.vetmic.2021.109021

Telhig, S., Ben Said, L., Zirah, S., Fliss, I., and Rebuffat, S. (2020). Bacteriocins to thwart bacterial resistance in gram negative bacteria. *Front. Microbiol.* 11:586433. doi: 10.3389/fmicb.2020.586433

Tschauner, K., Hornschemeyer, P., Muller, V. S., and Hunke, S. (2014). Dynamic interaction between the CpxA sensor kinase and the periplasmic accessory protein CpxP mediates signal recognition in *E. coli*. *PLoS One* 9:e107383. doi: 10.1371/journal.pone.0107383

Xu, Z., Zhou, Y., Li, L., Zhou, R., Xiao, S., Wan, Y., et al. (2008). Genome biology of *Actinobacillus pleuropneumoniae* JL03, an isolate of serotype 3 prevalent in China. *PLoS One* 3:e1450. doi: 10.1371/journal.pone.0001450

Yamamoto, K., and Ishihama, A. (2006). Characterization of copper-inducible promoters regulated by CpxA/CpxR in *Escherichia coli*. *Biosci. Biotechnol. Biochem.* 70, 1688–1695. doi: 10.1271/bbb.60024

Yan, K., Liu, T., Duan, B., Liu, F., Cao, M., Peng, W., et al. (2020). The CpxAR two-component system contributes to growth, stress resistance, and virulence of *Actinobacillus pleuropneumoniae* by upregulating *wecA* transcription. *Front. Microbiol.* 11:1026. doi: 10.3389/fmicb.2020.01026

Zhang, L., Luo, W., Xiong, R., Li, H., Yao, Z., Zhuo, W., et al. (2022). A combinatorial vaccine containing inactivated Bacterin and subunits provides protection against *Actinobacillus pleuropneumoniae* infection in mice and pigs. *Front Vet Sci* 9:902497. doi: 10.3389/fvets.2022.902497

frontiers | Frontiers in Microbiology

TYPE Original Research
PUBLISHED 11 January 2023
DOI 10.3389/fmicb.2022.1082712

OPEN ACCESS

EDITED BY
Qing Pan,
Qingdao Agricultural University, China

REVIEWED BY
Kunfeng Sun,
University of Pennsylvania,
United States
Yongtao Zhu,
Minnesota State University, Mankato,
United States
Cherry Fernandez-Colorado,
University of the Philippines Los Baños,
Philippines

*CORRESPONDENCE
Qinghai Hu
huqinghai@caas.cn

†These authors have contributed equally to this work

SPECIALTY SECTION
This article was submitted to Infectious Agents and Disease, a section of the journal Frontiers in Microbiology

RECEIVED 28 October 2022
ACCEPTED 28 December 2022
PUBLISHED 11 January 2023

CITATION
Wang J, Chen Y, He X, Du X, Gao Y, Shan X, Hu Z and Hu Q (2023) PaR1 secreted by the type IX secretion system is a protective antigen of *Riemerella anatipestifer*. *Front. Microbiol.* 13:1082712. doi: 10.3389/fmicb.2022.1082712

PaR1 secreted by the type IX secretion system is a protective antigen of *Riemerella anatipestifer*

Jialing Wang†, Yan Chen†, Xiaohua He, Xiaoli Du, Yongheng Gao, Xinggen Shan, Zhiqun Hu and Qinghai Hu*

Shanghai Veterinary Research Institute, Chinese Academy of Agricultural Sciences, Shanghai, China

Riemerella anatipestifer mainly infects domestic ducks, geese, turkeys, and other birds, and causes considerable economic losses to the global duck industry. Previous studies have shown that concentrated cell-free culture filtrates of *R. anatipestifer* induce highly significant protection against homologous challenge. In this study, 12 immunogenic proteins were identified in the culture supernatant of *R. anatipestifer* strain Yb2 with immunoproteomic analysis. Of these, three immunogenic proteins, AS87_RS06600 (designated "PaR1" in this study), AS87_RS09020, and AS87_RS09965, which appeared in more than three spots on the western-blotted membrane, were expressed in *Escherichia coli* and purified. Animal experiments showed that the recombinant PaR1 (rPaR1) protein protected 41.67% of immunized ducklings against challenge with virulent Yb2, whereas rAS87_RS09020 or rAS87_RS09965 did not, and that ducklings immunized once with rPaR1 were 20, 40, and 0% protected from challenge with *R. anatipestifer* strains WJ4 (serotype 1), Yb2 (serotype 2), and HXb2 (serotype 10), respectively. In addition, rPaR1 immunized rabbit serum showed bactericidal activity against strain Yb2 at a titer of 1:8. These results indicate that rPaR1 of strain Yb2 protects against homologous challenge. Amino acid homology analysis show that PaR1 is a non-serotype-specific protein among different *R. anatipestifer* serotypes. Furthermore, PaR1 is mainly secreted outside the cell through the T9SS. Overall, our results demonstrate that *R. anatipestifer* PaR1 is a non-serotype-specific protective protein secreted by the T9SS.

KEYWORDS

***Riemerella anatipestifer*, protective antigen, subcellular localization, the type IX secretion system (T9SS), PaR1**

Introduction

Riemerella anatipestifer, the type species of the genus *Riemerella* in the family *Weeksellaceae* within the order *Flavobacteriales* in the phylum *Bacteroidetes* (Garcia-Lopez et al., 2019), is the causative agent of septicemia anserum exsudativa (Segers et al., 1993). It infects domestic ducks, geese, turkeys, and other birds. *R. anatipestifer* infection is probably the most economically important disease of farmed ducks worldwide. Once the bacterium infects a duck flock, it can become endemic and eradication can be difficult, with repeated infectious episodes possible. Currently, at least 21 serotypes of *R. anatipestifer* have been identified (Bisgaard, 1982; Pathanasophon et al., 2002; Cheng et al., 2003), but no or only little cross-protection has been observed among different serotypes of *R. anatipestifer* (Sandhu, 1979; Pathanasophon et al., 1996). Thus far, little is known about the protective antigens of *R. anatipestifer*.

Bacterial outer-membrane proteins are exposed on the cell surface, in direct contact with the host immune system, so some are potentially immunogenic antigens. The outer-membrane protein OmpA was the first immunogenic protein (Subramaniam et al., 2000) and virulence factor (Hu et al., 2011) identified in *R. anatipestifer*. The full length of the *ompA* gene is 1,467 bp, encoding 488 amino acids, and a 1,164 bp open reading frame (ORF) occurs within *ompA* at nucleotides (nt) 303–1,467. However, recombinant OmpA (residues 101–488) of serotype 15 *R. anatipestifer* strain 110/89 did not protect against challenge with this virulent serotype 15 strain, although specific antibodies were detected in the infected ducks (Huang et al., 2002). However, recombinant OmpA (residues 33–466) of serotype 2 *R. anatipestifer* strain Rf153 reportedly induced protection against challenge with both homologous and heterologous strains (60 and 50% protection against serotype 2 strain Rf153 and serotype 1 strain Rf63, respectively) (Zhai et al., 2013). In a recent study, we showed that the soluble recombinant protein rOmpA1164 (amino acids 102–488, encoded by a 1,164 bp ORF within *ompA*) but not rOmpA1467 (amino acids 1–488), provided partial protective immunity against homologous challenge (Xu et al., 2020). Outer-membrane protein GroEL is another immunogenic protein expressed by *R. anatipestifer*. Ducklings immunized with rGroEL were 50, 37.5, and 37.5% protected from the challenge with RA strains WJ4 (serotype 1), Th4 (serotype 2), and YXb-2 (serotype 10) (Han et al., 2012). In our previous study, an immunoproteomic analysis using duck antiserum against *R. anatipestifer* identified 34 immunogenic proteins, including OmpA and GroEL, among the whole-cell bacterial proteins of serotype 2 *R. anatipestifer* strain Th4, and the TonB-dependent outer-membrane receptor TbdR1 was shown to be a cross-immunogenic antigen among serotypes 1, 2, and 10 of *R. anatipestifer* (Hu et al., 2012). Further studies showed that TbdR1 is involved in hemin iron acquisition and necessary for optimal bacterial virulence (Lu et al., 2013). In another study, 12 immunoreactive proteins were identified in whole cells of *R. anatipestifer* serotype 2 strain RAf153 with an immunoproteomic analysis using rabbit antiserum against *R. anatipestifer*. One of these proteins, recombinant elongation factor G, responded to serum against strain RAf153, but not that from serotype 1 strain RjR1 (Zhai et al., 2012).

Formalin-inactivated *R. anatipestifer* bacterin has been shown to protect against challenge with virulent strains of homologous serotypes (Sandhu, 1979; Layton and Sandhu, 1984), whereas broth culture bacterin prepared from strains of serotypes 1, 6, 11, 14, and 19 conferred no significant protection against challenge with strains of heterologous serotypes. However, concentrated cell-free culture filtrates prepared from strain 1,081 of serotype 1 and strain 328 of serotype 19 induced highly significant protection against homologous challenge (Pathanasophon et al., 1996), indicating that the protective antigens exist on the outer membrane and in the culture supernatant of *R. anatipestifer*. In this study, the immunogenic proteins in the culture supernatant of *R. anatipestifer* strain Yb2 were identified with an immunoproteomic analysis, and PaR1, which is secreted by the T9SS, was identified as a novel protective antigen of *R. anatipestifer*.

Materials and methods

Bacterial strains, plasmids, and culture conditions

Riemerella anatipestifer strains WJ4 (serotype 1), Yb2 (serotype 2), and HXb2 (serotype 10) were isolated by Qinghai Hu from sick ducks in China in 2000 (Hu et al., 2010), and their full genome sequences have been deposited in GenBank under the accession number CP041029, CP007204, and CP011859. The suicide plasmid pYT354 (Zhu et al., 2017) was generously provided by Professor Mark J. McBride (University of Wisconsin–Milwaukee, Milwaukee, WI, USA). The *R. anatipestifer* strains and their derivatives were routinely grown in tryptic soybean broth (TSB; Difco, Detroit, MI, USA) at 37°C with shaking or on tryptic soybean agar (TSA). *Escherichia coli* cells were routinely grown in Luria–Bertani (*LB*) *broth* (Difco) at 37°C with shaking. The strains, plasmids, and primers used in this study are listed in **Table 1**. When required, antibiotics were added at the following concentrations: ampicillin (100 μg/mL), chloramphenicol (50 μg/mL), erythromycin (0.5 μg/mL), or kanamycin (50 μg/mL).

Precipitation of cell-free culture supernatant of *R. anatipestifer* strain Yb2

The proteins in the culture supernatant of strain Yb2 were precipitated with the trichloroacetic acid (TCA)–acetone

method, as described previously (Flaugnatti and Journet, 2017), with some modification. Briefly, *R. anatipestifer* strain Yb2 was grown to mid-log phase, at an optical density at a wavelength of 600 nm (OD_{600}) of 1.0, in TSB at 37°C with shaking. The cells were pelleted by centrifugation at 7,000 × g for 10 min, and the culture supernatant was filtered through a 0.22 μm pore-size polyvinylidene difluoride (PVDF) filter (Merck Millipore, Darmstadt, Germany) to remove residual cells. TCA was then added to the filtered culture supernatant to a final concentration of 10% (w/v), mixed gently, and incubated at 4°C overnight. The precipitated proteins were collected by centrifugation at 16,000 × g for 1 h at 4°C, and the pellet was washed with cold acetone. The pellets were air dried and resuspended in solubilization buffer (7 M urea, 2 M thiourea, 4% CHAPS). The precipitated proteins were quantified with the Bradford method using Bio-Rad Protein Assay Dye Reagent (Bio-Rad, Hercules, CA, USA), and the samples were stored at -80°C until further analysis.

Immunoproteomic analysis of proteins precipitated from culture supernatant

Samples containing 200 μg of proteins precipitated from culture supernatants were passively rehydrated onto 13 cm immobilized pH gradient IPG strips (GE Healthcare Life Sciences, Piscataway, NJ, USA) in a pH range of 3–10 for 12–16 h. The immunoproteomic analysis of the precipitated proteins was performed as described previously (Hu et al., 2012), and included isoelectric focusing (IEF), sodium dodecyl sulfate-polyacrylamide gel electrophoresis (SDS-PAGE), western blotting, image processing, matrix-assisted laser desorption/ionization time of flight mass spectrometry (MALDI-TOF MS), database searches, and bioinformatic analyses. Convalescent duck serum against *R. anatipestifer* strain Yb2 was used in the western blotting analysis.

Expression and purification of selected proteins

In this study, proteins AS87_RS06600 (designated "PaR1"), AS87_RS09020, and AS87_RS09965 appeared in more than three spots on the western-blotted membrane in the immunoproteomic analysis. The genes encoding the three proteins were amplified from serotype 2 *R. anatipestifer* strain Yb2 and cloned into the pET28a vector (Novagen, Darmstadt, Germany). The recombinant proteins were expressed in *E. coli* BL21(DE3) cells (Novagen, Darmstadt, Germany) and purified with Ni-IDA affinity chromatography (DetaiBio, Nanjing, China) as described previously (Xu et al., 2020). The recombinant proteins rPaR1, rAS87_RS09020, and rAS87_RS09965 were detected on western blots probed with convalescent duck serum directed against *R. anatipestifer* strain Yb2.

Evaluation of protective immunity induced by the recombinant proteins

One-day-old Cherry Valley ducklings were purchased from Lijia Duck Farm (Taixin, Jiangsu, China), and no serum antibodies against *R. anatipestifer* strains WJ4 (serotype 1), Yb2 (serotype 2), or HXb2 (serotype 10) were detected with a whole-cell ELISA (Prieto et al., 2003). The ducklings were housed in cages under a 12 h light/dark cycle with free access to food and water. All applicable international, national, and institutional guidelines for the care and use of the animals were followed. The protocol was approved by the Committee on the Ethics of Animal Experiments of Shanghai Veterinary Research Institute, Chinese Academy of Agricultural Sciences (permit number: SHVRI-ZD-2018-026).

Before immunization and challenge experiments, the median lethal doses (LD_{50s}) for *R. anatipestifer* strains WJ4 (serotype 1), Yb2 (serotype 2), and HXb2 (serotype 10) were measured in ducklings as 1.97×10^8 CFU, 1.07×10^6 CFU, and 1.89×10^5 CFU, respectively. In this study, the immunized ducklings were challenged with 10 LD50 doses of each strain.

To evaluate the protective immunity conferred by the recombinant proteins rPaR1, rAS87_RS09020, and rAS87_RS09965, 8 days-old Cherry Valley ducklings were divided into four groups (12 ducklings per group) and immunized once intramuscularly with 100 μg of each recombinant protein or phosphate-buffered saline (PBS), each emulsified with Montanide ISA 70 V adjuvant (Seppic, Paris, France). At 2 weeks postimmunization, all the ducklings were challenged with 1×10^7 CFU of wild-type Yb2. Ducklings that became moribund were killed humanely and counted as dead, and then subjected to *R. anatipestifer* identification. The mortality of the ducklings was recorded daily for a period of 10 days after challenge.

To investigate whether rPaR1-immunized ducklings were protected from virulent challenge with *R. anatipestifer* strains of different serotypes, 8 days-old Cherry Valley ducklings were immunized with ISA-70-V-adjuvant-emulsified rPaR1 (n = 30 ducklings for three groups), ISA-70-V-adjuvant-emulsified PBS (n = 30 ducklings for three groups), or ISA-70-V-adjuvant-emulsified inactivated Yb2 bacterin (n = 10 ducklings). On day 15, the sera of the immunized ducklings from each group were collected and screened for rPaR1 antibodies with an ELISA, using 1 μg/mL rPaR1 as the coating antigen and *horseradish* peroxidase (HRP)-labeled rabbit anti-duck IgY (IgG) (Biodragon, Suzhou, China) as the secondary detection antibody. The rPaR1- and PBS-immunized ducklings (10 rPaR1-immunized and 10 PBS-immunized ducklings for each strain) were challenged with 2×10^9 CFU of serotype 1 strain WJ4,

TABLE 1 Strains, plasmids, and primers used in this study.

Strains, plasmids or primers	Description[a]	References
Strains		
R. anatipestifer WJ4	The wild type strain, serotype 1, Kan^R	(Hu et al., 2010)
R. anatipestifer Yb2	The wild type strain, serotype 2, Kan^R	(Hu et al., 2010)
R. anatipestifer HXb2	The wild type strain, serotype 10, Kan^R	(Hu et al., 2010)
R. anatipestifer Yb2ΔgldL	*gldL* deletion mutant of strain Yb2, T9SS defective	This study
E. coli S-17-1	Lpir hsdR pro thi; chromosomal integrated RP4-2 Tc:Mu Km:Tn7	Biomedal
Plasmids		
pYT354	Suicide plasmid, Ap^R (Em^R)	(Zhu et al., 2017)
pYT354-gldL-LR	Recombinant suicide plasmid for deleting *gldL*	This study
Primers for construction of suicide plasmid		
gldL-L F	5′ TAGGATCCAGGATTGATAGGAGAATACCTTATTGA 3′ *Bam*HI site underlined	This study
gldL-L R	5′ CATGTCGACTACTACAGAAGCACCTACAGAGTAGAT 3′ *Sal*I site underlined	This study
gldL-R F	5′ AGTAGTCGACGCACTTTATGCATTACAGTTAGAA 3′ *Sal*I site underlined	This study
gldL-R R	5′ ATGCATGCTGTAAATCTAGTAGTTCCACATATCGT 3′ *Sph*I site underlined	This study
Primers for identification of the *gldL* deleted mutant		
16S rRNA F	5′ CAGCTTAACTGTAGAACTGC 3′	(Hu et al., 2011)
16S rRNA R	5′ TCGAGATTTGCATCACTTCG 3′	
ermF F	5′ GCCCGAAATGTTCAAGTTGT 3′	This study
ermF R	5′ TTTCCGAAATTGACCTGACC 3′	This study
gldL ORF F	5′ ATGAGACTAAATGATAAAACATTAAATT 3′	This study
gldL ORF R	5′ ATTTTATCCTTTCATCGCGTT 3′	This study

[a]Antibiotic resistance phenotypes are as follows: Kanamycin, Kan^R; ampicillin, Ap^R; erythromycin, Em^R.

10^7 CFU of serotype 2 strain Yb2, or 2×10^6 CFU of serotype 10 strain HXb2. Ten ducklings immunized with inactivated Yb2 bacterin were challenged with 10^7 CFU of Yb2. The mortality of the ducklings was recorded daily, as above.

Serum bactericidal assay

The natural ability of mouse complement (Sigma-Aldrich, St. Louis, MO, USA) and inactivated mouse complement (56°C for 30 min) to kill serotype 1 strain WJ4, serotype 2 strain Yb2, and serotype 10 strain HXb2, was determined. To each well of a 96-well flat-bottom plate (Corning, NY, USA) containing 45 μL of sterile PBS, 25 μL of mouse complement or inactivated mouse complement was added, and then 30 μL of each bacterial suspension (10^4 CFU/mL in PBS). After incubation at 37°C for 30 min, 100 μL of the mixture was plated onto TSA plates. Percentage killing was calculated as the geometric mean value of [1-(CFU remaining after mouse complement/CFU remaining after inactivated complement)] × 100 from three trials, and the strain for which the natural bactericidal rate of mouse complement was <15% at a complement concentration of 25% (Martin et al., 2005) was used in the next bactericidal assay. Rabbit antiserum against rPaR1 and naïve rabbit serum were inactivated at 56°C for 30 min and 2-fold serial diluted in PBS. Then the bactericidal activity against serotype 2 strain Yb2 was performed as described previously (Gu et al., 1996). For each well of a 96-well flat-bottom plate, 50 μL of diluted rabbit antiserum against rPaR1 or naïve rabbit serum, 30 μL of bacterial suspension (10^4 CFU/mL in PBS) and 15 μL of mouse complement serum were added. The plates were incubated at 37°C for 30 min, and 50 μL of the mixture in each well was spread onto TSA plates. The bactericidal assay was performed in triplicate. The highest serum dilution causing 50% killing was expressed as the bactericidal titer.

Sequences analysis of *paR1* from *R. anatipestifer* strains of different serotypes

The nucleotide acid sequence of *paR1* (AS87_RS06600) from *R. anatipestifer* strains of different serotypes were retrieved from the GenBank database. The derived amino acid sequences of PaR1 from these strains were aligned and analyzed with Clustal W in the MegAlign program of the Lasergene 7.01 software (DNASTAR Inc., Madison, WI, USA).

Preparation of rabbit antiserum against rPaR1

Rabbit antiserum against rPaR1 was obtained by immunizing 2 months-old New Zealand rabbits subcutaneously (s.c.) with 100 μg of purified rPaR1 protein emulsified with 50% (vol/vol) Montanide ISA 50 V adjuvant (Seppic) and boosted twice s.c. with 100 μg of rPaR1 at two weekly intervals. The rabbit sera were collected 7 days after the third immunization.

Construction of type IX secretion system (T9SS)-defective mutant of *R. anatipestifer* strain Yb2

Most members of the phylum Bacteroidetes secrete proteins across the outer membrane *via* the type IX secretion system (T9SS) (Sato et al., 2010; McBride and Zhu, 2013). T9SS is a multiprotein system consisting of at least 20 proteins, and GldL is one of the core components of T9SS (Hennell James et al., 2021). To construct a T9SS-defective mutant, a 444 bp (nt 58–501) fragment of the strain Yb2 *gldL* ORF (687 bp) was deleted in-frame with the suicide plasmid pYT354, as described previously (Barbier et al., 2020). Briefly, a 2,599 bp region corresponding to the first 57 bp of *gldL* together with the directly upstream region was amplified with primers gldL-L P1 and gldL-L P2. A 2,773 bp region corresponding to the final 186 bp of *gldL* together with the directly downstream region was amplified with primers gldL-R P1 and gldL-R P2. The two fragments were ligated into suicide vector pYT354, generating the recombinant suicide plasmid p354-gldL-LR. This plasmid was then transferred into wild-type Yb2 by conjugation, and transformants were selected on TSA agar containing erythromycin and kanamycin. One positive colony was grown in TSB without antibiotics at 37°C overnight, and the cells were then plated on TSA containing 8% sucrose. The positive mutant colonies were screened by PCR using primers gldL ORF F plus gldL ORF R, and 16S rRNA F plus 16S rRNA R, to detect the 16S rRNA, and *gldL* ORF, respectively. A *gldL* deletion mutant, which was positive for 16S rRNA and has a smaller PCR product (about 250 bp) for amplification of *gldL* ORF than that in the wild type Yb2, was designated as Δ*gldL*.

Subcellular localization analysis of PaR1

The subcellular localization of PaR1 predicted by PSORTb v.3.0[1] was "unknown," suggesting that *R. anatipestifer* may be not uniquely located.

To investigate whether the specific antibodies to rPaR1 in rabbit antiserum against rPaR1 could bound to the outer membrane of *R. anatipestifer* strainYb2, a whole-cell ELISA using whole Yb2 cells as the coating antigen was performed as described previously (Prieto et al., 2003). Naïve rabbit serum and convalescent duck serum against *R. anatipestifer* strain Yb2 were used as the negative and positive controls, and HRP-labeled goat anti-rabbit IgG (Solarbio, Beijing, China) and HRP-labeled rabbit anti-duck IgY (IgG) (Biodragon) as the secondary detection antibodies for detection of rabbit sera and duck serum, respectively. At the same time, PaR1-specific antibodies in the rPaR1 immunized rabbit serum and naïve rabbit serum were detected with an indirect ELISA using 1 μg/mL rPaR1 as the coating antigen. All samples were tested in triplicate. On the other hand, for indirect immunofluorescence assay, rabbit antiserum against rPaR1 was incubated with fresh whole Yb2 cells at room temperature for 2 h. After the cells were washed with PBS, the cells were incubated with Alexa Fluor 488-labeled goat anti-rabbit IgG antibody (ThermoFisher, USA) at room temperature for 1 h. After the washes, the cells were observed on a fluorescence microscope (Nikon Eclipse 80i, Japan). Rabbit serum against Yb2 and naïve rabbit serum were used as positive and negative controls.

The inner (cytoplasmic)-membrane proteins of wild-type Yb2 and the mutant Δ*gldL* were prepared as described previously (Spratt and Pardee, 1975), with some modification. Briefly, *R. anatipestifer* cells were grown to mid-log phase (OD_{600} = 1.0) in TSB at 37°C with shaking. The cells were centrifuged and washed twice with 0.01 M PBS (pH 7.0), and the pellet was resuspended in 0.01 M PBS (pH 7.0) containing 1 mM phenylmethanesulfonyl fluoride. After sonication, any unbroken cells were removed by centrifugation at 7,000 × g for 10 min. The membrane fraction was then collected by centrifugation at 100,000 × g for 30 min. The pellets were resuspended in 0.01 M PBS (pH 7.0) to which 1% (w/v) sarkosyl (Macklin, Shanghai, China) was added, and incubated at room temperature for 20 min. The membrane samples were then separated into the soluble (inner membrane) and insoluble (outer membrane) fractions by centrifugation at 100,000 × g for 30 min.

To determine whether protein PaR1 is secreted to the outside of *R. anatipestifer* cells through T9SS, the proteins in the culture supernatant of WT Yb2 and Δ*gldL* were precipitated with the TCA–acetone method, as described above. PaR1 was detected in the whole Yb2 cells, the inner membrane proteins, the normal cell-free culture supernatant, and the precipitated proteins in the culture supernatant with SDS-PAGE and western blotting, using rPaR1 immunized rabbit serum as the primary antibody. The blots were developed using an enhanced chemiluminescence detection kit (ECM Biotech, Suzhou, China).

1 https://www.psort.org/psortb/

Statistical analysis

GraphPad Prism 9.0.0 software (GraphPad Software, Inc., San Diego, CA, USA) was used for statistical analysis and preparation of graphs. The statistical significance of the survival curves was determined with a log-rank (Mantel–Cox) test, and the significant differences of ELISA results between groups were identified using the two-tailed Student's *t*-test. A probability (*p*) value of <0.05 was considered statistically significant.

Results

Immunoproteomics in the cell-free culture supernatant of *R. anatipestifer* strain Yb2

Samples containing 200 μg of proteins precipitated from the cell-free culture supernatant of *R. anatipestifer* strain Yb2 were separated with *two-dimensional* polyacrylamide gel electrophoresis (*2-DE)* and stained with Coomassie Brilliant Blue G-250 (Sigma-Adrich, MO, USA). The proteins were separated according to isoelectric point (PI) in the first dimension over a pH range of pH 3–10, and most proteins on the 2D gels had molecular weights (MWs) of 10–150 kDa (**Figure 1A**). The western blotting analysis detected 43 immunogenic protein spots when probed with convalescent duck serum against *R. anatipestifer* strain Yb2 (**Figure 1B**), but no appreciable spots appeared on the membrane probed with naïve duck serum (data not shown). Eleven immunogenic proteins were identified with MALDI-TOF-MS and a peptide mass fingerprinting (PMF) analysis (**Table 2**). Five proteins appeared in more than one spot, and of these, proteins AS87_RS06600 (PaR1), AS87_RS09020, and AS87_RS09965 appeared on 23, eight, and four spots, respectively. Moreover, both AS87_RS06600 and AS87_RS09020 were predicted to contain a type A carboxy-terminal domain (CTD) of the type IX secretion system (T9SS) (Kulkarni et al., 2017), suggesting they were secreted by T9SS. In addition, it is noteworthy that 11 immunogenic proteins identified in the culture supernatant of *R. anatipestifer* strain Yb2 in this study were not identified in the whole cells (Hu et al., 2012; Zhai et al., 2012) or culture supernatant (Zhai et al., 2013) of *R. anatipestifer* in immunoproteomic analyses in previous studies. The subcellular locations of these proteins predicted with the PSORTb v.3.0 software showed that six proteins (54.55%, 6/11) were extracellular proteins and the locations of five (45.45%, 5/11) were "unknown" (**Table 2**).

Expression and purification of PaR1, AS87_RS09020, and AS87_RS09965

In this study, three proteins (PaR1, AS87_RS09020, and AS87_RS09965), which appeared in more than three spots on PVDF membranes in a western blotting analysis, were expressed in *E. coli* and purified. The immunogenicity of the recombinant proteins was investigated with western blotting using duck antiserum against Yb2 as the primary antibody. The three recombinant proteins reacted with duck antiserum against Yb2 (**Supplementary Figure 1**), suggesting that they are immunogenic proteins of *R. anatipestifer*.

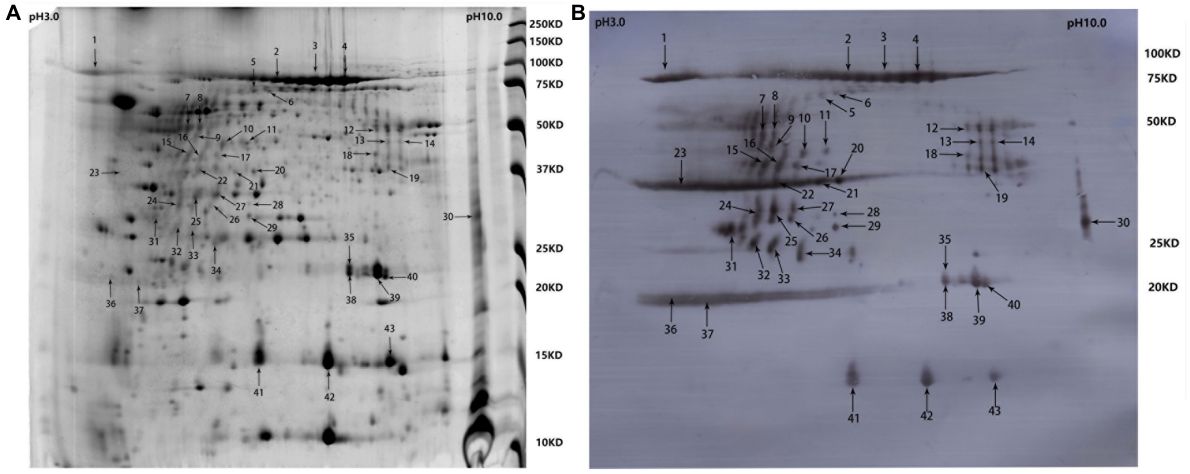

FIGURE 1
Two-dimensional electrophoresis (2-DE) gel and western blotting profile of cell-free culture supernatant of *R. anatipestifer* strain Yb2. **(A)** Separation of trichloroacetic acid (TCA)-precipitated proteins from the culture supernatant of *R. anatipestifer* Yb2 (200 μg) with 2-DE over pH 3–10 (stained with Coomassie Brilliant Blue G-250). Sites of excised spots are shown with arrows. **(B)** Western blotting analysis of the proteins on 2-DE gel, probed with convalescent duck serum against *R. anatipestifer* strain Yb2.

TABLE 2 Immunogenic proteins in the culture supernatant of *Riemerella anatipestifer* strain Yb2 identified by matrix-assisted laser desorption/ionization time of flight mass spectrometry (MALDI-TOF MS).

Spot no.	Protein name	GenBank accession no.	Locus tag on the Yb2 genome[a]	T9SS CTD[b]	Theoretical MW/PI	Protein score C. I. %	Subcellular location[c]
1–17, 19, 24–26, 30, 32	Hypothetical protein (PaR1)	AKQ40033.1	AS87_RS06600	Type A CTD	117222.2/8.44	99.552–100	Unknown
31, 33, 36, 41–43	Carbohydrate-binding protein	AKQ40508.1	AS87_RS09020	Type A CTD	28565.6/9.19	100	Extracellular
35, 38–40	ABC transporter substrate-binding protein	AKQ40692.1	AS87_RS09965	–	25301.6/8.46	100	Extracellular
20–21	Hypothetical protein	AKQ40507.1	AS87_RS09015	–	44256.6/6.08	100	Extracellular
28–29	Hypothetical protein	AKQ40504.1	AS87_RS09000	–	34729.2/6.02	100	Unknown
11	Peptidase M16	AKQ38937.1	AS87_RS00925	–	49795.2/6.07	100	Extracellular
18	Hypothetical protein	AKQ40440.1	AS87_RS08675	–	48715.7/8.51	100	Extracellular
23	Hypothetical protein	AKQ40669.1	AS87_RS09845	–	104859.6/4.88	100	Extracellular
27	Hypothetical protein	AKQ39770.1	AS87_RS05240	–	34176.2/5.65	100	Unknown
34	Succinate-CoAligase	AKQ39333.1	AS87_RS02975	–	29662.3/5.34	100	Unknown
37	Alkyl hydroperoxide reductase	AKQ38855.1	AS87_RS00505	–	23820.8/4.94	100	Unknown

[a]The GenBank accession number of *R. anatipestifer* strain Yb2: NZ_CP007204.
[b]Most proteins that are secreted by the type IX secretion system (T9SS) have conserved carboxy terminal domains (CTDs) that belong to the protein domain family TIGR04183 (type A CTDs) or TIGR04131 (type B CTDs). The conserved domains of proteins were screened by CD-search program (https://www.ncbi.nlm.nih.gov/Structure/cdd/wrpsb.cgi).
[c]Subcellular locations were predicted by the PSORTb v.3.0 software (http://www.psort.org/).

Recombinant protein rPaR1 induced protective immunity against challenge

As shown in **Figure 2A**, five (41.67%) of 12 ducklings immunized once with the soluble rPaR1 protein were protected from wild-type Yb2 challenge, whereas all the ducklings immunized with rAS87_RS09020, rAS87_RS09965, or PBS died within 4 days of challenge. There was a significant difference in the protective immunity conferred by rPaR1 and the PBS control ($p < 0.01$). To investigate whether rPaR1 conferred protective immunity against challenge with *R. anatipestifer* strains of different serotypes, ducklings were challenged with serotype 1 strain WJ4, serotype 2 strain Yb2, or serotype 10 strain HXb2 at 2 weeks after rPaR1 immunization. All the ducklings inoculated with PBS emulsified with ISA 70 V adjuvant died within 6 days of challenge with strains WJ4, Yb2, or HXb2, whereas 2/10 (20%), 4/10 (40%), and 0% of ducklings immunized with rPaR1 emulsified with ISA 70 V adjuvant survived challenge with serotype 1 strain WJ4 ($p > 0.05$, versus PBS group challenge with WJ4), serotype 2 strain Yb2 ($p < 0.05$, versus group challenge with Yb2), and serotype 10 strain HXb2 challenge, respectively (**Figure 2B**), suggesting that rPaR1 did not confer protection against serotype 10 strain HXb2 or serotype 1 strain WJ4. Before the challenge, the sera from the immunized ducklings were collected and the PaR1-specific antibodies measured with an ELISA using rPaR1 as the coating antigen. As shown in **Figure 2C**, the average OD_{490} values for antibodies to PaR1 in the serum samples obtained from ducks immunized with ISA-70 V-emulsified rPaR1 was 1.39 ± 0.17, whereas that in sera from ducklings immunized with ISA-70 V-emulsified inactivated Yb2 bacterin was 0.24 ± 0.06.

The bactericidal activity of rPaR1 immunized rabbit serum was also determined. A natural bactericidal activity assay showed that the natural bactericidal rates of mouse complement against serotype 1 strain WJ4, serotype 2 strain Yb2, and serotype 10 strain HXb2 were below zero, 8.5% (<30%), and 87.4% (>30%), respectively. Therefore, the mouse complement used in this study was only suitable for the analysis of the bactericidal activity against serotype 2 strain Yb2, but not against serotype 1 strain WJ4 and serotype 10 strain HXb2.

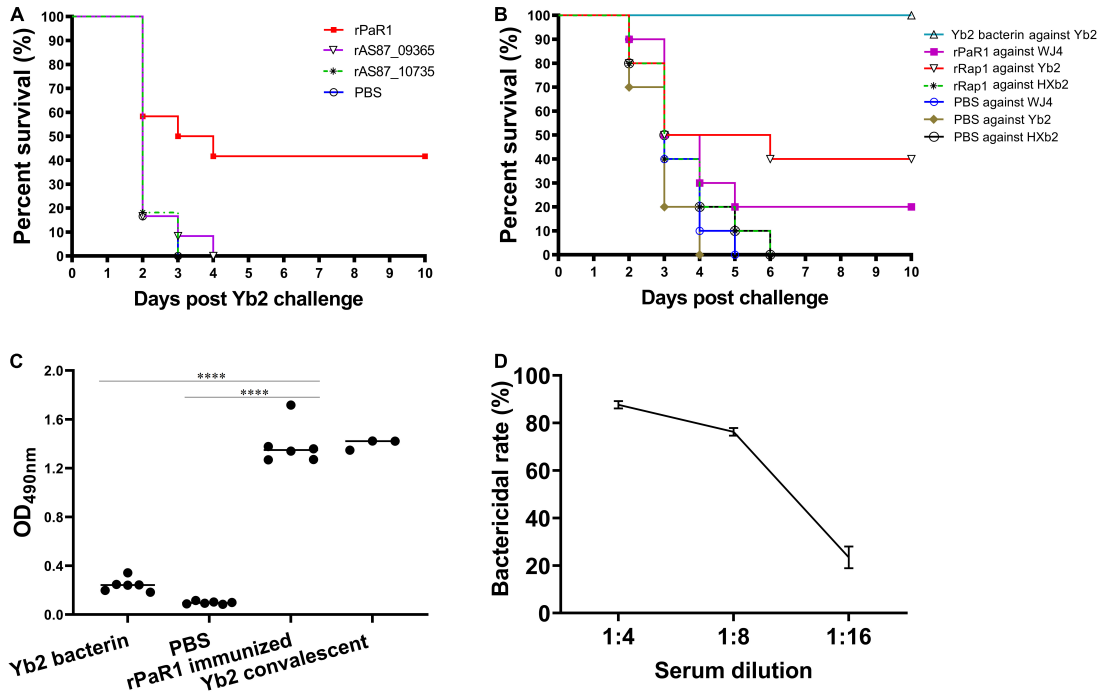

FIGURE 2
Recombinant protein recombinant PaR1 (rPaR1) confers protective immunity against Yb2 challenge. **(A)** Recombinant protein rPaR1, but not rAS87_RS09020 or rAS87_RS09965, conferred protective immunity against Yb2 challenge. **(B)** Recombinant protein rPaR1 conferred protective immunity against challenge with serotype 2 *R. anatipestifer* strain Yb2, but not serotype 1 strain WJ4 or serotype 10 strain HXb2. **(C)** ELISA scatter plots of antibodies to PaR1 detected in duck sera. Ducklings immunized with rPaR1, but not those immunized with inactivated Yb2 bacterin, displayed high levels of anti-PaR1 antibodies in their sera. Asterisks indicate statistically significant differences between two groups (**** <0.0001). **(D)** Bactericidal activity of rabbit serum against rPaR1. Rabbit antiserum against rPaR1 and naïve rabbit serum were inactivated at 56°C for 30 min and 2-fold serial diluted in PBS. Then the bactericidal activity against serotype 2 strain Yb2 was performed. The highest serum dilution causing 50% killing was expressed as the bactericidal titer.

The bactericidal assay showed rPaR1 immunized rabbit serum showed bactericidal activity against strain Yb2 at a titer of 1:8 (Figure 2D).

PaR1 is not a serotype-specific protein of *R. anatipestifer*

The *paR1* gene sequences of 33 *R. anatipestifer* strains of different serotypes were retrieved from GenBank. Among these, 26 strains carried one copy of the *paR1* gene, and the other seven strains (20190305E2-2, 20190109E1-1, 20190609E1-1, RCAD0416, 20190121E1-3, 20190507E1-1, 20190509E1-1) carried 2–3 copies of *paR1* homologous. A homology analysis showed that PaR1 of serotype 2 *R. anatipestifer* strain Yb2 shared 100% identity with those of strains RA-YM (serotype 1), RA-LZ01 (serotype 1), RA-GD (serotype 1), 17 (serotype 17), and RCAD0392, indicating that PaR1 is not a serotype-specific protein of *R. anatipestifer* (Supplementary Figure 2). In addition, PaR1 of strain Yb2 shared 99.9, 84.5, 83.8, and 85.5% identities with that of strains DSM15868 (= ATCC 11845, type strain), WJ4 (serotype 1), CH-2 (serotype 2), and HXb2 (serotype 10), respectively.

PaR1 Protein localized to the culture supernatant of *R. anatipestifer*

To determine whether PaR1 is located on the outer membrane of *R. anatipestifer*, whole Yb2 cells were used as the coating antigen in a whole-cell ELISA. The average OD_{490} values for rabbit antiserum against rPaR1 was 0.088 ± 0.001, which was close to that for naïve rabbit serum, whereas that for rabbit antiserum directed against rPaR1 was 1.28 ± 0.02 when rPaR1 protein was used as the coating antigen in ELISA (Figure 3A), indicating that the polyclonal antibodies against rPaR1 could not bind to the whole *R. anatipestifer* cells. Furthermore, no fluorescence was observed on the *R. anatipestifer* cells under fluorescence microscopy when rabbit antiserum against rPaR1 was used as the primary antibody and fluorescein-isothiocyanate-labeled goat anti-rabbit IgG antibody as the secondary antibody (data not shown). These results indicate PaR1 does not localize to the *R. anatipestifer* outer membrane.

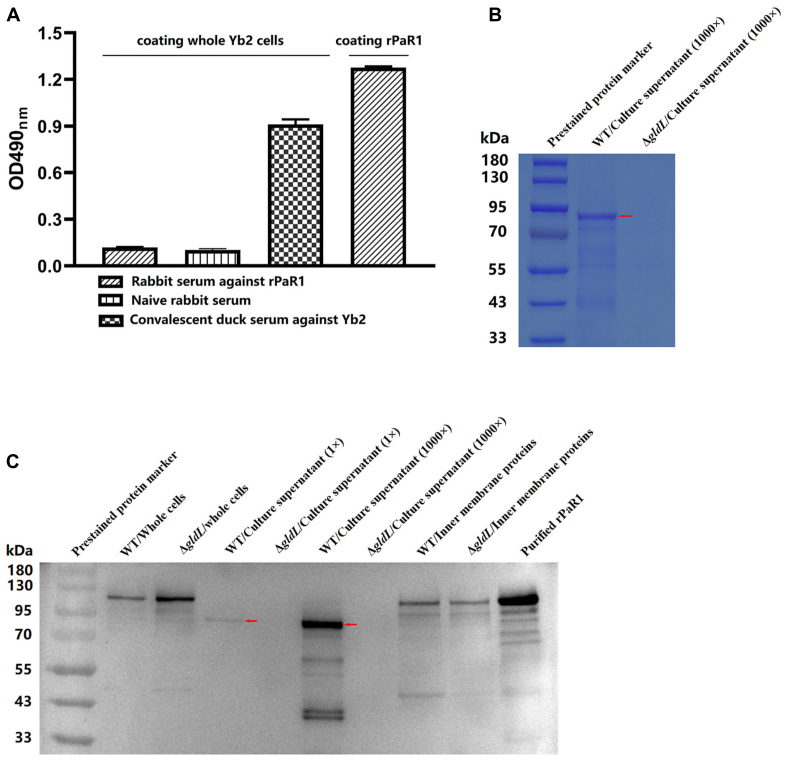

FIGURE 3
PaR1 protein localizes to the culture supernatant of *R. anatipestifer*. **(A)** Polyclonal antibodies against rPaR1 in immunized rabbit serum did not react with whole Yb2 cells in a whole-cell ELISA. **(B)** Protein secretion was defective in T9SS-defective mutant Δ*gldL*. *R. anatipestifer* cells were grown in TSB medium at 37°C with shaking and harvested in exponential phase (OD_{600} = 1.0). The cells were removed by centrifugation and filtered (0.22 μm). Equal volumes of cell-free culture supernatant of wild-type Yb2 (WT) and Δ*gldL* mutant were precipitated with TCA (concentrated 1,000-fold), and the proteins were separated with SDS-PAGE and stained with Coomassie Brilliant Blue G-250. The red arrow indicates the position of the main component in the trichloroacetic acid (TCA)-precipitated proteins from the culture supernatant of wild-type Yb2. **(C)** Mature PaR1 was detected with western blotting using rabbit antiserum against rPaR1 in the culture supernatant of wild-type Yb2, but not in that of T9SS-defective mutant Δ*gldL*. *R. anatipestifer* cells were grown in TSB medium at 37°C with shaking and harvested in exponential phase (OD_{600} = 1.0). Equal volumes of cultured WT and Δ*gldL* were used to prepared the whole cells, and inner membrane proteins. Proteins from equal volumes of cell-free culture supernatant of wild-type Yb2 (WT) and Δ*gldL* mutant were precipitated with TCA (concentrated 1,000-fold). The whole cells, normal cell-free culture supernatant, TCA-precipitated proteins from the culture supernatant (1,000-fold concentrated), and inner membrane proteins were analyzed for rPaR1 with SDS-PAGE and western blotting. The red arrows indicate the position of mature PaR1 in the TCA-precipitated proteins from the culture supernatant of wild-type Yb2.

The proteins in the culture supernatant of Yb2 and T9SS-defective mutant Δ*gldL* were detected by SDS-PAGE and western blotting. Compared to the wild type, the amount of proteins in the cell-free culture supernatant of Δ*gldL* mutant was obviously reduced (Figure 3B), indicating that T9SS-defective mutant Δ*gldL* was defective in extracellular protein secretion. PaR1 of wild-type Yb2 (proPaR1) was predicted to be 117 kDa in size, according to its amino acid sequence. As shown in Figure 3C, a band close in size to proPaR1 and rPaR1 was detected with rabbit antiserum against rPaR1 from the whole cells of Yb2 and Δ*gldL* mutant with western blotting. In contrast, as shown in Figures 3B, C, and PaR1 was the major protein component in the culture supernatant of wild-type Yb2, and mature PaR1, which is about 85 kDa, was detected in the normal or 1,000-fold-concentrated cell-free culture supernatant of WT Yb2. At least six other smaller bands, including two obvious bands of about 40 kDa, were also detected. However, PaR1 was absent from both the normal and 1,000-fold-concentrated culture supernatant of the T9SS-defective mutant Δ*gldL*, indicating that PaR1 protein is mainly secreted to the outside of wild-type strain Yb2 cells *via* the T9SS. In addition, PaR1 was also detected among the inner-membrane proteins of Yb2 and mutant Δ*gldL*, and the most obvious bands had a molecular mass close to those of proPaR1 and rPaR1 (Figure 3C), suggesting the CTD is not cleaved yet for the inner membrane PaR1. The N-terminal signal peptide guides the PaR1 protein across the inner membrane in the first step in its secretion from *R. anatipestifer* cells, therefore, most probably, the PaR1 on the inner membrane is a normal intermediate state of the secretion process. Overall, the localization of PaR1 is extracellular after secretion through T9SS.

Discussion

Identifying the immunogenic antigens is the first step in developing a novel generation of vaccines for *R. anatipestifer* infection and developing a method to detect the related antibody levels in duck sera. In general, bacterial outer-membrane proteins are considered potential immunogenic proteins and candidate protective antigens for vaccine development. However, in this study, our results showed that PaR1 is a protective antigen, although it is mainly secreted to the outside of *R. anatipestifer* by the T9SS.

The results in this study show that PaR1 of serotype 2 strain Yb2 shares 100% identity with that of other serotypes of *R. anatipestifer* strains, making cross-protection between different serotypes of *R. anatipestifer* strains possible. This is inconsistent with the long-held view that no or little cross-protection is afforded to *R. anatipestifer* strains of different serotypes (Sandhu, 1979; Pathanasophon et al., 1996). This may be attributable to the following factors: (1) The amino acid sequences of PaR1 may differ between two tested strains of different serotypes. Only when two PaR1 strains share the same protective antigenic epitope can there be cross-protection between two strains. (2) The localization of *R. anatipestifer* PaR1. PaR1 is mainly secreted outside the cell *via* T9SS, and the culture supernatant may be discarded during the preparation of inactivated *R. anatipestifer* bacterin. Therefore, no cross-protection induced by PaR1 was observed when ducklings were immunized with inactivated bacterin. For example, in the present study, the rPaR1-directed antibodies in the sera of ducklings immunized with Yb2 bacterin was very low. (3) The amount of PaR1 in the culture supernatant of *R. anatipestifer* was relatively low, so even when two *R. anatipestifer* strains shared 100% amino acid identity of PaR1, they did not induce enough cross-protection. Previous studies have shown that 10-fold-concentrated cell-free culture filtrates (10 × CF) of *R. anatipestifer* strains induced highly significant protection against homologous challenge (Pathanasophon et al., 1996). In the present study, high levels of antibodies to PaR1 were detected in the convalescent duck serum against *R. anatipestifer* strain Yb2 with an ELISA. Therefore, we speculate that if two different serotypes of attenuated *R. anatipestifer* vaccine strains, which have the same PaR1 amino acid sequence or the same protective antigenic epitope on PaR1, may provide cross-protection. Therefore, the amino acid sequence of PaR1 may be one of the factors to be considered when selecting attenuated candidate vaccine strains.

In this study, PaR1 was found to be the main immunogenic and protective protein in the cell-free culture supernatant, therefore, the effectiveness of concentrated culture supernatant in protecting against homologous challenge (Pathanasophon et al., 1996) may be attributable to PaR1, and thus this protection may be non-serotype-specific.

Proteins secreted by the T9SS have an N-terminal signal peptide that facilitates their export across the inner membrane by the Sec system and a conserved C-terminal domain (CTD), referred to as the CTD signal, that allows them to pass through the outer membrane *via* the T9SS (Kulkarni et al., 2017). In this study, the size of proPaR1 of strain Yb2 is about 117 kDa with an 18-amino-acid signal peptide at its N-terminus and a 78-amino-acid CTD (amino acids 962–1,039) at its C-terminus. Both the N-terminal signal peptide and the CTD are removed during the secretion of the protein into the culture supernatant *via* T9SS (Gorasia et al., 2015), and the remaining fragment is predicted to be 106 kDa, which is larger than the molecular mass of mature PaR1 in the culture supernatant (about 85 kDa). This suggests that the PaR1 protein in the culture supernatant had also been further proteolytically processed. Furthermore, at least six smaller and weaker bands were also detected with rabbit serum against rPaR1, suggesting that some of the mature PaR1 protein is further cleaved by protease(s). This explains why we detected PaR1 spots with different molecular mass in the immunoproteomic assay in this study. However, the protease that cleaves PaR1 and whether the smaller cleaved proteins have some other biological function remain unclear. This phenomenon is similar to that found in *Flavobacterium johnsoniae*, in which chitinase ChiA is also secreted by the T9SS. The predicted size of proChiA is 166 kDa, whereas that of secreted ChiA in spent medium is 92 kDa, and another 65 kDa band of ChiA was also detected (Kharade and McBride, 2014).

In summary, the results presented here demonstrate that *R. anatipestifer* PaR1 is a non-serotype-specific protective protein that is secreted outside *R. anatipestifer* cells *via* the T9SS.

Data availability statement

The original contributions presented in this study are included in the article/**Supplementary material**, further inquiries can be directed to the corresponding author.

Ethics statement

The animal study was reviewed and approved by the Committee on the Ethics of Animal Experiments of Shanghai Veterinary Research Institute, Chinese Academy of Agricultural Sciences (permit number: SHVRI-ZD-2018-026).

Author contributions

QH designed the experiments and revised the manuscript. JW wrote the manuscript, performed serum bactericidal assay, and subcellular localization analysis of PaR1 and sequence analysis. YC performed immunoproteomic analysis, protein expression and purification, and construction of T9SS-defective mutant of strain Yb2. XH, JW, and YC did the animal experiments for evaluating protective immunity induced by

the recombinant proteins. JW, XD, and YG analysis the data and drew the figures. XD, XS, and ZH participated in animal experiments and prepared the reagents and materials. All authors contributed to the article and approved the submitted version.

Funding

This work was supported by the National Natural Science Foundation of China (31772770, 31472224, and 31272590).

Conflict of interest

The authors declare that the research was conducted in the absence of any commercial or financial relationships that could be construed as a potential conflict of interest.

Publisher's note

All claims expressed in this article are solely those of the authors and do not necessarily represent those of their affiliated organizations, or those of the publisher, the editors and the reviewers. Any product that may be evaluated in this article, or claim that may be made by its manufacturer, is not guaranteed or endorsed by the publisher.

Supplementary material

The Supplementary Material for this article can be found online at: https://www.frontiersin.org/articles/10.3389/fmicb.2022.1082712/full#supplementary-material

SUPPLEMENTARY FIGURE 1
Confirmation of PaR1, AS87_RS09020, and AS87_RS09965 as immunogenic proteins of *R. anatipestifer*. The AS87_RS06600 (*paR1*), AS87_RS09020, and AS87_RS09965 ORFs of wild type Yb2 were cloned into the pET28a (+) vector and expressed in *E. coli* BL21(DE3) cells, respectively. The recombinant proteins were purified with Ni-IDA affinity chromatography. Then the purified recombinant proteins rPaR1, rAS87_RS09020, and rAS87_RS09965 were separated with SDS-PAGE and detected with western blotting using convalescent duck serum against *R. anatipestifer* strain Yb2.

SUPPLEMENTARY FIGURE 2
PaR1 is not a serotype-specific protein of *R. anatipestifer*. The *paR1* sequences of *R. anatipestifer* strains with different serotypes were retrieved from GenBank, and aligned and analyzed with Clustal W in the MegAlign program of the Lasergene 7.01 software. The locus tags of *paR1* in the genome of all bacterial strains, and their amino acid identities to PaR1 of *R. anatipestifer* strain Yb2, are listed.

References

Barbier, P., Rochat, T., Mohammed, H. H., Wiens, G. D., Bernardet, J. F., Halpern, D., et al. (2020). The type IX secretion system is required for virulence of the fish pathogen *Flavobacterium psychrophilum*. *Appl. Environ. Microbiol.* 86, e00799–20. doi: 10.1128/AEM.00799-20

Bisgaard, M. (1982). Antigenic studies on *Pasteurella anatipestifer*, species incertae sedis, using slide and tube agglutination. *Avian Pathol.* 11, 341–350. doi: 10.1080/03079458208436109

Cheng, A., Wang, M., Chen, X., Zhu, D., Huang, C., Liu, F., et al. (2003). Epidemiology and new serotypes of *Riemerella anatipestifer* isolated from ducks in China and studies in their pathogenic characteristics (in chinese). *Chin. J. Vet. Sci.* 23, 320–323.

Flaugnatti, N., and Journet, L. (2017). Identification of effectors: Precipitation of supernatant material. *Methods Mol. Biol.* 1615, 459–464. doi: 10.1007/978-1-4939-7033-9_31

Garcia-Lopez, M., Meier-Kolthoff, J. P., Tindall, B. J., Gronow, S., Woyke, T., Kyrpides, N. C., et al. (2019). Analysis of 1,000 type-strain genomes improves taxonomic classification of Bacteroidetes. *Front. Microbiol.* 10:2083. doi: 10.3389/fmicb.2019.02083

Gorasia, D. G., Veith, P. D., Chen, D., Seers, C. A., Mitchell, H. A., Chen, Y. Y., et al. (2015). *Porphyromonas gingivalis* type IX secretion substrates are cleaved and modified by a sortase-like mechanism. *PLoS Pathog.* 11:e1005152. doi: 10.1371/journal.ppat.1005152

Gu, X. X., Tsai, C. M., Ueyama, T., Barenkamp, S. J., Robbins, J. B., and Lim, D. J. (1996). Synthesis, characterization, and immunologic properties of detoxified lipooligosaccharide from nontypeable *Haemophilus influenzae* conjugated to proteins. *Infect. Immun.* 64, 4047–4053. doi: 10.1128/iai.64.10.4047-4053.1996

Han, X., Hu, Q., Ding, S., Chen, W., Ding, C., He, L., et al. (2012). Identification and immunological characteristics of chaperonin GroEL in *Riemerella anatipestifer*. *Appl. Microbiol. Biotechnol.* 93, 1197–1205. doi: 10.1007/s00253-011-3635-2

Hennell James, R., Deme, J. C., Kjr, A., Alcock, F., Silale, A., Lauber, F., et al. (2021). Structure and mechanism of the proton-driven motor that powers type 9 secretion and gliding motility. *Nat. Microbiol.* 6, 221–233. doi: 10.1038/s41564-020-00823-6

Hu, Q., Ding, C., Tu, J., Wang, X., Han, X., Duan, Y., et al. (2012). Immunoproteomics analysis of whole cell bacterial proteins of *Riemerella anatipestifer*. *Vet. Microbiol.* 157, 428–438. doi: 10.1016/j.vetmic.2012.01.009

Hu, Q., Han, X., Zhou, X., Ding, C., Zhu, Y., and Yu, S. (2011). OmpA is a virulence factor of *Riemerella anatipestifer*. *Vet. Microbiol.* 150, 278–283. doi: 10.1016/j.vetmic.2011.01.022

Hu, Q., Han, X., Zhou, X., Ding, S., Ding, C., and Yu, S. (2010). Characterization of biofilm formation by *Riemerella anatipestifer*. *Vet. Microbiol.* 144, 429–436. doi: 10.1016/j.vetmic.2010.02.023

Huang, B., Subramaniam, S., Frey, J., Loh, H., Tan, H. M., Fernandez, C. J., et al. (2002). Vaccination of ducks with recombinant outer membrane protein (OmpA) and a 41 kDa partial protein (P45N') of *Riemerella anatipestifer*. *Vet. Microbiol.* 84, 219–230. doi: 10.1016/s0378-1135(01)00456-4

Kharade, S. S., and McBride, M. J. (2014). *Flavobacterium johnsoniae* chitinase ChiA is required for chitin utilization and is secreted by the type IX secretion system. *J. Bacteriol.* 196, 961–970. doi: 10.1128/JB.01170-13

Kulkarni, S. S., Zhu, Y., Brendel, C. J., and McBride, M. J. (2017). Diverse C-terminal sequences involved in *Flavobacterium johnsoniae* protein secretion. *J. Bacteriol.* 199, e00884–16. doi: 10.1128/JB.00884-16

Layton, H. W., and Sandhu, T. S. (1984). Protection of ducklings with a broth-grown *Pasteurella anatipestifer* bacterin. *Avian Dis.* 28, 718–726.

Lu, F., Miao, S., Tu, J., Ni, X., Xing, L., Yu, H., et al. (2013). The role of TonB-dependent receptor TbdR1 in *Riemerella anatipestifer* in iron acquisition and virulence. *Vet. Microbiol.* 167, 713–718. doi: 10.1016/j.vetmic.2013.08.020

Martin, D., McCallum, L., Glennie, A., Ruijne, N., Blatchford, P., O'Hallahan, J., et al. (2005). Validation of the serum bactericidal assay for measurement of

functional antibodies against group B meningococci associated with vaccine trials. *Vaccine* 23, 2218–2221. doi: 10.1016/j.vaccine.2005.01.070

McBride, M. J., and Zhu, Y. (2013). Gliding motility and Por secretion system genes are widespread among members of the phylum bacteroidetes. *J. Bacteriol.* 195, 270–278. doi: 10.1128/JB.01962-12

Pathanasophon, P., Phuektes, P., Tanticharoenyos, T., Narongsak, W., and Sawada, T. (2002). A potential new serotype of *Riemerella anatipestifer* isolated from ducks in Thailand. *Avian Pathol.* 31, 267–270. doi: 10.1080/03079450220136576

Pathanasophon, P., Sawada, T., Pramoolsinsap, T., and Tanticharoenyos, T. (1996). Immunogenicity of *Riemerella anatipestifer* broth culture bacterin and cell-free culture filtrate in ducks. *Avian Pathol.* 25, 705–719. doi: 10.1080/03079459608419176

Prieto, C. I., Rodriguez, M. E., Bosch, A., Chirdo, F. G., and Yantorno, O. M. (2003). Whole-bacterial cell enzyme-linked immunosorbent assay for cell-bound *Moraxella bovis* pili. *Vet. Microbiol.* 91, 157–168.

Sandhu, T. (1979). Immunization of white Pekin ducklings against *Pasteurella anatipestifer* infection. *Avian Dis.* 23, 662–669.

Sato, K., Naito, M., Yukitake, H., Hirakawa, H., Shoji, M., McBride, M. J., et al. (2010). A protein secretion system linked to bacteroidete gliding motility and pathogenesis. *Proc. Natl. Acad. Sci. U.S.A.* 107, 276–281. doi: 10.1073/pnas.0912010107

Segers, P., Mannheim, W., Vancanneyt, M., De Brandt, K., Hinz, K. H., Kersters, K., et al. (1993). *Riemerella anatipestifer* gen. nov., comb. nov., the causative agent of septicemia anserum exsudativa, and its phylogenetic affiliation within the *Flavobacterium-Cytophaga* rRNA homology group. *Int. J. Syst. Bacteriol.* 43, 768–776. doi: 10.1099/00207713-43-4-768

Spratt, B. G., and Pardee, A. B. (1975). Penicillin-binding proteins and cell shape in *E. coli*. *Nature* 254, 516–517. doi: 10.1038/254516a0

Subramaniam, S., Huang, B., Loh, H., Kwang, J., Tan, H. M., Chua, K. L., et al. (2000). Characterization of a predominant immunogenic outer membrane protein of *Riemerella anatipestifer*. *Clin. Diagn. Lab. Immunol.* 7, 168–174. doi: 10.1128/CDLI.7.2.168-174.2000

Xu, X., Xu, Y., Miao, S., Jiang, P., Cui, J., Gong, Y., et al. (2020). Evaluation of the protective immunity of *Riemerella anatipestifer* OmpA. *Appl. Microbiol. Biotechnol.* 104, 1273–1281. doi: 10.1007/s00253-019-10294-3

Zhai, Z., Cheng, L., Tang, F., Lu, Y., Shao, J., Liu, G., et al. (2012). Immunoproteomic identification of 11 novel immunoreactive proteins of *Riemerella anatipestifer* serotype 2. *FEMS Immunol. Med. Microbiol.* 65, 84–95. doi: 10.1111/j.1574-695X.2012.00947.$\times$

Zhai, Z., Li, X., Xiao, X., Yu, J., Chen, M., Yu, Y., et al. (2013). Immunoproteomics selection of cross-protective vaccine candidates from *Riemerella anatipestifer* serotypes 1 and 2. *Vet. Microbiol.* 162, 850–857. doi: 10.1016/j.vetmic.2012.11.002

Zhu, Y., Thomas, F., Larocque, R., Li, N., Duffieux, D., Cladiere, L., et al. (2017). Genetic analyses unravel the crucial role of a horizontally acquired alginate lyase for brown algal biomass degradation by *Zobellia galactanivorans*. *Environ. Microbiol.* 19, 2164–2181. doi: 10.1111/1462-2920.13699

frontiers | Frontiers in Microbiology

TYPE Original Research
PUBLISHED 12 January 2023
DOI 10.3389/fmicb.2022.1082025

OPEN ACCESS

EDITED BY
Qing Pan,
Qingdao Agricultural University, China

REVIEWED BY
Xin Cao,
Jilin Agricultural University, China
Fusheng Si,
Shanghai Academy of Agricultural Sciences, China

*CORRESPONDENCE
Shuangbao Gun
✉ gunsbao056@126.com

SPECIALTY SECTION
This article was submitted to Infectious Agents and Disease, a section of the journal Frontiers in Microbiology

RECEIVED 11 November 2022
ACCEPTED 28 December 2022
PUBLISHED 12 January 2023

CITATION
Yang J, Zhang J, Yang Q, Huang X, Yan Z, Wang P, Gao X, Li J, Li N, Gao Y and Gun S (2023) LncRNA *EN-90756* promotes CPB2-induced proliferation and inhibits apoptosis in IPEC-J2 cells by affecting the JAK-STAT signaling pathway activation. *Front. Microbiol.* 13:1082025. doi: 10.3389/fmicb.2022.1082025

LncRNA *EN-90756* promotes CPB2-induced proliferation and inhibits apoptosis in IPEC-J2 cells by affecting the JAK-STAT signaling pathway activation

Jiaojiao Yang[1], Juanli Zhang[2], Qiaoli Yang[1], Xiaoyu Huang[1], Zunqiang Yan[1], Pengfei Wang[1], Xiaoli Gao[1], Jie Li[1], Na Li[3], Yi Gao[3] and Shuangbao Gun[1,4]*

[1]College of Animal Science and Technology, Gansu Agricultural University, Lanzhou, China, [2]College of Life Sciences and Technology, Longdong University, Qingyang, China, [3]Jilin Rongtai Agricultural Development Co., Ltd., Changchun, China, [4]Gansu Research Center for Swine Production Engineering and Technology, Lanzhou, China

Background: Long non-coding RNAs (lncRNAs), as key regulators, are closely associated with the development of a variety of disease. However, the mechanisms by which lncRNAs regulate *Clostridium perfringens* type C induced piglet diarrhea are unclear.

Methods: In the present study, we explored the expression and characterization of lncRNAs in a *C. perfringens* beta2 (CPB2) toxin-treated intestinal porcine epithelial cell line-J2 (IPEC-J2) using RNA-sequencing (RNA-seq).

Results: A total of 6,558 lncRNAs were identified, of which 49 lncRNAs were significantly differentially expressed between the control and CPB2 groups. Functional enrichment analysis showed that the target genes of differentially expressed lncRNA *EN-90756* were mainly associated with defense response to virus, and negative regulation of apoptotic process. LncRNA *EN-90756* was significantly up-regulated in IPEC-J2 cells at different time points after CPB2 treatment. Functionally, knockdown of lncRNA *EN-90756* might regulate the proliferation and apoptosis of IPEC-J2 cells by affecting the Janus kinase (JAK)-signal transducer and activator of transcription (STAT) signaling pathway. LncRNA *EN-90756* may be involved in CPB2 toxin-induced piglet diarrhea by regulating the expression of its target gene *MX1* (encoding MX dynamin like GTPase 1).

Conclusion: Long non-coding RNA *EN-90756* affected the antiviral ability of IPEC-J2 cells by regulating the expression of MX1. Meanwhile, lncRNA

EN-90756 might regulate cell proliferation and apoptosis by affecting JAK-STAT signaling pathway activation. These findings provide novel perspectives and directions for further exploration of the regulatory mechanisms of lncRNAs on CPB2 toxin-induced diarrhea in piglets.

KEYWORDS

RNA-seq, lncRNAs, IPEC-J2, CPB2 toxin, piglet diarrhea

1. Introduction

Piglet diarrhea has a high incidence and brings huge economic losses to pig farms (Silva et al., 2015). *Clostridium perfringens* type C is one of the main pathogens causing diarrhea in piglets, producing *C. perfringens* beta2 (CPB2) toxin that acts directly or indirectly on the intestines, causing intestinal damage and triggering an inflammatory response (Zeng et al., 2016). Several epidemiological studies suggested that CPB2 toxins are highly associated with intestinal diseases in domestic animals. NetB toxin and CPB2 toxin produced by *C. perfringens* are associated with subclinical necrotizing enteritis in laying hens (Timoney et al., 2005). CPB2 toxin might play a role in the pathogenesis of enterotoxaemia in calves (Lebrun et al., 2007). There is a significant association between CPB2-positive *C. perfringens* isolates and piglet diarrhea (Waters et al., 2003). CPB2 toxin is significantly cytotoxic to intestinal porcine epithelial cell line-J2 (IPEC-J2) cells inhibiting cell growth and increasing cell permeability in a concentration-dependent manner (Luo et al., 2020). CPB2 toxin induces apoptosis and increases inflammatory markers in IPEC-J2 cells and impairs intestinal barrier function (Gao et al., 2020).

Long non-coding RNAs (lncRNAs) are RNAs comprising more than 200 nucleotides that have almost no protein-coding capacity and play key roles in a variety of biological processes, including epigenetic regulation, transcriptional regulation, metabolism, and immune responses (Marzia et al., 2018). In recent years, studies have reported that lncRNAs have important functions in piglet resistance to pathogenic infections causing diarrhea. Down-regulation of lncRNA *FUT3-AS1* expression contributed to enhancing the resistance of IPEC-J2 cells to *Escherichia coli* F18 infection (Wu et al., 2022). Porcine endemic diarrhea virus (PEDV) infection modulates lncRNA expression patterns in the ileum of IPEC-J2 cell lines and piglets and activates the ileal immune system (Chen et al., 2019). In piglet diarrhea caused by *C. perfringens* type C, many lncRNAs and mRNAs modulate drug resistance and susceptibility in piglets through immune-related pathways (Huang et al., 2019). Although many lncRNAs have been reported to be associated pig diarrhea, few lncRNAs have been identified that are closely associated with CPB2 toxin-induced diarrhea in piglets.

Our previous study used CPB2 toxin (20 μg/ml) to treat IPEC-J2 cells for 24 h to construct an *in vitro* model of *C. perfringens* type C infected piglet diarrhea (Gao et al., 2020). In this study, we used RNA sequencing (RNA-seq) to perform transcriptome analysis of the CPB2 and control groups of IPEC-J2 cells and to identify differentially expressed lncRNAs in response to CBP2. We also analyzed the gene ontology (GO) enrichment of differential lncRNAs and carried out Kyoto Encyclopedia of Genes and Genomes (KEGG) pathway analysis with the aim of identifying possible molecular mechanisms of CPB2 toxin-induced diarrhea in piglets. We identified a key lncRNA, lncRNA *EN-90756*, which was highly expressed in CPB2-induced IPEC-J2 cells and applied a series of biological experiments to explore its regulatory mechanism. These results increase our understanding of the molecular mechanisms of lncRNAs in CPB2 toxin-induced diarrhea in piglets.

2. Materials and methods

2.1. Preparation and purification of the CPB2 toxin

The CPB2 toxin was extracted and purified according to Luo's method (Luo et al., 2020). Briefly, a recombinant plasmid containing the CPB2 gene, pET-28a-CPB2, was constructed transformed into BL21 *E. coli* cells for expression. The expressed CPB2 protein was purified using High Affinity Ni-Charged Resin FF (GenScript, Nanjing, China) and concentrated using PEG6000. Finally, a ToxOut^{TM} Rapid Endotoxin Removal Kit (AmyJet Scientific, Wuhan, China) was used to remove the endotoxin.

2.2. Cell culture and processing

Intestinal porcine epithelial cell line-J2 cells were provided by the BeNa Culture Collection (Beijing, China). Cells were cultured using Dulbecco's modified Eagle's medium (HyClone, Logan, UT, USA) containing 10% fetal bovine serum (Gibco, Grand Island, NY, USA) and 1% double antibodies (penicillin

and streptomycin) at 37°C in an atmosphere of 5% CO_2. The CPB2 group of cells was treated with the CPB2 toxin (20 μg/ml). Three replicates were set up for each group.

2.3. RNA-sequencing (RNA-seq) and data analysis

Total RNA was extracted from the control and CPB2-treated cells using RNAiso^{TM} Reagent (Invitrogen, Carlsbad, CA, USA). The total RNA quantity and purity were assessed using a Bioanalyzer 2100 and RNA 1000 Nano LabChip Kit (Agilent, Santa Clara, CA, USA), respectively. The RNA samples were of high quality with RNA integrity numbers > 7. Ribosomal RNA was removed using a Ribo-Zero^{TM} rRNA Removal Kit (Illumina, San Diego, CA, USA) and then reverse transcribed into cDNA. The cDNA libraries were constructed and sequenced on an Illumina NovaSeq^{TM} 6000 platform (Illumina, San Diego, CA, USA) using 2 × 150 bp paired-end sequencing. The raw data obtained from IPEC-J2 samples were stored in the NCBI SRA database (accession number: PRJNA749943).

The raw data were processed using FastQC software.[1] This step produced clean data by removing the reads with shifted connectors and low quality sequences (quality score < Q30). The reads were mapped against the pig genome assembly (*Sscrofa* 11.1) and the alignment results were assessed using HISAT2[2] (Kim et al., 2015). StringTie software[3] was used to estimate gene expression levels according to fragments per kilobase of transcript per million mapped reads (FPKM) (Trapnell et al., 2010). After all transcripts were obtained, transcripts smaller than 200 bp and known mRNAs were removed and lncRNA prediction was performed on the remaining transcripts using CPC, Pfam-sca, and CNCI (Kong et al., 2007; Sun et al., 2013). LncRNAs with fold change (FC) ≥ 2 and $p < 0.05$ were regarded as significantly differentially expressed.

Long non-coding RNA target genes were predicted using both *cis* and *trans* methods. LncRNA *cis*-regulatory target genes were mainly predicted based on positional relationships. The mRNAs that were differentially expressed within 100 kb upstream and downstream of the lncRNA were considered to be lncRNA *cis*-regulatory target genes. The *trans*-regulated target genes of lncRNAs were analyzed using RIsearch (Wenzel et al., 2012) software. Screening conditions included the formation of secondary structure free energy between the lncRNA and mRNA sequences (energy < −11) and the Pearson correlation coefficient ($r > 0.95$ or $r < -0.95$). Subsequently, GOSeq Release 2.12 and KO-BAS (V2.0) (Kanehisa et al., 2007; Young et al., 2010) were used to perform GO and KEGG pathway enrichment analyses of the target genes of the lncRNAs, respectively.

2.4. Quantitative real-time reverse transcription polymerase chain reaction (qRT-PCR)

Total RNA was extracted from IPEC-J2 cells (1×10^7) according to the method described in section "2.3 RNA-sequencing (RNA-seq) and data analysis." Cytoplasmic and nuclear RNAs of IPEC-J2 cells were isolated using a PARIS^{TM} Kit reagent kit (Ambion, Austin, TX, USA) according to the instructions provided by the supplier. Total RNA was reverse transcribed into cDNA using Evo M-MLV Mix Kit with gDNA Clean for qPCR AG11728 (Accurate Biotechnology, Hunan, China). The qRT-PCR assay was performed according to the instructions of SYBR Green assay (Accurate Biotechnology, Hunan, China) and performed on a Roche LightCycler 480 (Roche Applied Science, Mannheim, Germany). Gene expression levels were normalized to that encoding glyceraldehyde-3-phosphate dehydrogenase (*GAPDH*) to determine the relative expression using the $2^{-\Delta\Delta Ct}$ method (Ljvak, 2001). The PCR primers for transcripts and genes are listed in **Table 1**.

2.5. Single RNA fluorescent *in situ* hybridization (FISH)

The green fluorescent FAM-labeled probe for lncRNA *EN-9075* (lncRNA-FISH probe mix) was designed by GenePharma (Shanghai, China) and detected using a fluorescent *in situ* hybridization kit (GenePharma) according to the manufacturer's instructions. In short, IPEC-J2 cells were inoculated overnight in 48-well plates at a density of 1×10^4 cells/well and then treated with CPB2 toxin for 24 h. IPEC-J2 cells were then fixed with 4% (v/v) paraformaldehyde for 15 min at room temperature. The IPEC-J2 cells permeabilized in phosphate-buffered saline (PBS) containing 0.1% Triton X-100 for 15 min at room temperature and then blocked with pre-hybridization buffer for 30 min at 37°C. The IPEC-J2 cells were treated with the FAM-labeled probe in hybridization buffer (10 μL, 10 μM probe, and 90 μL hybridization buffer) the dark at 37°C for 14 h. The cells were then washed three times with wash buffer (4 × SSC/2 × SSC) in the dark and stained with 4′, 6-diamidino-2-phenylindole for 15 min. The IPEC-J2 cells were washed three times with PBS and then observed under a fluorescent microscope at 200× magnification (Olympus IX71, Tokyo, Japan).

1 www.bioinformatics.babraham.ac.uk/projects/fastqc/

2 ccb.jhu.edu/software/hisat2/

3 ccb.jhu.edu/software/stringtie/

TABLE 1 Quantitative real-time reverse transcription polymerase chain reaction (qRT-PCR) primers for amplifying specific genes.

GeneID/Gene name		Nucleotide sequence (5′–3′)	Product length (bp)
ENSSSCG00000041190	Forward	GAATCTGAACTTCTTGCCACA	112
	Reverse	TACTAACATTCCCTGCCCAT	
ENSSSCG00000047438	Forward	CATTATGTGCCACCGACGAA	178
	Reverse	TCACTGAAAGCCAAGTGTC	
ENSSSCG00000046898	Forward	TTTATTTGGAAGCGGACCCT	110
	Reverse	TCCCCTCATTCTCAGAGTCG	
ENSSSCG00000045823	Forward	CCTTGCCTCACTCGGTGT	239
	Reverse	GGATCCTATGCAGCAACCC	
LOC106507243	Forward	CGGCGCTTCACAGACTCC	143
	Reverse	GGCTCCAGGAACAAGTACCC	
LOC102162336	Forward	GCCCATCCCTTGAAAATGACGA	157
	Reverse	CCGCCCTTCCTCAACACC	
ENSSSCG00000041166	Forward	GAAACGAATCTGACTAGCACCC	165
	Reverse	TAATCCCTGGCCTCACTCGG	
ENSSSCG00000047080	Forward	CCCCGACCTGATAAGTCCT	105
	Reverse	AGGCCATCTTCCCTAATCCCT	
LOC106508476	Forward	GGAAACAGCCTAAATGGTCA	160
	Reverse	GGCCTCATGTAACAAGGACTCA	
ENSSSCG00000048701	Forward	AGACTCTGACGTGGTAGGACA	145
	Reverse	TTGGAGAAGTGTCACACCGT	
U6	Forward	TTATGGGTCCTAGCCTGAC	224
	Reverse	CACTATTGCGGGTCTGC	
MX1	Forward	CCACCTGAAGAAGGGCTAC	219
	Reverse	AACAGGGGCAGAGTTTTAC	
GAPDH	Forward	AGTATGATTCCACCCACGGC	139
	Reverse	TACGTAGCACCAGCATCACC	
Caspase 3	Forward	CCGAAATGTTTGCTGACGGC	152
	Reverse	CCGATCTCGAAGGAAGTCCA	
Caspase 8	Forward	CGGCTCTGAGCAAGACCTTTA	173
	Reverse	GCCGTAGATGATGCCCTTGT	

2.6. Cell transfection

The small interfering RNA targeting lncRNA *EN-90756* (si EN-90756) and the negative control siRNA (si NC) were obtained from GenePharma. IPEC-J2 cells (1×10^5 cells/ml) were grown overnight in six-well plates until they were 70% confluent for transfection. Lipofectamine 2000 (Invitrogen) was mixed with Opti-MEM medium (Invitrogen, CA, USA) and left for 5 min. Then, the solution was added to si EN-90756, si NC (1:1 ratio) diluted with Opti-MEM medium, mixed and left for 20 min. The prepared mixtures were added to IPEC-J2 cells separately and transfection was completed after 24 h.

2.7. Cell viability and proliferation assay

Intestinal porcine epithelial cell line-J2 (density of 5×10^3/well) were seeded in 96-well plates, with three replicates for each group. After treatment with CPB2 toxin, cell viability was determined according to the instructions of Cell Counting Kit-8 (Beyotime, Shanghai, China). IPEC-J2 cells (1×10^5 cells/ml) were grown in six-well plates and treated with CPB2 toxin or PBS. Cell proliferation was assayed using the BeyoClick^{TM} EdU Cell Proliferation Kit with Alexa Fluor 488 [5-ethynyl-2′-deoxyuridine (EdU), Beyotime]. Cell proliferation was observed under a fluorescence microscope at 200× magnification (Olympus IX71).

2.8. Flow cytometry

Intestinal porcine epithelial cell line-J2 cells (1×10^5 cells/ml) were grown in six-well plates, transfected with si NC or si EN-90756 for 24 h and then treated with CPB2 toxin for 24 h. Cells were collected and washed twice with PBS. Then, 1 ml of pre-cooled 70% ethanol was added to the cells, mixed with gentle shaking, and fixed at 4°C for 12 h. The ethanol was discarded, the cells were washed using PBS and collected by centrifugation. Then, the cells were incubated with Annexin V-fluorescein isothiocyanate and propidium iodide for 20 min at 25°C in the dark. Apoptosis was detected using a FACSCalibur flow cytometer (BD Biosciences, San Jose, CA, USA).

2.9. Mitochondrial membrane potential assay

Intestinal porcine epithelial cell line-J2 cells were transfected with si NC or si EN-90756 and treated with CPB2 toxin or PBS and then assayed for mitochondrial membrane potential ($\Delta\psi m$) according to the instructions of the mitochondrial membrane potential assay kit with JC-1 (Beyotime). Briefly, cells were incubated with JC-1 staining solution at 37°C for 20 min, washed two times with JC-1 staining buffer (1×) and then observed under a fluorescent microscope (Olympus IX71).

2.10. Western blotting

Total IPEC-J2 cell proteins were extracted using Radioimmunoprecipitation assay (Beyotime). The extracted proteins were quantified using a bicinchoninic acid protein analysis kit (Beyotime). Sodium dodecyl sulfate-polyacrylamide gel electrophoresis (12%) was used to separate equal amounts of proteins, which were then transferred to polyvinylidene fluoride membranes (Millipore, Billerica, MA, USA). The membranes were incubated with primary antibodies overnight at 4°C.

The primary antibodies comprised those recognizing: MX dynamin like GTPase 1 (MX1) (bsm-51528m, Bioss, Woburn, MA, USA; 1:1,000); Janus kinase 1 (JAK1) (bs-1439R, Bioss; 1:1,000); phosphorylated (p-JAK1) (bs-3238R, Bioss; 1:1,000); signal transducer and activator of transcription 3 (STAT3) (GB11176, Servicebio, Wuhan, China; 1:1,000); p-STAT3 (bs-1658R, Bioss; 1:1,000); and GAPDH (GB15002, Servicebio;

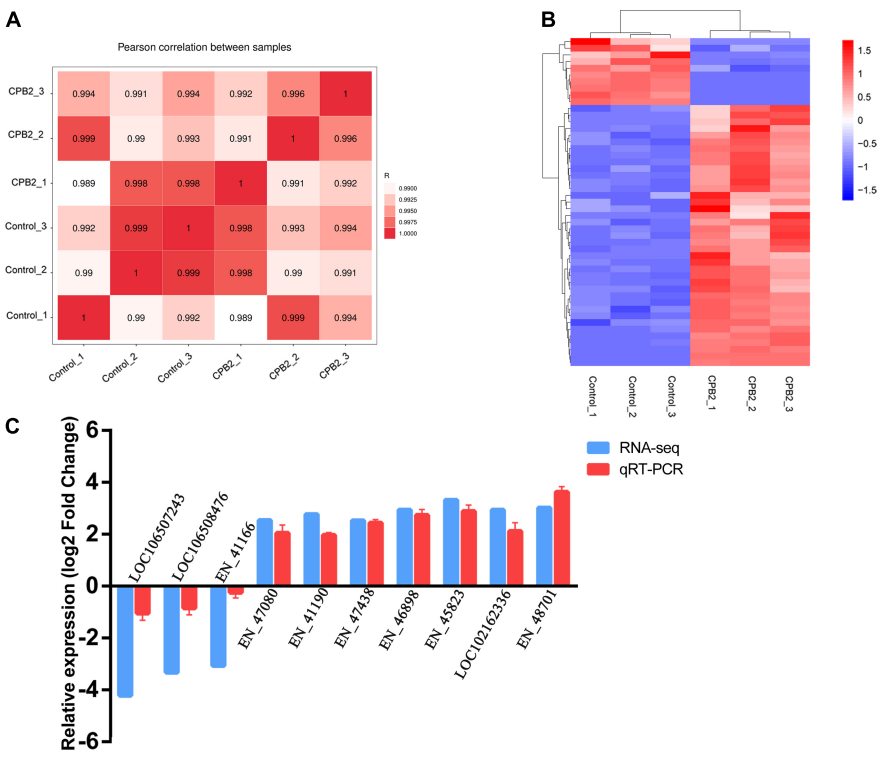

FIGURE 1
Quality analysis of the RNA-seq data. **(A)** Chart of the expression correlation between samples. *R* is Pearson's correlation coefficient. **(B)** A hierarchical heat map of differential long non-coding RNAs (lncRNAs) in the control and toxin-treated intestinal porcine epithelial cell line-J2 (IPEC-J2) cells. Data are expressed as the fragments per kilobase of transcript per million mapped reads. Different colors indicate different levels of gene expression, with colors ranging from blue through white to red indicating low to high expression. **(C)** Quantitative real-time reverse transcription polymerase chain reaction (qRT-PCR) validation of 10 differentially expressed lncRNAs.

1:2,000). After incubation with horseradish peroxidase-labeled secondary antibodies (GB23303, Servicebio; 1:5,000) or (GB25301, Servicebio; 1:5,000), the immunoreactive protein bands were observed using the enhanced chemiluminescence method (Thermo Fisher Scientific, Waltham, MA, USA).

2.11. Statistical analysis

The results were statistically analyzed using SPSS v.21 software (IBM Corp., Armonk, NY, USA). All experiments had three replicates, and the experimental data are expressed as the mean ± standard deviation (SD). Differences were determined using Student's *t*-test (two-tailed test). *P*-values < 0.05 were considered statistically significant.

3. Results

3.1. Quality analysis of the RNA-seq data

Six cDNA libraries of IPEC-J2 cells from the control and CPB2 groups were sequenced and Pearson's correlation coefficient between the two groups ranged from 0.98 to 0.99, indicating a high degree of similarity in expression patterns between the samples from the same group (**Figure 1A**). After quality control of the raw data, we obtained approximately 8.36 Gb of high quality data and the average GC content of the six libraries was approximately 53%; and the Q30 (sequencing error rate less than 0.001) per sample ranged from 95.34 to 96.14% (**Supplementary Table 1**). Over 70% of the clean reads were mapped to the porcine reference genome, containing approximately 60% of the unique mappings (**Supplementary Table 2**).

3.2. Identification of differentially expressed lncRNAs

A total of 6,558 lncRNAs were identified in IPEC-J2 cells in the control and CPB2 groups, among which 39 were significantly up-regulated and 10 were significantly down-regulated lncRNAs between the two groups of IPEC-J2 cells [*p*-value < 0.05 and $|(\log2\ (FC)| \geq 1)$] (**Figure 1B** and **Supplementary Table 3**).

Ten significantly differentially expressed lncRNAs were randomly selected for qRT-PCR validation of the accuracy of the sequencing results. The expression levels of lncRNAs *LOC106507243*, *LOC106508476*, and *EN-41166* were down-regulated after CPB2 treatment, while lncRNAs *EN-47080*, *EN-41190*, *EN-47438*, *EN-46898*, *EN-45823*, *LOC102162336*, and *EN-48701* were up-regulated after CPB2 treatment (**Figure 1C**). The results of qRT-PCR were consistent with the RNA-seq results, demonstrating that the sequencing results were reliable and reproducible.

3.3. GO terms and KEGG pathways analysis of lncRNA *EN-90756* target gene

To explore their functions, the 49 differentially expressed lncRNAs were subjected to target gene prediction. Consequently, genes associated with the immune response and viral defense (e.g., *CXCL2*, *MX1*, OASL) were identified among the target genes (**Figure 2A**) of the significantly differentially expressed lncRNA *EN-90756*. Further enrichment analysis revealed that significantly enriched GO terms were defense response to virus, negative regulation of viral genome replication, negative regulation of apoptotic process, and regulation of cell cycle (**Figure 2B**). The KEGG enrichment analysis identified Legionellosis, influenza A, Salmonella infection, and cellular senescence signaling pathways were significantly enriched (**Figure 2C**). Interestingly, the *MX1* gene was enriched in the defense response to virus, cellular response to type I interferon, and hepatitis C, influenza A, and measles signaling pathways. These results suggest that lncRNA *EN_90756* might be involved in the invasion of IPEC-J2 cells by CPB2 toxin through the regulation of target genes.

3.4. LncRNA *EN-90756* was highly expressed in CPB2-treated IPEC-J2 cells

The expression pattern of lncRNA *EN-90756* in CPB2-treated cells was determined at different time points (0, 12, 24, and 36 h) of CPB2 toxin treatment. The results showed that lncRNA *EN-90756* expression was significantly up-regulated during CPB2 toxin treatment and reached its highest level at 24 h (**Figure 3A**). The nuclear/cytosol separation assay showed that lncRNA *EN-90756* was mainly located in the cytoplasm, with a small amount in the nucleus (**Figure 3B**). RNA-FISH results also confirmed that the green fluorescent signal of lncRNA *EN-90756* was distributed in both the nucleus and the cytoplasm, but was mainly located in the cytoplasm (**Figure 3C**). These results suggest that lncRNA *EN-90756* might be an important regulator in the regulation of *C. perfringens* type C infection.

3.5. Knockdown of lncRNA *EN-90756* inhibited the proliferation of IPEC-J2 cells

Long non-coding RNA *EN-90756* was knocked down to investigate its role in CPB2-treated IPEC-J2 cells. The expression

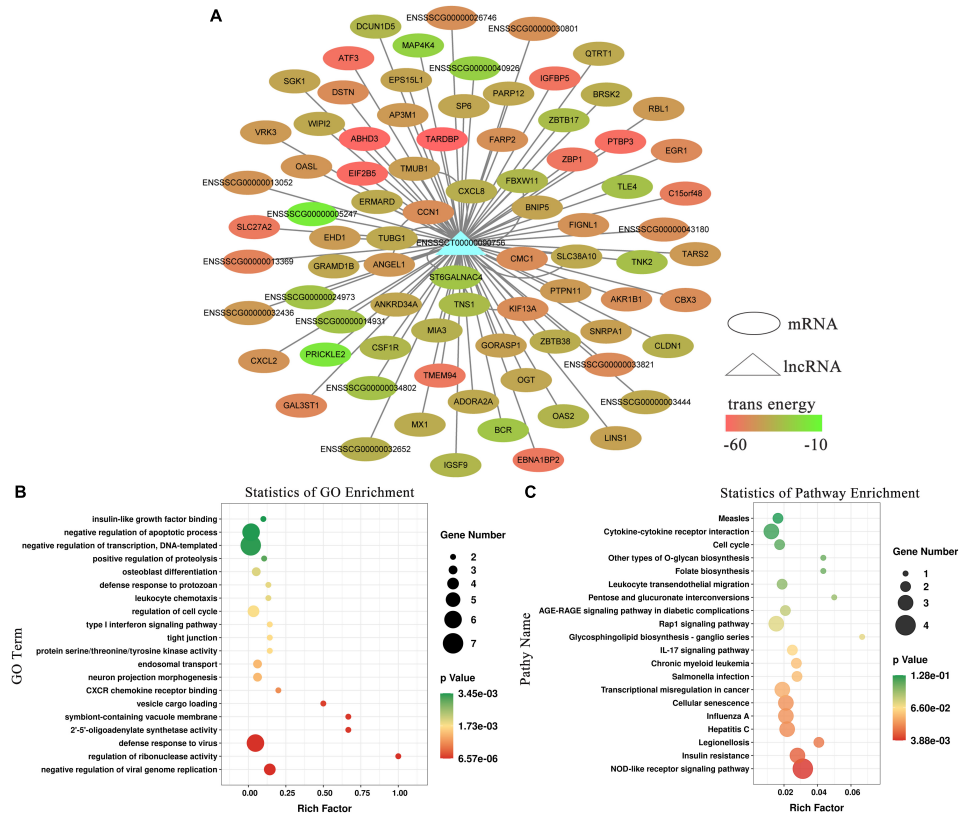

FIGURE 2
Functional enrichment analysis of long non-coding RNA (lncRNA) *EN-90756*. **(A)** Network between lncRNA *EN-90756* and differentially expressed mRNAs. The ellipse represents mRNAs, the triangle represents the lncRNA, and the color of the ellipse represents the formation of secondary structure free energy between the lncRNA and mRNA sequences. Functional enrichment analysis of lncRNA EN-90756 significantly differentially expressed target genes. **(B)** The top 20 significant gene ontology (GO) enrichment terms. **(C)** The top 20 enriched Kyoto Encyclopedia of Genes and Genomes (KEGG) pathways. In the scatter plot, the size of the dots represents the number of genes with significant differences, and the color of the dots represents the significance of the enrichment (*p*-value).

level of lncRNA *EN-90756* was significantly reduced after transfection with si EN-90756 (Figure 4A). Cell viability assays showed that knockdown of lncRNA *EN-90756* in CPB2-treated IPEC-J2 cells significantly reduced cell viability (to 78.75%) (Figure 4B). EdU analysis revealed that more EdU-positive cells were observed in the CPB2 and si NC + CPB2 groups, while fewer EdU-positive cells were observed in the si EN_90756 + CPB2 group (Figures 4C, D). These results indicated that down-regulation of lncRNA *EN-90756* inhibited the proliferation of IPEC-J2 cells.

3.6. Knockdown of lncRNA *EN-90756* promoted apoptosis in IPEC-J2 cells

JC-1 staining showed that after knocking down lncRNA *EN-90756*, the fluorescence turned almost entirely green in CPB2-treated IPEC-J2 cells, reflecting the collapse of the $\Delta\psi m$ (Figure 5A). This suggested that knockdown of lncRNA *EN-90756* exacerbated CPB2-induced loss of $\Delta\psi m$ in IPEC-J2 cells. Caspase 3 and Caspase 8, are key proteins in apoptosis, and qRT-PCR revealed that the mRNA expression levels of *Caspase 3* and *Caspase 8* were significantly elevated in CPB2-induced IPEC-J2 cells after knockdown of lncRNA *EN-90756* (Figures 5B, C). Furthermore, the results of flow cytometry showed that the apoptosis rate was 27.35% in the CPB2 group and 37.74% in the si EN_90756 + CPB2 group (Figure 5D). These results suggested that down-regulation of lncRNA *EN-90756* promoted apoptosis in IPEC-J2 cells.

3.7. Knockdown of lncRNA *EN-90756* promoted MX1 expression and inhibited the JAK-STAT signaling pathway

Long non-coding RNA *EN-90756* knockdown resulted in significant up-regulation of the expression of target gene *MX1*

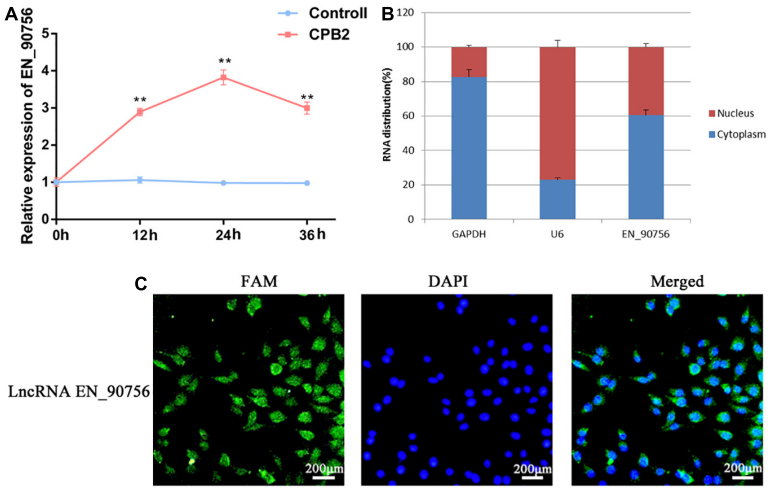

FIGURE 3
Clostridium perfringens beta2 (CPB2) toxin induction promotes high expression of long non-coding RNA (lncRNA) *EN-90756* in intestinal porcine epithelial cell line-J2 (IPEC-J2) cells. **(A)** Changes in lncRNA *EN-90756* expression from 0 to 36 h in IPEC-J2 cells treated with 20 μg/ml CPB2. **(B)** Nuclear/cytoplasmic isolation showed the distribution of lncRNA EN-90756 in the cells. **(C)** Fluorescent *in situ* hybridization (FISH) analysis of IPEC-J2 cells treated with CPB2 for 24 h using a FAM-labeled lncRNA EN-9075 probe (green) and 4′, 6-diamidino-2-phenylindole nuclear staining (blue). Scale bar = 200 μm. $^{**}p < 0.05$.

(**Figure 6A**) and its protein level (**Figures 6B, C**) in CPB2-induced IPEC-J2 cells. The JAK-STAT signaling pathway is involved in a variety of important biological processes, including cell proliferation and apoptosis. To explore the effect of lncRNA *EN-90756* on the JAK-STAT pathway, we examined the levels of JAK1 and STAT3 proteins and their phosphorylation. The results showed that JAK1 and p-JAK1 protein levels were significantly down-regulated in CPB2-induced IPEC-J2 cells after knockdown of lncRNA *EN-90756*. STAT3 and p-STAT3 proteins were barely detected in CPB2-induced IPEC-J2 cells after knockdown of lncRNA *EN-90756* (**Figures 6D, E**). The results suggested that lncRNA *EN-90756* regulates *MX1* expression and affects JAK-STAT pathway activation in CPB2-induced IPEC-J2 cells.

4. Discussion

Clostridium perfringens causes enteritis and enterotoxaemia in domestic animals, wildlife and humans, and its virulence is mainly due to its ability to produce toxins. CPB2 toxin is an important pathogenic factor causing necrotizing enteritis in animals. The correlation between neonatal piglet diarrhea and the presence of *C. perfringens* capable of producing CPB2 toxin in their intestine is extremely high (Bueschel et al., 2003). To further investigate the effects of CPB2 toxin on animal diarrhea, CPB2 toxin protein was isolated and purified. CPB2 toxin protein was moderately cytotoxic to human NCM460 intestinal epithelial cells (Zeng et al., 2016); and induced apoptosis and inflammation in porcine small intestinal epithelial cells, impairing the intestinal barrier function (Gao et al., 2020). However, the effects of host lncRNAs in CPB2 toxin-treated IPEC-J2 cells and how they are regulated are unclear. Here, IPEC-J2 cells from the CPB2 and control groups were analyzed using RNA-seq to search for lncRNAs affected by CPB2 toxin and to explore the function of these lncRNAs, which will inform studies on the effects of CPB2 toxin on piglet diarrhea.

Long non-coding RNAs have emerged as important regulators of various biological processes and diseases, interacting with other molecules and thus participating in the regulation of histone modifications, gene transcription, RNA stability, RNA splicing, and transcriptional or translational modifications. LncRNA *PVT1* promotes cancer initiation and progression by acting as a competing endogenous RNA (ceRNA), activating STAT3 signaling or KAT2A acetyltransferase, or interacting with myelocytomatosis oncogene (MYC) (Zhao J. et al., 2018; Jin et al., 2019; Sun et al., 2019). Systemic loss-of-function experiments demonstrate that long intergenic ncRNAs (lincRNAs) are involved in the molecular circuitry of embryonic stem cells and are required for the maintenance of embryonic stem cell pluripotency (Guttman et al., 2011). In recent years, numerous studies related to lncRNAs have been conducted in domestic animals. The 73 up-regulated and 68 down-regulated differentially expressed lncRNAs were identified in placentas from Meishan pigs at the establishment and expansion stages of placental fold development, and these differential lncRNAs were associated primarily with the placental fold development process (Deng et al., 2020). In the present study, we detected 49 significantly differentially expressed lncRNAs between control IPEC-J2 cells and CPB2 treated cells. The target genes of significantly different lncRNA *EN-90756* were mainly associated with

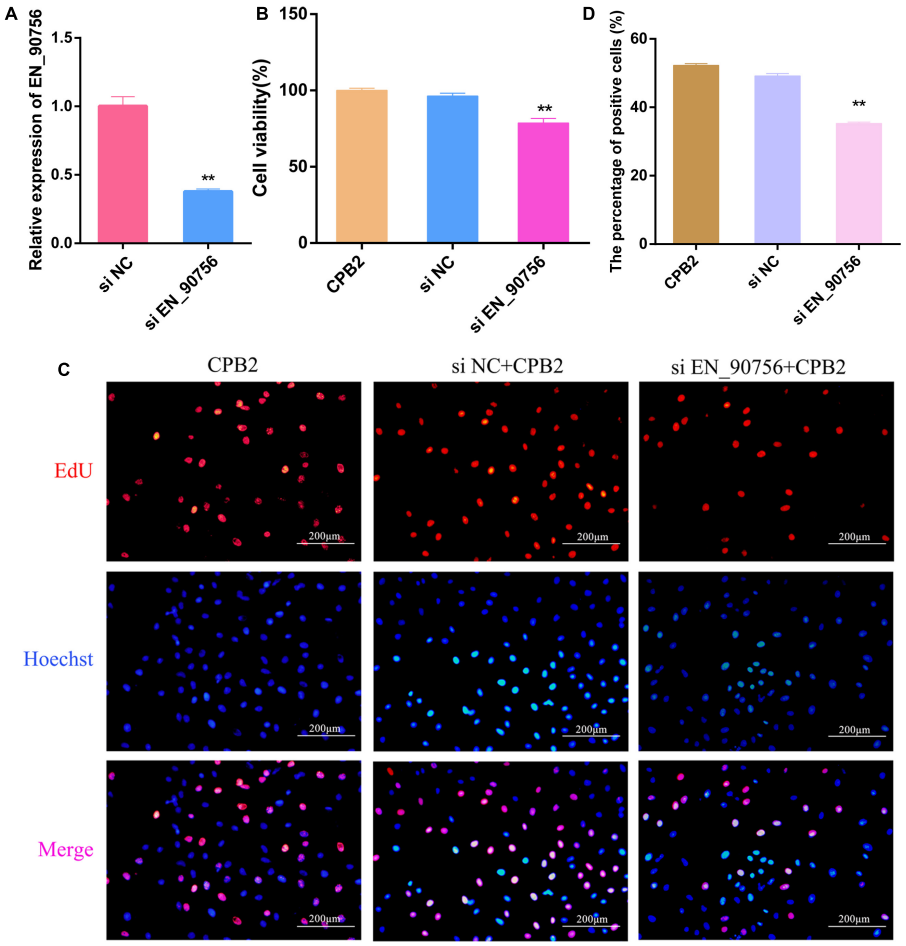

FIGURE 4
Knockdown of long non-coding RNA (lncRNA) *EN-90756* inhibits the proliferation of intestinal porcine epithelial cell line-J2 (IPEC-J2) cells. **(A)** Expression of lncRNA EN-90756 in *Clostridium perfringens* beta2 (CPB2) cells after transfection with si NC and si EN_90756. **(B)** Effect of lncRNA EN-90756 on the viability of CPB2-treated IPEC-J2 cells. **(C)** si NC or si *EN_90756* were transfected into CPB2-treated IPEC-J2 cells, followed by staining with 5-ethynyl-2′-deoxyuridine (EdU) (red) for DNA replication and Hoechst (blue) for nuclei. Scale bar = 200 μm. **(D)** The percentages of EdU-positive cells. $^{**}p < 0.05$.

defense responses to viruses, suggesting a possible regulatory role of lncRNA *EN-90756* in CPB2-treated cells.

Aberrant lncRNA expression is implicated in the pathogenesis of many diseases. Highly expressed lncRNA *LINC00707* mediates a range of biological functions in humans, including cell proliferation, apoptosis, metastasis, invasion, cell cycle arrest, inflammation, and even osteogenic differentiation (Yao et al., 2022). In present study, the expression of lncRNA *EN-90756* was significantly up-regulated with increasing treatment time of CPB2 toxin and reached its highest value at 24 h. EdU and cell viability assays showed that knockdown of lncRNA *EN-90756* inhibited the proliferation of CPB2-treated IPEC-J2 cells.

The ΔΨm plays a crucial role in many biological processes and is highly correlated with apoptosis (Tian et al., 2019). In epithelial cancer cells, ΔΨm is often abnormally higher than that in normal cells, which is associated with increased invasiveness of cancer cells *in vitro* and their increased metastatic potential *in vivo* (Begum et al., 2021). Instability of the ΔΨm leads to early reperfusion arrhythmias and systolic dysfunction (Ashok et al., 2020). Treatment with isoliquiritigenin increased apoptosis in human bladder cancer T24 cells in a concentration-dependent manner and caused a decrease in the ΔΨm in a time-dependent manner (Si et al., 2017). It has been reported that ΔΨm decreased in CPB2-treated IPEC-J2 cells (Luo et al., 2020). Here, we noted that knockdown of lncRNA *EN-90756* resulted in a significant decrease in the ΔΨm in IPEC-J2 cells, implying that the cells entered an early apoptotic phase. Initiator caspases (such as Caspase 8) are involved in early apoptotic signaling, and once Caspase 8 is activated, it can immediately initiate downstream effector caspases (e.g., Caspase 3) to promote

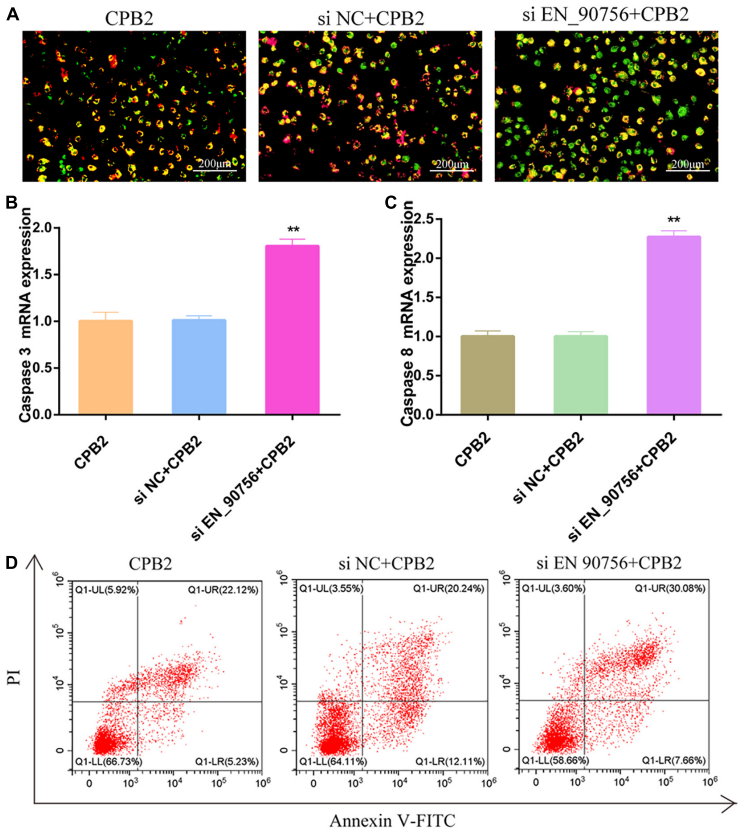

FIGURE 5
Knockdown of long non-coding RNA (lncRNA) *EN-90756* promoted apoptosis in intestinal porcine epithelial cell line-J2 (IPEC-J2) cells. **(A)** The $\Delta\psi$m was detected in IPEC-J2 cells treated with *Clostridium perfringens* beta2 (CPB2) for 24 h and stained using the JC-1 probe. Scale bar = 200 μm. The shift from red to green fluorescence represents a decrease in cell membrane potential. The mRNA expression of *caspase 3* **(B)** and *caspase 8* **(C)** in cells treated with 20 μg/ml CPB2 toxin for 24 h. **(D)** Apoptosis was detected using Annexin V-fluorescein isothiocyanate. $^{**}p < 0.05$.

apoptosis (O'Donnell et al., 2011; Willson, 2019; Zhaojun et al., 2022). We found that CPB2-induced the mRNA expression of apoptotic proteins *Caspase 3* and *Caspase 8* in IPEC-J2 cells, which was significantly increased after lncRNA *EN-90756* inhibition. Meanwhile, flow cytometry showed that down-regulation of lncRNA *EN-90756* expression promoted apoptosis in IPEC-J2 cells. In summary, knockdown of lncRNA *EN-90756* promoted apoptosis in CPB2-induced IPEC-J2 cells.

The localization of lncRNAs is closely related to their mode of regulation. Although most lncRNAs are transcribed by RNA polymerase II (Pol II) and have polyadenylate tails and m7G cap structures, they are processed and spliced less efficiently and exhibit significant cytosolic localization (Derrien et al., 2012; Tian and Manley, 2017; Guo et al., 2020). When localized in the nucleus, lncRNAs can interact with a variety of molecules such as DNA, RNA, and proteins to regulate chromosome structure and function, or regulate gene transcription in *cis* or *trans*, affecting mRNA splicing, stabilization, and translation (Fanucchi et al., 2019; Statello et al., 2020). LncRNAs localized in the cytoplasm are mainly involved in the regulation of gene expression in *trans* at the post-transcriptional level, such as the regulation of mRNA translation and degradation, or in the regulation of intracellular signaling pathways (Hartford and Lal, 2020). Special organelle-localized lncRNAs are involved in organelle function and metabolic regulation, such as the mitochondrial oxidative response and homeostatic balance (Mercer et al., 2011; Carlevaro-Fita et al., 2016; Noh et al., 2016). FISH analysis showed that lncRNA *EN-90756* was distributed in both the nucleus and cytoplasm, but mainly in the cytoplasm, suggesting that lncRNA *EN-90756* may be involved in post-transcriptional regulation. LncRNA *TINCR* regulates the stability of KRT80 by binding to STAU1 protein, thereby affecting epidermal cell differentiation (Kretz et al., 2013). The lncRNA AS Uchl1 controls the translation of Uchl1 *via* an embedded SINEB2 repeat sequence (Carrieri et al., 2012, 2015). No neighboring genes were found in the vicinity of lncRNA En-90756, suggesting that lncRNA En-90756 may function by regulating distal target genes. To further investigate the regulatory role of lncRNA EN-90756 in IPEC-J2 cells, we examined significantly differentially expressed

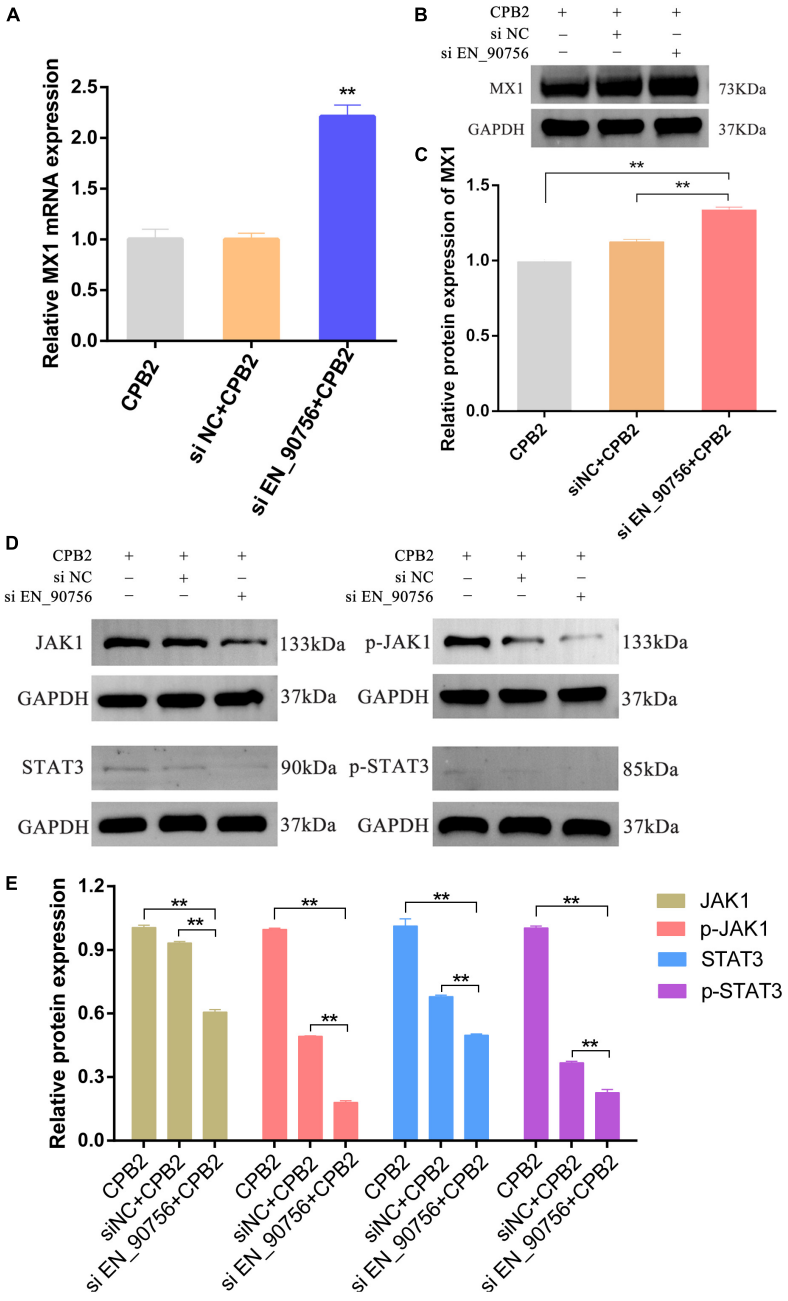

FIGURE 6
Inhibition of long non-coding RNA (lncRNA) *EN-90756* promoted MX1 expression and suppressed the Janus kinase (JAK)-signal transducer and activator of transcription (STAT) signaling pathway. The mRNA expression **(A)** and protein levels **(B,C)** of the target gene MX1 in *Clostridium perfringens* beta2 (CPB2)-induced intestinal porcine epithelial cell line-J2 (IPEC-J2) cells before and after lncRNA EN-90756 inhibition. **(D,E)** Western blotting analysis of JAK1, p-JAK1, STAT3, and p-STAT3 protein levels in IPEC-J2 cells after CPB2 stimulation by lncRNA *EN-90756* inhibition. $^{**}p < 0.05$.

target genes. We noted a significant up-regulation of MX1 expression after lncRNA EN-90756 knockdown. *MX1* is an interferon-stimulated gene that plays a role in the defense of mammalian cells against influenza A and other viruses by repressing viral gene transcription (Pavlovic et al., 1992; Holzinger et al., 2007; Raftery and Stevenson, 2017; Spitaels et al., 2019). MX1 represents a key component of the mouse innate immune system that protects mice from the highly lethal human H5N1 influenza virus (Tumpey et al., 2007). LncRNA *IVRPIE* promoted the host immune response against influenza A virus by regulating the expression of interferon β1 and MX1 (Zhao et al., 2020). These results suggest that lncRNA

EN-90756 might influence the immune response of IPEC-J2 cells by regulating MX1 expression, providing clues for disease resistance breeding and disease treatment in piglet diarrhea.

Previous studies confirmed that the JAK/STAT pathway plays an important role in mediating cell fate such as apoptosis, differentiation, and proliferation (Muoz-Cánoves et al., 2013; Richard and Stephens, 2014; O'Shea et al., 2015; Jia et al., 2016). The JAK family of receptor-associated tyrosine kinases act as primary transducers of multiple cytokine receptors and mediate a variety of their effects through the phosphorylation of STAT transcription factors (Derecka et al., 2012; Lee et al., 2016). LncRNA *FEZF1-AS1* promotes proliferation and inhibits apoptosis in ovarian cancer through activation of the JAK-STAT3 pathway (Zhao X. et al., 2018). Crizotinib could promote cell apoptosis of human lung cancer cell line H2228 by regulating the expression of JAK and STAT proteins in the JAK-STAT signaling pathway (Lu et al., 2018). LncRNA *MEG3* inhibited the migration of oral squamous cell carcinoma cells and promoted apoptosis by regulating the JAK-STAT pathway (Tan et al., 2019). Previous studies have shown that CPB2 toxin treatment of IPEC-J2 cells inhibits cell proliferation, promotes apoptosis, and accelerates the inflammatory response (Gao et al., 2020; Luo et al., 2020; Yang et al., 2022). Here, lncRNA *EN-90756* was able to alleviate CPB2 toxin-induced apoptosis and promote cell proliferation in IPEC-J2 cells. In addition, the JAK-STAT signaling pathway was regulated by lncRNA *EN-90756*, as inferred from the expression levels of related proteins. The above results suggested that lncRNA *EN-90756* might regulate the proliferation and apoptosis of IPEC-J2 cells by affecting the JAK-STAT pathway. However, the regulation of lncRNA is complex and the specific mechanism of regulation of JAK-STAT by lncRNA *EN-90756* needs to be further investigated.

In conclusion, this study identified differentially expressed lncRNAs in the CPB2 and control groups of IPEC-J2 cells. In addition, we found that CPB2 toxin treatment promoted significant differential lncRNA *EN-90756* expression up-regulation. Inhibition of lncRNA *EN-90756* suppressed the proliferation of CPB2-treated IPEC-J2 cells and promoted apoptosis. Mechanistically, lncRNA *EN-90756* might affect the antiviral ability of IPEC-J2 cells by regulating the expression of MX1. Meanwhile, lncRNA *EN-90756* might regulate CPB2-induced cell proliferation and apoptosis by affecting the JAK-STAT signaling pathway. These findings provide novel perspectives and directions for further exploration of the regulatory mechanisms of lncRNAs toward CPB2 toxin-induced diarrhea in piglets.

Data availability statement

The datasets presented in this study can be found in online repositories. The names of the repository/repositories and accession number(s) can be found below: https://www.ncbi.nlm.nih.gov/, PRJNA749943.

Author contributions

SG and JY: conceived and designed the study. JY, JZ, QY, XH, ZY, PW, and XG: experimental investigation and data analysis. JY, JL, NL, and YG: data curation. JY: writing—original draft. QY: writing—review and editing. All authors have read and agreed to the published version of the manuscript.

Funding

This research was funded by the National Natural Science Foundation of China (31960646) and breeding of new resistant local pig breeds (supporting lines) in the Northern Region (2021YFD1301204).

Acknowledgments

We thank LC-Bio Tech Co., Ltd. (Hangzhou, China) for their assistance with sequencing and data processing.

Conflict of interest

NL and YG were employed by Jilin Rongtai Agricultural Development Co., Ltd.

The remaining authors declare that the research was conducted in the absence of any commercial or financial relationships that could be construed as a potential conflict of interest.

Publisher's note

Supplementary material

The Supplementary Material for this article can be found online at: https://www.frontiersin.org/articles/10.3389/fmicb.2022.1082025/full#supplementary-material

References

Ashok, D., Papanicolaou, K., Liu, T., and O'Rourke, B. (2020). Reverse-mode mitochondrial Na^+/Ca^{2+} exchange, not the MCU, is the primary mode of Ca^{2+} import into the mitochondria during ischemia/reperfusion in neonatal cardiac myocytes. *Biophys. J.* 118:407a. doi: 10.1016/j.bpj.2019.11.2305

Begum, H. M., Mariano, C., Zhou, H., and Shen, K. (2021). E-cadherin regulates mitochondrial membrane potential in cancer cells. *Cancers* 13:5054. doi: 10.3390/cancers13205054

Bueschel, D. M., Jost, B. H., Billington, S. J., Trinh, H. T., and Songer, J. G. (2003). Prevalence of cpb2, encoding beta2 toxin, in *Clostridium perfringens* field isolates: Correlation of genotype with phenotype. *Vet. Microbiol.* 94, 121–129. doi: 10.1016/S0378-1135(03)00081-6

Carlevaro-Fita, J., Rahim, A., Guigó, R., Vardy, L. A., and Johnson, R. (2016). Cytoplasmic long noncoding RNAs are frequently bound to and degraded at ribosomes in human cells. *RNA* 22, 867–882. doi: 10.1261/rna.053561.115

Carrieri, C., Cimatti, L., Biagioli, M., Beugnet, A., Zucchelli, S., Fedele, S., et al. (2012). Long non-coding antisense RNA controls Uchl1 translation through an embedded SINEB2 repeat. *Nature* 491, 454–457. doi: 10.1038/nature11508

Carrieri, C., Forrest, A. R., Santoro, C., Persichetti, F., Carninci, P., Zucchelli, S., et al. (2015). Expression analysis of the long non-coding RNA antisense to Uchl1 (AS Uchl1) during dopaminergic cells' differentiation in vitro and in neurochemical models of Parkinson's disease. *Front. Cell. Neurosci.* 9:114. doi: 10.3389/fncel.2015.00114

Chen, J., Zhang, C., Zhang, N., and Liu, G. (2019). Porcine endemic diarrhea virus infection regulates long noncoding RNA expression. *Virology* 527, 89–97. doi: 10.1016/j.virol.2018.11.007

Deng, D., Tan, X., Han, K., Ren, R., Cao, J., and Yu, M. (2020). Transcriptomic and ChIP-seq integrative analysis reveals important roles of epigenetically regulated lncRNAs in placental development in Meishan pigs. *Genes* 11:397. doi: 10.3390/genes11040397

Derecka, M., Gornicka, A., Koralov, S. B., Szczepanek, K., Morgan, M., Raje, V., et al. (2012). Tyk2 and Stat3 regulate brown adipose tissue differentiation and obesity. *Cell Metab.* 16, 814–824. doi: 10.1016/j.cmet.2012.11.005

Derrien, T., Johnson, R., Bussotti, G., Tanzer, A., Djebali, S., Tilgner, H., et al. (2012). The GENCODE v7 catalog of human long noncoding RNAs: Analysis of their gene structure, evolution, and expression. *Genome Res.* 22, 1775–1789. doi: 10.1101/gr.132159.111

Fanucchi, S., Fok, E. T., Dalla, E., Shibayama, Y., Börner, K., Chang, E. Y., et al. (2019). Immune genes are primed for robust transcription by proximal long noncoding RNAs located in nuclear compartments. *Nat. Genet.* 51, 138–150. doi: 10.1038/s41588-018-0298-2

Gao, X., Yang, Q., Huang, X., Yan, Z., and Gun, S. (2020). Effects of *Clostridium perfringens* beta2 toxin on apoptosis, inflammation, and barrier function of intestinal porcine jejunum epithelial cells. *Microb. Pathog.* 147:104379. doi: 10.1016/j.micpath.2020.104379

Guo, C.-J., Ma, X.-K., Xing, Y.-H., Zheng, C.-C., Xu, Y.-F., Shan, L., et al. (2020). Distinct processing of lncRNAs contributes to non-conserved functions in stem cells. *Cell* 181, 621–636.e22. doi: 10.1016/j.cell.2020.03.006

Guttman, M., Donaghey, J., Carey, B. W., Garber, M., Grenier, J. K., Munson, G., et al. (2011). lincRNAs act in the circuitry controlling pluripotency and differentiation. *Nature* 477, 295–300. doi: 10.1038/nature10398

Hartford, C. C. R., and Lal, A. (2020). When long noncoding becomes protein coding. *Mol. Cell. Biol.* 40:e00528-19. doi: 10.1128/MCB.00528-19

Holzinger, D., Jorns, C., Stertz, S., Boisson-Dupuis, S., Thimme, R., Weidmann, M., et al. (2007). Induction of MxA gene expression by influenza A virus requires type I or type III interferon signaling. *J. Virol.* 81, 7776–7785. doi: 10.1128/JVI.00546-06

Huang, X. Y., Sun, W. Y., Yan, Z. Q., Shi, H. R., Yang, Q. L., Wang, P. F., et al. (2019). Novel insights reveal anti-microbial gene regulation of piglet intestine immune in response to *Clostridium perfringens* infection. *Sci. Rep.* 9:1963. doi: 10.1038/s41598-018-37898-5

Jia, Y., Liu, T., Zhou, L., Zhu, J., Wu, J., Sun, D., et al. (2016). Effects of di-(2-ethylhexyl) phthalate on lipid metabolism by the JAK/STAT pathway in rats. *Int. J. Environ. Res. Public Health* 13:1085. doi: 10.3390/ijerph13111085

Jin, K., Wang, S., Zhang, Y., Xia, M., Mo, Y., Li, X., et al. (2019). Long non-coding RNA PVT1 interacts with MYC and its downstream molecules to synergistically promote tumorigenesis. *Cell. Mol. Life Sci.* 76, 4275–4289. doi: 10.1007/s00018-019-03222-1

Kanehisa, M., Araki, M., Goto, S., Hattori, M., Hirakawa, M., Itoh, M., et al. (2007). KEGG for linking genomes to life and the environment. *Nucleic Acids Res.* 36(Suppl. 1), D480–D484. doi: 10.1093/nar/gkm882

Kim, D., Langmead, B., and Salzberg, S. L. (2015). HISAT: A fast spliced aligner with low memory requirements. *Nat. Methods* 12, 357–360. doi: 10.1038/nmeth.3317

Kong, L., Zhang, Y., Ye, Z.-Q., Liu, X.-Q., Zhao, S.-Q., Wei, L., et al. (2007). CPC: Assess the protein-coding potential of transcripts using sequence features and support vector machine. *Nucleic Acids Res.* 35(Suppl. 2), W345–W349. doi: 10.1093/nar/gkm391

Kretz, M., Siprashvili, Z., Chu, C., Webster, D. E., Zehnder, A., Qu, K., et al. (2013). Control of somatic tissue differentiation by the long non-coding RNA TINCR. *Nature* 493, 231–235. doi: 10.1038/nature11661

Lebrun, M., Filée, P., Mousset, B., Desmecht, D., Galleni, M., Mainil, J., et al. (2007). The expression of *Clostridium perfringens* consensus beta2 toxin is associated with bovine enterotoxaemia syndrome. *Vet. Microbiol.* 120, 151–157. doi: 10.1016/j.vetmic.2006.10.020

Lee, K., Um, S. H., Rhee, D. K., and Pyo, S. (2016). Interferon-alpha inhibits adipogenesis via regulation of JAK/STAT1 signaling. *Biochim. Biophys. Acta Gen. Subj.* 1860, 2416–2427. doi: 10.1016/j.bbagen.2016.07.009

Ljvak, K. (2001). Analysis of relative gene expression data using real time quantitative PCR and the $2^{-\Delta\Delta CT}$ method. *Methods* 25, 402–408. doi: 10.1006/meth.2001.1262

Lu, H., Wu, S., Chen, H., Huang, Y., Qiu, G., Liu, L., et al. (2018). Crizotinib induces apoptosis of lung cancer cells through JAK-STAT pathway. *Oncol. Lett.* 16, 5992–5996. doi: 10.3892/ol.2018.9387

Luo, R., Yang, Q., Huang, X., Yan, Z., Gao, X., Wang, W., et al. (2020). *Clostridium perfringens* beta2 toxin induced in vitro oxidative damage and its toxic assessment in porcine small intestinal epithelial cell lines. *Gene* 759:144999. doi: 10.1016/j.gene.2020.144999

Marzia, D., Andrea, P., Filomena, F. P., Giuseppe, P., Elisa, T., Claudio, L., et al. (2018). Long non-coding RNAs play a role in the pathogenesis of psoriatic arthritis by regulating MicroRNAs and genes involved in inflammation and metabolic syndrome. *Front. Immunol.* 9:1533. doi: 10.3389/fimmu.2018.01533

Mercer, T. R., Neph, S., Dinger, M. E., Crawford, J., Smith, M. A., Shearwood, A.-M. J., et al. (2011). The human mitochondrial transcriptome. *Cell* 146, 645–658. doi: 10.1016/j.cell.2011.06.051

Muoz-Cánoves, P., Scheele, C., Pedersen, B. K., and Serrano, A. L. (2013). Interleukin-6 myokine signaling in skeletal muscle: A double-edged sword? *FEBS Lett.* 280, 4131–4148. doi: 10.1111/FEBS.12338

Noh, J. H., Kim, K. M., Abdelmohsen, K., Yoon, J. H., Panda, A. C., Munk, R., et al. (2016). HuR and GRSF1 modulate the nuclear export and mitochondrial localization of the lncRNA RMRP. *Genes Dev.* 20, 1224–1239. doi: 10.1101/gad.276022.115

O'Donnell, M. A., Perez-Jimenez, E., Oberst, A., Ng, A., Massoumi, R., Xavier, R., et al. (2011). Caspase 8 inhibits programmed necrosis by processing CYLD. *Nat. Cell Biol.* 13, 1437–1442. doi: 10.1038/ncb2362

O'Shea, J. J., Schwartz, D. M., Villarino, A. V., Gadina, M., McInnes, I. B., and Laurence, A. (2015). The JAK-STAT pathway: Impact on human disease and therapeutic intervention. *Annu. Rev. Med.* 66, 311–328. doi: 10.1146/annurev-med-051113-024537

Pavlovic, J., Haller, O., and Staeheli, P. (1992). Human and mouse Mx proteins inhibit different steps of the influenza virus multiplication cycle. *J. Virol.* 66, 2564–2569. doi: 10.1016/0166-0934(92)90025-9

Raftery, N., and Stevenson, N. J. (2017). Advances in anti-viral immune defence: Revealing the importance of the IFN JAK/STAT pathway. *Cell. Mol. Life Sci.* 74, 2525–2535. doi: 10.1007/s00018-017-2520-2

Richard, A., and Stephens, J. M. (2014). The role of JAK-STAT signaling in adipose tissue function. *Biochim. Biophys. Acta* 1842, 431–439. doi: 10.1016/j.bbadis.2013.05.030

Si, L., Yang, X., Yan, X., Wang, Y., and Zheng, Q. (2017). Isoliquiritigenin induces apoptosis of human bladder cancer T24 cells via a cyclin-dependent kinase-independent mechanism. Corrigendum in. *Oncol. Lett.* 14, 241–249. doi: 10.3892/ol.2021.12529

Silva, R., Junior, C. O., Guedes, R., and Lobato, F. (2015). *Clostridium perfringens*: A review of the disease in pigs, horses and broiler chickens. *Ciec. Rural* 45, 1027–1034. doi: 10.1590/0103-8478cr20140927

Spitaels, J., Hoecke, L. V., Roose, K., Kochs, G., and Saelens, X. (2019). Mx1 in hematopoietic cells protects against thogoto virus infection. *J. Virol.* 93:e00193-19. doi: 10.1128/JVI.00193-19

Statello, L., Guo, C.-J., Chen, L. L., and Huarte, M. (2020). Gene regulation by long non-coding RNAs and its biological functions. *Nat. Rev. Mol. Cell Biol.* 22, 96–118. doi: 10.1038/s41580-020-00315-9

Sun, L., Luo, H., Bu, D., Zhao, G., Yu, K., Zhang, C., et al. (2013). Utilizing sequence intrinsic composition to classify protein-coding and long non-coding transcripts. *Nucleic Acids Res.* 41:e166. doi: 10.1093/nar/gkt646

Sun, Z.-Y., Jian, Y.-K., Zhu, H.-Y., and Li, B. (2019). lncRNAPVT1 targets miR-152 to enhance chemoresistance of osteosarcoma to gemcitabine through activating c-MET/PI3K/AKT pathway. *Pathol. Res. Pract.* 215, 555–563. doi: 10.1016/j.prp.2018.12.013

Tan, J., Xiang, L., and Xu, G. (2019). LncRNA MEG3 suppresses migration and promotes apoptosis by sponging miR-548d-3p to modulate JAK–STAT pathway in oral squamous cell carcinoma. *IUBMB Life* 71, 882–890. doi: 10.1002/iub.2012

Tian, B., and Manley, J. L. (2017). Alternative polyadenylation of mRNA precursors. *Nat. Rev. Mol. Cell Biol.* 18, 18–30. doi: 10.1038/nrm.2016.116

Tian, M., Sun, J., Dong, B., and Lin, W. (2019). Construction of mitochondria-nucleolus shuttling fluorescent probe for the reversible detection of mitochondrial membrane potential. *Sens. Actuators B Chem.* 292, 16–23. doi: 10.1016/j.snb.2019.04.118

Timoney, J., Hartmann, M., Fallon, L., Fallon, E., and Walker, J. (2005). Antibody responses of mares to prepartum vaccination with *Clostridium perfringens* bacterin and beta 2 toxin. *Vet. Rec.* 157, 810–812. doi: 10.1136/vr.157.25.810

Trapnell, C., Williams, B. A., Pertea, G., Mortazavi, A., Kwan, G., Van Baren, M. J., et al. (2010). Transcript assembly and quantification by RNA-Seq reveals unannotated transcripts and isoform switching during cell differentiation. *Nat. Biotechnol.* 28, 511–515. doi: 10.1038/nbt.1621

Tumpey, T. M., Szretter, K. J., Van Hoeven, N., Katz, J. M., Kochs, G., Haller, O., et al. (2007). The Mx1 gene protects mice against the pandemic 1918 and highly lethal human H5N1 influenza viruses. *J. Virol.* 81, 10818–10821. doi: 10.1128/JVI.01116-07

Waters, M., Savoie, A., Garmory, H. S., Bueschel, D., Popoff, M. R., Songer, J. G., et al. (2003). Genotyping and phenotyping of beta2-toxigenic *Clostridium perfringens* fecal isolates associated with gastrointestinal diseases in piglets. *J. Clin. Microbiol.* 41, 3584–3591. doi: 10.1128/JCM.41.8.3584-3591.2003

Wenzel, A., Akbasli, E., and Gorodkin, J. (2012). RIsearch: Fast RNA-RNA interaction search using a simplified nearest-neighbor energy model. *Bioinformatics* 28, 2738–2746. doi: 10.1093/bioinformatics/bts519

Willson, J. (2019). A matter of life and death for caspase 8. *Nat. Rev. Mol. Cell Biol.* 21:63. doi: 10.1038/s41580-019-0201-8

Wu, Z., Fan, H., Jin, J., Gao, S., Huang, R., Wu, S., et al. (2022). Insight into mechanisms of pig lncRNA FUT3-AS1 regulating *E. coli* F18-bacterial diarrhea. *PLoS Pathog.* 18:e1010584. doi: 10.1371/journal.ppat.1010584

Yang, J., Zhang, J., Gao, X., Luo, R., Xie, K., Wang, W., et al. (2022). FTO regulates apoptosis in CPB2-treated IPEC-J2 cells by targeting caspase 3 apoptotic protein. *Animals* 12:1644. doi: 10.3390/ani12131644

Yao, Q., Li, Z., and Chen, D. (2022). Review of LINC00707: A novel LncRNA and promising biomarker for human diseases. *Front. Cell Dev. Biol.* 10:813963. doi: 10.3389/fcell.2022.813963

Young, M. D., Wakefield, M. J., Smyth, G. K., and Oshlack, A. (2010). Gene ontology analysis for RNA-seq: Accounting for selection bias. *Genome Biol.* 11:R14. doi: 10.1186/gb-2010-11-2-r14

Zeng, J., Song, F., Yang, Y., Ma, C., Deng, G., Li, Y., et al. (2016). The generation and characterization of recombinant protein and antibodies of *Clostridium perfringens* beta2 toxin. *J. Immunol. Res.* 2016:5708468. doi: 10.1155/2016/5708468

Zhao, J., Du, P., Cui, P., Qin, Y., Hu, C. E., Wu, J., et al. (2018). LncRNA PVT1 promotes angiogenesis via activating the STAT3/VEGFA axis in gastric cancer. *Oncogene* 37, 4094–4109. doi: 10.1038/s41388-018-0250-z

Zhao, L., Xia, M., Wang, K., Lai, C., Fan, H., Gu, H., et al. (2020). A long non-coding RNA IVRPIE promotes host antiviral immune responses through regulating interferon β1 and ISG expression. *Front. Microbiol.* 20:260. doi: 10.3389/fmicb.2020.00260

Zhao, X., Cheng, Z., and Wang, J. (2018). Long noncoding RNA FEZF1-AS1 promotes proliferation and inhibits apoptosis in ovarian cancer by activation of JAK-STAT3 pathway. *Med. Sci. Monit.* 12, 8088–8095. doi: 10.12659/MSM.911194

Zhaojun, C., Lulin, T., Xin, F., Abdel-Nasser, S., Zunguo, L., and Xiong, L. (2022). Hydroxy-γ-sanshool from *Zanthoxylum bungeanum* (prickly ash) induces apoptosis of human colorectal cancer cell by activating P53 and Caspase 8. *Front. Nutr.* 1:914638. doi: 10.3389/fnut.2022.914638

frontiers | Frontiers in Microbiology

TYPE Original Research
PUBLISHED 17 January 2023
DOI 10.3389/fmicb.2022.1109606

OPEN ACCESS

EDITED BY
Qing Pan,
Chinese Academy of Agricultural Sciences, China

REVIEWED BY
Yuding Fan,
Chinese Academy of Fishery Sciences, China
Weiwei Zeng,
Foshan University, China
Ningqiu Li,
Chinese Academy of Fishery Sciences, China

*CORRESPONDENCE
Tong-Yan Lu
✉ lutongyan@hrfri.ac.cn

SPECIALTY SECTION
This article was submitted to Infectious Agents and Disease, a section of the journal Frontiers in Microbiology

RECEIVED 28 November 2022
ACCEPTED 26 December 2022
PUBLISHED 17 January 2023

CITATION
Zhao J-Z, Xu L-M, Ren G-M, Shao Y-Z, Liu Q, Teng C-B and Lu T-Y (2023) Comparative transcriptome analysis of rainbow trout gonadal cells (RTG-2) infected with U and J genogroup infectious hematopoietic necrosis virus. *Front. Microbiol.* 13:1109606. doi: 10.3389/fmicb.2022.1109606

Comparative transcriptome analysis of rainbow trout gonadal cells (RTG-2) infected with U and J genogroup infectious hematopoietic necrosis virus

Jing-Zhuang Zhao[1,2,3], Li-Ming Xu[2], Guang-Ming Ren[2], Yi-Zhi Shao[2], Qi Liu[2], Chun-Bo Teng[1] and Tong-Yan Lu[2]*

[1]Cell Biology Laboratory, College of Life Science, Northeast Forestry University, Harbin, China, [2]Heilongjiang River Fisheries Research Institute, Chinese Academy of Fishery Sciences, Harbin, China, [3]Key Laboratory of Aquatic Animal Diseases and Immune Technology of Heilongjiang Province, Harbin, China

Infectious hematopoietic necrosis virus (IHNV) is the causative pathogen of infectious hematopoietic necrosis, outbreaks of which are responsible for significant losses in rainbow trout aquaculture. Strains of IHNV isolated worldwide have been classified into five major genogroups, J, E, L, M, and U. To date, comparative transcriptomic analysis has only been conducted individually for the J and M genogroups. In this study, we compared the transcriptome profiles in U genogroup and J genogroup IHNV-infected RTG-2 cells with mock-infected RTG-2 cells. The RNA-seq results revealed 17,064 new genes, of which 7,390 genes were functionally annotated. Differentially expressed gene (DEG) analysis between U and J IHNV-infected cells revealed 2,238 DEGs, including 1,011 downregulated genes and 1,227 upregulated genes. Among the 2,238 DEGs, 345 new genes were discovered. The DEGs related to immune responses, cellular signal transduction, and viral diseases were further analyzed. RT-qPCR validation confirmed that the changes in expression of the immune response-related genes *trpm2*, *sting*, *itgb7*, *ripk2*, and *irf1*, cellular signal transduction-related genes *irl*, *cacnb2*, *bmp2l*, *gadd45α*, and *plk2*, and viral disease-related genes *mlf1, mtor, armc5*, *pik3r1*, and *c-myc* were consistent with the results of transcriptome analysis. Taken together, our findings provide a comprehensive transcriptional analysis of the differential virulence of the U and J genogroups of IHNV, and shed new light on the pathogenic mechanisms of IHNV strains.

KEYWORDS

rainbow trout gonadal cells, infectious hematopoietic necrosis virus, transcriptome analysis (RNAseq), U genogroup, J genogroup

1. Introduction

Rainbow trout is an important freshwater fish species in Chinese aquaculture that is valued for its nutrient-rich meat. However, rainbow trout farming is severely affected worldwide by viral diseases (MacWilliams et al., 2007; Ji et al., 2017; Zhao et al., 2017). One of the most severe viral diseases is infectious hematopoietic necrosis (IHN), which has caused significant losses in rainbow trout aquaculture since it was first reported in China (Niu and Zhao, 1988).

IHN disease is caused by infectious hematopoietic necrosis virus (IHNV) that contains a non-segmented single-stranded, negative-sense RNA and belongs to the genus *Novirhabdovirus* in the family *Rhabdoviridae* (Wargo et al., 2017). The viral genome is approximately 11 kb in length and contains five structural proteins and a non-virion protein (Kurath et al., 2003). Phylogenetic analyses have classified IHNV strains, isolated worldwide, into five major genogroups: J, E, L, M, and U (Xu et al., 2019). The genogroups U, M, and L were first detected in North America (Kurath et al., 2003; Black et al., 2016), and the E genogroup is prevalent in Europe (Enzmann et al., 2005; Cieslak et al., 2017). The first reported outbreak of IHN in Asia was from Japanese salmonid farming factories and it was associated with importation of sockeye salmon eggs from Alaska (Kimura and Yoshimizu, 1991; Nishizawa et al., 2006). Genetic typing analysis showed that the original IHNV in Japan was sockeye-specific U genogroup, but it jumped into rainbow trout as the virus spread in Japan (Nishizawa et al., 2006). During the 1980s, U genogroup evolved into J genogroup and became virulent in rainbow trout (Garver et al., 2006). Our study, along with previously reported studies, confirmed that all IHNV isolates from China belong to the J genogroup highly virulent in rainbow trout (Xu et al., 2019).

A few previous reports have detailed the pathogenic differences between J and U genogroup IHNV infection (Park et al., 2011; Xu et al., 2017), but the molecular mechanisms that underlie the pathogenic differences between these genogroups remain poorly understood. High-throughput sequencing technology, which is widely used in pathogenic and immune-related studies, permits genome wide transcriptomic analysis at high resolution. In the present study, we present the transcriptional sequencing libraries of U or J genogroup virus-infected, or PBS mock-infected rainbow trout gonadal (RTG-2) cells at 24 h post-infection. The different gene expression profiles were analyzed and identified by comparisons between the transcriptional sequencing libraries, and were then validated by RT-qPCR. A great number of genes that were differentially expressed upon J and U genogroup IHNV infection were identified and functionally annotated. This is the first report of transcriptional analysis between the U and J genogroups of IHNV. Our findings not only provide comprehensive transcriptional analysis, but also identify possible mechanisms associated with the differential virulence of the U and J genogroups of IHNV.

2. Materials and methods

2.1. Virus strains and cells

The RTG-2 cell line (CCL-55, ATCC) was cultured in Eagle's minimum essential medium (MEM, 8118228, Gibco, Suzhou, Jiangsu, China) with 10% fetal bovine serum (FBS) and 0.1 mg/ml streptomycin and penicillin. The U genogroup IHNV strain Blk94 (GenBank no: DQ164100) was kindly provided as a gift by Dr. Hong Liu of the Shenzhen Entry-exit Inspection and Quarantine Bureau, China. The J genogroup IHNV strain Sn1203 (GenBank no: KC660147.1) was isolated from moribund rainbow trout fry in China and was stored in our laboratory.

2.2. IHNV infection and samples collection

RTG-2 cells were infected with either IHNV virus (U or J genogroup IHNV) at a multiplicity of infection of 1.0, or mock infected with phosphate-buffered saline (PBS, control). After 1 h incubation, the treated RTG-2 cells were washed three times with PBS and then cultured in MEM with 2% FBS at 15°C. At 24 h post-IHNV-infection, the cells were collected and used for further analysis.

2.3. RNA extraction, and mRNA library construction and sequencing

Total RNA was extracted from RTG-2 cells treated with different IHNV strains using TRIzol reagent (15,596,026, Invitrogen, Carlsbad, California, United States) according to the manufacturer's instructions, and then digested with DNase I. The RNA integrity was determined using an Agilent 2,100 Bioanalyzer (Agilent Technologies, California, United States). The RNA samples that had a 28S/18S rRNA ratio of greater than 1.9 and an RNA integrity ≥8 were chosen for library construction (three individual samples per treatment group). The mRNA was isolated and fragmented from 1 μg of total RNA, followed by double-stranded cDNA synthesis. The 3′ end was repaired and adenylated for adapter ligation and finally, reverse PCR amplification. The final libraries for sequencing were analyzed using an Agilent 2,100 Bioanalyzer and quantified by qPCR using a Library Quantification Kit Illumina (KK4602, Kapa, Boston, Massachusetts, United States) according to the manufacturer's instructions.

2.4. Data processing and analysis of differential gene expression

Raw data were filtered by removing adaptor sequences and low quality sequences using SOAPnuke (v1.5.2) to obtain high

quality clean data. The clean data were then mapped to the *Oncorhynchus mykiss* genome sequence[1] using a HISAT2 comparison system (Kim et al., 2015). The mapped reads were assembled and quantified by StringTie comparisons (Pertea et al., 2015), and high quality data were used for downstream analysis. The mapped data were then annotated by BLAST against the NR, Swiss-Prot, COG, KOG, KEGG, GO, Pfam, eggNOG, and TrEMBL databases. Fragments Per Kilobase of transcript per Million fragments mapped (FPKM) served as a measured standard of the transcript or gene expression level. The screening criteria to identify significantly differentially expressed genes (DEGs) were a fold-change ≥ 2 and a false discovery rate (FDR) < 0.01. The DESeq2 software was used for DEG analysis involving three comparisons (Mock vs. U, Mock vs. J, and U vs. J).

2.5. RT-qPCR analysis of gene expression

To validate the results of RNA-seq analysis, 15 of the DEGs between the U and J groups relating to immune responses, cellular signal transduction, and viral diseases, were analyzed by RT-qPCR. The total RNA used for cDNA library construction was used for RT-qPCR analysis. The total RNA was first transcribed to cDNA using a PrimeScript RT Reagent Kit with gDNA Eraser (RR047A, Takara, Japan), and then a qPCR assay was performed using a TB Green Premix Ex Taq II Kit (RR820A, Takara). The primers used for RT-qPCR are listed in Supplementary Table 1, and β-actin was used as an internal control. The relative expression levels of different genes were calculated using the $2^{-\Delta\Delta CT}$ method.

2.6. Statistical analysis

The data were analyzed using the GraphPad Prism software (version 8.0) and are presented as the mean ± standard deviation (SD). The differences between groups were analyzed by a Student's *t*-test, and a statistically significant difference was defined as a *value of* $p < 0.05$.

3. Results

3.1. Quality analysis of transcriptome sequencing

In this study, nine cDNA libraries were obtained from RTG-2 cells after J-and U-IHNV infection. The quality control results showed that 63,513,756–66,846,372 raw reads and 60,573,286–63,305,380 clean reads were obtained from the nine cDNA libraries, and the ratio of clean reads ranged from 93.12 to 95.53%. The Q20 and Q30 values for all of the libraries were over 99.01 and 92.23%, respectively, and indicated the high quality of the RNA sequence data (Table 1). The raw sequence data have been deposited in the NCBI Sequence Read Archive, under accession number PRJNA895736. The obtained clean reads were mapped to the *O. mykiss* genome sequence and the mapping rates ranged from 88.58 to 93.71%, with most reads being mapped to exon regions within the *O. mykiss* genome.

3.2. Functional annotation and classification

The RNA-seq analysis revealed 17,064 new genes, 7,390 of which were functionally annotated. To understand the functions of these 7,390 genes, nine databases were used to annotate the unigenes. Of the 7,390 genes, the following numbers of genes were annotated using the following databases: 294 (3.98%) in COG, 3,729 (50.46%) in GO, 3,699 (50.05%) in KEGG, 1,320 (17.86%) in KOG, 2,248 (30.42%) in Pfam, 710 (9.61%) in Swiss-Prot, 7,053 (95.44) in TrEMBL, 3,701 (50.08%) in eggNOG, and 6,773 (91.65%) in Nr (Supplementary Table 2).

Among the COG functional annotations, 294 unigenes were classified into 20 categories, with the largest group being the mobilome: prophages, transposons (139, 47.28%), followed by translation, ribosomal structure and biogenesis (21, 7.14%), general function prediction only (18, 6.12%), and signal transduction mechanisms (18, 6.12%). Among the 25 categories in COG functional annotation, no unigenes were classified in RNA processing and modification, chromatin structure and dynamics, nuclear structure, cell motility, cytoskeleton, and extracellular structures (Figure 1A; Supplementary Table 2).

Among the GO functional annotation, the 3,729 unigenes were classified into 3 cellular components, 11 molecular functions, and 22 biological processes. The predominant category was cellular anatomical entity (1,749, 46.90%) in cellular component, binding (2,287, 61.33%) in molecular functions, and cellular process (2,172, 58.25%) in biological process. Of note, in the category biological process, there were 13 unigenes (0.35%) annotated in detoxification, 93 unigenes (2.49%) annotated in immune system process, and 593 unigenes (15.90%) annotated in response to stimulus (Figure 1B; Supplementary Table 2).

The KEGG pathway analysis revealed that 3,699 unigenes were categorized into 184 KEGG pathways, and the three predominant enriched categories were herpes simplex virus 1 infection (701, 18.95%), calcium signaling pathway (110, 2.97%), and protein processing in endoplasmic reticulum (105, 2.84%; Supplementary Table 2).

1 genoscope.cns.fr/trout/data/

TABLE 1 Summary of the quality analysis of RNA-seq data.

Sample name	Raw reads	Clean reads	Ratio of clean reads (%)	%≥Q20	%≥Q30	Mapped reads	Mapped rate (%)
Mock01	63,513,756	60,573,286	95.37	99.18	92.77	53,658,025	88.58
Mock02	65,146,218	61,991,656	95.16	99.06	92.23	54,945,172	88.63
Mock03	66,133,174	63,045,716	95.33	99.17	93.46	56,146,882	89.06
J24h01	66,352,932	61,787,254	93.12	99.45	93.86	57,719,634	93.42
J24h02	66,846,372	62,891,688	94.08	99.30	93.76	58,844,980	93.57
J24h03	64,442,328	61,562,360	95.53	99.45	93.87	57,690,477	93.71
U24h01	66,821,192	63,305,380	94.74	99.28	93.62	56,760,424	89.66
U24h02	66,062,330	62,792,522	95.05	99.25	93.52	56,232,737	89.56
U24h03	66,244,510	61,773,066	93.25	99.01	93.28	55,215,857	89.39

3.3. Identification of differentially expressed genes (DEGs) between the mock versus J and mock versus U groups

3.3.1. DEG analysis in the mock versus J group

DEG analysis revealed 8,296 DEGs in the Mock vs. J-IHNV infected group, including 4,058 up-regulated genes and 4,238 down-regulated genes (Figure 2A; Supplementary Table 3). Among the 8,296 DEGs, 1,056 new genes were discovered (Supplementary Table 3). Hierarchical clustering analysis showed that J-IHNV infection significantly changed the host gene expression levels compared with the Mock-infected group (Figure 2B). GO enrichment analysis revealed that 6,253 DEGs were annotated, and the top five enriched categories were binding (3,817, 61.04%), cellular process (3,062, 48.97%), cell (2,657, 42.49%), cell part (2,651, 42.40%), and single-organism process (2,466, 39.44%; Figure 2C; Supplementary Table 3). To better understand the effects of J-IHNV infection on pathway changes, KEGG analysis was performed and 6,000 DEGs were annotated into 248 pathways (Supplementary Table 3). The top 20 significantly enriched pathways included herpes simplex virus 1 infection, DNA replication, p53 signaling pathway, NOD-like receptor signaling pathway, and ubiquitin mediated proteolysis (Figure 2D; Supplementary Table 3).

3.3.2. DEG analysis in the mock versus U group

DEG analysis revealed 5,000 DEGs in the Mock vs. U-IHNV infected group, including 2,725 up-regulated genes and 2,275 down-regulated genes (Figure 3A; Supplementary Table 4). Among the 5,000 DEGs, 653 new genes were discovered (Supplementary Table 4). Hierarchical clustering analysis showed that U-IHNV infection significantly changed the host gene expression level compared with the Mock-infected group (Figure 3B). GO enrichment analysis showed that 3,808 DEGs were annotated and the top five enriched categories were the same as for the J-IHNV infection group (Figure 3C; Supplementary Table 4). KEGG analysis was performed and 3,627 DEGs were annotated into 229 pathways (Supplementary Table 4). The top 20 significantly enriched pathways included DNA replication, cell cycle, NOD-like receptor signaling pathway, mismatch repair, and hepatitis C (Figure 3D; Supplementary Table 4).

3.4. DEG analysis in the U versus J group

DEG analysis revealed 2,238 DEGs in the U vs. J IHNV infected group, including 1,227 up-regulated genes and 1,011 down-regulated genes (Figure 4A; Supplementary Table 5). Among the 2,238 DEGs, 345 new genes were discovered (Supplementary Table 5). Hierarchical clustering analysis showed that host gene expression levels were significantly changed between the U-and J-IHNV infection groups (Figure 4B). GO enrichment analysis revealed that 1,549 DEGs were annotated and the top five enriched categories were binding, cellular process, biological regulation, cell, and cell part (Figure 4C; Supplementary Table 5). KEGG analysis was performed and 1,525 DEGs were annotated into 187 pathways (Supplementary Table 5). The top 20 significantly enriched pathways included lysine degradation, herpes simplex virus 1 infection, relaxin signaling pathway, primary bile acid biosynthesis, platelet activation, and TGF-beta signaling pathway (Figure 4D; Supplementary Table 5).

3.4.1. Analysis of DEGs related to immune responses

The results showed that DEGs between U-and J-IHNV mapped to 187 KEGG pathways, and 15 of these pathways were significantly enriched ($p < 0.05$; Supplementary Table 5). Of particular interest, the DEGs between the U-and J-IHNV infection groups were enriched in immune-related pathways, such as the C-type lectin receptor signaling pathway, NOD-like receptor signaling pathway, RIG-I-like receptor signaling pathway, and Toll-like receptor signaling pathway (Supplementary Table 5). To further understand the DEGs between the U and J-IHNV infection groups, the top 30 DEGs related to immune responses were screened from the 187 KEGG pathways (Figure 5A). The

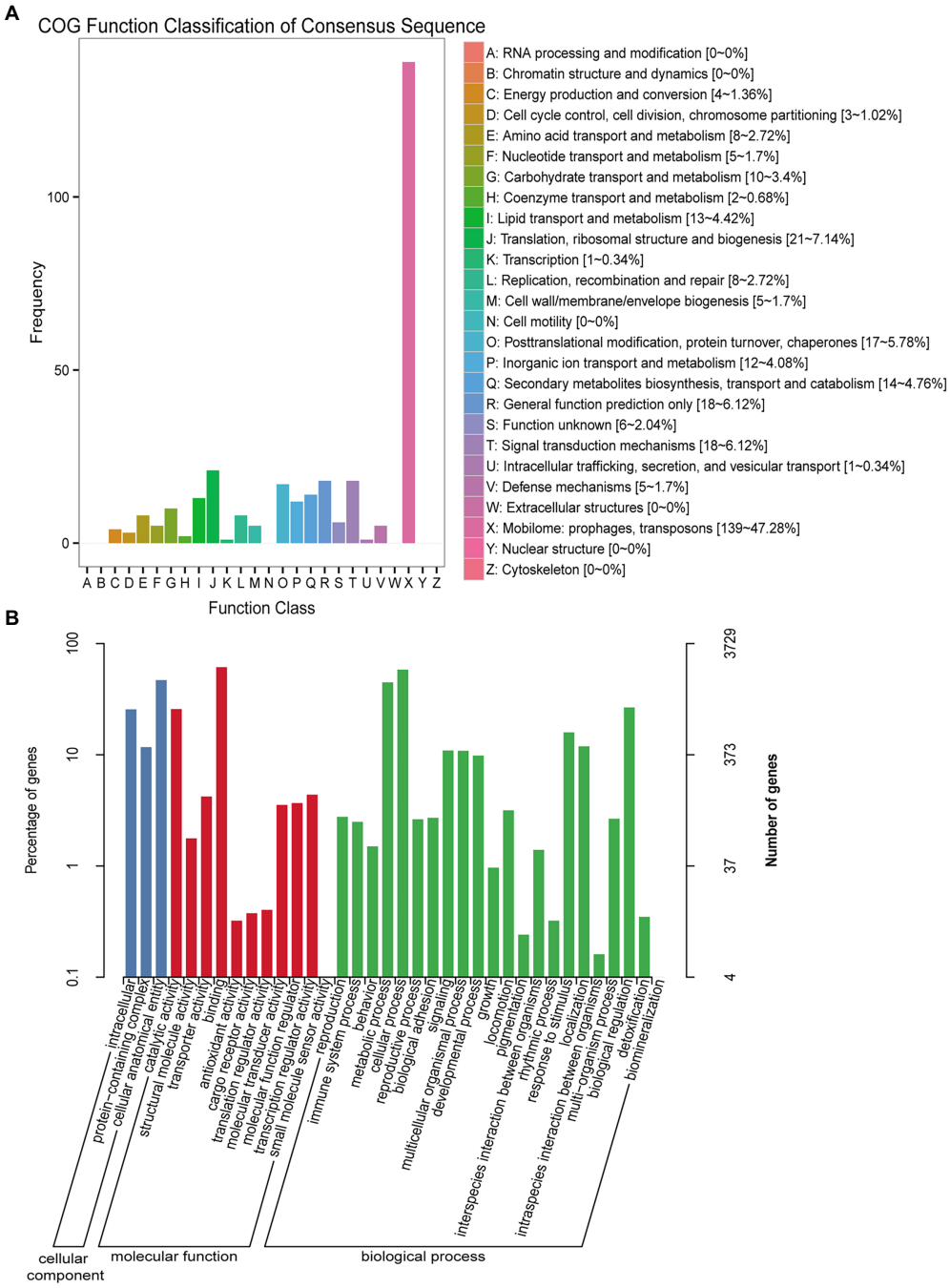

FIGURE 1
COG and GO function classification of unigenes from U-and J-IHNV-infected cells. **(A)** COG function classification of unigenes. **(B)** GO function classification of unigenes.

results showed that J-IHNV infection increased the expression of the transient receptor potential cation channel, subfamily M, member 2 (TRPM2) by 1.46-fold, stimulator of interferon genes protein-like (STING, LOC110487764) by 1.45-fold, integrin beta-7 (ITGB7, LOC110528101) by 1.20-fold, SLIT and NTRK-like protein 4 (SLITRK4, LOC110488543) by 1.12-fold, and anthrax toxin receptor 1 (ANTXR1, LOC110537215) by 1.11-fold compared with expression levels following U-IHNV infection. By contrast, the expression levels of anthrax toxin receptor 2 (ANTXR2, LOC110536457), arrestin domain-containing protein 2 (ARRDC2, LOC110492040), receptor-interacting serine/threonine-protein kinase 2 (RIPK2, LOC110526239), thioredoxin-interacting protein (TXNIP, LOC110496349), and interferon regulatory factor 1 (IRF1, LOC110533376) in the J-IHNV

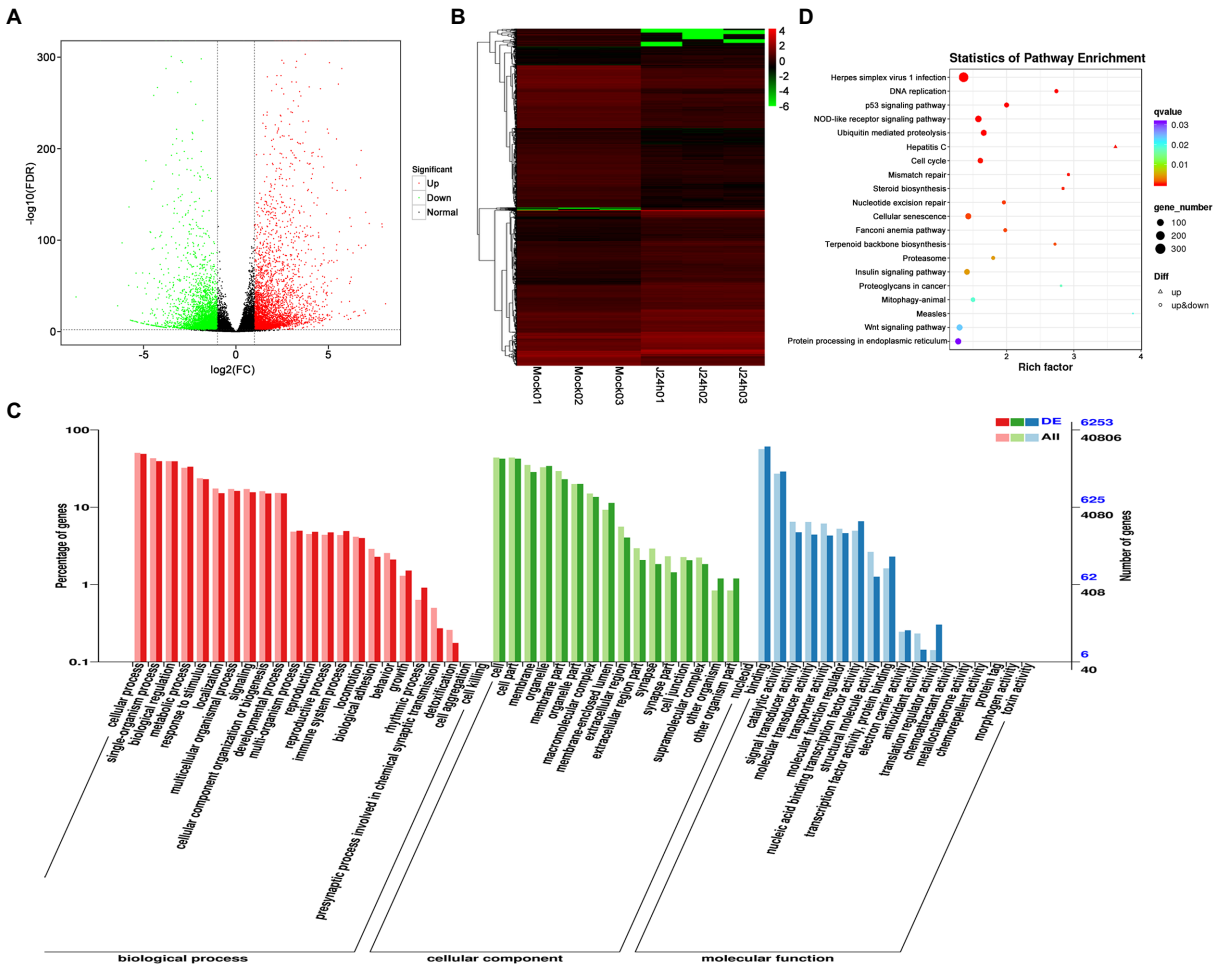

FIGURE 2
Comparison and enrichment analysis of DEGs in the Mock versus J-IHNV infection groups. **(A)** Volcano plot of DEGs. **(B)** Hierarchical clustering analysis of DEGs. **(C)** GO enrichment of DEGs. **(D)** KEGG enrichment analysis of DEGs.

infection group were decreased by 2.42-fold, 2.17-fold, 2.17-fold, 2.12-fold, and 1.86-fold, respectively, compared with the U-IHNV infection group (the fold change was represented as $\log_2^{FC}$; Supplementary Table 6).

3.4.2. Analysis of DEGs related to cellular signal transduction

The DEGs between the U and J IHNV infection groups were also enriched in signal transduction related pathways, such as the MAPK signaling pathway, Wnt signaling pathway, calcium signaling pathway, neuroactive ligand-receptor interaction pathway, and apelin signaling pathway (Supplementary Table 5). The top 40 DEGs related to signal transduction were screened to further understand the differences in signal transduction between the U and J IHNV infection groups (Figure 5B). The results showed that J-IHNV infection increased the expression of casein kinase I (CK1, LOC110502882) by 1.90-fold, insulin receptor-like (IRL, LOC110509203) by 1.84-fold, calcium channel voltage-dependent beta 2a (CACNB2, LOC110489951) by 1.74-fold, bone morphogenetic protein 2-like (BMP2L, LOC110491444) by 1.60-fold, and E3 ubiquitin-protein ligase RNF152 (RNF152, LOC110535571) by 1.56-fold compared with the expression levels following U-IHNV infection. By contrast, the expression levels of dual specificity protein phosphatase 4 (DUSP4, LOC110523806), transcription factor 7-like 1-A (TCF7L1A, LOC110526333), growth arrest and DNA damage-inducible protein GADD45 alpha (Gadd45α, LOC110530106), serine/threonine-protein kinase PLK2 (PLK2), and cellular communication network factor 2a (CCN2, LOC110522165) in the J-IHNV infection group were decreased by 2.31-fold, 1.86-fold, 1.85-fold, 1.81-fold, and 1.66-fold, respectively, compared with the U-IHNV infection group (the fold change was represented as $\log_2^{FC}$; Supplementary Table 6).

3.4.3. Analysis of DEGs related to viral diseases

The DEGs between the U and J IHNV infection groups were also enriched in viral disease-related genes, such as herpes simplex virus 1 infection, salmonella infection, and endocrine and metabolic disease (Supplementary Table 5). The top 30 DEGs

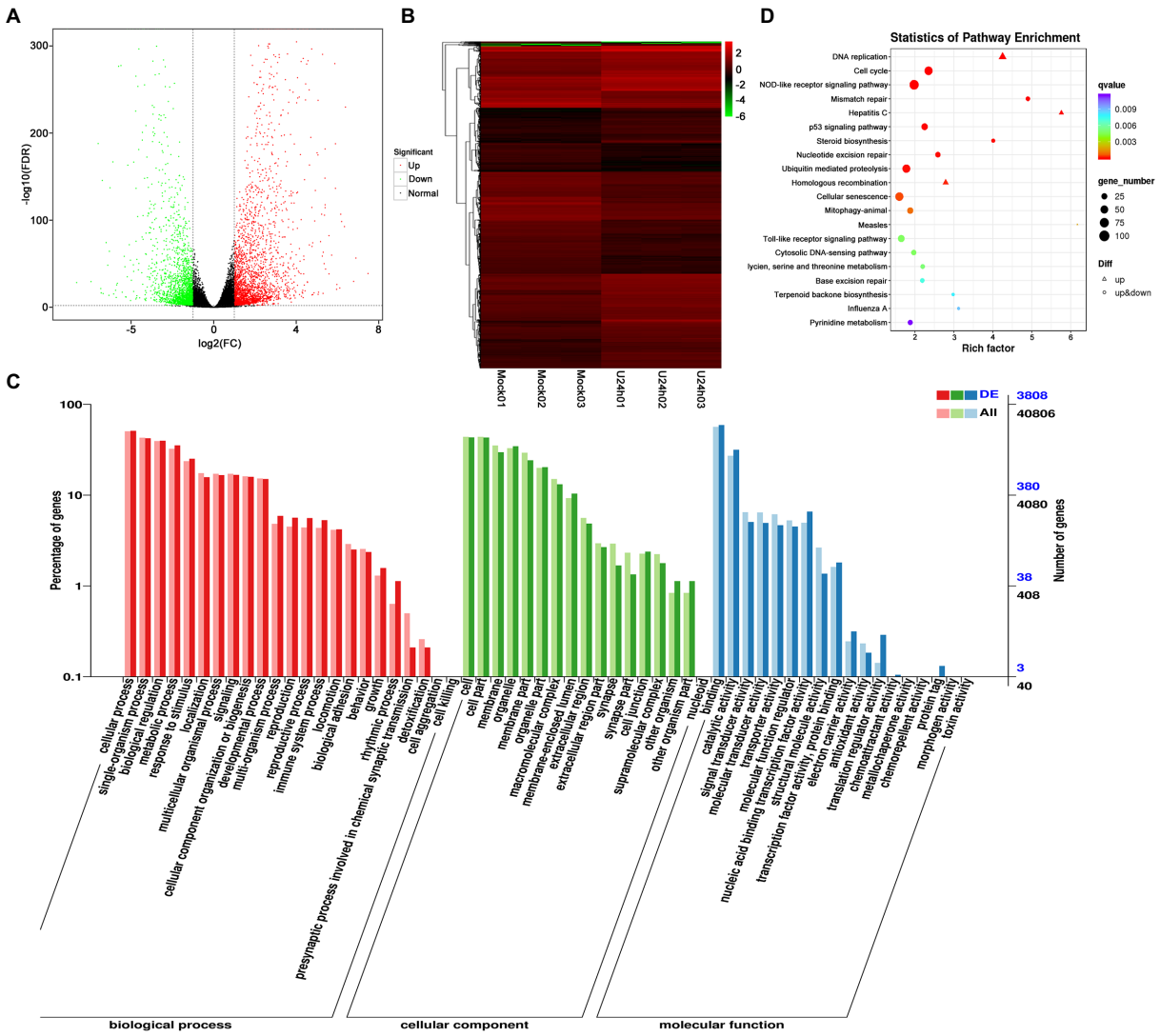

FIGURE 3
Comparison and enrichment analysis of DEGs in the Mock versus U-IHNV infection groups. **(A)** Volcano plot of DEGs. **(B)** Hierarchical clustering analysis of DEGs. **(C)** GO enrichment of DEGs. **(D)** KEGG enrichment analysis of DEGs.

related to disease were screened and analyzed (Figure 5C). The results showed that J-IHNV infection increased the expression of pleckstrin homology domain-containing family A member 6 (PLEKHA6) by 1.53-fold, tumor necrosis factor receptor superfamily member 14-like (TNFRSF14L, LOC110532771) by 1.19-fold, myeloid leukemia factor 1 (MLF1, LOC110507358) by 1.50-fold, myomesin-3-like (MYOM3L, LOC110534928) by 1.15-fold, and serine/threonine-protein kinase mTOR (LOC110491874) by 1.31-fold compared with the expression levels following U-IHNV infection. By contrast, the expression levels of CDC42 effector protein (Rho GTPase binding) 4b (CDC42EP4b, LOC110499240), armadillo repeat-containing protein 5 (ARMC5, LOC110538625), protein S100-A1 (S100-A1, LOC110520887), phosphatidylinositol 3-kinase regulatory subunit alpha (PIK3R1, LOC110526129), and transcriptional regulator Myc-like (c-Myc, LOC110535641) in the J-IHNV infection group were decreased by 1.32-fold, 2.14-fold, 1.89-fold, 1.33-fold, and 1.51-fold, compared with the U-IHNV infection group (the fold change was represented as $\log_2^{FC}$; Supplementary Table 6).

3.5. DEG validation by RT-qPCR

To validate the results of RNA-seq analysis, some of the DEGs between the U and J IHNV infection groups related to the immune response, signal transduction, and disease were analyzed by RT-qPCR. The results showed that immune response related genes *trpm2*, *sting*, and *itgb7*, signal transduction-related genes *irl*, *cacnb2*, and *bmp2l*, and disease-related genes *mlf1* and *mtor* were all up regulated, and immune response-related genes *ripk2* and

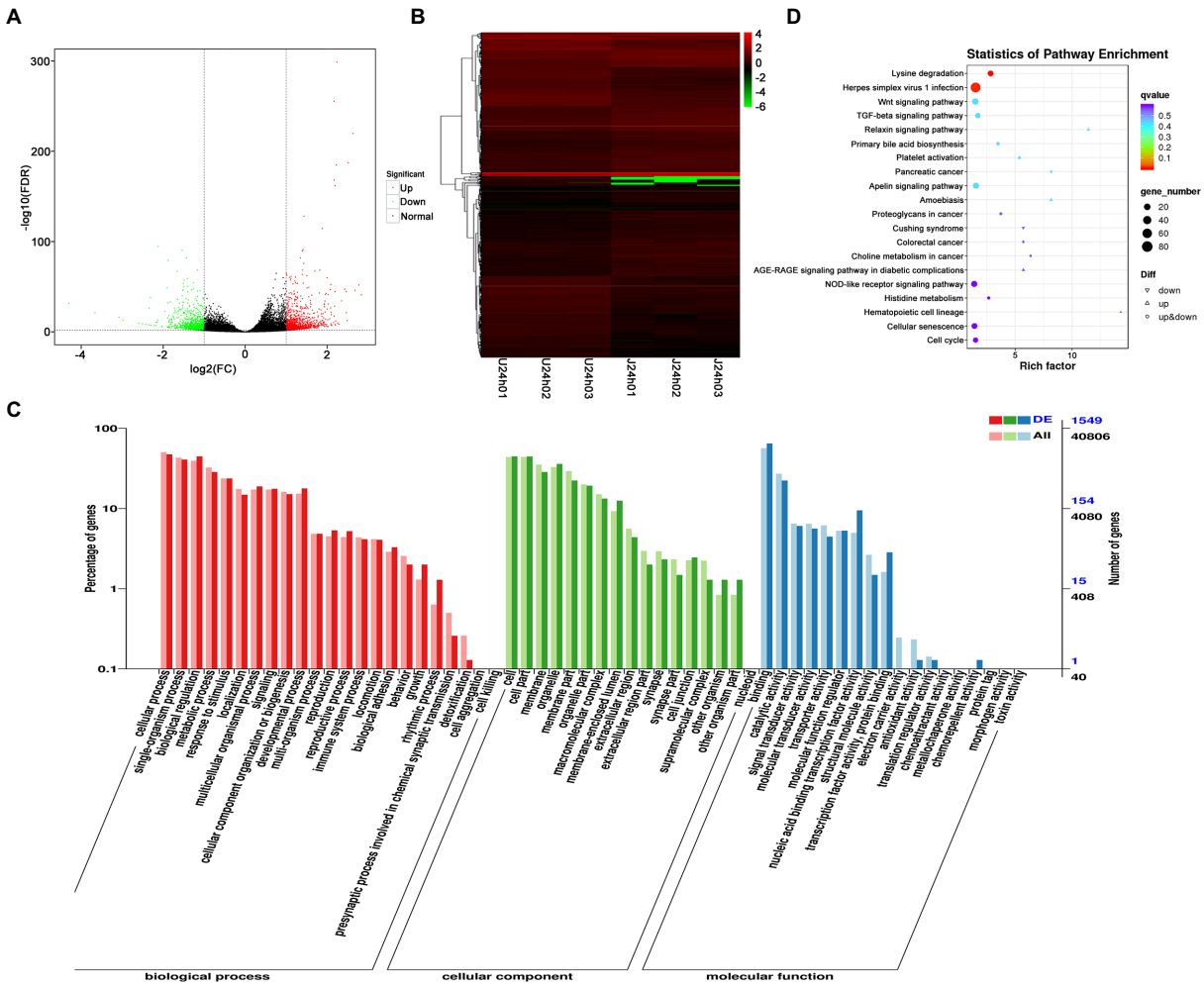

FIGURE 4
Comparison and enrichment analysis of DEGs in the U versus J-IHNV infection groups. **(A)** Volcano plot of DEGs. **(B)** Hierarchical clustering analysis of DEGs. **(C)** GO enrichment of DEGs. **(D)** KEGG enrichment analysis of DEGs.

irf1, signal transduction-related genes *gadd45α* and *plk2*, and disease-related genes *armc5*, *pik3r1* and *c-myc* were all down regulated in the J-IHNV group compared with the U-IHNV group (Figure 6). The fold-changes in DEGs determined by RT-qPCR were consistent with the changes derived from RNA-seq analysis, confirming the reliability of the RNA-seq data.

4. Discussion

Rainbow trout is an important cultured fish worldwide that significantly contributes to the economy of the fishery industry, but viral disease outbreaks severely reduce fish production. One of the most severe viral diseases of rainbow trout is caused by IHNV, which can result in a mortality rate of more than 90% (Zhao et al., 2019). Phylogenetic analyses classified IHNV strains, which have been isolated worldwide, into five major genogroups (Xu et al., 2019). IHNV isolates from China belong to the J genogroup, which has evolved from the U genogroup (Garver et al., 2006). The J genogroup virus is highly virulent in rainbow trout, whereas the U genogroup virus is lentogenic. Although some articles have investigated the pathogenicity of J and U genogroup IHNV, the molecular mechanisms that underlie the pathogenic differences remain poorly understood. To study the pathogenic mechanisms of these two viruses in detail, we conducted genome wide transcriptomic analysis at high resolution to assess viral-caused changes in immune responses, cellular signal transduction, and viral disease-related genes.

Host immune responses provide a critical biological barrier to protect the host against pathogen invasion, and many immune mechanisms are conserved among vertebrates. Given the crucial role of the immune response, immune system-related DEGs were further analyzed after U-and J-IHNV infection. The results showed that *trpm2*, *sting*, and *itgb7* in J-IHNV-infected cells were significantly up-regulated compared with U-IHNV-infected cells, and the *ripk2* and *irf1* genes were significantly down-regulated

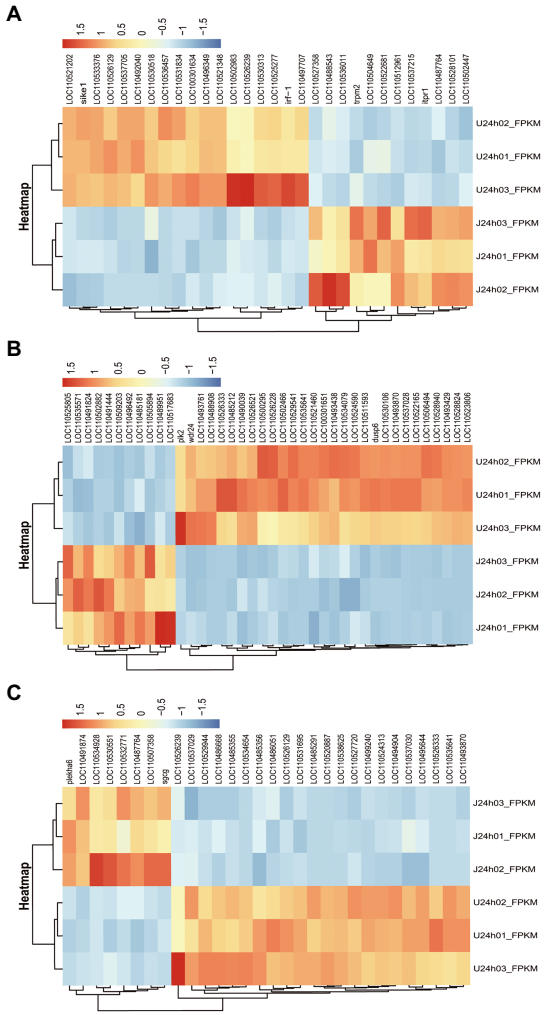

FIGURE 5
DEG analysis of the U versus J-IHNV infection groups for genes related to immune responses, cellular signal transduction, and viral diseases. **(A)** Top 30 DEGs related to immune responses. **(B)** Top 40 DEGs related to cellular signal transduction. **(C)** Top 30 DEGs related to viral diseases.

(Figure 6). TRPM2 is a reactive oxygen species-sensitive protein that is widely distributed and played an important role in the immune system (Xia et al., 2019). It was previously reported that HBV infection promotes TRPM2 expression to facilitate virus replication, while the inhibition of TRPM2 protects cells from H9N2 virus-induced damage (Wang et al., 2020; Chen et al., 2022). ITGB7 is a protein that associates with ITGA4 to form LPAM-1 dimer that functions as a T cell and B cell adhesion receptor and is important for intestinal immunity (Ballet et al., 2021). A study on Epstein–Barr virus (EBV) showed that virus infection induced the expression of ITGB7, which was beneficial for EBV infection (Delecluse et al., 2019). These results indicated that the TRPM2 and ITGB7 proteins may facilitate virus replication, and suggested that the induced high-level expression of TRPM2 and ITGB7 may facilitate higher replicative ability and pathogenicity of J-IHNV. STING is an important innate immune response protein that is reported to exert antiviral effects through numerous DNA and RNA-sensing pattern recognition receptors, and loss of STING caused a reduction in IFN production (Ma and Damania, 2016; Bao et al., 2021). STING mediated an IFN response to DNA virus and restricted RNA viruses (such as adenovirus, poxvirus, and vesicular stomatitis virus) by mediating translation inhibition (Lam and Falck-Pedersen, 2014; Franz et al., 2018; Georgana et al., 2018; Lee et al., 2019). Considering that J-IHNV is more virulent than U-IHNV, it may invoke a stronger immune response, including an increase in STING protein, to inhibit pathogen invasion. Although virus invasion results in an enhanced immune response, viruses have evolved in many ways to evade immunity, such as inhibiting the expression levels of some immune-related genes. RIPK2, also known as RIP2, is a protein used by NOD1 and NOD2 to direct the innate immune response against viral and bacterial infections (Hofmann et al., 2021). Research on influenza A virus showed that knockout of RIPK2 caused increased mortality after virus infection and indicated that RIPK2 protects the host against severe influenza A virus infection (Lupfer et al., 2013). IRF1 is a member of the interferon regulatory factor family, which binds to and activates

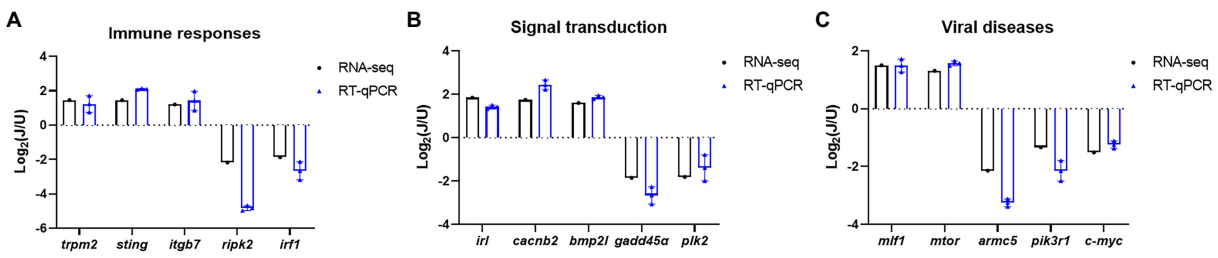

FIGURE 6
Validation of selected DEGs related to immune responses, cellular signal transduction, and viral diseases. **(A)** DEG expression levels for genes related to immune responses. **(B)** DEG expression levels for genes related to cellular signal transduction. **(C)** DEG expression levels for genes related to viral diseases.

type I interferon gene promoters (Feng et al., 2021). In recent years, IRF1 has been shown to mediate inducible and constitutive host defenses against virus infection, such as Sendai virus (Motz et al., 2013), dengue virus (Odendall et al., 2014), and hepatitis A virus (Yamane et al., 2019). In this study, we found that the expression levels of *ripk2* and *irf1* were downregulated in J-IHNV infection group, indicating that this virus has a stronger inhibitory effect on the immune system than U-IHNV.

Cells respond to a variety of extracellular changes by activating intracellular signal transduction pathways (Ludwig et al., 2021). Viruses are regarded as the extracellular stimuli that can lead to activated signal transduction. The successful activation of signal transduction facilitates various cellular responses against infection and is an important part of the host antiviral response. However, viruses have evolved many mechanisms to misuse or suppress antiviral signal transduction to promote their own replication. Therefore, we analyzed the signal transduction pathway-related DEGs after U and J genogroup IHNV infection. The results showed that the *ck1* and *RNF152* genes were significantly upregulated in J genogroup IHNV-infected cells compared with U IHNV-infected cells and the *dusp4*, *gadd45α*, *plk2*, and *ccn2* genes were significantly down-regulated (Figure 6). The CK1 family is a Ser/Thr protein kinase family reported to serve as regulators in the signal transduction of eukaryotic cells, as well as playing a role in many biological processes, such as regulating the Wnt signal, nucleus-cytoplasm shuttling of transcriptional factors, and DNA repair (Wang et al., 2014). During influenza A virus infection, viral HA protein induced IFN receptor degradation *via* CK1 to promote virus replication (Xia et al., 2018). CK1 regulated barley yellow striate mosaic virus-induced liquid–liquid phase separation and inhibited virus replication (Fang et al., 2022). These findings indicated that CK1 plays different roles in virus infection, and its role may vary from virus to virus. Although *ck1* gene expression in J-IHNV-infected cells was significantly upregulated compared with U-IHNV-infected cells, the exact role of *ck1* during IHNV infection remains to be clarified. RNF152 was reported as a positive regulator of TLR/IL-1R-mediated signaling and potentiates LPS-and IL-1β-induced activation of NF-κB in a ubiquitination-independent manner (Xiong et al., 2020). DUSPs are negative regulators of MAPK signal pathways, and DUSP1 and DUSP4 are believed to have similar specificities for the dephosphorylation of protein (Lin et al., 2020). Research showed that EBV infection significantly down-regulated DUSPs, including DUSP1 and DUSP4 (Lin et al., 2020). DUSP1 silencing increased the IFN antiviral effect against hepatitis C virus (HCV) by increasing the phosphorylation and nuclear translocation of STAT1 (Choi et al., 2015). Gadd45 proteins function as stress sensors in response to various environmental and physiological stressors, including bacterial and viral infection (Schmitz, 2013). HCV infections inhibited the mRNA transcription and protein expression levels of Gadd45 (Chen et al., 2016). PLK2 was a cell cycle regulator and also an apoptotic effector (Liu et al., 2015). Avian metapneumovirus subtype C (aMPV/C) infection significantly upregulated PLK2 expression and contributed to p53-mediated apoptosis to promote virus replication in Vero cells (Quan et al., 2020). However, in some cases, the inhibition of apoptosis may increase the viral titer by increasing the survival of infected cells. CCN2 is a matrix protein that can enhance immune cell migration and proinflammatory cytokine production to facilitate inflammatory responses (Kubota and Takigawa, 2015). Porcine reproductive and respiratory syndrome virus (PRRSV) infection inhibited the mRNA transcription of CCN2 to facilitate virus replication (Park and Chun, 2020). Collectively, compared with U-IHNV, J-IHNV infection caused down-regulation of the *dusp4*, *gadd45α*, *plk2*, and *ccn2* genes in a similar manner to EBV, HCV, aMPV/C, and PRRSV, suggesting that these genes may perform the same role during different virus infections, but the exact role within IHNV remains to be clarified.

In certain cases, virus infection can result in cancer, immune deficiency, drug resistance, endocrine and metabolic disorder, or even death. IHNV infection causes clinical signs in fish that include a darkened body, pale gills, exophthalmos, and hematopoietic tissue necrosis (Enzmann et al., 2010). To better understand the difference between J-IHNV and U-IHNV, the disease-related DEGs were analyzed. We found that in J-IHNV infection, the *tnfrsf14* and *mlf1* genes were significantly up-regulated compared with U-IHNV infection (Figure 6). TNFRSF14 is a cell surface molecule belonging to the TNF receptor superfamily that functions as an activator of cell survival genes *via* NF-kB transcription factors (Ware and Sedy, 2011). In recent years, TNFRSF14 was recognized as an alternative entry receptor for herpes simplex virus, and high protein levels facilitated viral replication (Taylor et al., 2007). MLF1 was first identified from a chromosomal rearrangement that caused acute myeloid leukemia and myelodysplastic syndrome, and functioned in the regulation of primitive hematopoietic cell development (Matsumoto et al., 2000). Based on the function of the TNFRSF14 and MLF1 proteins, we supposed that J-IHNV may induced higher protein levels to ensure the survival of the infected host to achieve increased viral titers, but the exact role of TNFRSF14 and MLF1 still needed to be clarified. However, research showed that MLF1 plays an antiviral role in white spot syndrome virus infection (Feng et al., 2017), so the role of MLF1 in IHNV infection requires in-depth analysis. ARMC5 is a cytosolic protein that was first identified as a tumor suppressor protein in 2013 (Assie et al., 2013), and knockout of the *armc5* gene in mice led to compromised T cell differentiation and proliferation that resulted in a compromised T cell immune response (Hu et al., 2017). PIK3R1 was also downregulated in nervous necrosis virus-infected sea bream larvae (Peruzza et al., 2021). During J-IHNV infection, the *armc5* and *pik3r1* genes were down-regulated compared with U-IHNV infection, and this may suggest that the virulent virus has a stronger inhibitory effect on these genes.

5. Conclusion

In this study, a transcriptional analysis of U and J genogroup IHNV-infected RTG-2 cells was performed to explore the molecular mechanisms responsible for the pathogenic differences between U and J IHNV infection. The DEGs induced by IHNV infection were identified and analyzed, and were related to the immune response, signal transduction, and diseases. This report not only provides a comprehensive transcriptional analysis, but also identifies possible mechanisms associated with the differential virulence of U and J genogroup IHNV. Our findings may shed new light on strategies for the prevention of IHNV.

Data availability statement

The datasets presented in this study can be found in online repositories. The names of the repository/repositories and accession number(s) can be found at: https://www.ncbi.nlm.nih.gov/, PRJNA895736.

Author contributions

J-ZZ: experiment design, data analysis, and manuscript writing. L-MX: English improvement. G-MR: data curation. Y-ZS: RT-qPCR validation. QL: statistical analysis. C-BT and T-YL: conceptualization, and review and editing. All authors contributed to the article and approved the submitted version.

Funding

This study was supported by the National Key Research and Development Program of China [2019YFE0115500], the Central Public-interest Scientific Institution Basal Research Fund, Chinese Academy of Fishery Sciences [HSY202204M and 2020TD43], the National Natural Science Foundation of China [32202988], and the Key Research and Development Program of Heilongjiang Province [JD22A017].

Conflict of interest

The authors declare that the research was conducted in the absence of any commercial or financial relationships that could be construed as a potential conflict of interest.

Publisher's note

All claims expressed in this article are solely those of the authors and do not necessarily represent those of their affiliated organizations, or those of the publisher, the editors and the reviewers. Any product that may be evaluated in this article, or claim that may be made by its manufacturer, is not guaranteed or endorsed by the publisher.

Supplementary material

The Supplementary material for this article can be found online at: https://www.frontiersin.org/articles/10.3389/fmicb.2022.1109606/full#supplementary-material

References

Assie, G., Libe, R., Espiard, S., Rizk-Rabin, M., Guimier, A., Luscap, W., et al. (2013). ARMC5 mutations in macronodular adrenal hyperplasia with Cushing's syndrome. *N. Engl. J. Med.* 369, 2105–2114. doi: 10.1056/NEJMoa1304603

Ballet, R., Brennan, M., Brandl, C., Feng, N., Berri, J., Cheng, J., et al. (2021). A CD22-Shp1 phosphatase axis controls integrin beta7 display and B cell function in mucosal immunity. *Nat. Immunol.* 22, 381–390. doi: 10.1038/s41590-021-00862-z

Bao, T., Liu, J., Leng, J., and Cai, L. (2021). The cGAS-STING pathway: more than fighting against viruses and cancer. *Cell Biosci.* 11:209. doi: 10.1186/s13578-021-00724-z

Black, A., Breyta, R., Bedford, T., and Kurath, G. (2016). Geography and host species shape the evolutionary dynamics of U genogroup infectious hematopoietic necrosis virus. *Virus Evol.* 2:vew034. doi: 10.1093/ve/vew034

Chen, W., Li, X. M., Li, A. L., Yang, G., and Hu, H. N. (2016). Hepatitis C virus increases free fatty acids absorption and promotes its replication via down-regulating GADD45α expression. *Med. Sci. Monit.* 22, 2347–2356. doi: 10.12659/msm.899591

Chen, L., Zhu, L., Lu, X., Ming, X., and Yang, B. (2022). TRPM2 regulates autophagy to participate in hepatitis B virus replication. *J. Viral Hepat.* 29, 627–636. doi: 10.1111/jvh.13710

Choi, J. E., Kwon, J. H., Kim, J. H., Hur, W., Sung, P. S., Choi, S. W., et al. (2015). Suppression of dual specificity phosphatase I expression inhibits hepatitis C virus replication. *PLoS One* 10:e0119172. doi: 10.1371/journal.pone.0119172

Cieslak, M., Wahli, T., Diserens, N., Haenen, O., and Schutze, H. (2017). Phylogeny of the infectious hematopoietic necrosis virus in European aquaculture. *PLoS One* 12:e0184490. doi: 10.1371/journal.pone.0184490

Delecluse, S., Tsai, M. H., Shumilov, A., Bencun, M., Arrow, S., Beshirova, A., et al. (2019). Epstein-Barr virus induces expression of the LPAM-1 integrin in B cells in vitro and in vivo. *J. Virol.* 93:e01618. doi: 10.1128/JVI.01618-18

Enzmann, P. J., Castric, J., Bovo, G., Thiery, R., Fichtner, D., Schutze, H., et al. (2010). Evolution of infectious hematopoietic necrosis virus (IHNV), a fish rhabdovirus, in Europe over 20 years: implications for control. *Dis. Aquat. Org.* 89, 9–15. doi: 10.3354/dao02182

Enzmann, P. J., Kurath, G., Fichtner, D., and Bergmann, S. M. (2005). Infectious hematopoietic necrosis virus: monophyletic origin of European isolates from north American genogroup M. *Dis. Aquat. Org.* 66, 187–195. doi: 10.3354/dao066187

Fang, X. D., Gao, Q., Zang, Y., Qiao, J. H., Gao, D. M., Xu, W. Y., et al. (2022). Host casein kinase 1-mediated phosphorylation modulates phase separation of a rhabdovirus phosphoprotein and virus infection. *elife* 11:e74884. doi: 10.7554/eLife.74884

Feng, X. W., Huo, L. J., Sun, J. J., Xu, J. D., Niu, G. J., Wang, J. X., et al. (2017). Myeloid leukemia factor functions in anti-WSSV immune reaction of kuruma shrimp, Marsupenaeus japonicus, Fish Shellfish. *Immunol.* 70, 416–425. doi: 10.1016/j.fsi.2017.09.028

Feng, H., Zhang, Y. B., Gui, J. F., Lemon, S. M., and Yamane, D. (2021). Interferon regulatory factor 1 (IRF1) and anti-pathogen innate immune responses. *PLoS Pathog.* 17:e1009220. doi: 10.1371/journal.ppat.1009220

Franz, K. M., Neidermyer, W. J., Tan, Y. J., Whelan, S., and Kagan, J. C. (2018). STING-dependent translation inhibition restricts RNA virus replication. *Proc. Natl. Acad. Sci. U. S. A.* 115, E2058–E2067. doi: 10.1073/pnas.1716937115

Garver, K. A., Batts, W. N., and Kurath, G. (2006). Virulence comparisons of infectious hematopoietic necrosis virus U and M genogroups in sockeye salmon and rainbow trout. *J. Aquat. Anim. Health* 18, 232–243. doi: 10.1577/H05-038.1

Georgana, I., Sumner, R. P., Towers, G. J., and Maluquer, D. M. C. (2018). Virulent poxviruses inhibit DNA sensing by preventing STING activation. *J. Virol.* 92, e02145–e02117. doi: 10.1128/JVI.02145-17

Hofmann, S. R., Girschick, L., Stein, R., and Schulze, F. (2021). Immune modulating effects of receptor interacting protein 2 (RIP2) in autoinflammation and immunity. *Clin. Immunol.* 223:108648. doi: 10.1016/j.clim.2020.108648

Hu, Y., Lao, L., Mao, J., Jin, W., Luo, H., Charpentier, T., et al. (2017). Armc5 deletion causes developmental defects and compromises T-cell immune responses. *Nat. Commun.* 8:13834. doi: 10.1038/ncomms13834

Ji, F., Zhao, J. Z., Liu, M., Lu, T. Y., Liu, H. B., Yin, J., et al. (2017). Complete genomic sequence of an infectious pancreatic necrosis virus isolated from rainbow trout (Oncorhynchus mykiss) in China. *Virus Genes* 53, 215–225. doi: 10.1007/s11262-016-1408-9

Kim, D., Langmead, B., and Salzberg, S. L. (2015). HISAT: a fast spliced aligner with low memory requirements. *Nat. Methods* 12, 357–360. doi: 10.1038/nmeth.3317

Kimura, T., and Yoshimizu, M. (1991). Viral diseases of fish in Japan. *Annu. Rev. Fish Dis.* 1, 67–82. doi: 10.1016/0959-8030(91)90023-D

Kubota, S., and Takigawa, M. (2015). Cellular and molecular actions of CCN2/CTGF and its role under physiological and pathological conditions. *Clin. Sci. (Lond.)* 128, 181–196. doi: 10.1042/CS20140264

Kurath, G., Garver, K. A., Troyer, R. M., Emmenegger, E. J., Einer-Jensen, K., and Anderson, E. D. (2003). Phylogeography of infectious haematopoietic necrosis virus in North America. *J. Gen. Virol.* 84, 803–814. doi: 10.1099/vir.0.18771-0

Lam, E., and Falck-Pedersen, E. (2014). Unabated adenovirus replication following activation of the cGAS/STING-dependent antiviral response in human cells. *J. Virol.* 88, 14426–14439. doi: 10.1128/JVI.02608-14

Lee, J., Ghonime, M. G., Wang, R., and Cassady, K. A. (2019). The antiviral apparatus: STING and oncolytic virus restriction. *Mol. Ther. Oncolytics* 13, 7–13. doi: 10.1016/j.omto.2019.02.002

Lin, K. M., Lin, S. J., Lin, J. H., Lin, P. Y., Teng, P. L., Wu, H. E., et al. (2020). Dysregulation of dual-specificity phosphatases by Epstein-Barr virus LMP1 and its impact on lymphoblastoid cell line survival. *J. Virol.* 94, e01837–e01819. doi: 10.1128/JVI.01837-19

Liu, L. Y., Wang, W., Zhao, L. Y., Guo, B., Yang, J., Zhao, X. G., et al. (2015). Silencing of polo-like kinase 2 increases cell proliferation and decreases apoptosis in SGC-7901 gastric cancer cells. *Mol. Med. Rep.* 11, 3033–3038. doi: 10.3892/mmr.2014.3077

Ludwig, S., Hrincius, E. R., and Boergeling, Y. (2021). The two sides of the same coin-influenza virus and intracellular signal transduction. *Cold Spring Harb. Perspect. Med.* 11:a038513. doi: 10.1101/cshperspect.a038513

Lupfer, C., Thomas, P. G., Anand, P. K., Vogel, P., Milasta, S., Martinez, J., et al. (2013). Receptor interacting protein kinase 2-mediated mitophagy regulates inflammasome activation during virus infection. *Nat. Immunol.* 14, 480–488. doi: 10.1038/ni.2563

Ma, Z., and Damania, B. (2016). The cGAS-STING defense pathway and its counteraction by viruses. *Cell Host Microbe* 19, 150–158. doi: 10.1016/j.chom.2016.01.010

MacWilliams, C., Johnson, G., Groman, D., and Kibenge, F. S. (2007). Morphologic description of infectious salmon anaemia virus (ISAV)-induced lesions in rainbow trout Oncorhynchus mykiss compared to Atlantic salmon Salmo salar. *Dis. Aquat. Org.* 78, 1–12. doi: 10.3354/dao01866

Matsumoto, N., Yoneda-Kato, N., Iguchi, T., Kishimoto, Y., Kyo, T., Sawada, H., et al. (2000). Elevated MLF1 expression correlates with malignant progression from myelodysplastic syndrome. *Leukemia* 14, 1757–1765. doi: 10.1038/sj.leu.2401897

Motz, C., Schuhmann, K. M., Kirchhofer, A., Moldt, M., Witte, G., Conzelmann, K. K., et al. (2013). Paramyxovirus V proteins disrupt the fold of the RNA sensor MDA5 to inhibit antiviral signaling. *Science* 339, 690–693. doi: 10.1126/science.1230949

Nishizawa, T., Kinoshita, S., Kim, W. S., Higashi, S., and Yoshimizu, M. (2006). Nucleotide diversity of Japanese isolates of infectious hematopoietic necrosis virus (IHNV) based on the glycoprotein gene. *Dis. Aquat. Org.* 71, 267–272. doi: 10.3354/dao071267

Niu, L., and Zhao, Z. (1988). The epidemiology of IHN and IPN of rainbow trout in Northeast China. *J. Fish. China* 12, 327–332.

Odendall, C., Dixit, E., Stavru, F., Bierne, H., Franz, K. M., Durbin, A. F., et al. (2014). Diverse intracellular pathogens activate type III interferon expression from peroxisomes. *Nat. Immunol.* 15, 717–726. doi: 10.1038/ni.2915

Park, I. B., and Chun, T. (2020). Porcine reproductive and respiratory syndrome virus (PRRSV) non-structural protein (NSP)1 transcriptionally inhibits CCN1 and CCN2 expression by blocking ERK-AP-1 axis in pig macrophages in vitro. *Res. Vet. Sci.* 132, 462–465. doi: 10.1016/j.rvsc.2020.07.029

Park, J. W., Moon, C. H., Harmache, A., Wargo, A. R., Purcell, M. K., Bremont, M., et al. (2011). Restricted growth of U-type infectious haematopoietic necrosis virus (IHNV) in rainbow trout cells may be linked to casein kinase II activity. *J. Fish Dis.* 34, 115–129. doi: 10.1111/j.1365-2761.2010.01225.x

Pertea, M., Pertea, G. M., Antonescu, C. M., Chang, T. C., Mendell, J. T., and Salzberg, S. L. (2015). String tie enables improved reconstruction of a transcriptome from RNA-seq reads. *Nat. Biotechnol.* 33, 290–295. doi: 10.1038/nbt.3122

Peruzza, L., Pascoli, F., Dalla, R. G., Franch, R., Ferraresso, S., Babbucci, M., et al. (2021). Transcriptome analysis reveals a complex response to the RGNNV/SJNNV reassortant nervous necrosis virus strain in sea bream larvae. *Fish Shellfish Immunol.* 114, 282–292. doi: 10.1016/j.fsi.2021.04.021

Quan, R., Wei, L., Hou, L., Wang, J., Zhu, S., Li, Z., et al. (2020). Proteome analysis in a mammalian cell line reveals that PLK2 is involved in avian metapneumovirus type C (aMPV/C)-induced apoptosis. *Viruses* 12:375. doi: 10.3390/v12040375

Schmitz, I. (2013). Gadd 45 proteins in immunity. *Adv. Exp. Med. Biol.* 793, 51–68. doi: 10.1007/978-1-4614-8289-5_4

Taylor, J. M., Lin, E., Susmarski, N., Yoon, M., Zago, A., Ware, C. F., et al. (2007). Alternative entry receptors for herpes simplex virus and their roles in disease. *Cell Host Microbe* 2, 19–28. doi: 10.1016/j.chom.2007.06.005

Wang, Y., Hu, L., Tong, X., and Ye, X. (2014). Casein kinase 1gamma1 inhibits the RIG-I/TLR signaling pathway through phosphorylating p65 and promoting its degradation. *J. Immunol.* 192, 1855–1861. doi: 10.4049/jimmunol.1302552

Wang, S., Liang, T., Luo, Q., Li, P., Zhang, R., Xu, M., et al. (2020). H9N2 swine influenza virus infection-induced damage is mediated by TRPM2 channels in mouse pulmonary microvascular endothelial cells. *Microb. Pathog.* 148:104408. doi: 10.1016/j.micpath.2020.104408

Ware, C. F., and Sedy, J. R. (2011). TNF superfamily networks: bidirectional and interference pathways of the herpesvirus entry mediator (TNFSF14). *Curr. Opin. Immunol.* 23, 627–631. doi: 10.1016/j.coi.2011.08.008

Wargo, A. R., Scott, R. J., Kerr, B., and Kurath, G. (2017). Replication and shedding kinetics of infectious hematopoietic necrosis virus in juvenile rainbow trout. *Virus Res.* 227, 200–211. doi: 10.1016/j.virusres.2016.10.011

Xia, S., Wang, L., Fu, T. M., and Wu, H. (2019). Mechanism of TRPM2 channel gating revealed by cryo-EM. *FEBS J.* 286, 3333–3339. doi: 10.1111/febs.14939

Xia, C., Wolf, J. J., Vijayan, M., Studstill, C. J., Ma, W., and Hahm, B. (2018). Casein kinase 1α mediates the degradation of receptors for type I and type II interferons caused by hemagglutinin of influenza a virus. *J. Virol.* 92, e00006–e00018. doi: 10.1128/JVI.00006-18

Xiong, M. G., Xu, Z. S., Li, Y. H., Wang, S. Y., Wang, Y. Y., and Ran, Y. (2020). RNF152 positively regulates TLR/IL-1R signaling by enhancing MyD88 oligomerization. *EMBO Rep.* 21:e48860. doi: 10.15252/embr.201948860

Xu, L., Zhao, J., Liu, M., Kurath, G., Breyta, R. B., Ren, G., et al. (2019). Phylogeography and evolution of infectious hematopoietic necrosis virus in China. *Mol. Phylogenet. Evol.* 131, 19–28. doi: 10.1016/j.ympev.2018.10.030

Xu, L., Zhao, J., Liu, M., Kurath, G., Ren, G., Lapatra, S. E., et al. (2017). A effective DNA vaccine against diverse genotype J infectious hematopoietic necrosis virus strains prevalent in China. *Vaccine* 35, 2420–2426. doi: 10.1016/j.vaccine.2017.03.047

Yamane, D., Feng, H., Rivera-Serrano, E. E., Selitsky, S. R., Hirai-Yuki, A., Das, A., et al. (2019). Basal expression of interferon regulatory factor 1 drives intrinsic hepatocyte resistance to multiple RNA viruses. *Nat. Microbiol.* 4, 1096–1104. doi: 10.1038/s41564-019-0425-6

Zhao, J. Z., Xu, L. M., Liu, M., Cao, Y. S., LaPatra, S. E., Yin, J. S., et al. (2017). Preliminary study of an oral vaccine against infectious hematopoietic necrosis virus using improved yeast surface display technology. *Mol. Immunol.* 85, 196–204. doi: 10.1016/j.molimm.2017.03.001

Zhao, J. Z., Xu, L. M., Zhang, Z. Y., Liu, M., Cao, Y. S., Yin, J. S., et al. (2019). Recovery of recombinant infectious hematopoietic necrosis virus strain Sn1203 using the mammalian cell line BHK-21. *J. Virol. Methods* 265, 84–90. doi: 10.1016/j.jviromet.2019.01.002

frontiers | Frontiers in Microbiology

TYPE Original Research
PUBLISHED 26 January 2023
DOI 10.3389/fmicb.2022.1067235

OPEN ACCESS

EDITED BY
Zhenyu Zhang,
University of Wisconsin-Madison,
United States

REVIEWED BY
Miles D. Lange,
Aquatic Animal Health Research,
Agricultural Research Service (USDA),
United States
Ming-Chi Li,
National Cheng Kung University,
Taiwan

*CORRESPONDENCE
Andrew P. Desbois
✉ andrew.desbois@stir.ac.uk

†These authors have contributed equally to this work and share first authorship

SPECIALTY SECTION
This article was submitted to Infectious Agents and Disease, a section of the journal Frontiers in Microbiology

RECEIVED 12 October 2022
ACCEPTED 19 December 2022
PUBLISHED 26 January 2023

CITATION
Bartie KL, Ngô TPH, Bekaert M, Hoang Oanh DT, Hoare R, Adams A and Desbois AP (2023) *Aeromonas hydrophila* ST251 and *Aeromonas dhakensis* are major emerging pathogens of striped catfish in Vietnam. *Front. Microbiol.* 13:1067235. doi: 10.3389/fmicb.2022.1067235

Aeromonas hydrophila ST251 and *Aeromonas dhakensis* are major emerging pathogens of striped catfish in Vietnam

Kerry L. Bartie[1†], Thao P. H. Ngô[2†], Michaël Bekaert[1†], Dang Thi Hoang Oanh[3], Rowena Hoare[1], Alexandra Adams[1] and Andrew P. Desbois[1*]

[1]Institute of Aquaculture, Faculty of Natural Sciences, University of Stirling, Stirling, United Kingdom, [2]Aquacultural Biotechnology Division, Biotechnology Center of Ho Chi Minh City, Ho Chi Minh City, Vietnam, [3]Department of Aquatic Pathology, Can Tho University, Can Tho, Vietnam

Introduction: Aeromonads are ubiquitous in aquatic environments and several species are opportunistic pathogens of fish. Disease losses caused by motile *Aeromonas* species, particularly *Aeromonas hydrophila*, can be challenging in intensive aquaculture, such as at striped catfish (*Pangasianodon hypophthalmus*) farms in Vietnam. Outbreaks require antibiotic treatments, but their application is undesirable due to risks posed by resistance. Vaccines are an attractive prophylactic and they must protect against the prevalent strains responsible for ongoing outbreaks.

Methods: This present study aimed to characterize *A. hydrophila* strains associated with mortalities in striped catfish culture in the Mekong Delta by a polyphasic genotyping approach, with a view to developing more effective vaccines.

Results: During 2013–2019, 345 presumptive *Aeromonas* spp. isolates were collected at farms in eight provinces. Repetitive element sequence-based PCR, multi-locus sequence typing and whole-genome sequencing revealed most of the suspected 202 *A. hydrophila* isolates to belong to ST656 (n = 151), which corresponds to the closely-related species *Aeromonas dhakensis*, with a lesser proportion belonging to ST251 (n = 51), a hypervirulent lineage (vAh) of *A. hydrophila* already causing concern in global aquaculture. The *A. dhakensis* ST656 and vAh ST251 isolates from outbreaks possessed unique gene sets compared to published *A. dhakensis* and vAh ST251 genomes, including antibiotic-resistance genes. The sharing of resistance determinants to sulphonamides (*sul1*) and trimethoprim (*dfrA1*) suggests similar selection pressures acting on *A. dhakensis* ST656 and vAh ST251 lineages. The earliest isolate (a vAh ST251 from 2013) lacked most resistance genes, suggesting relatively recent acquisition and selection, and this underscores the need to reduce antibiotics use where possible to prolong their effectiveness. A novel PCR assay was designed and validated to distinguish *A. dhakensis* and vAh ST251 strains.

Discussion: This present study highlights for the first time *A. dhakensis*, a zoonotic species that can cause fatal human infection, to be an emerging pathogen in aquaculture in Vietnam, with widespread distribution in recent outbreaks of motile *Aeromonas* septicaemia in striped catfish. It also confirms

vAh ST251 to have been present in the Mekong Delta since at least 2013. Appropriate isolates of *A. dhakensis* and vAh should be included in vaccines to prevent outbreaks and reduce the threat posed by antibiotic resistance.

KEYWORDS

antibiotic resistance, antimicrobial resistance (AMR), aquaculture, comparative genomics, hypervirulent *Aeromonas hydrophila* (vAh), motile *Aeromonas* septicaemia, pangasius, *Pangasianodon hypophthalmus*

1. Introduction

Aeromonas spp. are ubiquitous members of autochthonous communities in aquatic environments, while some species are opportunistic pathogens of animals and humans (Janda and Abbott, 2010; Batra et al., 2016; Pessoa et al., 2019; Fernández-Bravo and Figueras, 2020) meaning they can present a One Health challenge (Lamy et al., 2021). Infections caused by *Aeromonas* spp. can be particularly challenging at aquaculture sites where aquatic animals are farmed intensively, as these provide ideal conditions for a disease outbreak. Vietnam is a major aquaculture producer with several species dominating output, including the striped catfish *Pangasianodon hypophthalmus* (Sauvage, 1878), which is exported around the world as pangasius (Phuong and Oanh, 2010). Striped catfish production is concentrated in the Mekong Delta region where these fish are cultured primarily in freshwater ponds and the sector provides significant support to the regional economy with exports worth >USD 1.7 bn, thereby securing livelihoods and employment (Phuong and Oanh, 2010; Nguyen and Jolly, 2020; Hasan and Shipton, 2021). However, bacterial disease outbreaks can disrupt production, with the most important pathogens being *Edwardsiella ictaluri*, which causes bacillary necrosis of pangasius (BNP), and motile species of *Aeromonas*, particularly *A. hydrophila*, which are responsible for motile *Aeromonas* septicaemia (MAS), also known as haemorrhagic or red spot disease (Phu et al., 2016; Hoa et al., 2021). In striped catfish, MAS manifests clinically with hemorrhage, abscess, ulcers, ascitic fluid, and anemia, and outbreaks result typically in high rates of mortality (Anyanwu et al., 2015; Phu et al., 2016).

An injectable vaccine is available commercially in Vietnam to protect against BNP and MAS, and it contains an inactivated isolate of *E. ictaluri* and two biotypes of *A. hydrophila* (ALPHA JECT® Panga 2, PHARMAQ; Tung et al., 2014); however, uptake by farmers is far from universal with cost cited as a barrier because specialized teams and equipment are needed to administer the vaccine (Adams, 2019; Kayansamruaj et al., 2020). Consequently, treatment with antibiotics is needed when outbreaks occur (Rico et al., 2013; Ström et al., 2019), but this is undesirable due to risks associated with the selection and enrichment of antibiotic-resistant strains in the environment and in people and animals exposed to these agents (Mo et al., 2015; Phu et al., 2016; Brunton et al., 2019; Hoa et al., 2021). Therefore, the implementation of preventative measures to counter infectious diseases, including easy to administer and less costly vaccines, is a priority, with oral and immersion-based vaccines showing promise and in advanced development (Mzula et al., 2019; Ngo et al., 2022). Nevertheless, to ensure greatest efficacy, it is critical that newly developed vaccines protect against the most prevalent disease-causing lineages in circulation, thus underlining a need for regular surveillance.

Due to long standing misidentification issues and the high heterogeneity present within the *Aeromonas* genus (Pessoa et al., 2019), the strains affecting striped catfish deserve special attention. Several approaches can be applied to differentiate strains of *Aeromonas*, although even speciation within this genus can be a challenge due to traditional phenotypic markers lacking sufficient discrimination (Pessoa et al., 2019; Fernández-Bravo and Figueras, 2020). Indeed, the molecular epidemiology of MAS outbreaks affecting striped catfish in the Mekong Delta is not well described, and many studies have relied solely on traditional biochemical tests to identify presumed *Aeromonas* spp. (Nguyen et al., 2014), with identification of *A. hydrophila* reliant on single genetic markers based on amplification of the aerolysin gene (Pollard et al., 1990; Hoa et al., 2021). More recently, genetic methods of characterisation for *Aeromonas* spp. based on housekeeping gene phylogeny and multi-locus sequence typing (MLST) have proven popular and these can provide more reliable species placement and strain resolution (Martino et al., 2011; Navarro and Martínez-Murcia, 2018). Still, instances of ambiguous species attribution have been documented based on MLST (de Melo et al., 2019), with whole genome sequencing (WGS) providing the most definitive differentiation of species and strains (Bayliss et al., 2017). Such genomic studies have revealed the presence of a hypervirulent lineage (vAh) of *A. hydrophila* [sequence type (ST) 251] that is prompting serious concern in global aquaculture due to its role in causing MAS outbreaks in farmed channel catfish and carp in the USA and China, respectively (Pang et al., 2015; Rasmussen-Ivey et al., 2016; Awan et al., 2018), whilst vAh ST251 isolates have been detected recently in two provinces farming striped catfish in Vietnam (Ngo et al., 2022). Application

of a comprehensive suite of strain typing methods to isolates associated with MAS outbreaks in Vietnam would allow for the identification of the predominant strains in circulation for inclusion into more effective vaccines, whilst providing insight into the most suitable methods for future surveillance to ensure their continued effectiveness.

Therefore, the aim of the present study was to characterize the circulating *A. hydrophila* strains associated with mortality losses in striped catfish culture in the Mekong Delta, Vietnam by a polyphasic genotyping approach, with a view to applying this knowledge to the development of new vaccines offering greater protection against this pathogen.

2. Materials and methods

2.1. Reference and type strains

Five *A. hydrophila* isolates of varied host origin were used for reference purposes and these isolates originated from Thailand (isolate F2D20 from *Rana rugulosa*), Bangladesh (isolate T4 from *Labeo rohita* and isolate B2/12 from an unknown host), India (isolate VDS from *Ictalurus punctatus*), and USA (isolate AL09-71 from *I. punctatus*). A further reference isolate, *Aeromonas veronii* biovar *sobria* LMG 13067 (originating from an unspecified frog host in the USA), and 12 type strains of *Aeromonas* spp. were also included (Supplementary Table 1).

2.2. Sampling sites and primary isolation of *Aeromonas* spp. field isolates

P. hypophthalmus exhibiting classical signs of MAS, including reddened fins and external and/or internal hemorrhage, were sampled from disease outbreaks in the Mekong Delta region (An Giang, Ben Tre, Can Tho, Dong Thap, Hậu Giang, Tien Giang, and Vinh Long provinces) and Dong Nai province during 2013–2019. For each sampling occasion, at least two representative field isolates were included that had been derived from separate farms located in the same geographic area. Additionally, nine farms from five regions were sampled more extensively between 2018 and 2019, where multiple fish, internal organs and isolates per culture plate were collected. After disinfecting the fish surface with 70% ethanol in water, the internal organs (liver, spleen, and head kidney) were dissected out aseptically, streaked on to Rimler-Shotts agar (RS; Himedia, India) or *Aeromonas* medium (supplemented with ampicillin; Thermo Fisher Scientific, UK) and incubated overnight at 28°C. Smooth, convex, round, and yellow (or dark green on *Aeromonas* medium) single colonies presumed to be *Aeromonas* spp. were sub-cultured in tryptone soya broth (TSB; Himedia) at 28°C for 16–20 h at 240 rpm. All isolates, samples and locations are listed in Supplementary Table 1. Cultures were cryopreserved at −80°C in TSB medium supplemented with 20% glycerol (Merck, USA).

2.3. Diagnostic PCR to confirm colonies to be *A. hydrophila*

Genomic DNA was extracted from the culture pellet of each isolate using the GeneJET Genomic DNA Purification kit (Thermo Scientific, USA). PCR was performed against the *16S rRNA* gene using the primers of Trakhna et al. (2009), and this assay yields an amplicon of 103 bp in the presence of genomic DNA from *A. hydrophila*. This *16S rRNA* PCR assay was chosen to identify *A. hydrophila* instead of the more traditional aerolysin gene PCR (Pollard et al., 1990), as initial evaluations found equivalent PCR outcomes with reference isolates within the *Aeromonas* genus whilst avoiding the presence of non-specific artifact products that appeared for a small proportion of aerolysin PCR-negative samples collected from the field (e.g., isolate TN120 from An Giang and isolates TN103 and TN117 from Dong Thap; data not shown). Each PCR contained 10 ng genomic DNA in a 10 μL total volume containing 1× MyTaq HS PCR master mix (Meridian Bioscience, UK) and 0.2 μM of each primer. The amplification conditions were as follows: initial denaturation at 95°C for 3 min, followed by 30 cycles of 95°C for 15 s, 55°C for 15 s, and 72°C for 10 s. PCR amplicons were electrophoresed through 1% agarose gel (Meridian Bioscience, UK) containing 0.1 mg/mL ethidium bromide in 0.5× TAE (20 mM Tris, 10 mM acetic acid, and 0.5 mM EDTA). The gel was observed under UV light using the InGenius gel imaging system (Syngene, UK) for the presence of the expected band.

2.4. Repetitive element sequence-based PCR (rep-PCR)

Each field isolate was genotyped using a rep-PCR based on the single $(GTG)_5$ repetitive primer, as described previously (Bartie et al., 2012). Field isolates negative by *16S rRNA* PCR were included to see whether lineages of non-*A. hydrophila* species associated strongly with MAS outbreaks (Supplementary Table 2). Five microlitres of each PCR reaction was separated on a 1.5% UltraPure Agarose-1000 gel (Invitrogen, Thermo Fisher Scientific) in chilled 0.5× TAE buffer. A GeneRuler 100 bp Plus DNA Ladder (Thermo Fisher Scientific) was used to aid DNA profile comparisons. Following electrophoresis, the gels were stained for 30 min in 1 mg/mL ethidium bromide and de-stained in Milli-Q water (Merck Millipore, UK) for 1 h. DNA profiles resulting from the rep-PCR were visualized and gel images captured using the InGenius system (Syngene, UK). Numerical analysis of the DNA fingerprints was performed using Gel Compar II software

(Applied Maths NV, Belgium). Dendrograms were constructed using the unweighted pair group method with arithmetic mean (UPGMA) and Pearson similarity coefficient. Clusters of similar banding profiles (similarity of at least 95%) were defined as an equivalent rep-PCR type where the banding patterns were considered indistinguishable by manual inspection of the respective rep-PCR gel profiles.

2.5. Phenotypic characterisation of suspected *A. hydrophila* isolates

A subset of 12 field isolates positive by *16S rRNA* PCR, representative of the main groups by rep-PCR and collected from different provinces and sampling times, were analyzed by API 20E biochemical profiling (bioMérieux, USA) and oxidase test (Oxoid) to further support the species identification (Supplementary Table 2). *A. hydrophila* subsp. *hydrophila* ATCC 7966^{T} was included for comparison.

2.6. Next-generation sequencing multi-locus sequence typing (ngsMLST)

A subset of 132 field isolates were selected for ngsMLST profiling such that they represented the diversity of *A. hydrophila* diagnostic PCR outcomes, rep-PCR profiles and sample sites. Four *A. hydrophila* reference isolates of varied host origin and six type strains of *Aeromonas* spp. were included as control material for ngsMLST library preparation (Supplementary Table 2). A total of nine MLST loci and the full-length *16S rRNA* gene (Weisburg et al., 1991) were amplified by PCR, barcoded, and sequenced using the high-throughput sequencing HiSeq platform (Illumina, USA) in order to assess the genetic variation within the field isolate collection. Six loci were included (*gyrB*, *groL*, *glt*A, *met*G, *ppsA*, *recA*) based on the MLST scheme of Martino et al. (2011) with three additional markers (*rpoD*, *dnaX*, *dnaJ*) selected for their ability to inform phylogeny within the *Aeromonas* genus (Nhung et al., 2007; Martinez-Murcia et al., 2011). Primer sequences of the MLST loci and full-length *16S rRNA* gene are listed in Supplementary Table 3.

2.7. ngsMLST library preparation

The ten loci of interest were amplified individually in a 5-μL PCR containing 1× MyTaq HS mix (Meridian Bioscience, UK), 0.2 μM of each primer pair and 2.5 ng genomic DNA template. The touchdown cycling protocol consisted of an initial denaturation at 95°C for 3 min; then 10 cycles of 95°C for 15 s, annealing at 65°C (with this temperature decreasing by 1°C each cycle), and extension at 72°C for 30 s; followed by eight PCR cycles performed at an annealing temperature of 55°C. The full-length *16S rRNA* gene PCR was conducted in the same PCR master mix conditions with an initial 3 min denaturation step at 95°C; 15 cycles of 95°C for 15 s, 45°C for 30 s, and 72°C for 45 s; and a final extension at 72°C for 5 min.

Amplicons were visualized on a 1.5% TAE agarose gel and the PCR products from each isolate combined to normalize total DNA template according to band intensity and size. Samples were purified by AxyPrep Mag PCR bead clean-up kit (Axygen Biosciences, USA) at a bead ratio of 0.6× and diluted to 0.2 ng/μL according to Qubit dsDNA HS quantification (Invitrogen; Thermo Fisher Scientific). Libraries were constructed in a miniaturized volume modified from an existing Illumina Nextera XT Library Preparation protocol (Illumina, USA), starting with 0.1 ng DNA template in a 2.5 μL tagmentation mixture and 5 μL barcoding PCR. Then libraries were cleaned up by AxyPrep magnetic beads (Axygen Biosciences, USA) at a 1:1 ratio. Finally, quantified libraries (Qubit dsDNA HS) were normalized by abundance of DNA, divided into four pools, and submitted for sequencing on a NovaSeq 6000 sequencing platform (Illumina, USA) at PE250 reads (Novogene, UK).

2.8. ngsMLST data analysis

Mass-parallel molecular typing data (ngsMLST sequences) were filtered for quality (QC > 20), length (150 nt), and absence of primers/adaptors and complexity (entropy > 15) using fastp (Chen et al., 2018). Gene sequence assemblies and typing were performed using SRST2 v0.2.0 (Inouye et al., 2014) and PubMLST (Jolley and Maiden, 2012). The resulting sequences of nine MLST loci and the full-length *16S rRNA* gene with average coverage above 400× were concatenated and aligned using GramAlign v3.0 (Russell, 2014). A phylogenetic tree was generated by PhyML v3.3.20200621 (Guindon et al., 2010) and this included concatenated ngsMLST sequences derived from published genomes of two reference isolates (vAh ST251 strain AL09-71 and *A. veronii* biovar *sobria* LMG 13067) and 12 *Aeromonas* spp. type strains (Supplementary Table 2).

2.9. Whole-genome sequencing

Fourteen isolates positive by the *A. hydrophila 16S rRNA* diagnostic PCR from the predominant rep-PCR types, and the reference isolate *A. hydrophila* T4 that originated from *L. rohita* in Bangladesh (Poobalane et al., 2010), were selected for WGS. Genomic DNA samples were submitted for DNA library preparation and microbial WGS (Novogene, UK) on the

NovaSeq 6000 sequencing platform (Illumina, USA) at PE150 read length.

2.10. Genome analysis

Reads from the 15 sequencing libraries were used separately during the assembly process and reads were filtered as described in Section 2.8. Raw data were assembled using Spades v3.14.0 (Bankevich et al., 2012) and the Unicycler-pipeline v0.4.8 (Wick et al., 2017). The initial *de novo* output was re-aligned against both *A. dhakensis* CIP 107500^T (assembly GCF_000820305.1), a closely related species frequently misidentified as *A. hydrophila*, and *A. hydrophila* subsp. *hydrophila* ATCC 7966^T (assembly GCF_000014805.1), using CONTIGuator v2.7.5 (Galardini et al., 2011) to order the contigs when continuity was incomplete. Finally, Pilon v1.23 (Walker et al., 2014) was used for polishing and correcting sequencing errors and to recover closed circular plasmid sequences. Subsequently, all genomes were annotated by DFAST v1.2.4 (Tanizawa et al., 2018) and plasmids identified using blastN v2.11.0 (Nowicki et al., 2018) against the National Center for Biotechnology Information (NCBI) plasmid database [2021–12–01]. Furthermore, genome sequences (including complete sequences, draft assemblies, and raw reads) of 116 publicly available *A. dhakensis* and *A. hydrophila* strains, and four other *Aeromonas* spp. to act as outgroups, were downloaded from the European Bioinformatics Institute (Supplementary Table 4). Unassembled samples were assembled according to the same process as the newly sequenced isolates.

2.11. Species affiliation by average nucleotide identity (ANI)

To support species assignments, FastANI v1.33 (Jain et al., 2018) was applied to the genome sequences to calculate an ANI index against several type strains, specifically *A. dhakensis* CECT 7289^T and CIP 107500^T (assemblies GCF_000819705.1 and GCF_000820305.1, respectively), and *A. hydrophila* subsp. *hydrophila* ATCC 7966^T (GCF_000014805.1). An ANI value of more than 0.96 was selected as the species threshold (Ciufo et al., 2018).

2.12. MLST typing and ST-eBurst

MLST types were determined for each genome with mlst v2.19.0 (Seemann, 2022) and PubMLST (Jolley and Maiden, 2012). The Phyloviz v2.0a (Nascimento et al., 2017) tool was used to run the goeBURST nLV algorithm and visualize trees based on the probable patterns of evolutionary descent between allelic profiles.

2.13. Core and accessory genomes

PIRATE v1.0.4 (Bayliss et al., 2019) was used to create a detailed pan-genome and to classify the core and accessory genomes of all available *A. dhakensis* and *A. hydrophila* isolates. Analysis of pan-genome outputs was performed using R v4.0.0 (R Core Team, 2022). Data on clustering and presence/absence, and trees from PIRATE, were visualized using panX release bb56978 (Ding et al., 2018) and phandango v1.3.0 (Hadfield et al., 2018).

2.14. Screening for antibiotic resistance genes

Screening for the presence of antibiotic resistance genes was conducted for the genomes with ABRicate v1.0.0 (Seemann, 2020), using multiple databases [2021–12–01]: NCBI (Feldgarden et al., 2020) and PlasmidFinder (Carattoli et al., 2014).

2.15. Design and validation of primers to distinguish the main groups of strains

Core genes of the two most prevalent groups of strains observed in this present study were used to design pairs of discriminating primers, with conserved regions within core genes used to identify sites for the anchoring primers. Then, whole genomes were scanned to confirm the specificity of the primer sets using ecoPrimer v0.5 (Riaz et al., 2011). Candidate PCR primer pairs (targeting sequences in *yjcS* and *intA_5* genes) were evaluated against a panel of field isolates and reference and type strains to confirm their specificity (Supplementary Table 2). Each PCR contained 5 ng genomic DNA in a 10 μL total volume containing MyTaq HS mix (Meridian Bioscience, UK) and 0.2 μM of each primer. Initial specificity testing was conducted using the following amplification conditions: denaturation at 95°C for 3 min; followed by 30 cycles of 95°C for 15 s, 52°C for 15 s, and 72°C for 10 s. PCR amplicons were separated through a 1% agarose gel (Meridian Bioscience, UK) containing 0.1 mg/mL ethidium bromide and visualized. A gradient PCR between 52°C and 62°C was conducted to optimize the PCR conditions and confirm the differential amplification of DNA from isolates representing the different groups of strains.

3. Results

3.1. Collection of field isolates

In total, 345 presumptive *Aeromonas* spp. colonies were recovered on isolation agar plates from *P. hypophthalmus*

individuals exhibiting classical signs of MAS. Of these presumed *A. hydrophila* isolates, 58.6 (202/345) yielded the expected 103-bp amplicon in the PCR of Trakhna et al. (2009) that targets specifically the *16S rRNA* gene of *A. hydrophila*, thus indicating the presence of this species (Supplementary Table 2). Of the nine farm sites sampled between 2018 and 2019, PCR-positive isolates suspected to be *A. hydrophila* were detected at seven sites, including co-isolation with PCR-negative colonies at six of these sites, indicative of the presence of other *Aeromonas* spp. Notably, of the 40 fish from which more than one isolate was recovered from the internal organs, in eight cases PCR-positive and negative colonies were isolated, indicating the presence of more than one *Aeromonas* spp. (e.g., Site 3, Fish 1; Supplementary Tables 1, 2).

A summary of the analyses performed for isolates included in this present study can be found in Supplementary Figure 1.

3.2. Repetitive PCR (rep-PCR) genotyping

Analysis of the 345 field isolates by rep-PCR revealed complex DNA profiles consisting of 12–14 fragments, with each ranging from ca. 300–3,000 bp (Supplementary Figure 2). Of the 202 isolates positive by *16S rRNA* PCR and thus suspected to be *A. hydrophila*, two distinct profiles were dominant: these were confirmed by manual inspection and numerical analysis and termed rep-PCR types A and B (Supplementary Table 2). Rep-PCR types A and B were widely distributed across the eight provinces sampled (Supplementary Figure 2), with rep-PCR type A being most prevalent (151/202; 74.8%) among the suspected *A. hydrophila* isolates, especially in samples collected more recently. Of note, from one fish (Site 3, Fish 3) was isolated three PCR-positive colonies, where two isolates clustered within rep-PCR type A whilst the third was rep-PCR type B (Supplementary Tables 1, 2).

More variable rep-PCR profiles were observed for the colonies isolated on Aeromonas selective medium that were negative by the *16S rRNA* PCR (Supplementary Table 2, Supplementary Figure 3), and these presumed *Aeromonas* spp. isolates formed relatively diffuse clusters (Supplementary Figure 2) compared to the tight clusters corresponding to the two main rep-PCR types, A and B of suspected *A. hydrophila* isolates that tested positive by *16S rRNA* PCR.

3.3. Phenotypic characterisation of suspected *A. hydrophila* isolates

Biochemical characterisation of *A. hydrophila* subsp. *hydrophila* ATCC 7966^T and 12 field isolates, suspected to be *A. hydrophila* by *16S rRNA* PCR and representative of rep-PCR types A and B, revealed identical API-20E biochemical profiles (704126) matching *A. hydrophila*, according to BacDive [https://bacdive.dsmz.de/api-test-finder].

3.4. ngsMLST phylogeny

To provide greater confidence into the identities and relatedness of the field isolates, ngsMLST was performed whereby fragments (between 477 and 1,496 bp) at each of the 10 loci were amplified for 132 representative field isolates, four *A. hydrophila* reference isolates from varied hosts, and six *Aeromonas* spp. type strains. These isolates were used as template for ngsMLST library preparation and were selected for diversity of sampling location, and the outcomes of *16S rRNA* PCR and rep-PCR assays (Supplementary Table 2). After applying the selected depth threshold, a phylogenetic tree was generated for 92 libraries (87 field isolates, three reference isolates, and two type strains) based on the concatenated sequence (ca. 6,910 bp in length) from each isolate (Figure 1). Amongst the field isolates suspected to be *A. hydrophila* (i.e., positive by *16S rRNA* PCR), two major clusters formed according to multilocus phylogenetic analysis (MLPA). Application of the PubMLST scheme and allelic profiling of the six housekeeping genes (*gyrB*, *groL*, *gltA*, *metG*, *ppsA*, and *recA*) permitted the assignment of sequence types (STs) to each of these two main clusters, namely ST656 (n = 39) and ST251 (n = 13), which corresponded to rep-PCR types A and B respectively. ST656 is associated with *A. dhakensis* (Jolley et al., 2010), a species closely related to *A. hydrophila* (Beaz-Hidalgo and Figueras, 2013), while ST251 is a hypervirulent lineage of *A. hydrophila* (vAh). In contrast, the PCR-negative *Aeromonas* spp. isolates clustered more variably and distinctly from the main *A. dhakensis* and vAh ST251 clades and formed a diffuse cluster that affiliated most closely to published loci of *A. veronii* NCIMB 13015^T (n = 26) with a minor sub-cluster related to *A. jandaei* CECT 4228 and *A. sobria* NCIMB 12065^T (n = 9; Figure 1). The remaining three field isolates from *P. hypophthalmus* presented as outlier groups according to MLPA. The majority of the allelic profiles of these *Aeromonas* spp. isolates did not match any ST in the PubMLST *Aeromonas* database (Supplementary Table 2).

3.5. Genome assemblies and ANI

Genome sequencing generated a mean of 12 million short-reads for each of 14 representative field isolates and the *A. hydrophila* T4 reference strain (Table 1). The genomes ranged between 4.82 and 4.98 Mb, with GC ratios ranging from 60.9 to 61.4%; several closed plasmids were detected consistently (Table 2). All genomes were (re-)annotated for gene location consistency using DFAST (Supplementary Table 4), aligned against selected type strains

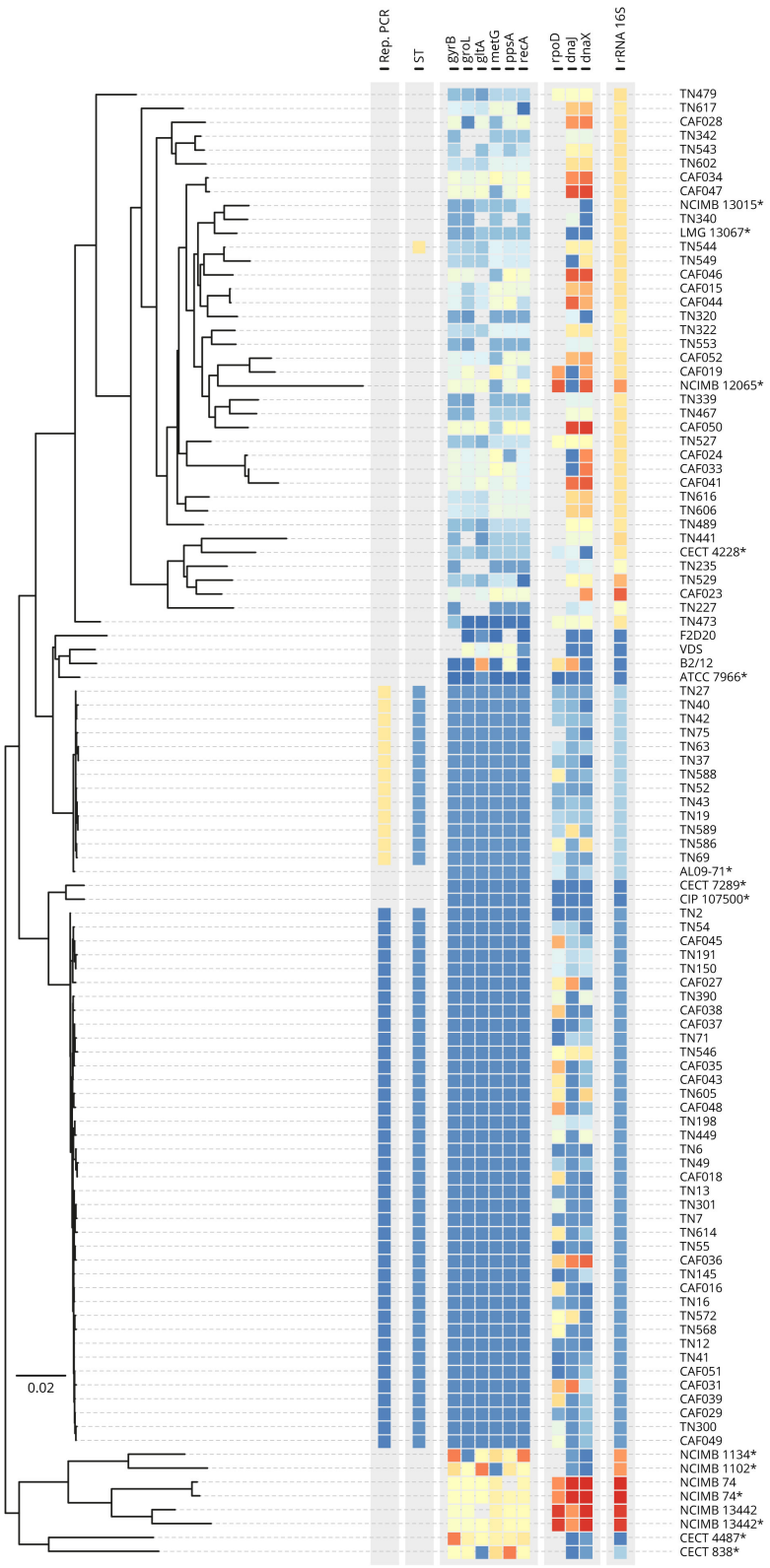

FIGURE 1
Multilocus phylogenetic analysis by sequence comparison of concatenated housekeeping genes at 10 loci for 87 representative field isolates of *Aeromonas* from striped catfish, five reference isolates, and 12 type strains. rep-PCR type, sequence type (ST), and alleles derived from ngsMLST analysis of 10 genes including *16S rRNA* are color coded. *Gene sequences (when available) were retrieved from the genome assembly at NCBI.

TABLE 1 Field isolate genomes sequenced in this present study.

Isolate	Year	Country	Province	Host	Rep-PCR type	Read number	Run Acc.
T4	1994	Bangladesh	–	*L. rohita*	*n.d.*	15,048,804	ERR4911987
TN1	2013	Vietnam	AG	*P. hypophthalmus*	B	18,305,234	ERR4911995
TN3	2013	Vietnam	AG	*P. hypophthalmus*	A	14,958,648	ERR4911948
TN4	2014	Vietnam	AG	*P. hypophthalmus*	A	14,771,162	ERR4911656
TN5	2013	Vietnam	AG	*P. hypophthalmus*	A	6,820,380	ERR4911952
TN10	2014	Vietnam	AG	*P. hypophthalmus*	A	7,456,818	ERR4911957
TN11	2014	Vietnam	AG	*P. hypophthalmus*	A	18,000,280	ERR4911967
TN14	2013	Vietnam	AG	*P. hypophthalmus*	A	8,281,592	ERR4911973
TN22	2014	Vietnam	CT	*P. hypophthalmus*	B	16,909,614	ERR4912005
TN27	2014	Vietnam	DT	*P. hypophthalmus*	B	7,555,950	ERR4912016
TN42	2015	Vietnam	BT	*P. hypophthalmus*	B	14,792,042	ERR4912885
TN45	2018	Vietnam	TG	*P. hypophthalmus*	A	10,315,308	ERR4911633
TN46	2015	Vietnam	DN	*P. hypophthalmus*	B	8,067,104	ERR4912011
TN49	2015	Vietnam	AG	*P. hypophthalmus*	A	7,221,844	ERR4911978
TN50	2015	Vietnam	AG	*P. hypophthalmus*	A	8,292,598	ERR4911638

For each isolate the year sampled, country of origin and province (AG, An Giang; CT, Can Tho; DT, Dong Thap; DN, Dong Nai; BT, Ben Tre; TG, Tien Giang), host, rep-PCR genotype (rep-PCR type A of *A. dhakensis* ST656 and rep-PCR type B of vAh ST251), total reads, and data accession number (Run Acc.) is provided. *n.d.*, not determined.

TABLE 2 Genome assembly summary of 15 field isolate genomes.

Isolate	Species	MLST type	Chromosome size (bp)	a	b	c	d	e	f	g	h	Assembly acc.
T4	*A. hydrophila*	u3	4,891,336									GCA_905132965
TN1	*A. hydrophila*	vAh ST251	4,957,116							●	●	GCA_905132985
TN3	*A. dhakensis*	ST656	4,850,229	●	●	●	●					GCA_905132935
TN4	*A. dhakensis*	ST656	4,850,407	●	●	●	●					GCA_905132895
TN5	*A. dhakensis*	ST656	4,850,228	●	●	●	●					GCA_905132915
TN10	*A. dhakensis*	ST656	4,850,407	●	●	●	●					GCA_905132905
TN11	*A. dhakensis*	ST656	4,850,231	●	●	●	●					GCA_905132845
TN14	*A. dhakensis*	ST656	4,847,439	●	○	●	○					GCA_905132925
TN22	*A. hydrophila*	vAh ST251	4,977,638					●	●			GCA_905132975
TN27	*A. hydrophila*	vAh ST251	4,977,339					○	●			GCA_905132955
TN42	*A. hydrophila*	vAh ST251	4,978,631					▲	●			GCA_905132945
TN45	*A. dhakensis*	ST656	4,820,690	●	●	●	●					GCA_905132775
TN46	*A. hydrophila*	vAh ST251	4,977,942					●	●			GCA_905132995
TN49	*A. dhakensis*	ST656	4,850,028	●	●	●	●					GCA_905132875
TN50	*A. dhakensis*	ST656	4,847,436	●	●	●	●					GCA_905132865

For each isolate the species assignment, multi-locus sequence type, chromosome size, presence of plasmids and assembly accession number is provided. ●, circular/complete plasmid sequence identified; ○, partial plasmid sequence found; ▲, present with extra insertion (5,640 bp). a, p6.4-Qnr (6,386 bp); b, p6.3-RelE (6,276 bp); c, p6.2-StbE (6,162 bp); d, p4.7-HicB (4,678 bp); e, p5.0-YhdJ (5,092 bp); f, p3.6-parDE (3,663 bp); g, p6.2-ParE (6,214 bp); h, p4.1-Rec (4,140 bp).

to determine ANI (Supplementary Table 5), and re-classified (Figure 2). Field isolates fell within two clades that associated with either *A. dhakensis* or the clonal vAh ST251 lineage within *A. hydrophila*, respectively. Moreover, the ANI calculations supported the existence of these two predominant species amongst the isolates collected from *P. hypophthalmus* (Figure 2,

Supplementary Table 5). ANI values of 97.1–97.2% were estimated for nine of the genomes (all rep-PCR type A) against the two *A. dhakensis* type strains (CECT 7289^T and CIP 107500^T). Similarly, the five vAh ST251 genomes (all rep-PCR type B) associated most closely with the *A. hydrophila* subsp. *hydrophila* ATCC 7966^T type strain (mean ANI value of 96.8%). The reference strain, *A. hydrophila* T4, was also placed within the major *A. hydrophila* clade (ANI values of 97.0% compared to *A. hydrophila* subsp. *hydrophila* ATCC 7966^T), although separately from the ST251 lineage.

3.6. Genome-based MLST and ST-eBurst analysis

Genomes generated in this present study and all those publicly available for *A. dhakensis* and *A. hydrophila* were analyzed by MLST for the *Aeromonas* genus to identify STs and perform network analysis. Most of the genomes had profiles corresponding to a known ST, although 64 out of 135 analyzed genomes presented with novel gene sequences and MLST associations (denoted by "u" in Figure 3 and Supplementary Table 5). Network eBurst analysis based on sequence distance (Figure 3) revealed high diversity within and between the *A. dhakensis* and *A. hydrophila* species, thus supporting their separation into two species. For both species, strain STs were distributed typically as part of a network of single locus variants or less commonly as unique doublets or singletons (Figure 3). The *A. dhakensis* ST656 isolates associated with *P. hypophthalmus* were located within the main clonal complex of *A. dhakensis* strains; conversely, *A. hydrophila* ST251 isolated from *P. hypophthalmus* presented as a singleton.

3.7. Core and accessory genomes

Core (n = 2,517) and accessory genes (n = 33,952) were inferred to create a detailed pan-genome and to classify core and accessory genomes using all available *A. dhakensis* and *A. hydrophila* genomes (threshold of 95% presence in available genomes; Figure 4). When analyzing *A. dhakensis*, *A. dhakensis* ST656, *A. hydrophila* and *A. hydrophila* vAh ST251 pan-genomes separately, there were 2,196 shared core genes identified between the groups (threshold of 95% presence in available genomes for each group; Supplementary Figure 4). A characteristic pattern of genes within the core genomes distinguished the two closely related species of *A. dhakensis* (n = 1,505 unique genes not found in *A. hydrophila*) and *A. hydrophila* (n = 923 unique genes not found in *A. dhakensis*). Strain-specific regions associated with the *A. dhakensis* ST656 (n = 769 genes) and vAh ST251 (n = 425 genes) genotypes were detected when compared to all published *A. dhakensis* and *A. hydrophila* genomes, respectively (Supplementary Figure 4).

3.8. Antibiotic resistance genes

Screening for antibiotic resistance genes was conducted for each of the 135 *A. dhakensis* and *A. hydrophila* available genomes, including four *Aeromonas* spp. genomes as outliers (Figure 2, Supplementary Table 5). Interestingly, the genomes of the field isolates possessed sets of genes implicated in a multi-drug resistance trait and in patterns not detected in closely-related *A. dhakensis* and vAh ST251 counterparts (Figure 2, Supplementary Table 5). The nine field isolates of *A. dhakensis* ST656 each included resistance determinants to sulphonamides (*sul1*), trimethoprim (*dfrA1*), tetracycline (*tetA*), and a plasmid-mediated quinolone resistance gene (*qnrS2*). Of note, the sulphonamide (*sul1*) and trimethoprim (*dfrA1*) resistance genes were detected in both *A. dhakensis* ST656 and vAh ST251 outbreak genomes. Four of the vAh ST251 field isolates originating from multiple provinces in 2014 and 2015 also contained additional genetic elements conferring reduced susceptibility to gentamicin [*aac(6′)-Ib4*] and rifamycin (*arr-2*). Intriguingly, the earliest vAh ST251 isolate (TN1 collected in 2013) lacked most of these additional antibiotic-resistance determinants (Figure 2).

Gene determinants encoding reduced susceptibility to β-lactams and carbapenems were common in all *A. dhakensis* and *A. hydrophila* genomes, including in field isolates. The β-lactamase gene, bla$_{AQU}$, was found uniquely in *A. dhakensis*, including the ST656 outbreak strains isolated from striped catfish, while the chromosomally mediated Class D OXA β-lactamase genes, bla$_{OXA-726}$ or related bla$_{OXA-724}$, were common to genomes of both species. Sequences with homology to CphA-type carbapenemases, belonging to metallo-β-lactamases subclass B2, were also shared amongst the two species, with the cphA3 subtype associated with vAh ST251, including in the five genomes of the vAh ST251 field isolates sequenced in this present study. In contrast, a predicted cephalosporin-resistant phenotype was limited to *A. hydrophila*, including in the vAh ST251 field isolates (*cepH*) and in the *A. hydrophila* T4 reference genome (*cepS*). Markers for reduced susceptibility to chloramphenicol, aminoglycosides, macrolides and quinolones were present but distributed more sporadically across the entirety of genomes examined.

3.9. Design and validation of primers to distinguish *A. dhakensis* and vAh ST251

Two primer sets based on the core genes in the *A. dhakensis* and vAh ST251 genomes were evaluated for their ability to distinguish these two key strain groups (Supplementary Table 6). To confirm the specificity of each set of primers, the two pairs

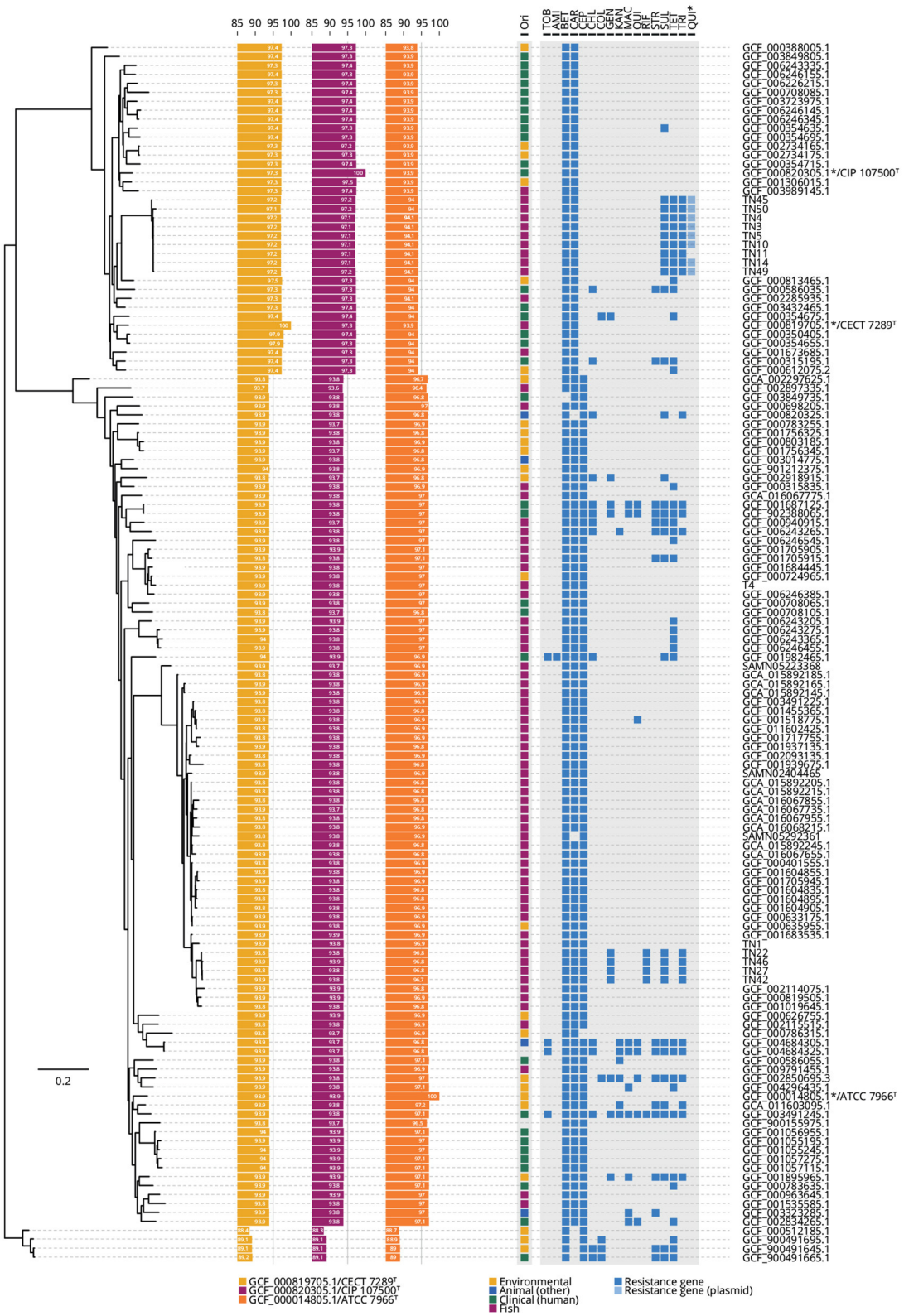

FIGURE 2
Phylogenetic tree of 14 field isolates, one reference isolate, and 116 published *A. hydrophila* and *A. dhakensis* genomes. Four *Aeromonas* spp. genomes are included in the analysis as an outlier group. Tree is based on the pan-genome analysis. Average nucleotide identity (ANI) values

(Continued)

FIGURE 2 (Continued)
were calculated compared to the three labeled type strains (*A. dhakensis* CECT 7289^T assembly GCF_000819705.1; *A. dhakensis* CIP 107500^T assembly GCF_000820305.1; and *A. hydrophila* subsp. *hydrophila* ATCC 7966^T assembly GCF_000014805.1). The origin (Ori) of each isolate and the presence/absence of 17 antibiotic resistance genes in the pan-genome analysis is provided. *The quinoline resistance gene was found on a plasmid and plasmid sequences were available only for the genomes sequenced in this present study. Full list of the abbreviations and detailed gene names is provided in Supplementary Table 5.

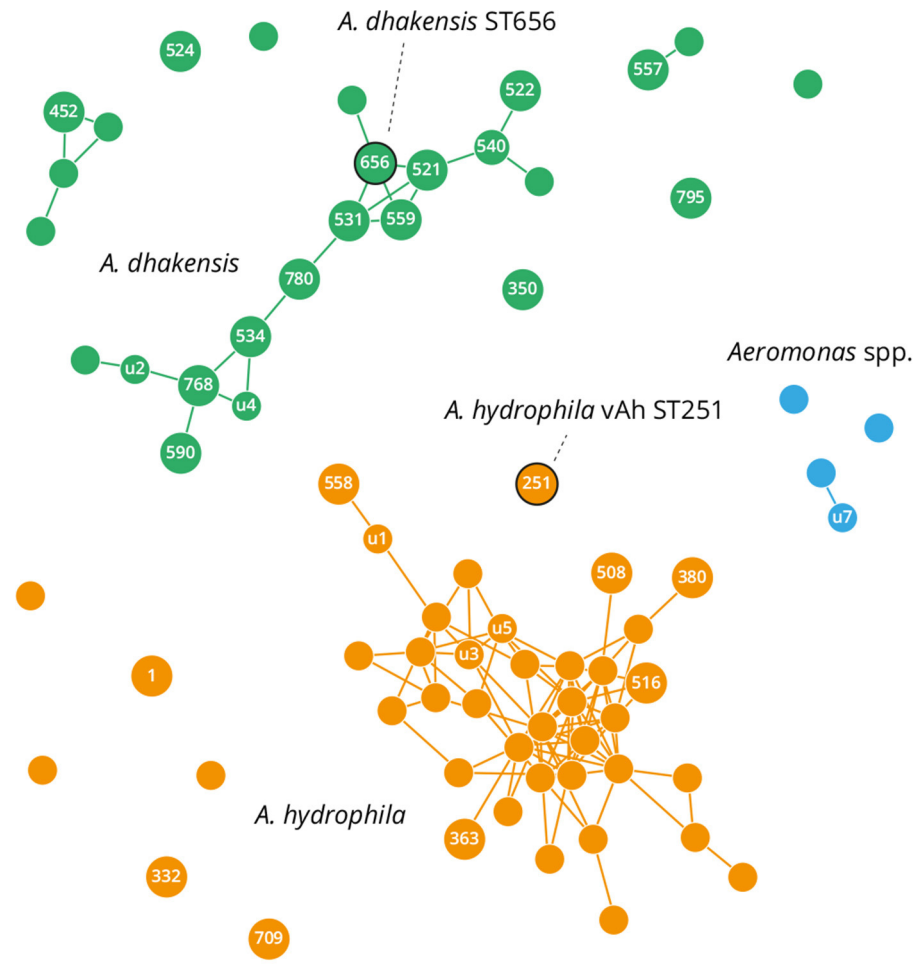

FIGURE 3
eBurst network based on multilocus sequence typing (MLST) patterns of publicly available *A. hydrophila* and *A. dhakensis* genomes. Circles denote a distinct MLST: small and unlabelled if undefined and unique; small and labeled if undefined but identified multiple times ("u"); and larger and labeled if present in the PubMLST database. Links show single allele variants. Sequence types (STs) containing field isolates are outlined in black and these correspond to *A. hydrophila* vAh ST251 and *A. dhakensis* ST656.

were screened in an initial evaluation against a panel of 14 *Aeromonas* isolates that included field isolates of *A. dhakensis* ST656 ($n = 2$) and vAh ST251 ($n = 2$), non-vAh *A. hydrophila* reference strains ($n = 2$), *A. hydrophila* subsp. *hydrophila* ATCC 7966^T, the *A. dhakensis* type strains ($n = 2$), and type strains of other *Aeromonas* spp. ($n = 5$). The PCR assay designed to target *yjcS*, which encodes a metallo-β-hydrolase in the *A. dhakensis* genome, yielded the predicted 223-bp amplicon at 62°C only for the DNA samples derived from the two *A. dhakensis* isolates collected from striped catfish in this present study (TN5 and TN49) and the two *A. dhakensis* type strains (CIP 107500^T and CECT 7289^T). Similarly, a PCR assay targeting the *intA_5* integrase gene in the vAh ST251 genome yielded a 283-bp amplicon at the optimum 58°C annealing temperature for only the two vAh ST251 field isolates collected herein (TN1 and TN27). No amplification in either assay was observed for any non-target isolates (Supplementary Figure 5).

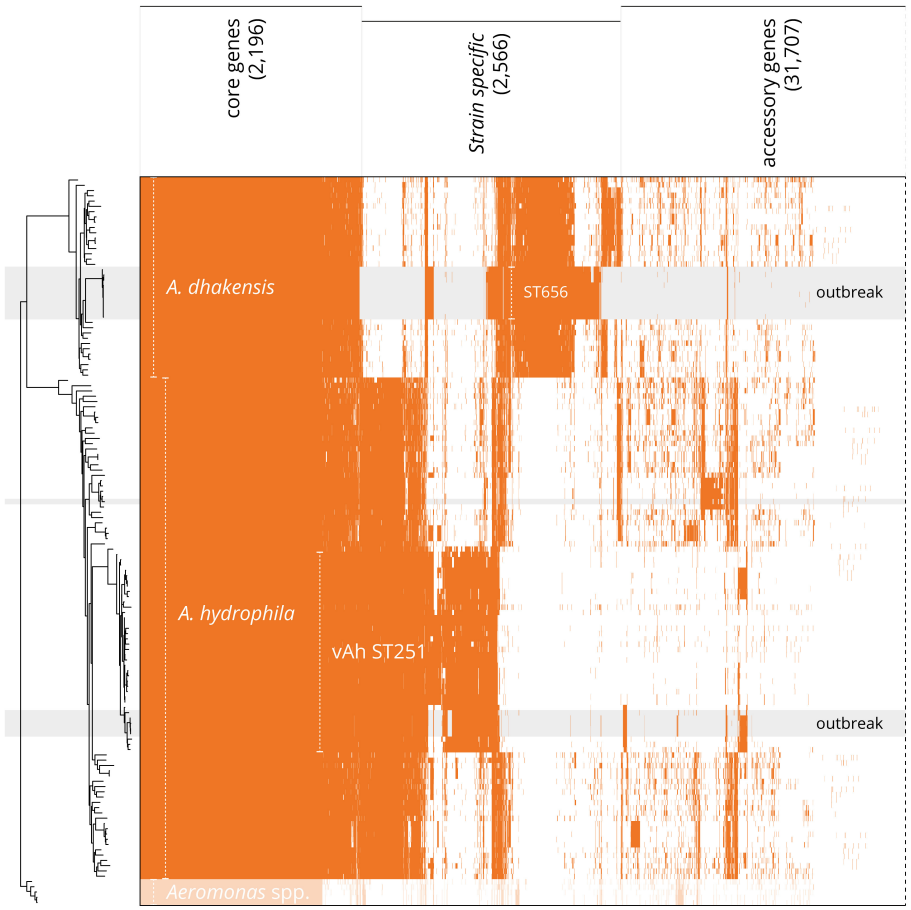

FIGURE 4
Distribution of protein-encoding genes in the pan-genome of *A. hydrophila* and *A. dhakensis*. Tree is based on pan-genome analysis, calculated by PIRATE using the accessory genes. Gray background indicates isolates sequenced *de novo* in this present study, with field isolates labeled "outbreak". Shared protein-encoding genes constitute the core genome (95% presence; 2,517 genes). *A. dhakensis* has species-specific genes (698 genes) whilst the outbreak strains (ST656, from this present study) share a cluster of clone-specific genes (additional 769 genes). Similarly, *A. hydrophila* possesses 439 unique genes (95% presence), whilst the vAh ST251 strains exhibit a specific gene cluster distinct from all other specimens (additional 425 genes). A 4-way Venn diagram of the separate pan-genomes for *A. dhakensis*, *A. dhakensis* ST656, *A. hydrophila* and *A. hydrophila* vAh ST251 is available in Supplementary Figure 4.

4. Discussion

This present study aimed to characterize the predominant strains of *A. hydrophila* causing MAS in striped catfish in the Mekong Delta, Vietnam to inform the selection of isolates for inclusion into new vaccine formulations. A polyphasic approach was taken to provide insight into the most appropriate methods for discriminating the strains sufficiently. Following selective culture of MAS-affected fish tissues on agar, biochemical profiling, species-specific PCR, rep-PCR, ngsMLST, and WGS, the main strains responsible for recent MAS outbreaks were determined to be clonal lineages of two emerging pathogens, specifically a hypervirulent clone of *A. hydrophila* (vAh ST251) and a predominant single clone of the closely related species *A. dhakensis* (ST656).

Isolates of *A. dhakensis* were most prevalent in the samples collected from striped catfish, with this species representing 151/202 of the field isolates testing positive by the *16S rRNA* PCR of Trakhna et al. (2009). This present study is the first to report *A. dhakensis* to be a major pathogen affecting the striped catfish sector in the Mekong Delta, Vietnam. *A. dhakensis* isolates were collected from all eight provinces during 2013-2019, and these isolates clustered within the rep-PCR type A group and belonged to ST656. The detection and clonal nature of *A. dhakensis* was unexpected because *A. hydrophila* is often cited to be the most important pathogen responsible for MAS in striped catfish in Vietnam (Ngo et al., 2022). However, given that *A. dhakensis* (Aravena-Román et al., 2011) and *A. hydrophila* (Beaz-Hidalgo et al., 2013) are frequently misidentified due to overlapping phenotypic traits, shifting classification schemes and a lack of

reliable discriminatory tools (Awan et al., 2018; da Silva Filho et al., 2021), it is highly likely that *A. dhakensis* is an under-reported cause of mortality in aquatic animals, with disease outbreaks attributed instead to *A. hydrophila* (Aravena-Román et al., 2011). Previously, *A. dhakensis* (formerly *Aeromonas aquariorum*) has been reported in disease events of ornamental fish in Portugal (Martinez-Murcia et al., 2008) and Sri Lanka (Jagoda et al., 2014), and in eels in Spain (Esteve et al., 2012) and China (Guo et al., 2016). Moreover, *A. dhakensis* was the predominant species isolated from freshwater fish with MAS symptoms in Malaysia (Azzam-Sayuti et al., 2021), and this species was also implicated in disease outbreaks in farmed tilapia in Mexico (Soto-Rodriguez et al., 2013).

The remaining 51/202 field isolates that tested positive by the Trakhna et al. (2009) PCR grouped together as rep-PCR type B and were identified as vAh ST251. Isolates of this hypervirulent clone were found in the earliest samples analyzed, which confirms its presence in the striped catfish sector in the Mekong Delta since at least 2013 (TN1 was isolated in 2013; AG-2013-AG1 in Ngo et al., 2022). Furthermore, vAh ST251 isolates showed widespread geographical and temporal distribution through to 2019 when the most recent samples were cultured (Supplementary Table 1), demonstrating the persistence of this clone within the industry and supporting a major role for *A. hydrophila* in the etiology of MAS in striped catfish (Stratev and Odeyemi, 2017). Lineages of vAh ST251 have been implicated in significant MAS outbreaks worldwide including those affecting the catfish industry in the USA and carp production in China (Pang et al., 2015; Rasmussen-Ivey et al., 2016), and further sampling may reveal this clone to be responsible for disease outbreaks elsewhere. The restricted singleton presentation of vAh ST251 is unusual given the high strain diversity typically encountered in *A. hydrophila*. Further, the global dissemination of the vAh ST251 epidemic strain is limited to fish hosts thus far, and the pan-genomic analysis presented herein supports the existence of vAh-specific regions within core and accessory genomes that could explain the hypervirulence and host specificity phenotype (Pang et al., 2015; Rasmussen-Ivey et al., 2016; da Silva Filho et al., 2021). Indeed, gene clusters unique to the vAh ST251 lineage have been described previously in relation to prophages, O-antigen biosynthesis and fucose and myo-inositol metabolism (Hossain et al., 2013; Rasmussen-Ivey et al., 2016; Ngo et al., 2022).

This present study showed that only rep-PCR, MLST, and WGS had sufficient discriminatory power to distinguish the two main groups of isolates effectively, specifically vAh ST251 and *A. dhakensis*. Indeed, the vAh ST251 and *A. dhakensis* isolates were indistinguishable by colony appearance on RS agar, API20E biochemical profiles and the *16S rRNA* PCR (Supplementary Table 2). The inability of the Trakhna et al. (2009) primers to discriminate *A. dhakensis* from *A. hydrophila* is not entirely unexpected given the close genetic relatedness of these species (Awan et al., 2018). Nevertheless, that *A. dhakensis* ST656 returned an identical API20E profile to vAh ST251 (*i.e.*, 704126) was unexpected because the inability of *A. dhakensis* to ferment L-arabinose (API20E profile, 7047125) has been applied to discriminate these species previously (Esteve et al., 2012). Still, the high strain diversity within the *Aeromonas* genus has resulted in isolates with atypical phenotypes being encountered, such as *A. dhakensis* 1P11S3 from striped catfish in Malaysia that utilized myo-inositol similar to vAh ST251 (Azzam-Sayuti et al., 2022). The inability of *A. dhakensis* to assimilate urocanic acid or to produce acid from L-fucose are other phenotypic markers that have been applied to distinguish *A. hydrophila* and *A. dhakensis* (Huys et al., 2002), but the observations in this present study further underscore the need for more effective discriminatory genotyping tools to differentiate *Aeromonas* species. Rep-PCR with a single repetitive primer such as $(GTG)_5$ has long been exploited in bacterial strain typing due to the relative simplicity, low cost, and discriminative power of the assay to subspecies level (Ishii and Sadowsky, 2009), and the continued relevance of this genotyping methodology was demonstrated. Although rep-PCR performed well to describe the population structure of strains associated with the MAS outbreaks, MLST provides a more objective approach to genotyping and a scheme has been established for the *Aeromonas* genus (Martino et al., 2011; Du et al., 2021). MLST allows the assignment of definitive genotypes for reliable comparisons to previous studies, but the approach can be relatively costly through reliance on Sanger sequencing technology. To counter this shortcoming, in this present study a ngsMLST sequencing protocol was devised to create multiplexed miniaturized libraries from the PCR amplicons of each isolate at each MLST locus, followed by high-throughput sequencing as applied in yeast (Chen et al., 2015). This method allows for cost effective, large-scale strain characterization compared to more laborious traditional sequencing methods, and offers a highly discriminative approach for future surveillance efforts of bacterial pathogens, including those associated with MAS outbreaks as demonstrated in this present study. Further to this, to enable a rapid and inexpensive method to discriminate *A. dhakensis* from *A. hydrophila* and vAh ST251, a simple endpoint PCR was designed based on the core genomes. The primers were validated experimentally to confirm their specificity against a panel of strains that included field isolates, non-vAh isolates, and type strains of *A. dhakensis*, *A. hydrophila* subsp. *hydrophila* and several other *Aeromonas* spp. However, it is unclear whether these primers can differentiate between other strains of *A. dhakensis*, vAh ST251 of varied origin or *Aeromonas* species, and further work is required to confirm this. Even so, this *yjcS* PCR assay represents a novel tool that could be applied to improve detection of *A. dhakensis* and avoid misidentification as *A. hydrophila*, particularly for MAS outbreaks in striped catfish in the Mekong delta. Similar assays to the *intA_5* PCR used to identify vAh ST251 in this present study have been reported to target specific sequences unique to the strains from the United States (Griffin et al., 2013), as well

as vAh lineages from outbreaks in Asia (Rasmussen-Ivey et al., 2016).

WGS provided the greatest discriminatory power and phylogenetic insight, and sequencing of 14 genomes representative of the two main clusters of striped catfish isolates confirmed definitively the respective species affiliations, their clonal nature and separation into two distinct lineages. The genomes for the *A. dhakensis* ST656 isolates generated in this present study are the first to be reported from striped catfish and are a welcome supplement to the relatively few genomes available for this species, compared to *A. hydrophila*. However, *A. dhakensis* is attracting increasing attention as an emerging pathogen with zoonotic potential, especially in Asia, where this species has been associated with serious infections and fatalities in humans (Huys et al., 2002; Wu et al., 2012; Chen et al., 2016; Khor et al., 2018; Kitagawa et al., 2019; Lau et al., 2020; Sun et al., 2021). Interestingly, though ST656 has been recovered exclusively so far from fish hosts, this clone was placed within a larger clonal complex of *A. dhakensis* strains originating from human clinical cases (Figure 3), meaning outbreaks of disease due to *A. dhakensis* in fish hosts present a theoretical risk to susceptible individuals interacting with infected stocks. Of note, a fatal case of necrotising fasciitis involving *A. dhakensis* was recorded in Australia after exposure to pond water (Melo-Bolivar et al., 2019). Pan-genomic analyses of the WGS data revealed genomic regions unique to *A. dhakensis* and a relatively large abundance of genes associated distinctively with the ST656 genotype, which could have a role in disease progression and host specificity (Supplementary Figure 4). Additional genomes for *A. dhakensis* and *A. hydrophila* and their analysis will enhance our understanding of zoonotic potential and the success of epidemic strains.

The genomic analyses confirmed the presence of antimicrobial resistance determinants in the field isolates of both species, which can reduce therapeutic treatment options and underlines the need for greater uptake of control measures by striped catfish farmers such as vaccines (Dien et al., 2022). The inherent reduced susceptibility of *Aeromonas* isolates to β-lactams is well recognized (Awan et al., 2018), but the genomes of the isolates collected from the striped catfish revealed the co-occurrence of resistance genes to sulphonamides, trimethoprim, tetracycline and quinolines in *A. dhakensis*, and to sulphonamides, trimethoprim, gentamicin, and rifamycin in vAh ST251. Of particular concern, the *qnrS2* gene that confers resistance to quinoline was detected on a 6.4 kb plasmid in *A. dhakensis*, which indicates a propensity for likely transmission between strains, as shown before for *Aeromonas* spp. isolates in this study arena (Nguyen et al., 2014). Notably, *A. hydrophila* T4 (isolated in 1994 from an Asian carp in Bangladesh) and the earliest vAh ST251 field isolate in this present study (TN1 sampled from a diseased pangasius catfish in 2013; Ngo et al., 2022) did not possess most of the additional antimicrobial resistance genes, in stark contrast with the more recent vAh ST251 genomes, thereby suggesting relatively recent acquisition and/or selection. The emergence of the multi-resistant strains has likely occurred in response to selective pressure exerted by exposure to antibiotics applied in the Mekong Delta region (Phu et al., 2016; Truong et al., 2019; Dang et al., 2021). Still, antibiotic susceptibility testing is needed to verify the reduced susceptibility phenotypes of the field isolates. Amongst the *Aeromonas* genomes, the frequent presence of resistance elements to agents reserved as treatments of last resort for Gram-negative infections in humans is of concern, particularly genes encoding resistance against carbapenems (*cphA*). Likewise, the frequent carriage of the chromosomal class C β-lactamase bla$_{AQU}$ in *A. dhakensis*, including in the genomes of field isolates from striped catfish, has reduced therapeutic options in cases of septicaemia in humans (Wu et al., 2013), and *A. dhakensis* is postulated to be a reservoir of β-lactamase-encoding genes Yi et al. (2014).

Amongst the field isolates that tested negative by the *16S rRNA* PCR, high strain diversity was detected by rep-PCR and ngsMLST both within and between sampling sites (Supplementary Figure 2, Figure 1). Thus, the molecular epidemiology of *Aeromonas* strains causing MAS in striped catfish appears to be complex and this fits with a more opportunistic and sporadic population structure for these other species. Similar to the varied rep-PCR profiles encountered, the extensive strain diversity of other *Aeromonas* species relative to the single clonal lineages of *A. dhakensis* and vAh ST251 was indicated by less well-defined clusters in the MLPA of the concatenated housekeeping gene sequences and inability to assign isolates to an existing ST. The species identification for these *Aeromonas* spp. isolates was less certain, with closest homology to members of the *A. veronii* complex noted in the main MLPA cluster of suspected *Aeromonas* spp. isolates, and a minor group related to *A. jandaei* and *A. sobria* (Figure 1). This is consistent with other studies that have implicated species other than *A. hydrophila* in MAS outbreaks, including *A. veronii* in channel catfish in Vietnam (Hoai et al., 2019) and carp in China (Ran et al., 2018), and *A. veronii* and *A. jandaei* in tilapia in Thailand (Dong et al., 2017; Sakulworakan et al., 2021). This present study relied on opportunistic sampling and a structured epidemiological approach is necessary to understand the relative contributions of *A. hydrophila* including vAh ST251, *A. dhakensis* and other *Aeromonas* species and strains to MAS outbreaks in striped catfish in Vietnam. Moreover, isolation of more than one *Aeromonas* sp. from the fish sampled in this present study indicates that co-infections may be common in striped catfish, as has been reported for carp (Ran et al., 2018). In this present study, co-isolation of more than one *Aeromonas* sp. isolate was detected in 9/40 fish from which multiple isolates were collected, and this included a single fish (Site 3, Fish 3) from which both *A. dhakensis* ST656 and vAh ST251 were isolated (Supplementary Tables 1, 2). Furthermore, the presence of *Aeromonas* spp. with non-aeromonads in clinical infections

is also not unusual (Fernández-Bravo and Figueras, 2020), with both *A. hydrophila* and *E. ictaluri* co-isolated from individual fish at nurseries in Vietnam (Hoa et al., 2021).

In conclusion, two epidemic lineages of *Aeromonas* were associated with recent outbreaks of MAS in striped catfish in the Mekong Delta of Vietnam, specifically *A. dhakensis* ST656 and vAh ST251. An endpoint PCR to differentiate these strains was designed and validated. The most appropriate and practical methods for continued surveillance of the strains underlying MAS outbreaks include rep-PCR and MLST, where a new approach relying on next-generation sequencing was developed (ngsMLST). Representative isolates of these two key pathogens can be used to develop improved vaccine formulations, including novel vaccines for mucosal delivery, and this forms the focus of a forthcoming study. Such vaccines delivered in feed or by bathing should assist efforts to increase vaccine uptake by farmers in Vietnam, thus reducing need for antibiotic therapy and consequent problems associated with bacterial antibiotic resistance. In turn, this will aid efforts to enhance the environmental sustainability of the striped catfish sector in Vietnam, which supports livelihoods and provides a nutritious animal protein source for people across the world.

Data availability statement

The datasets presented in this study can be found in online repositories. The names of the repository/repositories and accession number(s) can be found in the article/Supplementary material.

Ethics statement

The animal study was reviewed and approved by the University of Stirling Animal Welfare and Ethical Review Body.

Author contributions

KB: conceptualisation, methodology, formal analysis, investigation, data curation, writing—original draft, writing—review and editing, visualization, and funding acquisition. TN: conceptualisation, investigation, resources, writing—review and editing, supervision, project administration, and funding acquisition. MB: conceptualisation, methodology, formal analysis, investigation, data curation, writing—original draft, writing—review and editing, and visualization. DH: investigation, resources, writing—review and editing, and funding acquisition. RH: conceptualisation and writing—review and editing. AA: conceptualisation, methodology, writing—review and editing, supervision, project administration, and funding acquisition. AD: conceptualisation, methodology, formal analysis, data curation, writing—original draft, writing—review and editing, visualization, supervision, project administration, and funding acquisition. All authors contributed to the article and approved the submitted version.

Funding

This work was supported by the GCRF Networks in Vaccines Research and Development which was co-funded by the MRC and BBSRC and is supported by the International Veterinary Vaccinology Network (IVVN). This project was funded by an IVVN Pump-priming Grant.

Conflict of interest

The authors declare that the research was conducted in the absence of any commercial or financial relationships that could be construed as a potential conflict of interest.

Publisher's note

Supplementary material

The Supplementary Material for this article can be found online at: https://www.frontiersin.org/articles/10.3389/fmicb.2022.1067235/full#supplementary-material

References

Adams, A. (2019). Progress, challenges and opportunities in fish vaccine development. *Fish Shellfish Immunol.* 90, 210–214. doi: 10.1016/j.fsi.2019.04.066

Anyanwu, M. U., Chah, K. F., and Shoyinka, V. S. (2015). Evaluation of pathogenicity of motile *Aeromonas species* in African catfish. *Int. J. Fish. Aquat. Stud.* 2, 93–98.

Aravena-Román, M., Harnett, G. B., Riley, T. V., Inglis, T. J. J., and Chang, B. J. (2011). *Aeromonas aquariorum* is widely distributed in clinical and environmental specimens and can be misidentified as *Aeromonas hydrophila*. *J. Clin. Microbiol.* 49, 3006–3008. doi: 10.1128/JCM.00472-11

Awan, F., Dong, Y., Liu, J., Wang, N., Mushtaq, M. H., Lu, C., et al. (2018). Comparative genome analysis provides deep insights into *Aeromonas hydrophila* taxonomy and virulence-related factors. *BMC Genomics* 19, 712. doi: 10.1186/s12864-018-5100-4

Azzam-Sayuti, M., Ina-Salwany, M. Y., Zamri-Saad, M., Annas, S., Liles, M. R., Xu, T., et al. (2022). Draft genome sequence of myo-inositol utilizing *Aeromonas dhakensis* 1P11S3 isolated from striped catfish (*Pangasianodon hypopthalmus*) in a local fish farm in Malaysia. *Data Brief* 41, 107974. doi: 10.1016/j.dib.2022.107974

Azzam-Sayuti, M., Ina-Salwany, M. Y., Zamri-Saad, M., Yusof, M. T., Annas, S., Najihah, M. Y., et al. (2021). The prevalence, putative virulence genes and antibiotic resistance profiles of *Aeromonas* spp. isolated from cultured freshwater fishes in peninsular Malaysia. *Aquaculture* 540, 736719. doi: 10.1016/j.aquaculture.2021.736719

Bankevich, A., Nurk, S., Antipov, D., Gurevich, A. A., Dvorkin, M., Kulikov, A. S., et al. (2012). SPAdes: a new genome assembly algorithm and its applications to single-cell sequencing. *J. Comput. Biol.* 19, 455–477. doi: 10.1089/cmb.2012.0021

Bartie, K. L., Austin, F. W., Diab, A., Dickson, C., Dung, T. T., Giacomini, M., et al. (2012). Intraspecific diversity of *Edwardsiella ictaluri* isolates from diseased freshwater catfish, *Pangasianodon hypophthalmus* (Sauvage), cultured in the Mekong Delta, Vietnam. *J. Fish Dis.* 35, 671–682. doi: 10.1111/j.1365-2761.2012.01376.x

Batra, P., Mathur, P., and Misra, M. C. (2016). *Aeromonas* spp.: an emerging nosocomial pathogen. *J. Lab. Phys.* 8, 1–4. doi: 10.4103/0974-2727.176234

Bayliss, S. C., Thorpe, H. A., Coyle, N. M., Sheppard, S. K., and Feil, E. J. (2019). PIRATE: a fast and scalable pangenomics toolbox for clustering diverged orthologues in bacteria. *GigaScience* 8, giz119. doi: 10.1093/gigascience/giz119

Bayliss, S. C., Verner-Jeffreys, D. W., Bartie, K. L., Aanensen, D. M., Sheppard, S. K., Adams, A., et al. (2017). The promise of whole genome pathogen sequencing for the molecular epidemiology of emerging aquaculture pathogens. *Front. Microbiol.* 8, 121. doi: 10.3389/fmicb.2017.00121

Beaz-Hidalgo, R., and Figueras, M. J. (2013). *Aeromonas* spp. whole genomes and virulence factors implicated in fish disease. *J. Fish Dis.* 36, 371–388. doi: 10.1111/jfd.12025

Beaz-Hidalgo, R., Martínez-Murcia, A., and Figueras, M. J. (2013). Reclassification of *Aeromonas hydrophila* subsp. *dhakensis* Huys et al. 2002 and *Aeromonas aquariorum* Martínez-Murcia et al. 2008 as *Aeromonas dhakensis* sp. nov. comb nov. and emendation of the species *Aeromonas hydrophila*. *Syst. Appl. Microbiol.* 36, 171–176. doi: 10.1016/j.syapm.2012.12.007

Brunton, L. A., Desbois, A. P., Garza, M., Wieland, B., Mohan, C. V., Hsler, B., et al. (2019). Identifying hotspots for antibiotic resistance emergence and selection, and elucidating pathways to human exposure: application of a systems-thinking approach to aquaculture systems. *Sci. Total Environ.* 687, 1344–1356. doi: 10.1016/j.scitotenv.2019.06.134

Carattoli, A., Zankari, E., García-Fernández, A., Larsen, M. V., Lund, O., Villa, L., et al. (2014). *In silico* detection and typing of plasmids using PlasmidFinder and plasmid multilocus sequence typing. *Antimicrob. Agents Chemother.* 58, 3895–3903. doi: 10.1128/AAC.02412-14

Chen, P.-L., Lamy, B., and Ko, W.-C. (2016). *Aeromonas dhakensis*, an increasingly recognized human pathogen. *Front. Microbiol.* 7, 793. doi: 10.3389/fmicb.2016.00793

Chen, S., Zhou, Y., Chen, Y., and Gu, J. (2018). fastp: an ultra-fast all-in-one FASTQ preprocessor. *Bioinformatics* 34, i884-i890. doi: 10.1093/bioinformatics/bty560

Chen, Y., Frazzitta, A. E., Litvintseva, A. P., Fang, C., Mitchell, T. G., Springer, D. J., et al. (2015). Next generation multilocus sequence typing (NGMLST) and the analytical software program MLSTEZ enable efficient, cost-effective, high-throughput, multilocus sequencing typing. *Fungal Genet. Biol.* 75, 64–71. doi: 10.1016/j.fgb.2015.01.005

Ciufo, S., Kannan, S., Sharma, S., Badretdin, A., Clark, K., Turner, S., et al. (2018). Using average nucleotide identity to improve taxonomic assignments in prokaryotic genomes at the NCBI. *Int. J. Syst. Evol. Microbiol.* 68, 2386–2392. doi: 10.1099/ijsem.0.002809

da Silva Filho, A. C., Marchaukoski, J. N., Raittz, R. T., De Pierri, C. R., de Jesus Soares Machado, D., Fadel-Picheth, C. M. T., et al. (2021). Prediction and analysis *in silico* of genomic islands in *Aeromonas hydrophila*. *Front. Microbiol.* 12, 769380. doi: 10.3389/fmicb.2021.769380

Dang, L. T., Nguyen, L.-H. T., Pham, V. T., and Bui, H. T. T. (2021). Usage and knowledge of antibiotics of fish farmers in smallscale freshwater aquaculture in the Red River Delta, Vietnam. *Aquacult. Res.* 52, 3580–3590. doi: 10.1111/are.15201

de Melo, B. S. T., Mendes-Marques, C. L., de Lima Campos, T., de Almeida, A. M. P., Leal, N. C., and Xavier, D. E. (2019). High-resolution genome-wide analysis is essential for the identification of ambiguous *Aeromonas strains*. *FEMS Microbiol. Lett.* 366, fnz245. doi: 10.1093/femsle/fnz245

Dien, L. T., Ngo, T. P. H., Nguyen, T. V., Kayansamruaj, P., Salin, K. R., Mohan, C. V., et al. (2022). Nonantibiotic approaches to combat motile *Aeromonas* infections in aquaculture: current state of knowledge and future perspectives. *Rev. Aquac.* 15, 333–366. doi: 10.1111/raq.12721

Ding, W., Baumdicker, F., and Neher, R. A. (2018). panX: pan-genome analysis and exploration. *Nucleic Acids Res.* 46, e5. doi: 10.1093/nar/gkx977

Dong, H. T., Techatanakitarnan, C., Jindakittikul, P., Thaiprayoon, A., Taengphu, S., Charoensapsri, W., et al. (2017). *Aeromonas jandaei* and *Aeromonas veronii* caused disease and mortality in Nile tilapia, *Oreochromis niloticus* (L.). *J. Fish Dis.* 40, 1395–1403. doi: 10.1111/jfd.12617

Du, X., Wang, M., Zhou, H., Li, Z., Xu, J., Li, Z., et al. (2021). Comparison of the multiple platforms to identify various *Aeromonas species*. *Front. Microbiol.* 11, 625961. doi: 10.3389/fmicb.2020.625961

Esteve, C., Alcaide, E., and Blasco, M. D. (2012). *Aeromonas hydrophila* subsp. dhakensis isolated from feces, water and fish in mediterranean Spain. *Microbes Environ.* 27, 367–373. doi: 10.1264/jsme2.ME12009

Feldgarden, M., Brover, V., Haft, D. H., Prasad, A. B., Slotta, D. J., Tolstoy, I., et al. (2020). Validating the AMRFinder tool and resistance gene database by using antimicrobial resistance genotype-phenotype correlations in a collection of isolates. *Antimicrob. Agents Chemother.* 64, e00483-e00419. doi: 10.1128/AAC.00361-20

Fernández-Bravo, A., and Figueras, M. J. (2020). An update on the genus *Aeromonas*: taxonomy, epidemiology, and pathogenicity. *Microorganisms* 8, 129. doi: 10.3390/microorganisms8010129

Galardini, M., Biondi, E. G., Bazzicalupo, M., and Mengoni, A. (2011). CONTIGuator: a bacterial genomes finishing tool for structural insights on draft genomes. *Source Code Biol. Med.* 6, 11. doi: 10.1186/1751-0473-6-11

Griffin, M. J., Goodwin, A. E., Merry, G. E., Liles, M. R., Williams, M. A., Ware, C., et al. (2013). Rapid quantitative detection of *Aeromonas hydrophila* strains associated with disease outbreaks in catfish aquaculture. *J. Vet. Diagn. Invest.* 25, 473–481. doi: 10.1177/1040638713494210

Guindon, S., Dufayard, J.-F., Lefort, V., Anisimova, M., Hordijk, W., and Gascuel, O. (2010). New algorithms and methods to estimate maximum-likelihood phylogenies: assessing the performance of PhyML 3.0. *Syst. Biol.* 59, 307–321. doi: 10.1093/sysbio/syq010

Guo, S., Yang, Q., Feng, J., Duan, L., and Zhao, J. (2016). Phylogenetic analysis of the pathogenic genus *Aeromonas* spp. isolated from diseased eels in China. *Microb. Pathog.* 101, 12–23. doi: 10.1016/j.micpath.2016.10.016

Hadfield, J., Croucher, N. J., Goater, R. J., Abudahab, K., Aanensen, D. M., and Harris, S. R. (2018). Phandango: an interactive viewer for bacterial population genomics. *Bioinformatics* 34, 292–293. doi: 10.1093/bioinformatics/btx610

Hasan, M. R., and Shipton, T. A. (2021). Aquafeed value chain analysis of striped catfish in Vietnam. *Aquaculture* 541, 736798. doi: 10.1016/j.aquaculture.2021.736798

Hoa, T. T. T., Boerlage, A. S., Duyen, T. T. M., Thy, D. T. M., Hang, N. T. T., Humphry, R. W., et al. (2021). Nursing stages of striped catfish (*Pangasianodon hypophthalmus*) in Vietnam: pathogens, diseases and husbandry practices. *Aquaculture* 533, 736114. doi: 10.1016/j.aquaculture.2020.736114

Hoai, T. D., Trang, T. T., Tuyen, N. V., Giang, N. T. H., and Van, K. V. (2019). *Aeromonas veronii* caused disease and mortality in channel catfish in Vietnam. *Aquaculture* 513, 734425. doi: 10.1016/j.aquaculture.2019.734425

Hossain, M. J., Waldbieser, G. C., Sun, D., Capps, N. K., Hemstreet, W. B., Carlisle, K., et al. (2013). Implication of lateral genetic transfer in the emergence of *Aeromonas hydrophila* isolates of epidemic outbreaks in channel catfish. *PLoS ONE* 8, e80943. doi: 10.1371/journal.pone.0080943

Huys, G., Kmpfer, P., Albert, M. J., Khn, I., Denys, R., and Swings, J. (2002). *Aeromonas hydrophila* subsp. *dhakensis* subsp. *nov*., isolated from children with diarrhoea in Bangladesh, and extended description of *Aeromonas hydrophila* subsp. *hydrophila* (Chester 1901) Stanier 1943 (approved lists 1980). *Int. J. Syst. Evol. Microbiol.* 52 (Pt. 3), 705–712. doi: 10.1099/00207713-52-3-705

Inouye, M., Dashnow, H., Raven, L.-A., Schultz, M. B., Pope, B. J., Tomita, T., et al. (2014). SRST2: rapid genomic surveillance for public health and hospital microbiology labs. *Genome Med.* 6, 90. doi: 10.1186/s13073-014-0090-6

Ishii, S., and Sadowsky, M. J. (2009). Applications of the rep-PCR DNA fingerprinting technique to study microbial diversity, ecology and evolution. *Environ. Microbiol.* 11, 733–740. doi: 10.1111/j.1462-2920.2008.01856.x

Jagoda, S., Wijewardana, T., Arulkanthan, A., Igarashi, Y., Tan, E., Kinoshita, S., et al. (2014). Characterization and antimicrobial susceptibility of

motile aeromonads isolated from freshwater ornamental fish showing signs of septicaemia. *Dis. Aquat. Organ*. 109, 127–137. doi: 10.3354/dao02733

Jain, C., Rodriguez,-R, L. M., Phillippy, A. M., Konstantinidis, K. T., and Aluru, S. (2018). High throughput ANI analysis of 90K prokaryotic genomes reveals clear species boundaries. *Nat. Commun*. 9, 5114. doi: 10.1038/s41467-018-07641-9

Janda, J. M., and Abbott, S. L. (2010). The genus *Aeromonas*: taxonomy, pathogenicity, and infection. *Clin. Microbiol. Rev*. 23, 35–73. doi: 10.1128/CMR.00039-09

Jolley, K. A., Bliss, C. M., Bennett, J. S., Bratcher, H. B., Brehony, C., Colles, F. M., et al. (2012). Ribosomal multilocus sequence typing: universal characterization of bacteria from domain to strain. *Microbiology* 158(Pt. 4), 1005–1015. doi: 10.1099/mic.0.055459-0

Jolley, K. A., and Maiden, M. C. J. (2010). BIGSdb: scalable analysis of bacterial genome variation at the population level. *BMC Bioinformatics* 11, 595. doi: 10.1186/1471-2105-11-595

Kayansamruaj, P., Areechon, N., and Unajak, S. (2020). Development of fish vaccine in Southeast Asia: a challenge for the sustainability of SE Asia aquaculture. *Fish Shellfish Immunol*. 103, 73–87. doi: 10.1016/j.fsi.2020.04.031

Khor, W. C., Puah, S. M., Koh, T. H., Tan, J. A. M. A., Puthucheary, S. D., and Chua, K. H. (2018). Comparison of clinical isolates of *Aeromonas* from Singapore and Malaysia with regard to molecular identification, virulence, and antimicrobial profiles. *Microb. Drug Resist*., 24, 469–478. doi: 10.1089/mdr.2017.0083

Kitagawa, H., Ohge, H., Yu, L., Kayama, S., Hara, T., Kashiyama, S., et al. (2019). *Aeromonas dhakensis* is not a rare cause of *Aeromonas bacteremia* in Hiroshima, Japan. *J. Infect. Chemother*. 26, 316–320. doi: 10.1016/j.jiac.2019.08.020

Lamy, B., Baron, S., and Barraud, O. (2021). *Aeromonas*: the multifaceted middleman in the one health world. *Curr. Opin. Microbiol*. 65, 24–32. doi: 10.1016/j.mib.2021.09.012

Lau, T. T. V., Tan, J.-A. M. A., Puthucheary, S. D., Puah, S.-M., and Chua, K.-H. (2020). Genetic relatedness and novel sequence types of clinical *Aeromonas dhakensis* from Malaysia. *Braz. J. Microbiol*. 51, 909–918. doi: 10.1007/s42770-020-00239-8

Martinez-Murcia, A. J., Monera, A., Saavedra, M. J., Oncina, R., Lopez-Alvarez, M., Lara, E., et al. (2011). Multilocus phylogenetic analysis of the genus *Aeromonas*. *Syst. Appl. Microbiol*. 34, 189–199. doi: 10.1016/j.syapm.2010.11.014

Martinez-Murcia, A. J., Saavedra, M. J., Mota, V. R., Maier, T., Stackebrandt, E., and Cousin, S. (2008). *Aeromonas aquariorum* sp. nov., isolated from aquaria of ornamental fish. *Int. J. Syst. Evol. Microbiol*. 58 (Pt. 5), 1169–1175. doi: 10.1099/ijs.0.65352-0

Martino, M. E., Fasolato, L., Montemurro, F., Rosteghin, M., Manfrin, A., Patarnello, T., et al. (2011). Determination of microbial diversity of *Aeromonas* strains on the basis of multilocus sequence typing, phenotype, and presence of putative virulence genes. *Appl. Environ. Microbiol*. 77, 4986–5000. doi: 10.1128/AEM.00708-11

Melo-Bolivar, J. F., Sinclair, H. A., and Sidjabat, H. E. (2019). Draft genome sequence of *Aeromonas dhakensis*, isolated from a patient with fatal necrotizing fasciitis. *Microbiol. Resour. Announc*. 8, e00009–19. doi: 10.1128/MRA.00009-19

Mo, W. Y., Chen, Z., Leung, H. M., and Leung, A. O. W. (2015). Application of veterinary antibiotics in China's aquaculture industry and their potential human health risks. *Environ. Sci. Pollut. Res*. 24, 8978–8989. doi: 10.1007/s11356-015-5607-z

Mzula, A., Wambura, P. N., Mdegela, R. H., and Shirima, G. M. (2019). Current state of modern biotechnological-based *Aeromonas hydrophila* vaccines for aquaculture: a systematic review. *Biomed Res. Int*. 2019, 3768948. doi: 10.1155/2019/3768948

Nascimento, M., Sousa, A., Ramirez, M., Francisco, A. P., Carriço, J. A., and Vaz, C. (2017). PHYLOViZ 2.0: providing scalable data integration and visualization for multiple phylogenetic inference methods. *Bioinformatics* 33, 128–129. doi: 10.1093/bioinformatics/btw582

Navarro, A., and Martínez-Murcia, A. (2018). Phylogenetic analyses of the genus *Aeromonas* based on housekeeping gene sequencing and its influence on systematics. *J. Appl. Microbiol*. 125, 622–631. doi: 10.1111/jam.13887

Ngo, T. P., Vu, H. T., Le, T. T., Bui, H. C., Liles, M. R., and Rodkhum, C. (2022). Comparative genomic analysis of hypervirulent *Aeromonas hydrophila* strains from striped catfish (*Pangasianodon hypophthalmus*) in Vietnam. *Aquaculture* 558, 738364. doi: 10.1016/j.aquaculture.2022.738364

Nguyen, H. N. K., Van, T. T. H., Nguyen, H. T., Smooker, P. M., Shimeta, J., and Coloe, P. J. (2014). Molecular characterization of antibiotic resistance in *Pseudomonas* and *Aeromonas* isolates from catfish of the Mekong Delta, Vietnam. *Vet. Microbiol*. 171, 397–405. doi: 10.1016/j.vetmic.2014.01.028

Nguyen, T. A. T., and Jolly, C. M. (2020). Global value chain and food safety and quality standards of Vietnam pangasius exports. *Aquacult. Rep*. 16, 100256. doi: 10.1016/j.aqrep.2019.100256

Nhung, P. H., Hata, H., Ohkusu, K., Noda, M., Shah, M. M., Goto, K., et al. (2007). Use of the novel phylogenetic marker dnaJ and DNA-DNA hybridization to clarify interrelationships within the genus *Aeromonas*. *Int. J. Syst. Evol. Microbiol*. 57, 1232–1237. doi: 10.1099/ijs.0.64957-0

Nowicki, M., Bzhalava, D., and BaLa, P. (2018). Basic local alignment search tool. *J. Comput. Biol*. 25, 403–410. doi: 10.1089/cmb.2018.0079

Pang, M., Jiang, J., Xie, X., Wu, Y., Dong, Y., Kwok, A. H. Y., et al. (2015). Novel insights into the pathogenicity of epidemic *Aeromonas hydrophila* ST251 clones from comparative genomics. *Sci. Rep*. 5, 9833. doi: 10.1038/srep09833

Pessoa, R. B. G., de Oliveira, W. F., Marques, D. S. C., dos Santos Correia, M. T., de Carvalho, E. V. M. M., and Coelho, L. C. B. B. (2019). The genus *Aeromonas*: a general approach. *Microb. Pathog*. 130, 81–94. doi: 10.1016/j.micpath.2019.02.036

Phu, T. M., Phuong, N. T., Dung, T. T., Hai, D. M., Son, V. N., Rico, A., et al. (2016). An evaluation of fish health-management practices and occupational health hazards associated with *Pangasius* catfish (*Pangasianodon hypophthalmus*) aquaculture in the Mekong Delta, Vietnam. *Aquacult. Res*. 47, 2778–2794. doi: 10.1111/are.12728

Phuong, N. T., and Oanh, D. T. H. (2010). "Striped catfish aquaculture in Vietnam: a decade of unprecedented development," in *Success Stories in Asian Aquaculture*. Eds. S. S. De Silva and F. B. Davy (Dordrecht: Springer), 131–147. doi: 10.1007/978-90-481-3087-0_7

Pollard, D. R., Johnson, W. M., Lior, H., Tyler, S. D., and Rozee, K. R. (1990). Detection of the aerolysin gene in *Aeromonas hydrophila* by the polymerase chain reaction. *J. Clin. Microbiol*. 47, 2477–2481. doi: 10.1128/jcm.28.11.2477-2481.1990

Poobalane, S., Thompson, K. D., Ardó, L., Verjan, N., Han, H.-J., Jeney, G., et al. (2010). Production and efficacy of an *Aeromonas hydrophila* recombinant S-layer protein vaccine for fish. *Vaccine* 28, 3540–3547. doi: 10.1016/j.vaccine.2010.03.011

R Core Team (2022). *R: A Language and Environment for Statistical Computing*. R Foundation for Statistical Computing, v4.2.0. Available online at: https://www.r-project.org/

Ran, C., Qin, C., Xie, M., Zhang, J., Li, J., Xie, Y., et al. (2018). *Aeromonas veronii* and aerolysin are important for the pathogenesis of motile aeromonad septicemia in cyprinid fish. *Environ. Microbiol*. 20, 3442–3456. doi: 10.1111/1462-2920.14390

Rasmussen-Ivey, C. R., Hossain, M. J., Odom, S. E., Terhune, J. S., Hemstreet, W. G., Shoemaker, C. A., et al. (2016). Classification of a hypervirulent *Aeromonas hydrophila* pathotype responsible for epidemic outbreaks in warm-water fishes. *Front. Microbiol*. 7, 1615. doi: 10.3389/fmicb.2016.01615

Riaz, T., Shehzad, W., Viari, A., Pompanon, F., Taberlet, P., and Coissac, E. (2011). ecoPrimers: inference of new DNA barcode markers from whole genome sequence analysis. *Nucleic Acids Res*. 39, e145-e145. doi: 10.1093/nar/gkr732

Rico, A., Phu, T. M., Satapornvanit, K., Min, J., Shahabuddin, A., Henriksson, P. J., et al. (2013). Use of veterinary medicines, feed additives and probiotics in four major internationally traded aquaculture species farmed in Asia. *Aquaculture* 412–413, 231–243. doi: 10.1016/j.aquaculture.2013.07.028

Russell, D. J. (2014). "GramAlign: fast alignment driven by grammar-based phylogeny," in *Multiple Sequence Alignment Methods, Vol. 1079*, ed D. J. Russell (Totowa, NJ: Humana Press), 171–189. doi: 10.1007/978-1-62703-646-7_11

Sakulworakan, R., Chokmangmeepisarn, P., Dinh-Hung, N., Sivaramasamy, E., Hirono, I., Chuanchuen, R., et al. (2021). Insight into whole genome of *Aeromonas veronii* isolated from freshwater fish by resistome analysis reveal extensively antibiotic resistant traits. *Front. Microbiol*. 12, 733668. doi: 10.3389/fmicb.2021.733668

Seemann, T. (2020). *ABRicate. Github, v1.0.0.0*. Available online at: https://github.com/tseemann/abricate

Seemann, T. (2022). *MLST. Github*, *v2.19.0*. Available online at: https://github.com/tseemann/mlst

Soto-Rodriguez, S., Cabanillas-Ramos, J., Alcaraz, U., Gomez-Gil, B., and Romalde, J. (2013). Identification and virulence of *Aeromonas dhakensis, Pseudomonas mosselii* and *Microbacterium paraoxydans* isolated from Nile tilapia, *Oreochromis niloticus*, cultivated in Mexico. *J. Appl. Microbiol*. 115, 654–662. doi: 10.1111/jam.12280

Stratev, D., and Odeyemi, O. A. (2017). An overview of motile *Aeromonas septicaemia* management. *Aquacult. Int*. 25, 1095–1105. doi: 10.1007/s10499-016-0100-3

Ström, G. H., Björklund, H., Barnes, A. C., Da, C. T., Nhi, N. H. Y., Lan, T. T., et al. (2019). Antibiotic use by small-scale farmers for freshwater aquaculture in the upper Mekong Delta, Vietnam. *J. Aquat. Anim. Health* 31, 290–298. doi: 10.1002/aah.10084

Sun, Y., Zhao, Y., Xu, W., Fang, R., Wu, Q., He, H., et al. (2021). Taxonomy, virulence determinants and antimicrobial susceptibility of *Aeromonas* spp. isolated from bacteremia in southeastern China. *Antimicrob. Resist. Infect. Control* 10, 43. doi: 10.1186/s13756-021-00911-0

Tanizawa, Y., Fujisawa, T., and Nakamura, Y. (2018). DFAST: a flexible prokaryotic genome annotation pipeline for faster genome publication. *Bioinformatics* 34, 1037–1039. doi: 10.1093/bioinformatics/btx713

Trakhna, F., Harf-Monteil, C., AbdelNour, A., Maaroufi, A., and Gadonna-Widehem, P. (2009). Rapid *Aeromonas hydrophila* identification by TaqMan PCR assay: comparison with a phenotypic method. *Lett. Appl. Microbiol.* 49, 186–190. doi: 10.1111/j.1472-765X.2009.02635.x

Truong, D. B., Doan, H. P., Tran, V. K. D., Nguyen, V. C., Bach, T. K., Rueanghiran, C., et al. (2019). Assessment of drivers of antimicrobial usage in poultry farms in the Mekong Delta of Vietnam: a combined participatory epidemiology and Q-sorting approach. *Front. Vet. Sci.* 6, 84. doi: 10.3389/fvets.2019.00084

Tung, V. T., Phuong, T. D., Phuong, L. T. K., Phuc, N. T., Nygaard, A., Hunderholdt, L. B., et al. (2014). *Immunogenic Composition Against Aeromonas hydrophila*. International Patent No WO 2014/064217 A1. World International Patent Organization.

Walker, B. J., Abeel, T., Shea, T., Priest, M., Abouelliel, A., Sakthikumar, S., et al. (2014). Pilon: an integrated tool for comprehensive microbial variant detection and genome assembly improvement. *PLoS ONE* 9, e112963. doi: 10.1371/journal.pone.0112963

Weisburg, W. G., Barns, S. M., Pelletier, D. A., and Lane, D. J. (1991). 16s ribosomal DNA amplification for phylogenetic study. *J. Bacteriol.* 173, 697–703. doi: 10.1128/jb.173.2.697-703.1991

Wick, R. R., Judd, L. M., Gorrie, C. L., and Holt, K. E. (2017). Unicycler: resolving bacterial genome assemblies from short and long sequencing reads. *PLoS Comput. Biol.* 13, e1005595. doi: 10.1371/journal.pcbi.1005595

Wu, C.-J., Wang, H.-C., Chen, C.-S., Shu, H.-Y., Kao, A.-W., Chen, P.-L., et al. (2012). Genome sequence of a novel human pathogen, *Aeromonas aquariorum*. *J. Bacteriol.* 194, 4114–4115. doi: 10.1128/JB.00621-12

Wu, C.-J., Wang, H.-C., Chen, P.-L., Chang, M.-C., Sun, H. S., Chou, P.-H., et al. (2013). AQU-1, a chromosomal class C β-lactamase, among clinical *Aeromonas dhakensis* isolates: distribution and clinical significance. *Int. J. Antimicrob. Agents* 42, 456–461. doi: 10.1016/j.ijantimicag.2013.08.002

Yi, S.-W., Chung, T.-H., Joh, S.-J., Park, C., Park, B.-Y., and Shin, G.-W. (2014). High prevalence of BlaCTX-M group genes in *Aeromonas dhakensis* isolated from aquaculture fish species in South Korea. *J. Vet. Med. Sci.* 76, 1589–1593. doi: 10.1292/jvms.14-0274

frontiers | Frontiers in Microbiology

TYPE Original Research
PUBLISHED 16 February 2023
DOI 10.3389/fmicb.2023.1101111

OPEN ACCESS

EDITED BY
Zhenyu Zhang,
University of Wisconsin-Madison,
United States

REVIEWED BY
Edward Pajarillo,
Florida Agricultural and Mechanical University,
United States
Sooyeon Song,
Jeonbuk National University,
Republic of Korea

*CORRESPONDENCE
Wenbin Bao
✉ wbbao@yzu.edu.cn

†These authors have contributed equally to this work

SPECIALTY SECTION
This article was submitted to Infectious Agents and Disease, a section of the journal Frontiers in Microbiology

RECEIVED 20 November 2022
ACCEPTED 30 January 2023
PUBLISHED 16 February 2023

CITATION
Qin W, Xie Y, Ren Z, Xu C, Sun M-a, Yin Z and Bao W (2023) Integrative ATAC-seq and RNA-seq analyses of IPEC-J2 cells reveals porcine transcription and chromatin accessibility changes associated with *Escherichia coli* F18ac inhibited by *Lactobacillus reuteri*. *Front. Microbiol.* 14:1101111. doi: 10.3389/fmicb.2023.1101111

Integrative ATAC-seq and RNA-seq analyses of IPEC-J2 cells reveals porcine transcription and chromatin accessibility changes associated with *Escherichia coli* F18ac inhibited by *Lactobacillus reuteri*

Weiyun Qin[1,2†], Yunxiao Xie[1†], Zhanshi Ren[1], Chao Xu[1], Ming-an Sun[2], Zongjun Yin[3] and Wenbin Bao[1*]

[1]College of Animal Science and Technology, Yangzhou University, Yangzhou, China, [2]College of Veterinary Medicine, Institute of Comparative Medicine, Yangzhou University, Yangzhou, China, [3]College of Animal Science and Technology, Anhui Agricultural University, Hefei, Anhui, China

Escherichia coli is the main cause of postweaning diarrhea in pigs, leading to economic loss. As a probiotic, *Lactobacillus reuteri* has been used to inhibit *E. coli* in clinical applications; however, its integrative interactions with hosts remain unclear, especially in pigs. Here, we found that *L. reuteri* effectively inhibited *E. coli* F18ac adhering to porcine IPEC-J2 cells, and explored the genome-wide transcription and chromatin accessibility landscapes of IPEC-J2 cells by RNA-seq and ATAC-seq. The results showed that some key signal transduction pathways, such as PI3K-AKT and MAPK signaling pathways, were enriched in the differentially expressed genes (DEGs) between *E. coli* F18ac treatment with and without *L. reuteri* groups. However, we found less overlap between RNA-seq and ATAC-seq datasets; we speculated that this might be caused by histones modification through ChIP-qPCR detection. Furthermore, we identified the regulation of the actin cytoskeleton pathway and a number of candidate genes (*ARHGEF12*, *EGFR*, and *DIAPH3*) that might be associated with the inhibition of *E. coli* F18ac adherence to IPEC-J2 cells by *L. reuteri*. In conclusion, we provide a valuable dataset that can be used to seek potential porcine molecular markers of *E. coli* F18ac pathogenesis and *L. reuteri* antibacterial activity, and to guide the antibacterial application of *L. reuteri*.

KEYWORDS

diarrhea, *Lactobacillus reuteri*, *Escherichia coli* F18ac, chromatin accessibility, transcriptome

1. Introduction

Bacterial diarrhea is one of the most serious causes of postweaning diarrhea (PWD), which endangers the sustainable development of the pig industry in China and is especially harmful to the health of piglets (Wu et al., 2016). Bacterial diarrhea is mainly caused by pathogenic *Escherichia coli* F18. Several of its common clinical symptoms include diarrhea, decreased growth velocity, weight loss, and death (Moxley and Duhamel, 1999). Porcine pathogenic *E. coli* strains harbor specific colonization factors, including fimbrial adhesins F18 and F4 (K88; Fairbrother et al., 2005). There are 2 closely related antigenic variants of F18, F18ab, and F18ac. While F18ab-positive strains are known to be associated with edema disease, *E. coli*-carrying F18ac are known to cause diarrhea

(DebRoy et al., 2009). The development of resistance to widely used antibiotics in a variety of *E. coli*, as well as the increased prevalence and gravity of postweaning syndrome, urgently require the use of alternative strategies to control them (Fairbrother et al., 2005). Of the probiotics and postbiotics used as substitutes for antibiotics, of particular interest are the bacteriocinogenic probiotics, that is, bacterial strains capable of producing bacteriocins that confer health benefits to the host.

Lactobacillus reuteri is a gram-positive bacterium belong to *Firmicutes*, *Bacilli*, *Lactobacillales*, *Lactobacillaceae*, *Limosilactobacillus* (Zheng et al., 2020), which can colonize in gastrointestinal tract and then has a variety of beneficial effects on diarrhea, intestinal infection, inflammatory bowel syndrome (IBS), inflammatory bowel disease (IBD), and colorectal cancer (Lebeer et al., 2008; Dore et al., 2014; Mu et al., 2018; Dore et al., 2019). *L. reuteri* may be a useful, safe, and supportive measure for the treatment and prevention of diarrhea, reducing both the duration and the intensity of diarrhea symptoms, having beneficial health effects (Szajewska et al., 2014). *L. reuteri* ATCC 53608, isolated from pig intestines also has a similar antibacterial effect, which against pathogenic (*Staphylococcus aureus Salmonella enterica* ssp. *enterica*, and *Listeria monocytogenes*), and pathogen surrogate (*Escherichia coli* DH5α) microorganisms (Ortiz-Rivera et al., 2017). However, our understanding of its specific intestinal protection and antibacterial mechanisms is still limited. Notably, oral administration of *L. reuteri* to healthy breastfed mice promoted intestinal immune tolerance and was linked to the proliferation of beneficial gut microbiota (Liu et al., 2019). *L. reuteri* also induced an anti-inflammatory response by affecting the secretion of macrophage-derived cytokines (Dias et al., 2021). Additionally, *L. reuteri*, together with a tryptophan-rich diet, could reprogram intraepithelial CD4(+) T cells into immunoregulatory T cells (Cervantes-Barragan et al., 2017). *L. reuteri* protected the intestinal mucosal barrier integrity by moderately modulating the Wnt/β-catenin pathway to avoid overactivation (Wu et al., 2020). The understanding of these mechanisms and of regulatory changes at the genomic chromatin level remains incomplete.

With the popularization of high-throughput sequencing, revealing changes in host genome-wide chromatin has become possible using sequencing; as a tool, accessible chromatin with next-generation sequencing (ATAC-seq) can be used to detect the unique chromatin landscape associated with a cell type and how it may be altered by perturbation or disease (Grandi et al., 2022). The advantage of ATAC-seq is that it requires only a small number of viable cells and does not require knowledge about transcription factors or epigenetics. In this study, ATAC-seq helped us to actively understand the epigenetic changes that regulate the host during the pathogenic process of *E. coli* F18ac, and how *L. reuei* inhibits *E. coli* F18ac to protect the host cells. We aimed provide unique insights into further understanding of the mechanisms of bacterial interaction with the host at the chromatin level by using ATAC-seq combined with RNA-seq. Our findings also provide a strong reference and basis for the efficient use of the antibacterial properties of *L. reuteri*.

2. Materials and methods

2.1. Bacterial culture

We purchased *L. reuteri* (ATCC 53608) from the China Center of Industrial Culture Collection (CICC) (Beijing, China), which we grew in de Man, Rogosa, and Sharpe (MRS) medium at 37°C for 24 h under anaerobic conditions. *E. coli* F18ac was offered by the veterinary laboratory at the University of Pennsylvania, and was inoculated in Luria-Bertani (LB) medium at 37°C for 24 h. For subsequent cell assays, we collected bacterial cells by centrifugation at 4000 *r*/min for 5 min and washed with phosphate-buffered saline (PBS) buffer three times. Finally, we used Dulbecco's modified eagle medium (DMEM) with 10% fetal bovine serum to resuspend the bacterial cells, which we adjusted to a density of 1×10^7 colony forming units (CFU)/mL *E. coli* F18ac and 1×10^8 CFU/ml of *L. reuteri*.

2.2. Zone of inhibition assay

We evenly distributed *E. coli* F18ac over the surface of the LB plate. After the plate was dried, 200 μL of *L. reuteri* fermentation broth was added into each Oxford cup before the pH was adjusted to 6.0 using NaOH solution, which we transferred to a 37°C incubator for overnight. We compared the inhibition zone diameter values with the prescribed Kirby-Bauer antibiotic testing standard values to determine whether they were resistive, susceptible, or intermediate (Cockerill, 2010).

2.3. Assay of adhesion ability of bacteria to IPEC-J2 cells

We seeded IPEC-J2 cells at a density of 0.7×10^6 cells/mL with DMEM, which we then supplemented with 10% fetal bovine serum. We grew cells to complete confluence, which we subsequently washed three times with PBS and incubated for 4 h in DMEM with *E. coli* F18ac or simultaneously added extra *L. reuteri* (Skjolaas et al., 2007; Liu et al., 2017; Yi et al., 2018). For the control group, we replaced the medium only. We washed unadhered bacteria with PBS five times; then, we digested the culture cells with trypsin. We used colony counting to calculate the number of bacteria.

2.4. Sample collection

Figure 1 shows our sample treatment and sequencing process. We divided 18 samples into three 3: control (CTL) group, *E. coli* F18ac (EC), *L. reuteri* and *E. coli* F18ac (LR + EC) groups. IPEC-J2 cells were seeded into 25 cm^2 cell culture flask at a density of 0.7×10^6 cells/mL. Cells were maintained with DMEM supplemented with 10% fetal bovine serum in a cell incubator (37°C, under 5% CO_2). When the cells were grown to complete confluence, they were incubated for 4 h in DMEM with *E. coli* F18ac or extra *L. reuteri* were simultaneously added, without antibiotics (Skjolaas et al., 2007; Liu et al., 2017; Yi et al., 2018). In the control group, only the medium was replaced. We collected three replicate samples for ATAC-seq and RNA-seq from each group. We subsequently IPEC-J2 cells collected for high-throughput sequencing.

2.5. RNA-seq library construction

We performed RNA-seq using the following method. Briefly, we generated the libraries with 3 μg of RNA per sample. We used an NEBNext® UltraTM RNA Library Prep Kit for Illumina® (NEB, United States) following the manufacturer's protocols. We used an AMPure XP system (Beckman Coulter, Beverly, United States) to purify

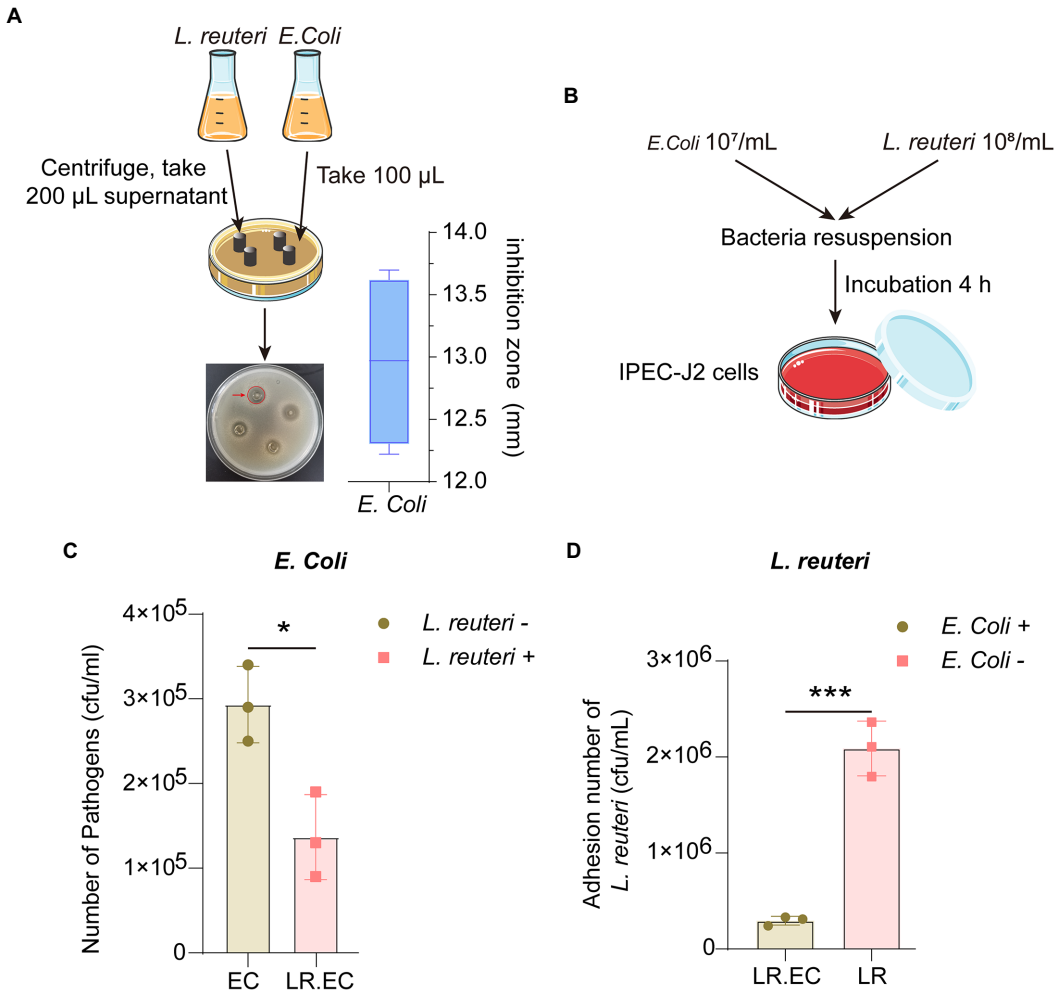

FIGURE 1
Antibacterial effect of *L. reuteri in vitro*. **(A)** Zone diameters of inhibition of *L. reuteri* against *E. coli* F18ac. **(B)** Workflow of adhesion ability assay of bacteria to IPEC-J2 cells. **(C)** Effect of *L. reuteri* on *E. coli* F18ac adhesion to IPEC-J2 cells. **(D)** Adhesion of *L. reuteri* to IPEC-J2 cells in *E. coli* F18ac (vs. control). *$p<0.01$; ***$p<0.001$.

the fragments, from which we selected lengths 250 and 300 bp. Then, we digested cDNA with USER Enzyme (NEB, United States), and subsequently performed PCR. We purified the PCR products and clustered the index-coded samples on an Agilent Bioanalyzer 2,100 system (Agilent Technologies, CA, United States) and a TruSeq PE Cluster Kit v3-cBot-HS (Illumina, CA, United States), respectively. Finally, we performed RNA-seq on an Illumina HiSeq platform according to standardized procedures.

2.6. RNA-seq data processing

We used Trimmomatic to process raw data, including cutting adapter and trimming low-quality bases. We calculated the Q20, Q30, and GC contents. All the subsequent analyses were based on the high-quality data after processing. We obtained the porcine reference genome and all gene annotation data from the Genome website. We built an index of the reference genome, and we aligned paired-end clean reads to the reference genome using Hisat2 (version 2.0.5). We counted the read numbers mapped to each gene. The threshold was set as follows: FDR < 0.05, |fold change| ≥ 2.

2.7. Gene ontology and Kyoto encyclopedia of genes and genomes enrichment analysis

We explored Gene ontology (GO) terms and Kyoto encyclopedia of genes and genomes (KEGG) pathways enriched by the differentially expressed genes (DEGs) or annotated genes from differentially accessible regions (DARs) through GO and KEGG analyses. GO and KEGG enrichment analyses are widely used to reflect the relationship between genes and GO terms and pathways. We calculated the significance level as previously described (Chen et al., 2016).

2.8. ATAC-seq library construction

We performed ATAC-seq for IPEC-J2 cells according to Buenrostro's method (Buenrostro et al., 2013), Briefly, we lysed cells with cold lysis buffer 10 mM tris–HCl (pH 7.4), 10 mM NaCl, 3 mM MgCl2, and 0.1% Tween 20. We enriched DNA sequences in open chromatin regions with Tn5 transcriptase. We suspended the cell nucleus with a Tn5 transcriptase reaction system, and we purified the DNA at 37°C for 30 min. Then, we performed the PCR amplification reaction.

We obtained cleaned up libraries through PCR amplification reactions and then conducted onboard sequencing with the Illumina platform.

2.9. ATAC-seq data analysis

We trimmed the reads in FASTQ format and aligned them to the reference genome of *sus scrofa* (Sscrofa11.1, INSDC Assembly: GCA_000003025.6) using the Bowtie2 software (Langmead and Salzberg, 2012). We used DeepTools (version 2.07; Ramirez et al., 2014) to map the density distribution of each gene. We used MACS2 (version 2.1.1; Zhang et al., 2008) for peak calling extraction. We estimated the empirical false detection rate (FDR), and selected FDR < 0.05 we as the identified peak. We used DESeq2 software (Love et al., 2014) for differential screening of the samples in each group. We used the ChIPseeker package (Yu et al., 2015) for the functional annotation of genome-wide peaks.

2.10. ChIP-qPCR

We fixed IPEC-J2 cells with 1% formaldehyde for 10 min, which we then quenched with 2.5 M glycine for 5 min, and sonicated to fragments of 200–500 bp in length. Subsequently, we incubated the chromatin fragments with anti-H3K4me3 and anti-H3K27ac, sequentially, which we then reverse-crosslinked. We purified ChIP-DNA for qPCR; the primer details are listed in Supplementary Table S1.

2.11. Indirect immunofluorescence assay

Cells were prepared using 24-well culture plates and fixed in 4% paraformaldehyde, blocked with 5% BSA for 2 h after 0.05% Triton X-100 treatment, and incubated 1 h with phalloidin-FITC (1:1000, Abcam). After washing, the cells were stained with DAPI (1,800, Beyotime Biotechnology), and observed and photographed with a fluorescence microscope.

2.12. Statistical analysis and data availability

All the replicates in each group are presented as the mean ± SD. A two-sided Student's *t*-test was used to analyze the differences between two groups. Standard analysis of variance (ANOVA) was used to analyze the differences among three groups. We considered differences as significant at * $p < 0.05$, ** $p < 0.01$, and *** $p < 0.001$.

3. Results

3.1. Effective inhibition of *Escherichia coli* F18ac by *Lactobacillus reuteri in vitro*

Because *L. reuteri* can effectively inhibit *E. coli in vitro*, we first investigated the efficiency of *L. reuteri* inhibition of *E. coli* F18ac *in vitro*. The Oxford cup results showed that the inhibition zone diameter reached 12.97 ± 0.69 mm, which is considered intermediate inhibition (Figure 1A). More importantly, *L. reuteri* acts as a probiotic that inhibits bacteria in the intestine and regulates host cell activity. As an effective intestinal epithelial cell model (Peterson and Artis, 2014), we used IPEC-J2 cells to perform bacterial adhesion assays (Figure 1B), effectively revealing that *L. reuteri* significantly reduced the adhesion level of *E. coli* F18ac to IPEC-J2 cells by *in vitro* occupancy ($p < 0.05$). In contrast, the adhesion level of *L. reuteri* also decreased ($p < 0.001$; Figures 1C,D). Our results indicated that *L. reuteri* effectively inhibited *E. coli* F18ac in IPEC-J2 cells.

3.2. RNA-seq reveals pathways regulated during bacteriostatic process of *Lactobacillus reuteri*

To thoroughly investigate the regulatory mechanism of the antibacterial activity of *L. reuteri*, we performed RNA-seq and ATAC-seq on IPEC-J2 cells with different treatments (Figure 2A). After quality control, we assessed the high-quality raw data (Supplementary Table S2) prior to downstream analysis. The results of PCA showed that each group could be well separated except for LR.EC sample 2 (Supplementary Figures S1A,D). The results of GO and KEGG enrichment analyses showed that the 373 DEGs in the *E. coli* F18a group compared with the control group were most enriched in the transmembrane receptor protein tyrosine kinase signaling pathway (Figure 2B) and the HIF-1 signaling pathway (Figure 2C). We screened only seven DEGs in *E. coli* F18a and *L. reuteri* co-incubation group compared with the *E. coli* F18a group; they were most enriched in cAMP-mediated signaling (Figure 2D) and viral protein interaction with cytokine and cytokine receptor (Figure 2E). Because a few DEGs were enriched after *L. reuteri* treatment, we performed GSEA to find pathways that play critical roles in the antibacterial process of *L. reuteri*. We found 97 upregulated pathways and 11 downregulated pathways between *E. coli* F18ac and the control groups (Figures 3A,C; Supplementary Table S3), and 8 upregulated pathways and 13 downregulated pathways between *E. coli* F18ac with or without *L. reuteri* groups (Figures 3B,D; Supplementary Table S4). Among these, we found 12 pathways that were upregulated after *E. coli* F18ac treatment, then were downregulated after *L. reuteri* treatment, and 4 pathways that were downregulated after *E. coli* F18ac treatment and then upregulated after *L. reuteri* treatment by examining the intersection (Supplementary Figure S2). These pathways may play an important role in the antibacterial process of *L. reuteri*.

3.3. Identification of accessible chromatin in IPEC-J2 cells using ATAC-Seq analysis

We detected the accessible chromatin alterations to explore the antibacterial mechanism of *L. reuteri* with ATAC-seq. The results showed that the density distribution of the reads around TSS were strongly enriched (Supplementary Figure S1E), indicating that the chromatin regions were successfully detected by ATAC-seq. We annotated 4,145 genes by the DARs between *E. coli* F18ac and control groups, and 1,481 genes between *E. coli* F18ac with and without *L. reuteri* groups (Supplementary Figures S1F–G). Then, we enriched these genes by GO and KEGG analyses. Genes in the *E. coli* F18a group compared with the control group were most enriched in the tube morphogenesis and the Human papillomavirus infection (Figures 4A,B). Genes in the *E. coli* F18a and *L. reuteri* coincubation group compared with the *E. coli* F18a group were most substantially enriched in the tumor necrosis factor production and the Human papillomavirus

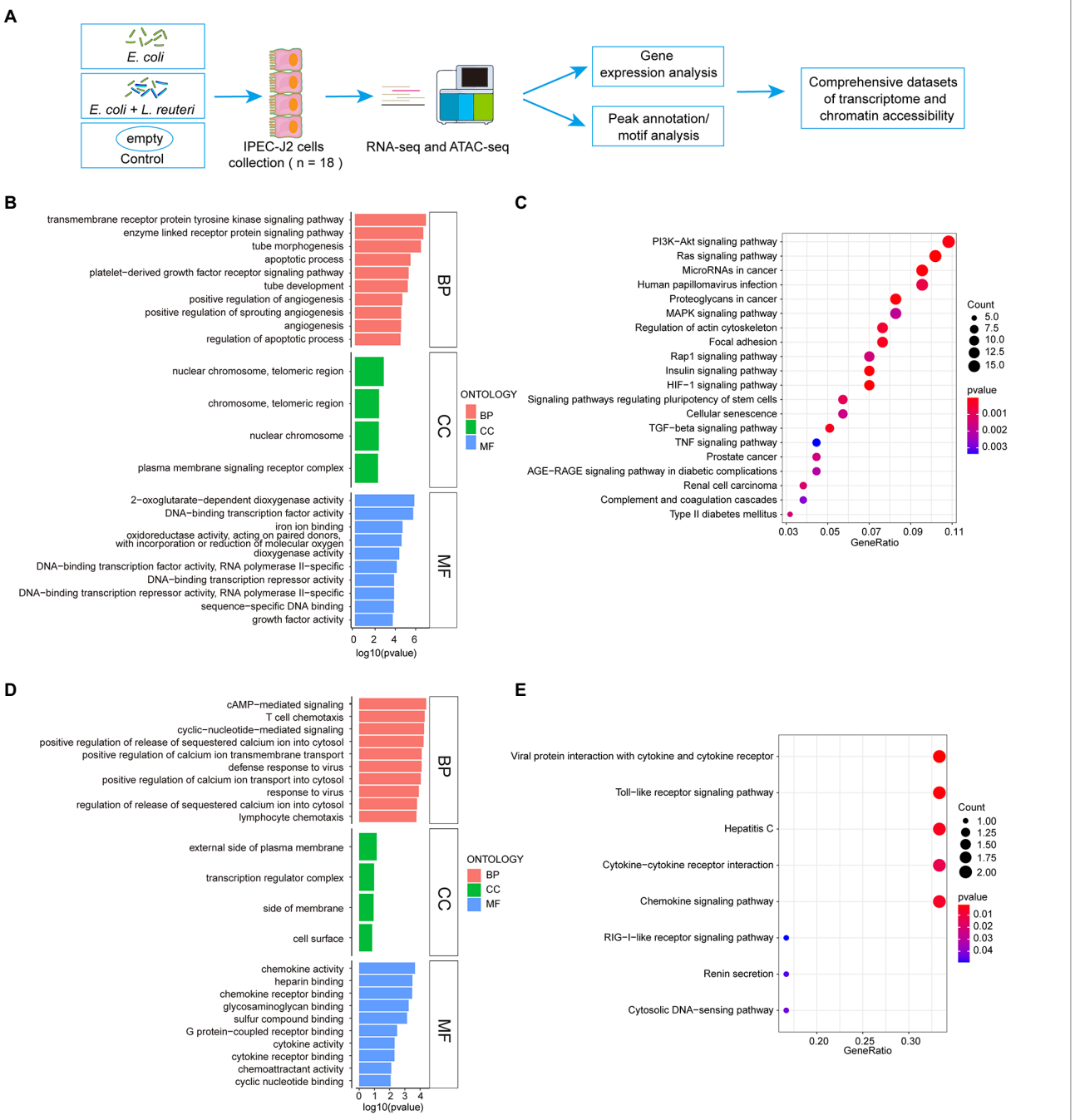

FIGURE 2
Workflow of sequence and enrichment analyses of RNA-seq dataset. **(A)** Workflow of experimental procedure and sequence analysis. **(B,C)** GO and KEGG enrichment analyses between *E. coli* F18ac and control groups. **(D,E)** GO and KEGG enrichment analyses between *E. coli* F18ac with and without *L. reuteri* groups. BP, Biological Process; CC, Cell Component; MF, Molecular Function.

infection (Figures 4C,D). We identified pathways such as the PI3K-AKT and MAPK signaling pathways that were also enriched in the RNA-seq analysis; these pathways are closely related to the cell cycle, apoptosis, and cell communication (Engelman et al., 2006; Ertel and Tozeren, 2008), which may be the important regulatory pathways for the antibacterial effect of *L. reuteri*. Furthermore, 14 genes were intersected between the DEGs and the genes annotated by DARs when we set the threshold at $p < 0.05$ (Figure 5A). The visualization of the DEGs' expression revealed that most of the genes were upregulated after *E. coli* F18ac treatment and downregulated after *L. reuteri*, indicating that *L. reuteri* likely inhibited *E. coli* F18ac by regulating these genes (Figure 5B). However, we noted a low overlap between RNA-seq and ATAC-seq datasets. H3K4me3 and H3K27ac are known to mark active promoters (Calo and Wysocka, 2013), which may lead to changes in chromatin accessibility but do not correspond to differential transcription. Therefore, we investigated the degree of histone H3K4me3 and H3K27ac enrichment of randomly selected genes to explain this phenomenon, and the results showed that H3K4me3 and H3K27ac enrichment increased in regions where chromatin accessibility was not increased, in line with our speculation (Figure 5C).

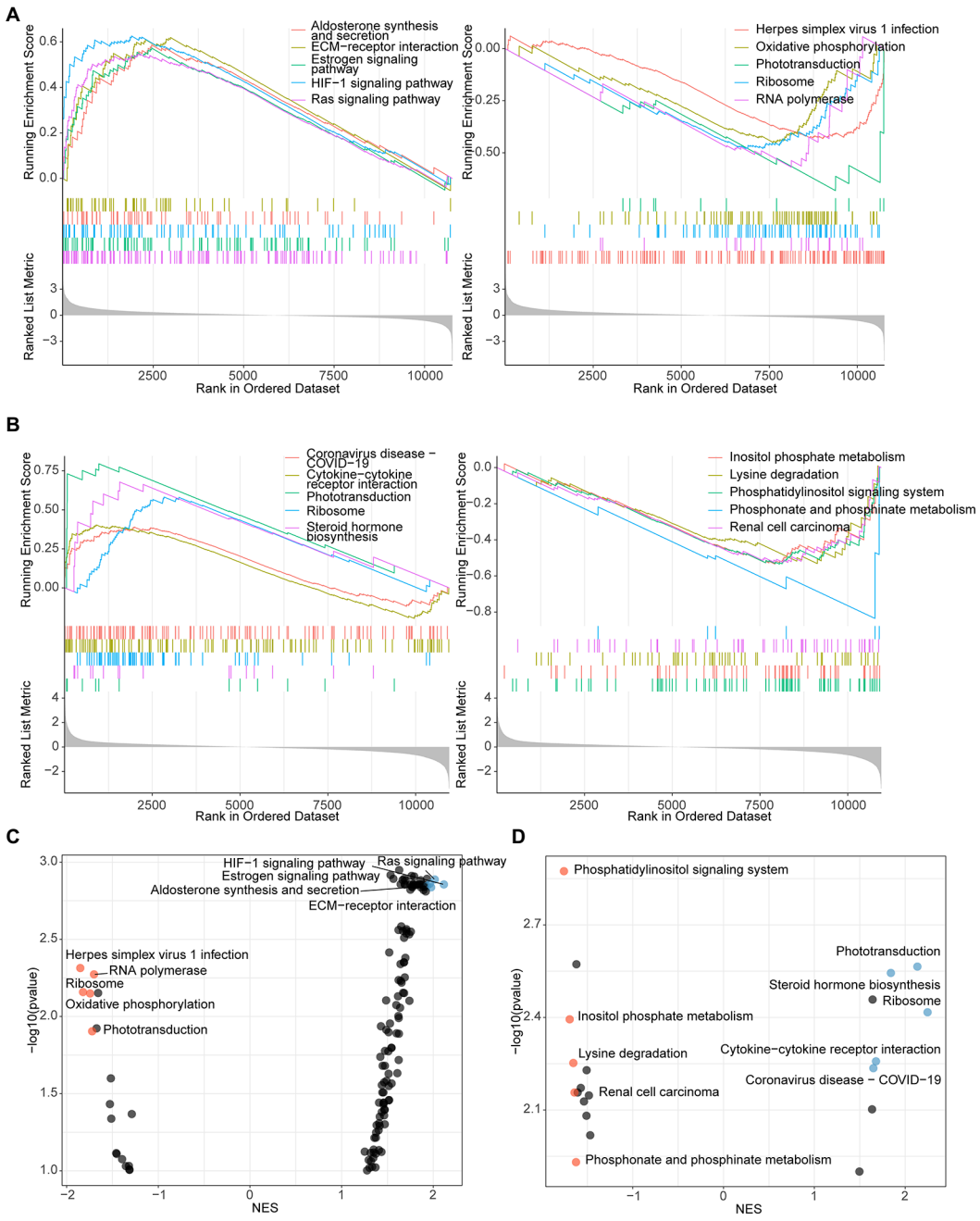

FIGURE 3
GSEA analysis identified pathways that participate in antibacterial process of *L. reuteri*. **(A)** Up- and downregulated enriched genes of top 5 pathways between *E. coli* F18ac and control groups. **(B)** Up- and downregulated enriched genes of top 5 pathways between *E. coli* F18ac with and without *L. reuteri* groups. Dot plots showing the up- and downregulated pathways in descending order on the y-axis by NES: left plot presents pathways compared between *E. coli* F18ac and control groups **(C)**; right plot represents pathways compared between *E. coli* F18ac with and without *L. reuteri* groups **(D)**. Blue and yellow dots indicate top 5 upregulated and downregulated pathways, respectively.

3.4. Regulation of actin cytoskeleton involved in regulation of *Lactobacillus reuteri* mediated bacteriostasis

We focused on the regulation of actin cytoskeleton, which was upregulated after *E. coli* F18ac treatment and downregulated after *L. reuteri* treatment in GSEA (Supplementary Figure S2); some peaks of the pathway genes were also notably altered (Figure 6A). We therefore surveyed the effect of different treatments on F-actin, which is the key downstream molecule. We found that considerably rearrangement and aggregation of F-actin occurred after *E. coli* F18ac treatment, which was alleviated by treatment with *L. reuteri* (Figure 6B). Accordingly, we hypothesized that the regulation of the actin cytoskeleton is one of the important regulatory pathways of *L. reuteri* mediated bacteriostasis. We thereafter visualized the genes of the regulation of the actin cytoskeleton both of the datasets, and then identified *ARHGEF12, EGFR*, and *DIAPH3* as potential key genes for which visualization revealed that their expressions were noticeably higher after *E. coli* F18ac

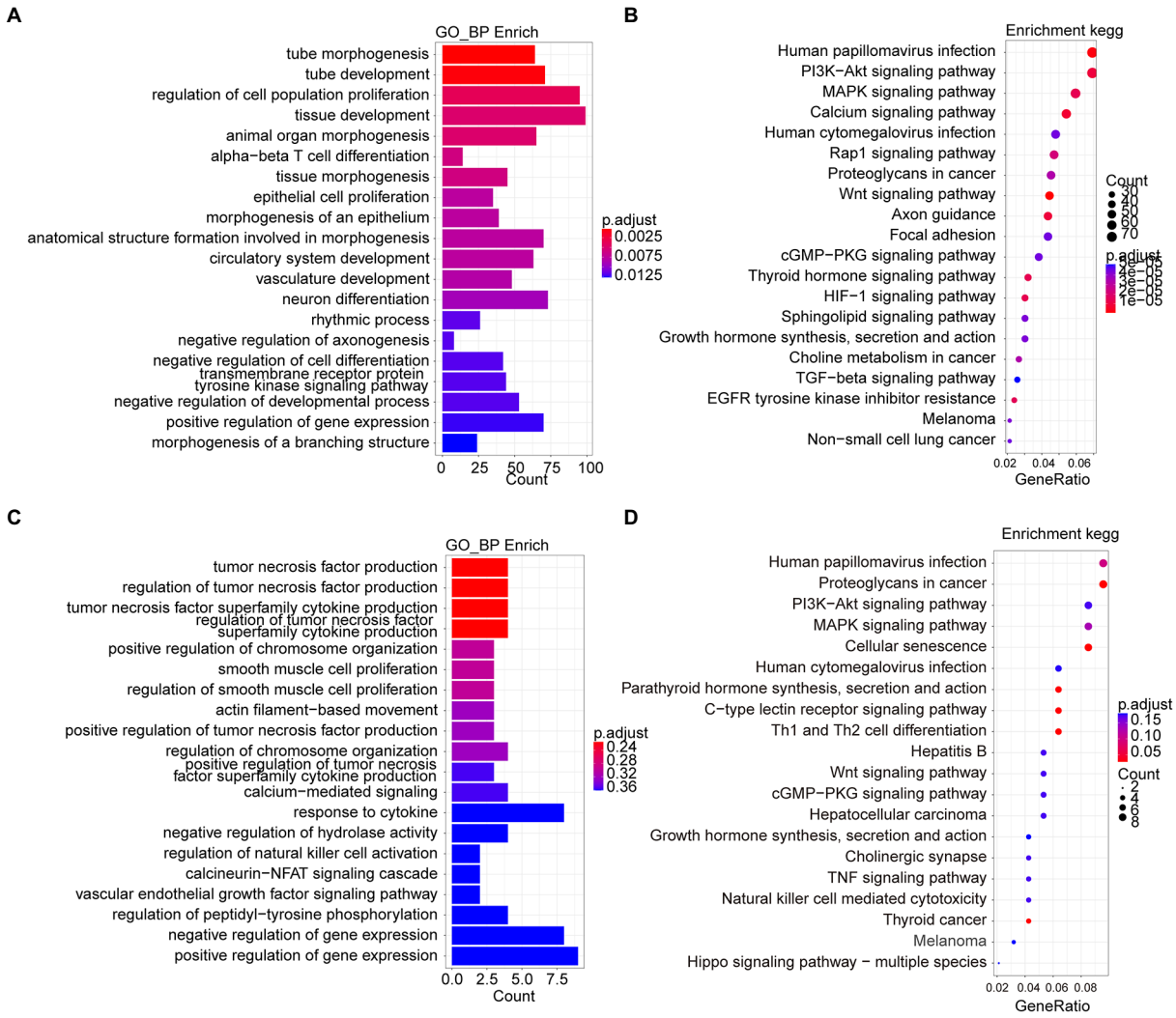

FIGURE 4
Go and KEGG enrichment analyses from ATAC-seq dataset reveal mechanism of antibacterial process of *L. reuteri*. **(A,B)** GO and KEGG enrichment analyses between *E. coli* F18ac and control groups. **(C,D)** GO and KEGG enrichment analyses between *E. coli* F18ac with and without *L. reuteri* groups. Enriched genes were annotated by DARs from ATAC-seq.

treatment. The application of *L. reuteri* restored their expressions (Figure 6C). Enteropathogenic *E. coli* effector EspH can specifically regulate the ARHGEF12 protein, thereby inhibiting the actin cytoskeleton regulated by small G proteins in host cells (Dong et al., 2010). EGFR was identified as a contributor to *E. coli* invasion of the BBB *in vitro* (Wang et al., 2016). Consequently, *ARHGEF12, EGFR,* and *DIAPH3* seem to be critical regulatory molecules in the process of *E. coli* F18ac inhibition by *L. reuteri* (Figure 6D).

4. Discussion

Lactobacillus reuteri, as a probiotic, can be effectively used in the treatment of diarrhea and other symptoms in children in clinical practice, but we do not have a sufficient understanding of the host regulation mechanism during its antibacterial process. In this study, we examined the transcriptome and chromatin accessibility landscape of IPEC-J2 induced by *E. coli* F18ac and the antibacterial process of *L. reuteri* using RNA-seq and ATAC-seq. To the best of our knowledge, this is the first report of the transcriptome and chromatin accessibility landscape, simultaneously showing differential responses of porcine IPEC-J2 cells to infection with *E. coli F*18ac as well as the inhibition by *L. reuteri*. We confirmed that *L. reuteri* has an inhibitory effect on *E. coli F18ac* through *in vitro* antibacterial experiments. *L. reuteri* can inhibit the growth of *E. coli* and thus inhibit the intestinal infections (Mu et al., 2018). IPEC-J2 cells are reference cellular substrates that can provide useful information about the intestinal interaction between host and enteric pathogens (Mariani et al., 2009). We were able to observe the molecule changes in the cellular responses induced by *E. coli* F18ac and *L. reuteri* with the IPEC-J2 model. We found that many of the *E. coli* F18ac induced DEGs and DARs were enriched in some key signaling pathways, one of which was the PI3K-AKT signaling pathway, which is one of the most important intracellular pathways that regulates cell growth, motility, survival, metabolism, and angiogenesis (Engelman et al., 2006; Alzahrani, 2019). Inhibition of the PI3K-AKT signaling pathway can lead to reduced cell proliferation and increased cell death (Hennessy et al., 2005). Another important pathway was the MAPK pathway, which is located downstream of many growth-factor receptors

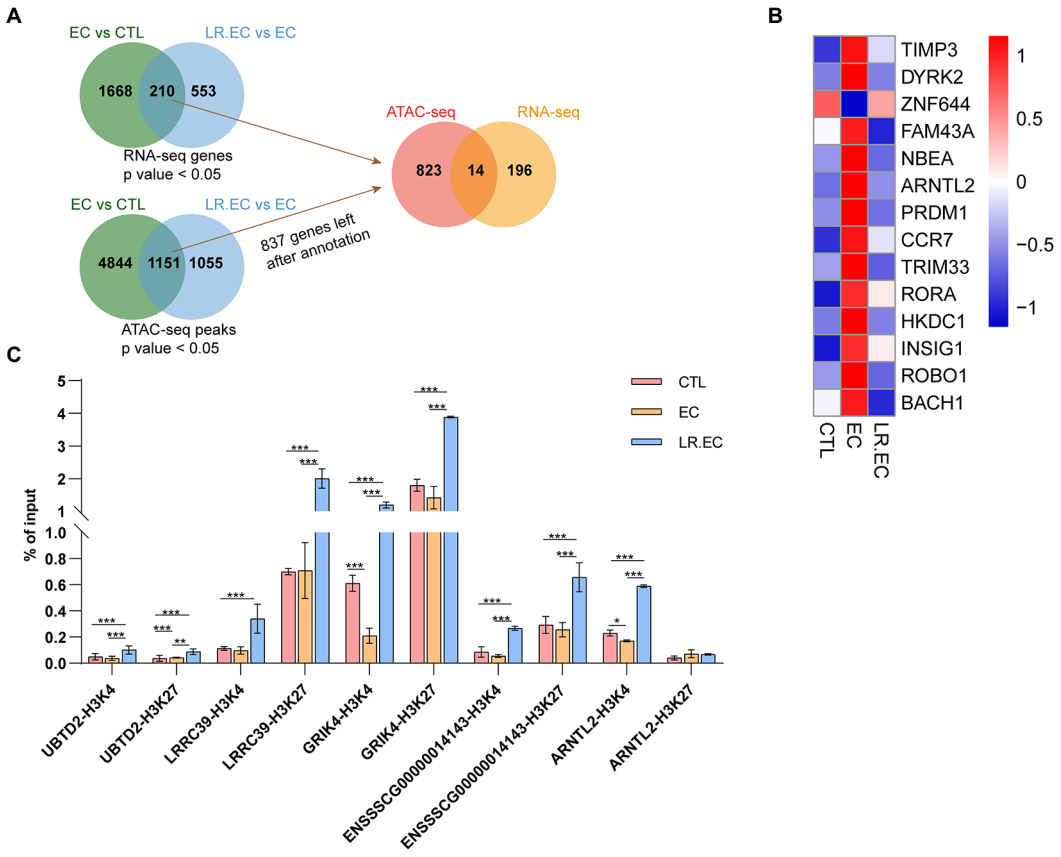

FIGURE 5
Integrative analysis of RNA-Seq and ATAC-Seq datasets. **(A)** Candidate gene were identified in two steps using overlap: the first step was overlap between different compared groups, and the second step was overlap between DEGs from RNA-seq dataset and annotated genes from ATAC-seq dataset. We set the threshold to a *p* value <0.05; we annotated ATAC-seq peaks to genomic features with the chipseeker package, and only 837 genes had gene names after annotation from DARs. **(B)** Heatmap of 14 overlapping genes in different groups. **(C)** Fold changes of histone H3K4me3 and H3K27ac were determined by ChIP-qPCR in chromatin accessible regions of *UBTD2*, *LRRC39*, *GRIK4*, *ENSSSCG00000014143*, and *ARNTL2*. Data are shown as mean±SD. *p<0.05; **p<0.01; ***p<0.001.

(Fang and Richardson, 2005) and hence mediates cell communication with extracellular environments (Ertel and Tozeren, 2008). The abundance of DEGs and DARs within the PI3K-AKT and MAPK pathways suggested that these pathways may be involved in *E. coli* F18ac infection and the antibacterial process of *L. reuteri*.

Next, we investigated transcriptional upstream DEGs, and some genes intersected between ATAC-seq and RNA-seq datasets. However, only 33 genes were intersected, which was unexpected. Among them, *TIMP3* and *CCR7* are involved in the regulation of PI3K/AKT pathway activity (Rodriguez-Fernandez and Criado-Garcia, 2020; Yang et al., 2022), and the PI3K/AKT pathway was also identified in our enrichment analysis. These results suggested that *E. coli* F18ac and *L. reuteri* might be involved in the regulation of PI3K/AKT pathway of host cells through regulation expression of *TIMP3* and *CCR7*. *HKDC1* could regulate the AMPK/mTOR signaling pathway to perform its biological function (Wang et al., 2020). *TRIM33* and *BACH1* could regulate the activation of activation of Wnt/β-catenin (Jiang et al., 2015; Li et al., 2022), and *L. reuteri* protect the intestinal mucosal barrier integrity by moderately modulating the Wnt/β-catenin pathway to avoid overactivation (Wu et al., 2020). *DYRK2*, *RORA* and other genes are also involved in the regulation of cell cycle (Lara-Chica et al., 2022), apoptosis (Li et al., 2022) and other activities. The above studies also fully confirmed that these candidate genes identified in this study may be potential regulatory molecules of *L. reuteri* to protect host cells against *E. coli* F18ac. We speculated that one of the reasons why so few genes overlap may be histone modification. Fan, Ren (Fan et al., 2021) also found fewer genes intersected when investigating the association between the specific chromatin-accessible regions and gene expression in murine ovarian GCs upon DON exposure. One potential mechanism is histone acetylation (acetyltransferases/deacetylases) and methylation (methyltransferases/demethylases) between histones and DNA regulating gene expression (Bhaumik et al., 2007). As H3K4me3 and H3K27ac are known to mark active promoters (Calo and Wysocka, 2013), this may lead to changes in chromatin accessibility but does not correspond to differential transcription, hence the lack of overlap in the genes between the two datasets. The ChIP-qPCR results were similar to expectations, and regions with increased chromatin accessibility did not have increased H3K4me3 and H3K27ac enrichment; the trend between the two was inconsistent. Besides, it has been reported that *Lactobacillus mucosae* strain LM1 caused a > 5.1-fold increase in different types of histones, this indicates a significant alteration in protein biosynthesis induced by *L. reuteri* in IPEC-J2 cells (Pajarillo et al., 2017). These both partially explained the reasons for the low overlap. In addition, DNA methylation can also affect gene

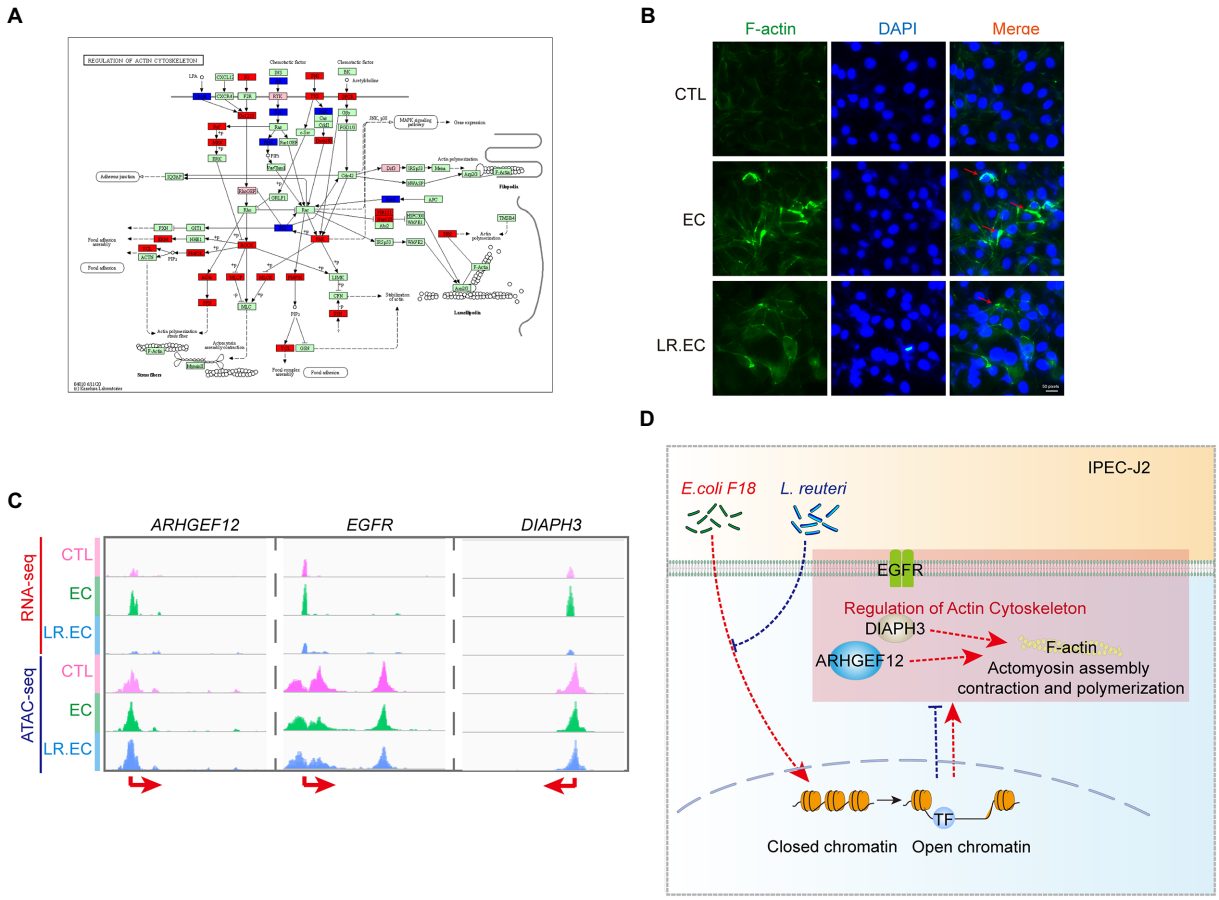

FIGURE 6
Regulation of actin cytoskeleton involved in regulation of *L. reuteri*-mediated bacteriostasis. **(A)** KEGG map of regulation of actin cytoskeleton. Red indicates genes identified by RNA-seq, blue indicates genes identified by ATAC-seq, and pink indicates genes identified by both. **(B)** IFA assay was used to visualize F-actin in different treatments. The red arrows represent the rearrangement and aggregation of F-actin. **(C)** Visualization of *ARHGEF12, EGFR,* and *DIAPH3* used by IGV in the two datasets. **(D)** Mechanism hypothesis diagram for the regulation of actin cytoskeleton involved in regulation of *L. reuteri*-mediated bacteriostasis. Red dashed lines represent the effect of *E. coli* F18ac, blue dashed lines and crosses represent the effect of *L. reuteri*.

transcription level. In this study, it was found that demethylated transferase lysine K-specific demethylase (KDM) family showed an overall increasing trend after *E. coli* F18ac infection, while a decreasing trend was showed after the addition of *L. reuteri* (Supplementary Table S5). However, this trend was not significant, and our study lacked data support at the protein level, which needed to be further explored. *L. reuteri* strongly regulates interleukin family members such as IL-1α, IL-6 IL-8, and IL-10 (Ma et al., 2004; Pena et al., 2004; Hoffmann et al., 2008). Therefore, we also investigated the transcriptional changes in interleukin-family genes and found that *E. coli* infection significantly increased the expressions of IL-1α, IL-11, NFIL-3, IL-16, and other cytokines. Zhou et al. identified 867 DEGs (including 30 immune-related genes) in IPECJ2 cells after infection with *E. coli* F18ac (Zhou et al., 2012). The number of DEGs in our study, especially the number of immune-related genes, was lower than that found by Zhou et al., which may have been due to differences in the MOI (we used 1×10^7 CFU/ml in this study, which is lower than the 1×10^8 CFU/ml used by Zhou et al.). Additionally, *L. reuteri* treatment did not reduce the uptrend in the levels of these cytokines, suggesting that porcine *L. reuteri* does not influence *E. coli* F18ac infection in IPEC-J2 cells by modulating interleukin release. The levels of important chemokines CXCL10, and CXCL11 increased only after *L. reuteri* treatment. CXCL10 and CXCL11 regulate immune cell migration, differentiation, and activation (Tokunaga et al., 2018), and the increased levels after *L. reuteri* treatment may have facilitated the recruitment of epithelial cells to immune cells.

Notably, the results of GO and KEGG enrichment analyses did not clearly describe the up- and downregulation changes in DEGs during the bacteriostatic process of *L. reuteri*. Therefore, we performed GSEA, through which we identified 12 pathways that were upregulated after *E. coli* F18ac infection and downregulated after *L. reuteri* treatment; we identified four pathways showing the opposite pattern. Among them, ECM–receptor interaction is involved in cellular–extracellular communication (Cui et al., 2018) and was reported to be associated with the infection process of *E. coli* (Zhou et al., 2012). The actin cytoskeleton can be manipulated by the effector proteins secreted by *E. coli* pathotypes (Selbach and Backert, 2005; Campellone, 2010; Navarro-Garcia et al., 2013). These pathways, which are closely associated with *E. coli* infection, may be a crucial bacteriostatic mechanism of *L. reuteri*. In this regard, we further found that the chromatin accessibility and expression levels of some key genes in the regulation of actin cytoskeleton were altered. The results of the IFA assay revealed that treatment with *E. coli* F18ac markedly augmented

actin aggregation, whereas *L. reuteri* treatment effectively lowered this aggregation, indicating that the regulation of the actin cytoskeleton is one of the important mechanisms through which *L. reuteri* inhibits *E. coli* F18ac infection. Additionally, *ARHGEF12* can be specifically regulated by EspH, a type III secretion system effector protein of *E. coli* (Dong et al., 2010), EGFR can also benefit *E. coli* invasion (Wang et al., 2016). Therefore, *ARHGEF12, EGFR,* and *DIAPH3* appear to be the key regulatory targets, which needs to be verified by further experiments.

In summary, our results fully displayed the chromatin accessibility and transcriptional landscape of the *E. coli* F18ac infection processes as well as the bacteriostatic action of *L. reuteri* in IPEC-J2 cells. We identified some key signaling pathways and node genes, revealing that *E. coli* F18ac triggers cellular activities in the host and can be generally regulated by *L. reuteri*. This study provides mechanistic guidance for the use of *L. reuteri* as a probiotic in livestock, poultry, and humans, as well as a theoretical basis for the development and use of *L. reuteri* and its synergistic drugs.

Data availability statement

The datasets presented in this study can be found in online repositories. The names of the repository/repositories and accession number(s) can be found below: NCBI - PRJNA767941.

Author contributions

WQ: conceptualization, methodology, and writing–original draft. YX: formal analysis and data curation. ZR: methodology. CX: software. M-aS: software. ZY: resources. WB: funding acquisition and writing–review and editing. All authors contributed to the article and approved the submitted version.

Funding

This study was supported by grants from the Jiangsu Agricultural Science and Technology Innovation Fund (CX(20)1003), Key Research and Development Project (Modern Agriculture) of Jiangsu Province (BE2019341), and the Priority Academic Program Development of Jiangsu Higher Education Institutions.

Conflict of interest

The authors declare that the research was conducted in the absence of any commercial or financial relationships that could be construed as a potential conflict of interest.

Publisher's note

All claims expressed in this article are solely those of the authors and do not necessarily represent those of their affiliated organizations, or those of the publisher, the editors and the reviewers. Any product that may be evaluated in this article, or claim that may be made by its manufacturer, is not guaranteed or endorsed by the publisher.

Supplementary material

The Supplementary material for this article can be found online at: https://www.frontiersin.org/articles/10.3389/fmicb.2023.1101111/full#supplementary-material

SUPPLEMENTARY FIGURE S1
Quality metrics and analysis for RNA-seq and ATAC-seq datasets. A. Principal component analysis (PCA) of all RNA-seq samples. B. Wayne diagram of DEGs between *E. coli* F18ac and control groups, C. Wayne diagram of DEGs between *E. coli* F18ac with and without *L. reuteri* groups. B and C, both with a threshold of fold change ≥ 2, adjusted P value < 0.05. D. Principal component analysis (PCA) of all ATAC-seq samples. E. ATAC-seq signal enrichment around 3 kb of the TSS for three representative samples. F. Wayne diagram of genes annotated by DARs between *E. coli* F18ac and control groups, G. Wayne diagram of genes annotated by DARs between *E. coli* F18ac with and without *L. reuteri* groups. F and G, both with a threshold of fold change ≥ 1, *P* value < 0.05.

SUPPLEMENTARY FIGURE S2
Overlapping pathways between different treatments reveal antibacterial process of *L. reuteri*. A. Overlapping pathways that were upregulated after *E. coli* F18ac treatment and downregulated after *L. reuteri* treatment. B. Overlapping pathways that were downregulated after *E. coli* F18ac treatment, and were upregulated after *L. reuteri* treatment.

SUPPLEMENTARY TABLE S1
Details of primers for CHIP-qPCR.

SUPPLEMENTARY TABLE S2
Metadata and mapping statistics for RNA-seq and ATAC-seq.

SUPPLEMENTARY TABLE S3
Pathways enriched by GSEA analysis between E. coli F18ac and control groups.

SUPPLEMENTARY TABLE S4
Pathways enriched by GSEA analysis between E. coli F18ac with and without L. reuteri groups.

References

Alzahrani, A. S. (2019). PI3K/Akt/mTOR inhibitors in cancer: at the bench and bedside. *Semin. Cancer Biol.* 59, 125–132. doi: 10.1016/j.semcancer.2019.07.009

Bhaumik, S. R., Smith, E., and Shilatifard, A. (2007). Covalent modifications of histones during development and disease pathogenesis. *Nat. Struct. Mol. Biol.* 14, 1008–1016. doi: 10.1038/nsmb1337

Buenrostro, J. D., Giresi, P. G., Zaba, L. C., Chang, H. Y., and Greenleaf, W. J. (2013). Transposition of native chromatin for fast and sensitive epigenomic profiling of open chromatin, DNA-binding proteins and nucleosome position. *Nat. Methods* 10, 1213–1218. doi: 10.1038/nmeth.2688

Calo, E., and Wysocka, J. (2013). Modification of enhancer chromatin: what, how, and why? *Mol. Cell* 49, 825–837. doi: 10.1016/j.molcel.2013.01.038

Campellone, K. G. (2010). Cytoskeleton-modulating effectors of enteropathogenic and enterohaemorrhagic *Escherichia coli*: Tir, EspFU and actin pedestal assembly. *FEBS J.* 277, 2390–2402. doi: 10.1111/j.1742-4658.2010.07653.x

Cervantes-Barragan, L., Chai, J. N., Tianero, M. D., Di Luccia, B., Ahern, P. P., Merriman, J., et al. (2017). *Lactobacillus reuteri* induces gut intraepithelial CD4(+) CD8alphaalpha(+) T cells. *Science* 357, 806–810. doi: 10.1126/science.aah5825

Chen, L., Zhang, Y. H., Zheng, M. Y., Huang, T., and Cai, Y. D. (2016). Identification of compound-protein interactions through the analysis of gene ontology, KEGG enrichment for proteins and molecular fragments of compounds. *Mol. Gen. Genomics.* 291, 2065–2079. doi: 10.1007/s00438-016-1240-x

Cockerill, F. R. (2010). Performance standards for antimicrobial susceptibility testing twenty-first informational supplement[M]. Clinical and Laboratory Standards Institute, 2010.

Cui, X., Morales, R. T., Qian, W., Wang, H., Gagner, J. P., Dolgalev, I., et al. (2018). Hacking macrophage-associated immunosuppression for regulating glioblastoma angiogenesis. *Biomaterials* 161, 164–178. doi: 10.1016/j.biomaterials.2018.01.053

DebRoy, C., Roberts, E., Scheuchenzuber, W., Kariyawasam, S., and Jayarao, B. M. (2009). Comparison of genotypes of *Escherichia coli* strains carrying F18ab and F18ac fimbriae from pigs. *J. Vet. Diagn. Investig.* 21, 359–364. doi: 10.1177/104063870902100310

Dias, A. M. M., Douhard, R., Hermetet, F., Regimbeau, M., Lopez, T. E., Gonzalez, D., et al. (2021). *Lactobacillus* stress protein GroEL prevents colonic inflammation. *J. Gastroenterol.* 56, 442–455. doi: 10.1007/s00535-021-01774-3

Dong, N., Liu, L., and Shao, F. (2010). A bacterial effector targets host DH-PH domain RhoGEFs and antagonizes macrophage phagocytosis. *EMBO J.* 29, 1363–1376. doi: 10.1038/emboj.2010.33

Dore, M. P., Bibbò, S., Loria, M., Salis, R., Manca, A., Pes, G. M., et al. (2019). Twice-a-day PPI, tetracycline, metronidazole quadruple therapy with Pylera (R) or *Lactobacillus reuteri* for treatment naive or for retreatment of *Helicobacter pylori*. Two randomized pilot studies. *Helicobacter* 24:e12659. doi: 10.1111/hel.12659

Dore, M. P., Cuccu, M., Pes, G. M., Manca, A., and Graham, D. Y. (2014). *Lactobacillus reuteri* in the treatment of helicobacter pylori infection. *Intern. Emerg. Med.* 9, 649–654. doi: 10.1007/s11739-013-1013-z

Engelman, J. A., Luo, J., and Cantley, L. C. (2006). The evolution of phosphatidylinositol 3-kinases as regulators of growth and metabolism. *Nat. Rev. Genet.* 7, 606–619. doi: 10.1038/nrg1879

Ertel, A., and Tozeren, A. (2008). Switch-like genes populate cell communication pathways and are enriched for extracellular proteins. *BMC Genomics* 9:3. doi: 10.1186/1471-2164-9-3

Fairbrother, J. M., Nadeau, E., and Gyles, C. L. (2005). *Escherichia coli* in postweaning diarrhea in pigs: an update on bacterial types, pathogenesis, and prevention strategies. *Anim. Health Res. Rev.* 6, 17–39. doi: 10.1079/AHR2005105

Fan, H., Ren, Z., Xu, C., Wang, H., Wu, Z., Rehman, Z. U., et al. (2021). Chromatin accessibility and transcriptomic alterations in murine ovarian granulosa cells upon Deoxynivalenol exposure. *Cells* 10:2818. doi: 10.3390/cells10112818

Fang, J. Y., and Richardson, B. C. (2005). The MAPK signalling pathways and colorectal cancer. *Lancet Oncol.* 6, 322–327. doi: 10.1016/S1470-2045(05)70168-6

Grandi, F. C., Modi, H., Kampman, L., and Corces, M. R. (2022). Chromatin accessibility profiling by ATAC-seq. *Nat. Protoc.* 17, 1518–1552. doi: 10.1038/s41596-022-00692-9

Hennessy, B. T., Smith, D. L., Ram, P. T., Lu, Y. L., and Mills, G. B. (2005). Exploiting the PI3K/AKT pathway for cancer drug discovery. *Nat. Rev. Drug Discov.* 4, 988–1004. doi: 10.1038/nrd1902

Hoffmann, M., Rath, E., Holzlwimmer, G., Quintanilla-Martinez, L., Loach, D., Tannock, G., et al. (2008). *Lactobacillus reuteri* 100-23 transiently activates intestinal epithelial cells of mice that have a complex microbiota during early stages of colonization. *J. Nutr.* 138, 1684–1691. doi: 10.1093/jn/138.9.1684

Jiang, L., Yin, M., Wei, X., Liu, J., Wang, X., Niu, C., et al. (2015). Bach1 represses Wnt/beta-catenin signaling and angiogenesis. *Circ. Res.* 117, 364–375. doi: 10.1161/CIRCRESAHA.115.306829

Langmead, B., and Salzberg, S. L. (2012). Fast gapped-read alignment with bowtie 2. *Nat. Methods* 9, 357–359. doi: 10.1038/nmeth.1923

Lara-Chica, M., Correa-Saez, A., Jimenez-Izquierdo, R., Garrido-Rodriguez, M., Ponce, F. J., Moreno, R., et al. (2022). A novel CDC25A/DYRK2 regulatory switch modulates cell cycle and survival. *Cell Death Differ.* 29, 105–117. doi: 10.1038/s41418-021-00845-5

Lebeer, S., Vanderleyden, J., and De Keersmaecker, S. C. (2008). Genes and molecules of *lactobacilli* supporting probiotic action. *Microbiol. Mol. Biol. Rev.* 72, 728–764. doi: 10.1128/MMBR.00017-08

Li, D., Liu, G., and Wu, Y. (2022). RORA alleviates LPS-induced apoptosis of renal epithelial cells by promoting PGC-1alpha transcription. *Clin. Exp. Nephrol.* 26, 512–521. doi: 10.1007/s10157-022-02184-2

Li, J., Wang, X., Su, Y., Hu, S., and Chen, J. (2022). TRIM33 modulates inflammation and airway remodeling of PDGF-BB-induced airway smooth-muscle cells by the Wnt/beta-catenin pathway. *Int. Arch. Allergy Immunol.* 183, 1127–1136. doi: 10.1159/000524574

Liu, H. B., Hou, C. L., Wang, G., Jia, H. M., Yu, H. T., Zeng, X. F., et al. (2017). *Lactobacillus reuteri* I5007 modulates intestinal host defense peptide expression in the model of IPEC-J2 cells and neonatal piglets. *Nutrients* 9:559. doi: 10.3390/nu9060559

Liu, Y. Y., Tian, X. J., He, B. K., Hoang, T. K., Taylor, C. M., Blanchard, E., et al. (2019). *Lactobacillus reuteri* DSM 17938 feeding of healthy newborn mice regulates immune responses while modulating gut microbiota and boosting beneficial metabolites. *Am. J. Physiol. Gastr. L.* 317, G824–G838. doi: 10.1152/ajpgi.00107.2019

Love, M. I., Huber, W., and Anders, S. (2014). Moderated estimation of fold change and dispersion for RNA-seq data with DESeq2. *Genome Biol.* 15:550. doi: 10.1186/s13059-014-0550-8

Ma, D. L., Forsythe, P., and Bienenstock, J. (2004). Live *lactobacillus reuteri* is essential for the inhibitory effect on tumor necrosis factor alpha-induced interleukin-8 expression. *Infect. Immun.* 72, 5308–5314. doi: 10.1128/Iai.72.9.5308-5314.2004

Mariani, V., Palermo, S., Fiorentini, S., Lanubile, A., and Giuffra, E. (2009). Gene expression study of two widely used pig intestinal epithelial cell lines: IPEC-J2 and IPI-2I. *Vet. Immunol. Immunopathol.* 131, 278–284. doi: 10.1016/j.vetimm.2009.04.006

Moxley, R. A., and Duhamel, G. E. (1999). Comparative pathology of bacterial enteric diseases of swine. *Adv. Exp. Med. Biol.* 473, 83–101. doi: 10.1007/978-1-4615-4143-1_7

Mu, Q., Tavella, V. J., and Luo, X. M. (2018). Role of *Lactobacillus reuteri* in human health and diseases. *Front. Microbiol.* 9:757. doi: 10.3389/fmicb.2018.00757

Navarro-Garcia, F., Serapio-Palacios, A., Ugalde-Silva, P., Tapia-Pastrana, G., and Chavez-Duenas, L. (2013). Actin cytoskeleton manipulation by effector proteins secreted by diarrheagenic *Escherichia coli* pathotypes. *Biomed. Res. Int.* 2013:374395. doi: 10.1155/2013/374395

Ortiz-Rivera, Y., Sanchez-Vega, R., Gutierrez-Mendez, N., Leon-Felix, J., Acosta-Muniz, C., and Sepulveda, D. R. (2017). Production of reuterin in a fermented milk product by *Lactobacillus reuteri*: inhibition of pathogens, spoilage microorganisms, and lactic acid bacteria. *J. Dairy Sci.* 100, 4258–4268. doi: 10.3168/jds.2016-11534

Pajarillo, E. A. B., Kim, S. H., Valeriano, V. D., Lee, J. Y., and Kang, D. K. (2017). Proteomic view of the crosstalk between *Lactobacillus mucosae* and intestinal epithelial cells in co-culture revealed by Q Exactive-based quantitative proteomics. *Front. Microbiol.* 8:2459. doi: 10.3389/fmicb.2017.02459

Pena, J. A., Li, S. Y., Wilson, P. H., Thibodeau, S. A., Szary, A. J., and Versalovic, J. (2004). Genotypic and phenotypic studies of murine intestinal *lactobacilli*: species differences in mice with and without colitis. *Appl. Environ. Microbiol.* 70, 558–568. doi: 10.1128/Aem.70.1.558-568.2004

Peterson, L. W., and Artis, D. (2014). Intestinal epithelial cells: regulators of barrier function and immune homeostasis. *Nat. Rev. Immunol.* 14, 141–153. doi: 10.1038/nri3608

Ramirez, F., Dundar, F., Diehl, S., Gruning, B. A., and Manke, T. (2014). deepTools: a flexible platform for exploring deep-sequencing data. *Nucleic Acids Res.* 42, W187–W191. doi: 10.1093/nar/gku365

Rodriguez-Fernandez, J. L., and Criado-Garcia, O. (2020). The chemokine receptor CCR7 uses distinct signaling modules with biased functionality to regulate dendritic cells. *Front. Immunol.* 11:528. doi: 10.3389/fimmu.2020.00528

Selbach, M., and Backert, S. (2005). Cortactin: an Achilles' heel of the actin cytoskeleton targeted by pathogens. *Trends Microbiol.* 13, 181–189. doi: 10.1016/j.tim.2005.02.007

Skjolaas, K. A., Burkey, T. E., Dritz, S. S., and Minton, J. E. (2007). Effects of *salmonella enterica serovar typhimurium*, or *serovar Choleraesuis*, *lactobacillus reuteri* and *bacillus licheniformis* on chemokine and cytokine expression in the swine jejunal epithelial cell line, IPECJ2. *Vet. Immunol. Immunopathol.* 115, 299–308. doi: 10.1016/j.vetimm.2006.10.012

Szajewska, H., Urbanska, M., Chmielewska, A., Weizman, Z., and Shamir, R. (2014). Meta-analysis: *Lactobacillus reuteri* strain DSM 17938 (and the original strain ATCC 55730) for treating acute gastroenteritis in children. *Benef. Microbes* 5, 285–293. doi: 10.3920/BM2013.0056

Tokunaga, R., Zhang, W., Naseem, M., Puccini, A., Berger, M. D., Soni, S., et al. (2018). CXCL9, CXCL10, CXCL11/CXCR3 axis for immune activation - a target for novel cancer therapy. *Cancer Treat. Rev.* 63, 40–47. doi: 10.1016/j.ctrv.2017.11.007

Wang, X., Maruvada, R., Morris, A. J., Liu, J. O., Wolfgang, M. J., Baek, D. J., et al. (2016). Sphingosine 1-phosphate activation of EGFR as a novel target for Meningitic *Escherichia coli* penetration of the blood-brain barrier. *PLoS Pathog.* 12:e1005926. doi: 10.1371/journal.ppat.1005926

Wang, X., Shi, B., Zhao, Y., Lu, Q., Fei, X., Lu, C., et al. (2020). HKDC1 promotes the tumorigenesis and glycolysis in lung adenocarcinoma via regulating AMPK/mTOR signaling pathway. *Cancer Cell Int.* 20:450. doi: 10.1186/s12935-020-01539-7

Wu, Z., Qin, W., Wu, S., Zhu, G., Bao, W., and Wu, S. (2016). Identification of microRNAs regulating *Escherichia coli* F18 infection in Meishan weaned piglets. *Biol. Direct* 11:59. doi: 10.1186/s13062-016-0160-3

Wu, H., Xie, S., Miao, J., Li, Y., Wang, Z., Wang, M., et al. (2020). *Lactobacillus reuteri* maintains intestinal epithelial regeneration and repairs damaged intestinal mucosa. *Gut Microbes* 11, 997–1014. doi: 10.1080/19490976.2020.1734423

Yang, D., Fan, L., Song, Z., Fang, S., Huang, M., and Chen, P. (2022). The KMT1A/TIMP3/PI3K/AKT circuit regulates tumor growth in cervical cancer. *Reprod. Biol.* 22:100644. doi: 10.1016/j.repbio.2022.100644

Yi, H. B., Wang, L., Xiong, Y. X., Wang, Z. L., Qiu, Y. Q., Wen, X. L., et al. (2018). *Lactobacillus reuteri* LR1 improved expression of genes of tight junction proteins via the MLCK pathway in IPEC-1 cells during infection with Enterotoxigenic *Escherichia coli* K88. *Mediat. Inflamm.* 20, 1–8. doi: 10.1155/2018/6434910

Yu, G., Wang, L. G., and He, Q. Y. (2015). ChIPseeker: an R/Bioconductor package for ChIP peak annotation, comparison and visualization. *Bioinformatics* 31, 2382–2383. doi: 10.1093/bioinformatics/btv145

Zhang, Y., Liu, T., Meyer, C. A., Eeckhoute, J., Johnson, D. S., Bernstein, B. E., et al. (2008). Model-based analysis of ChIP-Seq (MACS). *Genome Biol.* 9:R137. doi: 10.1186/gb-2008-9-9-r137

Zheng, J., Wittouck, S., Salvetti, E., Franz, C., Harris, H. M. B., Mattarelli, P., et al. (2020). A taxonomic note on the genus *lactobacillus*: description of 23 novel genera, emended description of the genus *lactobacillus* Beijerinck 1901, and union of *Lactobacillaceae* and *Leuconostocaceae*. *Int. J. Syst. Evol. Microbiol.* 70, 2782–2858. doi: 10.1099/ijsem.0.004107

Zhou, C., Liu, Z., Jiang, J., Yu, Y., and Zhang, Q. (2012). Differential gene expression profiling of porcine epithelial cells infected with three enterotoxigenic *Escherichia coli* strains. *BMC Genomics* 13:330. doi: 10.1186/1471-2164-13-330

frontiers | Frontiers in Microbiology

TYPE Original Research
PUBLISHED 24 February 2023
DOI 10.3389/fmicb.2023.1108197

OPEN ACCESS

EDITED BY
Zhenyu Zhang,
University of Wisconsin-Madison,
United States

REVIEWED BY
Susana María Martín-Orúe,
Autonomous University of Barcelona, Spain
Philippe Fravalo,
Conservatoire National des Arts et Métiers (CNAM), France
John Pluske,
The University of Melbourne, Australia
Elizabeth Maga,
University of California,
Davis, United States

*CORRESPONDENCE
Martin Peter Rydal
✉ martin.rydal@sund.ku.dk

SPECIALTY SECTION
This article was submitted to Infectious Agents and Disease, a section of the journal Frontiers in Microbiology

RECEIVED 26 November 2022
ACCEPTED 03 February 2023
PUBLISHED 24 February 2023

CITATION
Rydal MP, Gambino M, Castro-Mejia JL, Poulsen LL, Jørgensen CB and Nielsen JP (2023) Post-weaning diarrhea in pigs from a single Danish production herd was not associated with the pre-weaning fecal microbiota composition and diversity. *Front. Microbiol.* 14:1108197. doi: 10.3389/fmicb.2023.1108197

Post-weaning diarrhea in pigs from a single Danish production herd was not associated with the pre-weaning fecal microbiota composition and diversity

Martin Peter Rydal[1]*, Michela Gambino[1], Josue L. Castro-Mejia[2], Louise Ladefoged Poulsen[1], Claus Bøttcher Jørgensen[1] and Jens Peter Nielsen[1]

[1]Department of Veterinary and Animal Sciences, Faculty of Health and Medical Sciences, University of Copenhagen, Frederiksberg, Denmark, [2]Department of Food Science, Faculty of Science, University of Copenhagen, Frederiksberg, Denmark

Introduction: The association between the porcine pre-weaning gut microbiota composition and diversity, and subsequent post-weaning diarrhea (PWD) susceptibility is currently being studied. In this longitudinal study, we examined the association between pre-weaning fecal microbiome composition and diversity, and PWD development in a Danish sow herd.

Methods: Forty-five pigs were followed from birth until 7 days after weaning (post-natal day (PND) 33). At PND 33, the pigs were categorized as PWD cases or healthy controls based on fecal consistency. We compared their fecal microbiomes at PND 8, late lactation (PND 27) and 7 days post weaning (PND 33) using 16S rRNA V3 region high-throughput sequencing. At PND 27 and 33, we also weighed the pigs, assessed fecal shedding of hemolytic *Escherichia coli* by culture and characterized hemolytic isolates by ETEC virulence factors with PCR and by whole genome sequencing.

Results: A total of 25 out of 45 pigs developed PWD and one Enterotoxigenic *E. coli* strain with F18:LT:EAST1 virotype was isolated from most pigs. At PND 33, we found differences in beta diversity between PWD and healthy pigs (R^2 = 0.027, p = 0.009) and that body weight was associated with both alpha and beta diversity. Pre-weaning fecal microbiome diversity did not differ between PWD and healthy pigs and we found no significant, differentially abundant bacteria between them.

Conclusion: In the production herd under study, pre-weaning fecal microbiome diversity and composition were not useful indicators of PWD susceptibility.

KEYWORDS

gastrointestinal microbiome, enterotoxigenic *Escherichia coli*, diarrhea, piglet, post-weaning, F18 fimbriae, high-throughput sequencing, genetic marker

Introduction

The gut microbiota (GM) has an essential role in gut health (Wang et al., 2016). The composition of the microbial community is driven by host genetics (McKnite et al., 2012), diet (Frese et al., 2015), environmental conditions (Schmidt et al., 2011), and potentially physiological development (Leite et al., 2021). The rapid transition of diet in pig production, from milk as the primary nutrient source to solid feed at weaning, causes fast shifts in the GM composition and

its enzymatic functional capacities (Frese et al., 2015). Taken together with the early time of weaning in pig production at three to four weeks of age (Jensen and Recén, 1989), and the stress associated with changes of environment, the weaning period is a vast challenge that can lead to gut microbiota dysbiosis; a state of gut microbial imbalance (Gresse et al., 2017) that may favor opportunistic pathogens. Consequently, post-weaning diarrhea (PWD) is very common in pig production and constitutes a serious problem in terms of animal welfare, financial costs and antibiotic use, where metaphylatic treatments are often used to control the disease (Rhouma et al., 2017). Post-weaning diarrhea is a multifactorial condition and enterotoxigenic *Escherichia coli* (ETEC) is the primary pathogen isolated from outbreaks (Dubreuil et al., 2016). Enterotoxigenic *E. coli* cause secretory diarrhea and are distinguished by their fimbriae type and the types of enterotoxins they produce. The fimbriae types most frequently associated with ETEC-related PWD are F18 and F4 (Frydendahl, 2002).

Recently, there has been increasing attention to the role of the GM in relation to PWD. Research shows that the early life environment affects microbiome composition and stimulates the maturation of the immune system (Mulder et al., 2009). Dysbiosis caused by unfavorable environmental conditions, such as limited or compromised exposure to microbes in the natural environment (Mulder et al., 2009; Schmidt et al., 2011), or by antibiotics early in life (Fouhse et al., 2019) may have long lasting consequences to host immune response (Mulder et al., 2009; Fouhse et al., 2019). This may consequently affect vulnerability to later infections as shown in experimentally infected mice exposed to early-life antibiotics (Roubaud-Baudron et al., 2019). Dou and colleagues found that pigs with PWD, under experimental facility conditions in France, differed in fecal microbiome diversity indices and composition from healthy pigs as early as 1 week after birth (Dou et al., 2017). Healthy pigs showed less evenness and higher abundance of taxa belonging to the families *Lactobacillaceae* and *Ruminocaceae* and other commensals. In a recent Czech herd study (Karasova et al., 2021), researchers investigated the role of the fecal microbiota in late lactation (3 days before weaning) in pigs with and without PWD. Healthy and PWD affected pigs differed in fecal microbiota composition, 3 days before weaning, although no extensive differences were found based on principal coordinate analysis. These findings indicate that certain GM communities might be associated with subsequent PWD development. However, more research is needed to elucidate if cues in the pre-weaning fecal microbiome such as diversity indices and abundance of certain taxa can reveal risk of PWD development. This may especially be relevant in a herd setting where management factors and antibiotic use can influence the GM.

In this study, we used 16S rRNA V3 high-throughput sequencing to investigate the fecal microbiome at early preweaning (post-natal day (PND) 8), at late lactation (PND 27) and at 7 days after weaning (PND 33). We determined diversity indices and microbiome composition and investigated their association with PWD development in pigs.

Materials and methods

Ethical statement

The study was ethically assessed and approved by the Animal Ethics Institutional Review Board at the Department of Veterinary and Animal Sciences, University of Copenhagen. Approval number: 2022-02-PNH-006A.

Animals

A total of 45 female, Duroc x Landrace x Yorkshire pigs from 9 sows (5 pigs per sow) were included in the study. The herd of the study was part of the Danish SPF (Specific Pathogen Free) system, declared free from *Actinobacillus pleuropneumoniae* serotype 2, toxigenic *Pasteurella multocida*, *Brachyspira hyodysenteriae* and porcine reproductive and respiratory syndrome virus.

Female pigs, born on a single day, were weighed at birth. No crossfostering was performed in the pre-weaning period. Sow parity ranged from 2 to 5. The piglets were fed with milk formula through milk dispensers as a supplement to sow milk and were offered creep feed pre-weaning from PND 16. Pigs were weaned at PND 27 and received a standard weaner diet without added antimicrobials or medicinal zinc. All pigs had the same treatment history and received a single dose of amoxicillin trihydrate at post-natal day (PND) 1, Toltrazuril (anticoccidial) at PND 4, and metaphylatic lincomycin hydrochloride and spectinomycin sulfate (Linco-Spectin® Vet) treatment *via* drinking water during the entire study period after weaning. All 45 pigs were transported to and housed together at the nursery in a single pen, without additional pigs.

Experimental design

The study was an observational case–control study with pig as the study unit. The study population was randomized in blocks by litter where five female pigs (birthweight higher than 1 kg) from each of 9 litters were selected out of available female pigs of the litter. Rectal swabs for fecal microbiome analysis were collected longitudinally from the pigs at PND 8, at late lactation (PND 27) and at 7 days after weaning (PND 33). In addition, at PND 27 and 33, fecal samples were collected rectally from the pigs for assessment of diarrhea and shedding of hemolytic *E. coli* and ETEC. Pigs were grouped based on fecal consistency at PND 33 into "PWD-cases" or "healthy controls" to compare their fecal microbiomes at the three time points.

Fecal scoring and fecal dry matter content analysis

Feces were assessed using a visual fecal consistency score (1–4) (Pedersen and Toft, 2011) and diarrhea was defined as a fecal score greater than 2. Fecal dry matter content was determined by weighing feces before and after drying to constant weight, at 75°C for 18 h. Dried feces were kept in desiccators between weighings.

Bacteriological culturing of fecal samples

Feces collected at PND 27 and 33 were streaked on blood agar (BA, 5% calf blood in blood agar base, Oxoid CM0055, ThermoFischer) in three dilution zones. The BA plates were incubated at 37°C

overnight and semiquantitative assessment of hemolytic *E. coli* growth (%- hemolytic *E. coli* growth out of total growth, 0–100%) was performed. One haemolytic isolate per pig per timepoint was subjected to multiplex PCR to evaluate presence of the ETEC virulence factors F4, F18, STb, STa and LT with primers and protocol previously described (Zhang et al., 2007).

Whole genome sequencing of *Escherichia coli* F18, LT isolates

Five randomly chosen *E. coli* F18, LT isolates were subjected to whole genome sequencing (WGS) for further characterization and to investigate if one or more strains were present. Extraction of DNA was performed on Maxwell® RSC instrument with Maxwell RSC culture cell's DNA kit (Promega, Madison, USA) and WGS was performed at coverage of 30X, using 2×250 basepair V2 reagent kit with NGS-MiSeq (Illumina, University of Copenhagen, Denmark) platform, by service of Veterinary Clinical Microbiology at the Department of Veterinary and Animal Sciences, University of Copenhagen, Denmark. Raw sequencing reads were analyzed for virulence genes, serotypes and antibiotic resistance genes with the bioinformatics tools: VirulenceFinder (Version 2.0) (Joensen et al., 2014; Clausen et al., 2018; Tetzschner et al., 2020), SerotypeFinder (Version 2.0) (Joensen et al., 2015), and ResFinder (Version 4.1) (Zankari et al., 2017; Clausen et al., 2018; Bortolaia et al., 2020), hosted by the Center for Genomic Epidemiology (CGE) (www.genomicepidemiology.org).

16S rRNA V3 region high-throughput sequencing

Rectal swabs (Eswabs with Liquid Amies Medium, 490 CE.A, Copan Diagnostics Inc., Brescia, Italy) were stored at −80°C before DNA extraction. One rectal swab taken at PND 33 from a pig without PWD was missing before DNA extraction. Extraction of genomic DNA was carried out using Bead-Beat Micro AX Gravity kit (A&A Biotechnology, Gdynia, Poland) following the manufacturer's instructions. DNA concentration was measured using Qubit® dsDNA HS Assay Kit (Life Technologies, CA, USA) with Varioskan Flash Multimode Reader (Thermo Fischer Scientific, MA, USA). Extracted DNA was diluted 1:10 with sterile water before PCR amplification of the V3 region of the 16S rRNA gene. The following primers were used: nxt_338_F: 5′-CCTACGGGWGGCAGCAG-3′ and nxt_518_R: 5′-ATTACCGCGGCTGCTGG-3′ (Integrated DNA Technologies; Leuven, Belgium). Reaction mix for PCR1 contained 5 µL of PCRBIO buffer, 0.5 µL primer mix (10 µM of each primer), 0.25 µL PCRBIO HiFi polymerase (PCR Biosystems Ltd., London, United Kingdom), 1 µL bovine serum albumin, 1 µL formamide, 12.25 µL nuclease-free water and 5 µL genomic DNA (approximately 1 ng/µL), per sample. The following thermal cycling was used: 95°C for 2 min, then 33 cycles of 95°C for 15 s, 55°C for 15 s, 72°C for 20 s, and 1 cycle of 72°C for 4 min. PCR1 products were verified and quality checked on 1.5% agarose gels. Products from PCR1 were then purified using AMPure XP beads (Beckman Coulter Genomic, CA, USA) with Biomek 4,000 automated laboratory workstation. Afterwards, barcoding (PCR2) of purified PCR products was performed. Reaction mix for PCR2 contained 5 µL PCRBIO buffer, 0.25 µL PCRBIO HiFi polymerase, 4 µL barcode primers (2 µL P5 and 2 µL P7 primers, Nextera Index Kit), 13.75 µL nuclease-free water and 2 µL PCR product, per sample. The cycling conditions for PCR2 were: 95°C for 1 min, then 13 cycles of 95°C for 15 s, 55°C for 15 s, 72°C for 15 s, and finally, 1 cycle of 72°C for 5 min. The barcoded PCR products were subjected to cleaning and bead-based normalization with AMPure XP beads. DNA concentration was measured once more and samples were pooled in equimolar concentrations. Finally, high throughput Illumina MiSeq (Illumina, CA, USA) sequencing was performed following the manufacturer's instructions.

Gut microbiota sequencing

Quality-control of reads, de-replicating, purging from chimeric reads and constructing zero-radius Operational Taxonomic Units (zOTU) was conducted with the UNOISE pipeline (Edgar, 2018) and taxonomically assigned with Sintax (Edgar, 2016). Taxonomical assignments were obtained using the EZtaxon for 16S rRNA gene database. Description of the workflow can be found in: https://github.com/jcame/Fastq_2_zOTUtable.

FUT1 genotyping

All pigs were genotyped for the M307 mutation in FUT1. The M307 is a good marker for ETEC F18 resistant animals (Meijerink et al., 1997). Pig genomic DNA extraction was done from rectal swabs (Eswabs with Liquid Amies Medium, 490 CE.A, Copan Diagnostics Inc., Brescia, Italy). Genomic DNA was extracted from each swab using a crude DNA extraction method. Briefly, 100 µL medium was placed in a tube with 100 µL of NaOH solution (25 mM NaOH +2 mM EDTA). The sample was then heated at 100°C for 20 min. After centrifugation, the liquid phase was transferred and neutraliZed with 100 µL of Tris solution. The TaqMan SNP Genotyping assays were designed by Thermo Fisher Scientific (Waltham, Massachusetts, USA).

One µL of the crude DNA solution was used for TaqMan genotyping according to the manufacturer's instructions. Allele calling was performed on a Mx3000P qPCR System (Agilent, Santa Clara, California, USA).

Statistics

Statistical analysis was performed in R version 4.1.1 (R Core Team, 2022). p-values <0.05 were considered significant and < 0.10 a tendency.

Differences in fecal dry matter content and in shedding of hemolytic *E. coli* between diarrhea and non-diarrhea samples were evaluated with Wilcoxon rank sum test. Normal distribution of data was assessed using QQ-plots.

Association of litter and body weight with occurrence of PWD was evaluated with logistic regression.

For microbiome analysis and visualization, R packages vegan (Oksanen et al., 2022), phyloseq (McMurdie and Holmes, 2013), ANCOMBC (Mandal et al., 2015; Lin and Peddada, 2020), GUniFrac (Chen et al., 2022), lme4 (Bates et al., 2015), lmerTest (Kuznetsova et al., 2017), viridis (Garnier et al., 2021), tidyverse (Wickham et al.,

2019), ggtext (Wilke and Wiernik, 2022), cowplot (Wilke, 2020), ggplot2 (Wickham, 2016), and RColorBrewer (Neuwirth, 2022) were used. Four samples were removed due to low number of reads (<10,000), resulting in n = 44, 43, 43 samples at PND 8, PND 27, and PND 33, respectively. All samples were rarefied to the same sequencing depth of 10,000 reads/sample.

Group differences in Canberra and binary Soerensen-Dice distance matrices between healthy and PWD pigs were assessed with PERMANOVA at 999 permutations. Model selection was based on forward selection using ordiR2step function of vegan. Group differences were assessed at each timepoint, with litter included in the model as strata. At PND 33, body weight at PND 33 was also included as a fixed effect in the model. Multivariate homogeneity of group dispersions were checked with betadisper function. Ordination plots were generated from the full model using capscale (distance-based redundancy analysis) function of vegan.

Significant group differences in Shannon and Simpson indices and number of observed zOTUs were evaluated with linear mixed model with litter included in the model as a random effect. At PND 33, body weight at PND 33 was also included as a fixed effect in the model.

Mean relative abundance between groups were calculated at genus level and visualized for each time point. Pearson's correlation was calculated between relative abundance of *Prevotella* and body weight at PND 33.

Differential abundance analysis at each time point, was performed on amplicon counts at genus and zOTU level, using a taxon prevalence cut across samples of 10%, detecting structural zeros (using equation 1 in section 3.2 (Kaul et al., 2017)) and adjusting *p*-values with Holm–Bonferroni method. Data was analyzed with a univariable model (ANCOM-BC function) with PWD status as the explanatory variable and with a multivariable model (ANCOM function) where litter was added as random effect. At PND 33, body weight at PND 33 was also added to the model as fixed effect.

Results

Prevalence of diarrhea and risk factors for PWD

Just before weaning, at PND 27, only 1 out of 45 pigs had diarrhea. Four feces samples were missing at PND 27, as four pigs did not defecate at sample collection. Seven days after weaning, at PND 33, 25 out of the 45 pigs had diarrhea (Table 1). The majority of PWD samples were of watery consistency (16 out of 25 samples) indicative of severe diarrhea. Visual consistency scoring was confirmed by the significantly lower fecal dry matter content of PWD samples ($n = 25$) compared to non-diarrhea samples ($n = 20$) (Table 2, Wilcoxon test statistic (W) = 490, difference in medians = 12.33, 95% CI = 8.92;16.14, $p < 0.0001$).

Neither litter, birth weight (mean ± standard deviation (SD): 1.31 ± 0.18 kg and 1.38 ± 0.23 kg in PWD and healthy pigs, respectively) or body weight at PND 33 (mean ± SD: 8.8 ± 1.56 kg and 8.0 ± 1.6 kg in PWD and healthy pigs, respectively) had a significant association with PWD status in the pigs. A higher weaning weight was associated with slightly higher odds of PWD (mean weaning weight ± SD in PWD pigs were 8.66 ± 1.54 kg and 7.55 ± 1.69 kg in healthy, respectively, odds ratio = 1.54, 95% confidence interval (CI) = 1.05;2.4, $p = 0.02$).

Microbiological findings

At PND 27, shedding of hemolytic *E. coli* was detected in a non-diarrheic sample from a single animal. Otherwise, no shedding of hemolytic *E. coli* was found before weaning. At PND 33, non-diarrhea samples tended to have less growth of hemolytic *E. coli* than the post-weaning diarrhea samples (Tables 2, $W = 162$, difference in medians = −20.0, 95% CI = −4.0;3.7, $p = 0.06$). Genes encoding for F18 and LT were detected by PCR in the hemolytic *E. coli* isolate from PND 27 and the majority of isolates at PND 33. No genes encoding for F4 were detected. Whole genome sequencing of five randomly chosen F18, LT positive isolates revealed the same virotype, thus confirming an ETEC F18 associated outbreak caused by a single strain. The herd strain was identified as O8:H17, F18ac, LT, EAST-1, with a WGS-predicted phenotype resistant to lincomycin, but not spectinomycin.

Host genotype susceptibility to ETEC F18 using the FUT1-marker

Overall, 33 homozygous susceptible (SS), 11 heterozygous susceptible (RS) and 1 homozygous resistant (RR) pigs were identified by genotyping the FUT1-marker (Meijerink et al., 1997). The distribution of genotypes was similar between PWD cases and healthy controls (Table 3). Surprisingly, the single resistant pig was located in the PWD group which was confirmed by genotyping two independent samples from the same pig.

Microbiome analysis

Alpha diversity

In order to identify potential indicators for PWD early in pigs' lives, we processed all fecal samples at PND 8, 27 and 33 with 16S rRNA V3 amplicon sequencing. In analysis of alpha diversity (Shannon and Simpson's diversity index, and observed number of zOTUs), no statistically significant differences were found between the

TABLE 1 Prevalence of diarrhea and microbiological findings at late lactation (PND 27) and 7days post weaning (PND 33).

	PND 27	PND 33
E. coli F18, LT [number of positive samples/ samples total]	1/45	34/45
Pigs with diarrhea [*n* (%)]	1 (2%)	25 (55%)

TABLE 2 Clinical microbiology and fecal dry matter characteristics of feces at PND 33.

	Diarrhea	Non-diarrhea
Number of samples	25	20
Mean fecal dry matter ± SD [%]	11.3 ± 4.0	24.5 ± 6.6
Mean hemolytic *E. coli* shedding ± SD [% out of total growth]	76 ± 27	56 ± 33
E. coli F18, LT [number of positive samples/samples total]	18/25	16/20

TABLE 3 FUT1 genotypes for ETEC F18 susceptibility between PWD status groups.

Groups	Post weaning diarrhea			Healthy		
Genotype profile	RR	RS	SS	RR	RS	SS
Number of pigs	1	8	16	0	3	17

PWD group and healthy group at any timepoint (Figure 1). At PND 33, in the post weaning period, we found that the co-variable body weight was positively associated with increased alpha diversity. We did not find the same association between body weight and alpha diversity at PND 27 in the late lactation period.

Beta diversity

The analysis of beta diversity pre-weaning revealed no statistically significant differences at PND 8 (early lactation) nor at PND 27 (late lactation) based on PWD future status (Figure 2; Supplementary material 1). However at PND 33 (7 days after weaning), at the time of PWD occurrence, the fecal microbiotas of PWD pigs and healthy pigs had minor, but significant differences in their overall bacterial communities. In addition, we found that the co-variable body weight at PND 33 was also associated with differences in beta diversity at PND 33. In contrast, body weight was not associated with significant differences in beta diversity at PND 27 in the late lactation period.

There were no significant differences in dispersions between groups (Figure 2; Supplementary material 1) which confirmed that significant PERMANOVA results were due to location effects.

Differential abundance analysis

Shift in the composition of bacterial communities were further investigated with differential abundance analysis. The most abundant bacterial genera and their mean relative abundance grouped by PWD status are illustrated in Figure 3. Four genera are of particular interest because of their dynamics in time: *Lactobacillus*, *Escherichia/Shigella*, *Prevotella*, *Campylobacter*. *Lactobacillus* and *Escherichia/Shigella* were the most dominant genera before weaning, while after weaning, the mean relative abundance of *Prevotella* increased in both groups (from 2.94% at PND 27 to 6.69% at PND 33 in healthy; from 3.37% at PND 27 to 9.76% at PND 33 in PWD pigs), making it the second most abundant genus post weaning. Interestingly, despite the ongoing ETEC associated PWD outbreak, the mean relative abundance of *Escherichia/Shigella* decreased at PND 33 both in healthy (from 9.45% at PND 27 to 2.82% at PND 33) and PWD pigs (from 18.44% at PND 27 to 7.77% at PND 33).

Agglomerating amplicon counts and analyzing at genus level did not reveal any differentially abundant genera based on PWD status at any individual timepoint. When we analyzed the data at a lower taxonomic level (zOTU level) we found differences in composition of microbial communities, but only as differences in presence/absence of rare taxa between groups.

At PND 8, 12 zOTUs were detected as structural zeroes (complete absence in one of the groups) (Supplementary material 2). The zOTUs did not belong to top abundant genera, except for two zOTU identified as *Prevotella* (mean relative abundance across taxa and samples 0.003%) that was found present only in the PWD group, and one zOTU identified as *Lactobacillus animalis* (mean relative abundance across taxa and samples 0.002%) that was only present in the healthy control.

At PND 27, a total of 17 zOTUs were detected as structural zeroes (Supplementary material 3). Among these were three zOTUs identified as *Lactobacillus* spp. (*Lactobacillus sanfranciscensis* and *Lactobacillus rapi,* mean relative abundance across taxa and samples at PND 27 of 0.013%) that were present only in healthy pigs, a genus that also had numerically higher mean relative abundance in healthy pigs (Figure 3 –PND 27).

At PND 33, a total of 99 zOTUs (98 of which were detected as structural zeroes) were differentially abundant between healthy and PWD pigs in the univariable analysis (Supplementary material 4). In the multivariable model, only the 98 zOTUs detected as structural zeroes remained differentially abundant between healthy and PWD pigs (Supplementary material 4). Four zOTUs identified as *Campylobacter hyointestinalis subsp. Lawsonii* (mean relative abundance across taxa and samples at PND 33 of 0.238%) were present only in PWD pigs. *Campylobacter* spp. was one of the top genera that had numerically higher mean relative abundance in PWD case pigs at PND 33 (Figure 3 –PND 33). Several zOTUs identified as *Prevotella* spp. were only detected in PWD pigs and this genus also had numerically higher mean relative abundance in the PWD affected pigs (Figure 3 –PND 33). Relative abundance of *Prevotella* at PND 33 increased with body weight at PND 33 (Supplementary material 5). Thus, questioning if the presence of *Prevotella* and numerically higher mean relative abundance in the PWD group was simply due to the higher average body weight in this group.

In summary, findings were limited to presence/absence of rare taxa between groups. Most of these differences were detected at PND 33 in the post-weaning period, and the least differences were found at PND 8 in the early lactation period.

Discussion

In this study, we investigated whether PWD-case pigs and healthy pigs had different fecal microbiomes in the pre-weaning period. Such distinct patterns could be useful as early biomarkers for PWD susceptibility and give the scientific background for preventive measures. However, under our conditions, pigs that developed ETEC F18 associated PWD did not have distinguishable fecal microbiotas from their healthy counterparts before weaning.

This contrasts to the work of Dou and colleagues, who found that PWD pigs could be distinguished from healthy pigs that had lower evenness and higher abundance of *Ruminocacaceae*, *Prevotellaceae*, *Lachnospiraceae* and *Lactobacillaceae* already at PND 7 (Dou et al., 2017). An important difference from their study was that our study was performed in a herd setting with conditions close to reality at a farm. For example, as is common in pig farms to counteract umbilical cord infection, IM amoxicillin treatment was given to all pigs at PND 1. This may have perturbed the GM and made it harder to differentiate between PWD predisposed and healthy pigs 7 days after treatment. Transient perturbations of the GM has been observed in pigs receiving oral amoxicillin during the first 2 weeks of life (Fouhse et al., 2019). Immediate changes in the GM after IM amoxicillin has not been documented in pigs, but it was found to reduce bacterial community

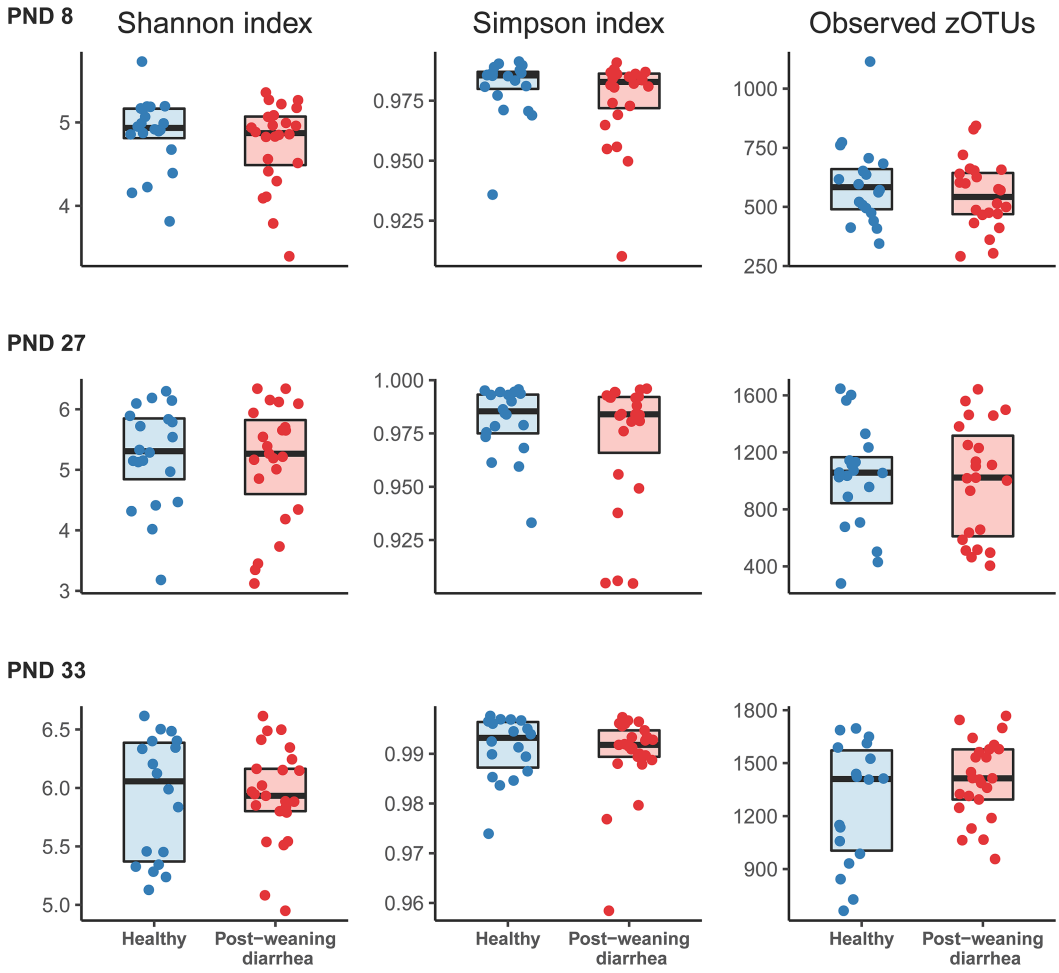

FIGURE 1
Comparison of alpha diversity indices based on post-weaning diarrhea (PWD) status. Groups were compared at post-natal day (PND) 8 (early lactation, healthy: *n*=20 pigs, PWD: *n*=24 pigs), at PND 27 (late lactation, healthy: *n*=20 pigs, PWD: *n*=23 pigs), and PND 33 (7days after weaning, healthy: *n*=18 pigs, PWD: *n*=25 pigs). Shannon and Simpson indices and number of observed zOTUs were based on a rarefied zOTU table generated from 16S rRNA V3 high throughput amplicon sequencing. Graphs show boxplots with medians marked with bold line. Statistical differences between groups were assessed with linear mixed models. No significant group differences were found for PWD status at any time point. At PND 33, the covariable body weight at PND 33 was positively associated with increased Shannon diversity (effect size: 0.13, 95% CI: [0.068; 0.208], p=0.0002), Simpson's diversity (effect size: 0.001, 95% CI: [−0.00012; 0.002], p=0.07), and number of observed zOTUs (effect size: 86.33, 95% CI: [46.27; 126.80], p=0.00009).

diversity in the colon 5 weeks after administration (Janczyk et al., 2007). However, in a recent herd study where pigs received creep feed with medicinal zinc pre-weaning and in-feed antibiotics (sulfamethoxazole and trimethoprim) after weaning, researchers still found several taxa in the fecal microbiome that were differentially abundant between their PWD-cases and healthy controls in the late pre-weaning period (Karasova et al., 2021). This suggests that it is possible to distinguish between PWD predisposed and healthy pigs regardless of previous and ongoing antimicrobial treatment. However, we found no obvious microbiome differences that could be used to identify PWD susceptible and resilient pigs in the pre-weaning period in our study. Although *Escherchia/Shigella* and *Lactobacillus* appeared more abundant based on the visualization of mean relative abundance at PND 27, we did not find these genera differentially abundant between future PWD cases and healthy controls when analyzing amplicon counts. At PND 27, a few low abundant zOTUs identified as *Lactobacillus* spp. were only present in healthy controls, but no significant differences in abundance were found in zOTUs related to this genus. Thereby, questioning if these structural zeros had any role the pre-weaning fecal microbiome of the healthy controls at PND 27. A possible explanation for the discrepancy between studies could also be that our study design and statistical analysis were more robust than previous studies.

In the present study, the sample size of pigs undergoing microbiome analysis was higher than in the two previous studies. In the study by Dou and colleagues, just 5 healthy and 5 diarrhoeic pigs were selected for bacterial 16S sequencing and compared. Karasova and colleagues, assessed slightly fewer pigs than us with 17 healthy and 17 pigs with PWD at each time point. The statistical analysis conducted in our study was also more conservative than previous studies. For example, we assessed confounding variables in our statistical analysis and accounted for the random effect of litter. Litter mates likely have bacterial compositions more similar to each other as their microbiota has been shaped in the same pen environment and they have the same mother (Grönlund et al., 2011). For the differential abundance analysis, we used ANCOM-BC and ANCOM which are

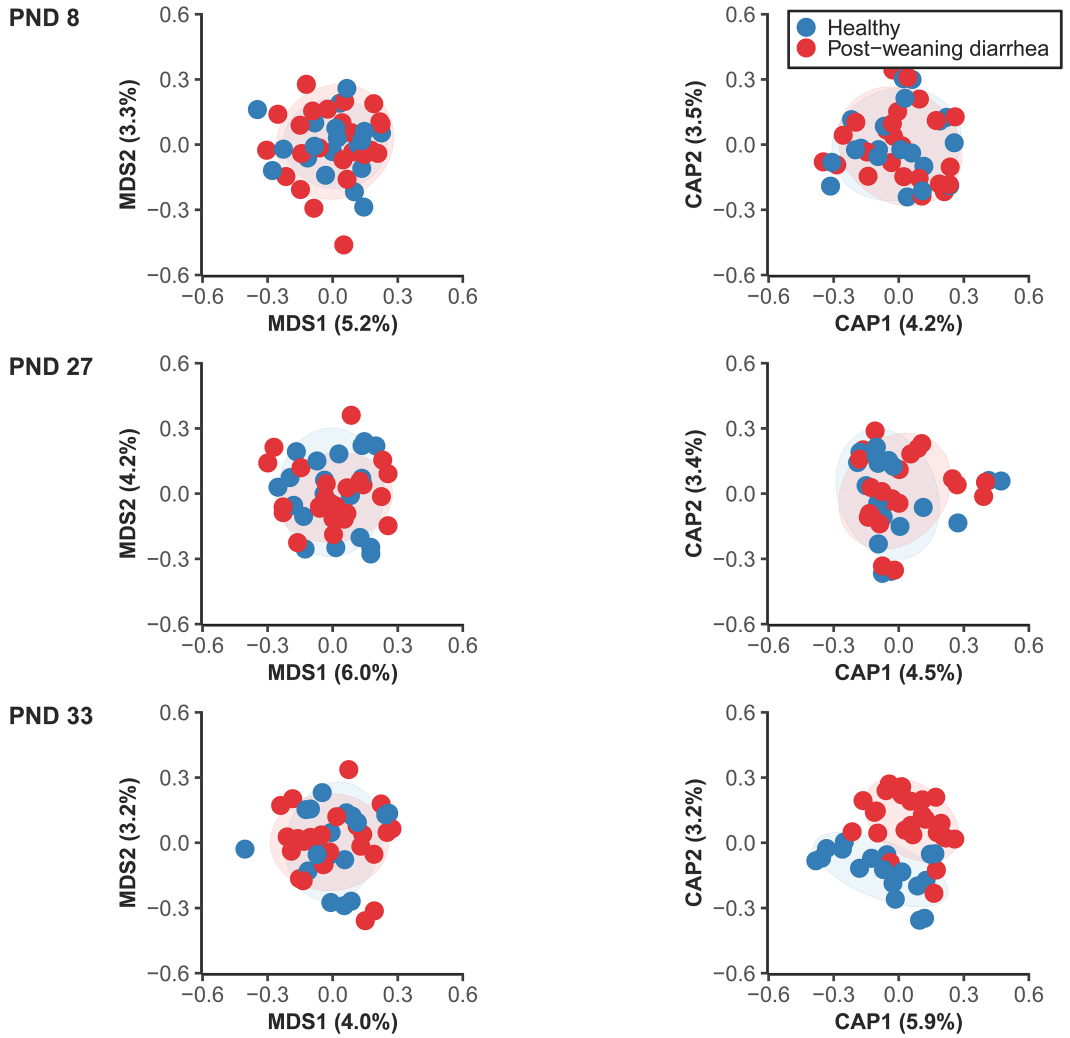

FIGURE 2
Unconstrained (left) and constrained ordination plots (right) of Canberra distance matrix of the fecal microbiome between healthy and post-weaning diarrhea (PWD) affected, at PND 8 (healthy: n=20 pigs, PWD: n=24 pigs), PND 27 (healthy: n=20 pigs, PWD: n=23 pigs), and PND 33 (healthy: n=18 pigs, PWD: n=25 pigs). Plots were created based on the rarefied zOTU table generated by 16S rRNA high throughput sequencing in the V3 region. Ellipses show 80% confidential areas assuming multivariate t-distribution. PERMANOVA was used to evaluate differences in distances at 999 permutations between the groups. Significant group difference in PWD status were found at PND 33: R^2=0.027, p=0.009. In addition, there was a significant effect of the covariable body weight at PND 33: R^2=0.028, p=0.003.

designed for analysis of microbiome data and may be more reliable in determining differentially abundant taxa (Nearing et al., 2022). Finally, an advantage of our study was that we supported our 16S sequencing data with clinical microbiology and found that an ETEC F18ac strain was associated with PWD occurrence in the study. This meant that we could assess FUT1 genotype of the pigs to get an idea of host susceptibility to ETEC F18. We found that the distribution of FUT1 susceptible pigs were similar between groups and could therefore exclude the possibility that healthy pigs were merely resistant toward ETEC F18. We found a single pig with ETEC F18 diarrhea that was FUT1 homozygous resistant and we can only speculate on reasons for this finding. In theory, viruses or other factors could also have been present at the same time as ETEC F18 and be involved in occurrence of the diarrhea, but we did not investigate for presence of viruses in the study. Even more speculative, it could be that the marker is not the true causative mutation for ETEC F18 susceptibility, although this statement contradicts with the existing literature (Meijerink et al., 2000). This assertion would call for additional studies and cannot be concluded from this study. Dou and colleagues also genotyped their pigs to rule out that differences in host susceptibility to "*Enterobacteriaceae*-associated diarrhea" were involved in prevalence of PWD. However, they only used MUC13 genotyping, which is merely a marker for ETEC F4ac susceptibility (Ren et al., 2012), and did not investigate if ETEC F4ac strain(s) were actually present or associated with PWD occurrence in their study.

In relation to the types of bacteria that were most abundant at the different time points our results were quite comparable with previous literature. At PND 8, we found the most abundant bacteria were *Lactobacillus* spp., *Prevotella* spp., *Enterococcus* spp., *Bacteroides* spp. which is comparable to the OTUs that contributed most to group discrimination at PND 7 described by Dou and colleagues (Dou et al., 2017). At PND 27 (late lactation),

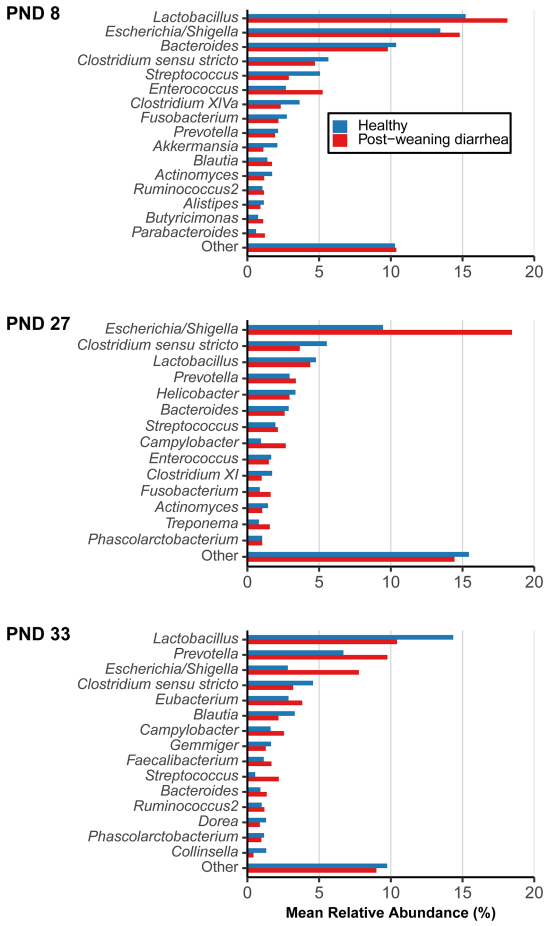

FIGURE 3
Mean relative abundance of most abundant genera, grouped by post-weaning diarrhea (PWD) status. Samples were collected longitudinally and the groups were compared at post-natal day (PND) 8 (early lactation, healthy: *n*=20 pigs, PWD: *n*=24 pigs), at PND 27 (late lactation, healthy: *n*=20 pigs, PWD: *n*=23 pigs), and PND 33 (7days after weaning, healthy: *n*=18 pigs, PWD: *n*=25 pigs) which was the time of active PWD where pigs were divided into PWD cases and healthy controls for comparison. Genera representing <1% mean relative abundance were pooled into "Other." Accumulated mean relative abundance of unassigned taxa (not shown) at genus level represented 20.00% (healthy) and 19.24% (PWD) at PND 8, 45.21% (healthy) and 37.62% (PWD) at PND 27, and 45.03% (healthy) and 41.36% (PWD) at PND 33.

we found family *Enterobacteriaceae*, *Lachnospiraceae, Ruminococcaeceae,* and *Lactobacillaeceae* (data not shown at family level, but described here for comparison) as the most abundant families, which were among the most abundant 3 days before weaning in the study by Karasova and colleagues (Karasova et al., 2021). We also observed a decrease of family *Enterobacteriaceae* and an increase in *Prevotellaceae* 7 days after weaning, similar to the observations by Karasova et al. at 4 days after weaning and to what has been described in literature (Frese et al., 2015; Mach et al., 2015).

As in previous studies, we did not collect fecal samples from the pigs every day in the 2 week period after weaning. Diarrhea occurring within this 2 week period is referred to as post-weaning diarrhea (Rhouma et al., 2017). Instead, we defined the pigs as PWD cases and healthy controls based on diarrhea occurrence at 7 days after weaning. This was the time where the farmer experienced problems with PWD in his herd and it was therefore decided to be the optimal sampling time. Diarrhea could also have occurred before or after our sampling, but it was not practically feasible at the herd to collect samples during the entire post weaning period and the same limitation apply to previous studies. Further, occurrence of diarrhea after weaning is not limited only to the first 2 weeks. However, we chose to focus on the period just after weaning, which is the period where classic, ETEC-associated post-weaning diarrhea occurs and where farmers experience most problems with diarrhea.

In the present study, the pigs with higher weaning weight had slightly higher odds of developing PWD. A possible explanation for this could be that the heavy weaners overate after weaning, which may result in increased risk for PWD (Hampson and Smith, 1986). We speculate that a higher solid feed intake of larger pigs results in more plant based substrate available and thereby promote and shape a gut microbiota with higher diversity of plant degrading bacteria (Tomova et al., 2019). This could also explain why we saw that increased body weight was associated with differences in beta diversity and a higher alpha diversity at PND 33. However, we did not measure feed intake after weaning which could have provided further insight in this. Another possible explanation for the higher odds of diarrhea in the heavier weaners could be that these pigs fought more to establish their position in the new hierarchy. This could result in additional stress and altered food and water intake (Coutellier et al., 2007) for the larger animals. It may be relevant for future similar studies to weigh the pigs at the time they are divided into disease cases and healthy controls to adjust for this potential confounder on microbiome diversity and composition.

In conclusion, the pre-weaning fecal microbiome did not contain biomarkers that could be used to identify PWD susceptible pigs in our herd. Instead, differences in the fecal microbiomes between PWD case pigs and healthy controls were first observed at 7 days after weaning. The lacking differences in the pre-weaning fecal microbiomes may be a result of similar poor gut microbiotas in both groups due to early life antibiotic treatments or be herd-specific. Alternatively, our findings may imply that the association between the pre-weaning fecal microbiome and PWD susceptibility has previously been overestimated perhaps due to small sample size and crude statistical analysis. More research is needed to assess if modulating the gut microbiota toward higher diversity and certain bacterial compositions in early-life pigs is a relevant strategy and investment for counteracting PWD.

Data availability statement

The datasets generated/analyzed for this study can be found in its supplementary information files (Supplementary material 2–4 and 6–9). Supplementary material referred to in the article can be found in the article/Supplementary material. The data presented in the study are deposited in online repositories, with the following accession numbers: Whole genome sequences of the ETEC isolates as SRA data can be found

at NCBI (BioProject: PRJNA905088) 16S amplicon sequence data as SRA data are available at NCBI (BioProject: PRJNA916113) SNPs can be found in the dbSNP data base: FUT1 (dbSNP:rs335979375).

Ethics statement

The animal study was reviewed and approved by Animal Ethics Institutional Review Board at the Department of Veterinary and Animal Sciences, University of Copenhagen. Approval number: 2022-02-PNH-006A. Written informed consent was obtained from the owners for the participation of their animals in this study.

Author contributions

MR designed the study, wrote the protocol, conducted the study, collected the data, did the statistical analysis, interpreted the data, and wrote the manuscript drafts. JN assisted in designing the study. MG, LP, and JN revised the protocol. MG and LP assisted and provided scientific input in microbiological assessment. JC-M provided scientific input for 16S rRNA sequencing, prepared the zOTU table and provided advice in statistical analysis of the microbiome data. CJ did FUT1 genotyping and assisted in interpretation of the genotyping results. All authors helped revising the manuscript drafts and approved the submitted version.

Funding

This work was supported by the Innovation fund Denmark (IFD) (File number: 7076-00038B). The funding body did not play a role in the design, analysis, and reporting of the study.

Acknowledgments

The authors thank Rasmus Jelle Syhler for assistance with animal procedures and Gitte Petersen for assistance with multiplex PCR. The authors thanks to Tina Bahrt Neergaard Mahler and Amanda Bastian Andersen for technical assistance on the FUT1 genotyping. The authors thanks to Denitsa Vladimirova Stefanova for technical assistance in DNA extraction and library preparation for 16S rRNA sequencing. The authors thank Tatjana Kristensen for technical assistance in whole genome sequencing. The authors also thank to Leonardo Victor de Knegt for statistical discussions on structural zeroes and random effects.

Conflict of interest

The authors declare that the research was conducted in the absence of any commercial or financial relationships that could be construed as a potential conflict of interest.

Publisher's note

Supplementary material

The Supplementary material for this article can be found online at: https://www.frontiersin.org/articles/10.3389/fmicb.2023.1108197/full#supplementary-material

SUPPLEMENTARY MATERIAL 1
Unconstrained (left) and constrained ordination plots (right) of binary Soerensens dice distance matrix of the fecal microbiome between healthy and post weaning diarrhea (PWD) affected, at PND 8 (healthy: n = 20 pigs, PWD: n = 24 pigs), PND 27 (healthy: n = 20 pigs, PWD: n = 23 pigs), and PND 33 (healthy: n = 18 pigs, PWD: n = 25 pigs). Plots were created based on the rarefied zOTU table generated by Illumina sequencing in the V3 region. Ellipses show 80 % confidential areas assuming multivariate t-distribution. PERMANOVA was used to evaluate differences in distances at 999 permutations between the groups. Significant group difference in PWD status were found at PND 33: R^2 = 0.03, p = 0.012. Additionally, an effect of body weight at PND 33 was found: R^2 = 0.038, p = 0.002.

SUPPLEMENTARY MATERIAL 2
Results from differential abundance analysis at post-natal day 8.

SUPPLEMENTARY MATERIAL 3
Results from differential abundance analysis at post-natal day 27.

SUPPLEMENTARY MATERIAL 4
Results from differential abundance analysis at post-natal day 33.

SUPPLEMENTARY MATERIAL 5
Pearson's correlation showed a positive correlation between relative abundance of genus *Prevotella* and body weight at PND 33: r = 0.32, 95 % confidence interval: [0.032;0.573], p = 0.03. n = 43 pigs.

SUPPLEMENTARY MATERIAL 6
Meta data for microbiome analysis.

SUPPLEMENTARY MATERIAL 7
zOTU table for microbiome analysis.

SUPPLEMENTARY MATERIAL 8
Taxonomy for microbiome analysis.

SUPPLEMENTARY MATERIAL 9
Data sheet for analysis of clinical data and microbiology.

References

Bates, D., Mächler, M., Bolker, B., and Walker, S. (2015). Fitting linear mixed-effects models using lme4. *J. Stat. Softw.* 67, 1–48. doi: 10.18637/jss.v067.i01

Bortolaia, V., Kaas, R. S., Ruppe, E., Roberts, M. C., Schwarz, S., Cattoir, V., et al. (2020). ResFinder 4.0 for predictions of phenotypes from genotypes. *J. Antimicrob. Chemother.* 75, 3491–3500. doi: 10.1093/JAC/DKAA345

Chen, J., Zhang, X., and Yang, L. (2022). GUniFrac: generalized UniFrac distances. R package version Available at: https://CRAN.R-project.org/package=GUniFrac

Clausen, P. T. L. C., Aarestrup, F. M., and Lund, O. (2018). Rapid and precise alignment of raw reads against redundant databases with KMA. *BMC Bioinform.* 19, 307–308. doi: 10.1186/s12859-018-2336-6

Coutellier, L., Arnould, C., Boissy, A., Orgeur, P., Prunier, A., Veissier, I., et al. (2007). Pig's responses to repeated social regrouping and relocation during the growing-finishing period. *Appl. Anim. Behav. Sci.* 105, 102–114. doi: 10.1016/j.applanim.2006.05.007

Dou, S., Gadonna-Widehem, P., Rome, V., Hamoudi, D., Rhazi, L., Lakhal, L., et al. (2017). Characterisation of early-life fecal microbiota in susceptible and healthy pigs to post-weaning diarrhoea. *PLoS One* 12:e0169851. doi: 10.1371/journal.pone.0169851

Dubreuil, J. D., Isaacson, R. E., and Schifferli, D. M. (2016). Animal enterotoxigenic *Escherichia coli*. *EcoSal Plus* 7:1128. doi: 10.1128/ecosalplus.ESP-0006-2016

Edgar, R. C. (2016). SINTAX: a simple non-Bayesian taxonomy classifier for 16S and ITS sequences. Preprint from bioRxiv. 074161. doi: 10.1101/074161.

Edgar, R. C. (2018). Updating the 97% identity threshold for 16S ribosomal RNA OTUs. *Bioinformatics* 34, 2371–2375. doi: 10.1093/bioinformatics/bty113

Fouhse, J. M., Yang, K., More-Bayona, J., Gao, Y., Goruk, S., Plastow, G., et al. (2019). Neonatal exposure to amoxicillin alters long-term immune response despite transient effects on gut-microbiota in piglets. *Front. Immunol.* 10:2059. doi: 10.3389/FIMMU.2019.02059/BIBTEX

Frese, S. A., Parker, K., Calvert, C. C., and Mills, D. A. (2015). Diet shapes the gut microbiome of pigs during nursing and weaning. *Microbiome* 3:28. doi: 10.1186/s40168-015-0091-8

Frydendahl, K. (2002). Prevalence of serogroups and virulence genes in *Escherichia coli* associated with postweaning diarrhoea and edema disease in pigs and a comparison of diagnostic approaches. *Vet. Microbiol.* 85, 169–182. doi: 10.1016/S0378-1135(01)00504-1

Garnier, S., Ross, N., Rudis, R., Camargo, A.P., Sciaini, M., and Scherer, C. (2021). Rvision – colorblind-friendly color maps for R. R package version 0.6.2.

Gresse, R., Forano, E., van de Wiele, T., Blanquet-Diot, S., Fleury, M. A., and Chaucheyras-Durand, F. (2017). Gut microbiota dysbiosis in postweaning piglets: understanding the keys to health. *Trends Microbiol.* 25, 851–873. doi: 10.1016/j.tim.2017.05.004

Grönlund, M.-M., Grześkowiak, Ł., Isolauri, E., and Salminen, S. (2011). Gut microbes influence of mother's intestinal microbiota on gut colonization in the infant. *Gut Microbes* 2, 227–233. doi: 10.4161/gmic.2.4.16799

Hampson, D. J., and Smith, W. C. (1986). Influence of creep feeding and dietary intake after weaning on malabsorption and occurrence of diarrhoea in the newly weaned pig. *Res. Vet. Sci.* 41, 63–69. doi: 10.1016/S0034-5288(18)30573-3

Janczyk, P., Pieper, R., Souffrant, W. B., Bimczok, D., Rothkötter, H.-J., and Smidt, H. (2007). Parenteral long-acting amoxicillin reduces intestinal bacterial community diversity in piglets even 5 weeks after the administration. *ISME J.* 1, 180–183. doi: 10.1038/ismej.2007.29

Jensen, P., and Recén, B. (1989). When to wean — observations from free-ranging domestic pigs. *Appl. Anim. Behav. Sci.* 23, 49–60. doi: 10.1016/0168-1591(89)90006-3

Joensen, K. G., Scheutz, F., Lund, O., Hasman, H., Kaas, R. S., Nielsen, E. M., et al. (2014). Real-time whole-genome sequencing for routine typing, surveillance, and outbreak detection of verotoxigenic Escherichia coli. *J. Clin. Microbiol.* 52, 1501–1510. doi: 10.1128/JCM.03617-13

Joensen, K. G., Tetzschner, A. M. M., Iguchi, A., Aarestrup, F. M., and Scheutz, F. (2015). Rapid and easy in silico serotyping of *Escherichia coli* isolates by use of whole-genome sequencing data. *J. Clin. Microbiol.* 53, 2410–2426. doi: 10.1128/JCM.00008-15

Karasova, D., Crhanova, M., Babak, V., Jerabek, M., Brzobohaty, L., Matesova, Z., et al. (2021). Development of piglet gut microbiota at the time of weaning influences development of postweaning diarrhea – a field study. *Res. Vet. Sci.* 135, 59–65. doi: 10.1016/j.rvsc.2020.12.022

Kaul, A., Mandal, S., Davidov, O., and Peddada, S. D. (2017). Analysis of microbiome data in the presence of excess zeros. *Front. Microbiol.* 8:2114. doi: 10.3389/FMICB.2017.02114/BIBTEX

Kuznetsova, A., Brockhoff, P. B., and Christensen, R. H. B. (2017). lmerTest package: tests in linear mixed effects models. *J. Stat. Softw.* 82, 1–26. doi: 10.18637/jss.v082.i13

Leite, G., Pimentel, M., Barlow, G. M., Chang, C., Hosseini, A., Wang, J., et al. (2021). Age and the aging process significantly alter the small bowel microbiome. *Cell Rep.* 36:109765. doi: 10.1016/j.celrep.2021.109765

Lin, H., and Peddada, S. D. (2020). Analysis of compositions of microbiomes with bias correction. *Nat. Commun.* 11, 3514–3511. doi: 10.1038/s41467-020-17041-7

Mach, N., Berri, M., Estellé, J., Levenez, F., Lemonnier, G., Denis, C., et al. (2015). Early-life establishment of the swine gut microbiome and impact on host phenotypes. *Environ. Microbiol. Rep.* 7, 554–569. doi: 10.1111/1758-2229.12285

Mandal, S., Van Treuren, W., White, R. A., Eggesbo, M., Knight, R., and Peddada, S. D. (2015). Analysis of composition of microbiomes: a novel method for studying microbial composition. *Microb. Ecol. Health Dis.* 11:27663. doi: 10.1038/s41467-020-17041-7

McKnite, A. M., Perez-Munoz, M. E., Lu, L., Williams, E. G., Brewer, S., Andreux, P. A., et al. (2012). Murine gut microbiota is defined by host genetics and modulates variation of metabolic traits. *PLoS One* 7:e39191. doi: 10.1371/JOURNAL.PONE.0039191

McMurdie, P. J., and Holmes, S. (2013). phyloseq: an R package for reproducible interactive analysis and graphics of microbiome census data. *PLoS One* 8:e61217. doi: 10.1371/journal.pone.0061217

Meijerink, E., Fries, R., Vögeli, P., Masabanda, J., Wigger, G., Stricker, C., et al. (1997). Two (1,2) fucosyltransferase genes on porcine chromosome 6q11 are closely linked to the blood group inhibitor (S) and Escherichia coli F18 receptor (ECF18R) loci. *Mamm. Genome* 8, 736–741. doi: 10.1007/s003359900556

Meijerink, E., Neuenschwander, S., Fries, R., Dinter, A., Bertschinger, H. U., Stranzinger, G., et al. (2000). A DNA polymorphism influencing alpha(1,2) fucosyltransferase activity of the pig FUT1 enzyme determines susceptibility of small intestinal epithelium to *Escherichia coli* F18 adhesion. *Immunogenetics* 52, 129–136. doi: 10.1007/s002510000263

Mulder, I. E., Schmidt, B., Stokes, C. R., Lewis, M., Bailey, M., Aminov, R. I., et al. (2009). Environmentally-acquired bacteria influence microbial diversity and natural innate immune responses at gut surfaces. *BMC Biol.* 7, 1–20. doi: 10.1186/1741-7007-7-79

Nearing, J. T., Douglas, G. M., Hayes, M. G., MacDonald, J., Desai, D. K., Allward, N., et al. (2022). Microbiome differential abundance methods produce different results across 38 datasets. *Nat. Commun.* 13, 342–316. doi: 10.1038/s41467-022-28034-z

Neuwirth, E. (2022). RColorBrewer: ColorBrewer palettes. R package version 1.1-3, Available at: https://CRAN.R-project.org/package=RColorBrewer (Accessed February 13, 2023).

Oksanen, J., Simpson, G., Blanchet, F., Kindt, R., Legendre, P., Minchin, P., et al. (2022). Vegan: community ecology package. R package version 2.6-2. Available at: https://CRAN.R-project.org/package=vegan (Accessed February 13, 2023).

Pedersen, K. S., and Toft, N. (2011). Intra- and inter-observer agreement when using a descriptive classification scale for clinical assessment of faecal consistency in growing pigs. *Prev. Vet. Med.* 98, 288–291. doi: 10.1016/j.prevetmed.2010.11.016

R Core Team (2022). *R: A language and Environment for Statistical Computing*. R Foundation for Statistical Computing, Vienna, Austria.

Ren, J., Yan, X., Ai, H., Zhang, Z., Huang, X., Ouyang, J., et al. (2012). Susceptibility towards enterotoxigenic *Escherichia coli* F4ac diarrhea is governed by the MUC13 gene in pigs. *PLoS One* 7:e44573. doi: 10.1371/JOURNAL.PONE.0044573

Rhouma, M., Fairbrother, J. M., Beaudry, F., and Letellier, A. (2017). Post weaning diarrhea in pigs: risk factors and non-colistin-based control strategies. *Acta Vet. Scand.* 59:31. doi: 10.1186/s13028-017-0299-7

Roubaud-Baudron, C., Ruiz, V. E., Swan, A. M. Jr., Vallance, B. A., Ozkul, C., Pei, Z., et al. (2019). Long-term effects of early-life antibiotic exposure on resistance to subsequent bacterial infection. *MBio* 10, e02820–e02819. doi: 10.1128/mBio.02820-19

Schmidt, B., Mulder, I. E., Musk, C. C., Aminov, R. I., Lewis, M., Stokes, C. R., et al. (2011). Establishment of normal gut microbiota is compromised under excessive hygiene conditions. *PLoS One* 6:e28284. doi: 10.1371/JOURNAL.PONE.0028284

Tetzschner, A. M. M., Johnson, J. R., Johnston, B. D., Lund, O., and Scheutz, F. (2020). In Silico genotyping of *Escherichia coli* isolates for extraintestinal virulence genes by use of whole-genome sequencing data. *J. Clin. Microbiol.* 58:e01269-20. doi: 10.1128/JCM.01269-20

Tomova, A., Bukovsky, I., Rembert, E., Yonas, W., Alwarith, J., Barnard, N. D., et al. (2019). The effects of vegetarian and vegan diets on gut microbiota. *Front. Nutr.* 6:47. doi: 10.3389/FNUT.2019.00047

Wang, M., Monaco, M. H., and Donovan, S. M. (2016). Impact of early gut microbiota on immune and metabolic development and function. *Semin. Fetal Neonatal Med.* 21, 380–387. doi: 10.1016/J.SINY.2016.04.004

Wickham, H. (2016). *ggplot2: Elegant Graphics for Data Analysis*. Springer-Verlag New York, NY

Wickham, H., Averick, M., Bryan, J., Chang, W., McGowan, L. D., François, R., et al. (2019). Welcome to the tidyverse. *J. Open Source Softw* 4:1686. doi: 10.21105/joss.01686

Wilke, C. (2020). cowplot: streamlined plot theme and plot annotations for 'ggplot2.' R package version 0.1.1. doi: 10.5281/zenodo.2533860

Wilke, C., and Wiernik, B. (2022). Ggtext: improved text rendering support for 'ggplot2.' R package version 0.1.2. Available at: https://CRAN.R-project.org/package=ggtext (Accessed February 13, 2023).

Zankari, E., Allesøe, R., Joensen, K. G., Cavaco, L. M., Lund, O., and Aarestrup, F. M. (2017). PointFinder: a novel web tool for WGS-based detection of antimicrobial resistance associated with chromosomal point mutations in bacterial pathogens. *J. Antimicrob. Chemother.* 72, 2764–2768. doi: 10.1093/JAC/DKX217

Zhang, W., Zhao, M., Ruesch, L., Omot, A., and Francis, D. (2007). Prevalence of virulence genes in *Escherichia coli* strains recently isolated from young pigs with diarrhea in the US. *Vet. Microbiol.* 123, 145–152. doi: 10.1016/j.vetmic.2007.02.018

frontiers | Frontiers in Microbiology

TYPE Original Research
PUBLISHED 22 March 2023
DOI 10.3389/fmicb.2023.1161287

OPEN ACCESS

EDITED BY
Kuan Zhao,
Hebei Agricultural University,
China

REVIEWED BY
Liying Chen,
Henan Agricultural University,
China
Nobalanda Mokoena,
Onderstepoort Biological Products,
South Africa

*CORRESPONDENCE
Yuanyi Peng
✉ pyy2002@sina.com
Chao Ye
✉ yechao123@swu.edu.cn

SPECIALTY SECTION
This article was submitted to Infectious Agents and Disease, a section of the journal Frontiers in Microbiology

RECEIVED 08 February 2023
ACCEPTED 02 March 2023
PUBLISHED 22 March 2023

CITATION
Chen J, Liu M, Li Y, Yang L, Tang Y, Dan R, Xie M, Fang R, Li N, Ye C and Peng Y (2023) Emergence and genomic analysis of a novel sublineage of bovine ephemeral fever virus in Southwest China.
Front. Microbiol. 14:1161287.
doi: 10.3389/fmicb.2023.1161287

Emergence and genomic analysis of a novel sublineage of bovine ephemeral fever virus in Southwest China

Jing Chen, Mengru Liu, Yixuan Li, Liu Yang, Yunhan Tang, Ruitong Dan, Muhan Xie, Rendong Fang, Nengzhang Li, Chao Ye* and Yuanyi Peng*

College of Veterinary Medicine, Southwest University, Chongqing, China

Introduction: Bovine ephemeral fever virus (BEFV), belonging to the genus *Ephemerovirus* under the family *Rhabdoviridae*, is the etiological cause for the bovine ephemeral fever (BEF) in cattle and water buffalo.

Methods: In this study, we report recent BEF outbreaks in Southwest China and sequence the complete genome sequence of one BEFV isolate BEFV/CQ1/2022.

Results and Discussion: Comparative genomic analyses between BEFV/CQ1/2022 and isolates available in GenBank revealed remarkable inter-isolate divergence. Meanwhile, the sequence divergence was related to the evolutionary relationships and geographical distribution of the isolates. Phylogenetic analysis indicated that the global BEFV isolates can be divided into 4 distinct lineages. The East Asia lineage was the most diverse and could be subdivided into 4 sublineages. Notably, BEFV/CQ1/2022 and other 10 recent isolates from Mainland China were found to be clustered in sublineage 2. Additionally, recombination analysis provided evidence of BEFV recombination among East Asian isolates for the first time. Taken together, a novel sublineage of the East Asian BEFV emerged in Southwest China, and large divergence and potential recombination among BEFV strains were investigated in this study, which may improve understanding of BEFV epidemiology and evolution.

KEYWORDS

bovine ephemeral fever virus, genomic analysis, phylogenetic analysis, sublineage, recombination

1. Introduction

Bovine ephemeral fever virus (BEFV) is an arthropod-borne rhabdovirus under the genus *Ephemerovirus* in the *Rhabdoviridae* (Murphy et al., 1972). Bovine ephemeral fever virus is considered to be the etiological cause for bovine ephemeral fever (BEF) of cattle and water buffaloes in tropical and subtropical regions including Africa, Asia, the Middle East, and Australia (Zheng and Qiu, 2012; Trinidad et al., 2014). Bovine ephemeral fever occurs seasonally in adjacent temperate zones and mosquitoes act as major vectors for BEFV spreading (Trinidad et al., 2014). The disease is characterized by high fever (triphasic), pneumonia, depression, stiffness, lameness, and paralysis. Although the BEF case mortality is thought to be very low, morbidity rate may go as high as 100% (Pyasi et al., 2020).

Bovine ephemeral fever virus is an enveloped virus with a bullet-like shape, which is structurally similar to other mammalian rhabdoviruses such as rabies virus and vesicular stomatitis

virus (Walker and Klement, 2015; Abayli et al., 2017). The genome of BEFV is a negative-sense single-stranded RNA with approximately 14.9 kb in length, mainly encoding 5 canonical rhabdovirus structural proteins in the following order: nucleoprotein (N), phosphoprotein (P), matrix protein (M), glycoprotein (G), and RNA-dependent RNA polymerase (L; Walker, 2005). The N protein is the most abundant element of virion that tightly associates with the genome, the P protein is essential for viral genome transcription and replication, the M protein encapsulates the nucleocapsid, the L protein is an RNA-dependent RNA polymerase that helps in the formation of transcription-replication complex, and the glycoprotein G is the only protein exposed to host cell surface during infection and acts as the major neutralizing antigen (Walker et al., 1991, 1992). Furthermore, a total of 4 independent antigenic sites (G1-G4) in the neutralizing G protein ectodomain have been identified. G1 (aa 487–503) is a linear antigenic site, G2 (aa 168–189) and G3 (aa 49–63, aa 215–231, and aa 262–271) are nonlinear conformational sites, however, the location of G4 has not yet been determined (Trinidad et al., 2014). In addition, a nonstructural glycoprotein (GNS) and several small accessory proteins (α1, α2, α3, β, and γ) are also located in the viral genome region between the G and L genes, but their functions are largely unknown (Walker, 2005).

Although the BEFV isolates are considered to be serologically related within a single cross-neutralizing serotype worldwide (Trinidad et al., 2014), phylogenetic analysis based on G gene sequences shows that the BEFV isolates worldwide can be classified into four different groups including the Australian, East Asian, Middle East and the relatively separate South African lineages (Kato et al., 2009; Zheng and Qiu, 2012; Omar et al., 2020). In China, BEF has been found endemic in Taiwan and 26 provinces in Mainland China since the first report in 1955 (Gao et al., 2017), and the first BEFV strain JB76H was isolated from an infected cow in Beijing in 1976 (Bai et al., 1987). Then, frequent epidemics of BEFV have been observed in Mainland China during the last two decades. For instance, the strain JT02L was isolated from dairy cattle in Zhejiang in southeast China in 2002 (Zheng et al., 2009), the LS11 and LYC11 strains were originated from dairy cattle in Henan in central China in 2011 (Zheng and Qiu, 2012), the 2011-Shandong isolate was from a cow with high fever in Shandong in eastern China in 2011 (Hou et al., 2012), and several isolates were collected in Guangdong and Guangxi provinces in Southern China in 2013–2017 (Kun et al., 2020). However, information on the nucleotide sequence variation of the BEFV isolates in Southwest China is still lacking.

In this study, we recently collected and analyzed clinical samples of BEF suspected cattle from outbreaks in Southwest China. Firstly, the complete G gene sequences of 4 samples from 3 different regions were obtained and they shared 100% homology. Then, the genome sequence of one sample (BEFV/CQ1/2022) was obtained by overlapping primer-based PCR and Sanger sequencing. Phylogenetic analysis based on BEFV complete sequences indicated that the current isolate BEFV/CQ1/2022 and one isolate BA/RZ/IR from Iran clustered within a sublineage of the East Asia lineage. Comparative genomic analysis suggested that large diversity existed among BEFV isolates with BEFV/CQ1/2022 highly similar to the East Asian strain JT02L but significantly different from isolates from other lineages. A phylogenetic tree based on G ectodomain encoding sequences indicated that the global BEFV isolates can be divided into 4 distinct lineages, and highlighted that the East Asia lineage was the most diverse and could be subdivided into four sublineages. Notably, BEFV/CQ1/2022 and other 10 recent isolates from Mainland China were clustered in the distinct sublineage 2. Recombination analysis showed that JT02L might be a minor parent-like strain of the Iranian strain BA/RZ/IR and BEFV/CQ1/2022 was more likely to be the major parent-associated strain with its ancestral strain as the actual major parent-like strain.

2. Materials and methods

2.1. Sample collection

In September 2022, the suspected outbreaks of bovine ephemeral fever in cattle occurred in Chongqing and Sichuan in Southwest China. With the owners' consent, clinical samples including blood, nasal swab and several tissues from the symptomatic cattle (Table 1) were collected with sterile collection tubes and immediately transported to our laboratory at temperatures between 2 and 8°C for routine diagnostic purposes. Our sampling procedures were approved by Institutional Animal Care and Use Committee of Southwest University, Chongqing, China (IACUC-20221114-03).

2.2. Etiological examinations of clinical samples

For etiological examinations, samples were either pooled or prepared separately, and then used for total RNA extraction by TRIzol reagent (Invitrogen, United States) according to the manufacturer's instructions. RNA samples were then subjected to cDNA synthesis using PrimeScript™RT reagent Kit with gDNA Eraser (TaKaRa, Dalian, China). And the primers BEFV-F (AGAGCTTGGTGTG AATAC) and BEFV-R (CCAACCTACAACAGCAGATA) were used to examine the presence of BEFV.

2.3. Genome sequencing of BEFV

For both amplifying the complete genome sequence and the G gene of BEFV, a set of primers (shown in Table 2) based on conserved regions of the viral genome was designed and used for obtaining the BEFV whole genome (Primer pairs 1–9) and the G gene sequences (Primer pairs 2–3) in BEFV-positive samples. The RT-PCR amplicons of expected sizes were extracted from agarose gels, cloned into the pMD-19 T vector (TaKaRa, Dalian, China), and sequenced by Sanger sequencing using the universal primers M13-47/M13-48. The complete genome and the G gene sequences were then assembled using SeqMan software (DNASTAR, Madison, WI, United States). Subsequently, the whole genomic cDNA sequences of BEFV/CQ1/2022 were submitted to NCBI GenBank database with accession no. OP887034.

2.4. Sequence annotation and protein-coding sequence alignments

The annotation of BEFV/CQ1/2022 was performed based on those annotations of the BEFV complete sequences available in the

TABLE 1 Clinical sample information in this study.

Samples No.	Collection date	Source	Geographical origin	PCR test results of BEFV
1	2022.9.14	Blood	Dianjiang, Chongqing	+ (test with pooled samples 1–3)
2	2022.9.14	Blood	Dianjiang, Chongqing	
3	2022.9.14	Blood	Dianjiang, Chongqing	
4	2022.9.14	Blood	Dianjiang, Chongqing	+ (test with pooled samples 4–6)
5	2022.9.14	Blood	Dianjiang, Chongqing	
6	2022.9.14	Blood	Dianjiang, Chongqing	
7	2022.9.14	Blood	Dianjiang, Chongqing	+ (test with pooled samples 7–9)
8	2022.9.14	Blood	Dianjiang, Chongqing	
9	2022.9.14	Blood	Dianjiang, Chongqing	
10	2022.9.14	Blood	Dianjiang, Chongqing	+ (test with pooled samples 10–12)
11	2022.9.14	Blood	Dianjiang, Chongqing	
12	2022.9.14	Blood	Dianjiang, Chongqing	
13	2022.9.14	Nasal swab	Dianjiang, Chongqing	+ (test with pooled samples 13–16)
14	2022.9.14	Nasal swab	Dianjiang, Chongqing	
15	2022.9.14	Nasal swab	Dianjiang, Chongqing	
16	2022.9.14	Nasal swab	Dianjiang, Chongqing	
17	2022.9.14	Nasal swab	Dianjiang, Chongqing	+ (test with pooled samples 17–18)
18	2022.9.14	Nasal swab	Dianjiang, Chongqing	
19	2022.9.14	Nasal swab	Dianjiang, Chongqing	+ (test with pooled samples 19–21)
20	2022.9.14	Nasal swab	Dianjiang, Chongqing	
21	2022.9.14	Nasal swab	Dianjiang, Chongqing	
22	2022.9.24	Lung	Fengdu, Chongqing	+
23	2022.9.24	Liver	Fengdu, Chongqing	–
24	2022.9.24	Spleen	Fengdu, Chongqing	–
25	2022.9.24	Kidney	Fengdu, Chongqing	–
26	2022.9.24	Heart	Fengdu, Chongqing	–
27	2022.9.24	Small intestine	Fengdu, Chongqing	–
28	2022.10.17	Lung	Meishan, Sichuan	+
29	2022.10.17	Liver	Meishan, Sichuan	–
30	2022.10.17	Spleen	Meishan, Sichuan	–
31	2022.10.17	Small intestine	Meishan, Sichuan	–
32	2022.10.17	Heart	Meishan, Sichuan	–

GenBank database. Then, the BEFV/CQ1/2022 genome was aligned with those of the representative isolates BA/RZ/IR (GenBank Accession No. MZ687779), JT02L (GenBank Accession No. KY315724), IND/IDR/BEFV/2019 (GenBank Accession No. MN905763), BB7721 (GenBank Accession No. AF234533) and RSA/OBP/BEF2008 (GenBank Accession No. MW463337). The multiple alignment was performed using the mVista LAGAN genomics analysis tool (Frazer et al., 2004). To investigate the diversity of each protein-coding sequences between isolates from different phylogenetic clusters, the corresponding amino acid alignments with the representative isolates (BEFV/CQ1/2022, JT02L, IND/IDR/BEFV/2019, BB7721 and RSA/OBP/BEF2008) were generated using MEGA 5.2 for sequence comparisons. Then, the amino acid variations unique to the corresponding sites of the BEFV/CQ1/2022 genome were identified and recorded in Table S1.

2.5. Phylogenetic analysis

The genomic sequence of BEFV isolate BEFV/CQ1/2022 was aligned with BEFV isolates available in the GenBank database using the MAFFT online server to investigate the genetic variation among BEFV isolates. Then, a phylogenetic tree was constructed using the MEGA 5.2 software and the maximum likelihood (ML) method and the Tamura-Nei model of nucleotide substitution with 1,000 bootstrap replications (Tamura et al., 2011).

TABLE 2 Primers used for Bovine ephemeral fever virus (BEFV) genome amplification in this study.

Primer pairs	Sequence (5′–3′)	Locations[a]	Length of amplicon (bp)
1	ACGAGAAAAAACAAAAAAACTAATTGATA	1–29	2,728
	GCAGTTCCGGTGAATTCTATTACCTCG	2,702–2,728	
2	TTCAAAACCAATAGAAAGAACAAC	2,522–2,545	1,698
	TAAGATCCGATCCCATAATGAT	4,198–4,219	
3	ACAGATAGAACAGAATTTGAAG	3,921–3,942	1754
	GCTTAATCAACTCTAGTCTAAT	5,653–5,674	
4	ATTATCCTCCTCCAAAGTGCGA	5,393–5,414	1,560
	TCAATATAATCCAAAATCCTAG	6,931–6,952	
5	AACAGGCAATGGAGAAAGG	6,815–6,833	2,368
	GTTTGAAACCTGCTAATTA	9,164–9,182	
6	GGACATAAGTGGACGGTGGATA	9,063–9,084	1967
	TTTCTCCTCTGATTGCTGGATT	11,008–11,029	
7	GGAACAATAAAGGGACTGCCAA	10,807–10,828	2018
	GTGAACTCTGATATAAATGATG	12,803–12,824	
8	GGTAGGTGATTCACTGTTAAGT	12,582–12,603	1,375
	AGCATGTCTAATATATTTGTA	13,935–13,956	
9	GAAACAGAATTCTATGATGATTGACCTGAT	13,767–13,788	1,133
	ACGAAGAAAAACAAATAAAATACAATTCCT	14,870–14,899	

[a]The location is determined based on the representative strain Bovine/China/Henan1/2012 (KM276084.1).

In addition, the ectodomain encoding sequence of G gene was most widely used for the phylogeny of BEFV. To understand the genetic diversity of BEFV worldwide, all the available G ectodomain encoding sequences (1,527 nt) were retrieved from NCBI GenBank database and analyzed together with the corresponding sequence of BEFV/CQ1/2022 collected in this study. Multiple sequence alignment was performed using the MUSCLE program implemented within the MEGA 5.2 software. Phylogenetic analysis based on the alignment of these G ectodomain encoding sequences were performed in MEGA5.2. A phylogeny was constructed by the neighbor-joining (NJ) method with the Kimura 2-parameter model. The reliability was evaluated by the bootstrap test with 1,000 replicates.

2.6. Antigenic sites analysis of BEFV G protein

In this study, the aa sequences deduced from BEFV G ectodomain encoding sequences were aligned in the MEGA 5.2 software, and the aa sequence variation within the G1, G2 and G3 sites were analyzed with the DNASTAR MegAlign software. The representative BEFV isolates were selected according to their positions in the phylogenetic tree based on G ectodomain encoding sequences.

2.7. Recombination analysis

All the 16 complete sequences of BEFV in this study were aligned using the MAFFT online server with the default parameter settings, then analyzed using two different types of software. Firstly, the RDP4.39 software was used to detect potential inter-isolate recombination events and the positions of breakpoints. Default parameter settings were used and the threshold value of p was set at 0.05 using the Bonferroni correction. To further validate the putative recombination events, the SimPlot 3.5.1 program was then used to identify the putative recombinant, which performed the bootscan analysis with a sliding window of 500 bp, a step size of 10 bp, gap stripped, and the Kimura 2-parameter substitution model. Phylogenetic trees were then constructed to validate the detected recombination signals when querying strain BA/RZ/IR, using the alignments of recombination region and non-recombination region divided by the predicted breakpoints, respectively.

3. Results

3.1. Etiological analysis of clinical samples

In this study, a total of 32 clinical samples including 12 blood samples, 9 nasal swabs, and 11 tissue samples were collected and used for RNA extraction and cDNA synthesis. Then, the cDNAs of 12 blood samples and 9 nasal swabs obtained from Dianjiang in Chongqing city were pooled by 2–4 samples for the subsequent BEFV detection. Finally, the results of PCR detection showed that all the tested samples were BEFV positive (Table 1). Meanwhile, the lung samples collected from Fengdu in Chongqing city and Meishan in Sichuan province were also tested to be BEFV positive by PCR, respectively. But the liver, spleen, kidney, heart and small intestine were found to be BEFV negative (Table 1). Furthermore, 4 samples collected from Dianjiang (2 blood samples), Fengdu (1 lung sample), and Meishan (1 lung

sample) were selected to obtain their G gene sequences by PCR and Sanger sequencing. The results showed that all the 4 samples shared 100% sequence homology (Data not shown), indicating that the recent BEF outbreaks in Southwest China may be caused by the same BEFV strain.

3.2. Comparative genomic analysis of BEFV isolates

To investigate the genomic characterization of the BEFV isolate BEFV/CQ1/2022, the genome of BEFV/CQ1/2022 was sequenced and found to be 14,925 bp in length. Moreover, the BEFV/CQ1/2022 genome has the same genomic composition as the other strains studied, however, several hypervariable regions in the P, M, G, GNS, and L genes were found in the multi-genome alignment of the BEFV strains (Figure 1). Compared to the relative diversity found between BEFV/CQ1/2022 and IND/IDR/BEFV/2019, BB7721 & RSA/OBP/BEF2008 isolates, the genomic diversity between the isolates (BEFV/CQ1/2022, BA/RZ/IR and JT02L) showed fewer differences (Figure 1). Furthermore, the similarities in their genomic sequences were generally consistent with their phylogenetic relationships. Phylogenetic analysis indicated that IND/IDR/BEFV/2019, BB7721, RSA/OBP/BEF2008 and JT02L clustered in the lineages of Middle East, Australia, Africa and East Asia, respectively (Figure 2). Meanwhile, the BEFV/CQ1/2022 and BA/RZ/IR isolates were closely related and clustered in a sublineage of the East Asia lineage (Figure 2). In addition, numerous aa mutations were found between BEFV/CQ1/2022 and the isolates from the Middle East, Australia and Africa lineages (Table S1). By contrast, the East Asian isolates BEFV/CQ1/2022 and JT02L showed a high degree of identity in their protein coding sequences (Table S1). Furthermore, due to the frequent occurrence of initiation and termination codons mutations, several aa insertions or deletions were found in BEFV-encoded proteins. Compared to BEFV/CQ1/2022, the α2 ORF of JT02L, the α3 ORF of IND/IDR/BEFV/2019, the β ORF of BB7721, the GNS ORF of RSA/OBP/BEF2008, and the L ORF of JT02L, IND/IDR/BEFV/2019 and BB7721 were truncated by 4 aa (MFGY), 20 aa (KIGHNAKRR SKFRLLSVAQH), 40 aa (EEYGVIDISIKVEPRGLRFLKRSSEIDICDIP RKVRVVPT), 8 aa (QRFFKLDY) and 3 aa (MKK), respectively; meanwhile, the α3 ORF of JT02L and BB7721 were elongated by 22 aa (QRELVMFGRCKETDINRVPESF) and 16 aa (QRELVVSGGHEKTN

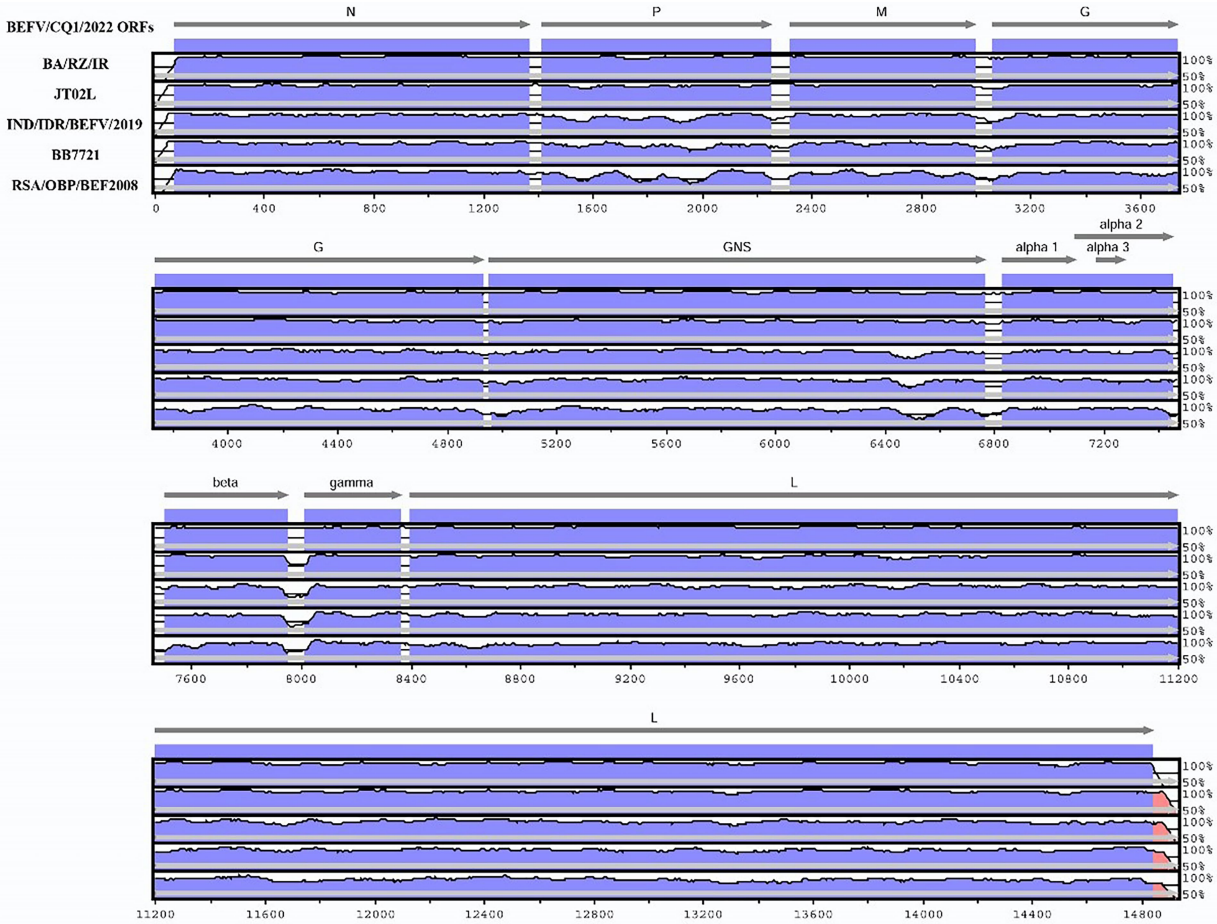

FIGURE 1
Genomic organization of Bovine ephemeral fever virus (BEFV) and comparison of sequence conservation within the BEFV/CQ1/2022, BA/RZ/IR, JT02L, IND/IDR/BEFV/2019, BB7721 and RSA/OBP/BEF2008 isolates. The mVISTA similarity plot showed sequence conservation among BEFV isolates BEFV/CQ1/2022, BA/RZ/IR, JT02L, IND/IDR/BEFV/2019, BB7721, and RSA/OBP/BEF2008. Sequence conservation was determined from a multiple sequence alignment, and the conservation score was plotted in a sliding 100-bp window.

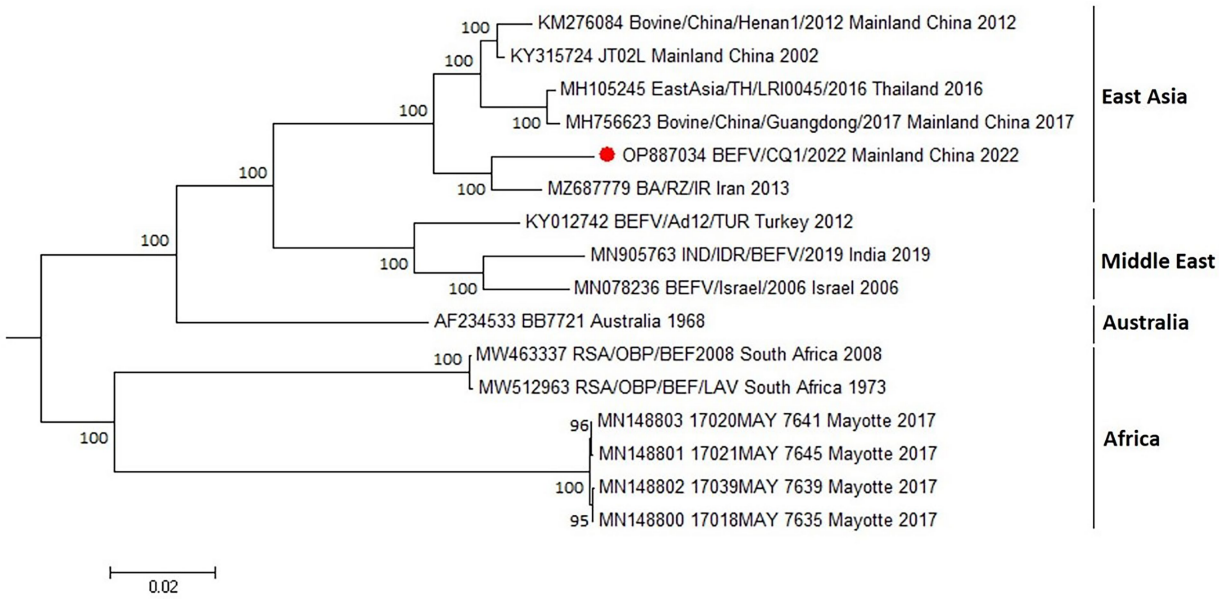

FIGURE 2
Phylogenetic tree construction based on the complete genome sequence of BEFV. The maximum likelihood (ML) method with bootstrap values (1,000 replicates) was used for phylogenetic tree construction with bootstrap values shown at the nodes. Bootstrap values less than 60% were not shown on the corresponding nodes. Red circle indicated the sample investigated in the current study. GenBank accession numbers along with isolates names, sample collection sites and year of the collection were indicated for reference viruses.

IN), respectively; additionally, the start codon alteration (ATG to GTG) was found in the α3 ORF of RSA/OBP/BEF2008, which might cause a translation defect in the α3 ORF of this BEFV isolate (Table S1).

3.3. Phylogeny of BEFVs based on G ectodomain encoding sequences

To predict the evolution of BEFVs worldwide, the 1,527 nt G ectodomain encoding sequence of BEFV/CQ1/2022 was aligned to the global data set deposited in the GenBank database. Then, the phylogenetic tree was constructed by the neighbor-joining (NJ) method. It showed that the global BEFV isolates were generally clustered geographically and divided into 4 large and distinct lineages (Figure 3). The East Asia lineage showed the greatest diversity and mostly consisted of isolates from Japan, Thailand, Mainland China and Taiwan with a few isolates from Turkey (3), Iran (3) and Egypt (1). By contrast, the Middle East lineage comprised isolates mostly from Middle East countries Turkey, Israel and Iran with only one isolate from India. Similarly, strains of the Australia lineage were all isolated in Australia. Additionally, the Africa lineage was composed of Australian and African isolates (Figure 3). Noticeably, the East Asia lineage could be subdivided into 4 sublineages (sublineage 1–4). Meanwhile, most of the isolates from Mainland China including BEFV/CQ1/2022 were found in sublineage 2, and the Middle East-derived isolates were found in sublineages 2 and 4 (Figure 3), suggesting a close evolutionary relationship between the recent East Asian isolates and Middle Eastern isolates.

3.4. Amino acid variation of the antigenic sites in BEFV G protein

As shown in Figure 4, the aa sequences of G1-G3 were relatively conserved among the BEFV isolates in the East Asia lineage, except for 15 aa substitutions in 11 isolates. Specifically, three residues at positions 490, 499, and 503 in the G1 sites were substituted from D to E, from S to N, and from K to T, respectively. And only two residues at positions 170 (T) and 187 (I) in the G2 sites were replaced with N and T, respectively. By contrast, a total of 10 substitutions (N53K, K215Q, R218K, E220A, E223D, T224I, E225D, E229G, E263G and Q271R) were found in the G3 sites (Figure 4). Additionally, compared to isolates from East Asia lineage, the aa sequences of G1-G3 among Middle East, Australia and Africa were significantly different. Most isolates from these lineages had their representative aa sequences in the antigenic sites, such as E223D and K503T in the Middle East lineage, R218K, E223D, T224K, S499N, K503R in the Australia lineage, K56R, T179A, R218M, N222D, E223D, S268A, F270L, V496I, K503N in the Africa lineage. In particular, some of the representative aa sequences were located at the putative glycosylation sites of G protein, which might influence the G protein antigenicity of isolates from these lineages (Figure 4).

3.5. Recombination analysis in BEFV isolates

To examine the potential recombination events in the BEFV genomes, we performed recombination analysis of the complete sequence alignment of BEFVs by the RDP and SimPlot softwares. The

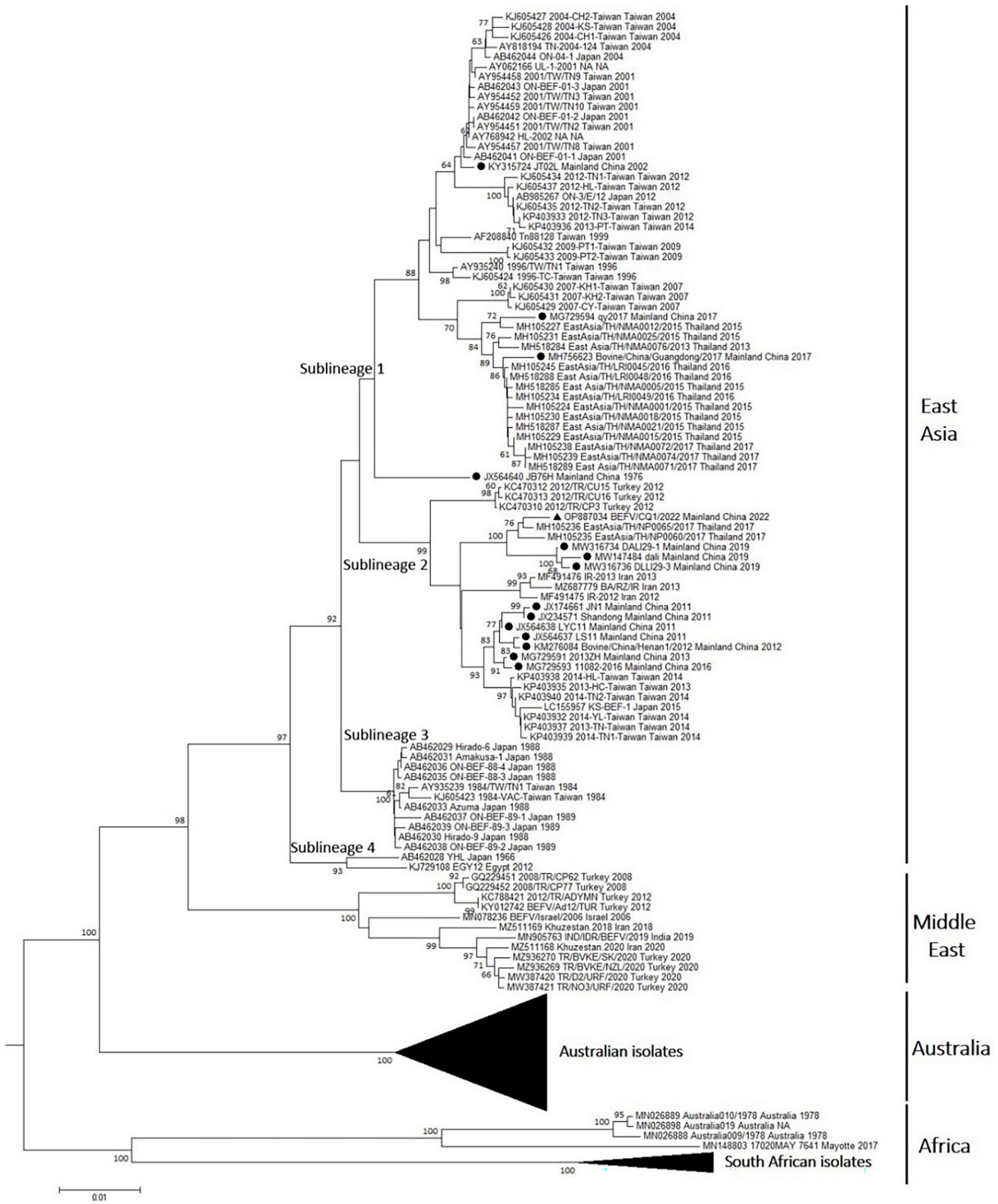

FIGURE 3
Phylogenetic tree of the BEFV isolates based on the comparison of G ectodomain encoding sequences. The phylogenetic tree of G ectodomain encoding sequences constructed by using neighbor-joining (NJ) method with Kimura 2-parameter model with bootstrap values of 1,000 replicates. The BEFV isolate BEFV/CQ1/2022 was indicated by black triangle, and other 14 BEFV strains from Mainland China were indicated by black circles. The details of Australian isolates in the Australia lineage and South African isolates in Africa lineage were not shown.

bootscan analysis was performed in SimPlot 3.5.1 software by the Kimura 2-parameter method, and the result showed that the BA/RZ/IR strain from Iran might be a putative recombinant. Furthermore, the BA/RZ/IR-like strain BEFV/CQ1/2022 was more likely to be the major parent-associated strain and JT02L might be the minor parent-like strain. In addition, according to the results of RDP, two putative recombination breakpoints were located at 10558 nt and 13,274 nt in the alignment, respectively; and the recombination region was located

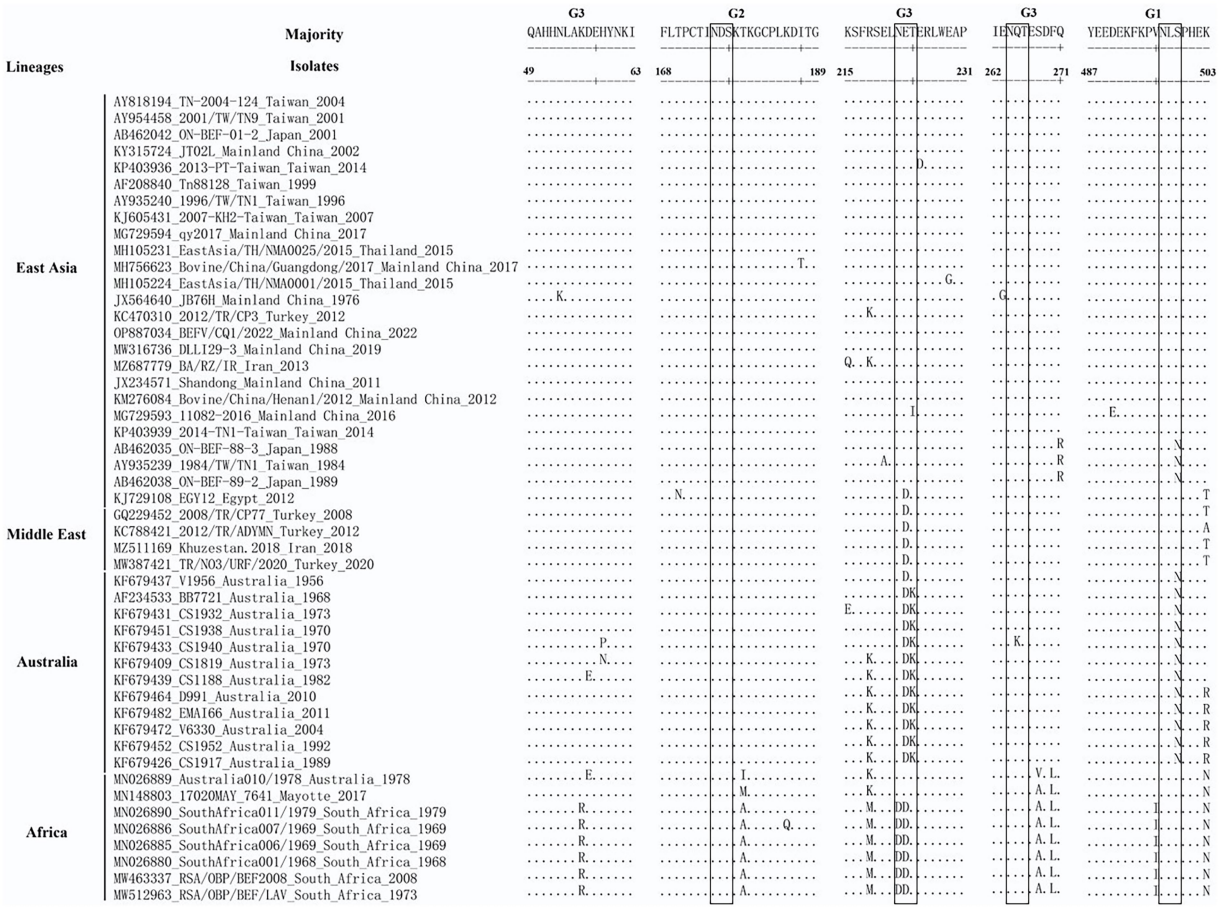

FIGURE 4
Comparison of antigenic sites of G protein among BEFV isolates. The amino acid residues differing from the sequences of the majority are denoted. Putative glycosylation sites are boxed.

in the BEFV L gene (Figure 5A). To further validate and confirm the putative recombination event, phylogenetic analyses of the recombination and non-recombination regions separated by recombination breakpoints were performed. Then, phylogenetic tree based on the non-recombination region indicated that BEFV/CQ1/2022 and BA/RZ/IR were clustered together in a relatively independent clade, however, JT02L and BA/RZ/IR showed more close phylogenetic relationship in the phylogeny based on the recombination region (Figure 5B), which further confirmed the putative recombination event.

4. Discussion

Bovine ephemeral fever virus (BEFV) is the causal agent of bovine ephemeral fever and is an economically important arthropod-borne virus of cattle and water buffaloes (Walker and Klement, 2015). In recent years, outbreaks of BEFVs have been reported in several provinces in China, which have caused a considerable economic losses to the livestock industry (Kun et al., 2020). In this study, the complete G gene sequences of several BEFV samples and the whole genome of BEFV/CQ1/2022 from BEF outbreaks in Southwest China were sequenced and compared with the BEFV sequences available in the GenBank database. It showed that the G gene sequences of 4 samples from 3 different outbreaks shared 100% homology, indicating the BEF outbreaks may be caused by the same BEFV strain. Genomic sequence alignment showed that BEFV/CQ1/2022 shared high sequence identity with BEFV BA/RZ/IR from Iran and JT02L from China. However, compared to the isolates from other lineages, several hypervariable regions were found in the multi-genome alignment of BEFV/CQ1/2022 and these BEFV isolates. More interestingly, frequent initiation and termination codon mutations were found among BEFV isolates, which further led to the occurrence of several aa insertions/deletions and even the α3 ORF translation defect in BEFV isolates. However, the effect of these aa mutations on the function of corresponding viral proteins needs to be explored in the future.

Phylogenetic analysis based on the BEFV genomic sequences indicated that the BEFV/CQ1/2022 and BA/RZ/IR isolates were closely related and clustered in a sublineage of the East Asia lineage, which was consistent with the finding of a previous study that several East Asian isolates together with the Iranian isolate could construct a separate lineage (Bakhshesh and Abdollahi, 2015). Moreover, one recent study showed that BEFV could be classified into 4 phylogenetic groups (Omar et al., 2020). In this study, a phylogenetic tree based on G ectodomain encoding sequences further revealed that the global BEFV isolates were clustered geographically and separated into four phylogenetic lineages with the African and several Australian isolates clustering in a distinct lineage separate from other lineages. Additionally, the isolates from East Asia lineage were found to be more

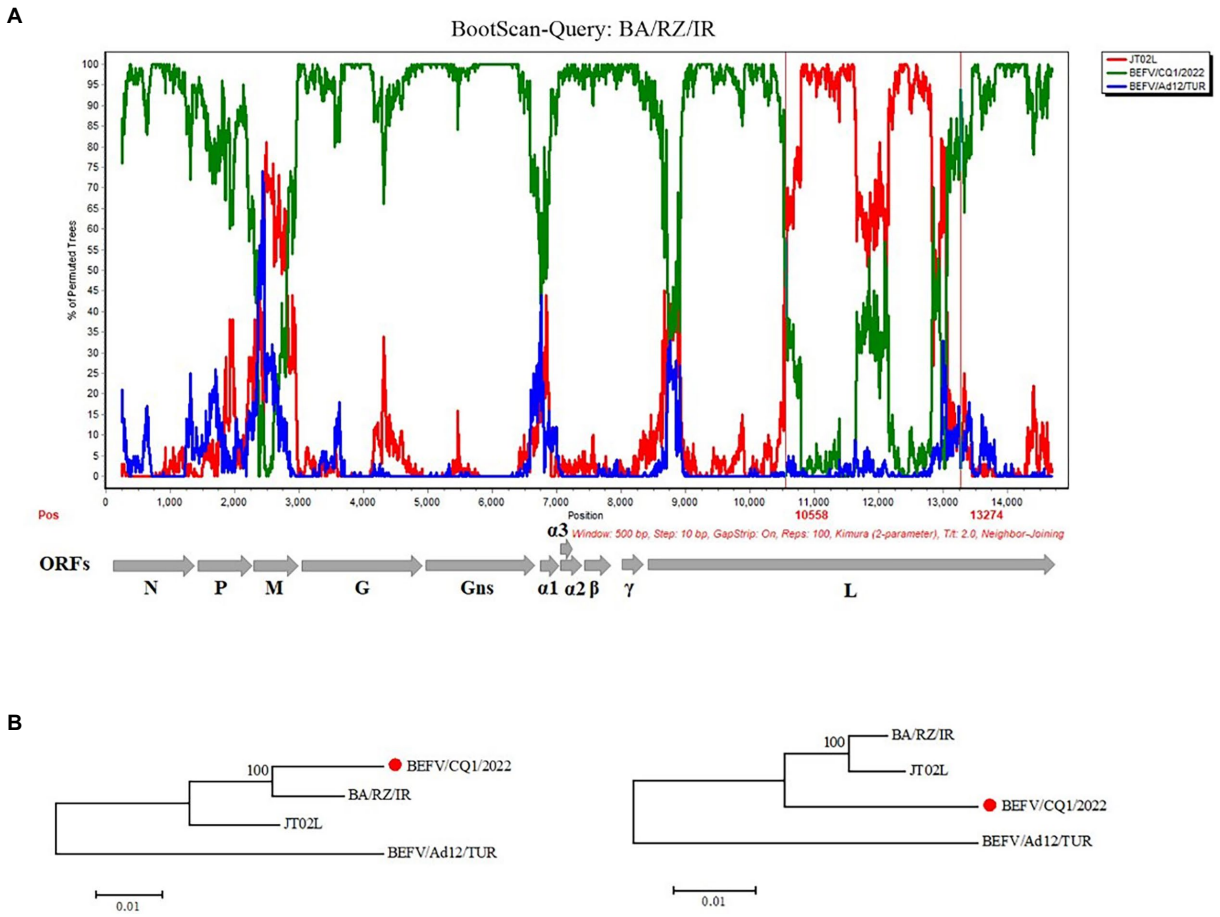

FIGURE 5
Recombination analysis of the BA/RZ/IR isolate. **(A)** BootScan analysis in the Simplot software was performed with BA/RZ/IR as the query sequence and BEFV/CQ1/2022 (green) and JT02L (red) as putative parental isolate and BEFV/Ad12/TUR (blue) as the outgroup isolate. The red vertical lines showed the potential breakpoints at position 10,558 and 13,274nt. **(B)** Phylogenetic trees of non-recombination region (the corresponding loci in the alignment: 1–10,558; 13,275-terminal site) and recombination region (the corresponding loci in the alignment: 10,559–13,274) were shown below, respectively. The phylogenetic trees were constructed using the neighbor joining (NJ) method in MEGA 5.2 software with 1,000 bootstrap replicates.

diverse and this lineage can be separated into four sublineages. Particularly, several Middle East-originated isolates from Turkey, Iran, and Egypt were found to be clustered in sublineages 2 and 4 of the East Asia lineage, indicating a close evolutionary relationship between the East Asian and Middle Eastern isolates.

Interestingly, the causative agents LYC11 and Shandong of the BEF outbreaks in China in 2011 were clustered in sublineage 2 of the East Asia lineage. Coincidentally, several Iran and Turkey-derived isolates collected in 2012–2013 were also clustered in sublineage 2, and Iran-derived isolates were closely related to the isolates LYC11 and Shandong from Mainland China. In addition, a molecular epidemiological study in Egypt reported that a BEFV isolate collected in 2005 was closely related to a 2004 isolate from Taiwan, suggesting that BEFV may have been imported through cattle trade from East Asia to the Middle East (Aziz-Boaron et al., 2012). Moreover, it had been reported that BEFV could spread *via* biological vectors through wind dispersal between East Asia and the Middle East (Chaisiririat et al., 2018). Hence, due to the relatively close geographical distance and frequent trade between East Asia and Middle East countries, more East Asia-originated isolates may have appeared and circulated in the Middle East countries. Similarly, an India-derived isolate was located in the Middle East lineage with the isolates from Middle East countries and several Australian isolates were found in the Africa lineage. The crossing of genetic relationships between isolates from different geographical origins suggests that the evolution and variation of BEFV are intensified globally, which requires extensive attention from all over the world.

The envelope glycoprotein (G) of BEFV has the capacity to induce the neutralizing immune response and then protect against experimental challenge in cattle. Neutralizing antigenic determinants of G protein have been identified as 4 independent antigenic sites (G1–G4). Furthermore, the amino acid (aa) sequences corresponding to G1, G2, and G3 have been determined. Here, the aa sequence differentiation in the antigenic sites G1-G3 of the BEFV isolates was analyzed. Overall, we found a certain amount of aa variation in the G1 to G3 antigenic sites between isolates used in this study. In the aa alignment of G protein among East Asian strains, aa variation sites were relatively scattered and the representative aa variation was not common. By contrast, consistent with the previous studies (Kato et al., 2009; Zheng and Qiu, 2012), the representative substitutions (E223D) and (T224K) in the putative glycosylation sites of G3 were found to be present in the majority of isolates in the Middle East and Australia lineage, respectively, which may play an important role in antigenic discrimination between the isolates of East Asia lineage and Middle

East & Australia lineages. More representative aa variation sites, including those (N222D and E223D) in the putative glycosylation sites, were also found in the Africa lineage. It can be speculated that these altered aa sites, especially the putative glycosylation sites, were likely to affect the conformation and antigenicity of G proteins, which may challenge the effectiveness of BEFV vaccines currently in use. However, further experiments using neutralizing monoclonal antibodies are still needed to determine the precise antigenic roles of this aa variation in the corresponding BEFV isolates.

Previously, He et al. had proposed that the East Asian BEFV was emerged by the recombination event between Middle East and Australia lineages, which provided the evidence of homologous recombination as one of genetic and variation mechanisms of BEFV (He et al., 2016). In this study, we performed a recombination analysis of geographically distinct BEFVs based on the whole genome sequences and found that potential recombination events might occur between these BEFV isolates. Furthermore, BEFV BA/RZ/IR collected from Iran was identified as a putative recombinant with the Chinese strain JT02L as its minor parent-like strain. In addition, considering that the major parent-associated strain BEFV/CQ1/2022 was isolated in Southwest China in 2022 and the putative recombinant BA/RZ/IR was collected in Iran in 2013, we assume that an ancestral strain of BEFV/CQ1/2022 may be the actual major parent-like strain of BA/RZ/IR. However, due to the absence of sequence information for earlier isolates in the sublineage of BEFV/CQ1/2022, the actual major parental isolate was not accurately deduced.

5. Conclusion

In conclusion, we sequenced the whole genome of one BEFV isolate in Southwest China and performed a comprehensive genetic and evolution analysis with the global BEFV sequences. Genomic analyses of the BEFV genomic sequences revealed remarkable inter-isolate divergence, and the sequence divergence strictly corresponded to evolutionary relationships between the isolates. Phylogenetic analysis indicated that isolates from East Asia lineage were diverse and the current isolate BEFV/CQ1/2022 clustered within a sublineage of the East Asia lineage. Additionally, recombination analysis provided an evidence of the recombination among BEFV isolates. These findings obtained in this study will increase understanding of the epidemiology and evolution of BEFV.

Data availability statement

The data presented in the study are deposited in the GenBank repository, accession number OP887034.

Ethics statement

The animal study was reviewed and approved by Institutional Animal Care and Use Committee of Southwest University, Chongqing, China (IACUC-20221114-03). Written informed consent was obtained from the owners for the participation of their animals in this study.

Author contributions

CY, YP, NL, and RF performed the conceptualization. JC, CY, and YP performed the formal analysis and funding acquisition. JC, CY, and ML wrote the manuscript. JC, ML, YL, LY, YT, RD, and MX executed experiments and analyzed the data. All authors contributed to the article and approved the submitted version.

Funding

This research was funded by the China Agriculture Research System of MOF and MARA (Beef/Yak Cattle, CARS-37), the Fundamental Research Funds for the Central Universities (SWU-KT22016), and the Chongqing postgraduate research and innovation project in 2022 (CYB22154).

Conflict of interest

The authors declare that the research was conducted in the absence of any commercial or financial relationships that could be construed as a potential conflict of interest.

Publisher's note

All claims expressed in this article are solely those of the authors and do not necessarily represent those of their affiliated organizations, or those of the publisher, the editors and the reviewers. Any product that may be evaluated in this article, or claim that may be made by its manufacturer, is not guaranteed or endorsed by the publisher.

Supplementary material

The Supplementary material for this article can be found online at: https://www.frontiersin.org/articles/10.3389/fmicb.2023.1161287/full#supplementary-material

References

Abayli, H., Tonbak, S., Azkur, A. K., and Bulut, H. (2017). Complete genome analysis of highly pathogenic bovine ephemeral fever virus isolated in Turkey in 2012. *Arch. Virol.* 162, 3233–3238. doi: 10.1007/s00705-017-3470-6

Aziz-Boaron, O., Klausner, Z., Hasoksuz, M., Shenkar, J., Gafni, O., Gelman, B., et al. (2012). Circulation of bovine ephemeral fever in the Middle East--strong evidence for transmission by winds and animal transport. *Vet. Microbiol.* 158, 300–307. doi: 10.1016/j.vetmic.2012.03.003

Bai, W. B., Tian, F. L., Wang, C., Jiang, C. L., and Zhang, Z. G. (1987). Preliminary studies of the complement fixation test to confirm the diagnosis of bovine ephemeral fever. *Aust. J. Biol. Sci.* 40, 137–141. doi: 10.1071/BI9870137

Bakhshesh, M., and Abdollahi, D. (2015). Bovine ephemeral fever in Iran: diagnosis, isolation and molecular characterization. *J. Arthropod-Borne Dis.* 9, 195–203.

Chaisiririrat, T., Sangthong, P., Arunvipas, P., Petcharat, N., Thangthamniyom, N., Chumsing, W., et al. (2018). Molecular characterization of bovine ephemeral fever virus in Thailand between 2013 and 2017. *Vet. Microbiol.* 227, 1–7. doi: 10.1016/j.vetmic.2018.10.013

Frazer, K. A., Pachter, L., Poliakov, A., Rubin, E. M., and Dubchak, I. (2004). VISTA: computational tools for comparative genomics. *Nucleic Acids Res.* 32, W273–W279. doi: 10.1093/nar/gkh458

Gao, S., Du, J., Tian, Z., Niu, Q., Zheng, F., Huang, D., et al. (2017). Complete genome sequence of a bovine ephemeral fever virus JT02L strain in mainland China. *Arch. Virol.* 162, 3555–3558. doi: 10.1007/s00705-017-3520-0

He, C. Q., Liu, Y. X., Wang, H. M., Hou, P. L., He, H. B., and Ding, N. Z. (2016). New genetic mechanism, origin and population dynamic of bovine ephemeral fever virus. *Vet. Microbiol.* 182, 50–56. doi: 10.1016/j.vetmic.2015.10.029

Hou, P., Yang, H., Wang, H., Liu, W., and He, H. (2012). Cloning and sequence analysis of the G gene of bovine ephemeral fever virus in Shandong Province (in Chinese). *Prog. Vet. Med.* 33, 1–5.

Kato, T., Aizawa, M., Takayoshi, K., Kokuba, T., Yanase, T., Shirafuji, H., et al. (2009). Phylogenetic relationships of the G gene sequence of bovine ephemeral fever virus isolated in Japan, Taiwan and Australia. *Vet. Microbiol.* 137, 217–223. doi: 10.1016/j.vetmic.2009.01.021

Kun, J., Rongrong, J., Xiangbin, W., Yan, Z., Yiping, D., Gang, L., et al. (2020). Genetic characterization of bovine ephemeral fever virus in southern China, 2013-2017. *Virus Genes* 56, 390–395. doi: 10.1007/s11262-020-01740-w

Murphy, F. A., Taylor, W. P., Mims, C. A., and Whitfield, S. G. (1972). Bovine ephemeral fever virus in cell culture and mice. *Arch. Gesamte Virusforsch.* 38, 234–249. doi: 10.1007/BF01249675

Omar, R., Van Schalkwyk, A., Carulei, O., Heath, L., Douglass, N., and Williamson, A. L. (2020). South African bovine ephemeral fever virus glycoprotein sequences are phylogenetically distinct from those from the rest of the world. *Arch. Virol.* 165, 1207–1210. doi: 10.1007/s00705-020-04568-9

Pyasi, S., Sahu, B. P., Sahoo, P., Dubey, P. K., Sahoo, N., Byrareddy, S. N., et al. (2020). Identification and phylogenetic characterization of bovine ephemeral fever virus (BEFV) of middle eastern lineage associated with 2018-2019 outbreaks in India. *Transbound. Emerg. Dis.* 7, 2226–2232. doi: 10.1111/tbed.13531

Tamura, K., Peterson, D., Peterson, N., Stecher, G., Nei, M., and Kumar, S. (2011). MEGA5: molecular evolutionary genetics analysis using maximum likelihood, evolutionary distance, and maximum parsimony methods. *Mol. Biol. Evol.* 28, 2731–2739. doi: 10.1093/molbev/msr121

Trinidad, L., Blasdell, K. R., Joubert, D. A., Davis, S. S., Melville, L., Kirkland, P. D., et al. (2014). Evolution of bovine ephemeral fever virus in the Australian episystem. *J. Virol.* 88, 1525–1535. doi: 10.1128/JVI.02797-13

Walker, P. J. (2005). Bovine ephemeral fever in Australia and the world. *Curr. Top. Microbiol. Immunol.* 292, 57–80. doi: 10.1007/3-540-27485-5_4

Walker, P. J., Byrne, K. A., Cybinski, D. H., Doolan, D. L., and Wang, Y. H. (1991). Proteins of bovine ephemeral fever virus. *J. Gen. Virol.* 72, 67–74. doi: 10.1099/0022-1317-72-1-67

Walker, P. J., Byrne, K. A., Riding, G. A., Cowley, J. A., Wang, Y., and McWilliam, S. (1992). The genome of bovine ephemeral fever rhabdovirus contains two related glycoprotein genes. *Virology* 191, 49–61. doi: 10.1016/0042-6822(92)90165-l

Walker, P. J., and Klement, E. (2015). Epidemiology and control of bovine ephemeral fever. *Vet. Res.* 46:124. doi: 10.1186/s13567-015-0262-4

Zheng, F., Lin, G., Qiu, C., Zhou, J., Cao, X., and Gong, X. (2009). Isolation and characteriztion of a field strain of bovine ephemeral fever virus in China. *J. Anim. Vet. Adv.* 26, 197–200. doi: 10.1016/j.fsi.2008.03.014

Zheng, F., and Qiu, C. (2012). Phylogenetic relationships of the glycoprotein gene of bovine ephemeral fever virus isolated from mainland China, Taiwan, Japan, Turkey, Israel and Australia. *Virol. J.* 9:268. doi: 10.1186/1743-422X-9-268

frontiers | Frontiers in Microbiology

TYPE Original Research
PUBLISHED 27 March 2023
DOI 10.3389/fmicb.2023.1118056

OPEN ACCESS

EDITED BY
Qing Pan,
Qingdao Agricultural University,
China

REVIEWED BY
Anusak Kerdsin,
Kasetsart University Chalermphrakiat Sakon Nakhon Province Campus,
Thailand
Yao Zhu,
Harbin Veterinary Research Institute,
Chinese Academy of Agricultural Sciences,
China
Hoa Ngo,
Oxford University Clinical Research Unit Vietnam (OUCRU-VN),
Vietnam

*CORRESPONDENCE
Xiaolu Shi
✉ shixiaolu831@163.com

†These authors have contributed equally to this work and share the first authorship

SPECIALTY SECTION
This article was submitted to Infectious Agents and Disease, a section of the journal Frontiers in Microbiology

RECEIVED 08 December 2022
ACCEPTED 14 February 2023
PUBLISHED 27 March 2023

CITATION
Ji L, Chen Z, Li F, Hu Q, Xu L, Duan X, Wu H, Xu S, Chen Q, Wu S, Qiu S, Lu H, Jiang M, Cai R, Qiu Y, Li Y and Shi X (2023) Epidemiological and genomic analyses of human isolates of *Streptococcus suis* between 2005 and 2021 in Shenzhen, China.
Front. Microbiol. 14:1118056.
doi: 10.3389/fmicb.2023.1118056

Epidemiological and genomic analyses of human isolates of *Streptococcus suis* between 2005 and 2021 in Shenzhen, China

Liyin Ji[1†], Zhigao Chen[2†], Fan Li[3†], Qinghua Hu[2], Liangcai Xu[4], Xiangke Duan[2], Hanguang Wu[3], Shiqin Xu[1], Qiongcheng Chen[2], Shuang Wu[2], Shuxiang Qiu[5], Huiqun Lu[5], Min Jiang[2], Rui Cai[2], Yaqun Qiu[2], Yinghui Li[2] and Xiaolu Shi[1,2]*

[1]School of Public Health, Shanxi Medical University, Taiyuan, China, [2]Shenzhen Center for Disease Control and Prevention, Shenzhen, China, [3]Shenzhen Institute of Quality and Safety Inspection and Research, Shenzhen, China, [4]Futian District Center for Disease Control and Prevention, Shenzhen, China, [5]School of Public Health, University of South China, Hengyang, China

Streptococcus suis (*S. suis*) is an important food-borne zoonotic pathogen that causes swine streptococcosis, which threatens human health and brings economic loss to the swine industry. Three-quarters of human *S. suis* infections are caused by serotype 2. A retrospective analysis of human *S. suis* cases in Shenzhen, a megacity in China, with high pork consumption, between 2005 and 2021 was conducted to understand its genomic epidemiology, pathogen virulence, and drug resistance characteristics. The epidemiological investigation showed that human cases of *S. suis* in Shenzhen were mainly associated with people who had been in close contact with raw pork or other swine products. Whole-genome sequence analysis showed that 33 human isolates in Shenzhen were dominated by serotype 2 (75.76%), followed by serotype 14 (24.24%), and the most prevalent sequence types (STs) were ST7 (48.48%) and ST1 (39.40%). ST242 (9.09%) and ST25 (3.03%), which were rarely reported, were also found. Phylogenetic analysis showed that the Shenzhen human isolates had close genetic relatedness to isolates from Guangxi (China), Sichuan (China), and Vietnam. We found a new 82KB pathogenicity island (PAI) in the serotype 2 isolate that may play a role in sepsis. Similarly, a serotype 14 isolate, containing 78KB PAI, was isolated from a patient presenting with streptococcal toxic shock syndrome (STSLS) who subsequently died. Multi-drug resistance (MDR) was high in human isolates of *S. suis* from Shenzhen. Most human isolates were resistant to tetracycline, streptomycin, erythromycin, and clindamycin, and 13 isolates had intermediate resistance to penicillin. In conclusion, swine importation from Guangxi, Sichuan, and Vietnam should be more closely monitored, and the use of antibiotics limited to reduce the potential for antimicrobial resistance (AMR).

KEYWORDS

***Streptococcus suis*, human, epidemiology, SNP-based phylogeny, pathogenicity island, antimicrobial resistance**

1. Introduction

Shenzhen is a megacity in China, with a population of approximately 20 million, and has a high consumption of pork due to its high nutritional value. There are no swine farms in Shenzhen, and live swine are imported from nearby provinces and cities and exported, for example, to Hong Kong and Macao. *Streptococcus suis* (*S. suis*) is a significant zoonotic pathogen that is localized in the upper respiratory tract of healthy swine (Goyette-Desjardins et al., 2014). In humans, *S. suis* can cause meningitis, septicemia, endocarditis, pneumonia, arthritis, and streptococcal toxic shock syndrome (STSLS), with pathogen transmission through broken skin contact with swine, pork, and pork-related derivatives or consumption of raw or undercooked pork products (Kerdsin et al., 2022). In severe cases, *S. suis* infection can lead to death (Goyette-Desjardins et al., 2014). China has had three outbreaks of *S. suis* serotype 2 in Jiangsu (1998), Sichuan (2005), and Guangxi (2016), which caused multiple infections and deaths, and brought serious economic loss to the localities (Tang et al., 2006; Huang et al., 2019b).

To date, 29 authentic *S. suis* serotypes (1–19, 21, 23–25, 27–31, and 1/2; Okura et al., 2016), serotype Chz (Pan et al., 2015), and 26 novel capsular polysaccharide loci (NCL) have been described (Zheng et al., 2015; Qiu et al., 2016; Zheng et al., 2017; Huang et al., 2019a), depending on the antigenicity of the capsular polysaccharide. Of human pathogenic isolates, 74.7% are *Streptococcus suis* serotype 2 (*S. suis* 2), which is the most common and virulent isolate across geographic regions (Goyette-Desjardins et al., 2014). In addition, *Streptococcus suis* serotype 14 (*S. suis* 14) has been isolated several times from human isolates (Huang et al., 2019b; Kerdsin et al., 2020; Thu et al., 2021). Multi-locus sequence typing (MLST) is commonly used to distinguish between pathogen isolate types. PubMLST shows that 1,962 different sequence types (STs) of *S. suis* have been identified worldwide, and new STs are constantly being discovered. Among them, ST7 is mostly endemic to China (Goyette-Desjardins et al., 2014). The 89 KB pathogenicity island (PAI) was discovered in the Chinese *S. suis* 2-ST7 isolates, 98HAH12, SC84, and 05ZYH33 (Ye et al., 2006; Chen et al., 2007) and contained several genomic components associated with pathogenicity. Such genomic components include three groups of ABC transport systems controlling substance transport, a two-component signal transduction system (TCS), three type IV secretory system (T4SS) component genes, a toxin-antitoxin system, and a Tn*916* transposon (Wu et al., 2011). These genomic components played an important role in STSLS and drove the *S. suis* outbreak in Jiangsu (1998) and Sichuan (2005) of China (Chen et al., 2007).

Both human and veterinary prevention of *S. suis* infection and disease treatment depends on the effective use of antibiotics, which are equivalent or belong to the same class (Yongkiettrakul et al., 2019). In recent years, however, antibiotic overuse on a global scale has caused bacteria to evolve antimicrobial resistance (AMR), and multi-drug resistance (MDR) is gradually increasing (Aradanas et al., 2021). There is a similar concern that *S. suis* may act as a streptococci community (pathogenic and non-pathogenic) reservoir for antibiotic resistance genes (ARGs; Palmieri et al., 2011). High-level AMR to tetracyclines, macrolides, and lincosamides has been reported in both human and swine isolates of *S. suis* (Gurung et al., 2015; Ichikawa et al., 2020; Aradanas et al., 2021). The ARGs, *tet*(O) and *erm*(B), are the most common genes associated with AMR (Princivalli et al., 2009; Chen et al., 2013b), and consequently, beta-lactamase and fluoroquinolone antibiotics are used to treat *S. suis* infections in both swine and human (Aradanas et al., 2021). However, non-penicillin and non-levofloxacin susceptible isolates of *S. suis* have also been reported worldwide (Varela et al., 2013; Bamphensin et al., 2021; Dechêne-Tempier et al., 2021). As treatment for *S. suis* infection in both humans and swine is dependent on antibiotics, monitoring antibiotic sensitivity will help to optimize antibiotic therapy.

A total of 43 human cases of *S. suis* infection were reported in the Shenzhen region over a 17-year time period[1]. The epidemiological characteristics of the infections remain undescribed, and the genetic relatedness among humans of Shenzhen and global *S. suis* isolates remains unclear. To understand the possible relationship between the human *S. suis* isolates of Shenzhen and the global isolates from a phylogenetic perspective, we collected and preserved isolates from 33 of the 43 cases from 2005 to 2021 and performed a genomic analysis. Antibiotic susceptibility testing was also performed to investigate the potential resistance of *S. suis* isolates in Shenzhen and provide a basis for clinical treatment of human *S. suis* infection.

2. Materials and methods

2.1. Sample collection, isolation, and identification

A total of 43 human cases of *S. suis* were reported in Shenzhen of China from 2005 to 2021, as determined using PulseNet China. Cerebrospinal fluid or blood was taken from each of the 43 patients at the time of hospitalization, and isolates from 33 of the 43 cases were obtained from sentinel hospitals (Supplementary Table S1) and sent to Shenzhen Center for Disease Control and Prevention. Clinical information and patient exposure history 1 week prior to disease onset were also collected from China Information System for Disease Control and Prevention. Samples ($n = 100$) of clinically healthy swine tonsils with quarantine certificates from Abattoir 2 in Shenzhen were collected in December 2021. Each swine tonsil tissue was aseptically cut into small pieces, then homogenized in 1 ml of PBS using a tissue homogenizer (MagNA Lyser Instrument, United States), delineated on Columbia blood agar medium (Detgerm Microbiogical Science Ltd., Guangzhou, China), and incubated at 37°C for 18–24 h in a 5% CO_2 incubator. From each sample, 1–2 small gray–white colonies with varying degrees of hemolysis were selected and inoculated on Columbia blood agar medium and incubated at 37°C for 18 to 24 h. A single colony was placed in an EP tube (1.5Ml) filled with 300 µl of pure water and bathed at 100°C for 15 min to extract nucleic acid. Using the *Streptococcus suis* detection kit (real-time PCR method; MABSKY, Shenzhen, China) for the conserved gene *gdh* of *S. suis*, individual suspected colonies were identified with a Ct value of ≤ 36 and a significant curve growth, which could be judged as positive isolates. There were 38 positively identified *S. suis* isolates from the swine samples. Including both the human and swine samples, a total of 71 *S. suis* isolates were included in the study.

1 https://10.249.6.18:8881/cdc/login

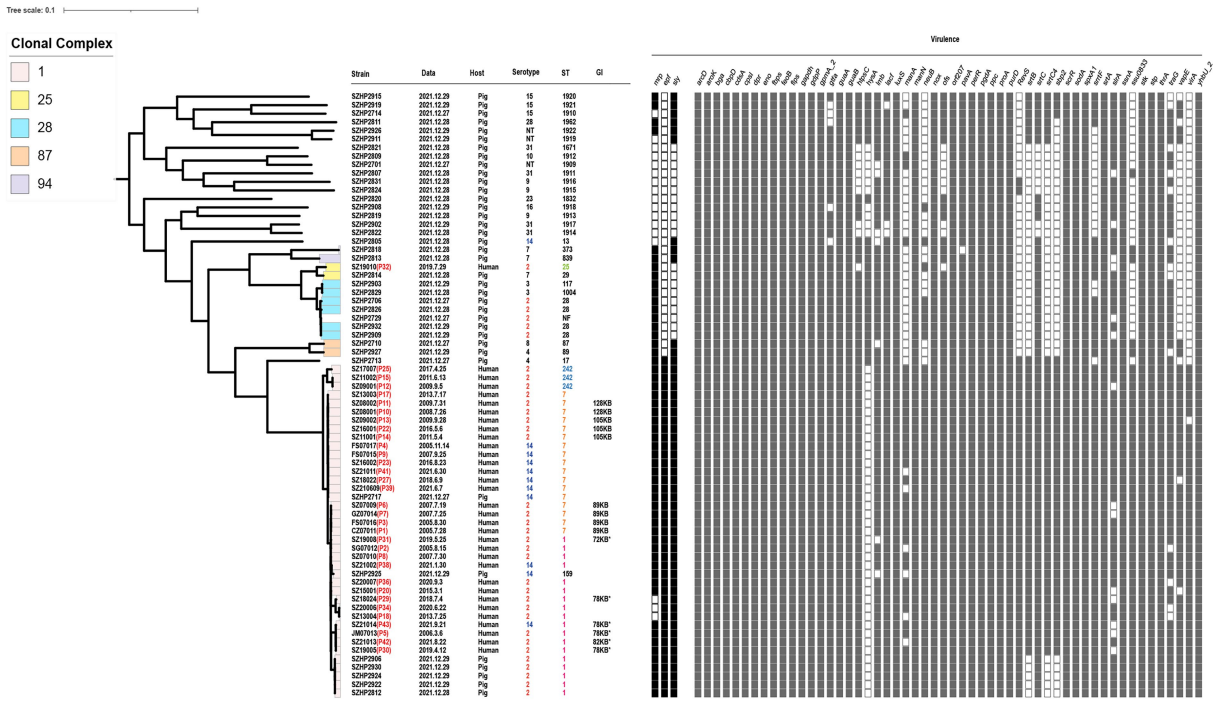

FIGURE 1
Information and virulence genes of 71 *Streptococcus suis* isolates in Shenzhen. The red font after the strain number is the patient number. Data mean the onset time of human isolates and the isolation time of swine isolates. Serotype, ST, clone complex, and host of 71 isolates are described. "*" indicates that it is derived from 89 KB PAI. Squares are filled with color when the corresponding virulence gene is present.

2.2. Genomic DNA preparation, whole-genome sequencing, assembly, and annotation

Genomic DNA was obtained from all 71 *S. suis* isolates using the Ezup Column Bacteria Genomic DNA Purification Kit (Sangon Biotech, Shanghai, China), after resuscitation and passaging using the Columbia Blood Plate. Pair-end libraries with a mean insert size of 350 bp were prepared using the NEB Ultra DNA Library Preparation Kit (NEB, Massachusetts, United States). Whole-genome sequencing was conducted using Illumina NovaSeq PE150 (Novogene Co. Ltd., Beijing, China); the average read length was 150 bp, yielding an average of 1 GB of clean reads per isolate. Short-read sequencing data for the Shenzhen isolates have been stored in the NCBI Sequence Read Archive under accession number PRJNA894855. In addition, 429 genome sequences of *S. suis* 2 and *S. suis* 14 isolates were downloaded from the NCBI SRA (375) and NCBI Assembly (54) for further analysis. Data information on 429 genome sequences is provided in Supplementary Table S2.

A total of 344 genome sequences downloaded from the NCBI SRA, and 71 pair-ended genome sequences in this study were filtered using the software trimmomatic v0.39 (Bolger et al., 2014), and then, Kraken2[2] was used to identify *S. suis*. SPAdes v1.1.0 (Bankevich et al., 2012) was used to perform *de-novo* genome assembly. Quast v5.0.2 (Gurevich et al., 2013) was used to check the quality of all 500 draft sequences, and Prokka 1.14.6 (Seemann, 2014) was used to perform gene annotation.

2.3. Serotyping and MLST

Streptococcus suis serotyping pipeline[3] was used for *S. suis* serotyping, used to identify the traditional 29 serotypes and differentiate between serotypes 2 and 1/2, and between serotypes 1 and 14. For serotypes other than the 29 traditional serotypes, a cps database was created based on published articles, containing serotype Chz (Pan et al., 2015) and NCL1-26-specific genes (Zheng et al., 2015, 2017; Qiu et al., 2016; Huang et al., 2019a). SRST2 (Inouye et al., 2014) was used to perform serotyping in comparison with the created database. The genome sequences of the isolates were submitted to the *S. suis* MLST database[4] for genotype determination, and then, clonal complex groups (CCs) were identified using goeBURST[5].

2.4. Phylogenetic tree building

Core-genome (regions present in >99% of isolates) single-nucleotide polymorphisms (core-SNPs) were identified using Snippy Pipeline v4.6.0[6]. SC84 (accession number: NC_012924.1) was used as the reference sequence for the Shenzhen isolate sequences (Figure 1) and *S. suis* 2 sequences (Figure 2), and JS14 (accession number: NC_017618.1) was used as the reference sequence for *S. suis* 14 sequences

2 https://ccb.jhu.edu/software/kraken2/

3 https://github.com/streplab/SsuisSerotyping_pipeline
4 https://pubmlst.org/ssuis/
5 https://online.phyloviz.net
6 https://github.com/tseemann/snippy

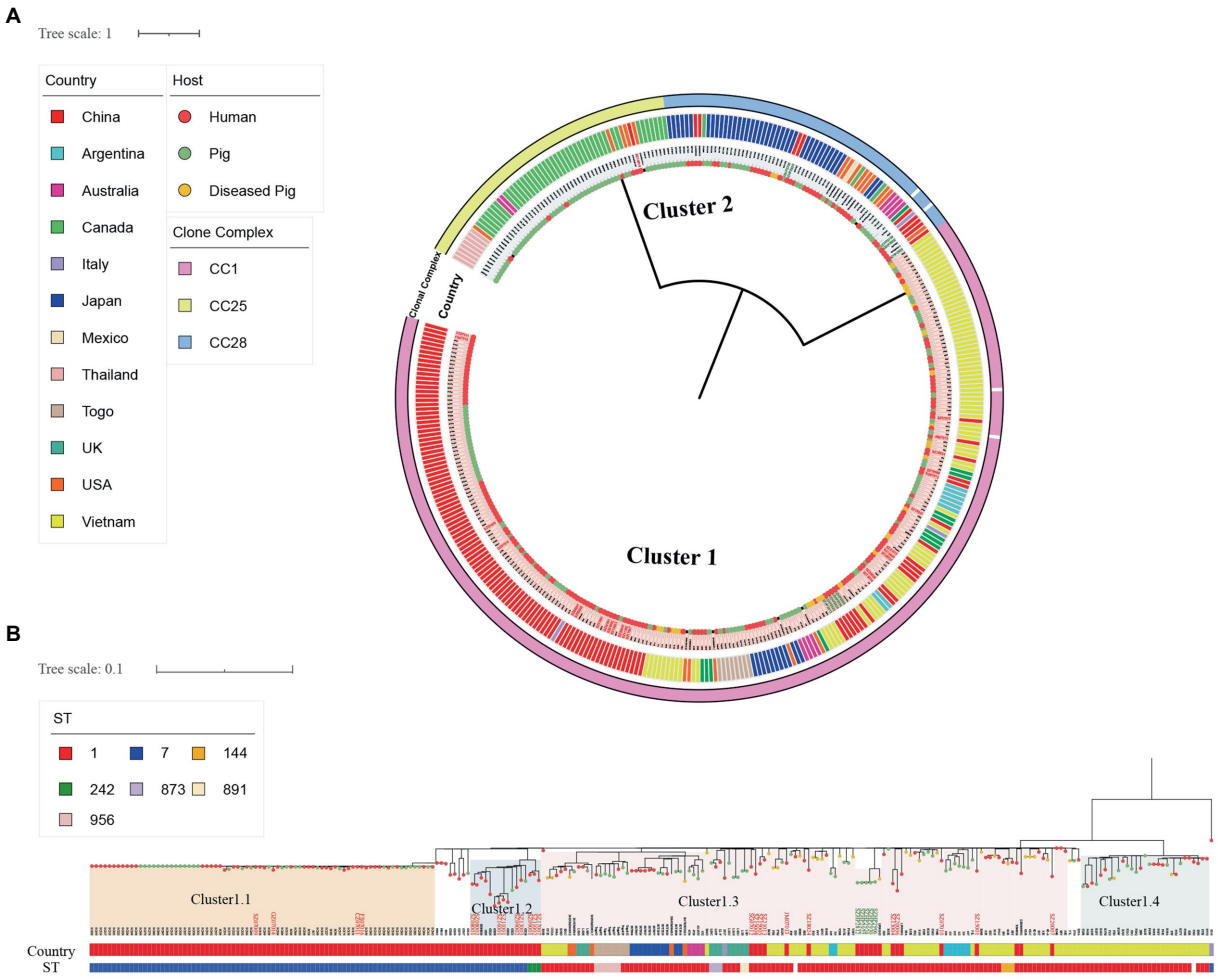

FIGURE 2
Single-nucleotide polymorphism-based global *S. suis* 2 Ml tree. **(A)** SNP-based global *S. suis* 2 Ml tree includes 25 human isolates (red font) and 10 swine isolates (green font) from Shenzhen, and 345 *S. suis* isolates downloaded from the NCBI database. The different colored circles on each branch represent different host sources, and the circles represent clonal complex, country, or cluster as indicated on the figure. **(B)** SNP-based global *S. suis* 2 Cluster1 ML tree includes 24 human isolates (red font) and five swine isolates (green font) from Shenzhen, and 224 *S. suis* isolates downloaded from the NCBI database. The country and host legends of the isolates are the same as on **(A)**. ST or cluster as indicated on the figure.

(Figure 3). Gubbins v2.4.1 (Croucher et al., 2015) was used to remove recombination, and SNP distance matrices were obtained for isolates using snp-dist v0.6.3[7], and then, non-repetitive core-SNPs were used to construct the three maximum-likelihood (ML) trees using FastTree v2.1.10 (Price et al., 2010), with the auto-detected best-fitting substitution model. iTOL[8] was used for modification and presentation (Figures 1–3).

2.5. Identification of virulence genes, plasmids, and prediction of gene islands

To identify virulence genes in the isolates, a database containing 84 virulence genes was created based on previously published data (Dong et al., 2015; Cucco et al., 2022), using Abricate[9] and in combination with the VFDB online database[10]. PlasmidFinder v2.1 (Carattoli et al., 2014) was used to detect plasmids. A database of *S. suis* gene island (GI) was also constructed, containing 89 K PAI present in epidemic isolate 05ZYH33 (Li et al., 2011), the 105 K GI found in the diseased swine isolate SC070731(Wu et al., 2014), and the 128 k GI found in CMGETZ080501 (Huang et al., 2016). Blast v2.5.0 (Camacho et al., 2009), with a cutoff value of ≥ 70% coverage and ≥ 80% identity was used to determine the presence of GI. The results were presented using Easyfig[11].

2.6. Antibiotic susceptibility testing and identification of ARGs

The antimicrobial susceptibility of isolates to 17 antibiotics across 10 classes (Aminoglycosides, Amphenicols, Sulfanilamides, Lincosamides, Macrolides, Tetracyclines, Oxazolidinones, Fluoroquinolones, β-lactams,

7 https://github.com/tseemann/snp-dists
8 https://itol.embl.de/
9 https://github.com/tseemann/abricate
10 http://www.mgc.ac.cn/VFs/
11 https://github.com/mjsull/Easyfig

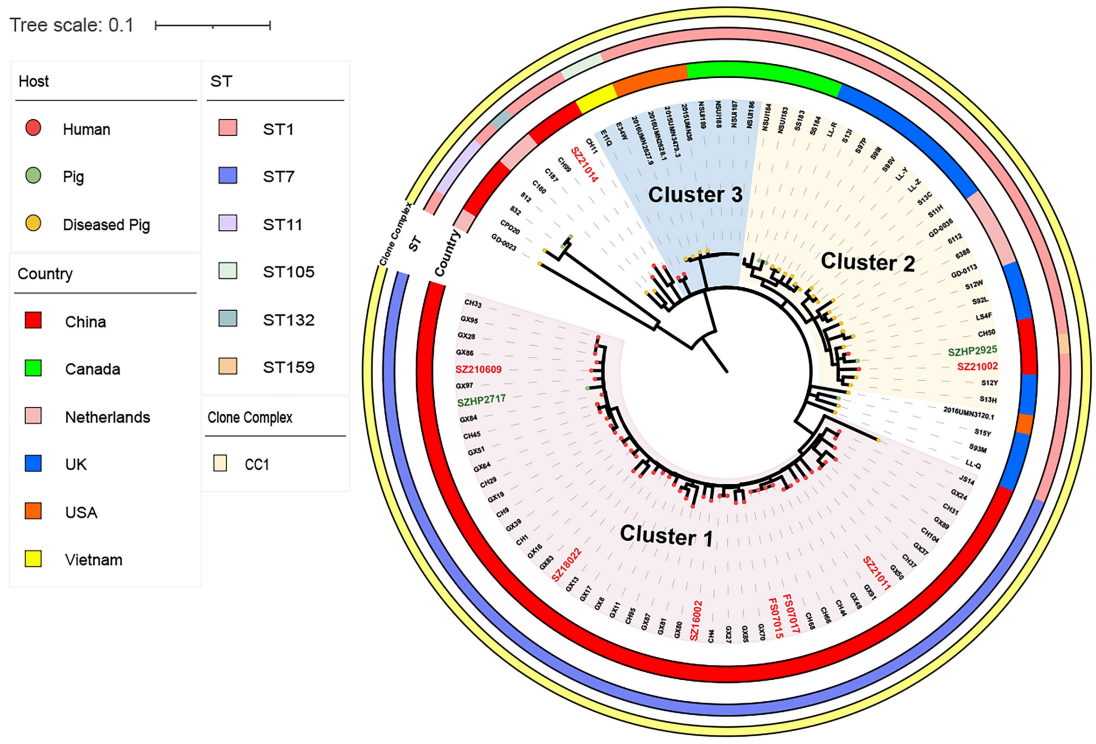

FIGURE 3
Single-nucleotide polymorphism (SNP)-based global *S. suis* 14 Ml tree includes eight human isolates (red font) and two swine isolates from Shenzhen (green font), and 86 *S. suis* isolates downloaded from the NCBI database. The different colored circles on each branch represent different host sources, the circles represent clonal complex, ST, or country, as indicated on the figure.

and Glycopeptides; Supplementary Table S3) was determined using the minimal inhibitory concentration (MIC) method. The broth microdilution method (FOSUN DIAGNOSTICS, Shanghai, China) was used to determine the antibiotic sensitivity of the *S. suis* isolates. Chloramphenicol (CPL), compound sulfamethoxazole (SMZco), clindamycin (DA), erythromycin (ERY), tetracycline (TC), linezolid (LZD), levofloxacin (LEV), moxifloxacin (MXF), penicillin (PG), cefepime (FEP), cefotaxime (CTX), meropenem (MEM), amoxicillin (AML), vancomycin (VA), and teicoplanin (TEC) were tested. The E-test method (Liofilchem, Italy) was used to determine the antibiotic sensitivity of the *S. suis* isolates to streptomycin (SM) and ceftriaxone (CRO). *Streptococcus pneumoniae* ATCC 49619 was used as a quality control isolate. Breakpoints for sensitive, intermediate, and resistant types were defined using the Clinical and Laboratory Standards Institute (CLSI) document M100 (31st edition; Humphries et al., 2021) when available, otherwise, EUCAST (v 13.0) clinical breakpoint cutoff values[12] were used. The reference breakpoint of SM was determined based on the high-level resistance values for SM in Streptococcus suis reported by Marie J. (Marie et al., 2002). In the absence of clinical breakpoints from CLSI or EUCAST, the values obtained were displayed. Resfinder 4.1 (Bortolaia et al., 2020) was used to identify ARGs.

2.7. Statistical analysis

Mean ± standard deviation (SD) and frequency were used to describe the characteristics of *S. suis* cases and isolates. Categorical variables were compared using the chi-square and Fisher's exact tests. A two-sample *t*-test was performed to access the differences between the two means. Wilcoxon rank-sum test was used when the continuous variables were not normally distributed. A consistency check was used to verify the consistency of the two methods. All analyses were performed using SPSS 27.0.1. *p*-values of less than 0.05 were considered statistically significant.

3. Results

3.1. Epidemiological and clinical features

Among the 43 cases of human *S. suis* reported in Shenzhen from 2005 to 2021, 34 cases were scattered across nine Shenzhen districts (Figure 4; Supplementary Table S1). There was a high prevalence of *S. suis* cases across the four districts of Longgang (27.91%), Longhua (18.60%), Baoan (11.63%), and Luohu (9.30%), though no obvious epidemiological association between them. Nine cases were imported from other cities in Guangdong of China, though seven of these cases had missing information. The remaining 36 cases had a minimum age of 22 years and a maximum age of 84 years, with a mean age of 50.14 (±12.96) years. A total of 31 (86.11%) of the *S. suis*-infected patients were male. Almost four-fifths of patients were cooks (41.67%), butchers (25.00%), and freelancers (16.67%) with close contact with raw pork or swine products. *S. suis* infections presented throughout the year, with a higher incidence in the hot and humid climate between April and September in Shenzhen.

12 www.EUCAST.org

FIGURE 4
Map of domestic sources of pork and the distribution of human cases of *S. suis* in Shenzhen, China. The orange area of the map of China (left) represents the source of pork imports to Shenzhen. The letters indicate the provinces of China: GX=Guangxi; HuN=Hunan; JX=Jiangxi; FJ=Fujian; GD=Guangdong; HN=Hainan; SZ=Shenzhen. The blue area (right) is an expanded representation of the Shenzhen region. The circles in the figure represent the distribution of cases in each district of Shenzhen.

Of the 36 patients with clinical information, we did not collect the clinical type of five of these patients, and 21 patients were diagnosed with meningitis (58.33%), four patients with sepsis (11.11%), and one patient with arthritis (2.78%). Three patients had meningitis complicated by sepsis (8.33%), and two patients had STSLS and died (5.56%). The mortality rate among 36 cases was 5.56%. Among the exposure history of the 36 patients, 28 patients had a history of raw pork exposure, of which 12 patients had wounds on their hands and did not use any personal protection when in contact with raw pork, and two patients had tasted raw pork or eaten pork from diseased swine. Exposure history data were lost from six patients. In addition, prior to the disease onset, 2 of the 30 patients had a history of exposure to chicken and duck meat only and had not been exposed to or consumed pork or related products. Patients' epidemiological and clinical data are provided in Supplementary Table S1.

3.2. *Streptococcus suis* serotyping, ST, and CCs identification in Shenzhen

Of the total 71 *S. suis* isolates in Shenzhen (Figure 1), three-quarters of the human isolates were *S. suis* 2 ($n=25$, 75.76%), and the remaining isolates were *S. suis* 14 ($n=8$, 24.24%). The swine isolates ($n=38$) carried a wide range of serotypes, though *S. suis* 2 was the most common ($n=10$, 26.32%). Other swine isolate serotypes included serotypes 2, 3, 4, 7, 8, 9, 10, 14, 15, 16, 23, 28, and 31, and non-typeable ones.

Multi-locus sequence typing (MLST) identified four STs in human isolates ($n=33$), which were present in differing prevalence. ST7 was the most prevalent (48.48%), followed by ST1 (39.40%), then ST242 (9.09%), and finally ST25 (3.03%). A total of 22 STs were identified in the swine isolates ($n=38$), among which ST1 (13.16%) and ST28 (10.53%) were the most prevalent. Eight new STs were identified in the swine isolates; ST1909, ST1911, ST1912, ST1913, ST1914, ST1917, ST1918, and ST1962, and a further isolate could not be genotyped. eBURST analysis showed that ST1, ST7, ST159, and ST242 belonged to CC1; ST25 and ST29 belonged to CC25; ST28, ST117, and ST1004 belonged to CC28; ST87 and ST89 belonged to CC87; ST373 and ST839 belonged to CC94; and other STs appeared in the single case form.

3.3. Phylogenetic analysis of Shenzhen human isolates with global *Streptococcus suis* isolates

To study the relationship between Shenzhen human *S. suis* 2 and global *S. suis* 2 isolates, we compared 25 human isolates of *S. suis* 2 in Shenzhen with 10 swine isolates of *S. suis* 2 from this study, and 345 global *S. suis* 2 isolates. Then, we constructed an *S. suis* 2 Ml tree of 380 isolates based on 7,370 SNPs in the core genome. The ML tree was divided into two clusters (Figure 2A), with Cluster1 containing CC1 isolates and Cluster2 containing CC25 and CC28 isolates. Shenzhen human isolates were mainly concentrated on Cluster1, which was further divided into four subgroups (Figure 2B). Within Cluster1, four ST7 (16.00%) Shenzhen human isolates isolated from 2005 to 2007 distributed to the Cluster1.1 subgroup were closely related to the Sichuan (China) isolates of 2005 ($0 \leq snp \leq 4$). Six ST7 (24.00%) and three ST242 (12.00%) Shenzhen human isolates isolated from 2008 to 2017 were distributed to the Cluster1.2 subgroup and were genetically close to the diseased swine isolate HN08324 of Henan (China;

8 ≤ snp ≤ 23) and Guangxi (China) human isolate GX9 (10 ≤ snp ≤ 23). In addition, 11 ST1 (44.00%) Shenzhen human isolates isolated from 2005 to 2021 in the Cluster1.3 subgroup were more closely related to the Vietnamese human isolates B34E and S8V(6 ≤ snp ≤ 19). Furthermore, a Shenzhen human isolate SZ19010 (4.00%), which belongs to ST25, is located in Cluster2 and was genetically distant (snp ≥ 5,622) from the remaining 24 (96.00%) Shenzhen human isolates of *S. suis* 2. SZ19010 had a closer genetic relationship with isolates from the United States, Canada, Thailand, and Australia (6 ≤ snp ≤ 68) and was most closely related to United States swine isolate NSUI012 and diseased swine isolates, 2014UMN2148.7 and 2016UMN1440.1 (snp = 6).

In the same way, we compared eight Shenzhen human and two swine *S. suis* 14 isolates from this study with 86 global *S. suis* 14 isolates. A *S. suis*14 ML tree was constructed with 96 isolates based on 1,688 SNPs in the core genome and divided into three clusters (Figure 3). Six ST7 (75.00%) Shenzhen human isolates isolated from 2005–2021 in Cluster1 were closely related to the Guangxi (China) human isolates GX8, GX17, and GX84 (17 ≤ snp ≤ 31), while the Shenzhen ST1 human isolate SZ21002 located in Cluster2 was closely related to the UK-diseased swine isolate LS4F (snp = 35) and Guangxi (China) human isolate CH29 (snp = 39), and the other ST1 human isolate SZ21014 isolated in 2021was closely related to Guangxi (China) human isolate CH11 (snp = 50). The information on genome sequences data is provided in Supplementary Table S2.

3.4. Virulence genes and plasmids of Shenzhen isolates and 89K PAI detection

A total of 57 virulence genes were detected in the genomes of 71 Shenzhen isolates (Figure 1). By the Wilcoxon rank-sum test, the CC1 carried more virulence genes (55.92 ± 0.17) than other CCs (45.53 ± 0.69; $p < 0.001$). Therefore, CC1 was defined as a cluster of highly virulent clones. It consisted of *S. suis* 2 and *S. suis* 14 isolates, containing 32 human isolates (96.97%) and seven swine isolates (18.42%). All isolates in CC1 showed *mrp* + *epf* + *sly* +, except for SZ13004, SZ18024, and SZ20006, which showed *mrp*- *epf* + *sly* +. For non-CC1 swine isolates, although some were *S. suis* 2 or *S. suis* 14, they only carried one of the three virulence genes. In addition, a swine serotype 4-ST17 isolate presented with *mrp* + *epf* + *sly* +. The only Shenzhen human *S. suis* 2-ST25 isolate SZ19010 belonging to CC25 showed *mrp* + *epf*–*sly*–.

In the CC1 human isolates, we found that the four *S. suis* 2-ST7 isolates that were genetically closely related to the Sichuan isolates (2005), had a complete 89 KB PAI. We also found 78 KB, 72 KB, and 82 KB PAI, which were derived from 89 KB PAI. Four *S. suis* 2-ST1 human isolates were found to have 78 KB PAI and retained most of the key factors associated with virulence, with only one group of ABC transporter proteins missing. We found a 72 KB PAI in a human isolate SZ19008, which lost the *SalR* gene in the TCS, in addition to a set of ABC transporter proteins. Clinical information indicated that the patient had STSLS and died. We identified an 82 KB PAI in a human isolate SZ21013, which had lost one of the TCS *SalK/SalR*, in comparison with the prevalent isolate 05ZYH33. In addition, many fragments in the Tn*916* transposon were lost, and TC resistance-related efflux pump gene *tet*(L) and the ISL3 family transposase IS1165 were inserted. The 78 KB PAI was also found in the *S. suis* 14 isolate SZ21014 from a patient presenting with STSLS. As the 78 KB PAI found in the *S. suis* 2 isolates, the one in *S. suis* 14 carried all the 89 KB PAIs except for a group of ABC transporter proteins (Figure 5). No plasmids were detected in the 71 Shenzhen isolates.

3.5. Antimicrobial resistance phenotype testing and gene detection

Drug susceptibility testing (Supplementary Table S3) showed that 33 human isolates of *S. suis* exhibited high levels of resistance to the

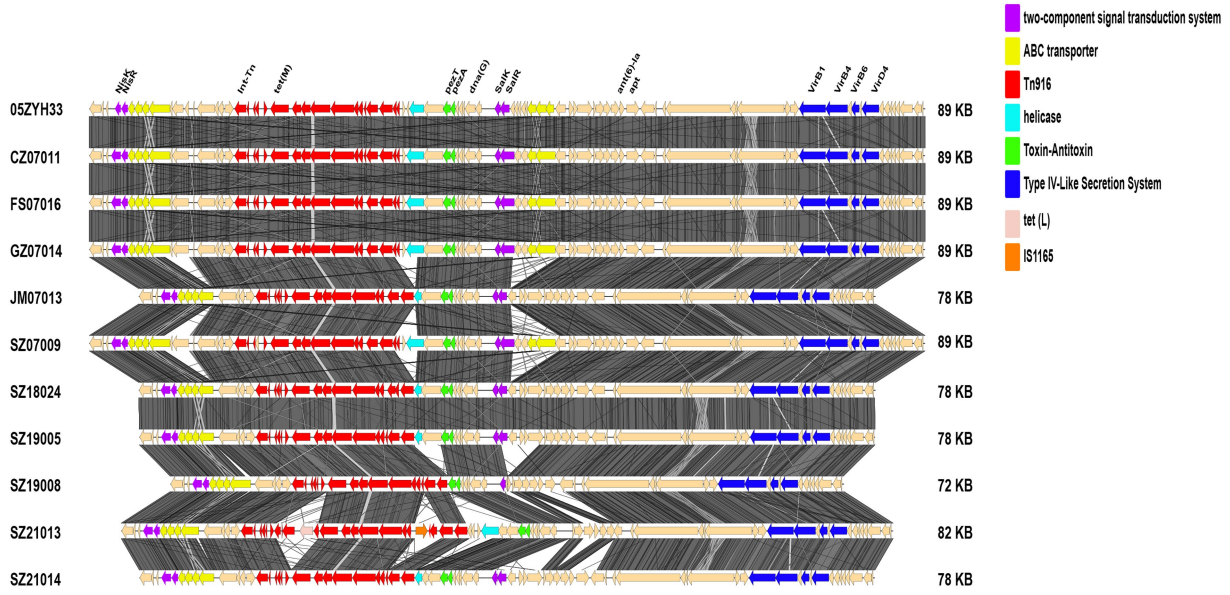

FIGURE 5
Structural diagram of the 89KB PAI and its variants found in the Shenzhen isolates.

TABLE 1 Phenotypic antimicrobial resistance (AMR) profiles of *Streptococcus suis* isolated from Shenzhen, China.

Phenotype	Human (n =33)		Swine (n =38)	
	n	%	n	%
Ami-Lin-Mac-Tet	10	30.30	6	15.79
Ami-Tet-Bla	6	18.18	0	0.00
Ami-Lin-Mac-Tet-Bla	2	6.06	1	2.63
Lin-Mac-Tet	4	12.12	21	55.26
Lin-Mac-Tet-Bla	2	6.06	0	0.00
Ami-Amp-Lin-Mac-Tet-Flq-Bla	0	0.00	1	2.63
Ami-Amp-Lin-Mac-Tet	0	0.00	1	2.63
Lin-Tet-Flq	0	0.00	1	2.63
Lin-Mac-Tet-Flq	0	0.00	1	2.63
Ami-Lin-Mac-Tet-Flq-Bla	0	0.00	1	2.63
Ami-Lin-Mac-Tet-Flq	0	0.00	1	2.63
Sum	24	72.73	34	89.47

Ami, Aminoglycosides; Lin, Lincosamides; Mac, Macrolides; Tet, Tetracyclines; Bla, β-lactams; Amp, Amphenicols; Flq, Fluoroquinolones.

antibiotics: TC ($n = 32$, 96.97%), SM ($n = 21$, 63.64%), ERY ($n = 18$, 54.55%), and DA ($n = 18$, 54.54%). In addition, 39.39% ($n = 13$) of the isolates demonstrated intermediate resistance to PG ($0.25 \leq MIC \leq 1$ μg/ml). A total of 38 swine isolates also exhibited high levels of resistance to the antibiotics TC ($n = 38$, 100%), DA ($n = 35$, 92.11%), and ERY ($n = 33$, 86.84%). In addition, swine isolates also had resistance to SM ($n = 9$, 23.68%), LEV ($n = 4$, 10.53%), and CPL ($n = 1$, 2.63%). Swine isolates demonstrated intermediate resistance to PG ($n = 5$, 13.16%), CPL ($n = 1$, 2.63%), and LEV ($n = 1$, 2.63%). By chi-square test, the resistance rate of the swine isolates to ERY and DA was higher than that of the human isolates ($p < 0.05$).

A total of 11 different resistance patterns were observed in this study (described in Table 1). The MDR rate of 33 human *S. suis* isolates was 72.73% ($n = 24$), and the main resistance patterns were Ami-Lin-Mac-Tet. Meanwhile, the MDR rate of 38 swine *S. suis* isolates reached 89.47% ($n = 34$), and the main resistance pattern was Lin-Mac-Tet.

A total of 20 ARGs were detected in the 71 isolates, including aminoglycosides ($n = 4$), amphenicols ($n = 2$), sulfonamides ($n = 1$), lincosamides ($n = 3$), macrolides ($n = 4$), and tetracyclines ($n = 6$; Figure 6). Among human isolates, *ant*(6)-*Ia* of aminoglycosides was the most common (63.64%), followed by *tet*(O) of tetracyclines (57.58%) and *erm*(B) of macrolides-lincosamides (54.55%). Among the swine isolates, macrolides-lincosamides *erm*(B) was the most common (86.84%), followed by tetracyclines *tet*(O) (78.95%) and aminoglycosides *ant*(6)-*Ia* (23.68%). Further comparison of human and swine *S. suis* 2 and *S. suis* 14 isolates by Fisher's exact test revealed that *ant*(6)-*Ia*, *tet*(40), *tet*(M), and *tet*(O) were distributed differently among hosts and serotypes ($p \leq 0.05$). Results showed that in human isolates, *ant*(6)-*Ia* was more predominant in *S. suis* 2 isolates and *tet*(40) was more predominant in *S. suis* 14 isolates. When comparing human and swine *S. suis* 2 isolates, *ant*(6)-*Ia* and *tet*(M) were more frequently present in human isolates, while *tet*(O) was found more frequently in swine isolates (Supplementary Table S4). By analyzing the consistency of antimicrobial resistance and phenotypes among 71 isolates in Shenzhen, it was found that there was a good agreement between resistance genotypes and phenotypes for SM, DA, ERY, TC, LZD, PG, CRO, FEP, CTX, MEM, AML, and VA (Kappa values = 1, $p < 0.001$).

4. Discussion and conclusion

Streptococcus suis S. suis infection can be fatal to humans and is transmitted from swine and related products. Based on phylogenetic results, we found that Shenzhen human isolates had close genetic relatedness to isolates from Guangxi (China), Sichuan (China), and Vietnam. ML Cluster1.1 was formed by the *S. suis* 2-ST7 Sichuan 2005 outbreak isolates (Li et al., 2011). Shenzhen human isolates in this cluster were endemic only for a short time in 2005–2007, potentially due to the quarantine and mass destruction of swine in response to the large-scale *S. suis* outbreak. In addition, from 2005–2021, the Shenzhen human *S. suis* isolates were mainly closely related to isolates from Guangxi and Vietnam. Most of the pork in Shenzhen comes from Guangxi, Guangdong, and other neighboring Chinese provinces (Zongyun and Guojian, 2019). Guangxi is close to Vietnam, and a private swine trade exists between them (Kedkovid et al., 2020). Huang et al. (2019b) demonstrated a close relationship between Guangxi and Vietnamese isolates of *S. suis* from a phylogenetic perspective. Meanwhile, the phenomenon of Vietnamese swine smuggling into Guangdong is also quite prominent (Magazine, 2014), which may enable the introduction of Vietnamese pathogen isolates into Guangxi and Guangdong and then into Shenzhen. Unfortunately, the Guangxi and Vietnam isolates that could be included in this study were human isolates, and the relationship between swine and humans could not be found, suggesting that we should strengthen the monitoring of the *S. suis* of swine.

Four human ST242 isolates have been found in human cases of meningitis, one in Guangxi (Jiang et al., 2020), and three in this study (distributed in Figure 2B Cluster1.2). There is no conclusive evidence of direct human-to-human *S. suis* transmission (Gottschalk et al., 2010). We only found one swine ST242 isolate (PubMLST), though there is no evidence that human ST242 isolates came from swine. ST242 has a certain pathogenicity, and the detection of ST242 in swine and human isolates could be strengthened for comparative analyses. In addition, the reported *S. suis* 2-ST25 isolates were mainly isolated from the United States, Australia, and Thailand (Kerdsin et al., 2018; Segura et al., 2020) and were relatively rare in China, with only one ST25 isolate recorded from a diseased swine (Zhu et al., 2013) and one from a patient in Hong Kong (Luey et al., 2007) have been reported. In this study, we found an ST25 isolate SZ19010 which was located in *S. suis* 2 Ml Cluster2 had close genetic relatedness to isolates from the USA. The import volume of frozen meat to Shenzhen ranks third in China and is mainly from the EU, the United Kingdom [13], Brazil, and the USA (Lowell et al., 2018; Zu et al., 2020). It suggests that the import of frozen meat also has the risk of human infection. In addition, we should sample the swine that are transported into Shenzhen to study the presence proportion and pathogenic ability of ST25 in Shenzhen swine.

Dong et al. (2021) divided China *S. suis* isolates into three lineages. Both lineagesIand III are ST7 isolates, with lineage I isolate containing 89 KB PAI. Lineage III represents a novel ST7, lacking 89 KB PAI but containing 128 KB GI, and lineage II is ST1 isolate, containing 78 KB PAI. Similar results were found in the human isolates from Shenzhen. Among the Shenzhen human isolates of *S. suis* 2, the ST7 isolates at Cluster1.2 were missing 89 KB PAI but had inserted 105 KB or 128 KB GI. In comparison, the ST7 isolates at Cluster1.1, carrying *ant*(6)-*Ia*, *aph*(3′)-*III*, *erm*(B), *mef*(A), *msr*(D), *tet*(O), and *tet*(40) ARGs, demonstrated MDR to the antibiotics SM, DA, ERY, and TC. In

13 https://agriculture.Ec.Europa.Eu/farming/animal-products/pork_en

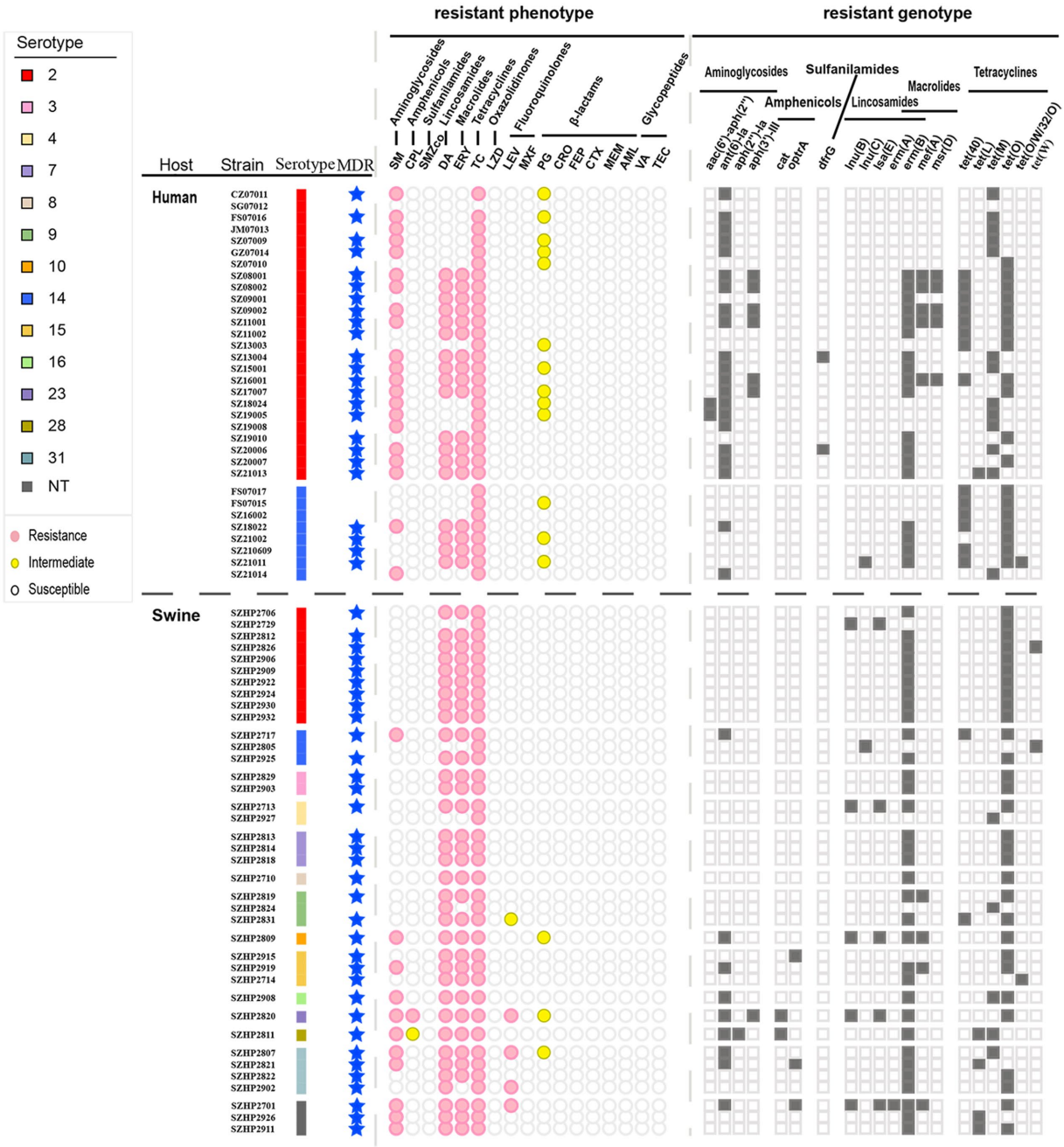

FIGURE 6
Different serotypes of Shenzhen *S. suis* isolates with resistance phenotype and resistance genotype distribution. MDR=multiple drug resistance. Circles or squares are filled with color when the corresponding resistance phenotype or resistance genotype is present.

addition, apart from ST1 isolates located in Cluster1.3, isolates contained 78 KB PAI with all the key factors associated with virulence in 89 KB PAI. Conversely, we found 72 KB and 82 KB PAI in *S. suis* 2 Cluster1.3, which were distinct from 89 KB PAI due to missing all or part of the *SalK/SalR*. *Tet*(L) and ISL3 family transposase IS1165 were found in 82 KB PAI. *Tet*(L) is usually carried in *Streptococcus* on small transmissible plasmids and was detected in the Tn*916* transposon of the Vietnamese human isolate BM407 (Holden et al., 2009). It is not present in isolates representative of the 2005 outbreak in China, such as SC84 and 05ZYH33 (Holden et al., 2009). While IS1165 was initially reported to be present in *Leuconostoc mesenteroides* subsp. *Cremoris* (Johansen and Kibenich, 1992), in this study, IS1165 was found for the first time in *S. suis* PAI. It is, therefore, necessary to further investigate the structure and function of *S. suis* 82 KB PAI fragments that may be responsible for changing pathogenicity and drug resistance. Further confirmation of relative pathogenicity is needed. 78 KB PAI was generally prevalent in *S. suis* 2 isolates (Dong et al., 2021), and we also found it in human isolates of *S. suis* 14. Therefore, we need to further study whether the pathogenicity of 78 KB PAI changes in different serotypes.

In this study, we found there was a good agreement between resistance genotypes and phenotypes for SM, DA, ERY, TC, LZD, PG, CRO, FEP, CTX, MEM, AML, and VA. This finding suggests that ARGs can therefore be used to predict resistant *S. suis* phenotypes. Currently, clinical treatment of *S. suis* infection is mainly with the antibiotics PG and CRO (Segura et al., 2020). We found that 13 isolates had intermediate resistance to PG. The emergence of isolates with intermediate resistance to PG suggests that the antibiotic treatment strategy should be promptly adjusted, and antibiotics used sparingly to avoid antibiotic resistance.

We found that carriage of *S. suis* was common in clinically healthy swine, and there was a diversity of serotypes and genotypes, including serotypes 2, 4, 7, 9, 14, 16, and 31, which are closely related to human infection (Liang et al., 2021; Wang et al., 2021). High virulence isolates were always found on the same branch (Chen et al., 2013a), and we found eight swine isolates clustered with 32 human isolates in Shenzhen, possessing the three key virulence factors *mrp*, *sly*, and *epf*. This indicates that healthy swine may act as reservoirs for *S. suis* that can then be transmitted to humans.

It is widely reported that the risk of *S. suis* infection is higher in people who come in close contact with swine and pork-related products, particularly with wound exposure (Feng et al., 2014; Lu et al., 2021). Most studies on *S. suis* have therefore focused on swine; however, we found two cases of *S. suis* infection resulting from exposure to, or consumption of chicken. In a study of Vietnamese chicken flocks, (Nhung et al., 2020) suggested that chickens may be a source of *S. suis* infection in humans and swine. These findings suggest that the carriage rate and genotype of *S. suis* should be monitored in poultry and swine.

To prevent human *S. suis* infection, meat should be bought with a quarantine certificate. In addition, personal and environmental hygiene should be maintained when handling raw meat and contact with diseased or dead swine and poultry, their excrement, and body fluids should be avoided. Occupational personnel working in direct contact with swine and poultry should wear protective gloves and clothing as well as rubber shoes. Workers with skin injuries should avoid contacting with swine, poultry, and their meat, and follow strict hygiene protocols, including covering wounds, wearing protective, and frequent hand washing. Cross-contamination of raw and cooked meat should also be avoided during food processing.

In summary, effective monitoring of imported swine and poultry from Guangxi and other provinces should be implemented to prevent the occurrence and spread of human *S. suis* disease in Shenzhen. At the same time, international cooperation should be strengthened to control the smuggling of live swine along with the China-Vietnam border. In addition, health education for relevant occupational groups should be increased to improve self-protection awareness, which can effectively avoid the occurrence of swine streptococcal disease. Finally, to reduce the burden of bacterial AMR, the rational use of antibiotics is urgently needed.

Data availability statement

The data presented in the study are deposited in the NCBI repository, accession number PRJNA894855.

Ethics statement

The studies involving human participants were reviewed and approved by the Ethics Committee of the Shenzhen Center for Disease Control and Prevention (QS2022110079). Written informed consent from the participants' legal guardians/next of kin was not required to participate in this study, in accordance with the national legislation and the institutional requirements.

Author contributions

LJ and XS conceived and designed the study. ZC collected case-related data. FL collected the swine samples. LJ, QH, LX, XD, HW, SX, QC, SW, SQ, HL, MJ, RC, YQ, and YL performed the experiments and data analysis. LJ drafted the manuscript. XS revised the manuscript. LJ, ZC, and FL contributed equally to this work. All authors contributed to the article and approved the submitted version.

Funding

This research was supported by the National Natural Science Foundation of China (No. 81773436), the Key Scientific and Technological Project of Shenzhen Science and Technology Innovation Committee (KCXFZ202002011006190), Shenzhen Key Medical Discipline Construction Fund (SZXK064), Non-profit Central Research Institute Fund of Chinese Academy of Medical Sciences (2020-PT330-006), and the Sanming Project of Medicine in Shenzhen (NO. SZSM201811071).

Conflict of interest

The authors declare that the research was conducted in the absence of any commercial or financial relationships that could be construed as a potential conflict of interest.

Publisher's note

Supplementary material

The Supplementary material for this article can be found online at: https://www.frontiersin.org/articles/10.3389/fmicb.2023.1118056/full#supplementary-material

References

Aradanas, M., Poljak, Z., Fittipaldi, N., Ricker, N., and Farzan, A. (2021). Serotypes, virulence-associated factors, and antimicrobial resistance of Streptococcus suis isolates recovered from sick and healthy pigs determined by whole-genome sequencing. *Front Vet Sci* 8:742345. doi: 10.3389/fvets.2021.742345

Bamphensin, N., Chopjitt, P., Hatrongjit, R., Boueroy, P., Fittipaldi, N., Gottschalk, M., et al. (2021). Non-penicillin-susceptible Streptococcus suis isolated from humans. *Pathogens* 10:1178. doi: 10.3390/pathogens10091178

Bankevich, A., Nurk, S., Antipov, D., Gurevich, A. A., Dvorkin, M., Kulikov, A. S., et al. (2012). SPAdes: a new genome assembly algorithm and its applications to single-cell sequencing. *J. Comput. Biol.* 19, 455–477. doi: 10.1089/cmb.2012.0021

Bolger, A. M., Lohse, M., and Usadel, B. (2014). Trimmomatic: a flexible trimmer for Illumina sequence data. *Bioinformatics* 30, 2114–2120. doi: 10.1093/bioinformatics/btu170

Bortolaia, V., Kaas, R. S., Ruppe, E., Roberts, M. C., Schwarz, S., Cattoir, V., et al. (2020). ResFinder 4.0 for predictions of phenotypes from genotypes. *J. Antimicrob. Chemother.* 75, 3491–3500. doi: 10.1093/jac/dkaa345

Camacho, C., Coulouris, G., Avagyan, V., Ma, N., Papadopoulos, J., Bealer, K., et al. (2009). BLAST+: architecture and applications. *BMC Bioinform.* 10:421. doi: 10.1186/1471-2105-10-421

Carattoli, A., Zankari, E., García-Fernández, A., Voldby Larsen, M., Lund, O., Villa, L., et al. (2014). In silico detection and typing of plasmids using PlasmidFinder and plasmid multilocus sequence typing. *Antimicrob. Agents Chemother.* 58, 3895–3903. doi: 10.1128/AAC.02412-14

Chen, L., Song, Y., Wei, Z., He, H., Zhang, A., and Jin, M. (2013b). Antimicrobial susceptibility, tetracycline and erythromycin resistance genes, and multilocus sequence typing of *Streptococcus suis* isolates from diseased pigs in China. *J. Vet. Med. Sci.* 75, 583–587. doi: 10.1292/jvms.12-0279

Chen, C., Tang, J., Dong, W., Wang, C., Feng, Y., Wang, J., et al. (2007). A glimpse of streptococcal toxic shock syndrome from comparative genomics of S. suis 2 Chinese isolates. *PLoS One* 2:e315. doi: 10.1371/journal.pone.0000315

Chen, C., Zhang, W., Zheng, H., Lan, R., Wang, H., Du, P., et al. (2013a). Minimum core genome sequence typing of bacterial pathogens: a unified approach for clinical and public health microbiology. *J. Clin. Microbiol.* 51, 2582–2591. doi: 10.1128/JCM.00535-13

Croucher, N. J., Page, A. J., Connor, T. R., Delaney, A. J., Keane, J. A., Bentley, S. D., et al. (2015). Rapid phylogenetic analysis of large samples of recombinant bacterial whole genome sequences using Gubbins. *Nucleic Acids Res.* 43:e15. doi: 10.1093/nar/gku1196

Cucco, L., Paniccià, M., Massacci, F. R., Morelli, A., Ancora, M., Mangone, I., et al. (2022). New sequence types and antimicrobial drug-resistant strains of *Streptococcus suis* in diseased pigs, Italy, 2017-2019. *Emerg. Infect. Dis.* 28, 139–147. doi: 10.3201/eid2801.210816

Dechêne-TEMPIER, M., Marois-Créhan, C., Libante, V., Jouy, E., Leblond-Bourget, N., and Payot, S. (2021). Update on the mechanisms of antibiotic resistance and the Mobile Resistome in the emerging zoonotic pathogen *Streptococcus suis*. *Microorganisms* 9:1765. doi: 10.3390/microorganisms9081765

Dong, X., Chao, Y., Zhou, Y., Zhou, R., Zhang, W., Fischetti, V. A., et al. (2021). The global emergence of a novel Streptococcus suis clade associated with human infections. *EMBO Mol. Med.* 13:e13810. doi: 10.15252/emmm.202013810

Dong, W., Ma, J., Zhu, Y., Zhu, J., Yuan, L., Wang, Y., et al. (2015). Virulence genotyping and population analysis of Streptococcus suis serotype 2 isolates from China. *Infect. Genet. Evol.* 36, 483–489. doi: 10.1016/j.meegid.2015.08.021

Feng, Y., Zhang, H., Wu, Z., Wang, S., Cao, M., Hu, D., et al. (2014). Streptococcus suis infection: an emerging/reemerging challenge of bacterial infectious diseases? *Virulence* 5, 477–497. doi: 10.4161/viru.28595

Gottschalk, M., Xu, J., Calzas, C., and Segura, M. (2010). Streptococcus suis: a new emerging or an old neglected zoonotic pathogen? *Future Microbiol.* 5, 371–391. doi: 10.2217/fmb.10.2

Goyette-Desjardins, G., Auger, J. P., Xu, J., Segura, M., and Gottschalk, M. (2014). Streptococcus suis, an important pig pathogen and emerging zoonotic agent-an update on the worldwide distribution based on serotyping and sequence typing. *Emerg. Microbes Infect.* 3:e45, 1–20. doi: 10.1038/emi.2014.45

Gurevich, A., Saveliev, V., Vyahhi, N., and Tesler, G. (2013). QUAST: quality assessment tool for genome assemblies. *Bioinformatics* 29, 1072–1075. doi: 10.1093/bioinformatics/btt086

Gurung, M., Tamang, M. D., Moon, D. C., Kim, S. R., Jeong, J. H., Jang, G. C., et al. (2015). Molecular basis of resistance to selected antimicrobial agents in the emerging zoonotic pathogen Streptococcus suis. *J. Clin. Microbiol.* 53, 2332–2336. doi: 10.1128/JCM.00123-15

Holden, M. T., Hauser, H., Sanders, M., Ngo, T. H., Cherevach, I., Cronin, A., et al. (2009). Rapid evolution of virulence and drug resistance in the emerging zoonotic pathogen Streptococcus suis. *PLoS One* 4:e6072. doi: 10.1371/journal.pone.0006072

Huang, J., Liu, X., Chen, H., Chen, L., Gao, X., Pan, Z., et al. (2019a). Identification of six novel capsular polysaccharide loci (NCL) from Streptococcus suis multidrug resistant non-typeable strains and the pathogenic characteristic of strains carrying new NCLs. *Transbound. Emerg. Dis.* 66, 995–1003. doi: 10.1111/tbed.13123

Huang, J., Ma, J., Shang, K., Hu, X., Liang, Y., Li, D., et al. (2016). Evolution and diversity of the antimicrobial resistance associated Mobilome in Streptococcus suis: a probable Mobile genetic elements reservoir for other streptococci. *Front. Cell. Infect. Microbiol.* 6:118. doi: 10.3389/fcimb.2016.00118

Huang, W., Wang, M., Hao, H., Yang, R., Xie, J., Su, J., et al. (2019b). Genomic epidemiological investigation of a Streptococcus suis outbreak in Guangxi, China, 2016. *Infect. Genet. Evol.* 68, 249–252. doi: 10.1016/j.meegid.2018.12.023

Humphries, R., Bobenchik, A. M., Hindler, J. A., and Schuetz, A. N. (2021). Overview of changes to the clinical and laboratory standards institute performance standards for antimicrobial susceptibility testing, M100, 31st edition. *J. Clin. Microbiol.* 59:e0021321. doi: 10.1128/JCM.00213-21

Ichikawa, T., Oshima, M., Yamagishi, J., Muramatsu, C., and Asai, T. (2020). Changes in antimicrobial resistance phenotypes and genotypes in Streptococcus suis strains isolated from pigs in the Tokai area of Japan. *J. Vet. Med. Sci.* 82, 9–13. doi: 10.1292/jvms.19-0449

Inouye, M., Dashnow, H., Raven, L. A., Schultz, M. B., Pope, B. J., Tomita, T., et al. (2014). SRST2: rapid genomic surveillance for public health and hospital microbiology labs. *Genome Med.* 6:90. doi: 10.1186/s13073-014-0090-6

Jiang, F., Guo, J., Cheng, C., and Gu, B. (2020). Human infection caused by Streptococcus suis serotype 2 in China: report of two cases and epidemic distribution based on sequence type. *BMC Infect. Dis.* 20:223. doi: 10.1186/s12879-020-4943-x

Johansen, E., and Kibenich, A. (1992). Isolation and characterization of IS1165, an insertion sequence of Leuconostoc mesenteroides subsp. cremoris and other lactic acid bacteria. *Plasmid* 27, 200–206. doi: 10.1016/0147-619X(92)90022-3

Kedkovid, R., Sirisereewan, C., and Thanawongnuwech, R. (2020). Major swine viral diseases: an Asian perspective after the African swine fever introduction. *Porcine Health Manag.* 6:20. doi: 10.1186/s40813-020-00159-x

Kerdsin, A., Akeda, Y., Takeuchi, D., Dejsirilert, S., Gottschalk, M., and Oishi, K. (2018). Genotypic diversity of Streptococcus suis strains isolated from humans in Thailand. *Eur. J. Clin. Microbiol. Infect. Dis.* 37, 917–925. doi: 10.1007/s10096-018-3208-8

Kerdsin, A., Segura, M., Fittipaldi, N., and Gottschalk, M. (2022). Sociocultural factors influencing human *Streptococcus suis* disease in Southeast Asia. *Foods* 11:1190. doi: 10.3390/foods11091190

Kerdsin, A., Takeuchi, D., Nuangmek, A., Akeda, Y., Gottschalk, M., and Oishi, K. (2020). Genotypic comparison between *Streptococcus suis* isolated from pigs and humans in Thailand. *Pathogens* 9:50. doi: 10.3390/pathogens9010050

Li, M., Shen, X., Yan, J., Han, H., Zheng, B., Liu, D., et al. (2011). GI-type T4SS-mediated horizontal transfer of the 89K pathogenicity island in epidemic *Streptococcus suis* serotype 2. *Mol. Microbiol.* 79, 1670–1683. doi: 10.1111/j.1365-2958.2011.07553.x

Liang, P., Wang, M., Gottschalk, M., Vela, A. I., Estrada, A. A., Wang, J., et al. (2021). Genomic and pathogenic investigations of Streptococcus suis serotype 7 population derived from a human patient and pigs. *Emerg. Microbes Infect.* 10, 1960–1974. doi: 10.1080/22221751.2021.1988725

Lowell, J. E., Schunke, E. D., Harsh, B. N., Bryan, E. E., Overholt, M. F., Stahl, C. A., et al. (2018). Correlation comparisons among early postmortem loin quality and aged loin and pork chop quality characteristics between finishing pigs from either Duroc or Pietrain sires. *J. Anim. Sci.* 96, 4644–4657. doi: 10.1093/jas/sky315

Lu, H., Li, X., Wang, G., Wang, C., Feng, J., Lu, W., et al. (2021). Baicalein ameliorates *Streptococcus suis*-induced infection *in vitro* and *in vivo*. *Int. J. Mol. Sci.* 22:5829. doi: 10.3390/ijms22115829

Luey, C. K., Chu, Y. W., Cheung, T. K., Law, C. C., Chu, M. Y., Cheung, D. T., et al. (2007). Rapid pulsed-field gel electrophoresis protocol for subtyping of *Streptococcus suis* serotype 2. *J. Microbiol. Methods* 68, 648–650. doi: 10.1016/j.mimet.2006.10.010

Magazine, N. F. T. (2014). The recent rampant smuggling Vietnam pork. *China Swine Industry* 9:67.

Marie, J., Morvan, H., Berthelot-Hérault, F., Sanders, P., Kempf, I., Gautier-Bouchardon, A. V., et al. (2002). Antimicrobial susceptibility of Streptococcus suis isolated from swine in France and from humans in different countries between 1996 and 2000. *J. Antimicrob. Chemother.* 50, 201–209. doi: 10.1093/jac/dkf099

Nhung, N. T., Yen, N. T. P., Cuong, N., Kiet, B. T., Hien, V. B., Campbell, J., et al. (2020). Carriage of the zoonotic organism Streptococcus suis in chicken flocks in Vietnam. *Zoonoses Public Health* 67, 843–848. doi: 10.1111/zph.12711

Okura, M., Osaki, M., Nomoto, R., Arai, S., Osawa, R., Sekizaki, T., et al. (2016). Current taxonomical situation of Streptococcus suis. *Pathogens* 5:45. doi: 10.3390/pathogens5030045

Palmieri, C., Varaldo, P. E., and Facinelli, B. (2011). Streptococcus suis, an emerging drug-resistant animal and human pathogen. *Front. Microbiol.* 2:235. doi: 10.3389/fmicb.2011.00235

Pan, Z., Ma, J., Dong, W., Song, W., Wang, K., Lu, C., et al. (2015). Novel variant serotype of streptococcus suis isolated from piglets with meningitis. *Appl. Environ. Microbiol.* 81, 976–985. doi: 10.1128/AEM.02962-14

Price, M. N., Dehal, P. S., and Arkin, A. P. (2010). FastTree 2--approximately maximum-likelihood trees for large alignments. *PLoS One* 5:e9490. doi: 10.1371/journal.pone.0009490

Princivalli, M. S., Palmieri, C., Magi, G., Vignaroli, C., Manzin, A., Camporese, A., et al. (2009). Genetic diversity of *Streptococcus suis* clinical isolates from pigs and humans in Italy (2003-2007). *Euro Surveill.* 14:19310. doi: 10.2807/ese.14.33.19310-en

Qiu, X., Bai, X., Lan, R., Zheng, H., and Xu, J. (2016). Novel capsular polysaccharide loci and new diagnostic tools for high-throughput capsular gene typing in Streptococcus suis. *Appl. Environ. Microbiol.* 82, 7102–7112. doi: 10.1128/AEM.02102-16

Seemann, T. (2014). Prokka: rapid prokaryotic genome annotation. *Bioinformatics* 30, 2068–2069. doi: 10.1093/bioinformatics/btu153

Segura, M., Aragon, V., Brockmeier, S. L., Gebhart, C., Greeff, A., Kerdsin, A., et al. (2020). Update on Streptococcus suis research and prevention in the era of antimicrobial restriction: 4th international workshop on S. suis. *Pathogens* 9:9. doi: 10.3390/pathogens9050374

Tang, J., Wang, C., Feng, Y., Yang, W., Song, H., Chen, Z., et al. (2006). Streptococcal toxic shock syndrome caused by *Streptococcus suis* serotype 2. *PLoS Med.* 3:e151. doi: 10.1371/journal.pmed.0030151

Thu, I. S. L., Tragoolpua, K., Intorasoot, S., Anukool, U., Khamnoi, P., Kerdsin, A., et al. (2021). Direct detection of Streptococcus suis from cerebrospinal fluid, positive hemoculture, and simultaneous differentiation of serotypes 1, 1/2, 2, and 14 within single reaction. *Pathogens* 10:996. doi: 10.3390/pathogens10080996

Varela, N. P., Gadbois, P., Thibault, C., Gottschalk, M., Dick, P., and Wilson, J. (2013). Antimicrobial resistance and prudent drug use for *Streptococcus suis*. *Anim. Health Res. Rev.* 14, 68–77. doi: 10.1017/S1466252313000029

Wang, X., Sun, J., Bian, C., Wang, J., Liang, Z., Shen, Y., et al. (2021). The population structure, antimicrobial resistance, and pathogenicity of *Streptococcus suis* cps31. *Vet. Microbiol.* 259:109149. doi: 10.1016/j.vetmic.2021.109149

Wu, Z., Li, M., Wang, C., Li, J., Lu, N., Zhang, R., et al. (2011). Probing genomic diversity and evolution of Streptococcus suis serotype 2 by NimbleGen tiling arrays. *BMC Genom.* 12:219. doi: 10.1186/1471-2164-12-219

Wu, Z., Wang, W., Tang, M., Shao, J., Dai, C., Zhang, W., et al. (2014). Comparative genomic analysis shows that Streptococcus suis meningitis isolate SC070731 contains a unique 105K genomic island. *Gene* 535, 156–164. doi: 10.1016/j.gene.2013.11.044

Ye, C., Zhu, X., Jing, H., Du, H., Segura, M., Zheng, H., et al. (2006). Streptococcus suis sequence type 7 outbreak, Sichuan, China. *Emerg. Infect. Dis.* 12, 1203–1208. doi: 10.3201/eid1708.060232

Yongkiettrakul, S., Maneerat, K., Arechanajan, B., Malila, Y., Srimanote, P., Gottschalk, M., et al. (2019). Antimicrobial susceptibility of Streptococcus suis isolated from diseased pigs, asymptomatic pigs, and human patients in Thailand. *BMC Vet. Res.* 15:5. doi: 10.1186/s12917-018-1732-5

Zheng, H., Ji, S., Liu, Z., Lan, R., Huang, Y., Bai, X., et al. (2015). Eight novel capsular polysaccharide synthesis gene loci identified in nontypeable Streptococcus suis isolates. *Appl. Environ. Microbiol.* 81, 4111–4119. doi: 10.1128/AEM.00315-15

Zheng, H., Qiu, X., Roy, D., Segura, M., Du, P., Xu, J., et al. (2017). Genotyping and investigating capsular polysaccharide synthesis gene loci of non-serotypeable Streptococcus suis isolated from diseased pigs in Canada. *Vet. Res.* 48:10. doi: 10.1186/s13567-017-0417-6

Zhu, W., Wu, C., Sun, X., Zhang, A., Zhu, J., Hua, Y., et al. (2013). Characterization of Streptococcus suis serotype 2 isolates from China. *Vet. Microbiol.* 166, 527–534. doi: 10.1016/j.vetmic.2013.06.009

Zongyun, L., and Guojian, L. (2019). Analysis and reflection on the investigation of pork thin in in Nanwan street farmers market in Longgang District, Shenzhen. *Modern Food* 2019, 186–189. doi: 10.16736/j.cnki.cn41-1434/ts.2019.13.057

Zu, E. E., Godar, J., Lathuillière, M. J., Löfgren, P., Gardner, T., Vasconcelos, A., et al. (2020). The origin, supply chain, and deforestation risk of Brazil's beef exports. *Proc. Natl. Acad. Sci. U. S. A.* 117, 31770–31779. doi: 10.1073/pnas.2003270117

frontiers | Frontiers in Microbiology

TYPE Original Research
PUBLISHED 27 April 2023
DOI 10.3389/fmicb.2023.1159590

OPEN ACCESS

EDITED BY
Qing Pan,
Qingdao Agricultural University, China

REVIEWED BY
Qin Zhao,
Northwest A&F University, China
Li Yanhua,
Northeast Agricultural University, China

*CORRESPONDENCE
Shujie Wang
✉ wangshujie@caas.cn
Xuehui Cai
✉ caixuehui@caas.cn

†These authors have contributed equally to this work

RECEIVED 06 February 2023
ACCEPTED 13 April 2023
PUBLISHED 27 April 2023

CITATION
Wang S, Xu M, Yang K, Zhang Y, Li S, Tang Y-D, Wang J, Leng C, An T and Cai X (2023) *Streptococcus suis* contributes to inguinal lymph node lesions in piglets after highly pathogenic porcine reproductive and respiratory syndrome virus infection. *Front. Microbiol.* 14:1159590. doi: 10.3389/fmicb.2023.1159590

Streptococcus suis contributes to inguinal lymph node lesions in piglets after highly pathogenic porcine reproductive and respiratory syndrome virus infection

Shujie Wang[1,2*†], Min Xu[3†], Kongbin Yang[4†], Ying Zhang[5], Siqi Li[1], Yan-Dong Tang[1], Jinliang Wang[5], Chaoliang Leng[6], Tongqing An[1] and Xuehui Cai[1*]

[1]State Key Laboratory for Animal Disease Control and Prevention, Harbin Veterinary Research Institute, Chinese Academy of Agricultural Sciences, Harbin, China, [2]Heilongjiang Provincial Key Laboratory of Veterinary Immunology, Harbin, China, [3]Sinopharm Animal Health Corporation Ltd., Wuhan, China, [4]Neurosurgery Department, The Fifth Affiliated Hospital of Guangzhou Medical University, Guangzhou, China, [5]Shandong Binzhou Animal Science and Veterinary Medicine Academy, Binzhou, China, [6]Henan Key Laboratory of Insect Biology in Funiu Mountain, Henan Provincial Engineering Laboratory of Insects Bio-Reactor, China-UK-NYNU-RRes Joint Laboratory of Insect Biology, Nanyang Normal University, Nanyang, China

The swine pathogens porcine reproductive and respiratory syndrome virus (PRRSV) and *Streptococcus suis* have both been reported to cause damage to the immune organs. Inguinal lymph node (ILN) injury has been reported in PRRSV-infected pigs with secondary *S. suis* infection, but not much is known about the mechanism. In this study, secondary *S. suis* infection after highly pathogenic (HP)-PRRSV infection caused more severe clinical symptoms, mortality, and ILN lesions. Histopathological lesions were seen in ILNs with a marked decrease in lymphocyte numbers. Terminal deoxynucleotidyl transferase (TdT)-mediated deoxyuridine triphosphate (dUTP)-biotin nick end-labeling (TUNEL) assays revealed that HP-PRRSV strain HuN4 alone induced ILN apoptosis, but dual-infection with *S. suis* strain BM0806 induced greater levels of apoptosis. Besides, we found that some HP-PRRSV-infected cells underwent apoptosis. Furthermore, anti-caspase-3 antibody staining confirmed that ILN apoptosis was mainly induced by a caspase-dependent pathway. Pyroptosis was also observed in HP-PRRSV-infected cells, and there was more pyroptosis in piglets infected with HP-PRRSV alone compared with those with secondary *S. suis* infection, and HP-PRRSV-infected cells underwent pyroptosis. Altogether, this is the first report to identify pyroptosis in ILNs and which signaling pathway is related to ILN apoptosis in single or dual-infected piglets. These results contribute to a better understanding of the pathogenic mechanisms during secondary *S. suis* infection.

KEYWORDS

HP-PRRSV, *Streptococcus suis*, inguinal lymph nodes, apoptosis, pyroptosis

Introduction

Porcine reproductive and respiratory syndrome virus (PRRSV) is a positive-sense, single-stranded, enveloped RNA virus (Firth et al., 2011; Wang et al., 2016) belonging to the family *Arteriviridae* and genus *Betaarterivirus* (Dokland, 2010; Ma et al., 2018). PRRSV was first discovered in the United States in 1987 (Rossow, 1998), whereas in China, classic PRRSV and highly pathogenic (HP)-PRRSV strains were isolated in 1996 and 2006 (Li et al., 2007; Jiang et al., 2020), respectively. Classic PRRSV can cause acute respiratory disease in piglets and fever, breathing difficulties and miscarriage in sows (Van Reeth, 1997; Johnson et al., 2004). HP-PRRSV is different from the classic strain, causing severe disease not only in piglets but also in adult pigs, with strong pathogenicity and high mortality resulting in huge economic losses for affected pig farms (Hu et al., 2013; Do et al., 2015; Chen et al., 2016).

Many studies have demonstrated the immunosuppressive nature of PRRSV (Fan et al., 2015; Zhou et al., 2021). PRRSV infection can cause atrophy of the thymus, in which a large number of $CD3^+$ T cells undergo apoptosis, decreasing the number of $CD4^+$ and $CD8^+$ T cells in peripheral blood (Li et al., 2014; Wang et al., 2015). PRRSV has a strong affinity for alveolar macrophages and can infect and replicate within them (Sun et al., 2022). Part of circulating antibodies can enhance viral infection and replication in macrophages (Shi et al., 2018, 2019). Meanwhile, PRRSV destroys macrophage function and inhibits their non-specific bactericidal activities (Jung et al., 2009), which can lead to serious secondary bacterial infections.

Inguinal lymph nodes (ILNs) are peripheral immune organs that defend against foreign bodies, producing antibodies and participating in the systemic immune response to pathogens (Sever et al., 2012). Immunosuppressive diseases are characterized by the destruction of immune organs (Wang et al., 2021), and PRRSV is known to damage immune organs including the thymus, bone marrow, spleen, and ILNs (Feng et al., 2001; Wang G. et al., 2020; Wang et al., 2022). Moreover, *Streptococcus suis* has also been reported to damage the thymus of pigs in recent years (Wang S. et al., 2020). However, reports of the mechanism for HP-PRRSV damage to peripheral immune organs such as ILNs, and specifically the involvement of secondary *S. suis* infection in ILN injury are less reported (Feng et al., 2001; Wang et al., 2014).

The purpose of this study was to explore the mechanism of ILN pathogenesis, both by HP-PRRSV alone or with secondary *S. suis* infection, and explore the differences in ILN apoptosis/pyroptosis in infected piglets.

Materials and methods

Ethics statement

All animal experiments were approved by the Committee on the Ethics of Animal Experiments of the Harbin Veterinary Research Institute of the Chinese Academy of Agricultural Sciences (CAAS), China. Piglet dual-infection experiments (approval number 200805-06) were carried out in the animal biosafety level 2 facilities at the Harbin Veterinary Research Institute, CAAS.

Bacterial and viral strains

The HP-PRRSV HuN4 strain (Wang et al., 2015) and *S. suis* serotype 7 strain BM0806 (Wang S. et al., 2020) used in the current study were stored in our lab. PRRSV HuN4 was passed three times on MARC-145 cells in Dulbecco's modified Eagle's medium (DMEM) with 8% fetal calf serum (Excel Bio, Shanghai, China) at 37°C. *Streptococcus suis* BM0806 was grown on sheep blood agar plates at 37°C for 20 h, and three colonies were inoculated into Todd-Hewitt broth (THB; HAIBO, Qingdao, China) and incubated for 12 h at 37°C with agitation.

Animal experiments

A total of 40, 21-day-old PRRSV- and *S. suis*-negative crossbred piglets were randomly divided into four groups and housed separately in isolation rooms. As shown in Figure 1, after 1 week (day 0), groups 1 ($n = 12$ piglets) and 2 ($n = 10$ piglets) were inoculated with 3 mL HP-PRRSV HuN4 (2×10^5 $TCID_{50}$ total, 2 mL intranasal and 1 mL intramuscular inoculation); groups 3 and 4 ($n = 9$ piglets each) were inoculated with 3 mL DMEM. On day 7, groups 1 and 4 were inoculated with 3 mL *S. suis* BM0806 (3×10^9 colony-forming units total, 2 mL intranasal and 1 mL intramuscular inoculation). Pigs were monitored daily for clinical signs including fever, lethargy, sneezing, joint swelling, lameness, central nervous system disease, and changes of skin. Three piglets from each group were humanely euthanized on day 7, 14, and 21. Lung and ILN samples were collected and macroscopic lesions were scored on a scale from 0 to 3 using the system outlined in Table 1. During the experiment, any piglets exhibiting extreme lethargy were euthanized humanely.

Histopathology examinations

Inguinal lymph node samples from sacrificed experimental animals were placed in 4% formalin in phosphate buffer and fixed for 7 days, embedded in paraffin and cut into 8-μm-thick slices prior to staining with hematoxylin and eosin (H&E). Tissue sections were observed by a professional pathologist on an inverted light microscope (Carl Zeiss, Munich, Germany). For morphometric analysis, the average number of lymphocytes in H&E sections was determined from counts of 10 microscope fields (400×). The mean number of lymphocytes per mm^2 was calculated.

Confocal microscopy

Inguinal lymph node samples from each group were collected and sectioned in 8-μm-thick slices for immunofluorescence. An *In situ* Cell Death Detection Kit (Roche, Mannheim, Germany) was used to detect apoptosis in ILNs by terminal deoxynucleotidyl transferase (TdT)-mediated deoxyuridine triphosphate (dUTP)-biotin nick end-labeling (TUNEL) assay. To identify the apoptosis signaling pathway, rabbit anti-mouse caspase-3 antibody (1:500, Cell Signaling, Danvers, United States), rabbit anti-mouse apoptosis-inducing factor (AIF) monoclonal antibody (1:50, Abcam, Cambridge, United Kingdom), and Alexa Fluor 568-conjugated goat anti-rabbit antibody (1:500, Sigma, Saint Louis, United States) were used. Rabbit polyclonal antiserum

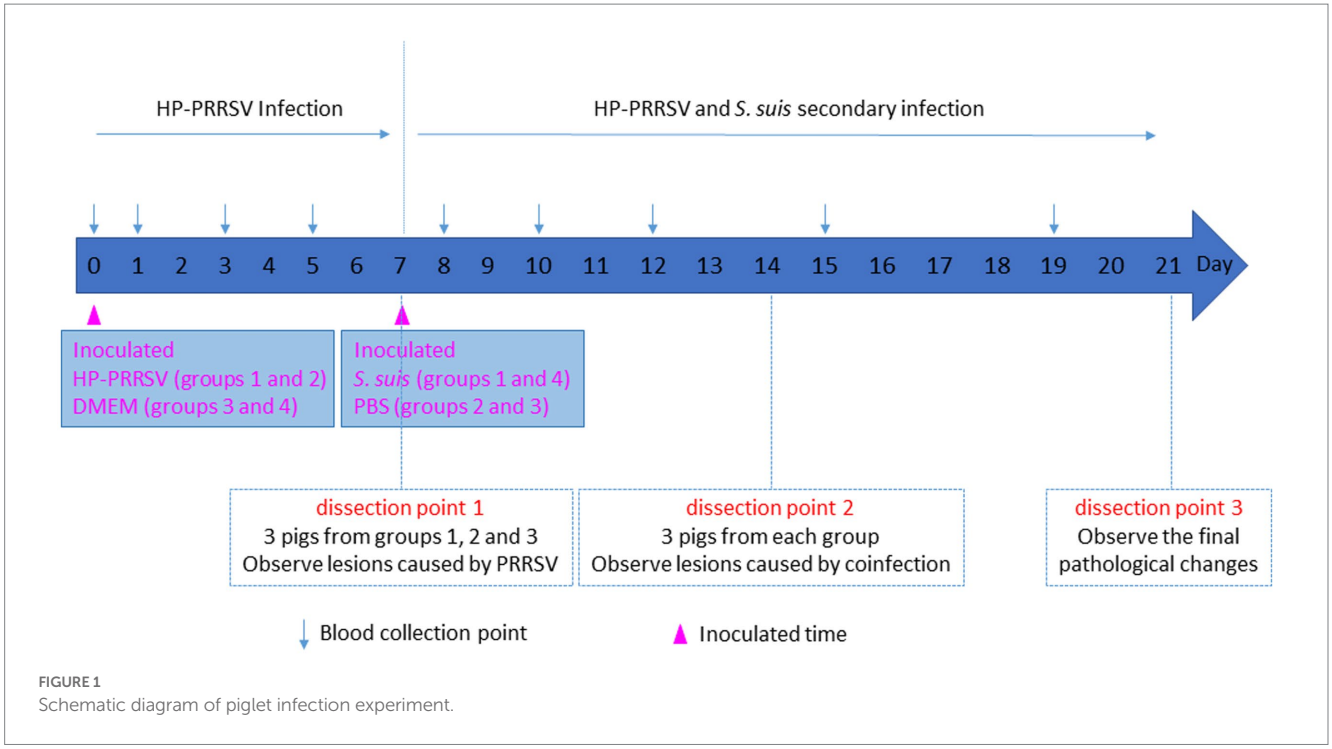

FIGURE 1
Schematic diagram of piglet infection experiment.

TABLE 1 Macroscopic pathohistological score.

Parameter	Score 0	Score 1	Score 2	Score 3
Lung	No visible lesions	Slight interstitial pneumonia or congestion	Interstitial pneumonia with local emphysema/ consolidation	Interstitial pneumonia with emphysema/ consolidation/ severe bleeding
ILN	No visible lesions	Slight enlargement	Swelling and hemorrhage	Swelling and severe hemorrhage

against *S. suis* serotype 7 (1:50, SSI, Denmark), FITC-conjugated goat anti-rabbit antibody (1:500, Sigma), monoclonal antibody (mAb) against HP-PRRSV N protein (1:500, produced in lab), and Alexa Fluor 488 rabbit anti-mouse antibody (1:1,000, Sigma) were used. To identify pyroptosis, rabbit anti-mouse gasdermin-D-N/C (GSDMD-N/C; 1:50, Abcam), mouse polyclonal antiserum against *S. suis* serotype 7 (1:50, made in lab) and Alexa Fluor 568/488-conjugated goat anti-rabbit/ mouse antibody (1:500, Sigma) were used. Nuclei were stained with 4-6-diamidino-2-phenylindole (DAPI, Sigma), and sections were observed by confocal laser scanning microscopy with fast airyscan LSM880 (Carl ZEISS, Jena, Germany). For morphometric analysis, the apoptotic or pyroptotic cells in 8 microscopy fields of the ILN sections were counted. The mean number of labeled cells per mm^2 was calculated.

Statistical analysis

Data were expressed as the mean ± standard deviation and analyzed by GraphPad Prism software (version 5.01; GraphPad Software Inc.). Differences between groups were assessed by one-way ANOVA and Tukey's multiple-comparison test or Fisher's exact test for categorical variables. A p value less than 0.05 was considered statistically significant.

Results

Dual-infection with *Streptococcus suis* caused more severe clinical symptoms and mortality in PRRSV-infected piglets

To investigate whether dual-infection with *S. suis* caused more severe clinical symptoms and mortality in PRRSV-infected piglets, we used *S. suis* BM0806 to infect PRRSV-infected piglets. As shown in Figure 2, piglets in the mock-infected control group did not show any clinical signs during the experiment. In the PRRSV HuN4-infected group, piglets developed symptoms of sneezing, cough, and diarrhea by 6 days post-infection (dpi), and anorexia, lying down, weight loss, wheezing, and muscle tremors at 11 dpi, one piglet died at 18, 21, and 22 dpi, respectively; mortality was 33%. In the group infected with *S. suis* BM0806 alone, several pigs (5/10) showed mild symptoms of cough and sneezing during first 3 days after infection. In the dual-infected group, piglets developed symptoms of anorexia, dyspnea, emaciation, tremors, and unsteadiness at 9 dpi, and three piglets died at 10 dpi, two piglets died at 12 dpi, one piglet died at 13 dpi with cyanotic limbs and ears, and one piglet exhibiting extreme lethargy was euthanized humanely on 15 dpi; overall mortality was 58.3%.

The rectal temperature of piglets in the PRRSV HuN4-infected group spiked (> 41.5°C) on day 9, remained above 40.7°C from day 10 to 18, and fell below 40°C on days 20 and 21 (Figure 3A). The rectal temperature of piglets in the dual-infected group rose above 40.2°C from day 8 to 15 (except on day 12), and reached the peak (40.7°C) on day 9.

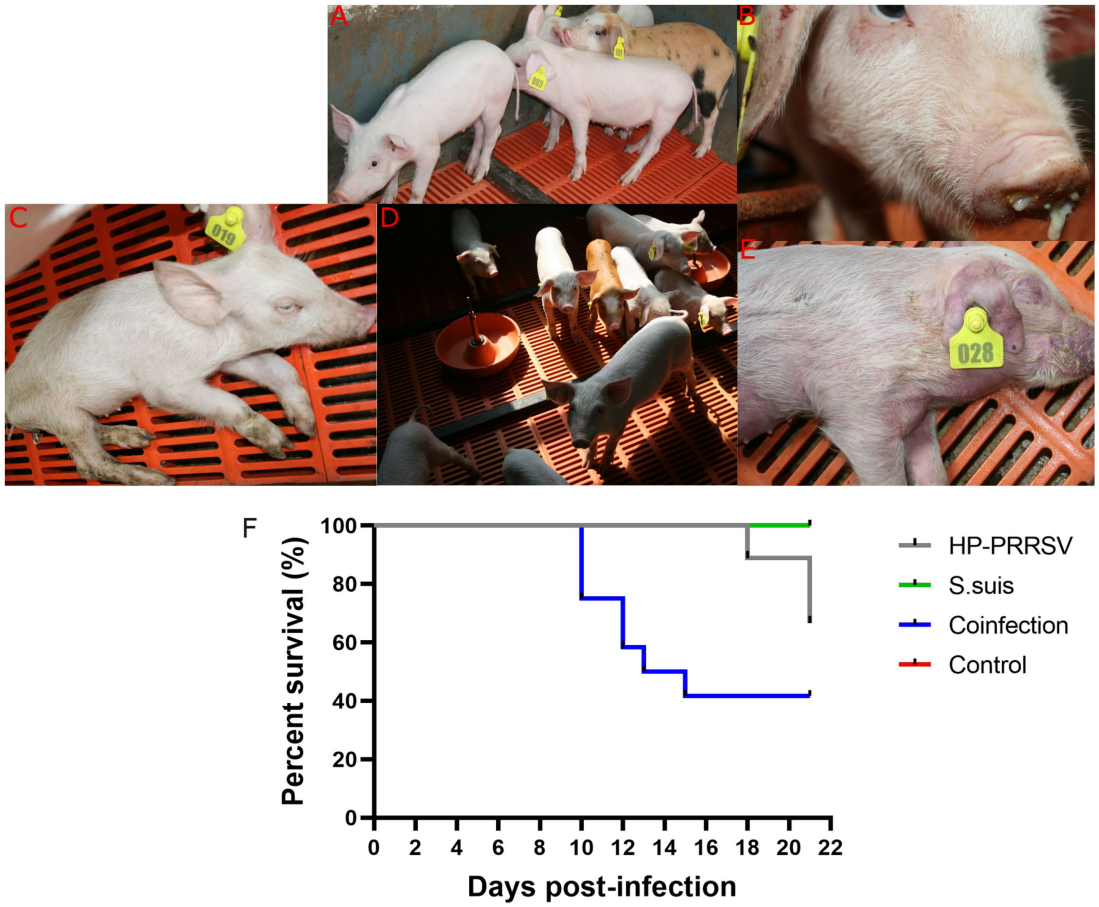

FIGURE 2
Clinical signs and mortality percent in piglets during the animal infection experiment. Clinical signs observed during experiment in **(A)** mock-infected control group; **(B)** Nasal discharge; **(C)** Anorexia, depression, and emaciation were seen in HP-PRRSV-infected piglets; **(D)** mild cough was seen in *Streptococcus suis*-infected group; **(E)** cyanotic limbs and ears were seen in co-infected group; **(F)** Survival percent in different experimental groups.

The temperature dropped below 40°C and remained stable from day 16 to 21. In the group infected with *S. suis* BM0806 alone, the rectal temperature of piglets was above 40.0°C from day 17 to 21. No significant increase in rectal temperature was observed in the control group.

More severe gross and histopathologic lesions in ILNs of dual-infected piglets

The macroscopic pathohistological score for lungs and ILNs in each experimental groups are presented in Table 2. The main visible organ lesions in PRRSV HuN4-infected piglets at 14 dpi were clearly found in lung (Figure 3B) and ILNs (Figure 3C). Piglets developed marked lobular interstitial pneumonia with fleshy consolidation in the sharp lobes of the lung. Gross lesions of the ILNs included swelling and hemorrhage. The main organ lesions found in the dual-infected piglets that died at 12 and 13 dpi were interstitial pneumonia with severe bleeding in the lungs and adhesions to the body cavity, severe bacterial infection and massive purulent fluid in the abdominal cavity, with swelling and hemorrhage in the ILNs. In the piglets infected with *S. suis* BM0806 alone, those sacrificed at 14 dpi had interstitial pneumonia or congestion with local emphysema in both lungs, hemorrhage and meningeal hemorrhage in the ILNs.

Representative histopathology for each treatment group is shown in Figure 4A. The main microscopic lesions in ILNs from PRRSV HuN4-infected piglets were a marked reduction in number of lymphocytes and visibly small vacuoles. In dual-infected piglets, the main ILN lesions were massive disintegration and necrosis of lymphocytes, macrophage infiltration and intense plasma cell proliferation. In piglets infected with *S. suis* BM0806 alone, the main ILN lesions were lymphocyte depletion and necrosis, lymph node nodules that were not obvious, and some eosinophilic infiltration into the paracortical areas. Compared with the control group, the lymphocytes in all three infected groups were significantly reduced on 14 dpi, but there was no statistical difference among them on 14 dpi (Figure 4B). On 21 dpi, the number of lymphocytes in the ILNs in single-infected pigs recovered, but there was no recovery in the dual-infected group, compared with the number of lymphocytes in the ILNs of the pigs on 14 dpi.

More apoptosis in ILNs of dual-infected piglet than PRRSV-infected piglets

In the following experiments, in order to explore the role of bacteria in ILN injury, we mainly compared the PRRSV

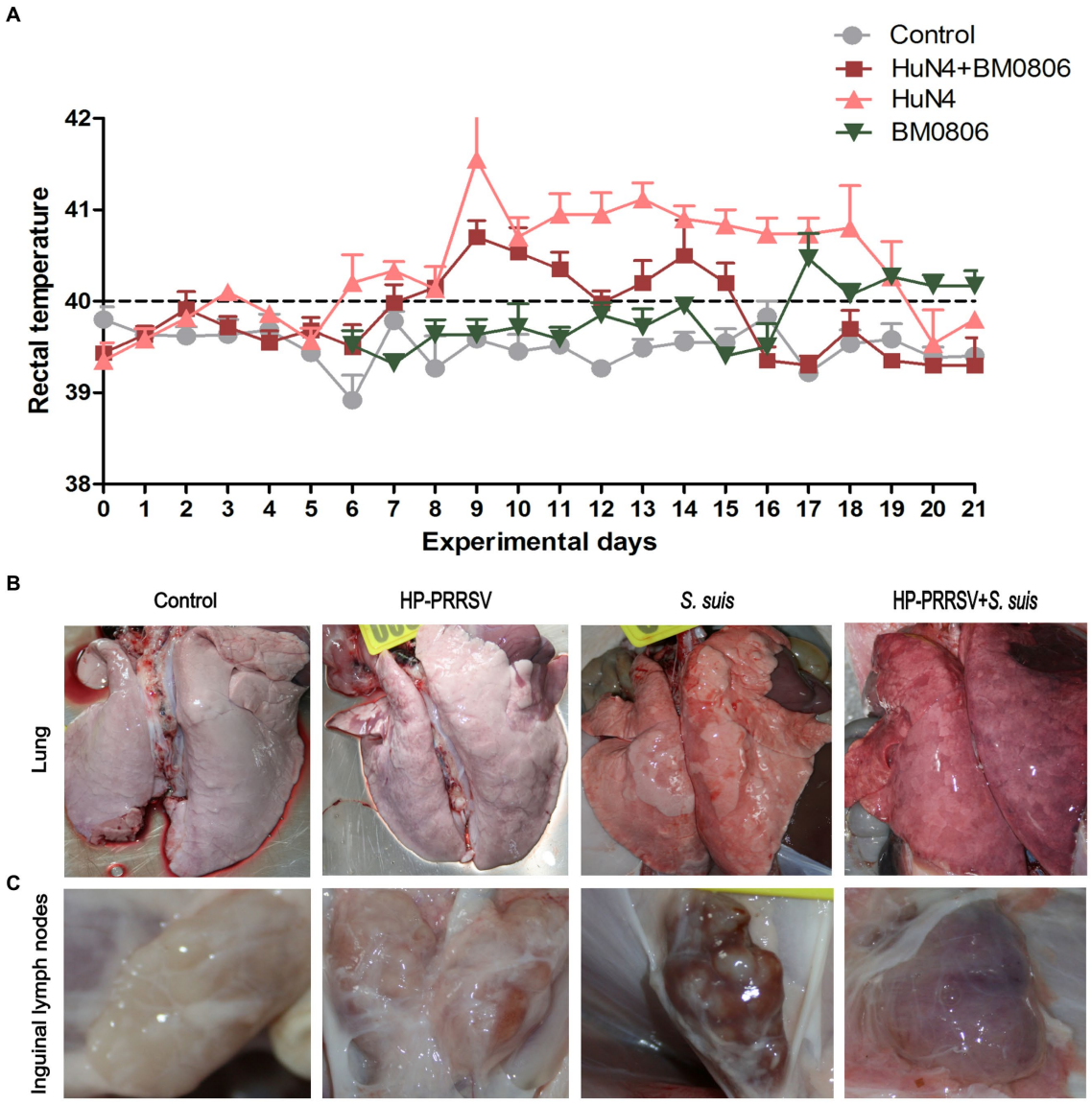

FIGURE 3
Gross lesions in lung and inguinal lymph nodes after infection with HP-PRRSV and/or *Streptococcus suis*. **(A)** Daily average rectal temperature of piglets from each treatment group. The mean±S.D. is plotted from all piglets on each experimental day. Piglets were mock infected (Control) or infected with HP-PRRSV and/or *S. suis*. Representative gross pathological lesions are depicted from **(B)** the lungs and **(C)** the inguinal lymph nodes of each experimental group.

TABLE 2 Macroscopic pathohistological score for lungs and ILNs.

Goups no. (*n*)	Designation	Lungs	ILNs
1 (12)	Co-infection	2.5^{A}	2.5^{A}
2 (10)	HP-PRRSV	2.2^{B}	2.0^{B}
3 (9)	PBS	0^{B}	0^{B}
4 (9)	*S. suis*	1.5^{C}	2.1^{B}

$^{A–C}$Different superscripts within a column indicate significant differences ($p < 0.05$) determined by Fisher's exact test.

single-infection group with the dual-infected. To investigate the cause of the massive decrease in the number of lymphocytes in the ILNs of infected piglets, apoptosis was detected using TUNEL assays. TUNEL-positive signals were observed in ILN sections from infected pigs (Figure 5A), and a large number of ILN cells underwent apoptosis in both the PRRSV-infected ($p < 0.01$) and dual-infected ($p < 0.001$) piglets compared with the mock-infected controls (Figure 5B). Moreover, the number of apoptotic cells in the dual-infected group was higher than in the group infected with PRRSV alone ($p < 0.01$).

Colocalization of PRRSV HuN4-infected cells and apoptotic cells

Double immunofluorescence staining was used to determine whether HP-PRRSV or *S. suis* signals colocalized with apoptotic cells. ILN sections were incubated with HP-PRRSV or *S. suis* polyclonal

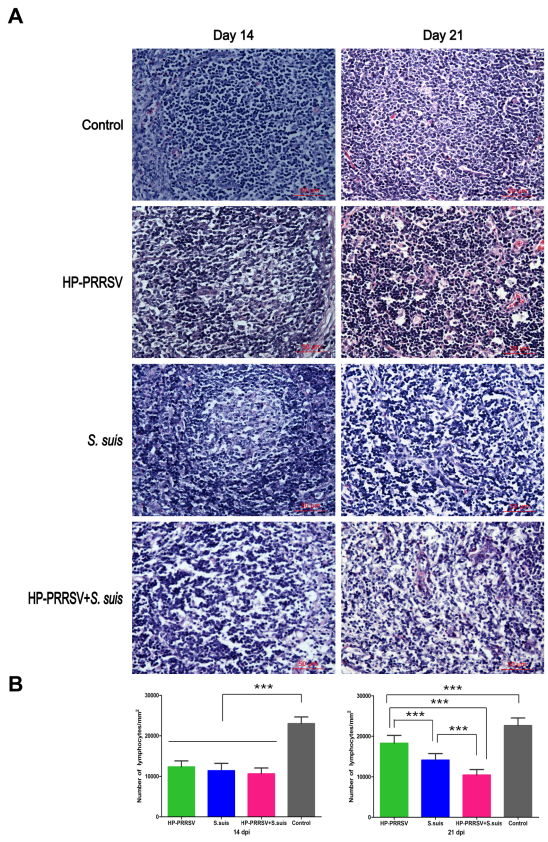

FIGURE 4
Histopathological lesions induced in the inguinal lymph nodes of infected piglets. **(A)** Representative hematoxylin & eosin staining in the inguinal lymph nodes of piglets mock infected (Control) or infected with HP-PRRSV and/or *Streptococcus suis*. **(B)** Number of lymphocytes in ILNs from different groups of pigs on 14 and 21dpi. On 14dpi, the number of lymphocytes decreased significantly in the inguinal lymph nodes from three infected groups compared with control group. On 21dpi, the number of lymphocytes in the single-infected groups recovered, with no significant recovery in dual-infected group. ***p <0.001.

antibodies, and apoptosis was detected using a TUNEL assay. HP-PRRSV-infected cells colocalized with apoptotic cells, indicating that HP-PRRSV-infected cells underwent apoptosis (Figure 6A). On the other hand, *S. suis*- and TUNEL-positive signal was not observed in the same cells, indicating a lack of apoptosis in *S. suis*-adhered cells (Figure 6B). Figure 6C is the ILN from control pig.

PRRSV HuN4 and *Streptococcus suis* BM0806 mainly induce caspase-dependent apoptosis in ILNs

Caspase-3 is considered a biochemical hallmark of apoptosis (Wang S. et al., 2020). We found caspase-3 expression in apoptotic cells in ILNs from piglets either infected with PRRSV alone, or dual-infected with *S. suis* (Figure 7A). Consistent with the TUNEL results, the number of apoptotic cells in the dual-infected group was greater than in the group infected with PRRSV alone (Figure 7B). Apoptosis-inducing factor (AIF) mainly mediates the p53 apoptosis pathway (Ding et al., 2018). We attempted to detect AIF protein expression in the infected groups, and no obvious difference of fluorescent signals was detected in ILNs of any of the infected piglets relative to mock-infected controls (data not shown). These results suggest that HP-PRRSV HuN4 induce caspase-dependent apoptosis in ILNs from infected piglets.

More pyroptosis signal was observed in ILNs of piglets infected by PRRSV alone

Pyroptosis is a form of programmed necrosis that is mediated by gasdermin D (GSDMD; Shi et al., 2017). To investigate whether pyroptosis occurred in the ILNs of HP-PRRSV-infected or PRRSV/*S. suis* dual-infected piglets, we used confocal microscopy to detect the GSDMD C-terminal domain in tissue sections. In contrast to mock-infected piglets, both PRRSV-infected and dual-infected piglets displayed ILN pyroptosis (Figure 8A), with much greater signal in those infected by PRRSV alone (Figure 8B).

To determine whether infected cells were undergoing pyroptosis, double immunofluorescence staining experiments were carried out using specific anti-PRRSV or anti-*S. suis* antibodies along with anti-GSDMD-N-terminal domain antibody. Some HP-PRRSV-infected cells colocalized with pyroptotic cells, whereas *S. suis*-adhered cells from ILNs of dual-infected piglets did not show any GSDMD-N signal (Figure 8C). These findings suggest that HP-PRRSV-infected cells may undergo pyroptosis.

Discussion

Porcine reproductive and respiratory syndrome virus is the most economically important pathogen in pigs worldwide (Lunney et al., 2016), and it has developed multiple mechanisms to evade the host immune response (Costers et al., 2008; Sang et al., 2011). After infecting alveolar macrophages in the lungs, PRRSV spreads to the macrophages present in tissues, resulting in destruction of lymphocytes and mucosal barriers. The synergistic pathogenesis of PRRSV and *S. suis* has been reported (Galina et al., 1994; Thanawongnuwech et al., 2000; Sun et al., 2020). In our study, the dual-infected group had a higher mortality rate (58.3%) than the PRRSV-infected group (33%), which is consistent with previous reports (Feng et al., 2001; Li et al., 2019). It could be that the ability of infected macrophages to engulf bacteria is compromised after the viral infection. Our observed mortality following infection with *S. suis* (58.3%) was comparable to that reported by Feng et al. (2001) (91%), who infected sows late in pregnancy to have PRRSV-infected piglets at birth, with bacterial challenge at 5 days-of-age. Any difference in mortality may stem from variation in piglet age and route of PRRSV or *S. suis* infection.

The results of the current study are similar to previous findings that piglets infected with HP-PRRSV or PRRSV develop ILN lesions (Rossow et al., 1995; Feng et al., 2001; Wang et al., 2014). Furthermore, we showed the impact of secondary *S. suis* infection on the ILN lesions induced by HP-PRRSV. In the acute infection period, the amount of lymphocyte depletion in all infected groups was very serious, however, after which the amount of lymphocyte in the single infection group including HP-PRRSV and *S. suis* infection alone was more recovery than in the dual-infection

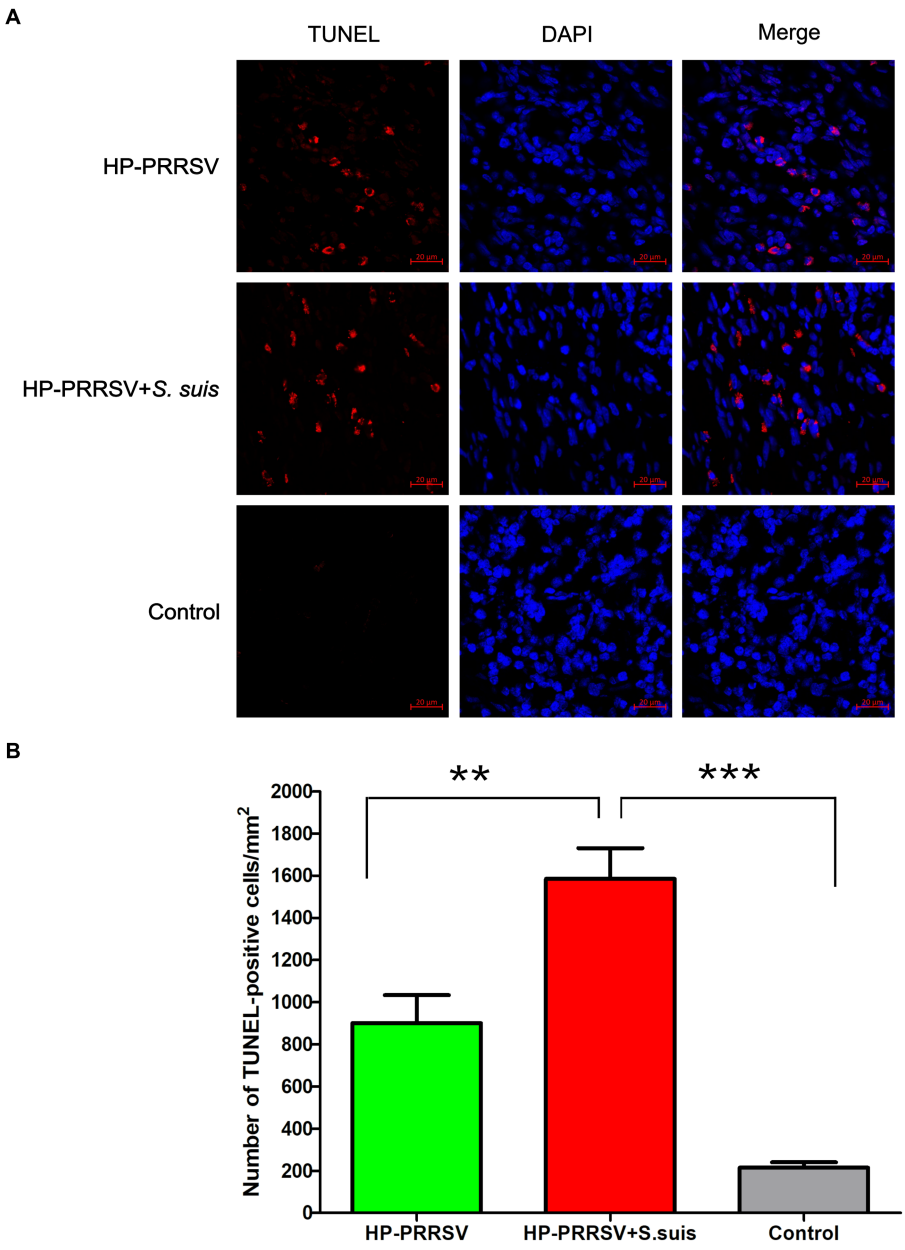

FIGURE 5
Identification of apoptotic cells in the inguinal lymph nodes of infected pigs. Sections of inguinal lymph node were prepared from piglets mock infected (Control) or infected by HP-PRRSV with or without *Streptococcus suis* dual-infection. **(A)** Apoptotic cells (TUNEL) were detected with the *In situ* Cell Death Detection Kit, and cell nuclei were stained with DAPI. **(B)** Number of apoptotic cells in ILNs from different groups of pigs. ***p* <0.01, ****p* <0.001.

group. The number of lymphocytes decreased from 14 to 21 dpi with almost no recovery in the dual-infection group. To sum up, *S. suis* contributes to lymphocyte depletion in the ILNs of piglets after HP-PRRSV infection.

HP-PRRSV HuN4 infection induced apoptosis in the ILNs of infected pigs that was enhanced by *S. suis* infection, which may be related to the lymphocyte depletion observed by histopathology. HP-PRRSV is a known immunosuppressive pathogen, reducing the number of lymphocytes in immune organs and in the peripheral blood. It is possible that HP-PRRSV-infected pigs could not clean bacteria in time in the case of lymphatic organs and macrophages damage when *S. suis* invaded, then the bacteria multiply inside the body. *S. suis* is also an immunosuppressive agent (Wang S. et al., 2020), which further destroys the host's immune organs, resulting in a more severe pathology in immune organs. Thus, our study helps to better understand the pathogenic mechanism of dual-infection commonly seen in the field.

Of the many ways to induce apoptosis (Ghobrial et al., 2005), we focused here on the caspase-3 mediated and the AIF-mediated p53 pathways, and our results revealed apoptosis mediated mainly by caspase-dependent pathways in all the infected piglets. This is the first report to identify which signaling pathway is related to

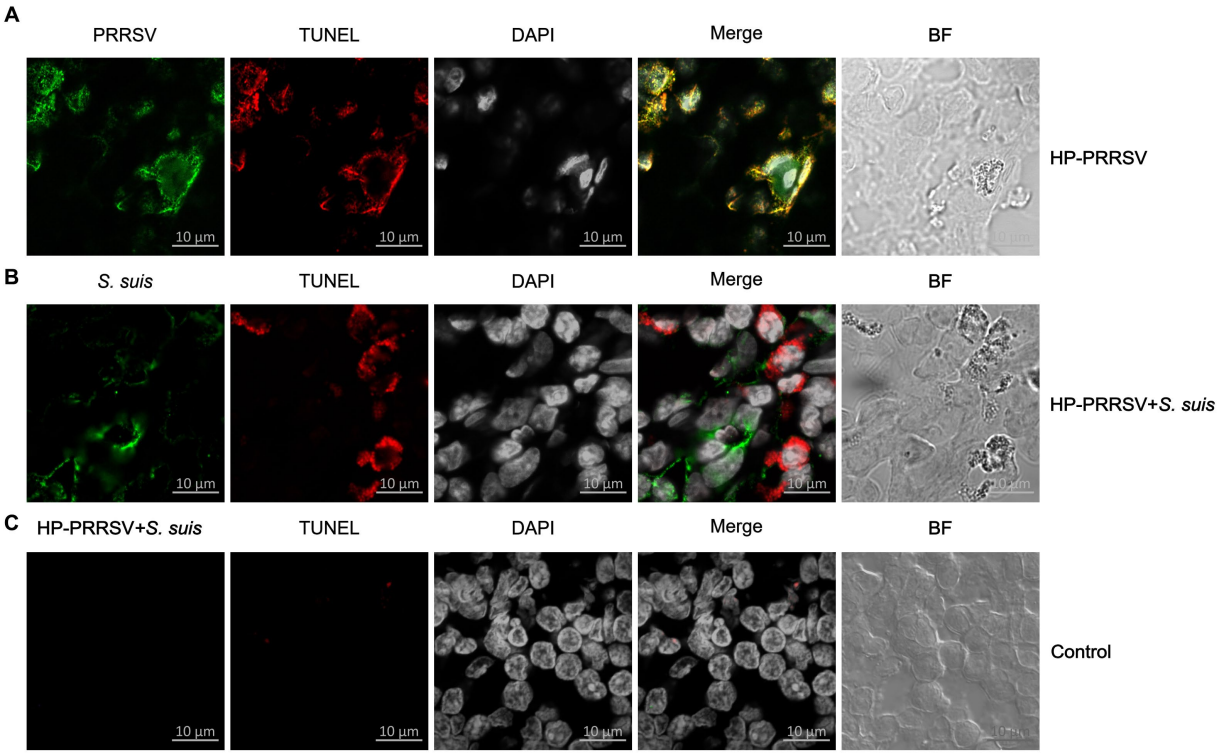

FIGURE 6
Colocalization of HP-PRRSV and *Streptococcus suis* in apoptotic inguinal lymph node cells. Sections of inguinal lymph node were prepared from piglets mock infected (Control) or infected by HP-PRRSV with or without *S. suis* dual-infection. Sections were incubated with antibodies against **(A)** HP-PRRSV N protein or **(B)** *S. suis* or **(C)** HP-PRRSV + *S. suis* and corresponding secondary antibodies. Apoptotic cells (TUNEL) were detected with the *In Situ* Cell Death Detection Kit, and cell nuclei were stained with DAPI. Bright field images are also included (BF).

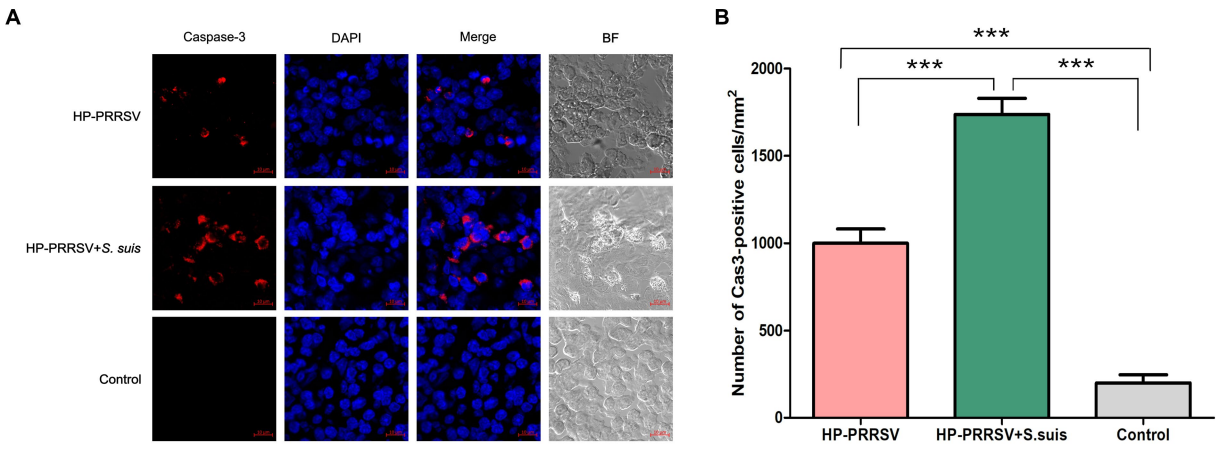

FIGURE 7
Porcine reproductive and respiratory syndrome virus (PRRSV) and *Streptococcus suis* induce caspase-dependent apoptosis in the inguinal lymph nodes of dual-infected piglets. Sections of inguinal lymph node were prepared from piglets mock infected (Control) or infected by HP-PRRSV with or without *S. suis* dual-infection. Cells were stained with **(A)** rabbit anti-mouse caspase-3 antibody and Alexa Fluor 568-conjugated goat anti-rabbit antibody. Nuclei were stained by DAPI; bright field images are also included (BF). **(B)** Number of caspase 3-positive cells in ILNs from different experimental groups. ***p <0.001, compared with control.

ILN apoptosis in single or dual-infected piglets. Moreover, the expression level of caspase-3 in the dual-infected piglets was significantly higher than in piglets infected with HP-PRRSV alone, indicating a synergy in the pathogenesis caused by *S. suis*. There are reports demonstrating that HP-PRRSV induces apoptosis in bystander cells in the thymus of infected piglets (Li et al., 2014). We found that the HP-PRRSV-infected cells underwent apoptosis, but we did not determine the type of cells (B/T cells or

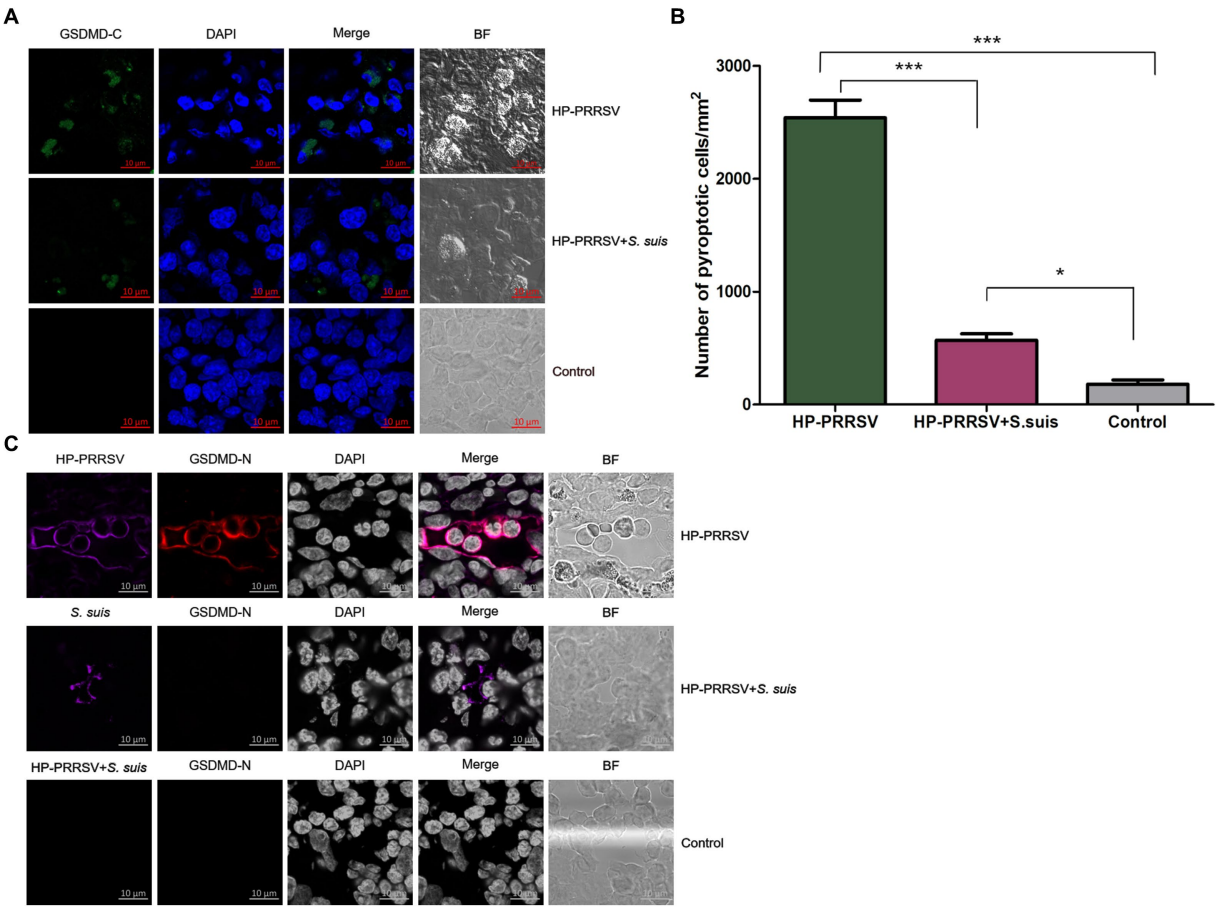

FIGURE 8
Characterization of pyroptosis in the inguinal lymph nodes of infected piglets. Sections of inguinal lymph node were prepared from piglets mock infected (Control) or infected by HP-PRRSV with or without *Streptococcus suis* dual-infection. Cells were stained with **(A)** rabbit anti-mouse GSDMD-C (green) antibody. **(B)** Number of pyroptotic cells in ILNs from different groups of pigs. **(C)** Cells were stained for mouse HP-PRRSV (purple) N protein mAb or *S. suis* (purple) mouse antibody and rabbit anti-mouse GSDMD-N (red). Nuclei were stained by DAPI; bright field images are also included (BF). *$p<0.05$, ***$p<0.001$.

macrophages) that were infected in the ILNs, which warrants further investigation.

Pyroptosis is an important mechanism contributing to pathogens clearance and antimicrobial immunity (Rathinam et al., 2019). Here, we report for the first time that PRRSV HuN4 induces pyroptosis in the ILNs of infected piglets, with fewer pyroptotic cells observed in dual-infected piglets. The levels of proinflammatory cytokines (e.g., IL-1β) in the serum were higher for pigs infected with PRRSV alone compared to pigs coinfected with virus and bacteria (Brockmeier et al., 2017), which is consistent with our results. As we all know, a large number of proinflammatory cytokines are released after pyroptosis. The HP-PRRSV infection group had high levels of proinflammatory cytokines due to the high number of pyroptosis, which warrants verification again in our future coinfection experiments. We theorize that the greater degree of damage to the immune organs observed during dual-infection diminished the host's ability to clear pathogens and mount an aggressive immune response, and the increased lesions may prevent the cells from mounting a pyroptotic signaling pathway. As a result, the clinical symptoms (cyanotic limbs and ears), gross lesions (interstitial pneumonia, swelling and hemorrhage in ILNs) and microscopic lesions (apoptosis) were more severe in dual-infected piglets than in those infected by HP-PRRSV alone.

Conclusion

Our results give mechanistic insights into how secondary *S. suis* infection after HP-PRRSV infection can aggravate disease development in affected piglets. We found more caspase-dependent apoptosis in the dual-infected group than in piglets infected with PRRSV alone. The increase in pyroptosis in piglets infected by PRRSV alone shows a clear impact of secondary bacterial infections on pathogen clearance and antimicrobial immunity.

Data availability statement

The original contributions presented in the study are included in the article/Supplementary material, further inquiries can be directed to the corresponding authors.

Ethics statement

The animal study was reviewed and approved by the Committee on the Ethics of Animal Experiments of the Harbin Veterinary Research Institute of the Chinese Academy of Agricultural Sciences (CAAS), China.

Author contributions

SW, MX, TA, and XC conceived the study and designed the experimental procedures. SW, MX, SL, and Y-DT performed the experiments. SW, KY, YZ, and JW analyzed the data. KY, YZ, JW, CL, and XC contributed the reagents and materials. SW, TA, Y-DT, and XC wrote the manuscript. All authors contributed to the article and approved the submitted version.

Funding

This work was supported by the National Key Research and Development Program of China (2022YFD1800304), National Natural Science Foundation of China (32273018), Central Public-interest Scientific Institution Basal Research Fund (No. 1610302022006), and the Key Program Foundation of Higher Education of Educational Commission of Henan Province (22A230016).

Conflict of interest

MX was employed by the company Sinopharm Animal Health Corporation Ltd., Wuhan, China.

The remaining authors declare that the research was conducted in the absence of any commercial or financial relationships that could be construed as a potential conflict of interest.

Publisher's note

References

Brockmeier, S. L., Loving, C. L., Palmer, M. V., Spear, A., Nicholson, T. L., Faaberg, K. S., et al. (2017). Comparison of Asian porcine high fever disease isolates of porcine reproductive and respiratory syndrome virus to United States isolates for their ability to cause disease and secondary bacterial infection in swine. *Vet. Microbiol.* 203, 6–17. doi: 10.1016/j.vetmic.2017.02.003

Chen, Y., He, S., Sun, L., Luo, Y., Sun, Y., Xie, J., et al. (2016). Genetic variation, pathogenicity, and immunogenicity of highly pathogenic porcine reproductive and respiratory syndrome virus strain XH-GD at different passage levels. *Arch. Virol.* 161, 77–86. doi: 10.1007/s00705-015-2597-6

Costers, S., Lefebvre, D. J., Delputte, P. L., and Nauwynck, H. J. (2008). Porcine reproductive and respiratory syndrome virus modulates apoptosis during replication in alveolar macrophages. *Arch. Virol.* 153, 1453–1465. doi: 10.1007/s00705-008-0135-5

Ding, L., Li, J., Li, W., Fang, Z., Li, N., Wu, S., et al. (2018). p53- and ROS-mediated AIF pathway involved in TGEV-induced apoptosis. *J. Vet. Med. Sci.* 80, 1775–1781. doi: 10.1292/jvms.18-0104

Do, T. D., Park, C., Choi, K., Jeong, J., Vo, M. K., Nguyen, T. T., et al. (2015). Comparison of pathogenicity of highly pathogenic porcine reproductive and respiratory syndrome virus between wild and domestic pigs. *Vet. Res. Commun.* 39, 79–85. doi: 10.1007/s11259-015-9628-3

Dokland, T. (2010). The structural biology of PRRSV. *Virus Res.* 154, 86–97. doi: 10.1016/j.virusres.2010.07.029

Fan, B., Liu, X., Bai, J., Li, Y., Zhang, Q., and Jiang, P. (2015). The 15N and 46R residues of highly pathogenic porcine reproductive and respiratory syndrome virus Nucleocapsid protein enhance regulatory T lymphocytes proliferation. *PLoS One* 10:e0138772. doi: 10.1371/journal.pone.0138772

Feng, W., Laster, S. M., Tompkins, M., Brown, T., Xu, J. S., Altier, C., et al. (2001). In utero infection by porcine reproductive and respiratory syndrome virus is sufficient to increase susceptibility of piglets to challenge by *Streptococcus suis* type II. *J. Virol.* 75, 4889–4895. doi: 10.1128/JVI.75.10.4889-4895.2001

Firth, A. E., Zevenhoven-Dobbe, J. C., Wills, N. M., Go, Y. Y., Balasuriya, U. B. R., Atkins, J. F., et al. (2011). Discovery of a small arterivirus gene that overlaps the GP5 coding sequence and is important for virus production. *J. Gen. Virol.* 92, 1097–1106. doi: 10.1099/vir.0.029264-0

Galina, L., Pijoan, C., Sitjar, M., Christianson, W. T., Rossow, K., and Collins, J. E. (1994). Interaction between *Streptococcus suis* serotype 2 and porcine reproductive and respiratory syndrome virus in specific pathogen-free piglets. *Vet. Rec.* 134, 60–64. doi: 10.1136/vr.134.3.60

Ghobrial, I. M., Witzig, T. E., and Adjei, A. A. (2005). Targeting apoptosis pathways in cancer therapy. *CA Cancer J. Clin.* 55, 178–194. doi: 10.3322/canjclin.55.3.178

Hu, S. P., Zhang, Z., Liu, Y. G., Tian, Z. J., Wu, D. L., Cai, X. H., et al. (2013). Pathogenicity and distribution of highly pathogenic porcine reproductive and respiratory syndrome virus in pigs. *Transbound. Emerg. Dis.* 60, 351–359. doi: 10.1111/j.1865-1682.2012.01354.x

Jiang, Y., Li, G., Yu, L., Li, L., Zhang, Y., Zhou, Y., et al. (2020). Genetic diversity of porcine reproductive and respiratory syndrome virus (PRRSV) from 1996 to 2017 in China. *Front. Microbiol.* 11:618. doi: 10.3389/fmicb.2020.00618

Johnson, W., Roof, M., Vaughn, E., Christopher-Hennings, J., Johnson, C. R., and Murtaugh, M. P. (2004). Pathogenic and humoral immune responses to porcine reproductive and respiratory syndrome virus (PRRSV) are related to viral load in acute infection. *Vet. Immunol. Immunopathol.* 102, 233–247. doi: 10.1016/j.vetimm.2004.09.010

Jung, K., Renukaradhya, G. J., Alekseev, K. P., Fang, Y., Tang, Y., and Saif, L. J. (2009). Porcine reproductive and respiratory syndrome virus modifies innate immunity and alters disease outcome in pigs subsequently infected with porcine respiratory coronavirus: implications for respiratory viral co-infections. *J. Gen. Virol.* 90, 2713–2723. doi: 10.1099/vir.0.014001-0

Li, Y., Wang, X., Bo, K., Wang, X., Tang, B., Yang, B., et al. (2007). Emergence of a highly pathogenic porcine reproductive and respiratory syndrome virus in the mid-eastern region of China. *Vet. J.* 174, 577–584. doi: 10.1016/j.tvjl.2007.07.032

Li, Y., Wang, G., Liu, Y., Tu, Y., He, Y., Wang, Z., et al. (2014). Identification of apoptotic cells in the thymus of piglets infected with highly pathogenic porcine reproductive and respiratory syndrome virus. *Virus Res.* 189, 29–33. doi: 10.1016/j.virusres.2014.04.011

Li, J., Wang, J., Liu, Y., Yang, J., Guo, L., Ren, S., et al. (2019). Porcine reproductive and respiratory syndrome virus NADC30-like strain accelerates *Streptococcus suis* serotype 2 infection in vivo and in vitro. *Transbound. Emerg. Dis.* 66, 729–742. doi: 10.1111/tbed.13072

Lunney, J. K., Fang, Y., Ladinig, A., Chen, N., Li, Y., Rowland, B., et al. (2016). Porcine reproductive and respiratory syndrome virus (PRRSV): pathogenesis and interaction with the immune system. *Annu. Rev. Anim. Biosci.* 4, 129–154. doi: 10.1146/annurev-animal-022114-111025

Ma, Z., Yang, L., and Zhang, Y. J. (2018). Porcine reproductive and respiratory syndrome virus: propagation and quantification. *Curr. Protoc. Microbiol.* 48, 15m.1.1–15m.1.14. doi: 10.1002/cpmc.51

Rathinam, V. A. K., Zhao, Y., and Shao, F. (2019). Innate immunity to intracellular LPS. *Nat. Immunol.* 20, 527–533. doi: 10.1038/s41590-019-0368-3

Rossow, K. D. (1998). Porcine reproductive and respiratory syndrome. *Vet. Pathol.* 35, 1–20. doi: 10.1177/030098589803500101

Rossow, K. D., Collins, J. E., Goyal, S. M., Nelson, E. A., Christopher-Hennings, J., and Benfield, D. A. (1995). Pathogenesis of porcine reproductive and respiratory syndrome virus infection in gnotobiotic pigs. *Vet. Pathol.* 32, 361–373. doi: 10.1177/030098589503200404

Sang, Y., Rowland, R. R., and Blecha, F. (2011). Interaction between innate immunity and porcine reproductive and respiratory syndrome virus. *Anim. Health Res. Rev.* 12, 149–167. doi: 10.1017/S1466252311000144

Sever, A. R., Mills, P., Hyvelin, J. M., Weeks, J., Gumus, H., Fish, D., et al. (2012). Percutaneous removal of sentinel lymph nodes in a swine model using a breast lesion excision system and contrast-enhanced ultrasound. *Eur. Radiol.* 22, 545–550. doi: 10.1007/s00330-011-2293-1

Shi, J., Gao, W., and Shao, F. (2017). Pyroptosis: Gasdermin-mediated programmed necrotic cell death. *Trends Biochem. Sci.* 42, 245–254. doi: 10.1016/j.tibs.2016.10.004

Shi, P., Su, Y., Li, Y., Zhang, L., Lu, D., Li, R., et al. (2019). The alternatively spliced porcine FcγRI regulated PRRSV-ADE infection and proinflammatory cytokine production. *Dev. Comp. Immunol.* 90, 186–198. doi: 10.1016/j.dci.2018.09.019

Shi, P., Zhang, L., Wang, J., Lu, D., Li, Y., Ren, J., et al. (2018). Porcine FcεRI mediates porcine reproductive and respiratory syndrome virus multiplication and regulates the inflammatory reaction. *Virol. Sin.* 33, 249–260. doi: 10.1007/s12250-018-0032-3

Sun, Y. F., Jiang, X., Zhang, A., Ma, J. F., Yu, X. X., Li, L. A., et al. (2020). Early infection of *Streptococcus suis* serotype 2 increases the virulence of highly pathogenic porcine reproductive and respiratory syndrome MLV-like virus in pigs. *Res. Vet. Sci.* 130, 68–72. doi: 10.1016/j.rvsc.2020.02.010

Sun, W., Wu, W., Jiang, N., Ge, X., Zhang, Y., Han, J., et al. (2022). Highly pathogenic PRRSV-infected alveolar macrophages impair the function of pulmonary microvascular endothelial cells. *Viruses* 14, 1–19. doi: 10.3390/v14030452

Thanawongnuwech, R., Brown, G. B., Halbur, P. G., Roth, J. A., Royer, R. L., and Thacker, B. J. (2000). Pathogenesis of porcine reproductive and respiratory syndrome virus-induced increase in susceptibility to *Streptococcus suis* infection. *Vet. Pathol.* 37, 143–152. doi: 10.1354/vp.37-2-143

Van Reeth, K. (1997). Pathogenesis and clinical aspects of a respiratory porcine reproductive and respiratory syndrome virus infection. *Vet. Microbiol.* 55, 223–230. doi: 10.1016/S0378-1135(96)01331-4

Wang, G., He, Y., Tu, Y., Liu, Y., Zhou, E. M., Han, Z., et al. (2014). Comparative analysis of apoptotic changes in peripheral immune organs and lungs following experimental infection of piglets with highly pathogenic and classical porcine reproductive and respiratory syndrome virus. *Virol. J.* 11:2. doi: 10.1186/1743-422X-11-2

Wang, Y., Kang, W., Yang, W., Zhang, J., Li, D., and Zheng, H. (2021). Structure of African swine fever virus and associated molecular mechanisms underlying infection and immunosuppression: a review. *Front. Immunol.* 12:715582. doi: 10.3389/fimmu.2021.715582

Wang, S., Lyu, C., Duan, G., Meng, F., Yang, Y., Yu, Y., et al. (2020). *Streptococcus suis* serotype 2 infection causes host immunomodulation through induction of Thymic atrophy. *Infect. Immun.* 88, 1–15. doi: 10.1128/IAI.00950-19

Wang, R., Wang, X., Ni, B., Huan, C. C., Wu, J. Q., Wen, L. B., et al. (2016). Syndecan-4, a PRRSV attachment factor, mediates PRRSV entry through its interaction with EGFR. *Biochem. Biophys. Res. Commun.* 475, 230–237. doi: 10.1016/j.bbrc.2016.05.084

Wang, S., Wang, G., Tang, Y. D., Li, S., Qin, L., Wang, M., et al. (2022). *Streptococcus suis* serotype 2 infection induces splenomegaly with Splenocyte apoptosis. *Microbiol. Spectr.* 10:e0321022. doi: 10.1128/spectrum.03210-22

Wang, G., Yu, Y., Cai, X., Zhou, E. M., and Zimmerman, J. J. (2020). Effects of PRRSV infection on the porcine Thymus. *Trends Microbiol.* 28, 212–223. doi: 10.1016/j.tim.2019.10.009

Wang, G., Yu, Y., Tu, Y., Tong, J., Liu, Y., Zhang, C., et al. (2015). Highly pathogenic porcine reproductive and respiratory syndrome virus infection induced apoptosis and autophagy in Thymi of infected piglets. *PLoS One* 10:e0128292. doi: 10.1371/journal.pone.0128292

Zhou, X., Ge, X., Zhang, Y., Han, J., Guo, X., Chen, Y., et al. (2021). Attenuation of porcine deltacoronavirus disease severity by porcine reproductive and respiratory syndrome virus coinfection in a weaning pig model. *Virulence* 12, 1011–1021. doi: 10.1080/21505594.2021.1908742

frontiers | Frontiers in Microbiology

TYPE Review
PUBLISHED 27 April 2023
DOI 10.3389/fmicb.2023.1139494

OPEN ACCESS

EDITED BY
Haili Zhang,
Jilin University, China

REVIEWED BY
Lauro Velazquez-Salinas,
Agricultural Research Service (USDA),
United States
Giulia Franzoni,
Experimental Zooprophylactic Institute of
Sardinia (IZS), Italy

*CORRESPONDENCE
Hu Shan
✉ shanhu67@163.com
Xiulei Cai
✉ xlcai_99@163.com

†These authors have contributed equally to this work and share first authorship

RECEIVED 07 January 2023
ACCEPTED 05 April 2023
PUBLISHED 27 April 2023

CITATION
Zhang H, Zhao S, Zhang H, Qin Z, Shan H and Cai X (2023) Vaccines for African swine fever: an update.
Front. Microbiol. 14:1139494.
doi: 10.3389/fmicb.2023.1139494

Vaccines for African swine fever: an update

Hongliang Zhang[1†], Saisai Zhao[1,2†], Haojie Zhang[1], Zhihua Qin[1], Hu Shan[1*] and Xiulei Cai[1*]

[1]Shandong Collaborative Innovation Center for Development of Veterinary Pharmaceuticals, College of Veterinary Medicine, Qingdao Agricultural University, Qingdao, China, [2]College of Animal Science and Technology, Shandong Agricultural University, Tai'an, China

African swine fever (ASF) is a fatal infectious disease of swine caused by the African swine fever virus (ASFV). Currently, the disease is listed as a legally notifiable disease that must be reported to the World Organization for Animal Health (WOAH). The economic losses to the global pig industry have been insurmountable since the outbreak of ASF. Control and eradication of ASF are very critical during the current pandemic. Vaccination is the optimal strategy to prevent and control the ASF epidemic, but since inactivated ASFV vaccines have poor immune protection and there aren't enough cell lines for efficient *in vitro* ASFV replication, an ASF vaccine with high immunoprotective potential still remains to be explored. Knowledge of the course of disease evolution, the way of virus transmission, and the breakthrough point of vaccine design will facilitate the development of an ASF vaccine. In this review, the paper aims to highlight the recent advances and breakthroughs in the epidemic and transmission of ASF, virus mutation, and the development of vaccines in recent years, focusing on future directions and trends.

KEYWORDS

African swine fever virus, epidemic and spread, vaccine, progress, review

1. Introduction

African swine fever (ASF) is a highly contagious swine disease caused by the African swine fever virus (ASFV), in which the only natural host is swine (Wang et al., 2019). It is also the only large double-stranded DNA virus that infects domestic swine, wild boar, and blunt-edge ticks (Dixon et al., 2019). The virus has an icosahedral symmetry with a diameter of 200 nm and a concentric circle (Rowlands et al., 2009). Further, the ASFV genome contains a variable number of open reading frames (ORFs), ranging from 160 to 175, with approximately 125 conserved ORFs encoding more than 50 functional proteins (Sánchez-Vizcaíno et al., 2015a; Simões et al., 2019). The clinical symptoms of ASF are classified as acute, subacute, and chronic. Acute ASF has a rapid onset and short duration and is characterized by high fever, loss of appetite, cyanosis, severe internal bleeding, and a nearly 100% mortality rate (Pietschmann et al., 2015; Gaudreault et al., 2020), while less virulent strains cause milder clinical symptoms. ASF originated in Africa in the 1920s, and the disease spread to the Caucasus region of Georgia in 2007. From there, ASFV gradually spread to neighboring countries (i.e., Armenia, Azerbaijan, Russia, and Belarus), affecting both domestic and wild swine (Rowlands et al., 2008; Costard et al., 2009). Since August 2018, it has been detected in China as a genotype II highly virulent strain (Ge et al., 2018; Wen et al., 2019; Zhao et al., 2019). More than 40 outbreaks have occurred successively in the northeastern regions of Liaoning, Inner Mongolia, and Heilongjiang, causing unprecedented losses to the pig farming industry in China and seriously affecting national production and diet

structure. Significant steps have been taken in recent years to curb the virus spread with the economy and international trade continued growth. Knowing the worldwide situation, prevalence, and transmission routes of ASFV is crucial for preventing the outbreak of diseases.

Genotype I was also known as the ESAC-WA genotype after 1957 when it was colonized in Europe, South America, and the Caribbean. By 2007, all countries (except Italy and Africa) had declared the eradication of ASF. Since the outbreak of ASFV genotype II in 2007, the world has been against ASF again, including Russia (2007), Ukraine (2012), Poland (2014), Belgium (2018), China (2018), Vietnam (2019), India (2020), and many other countries. Besides the wide range of transmissions, transmission routes are also very diverse. ASF is a viral disease transmitted via contact with infected swine and feces, either direct or indirect contact. Biological vectors such as ticks also accelerate the virus's spread. Mechanical agents such as vehicles, tools, and human activities, as well as pig processing products, are also causative factors. Biological control is currently the most direct and efficient method of preventing ASF, which is superior to a vaccine.

The inactivated vaccines that are ineffective against ASF have been proven. Surprisingly, one of the attenuated live vaccines, ASFV-G-ΔI177L in Vietnam, is the first commercial ASF vaccine in the world (Tran et al., 2022a). However, live attenuated vaccine development is characterized by high costs, long cycles, and instability, which limit their rapid development. Researchers are currently focusing on genetically engineered vaccines such as subunit vaccines, vector vaccines, and DNA vaccines, while most experiments were limited to immunogenicity and did not carry out challenge experiments. Thus, developing a safe and effective ASFV vaccine is one of the top priorities against the virus. This review of the ASFV vaccine highlights the recent advances' strengths and weaknesses and provides new research directions for promising progress.

2. Global scenario and prevalence of ASF

ASF is native to Africa, which maintains the virus by an ancient sylvatic cycle involving the natural hosts and vectors of the disease as well as domestic cycles with or without the involvement of natural vectors (Mulumba-Mfumu et al., 2019), has been recently reported in 32 countries since 2005. In Sardinia, there is genotype I, which is still endemic (Franzoni et al., 2020), whereas genotype II outbreaks occurred in Georgia in 2007, and from there, ASFV genotype II spread to neighboring countries, including Armenia, Azerbaijan, Russia, and Belarus, where it infected domestic swine and wild boar with a highly virulent strain of ASFV (Karger et al., 2019). A total of 9 countries in the continental European Union, such as Estonia, Lithuania, Latvia, Poland, the Czech Republic, Bulgaria, Belgium, Romania, and Hungary, have been severely affected by ASF from 2014 to 2018, and it persistently maintains spreading despite the efforts to control it. It caused high case-fatality rates in wild boar typical of the acute and subacute forms of the infection, particularly in newly infected areas (Martínez-Avilés et al., 2020). In just 2 years, from 2020 to 2022, a total of 16 EU countries reported the disease. Significantly, ASF was successfully eradicated from Belgium (March 2020) and the Czech Republic (April 2018; Baños et al., 2022). In August 2018, ASF was first proven in China (Liu Y. et al., 2021), and it quickly continued to spread to 31 provinces within a few months, resulting in a total of 178 ASF outbreaks. In 2019/2020, the disease spread to Oceania, with ASF reported in Timor-Leste, resulting in high mortalities in affected animals of small-scale pig farming (Berends et al., 2021; Phillips et al., 2021) and Papua New Guinea (Mighell and Ward, 2021). In early 2020, the first occurrence of ASF with high mortality in domestic swine in India (Arunachal Pradesh and Assam) was described, which is similar with the post-2007-p72-genotype II viruses reported from Asia and Europe, indicating the transboundary infection tendency of ASF outbreaks in the region (Rajukumar et al., 2021). In July 2021, ASF reappeared in the Americas after nearly 40 years of absence, first in the Dominican Republic and then in Haiti, with threats to animal health, livestock markets, and producer livelihoods (Jean-Pierre et al., 2022). Similarly, in January 2022, the Italian continent also notified the occurrence of ASFV genotype II after an absence of about 40 years (Beato et al., 2022; Iscaro et al., 2022). Meanwhile, two new countries have been affected: one of two in North Macedonia, caused by farms that were predominantly small-scale with high rates of turnover and the highest frequency of wild boar sightings (O'Hara et al., 2021), and the other of two in Thailand, caused by infected live and dead pigs, pork products, and wild boar semen, contaminated feed, and fomites (Thanapongtharm et al., 2022). The first reported ASF occurrence in Nepal was in March 2022, although the government had already banned the import of pigs and pork products from countries infected with ASFV on January 28, 2019 (Acharya and Wilson, 2020; Figure 1).

As shown in Table 1, since January 2020, ASF has been reported in five different regions involving 45 countries, affecting over 1,129,000 swine and 36,000 feral wild boars, with more than 1,931,000 animal losses (data from Immediate notifications and follow-up reports). The global outbreak of ASF has led to a sharp decline in the global swine production capacity, and the pig industry has been devastated. Due to the insidious and complex nature of ASFV infection, the current epidemic is still unclear. It is prospective that it will be difficult to recover to the previous level in 3–5 years.

3. Transmission routes of ASFV

The ASFV of a wide range of transmission routes, including direct and indirect transmission, complicates ASF prevention and control (Figure 2). Wild boars and ticks are the natural hosts of ASFV and play a pivotal role in the spread via the forest cycle (Sánchez-Vizcaíno et al., 2015a; Śmietanka et al., 2016; Galindo and Alonso, 2017). The presence of an omnipresent herd of wild boar poses a significant barrier to the control and eradication of ASF in areas where it occurs. Sick and dead wild boars were the dominant source of the virus in Europe, which is susceptible to different ASFV genotypes, especially genotype II isolates (Blome et al., 2012), and they are vital vectors as direct or indirect carriers of the disease (Probst et al., 2017). Previous research has hinted that the virus can be transmitted by the wild-domestic swine route, which exacerbates infection in both swine and wild boars and between same-breed populations (Costard et al., 2013). In the domestic cycle, domestic swine are the sole hosts and carriers of the virus, which remains permanently infected, including swine' feces and secretions (Guinat et al., 2016). Indeed, other animals that could also become virus

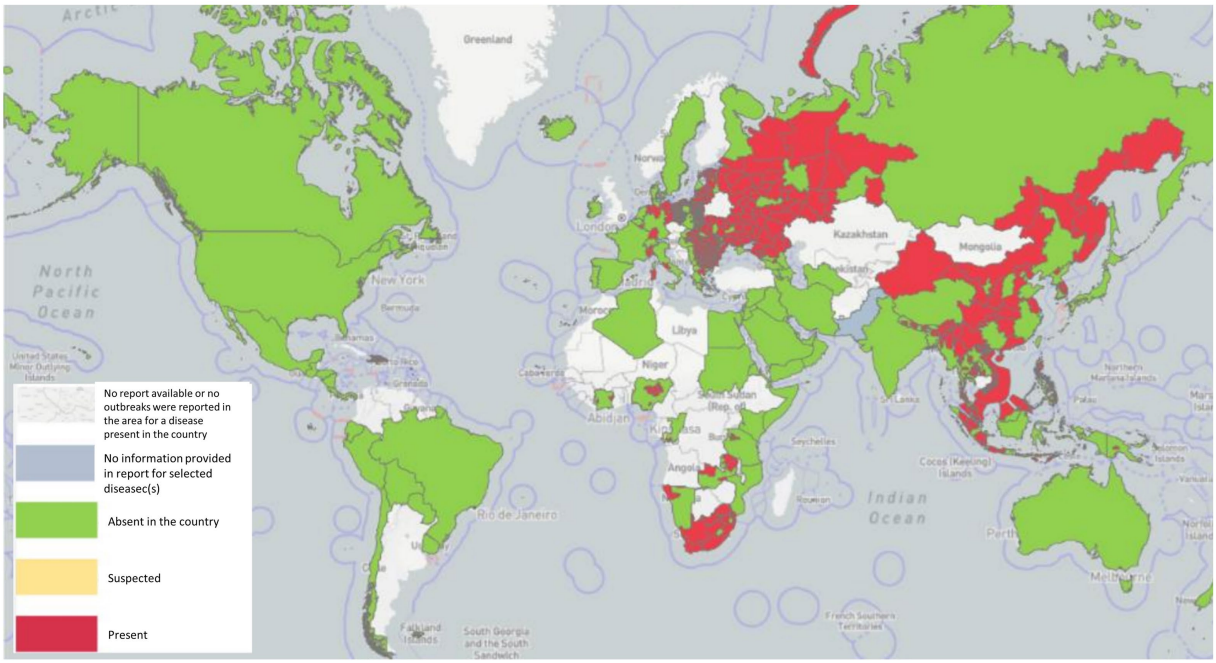

FIGURE 1
ASF has been reported in 45 countries globally since 2020 as of 29 September 2022 (Source: World Organization for Animal Health, World Health Organization, October 2022 line visit).

TABLE 1 Number of outbreaks, cases, and animal losses caused by ASF in different regions worldwide (2020, 01–2022, 09; Source: World Organization for Animal Health, World Health Organization, October 2022 line visit).

	Outbreaks		Cases		Losses*
	Domestic swine	Wild boar	Domestic swine	Wild boar	Domestic swine
Africa	201		16,177		23,208
Americas	255		9,594		17,798
Asia	1,298	2,105	101,482	2,765	438,492
Europe	3,703	20,518	1,001,921	34,159	1,452,045
Oceania	4		500		397
Total	5,461	22,623	1,129,674	36,924	1,931,930

*Loss (number of deaths + animals killed and disposed of): this figure refers to the loss of farms affected by the outbreak and does not include animals culled in the outbreak area to control the disease.

carriers through mechanical transmission over long distances have been reported in several studies, such as flies, leeches, and birds, including vultures (Brown and Bevins, 2018; Olesen et al., 2018; Karalyan et al., 2019; Bonnet et al., 2020).

In addition, human activities facilitated the influx of the virus into swine farms, exacerbating the extent of virus transmission. An important route for the spread of ASFV is through the illegal transportation of infected pork products and contaminated items, including feed, equipment, vehicles, and clothing (Costard et al., 2013). Other critical factors of epidemiology, including the transport of contaminated pork products and the feeding of swilling, have caused outbreaks of ASF in the Caucasus, the Russian Federation, and China (Gogin et al., 2013). The inherent properties of ASFV are highly resistant to a wide variety of environmental conditions such as temperature, pH, and so on, resulting in the virus positively existing in the environment and sustaining to spread to distant areas (Davies et al., 2017; Schulz et al., 2017; Mazur-Panasiuk et al., 2019; Petrini et al., 2019; Zani et al., 2020). Interestingly, several studies have proven that ASFV can survive in animal feed on transatlantic routes under specific conditions (Dee et al., 2019; Stoian et al., 2019). Moreover, though frozen meat and processed pork products contaminated with the virus are not causing human infection, they may be a potential factor for virus transmission to new regions after long-distance transport due to the long-term survival of the virus (Schulz et al., 2017).

4. Genetic variability of ASFV

The study of the genetic evolution of the ASFV genome has entered a new phase following the sustainable development of ASFV typing techniques. Up until now, ASFV has been classified into 24

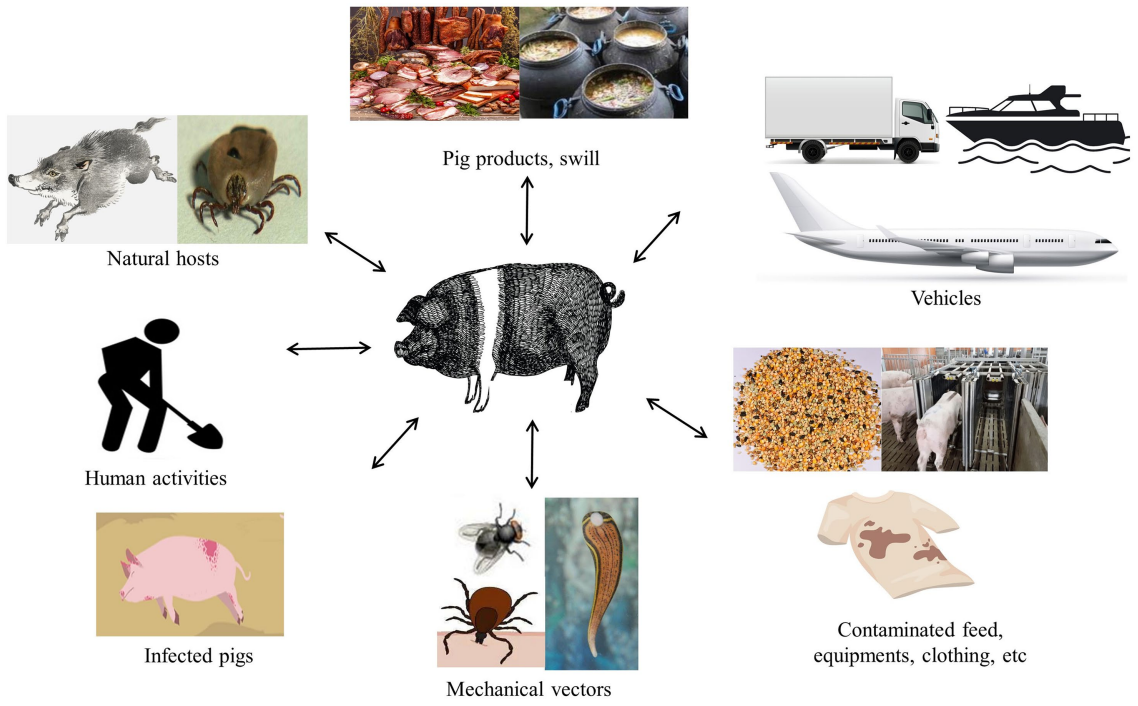

FIGURE 2
Potential ASFV routes of transmission to swine.

genotypes (Achenbach et al., 2017) or 8 serogroups (Malogolovkin et al., 2015). The depth of research on ASFV genotyping can facilitate tracing the origin of the virus causing the outbreak at the molecular level, understanding the potential transmission routes and possible modes of transmission, and screening potential vaccine candidates.

The ASFV genome is a linear double-stranded DNA, including left variable regions (LVR), a central conserved region (C region), and a right variable region (RVR; Van Etten, 2009). The genomic sequences of different strains may differ significantly in locations, for instance, the multigene family (MGF) within the LVR, the central variable region (CVR), and the EP402R gene (expressing the CD2v protein) within the C region. The various regions provide an advantageous condition for the evolutionary analysis of ASFV, especially for genetic evolution.

4.1. Genotype I strain of ASFV

Genotype I virus was first found and caused an outbreak in Portugal outside Africa in 1957 (Revilla et al., 2018). Since then it was prevalent in Portugal, Spain, Cuba, Brazil, and other countries during the 1950s to 1990s (Sánchez-Vizcaíno et al., 2015b; Galindo and Alonso, 2017). As the first case reported in the Asian region, the genotype I strain was first detected in clinical samples in China in 2021 (Sun et al., 2021). Currently, genotype I virus is still dominating in some West African countries, while no outbreak was reported in North Africa (Mulumba-Mfumu et al., 2019). In Central Africa, genotypes I and II are predominating at the same time. The specific strain information of ASFV is shown in Table 2.

Portugal et al. sequenced the genomes of the high-virulence strain Lisboa60 (L60) and the low-virulence strain NH/P68 (NHV) of ASFV, comparing the differential fraction with other strains of known virulence. The analysis showed that L60 and NHV are most recently related to p72 genotype I ASFV strains from Europe and West Africa, supporting the hypothesis that the European strains originated in West Africa. Due to the long interval and geographical distance between L60 and NHV, hinting that this is due to the extensive spread of the Portuguese isolate in tissue culture (Portugal et al., 2015). The team compared gene sequences between the high-virulence Lisboa60 (L60) and the low-virulence NH/P68 (NHV) of ASFV to overcome the restrictions of virus-host interaction research, uncovering further understanding of the virus evolution (Portugal et al., 2020).

Since the introduction of genotype II ASFV in Georgia in 2007, the world has been drifting into a war against the genotype II epidemic. The ASFV genotype I strain, which differs vastly from the currently prevalent genotype II strain. Two strains of ASFV genotype I SD/DY-I/21 and HeN/ZZ-P1/21 without porcine erythrocyte adsorption activity were isolated from clinical samples of pigs in Shandong and Henan farms. Whole-genome analyses exhibited that these two strains were highly similar to the genotype I low-lethal strains NH/P68 and OURT88/3 isolated in Portugal in the 20th century and differed significantly from the genotype I high-virulent strains L60 and Benin 97 isolated in Europe and Africa in the early years. The SD/DY-I/21 and HeN/ZZ-P1/21 strains have meaningful differences in some genes despite high genome-wide sequence similarity, suggesting the possibility that they belong to different invasive sources (Sun et al., 2021). The co-existence of genotype I and genotype II strains in China emphasized that the current prevention and control situation has become more severe, accelerating the development of vaccines.

TABLE 2 The specific strain information of ASFV (Source: National Center for Biotechnology Information. https://www.ncbi.nlm.nih.gov/).

Time	Country	Strain	Genbank	Gene length (bp)	Isolate gene
1957	Portugal	Lisbon 57	AF301537	415	VP72
1960	Portugal	Lisbon 60	AF301539	415	VP72
1962	Spain Espana	Madrid/62	AF449461	404	VP72
1964	France	Fr64	FJ174374	404	B646L
1968	Portugal	NH/P68	DQ028313	536	B646L
1979	Brazil	Brazil/79	AF302809	415	VP72
1979	Caribbean	DomRep/79	AF301810	392	MK4s2209
1985	Belgium	BEL/85	AF449466	404	VP72
1988	Portugal	OUR T88/3	AM712240	171,719	Complete

4.2. Genotype II strain of ASFV

The ASFV genomic study has made satisfactory progress since the rapid development of gene cloning, PCR, and sequencing technologies. p72 genotyping is the gold standard that is now widely used for ASFV genotyping. Gonzague et al. confirmed that the ASFV Malagasy strain isolated in 1999 was 99.2% related to the Mozambique strain isolated in 1994 with a highly conserved fragment of the p72 gene (Gonzague et al., 2001). In 2003, Bastos et al. first used the C-terminal end of the p72 protein to classify ASFV into 10 genotypes (Bastos et al., 2003). In 2005, Lubisi et al. further classified ASFV into 16 genotypes (Lubisi et al., 2005). In 2007, Boshoff et al. conducted a study of 43 strains of ASFV (1973–1999) isolates from South Africa (Boshoff et al., 2007). In 2016, Achenbach et al. conducted a comparative analysis of ASFV isolated in Ethiopia (2011–2014) and again identified one genotype (Achenbach et al., 2017). In 2017, Quembo et al. analyzed ASFV with 19 isolated strains from soft tick samples collected in Gorongosa National Forest Park, Mozambique. An evolutionary tree-specific analysis revealed that five strains belonged to a new evolutionary branch (Quembo et al., 2018). Thus, a total of 24 genotypes of ASFV were completely identified.

To improve our understanding of the evolutionary trends of similar strains, Gallardo et al. found that the whole ASFV genome has different combinations of tandem repeat sequences (TRS) in the intergenic region (IGR) of the I73R and I329L genes. For example, the IGR of the Polish and Lithuanian ASFV isolates was the same as that of the Belarusian and Ukrainian isolates but different from that of the Russian isolates, suggesting that the prevalent strains of ASFV in Poland and Lithuania may have originated in Belarus (Gallardo et al., 2014). Later, it was found that the virus strain in Russia had changed at the IGR site since 2012, inferring that the epidemic strain of ASFV in the EU might originate from Russia. In 2019, the virus strain (China/Guangxi/2019), which had two tandem repeat sequences at the IGR site and was primarily claimed in China, was named IGR-III (Ge et al., 2019). Subsequently, this virus strain also appeared successively in Korea (Kim et al., 2021) and Vietnam (Nguyen et al., 2022). A viral strain (Warminsko-Mazurskie, 2019) with three tandem repeat sequences, namely the IGR-IV, was also identified in Poland (Mazur-Panasiuk et al., 2020). The DNA polymerase PolX gene O174L at the 3′ end of the German ASFV pandemic strain can be distinguished in 2020 into five distinct lineages with at least 10 different mutations, suggesting that the mutation results in a pathogenic effect of the altered gene (Forth et al., 2023). The Indonesian Veterinary Science Research Center collected samples from pig farms in Bogor district, West Java province, that same year. The ASF positivity rate was 16/19, and genomic analysis revealed that this genotype of ASFV was identical to genotype II from domestic swine in Vietnam, China, and Russia (Dharmayanti et al., 2021). Senthilkumar et al. were the first to reveal the genomic analysis of the Indian strain, which is distantly linked to the Asian endemic strain. One important characteristic that could help identify the Asian endemic strain is the Mismatch between the I73R and I329L genes (Senthilkumar et al., 2022). ASFV genotyping in Sabah in 2021 revealed that this strain is comparable to the endemic strains in China, Vietnam, and Indonesia (Khoo et al., 2021).

Therefore, genomic surveillance of ASFV at the genome-wide level should be emphasized in the future, which is conducive to grasping the epidemiological pattern of ASFV, studying the disease evolution, and screening ideal vaccine candidates.

5. Research progress of ASFV vaccines

5.1. Inactivated vaccines

Inactivated ASF vaccines were first developed in the 1960s. Viral inactivation included physical and chemical methods such as heating, toluene, formaldehyde, and crystalline violet; evaluation of vaccine efficacy; and addition of adjuvants (Gómez-Puertas et al., 1997; Blome et al., 2014).

Walczak et al. indicated that anti-ASFV antibodies alone are not able to inhibit virus replication by analyzing the possibility of neutralization of the ASFV using collected sera from ASF-survivor animals (Walczak et al., 2022). However, researchers have indicated that it is impractical to use inactivated ASFV as a vaccine (Blome et al., 2014; Rock, 2017), which may be attributed to the non-neutralizing ASFV-specific antibodies (Cadenas-Fernández et al., 2021). Gomez-Puertas et al. reported that phosphatidylinositol is necessary for the correct epitope presentation of neutralizing antibodies (Gómez-Puertas et al., 1997). The viral membrane lipid composition plays an important role in antibody protein recognition, but unfortunately, it failed to detect effective specific antibodies. Multiple inactivations of inactivated vaccines do not induce effective cellular immunity in the host's innate immune system, and with the increasing understanding

of ASFV, the protective rate of inactivated ASFV vaccines is expected to improve by adding reliable adjuvants (Sang et al., 2020). The authors tested the immune efficacy of inactivated ASFV vaccines using "Polygen" and "Emulsigen D" as adjuvants, respectively, and immunized six weaned piglets twice at 21-day intervals. The animals were challenged with the homologous, extremely virulent Armenia 08 virus 42 days after the initial vaccination, both generated ASFV antibodies without neutralizing activity, and acute clinical signs appeared quickly (Blome et al., 2014). Although inactivated vaccines are antigenic, they cannot elicit a complete cellular immune response, resulting in incomplete protection (Tlaxca et al., 2015). The gamma-irradiated ASFV "Estonia 2014" has been shown to be ineffective when adjuvanted with Polygen™ or Montanide™ ISA 201 VG, respectively. Pikalo et al. demonstrated that the highly virulent "Armenia 2008" ASFV strain was not protective by inoculating weaned piglets separately with the inoculated vaccine and subjecting them to the highly virulent "Armenia 2008" strain after 42 days, showing that vaccinated animals contained specific IgG but no protection (Pikalo et al., 2022). Notably, animals inoculated with the ASFV-989 strain showed full clinical protection after 2 weeks of receiving the parental strain Georgia 2007/1. ASFV-989 could serve as a promising attenuated vaccine candidate against the challenge of homologous strains (Bourry et al., 2022). The above tests obtained similar conclusions, which may prove that currently available data suggest challenges in developing an effective inactivated ASFV vaccine using the existing methods.

5.2. Live attenuated vaccines

5.2.1. LAVs based on naturally attenuated virus isolates

Live attenuated ASFV vaccine is developed using natural or artificial methods *in vitro*. The vaccine contains a highly viable and strongly immunogenic treated pathogen, which may increase virulence.

Some naturally weak ASFV strains can be used to develop attenuated vaccines (Chen et al., 2020). Naturally attenuated ASFV strains have been isolated from soft ticks and chronically infected swine, such as the OURT88/3, NH/P68, and Lv17/WB/Rie1 strains (Boinas et al., 2004; Gil et al., 2008; Arias et al., 2017). Live attenuated vaccines prepared from OURT88/3 were protective against homologous strains against pigs, but the protective rate was not satisfactory due to individual differences of swine, vaccination doses, and attacking strains (Chen et al., 2020). In the mid-20th century, an attenuated vaccine against ASFV serotypes I-V developed by the Federal Center for Virology and Microbiology Research protected against strains of homologous serotypes for at least 4 months on day 14 after vaccination (Sereda et al., 2020). Swine vaccinated with naturally attenuated vaccines manifest severe toxic side effects, such as fever, abortion, and chronic or persistent infection (Netherton et al., 2019). Fortunately, Gallardo et al. successfully isolated a non-HAD-ASFV (genotype II) strain, Lv17/WB/Rie1, from a wild boar in Latvia, and experimental swine, which survived received a strong hemadsorbent strain, infected with this strain showed non-specific or subclinical signs (Gallardo et al., 2019). This study reported the non-HAD-cross-protective reinfection pattern of ASFV, suggesting the long-term persistence of ASFV in wild boar herds. The fact that animals immunized with naturally attenuated strains exhibit significant side effects such as fever, skin damage, and joint swelling, which hinder the development of naturally attenuated strains of the ASFV vaccine (Leitão et al., 2001; Mulumba-Mfumu et al., 2016).

However, the immunoprotective effect of different attenuated strains varies, which is related to the type of attacking virus as well as the dose and route of administration. The naturally attenuated strain NH/P68 (genotype I) protected 100% of the virulent strain L60 (genotype I) against heterologous attack by Arm/07 (genotype II; Gallardo et al., 2018). Further, initial vaccination with OURT88/3, followed by a booster immunization with the OURT88/1 strain, resulted in 85% immune protection. Exposure to Benin 97/1 and Uganda 1965 strains resulted in 7 and 100% immune protection, respectively. Immunization against naturally attenuated strains can overcome the challenge of non-homologous ASFV strains (King et al., 2011). Subsequently, Gallardo et al. used intramuscular injection or direct contact methods to infect domestic swine with two blood-sucking ASFV (HAD strains) from Poland (Pol16/DP/OUT21) and Estonia (Est16/WB/Viru8) and three genotypes of non-HAD ASFV from Latvia (Lv17/WB/Rie1; Gallardo et al., 2021). The ASFV from Poland rapidly induced fatal and acute disease, while the ASFV from Estonia caused acute to subacute infections, with two-thirds of animals surviving. In contrast, animals infected with ASFV from virus strain of Lv17/WB/Rie1 developed a more subtle, mild, or even subclinical disease. This study provides quantitative data regarding the transmission and excretion of different strains among domestic swine and increases the focus on supervisory activities. An experiment also demonstrated that factors such as delivery route, including intramuscular and intranasal routes, and dose at low and moderate doses (10^3 and 10^4 $TCID_{50}$), influence the outcome of immunization with the naturally attenuated isolate OURT88/3 (Sánchez-Cordón et al., 2017).

At present, determining whether using the Lv17/WB/Rie1 naturally attenuated strain as a vaccine prototype is an ideal strategy to control wild boar population transmission needs further research (Barasona et al., 2021). However, vaccines developed from naturally weak strains exhibit numerous side effects as well as the risk of re-dissemination of the virus, which limits their use in the clinical setting (Chen et al., 2020). Further, immune protection by natural LAVs has yet to be elucidated.

Advances in live-attenuated vaccines have recently made remarkable progress all over the world (Liu L. et al., 2021). Artificially attenuated vaccines are created by deleting specific virulence genes (O'Donnell et al., 2016; Zhang J. et al., 2021). Compared with other types of ASF vaccines, LAVs provide fully homologous and partially heterologous protection (Teklue et al., 2020a) and are ideal tools to dissect the mechanisms involved in cross-protection (Lacasta et al., 2015; Lopez et al., 2020), but virulence, immunogenicity, and, more importantly, viral phenotype and antigen diversity issues continue to affect ASF live attenuated vaccines (Revilla et al., 2018).

5.2.2. LAVs based on cell passages

The cell-passaged attenuated vaccine is a LAV that causes spontaneous deletion of part of the viral genome after ASFV has been adapted to a cultured cell line, thereby reducing the virulence of the virus. In the 1960s, a laboratory study reported that a weak ASFV vaccine, weakened by transmission from porcine bone marrow (PBM) cells, protected against an attack by a strong strain. Nevertheless, Krug

et al. reported that the strong strain (ASFV-G) was completely attenuated after 110 successive passages in Vero cells, and pigs immunized with the attenuated strain were not protected against it (Krug et al., 2015). In addition, ASFV passaged cultures can be adapted to cell lines such as 293 and Vero, but the virulence and antigenicity of the adapted strains are diminished, and the adapted strains do not provide effective protection after the immunization of pigs (Krug et al., 2015; Wang et al., 2021).

ASFV LAVs *in vitro* are generally based on primary cells, mainly consisting of porcine alveolar macrophages (PAMs) and PBM cells, but primary cells are not conducive to the large-scale production of LAVs. Given the failure of LAVs, additional tools are yet needed for studies involving LAVs. In 2021, Borca et al. reported that ASFV-G-ΔI177L/ΔLVR, which maintains the same attenuation level, immunogenicity profile, and protective efficacy as ASFV-G-ΔI177L, was efficiently replicated in stable porcine cell lines that could overcome the production limitations of primary porcine macrophages only (Borca et al., 2021a,b). Satisfactory discoveries revealed that the ASFV MGF-110-9L gene has a significantly reduced ability to replicate *in vitro* in primary swine macrophage cell cultures, implying the capacity of the ASFV MGF-110-9L strain for further development of ASF control strategies (Li et al., 2021a) and that a relationship involving the cGAS-STING pathway and ASFV MGF-505-7R contributed to uncovering the molecular mechanisms of ASFV (Li et al., 2021b).

Some ASFV genes' mechanisms of action have been revealed, such as the MGF360-9L gene, which is involved in the down-regulation of interferon expression, and the I267L gene, which inhibits RNA Pol-III-RIG-I-mediated innate antiviral responses and leads to severe and lethal disease in animals vaccined (Zhang et al., 2021a; Ran et al., 2022; Zhang K. et al., 2022). Ramirez-Medina et al. assessed the role of the MGF110-5L-6L gene during virus replication in cell cultures and experimental infection in swine in 2022 and showed that deletion of MGF110-5L-6L does not impact virulence or virus replication (Ramirez-Medina et al., 2022a). In 2021 and 2022, uncharacterized protein F317L of ASFV with the function of inhibiting host innate immune response and other uncharacterized proteins EP364R and C129R with the function of inhibiting type I interferon signaling was first discovered, respectively, providing novel insights for understanding how ASFV inhibits host innate immune response and developing an ASFV live-attenuated vaccine (Yang et al., 2021; Dodantenna et al., 2022). Borca et al. claimed that the CRISPR/Cas9 gene editing system can edit target sequences in the genome with high precision, improving the purification efficiency of recombinant ASFV and providing a method for the development of recombinant ASFV LAVs (Borca et al., 2018). Although ASF LAVs have made some progress, many issues will be studied and solved in the future.

5.2.3. LAVs based on deleting specific genes

5.2.3.1. Single deleted genes LAVs

Approaches to the ASFV vaccine's design currently focus on the development of modified live vaccines by targeted gene deletion from different isolates (Turlewicz-Podbielska et al., 2021).

5.2.3.1.1. Benin 97/1/DP148R gene

Reis et al. found that the ΔP148R gene was transcribed early after infection and that deletion of this gene did not affect virus replication in macrophages, indicating that this gene is non-essential (Reis et al., 2017). Based on these findings, the virulent strain BeninΔP148R was obtained by deleting the gene of the virulent isolate Benin 97/1. All swine infected with the modified strain survived. Infection with BeninΔP148R caused only mild clinical signs in pigs and induced a high degree of protection against a homologous virulent virus challenge. Thus, BeninΔP148R could provide a target for rational vaccine development.

5.2.3.1.2. NH/P68/A238L, A224L, A276R, EP153R

The A238L gene is involved in NFκB and NFAT regulation, the A224L gene is involved in apoptosis inhibition, the A276R gene is involved in type I interferon regulation, and the EP153R gene is a regulator of MHC-I antigen presentation. Gallardo et al. constructed recombinant NH/P68 attenuated strains by deleting these genes, respectively, with a view to developing a LAV (Gallardo et al., 2018). The results of the challenge showed that the vaccine candidate was fully effective against a homologous attack of L60 but not against genotype II Arm07, although one pig immunized with NH/P68DA224L survived.

5.2.3.1.3. SY18/L7L-L11L gene

Zhang et al. constructed a deletion strain SY18ΔL7-11 of the L7L-L11L gene to investigate the biology of the gene against ASFV and to gauge its potential as a vaccine candidate (Zhang J. et al., 2021). 11 of 15 pigs survived after 28 days of immunization with 10^3 $TCID_{50}$ and 10^6 $TCID_{50}$. Biological characterization indicated that deletion of the L7L-L11L gene did not affect virus replication *in vitro*. Overall, SY18ΔL7-11 can be researched in more depth as a safe vaccine strain.

5.2.3.1.4. ASFV-G/I177L gene

ASFV-G-ΔI177L was an ideal candidate, as proved by a previous study (Borca et al., 2021a,b). Here, Tran et al. evaluated the safety of ASFV-G-ΔI177L in vaccinated 6 to 8-week-old pigs, which did not cause general ASF symptoms and showed only sporadic, transient clinical signs such as mild cough and soft stools (Tran et al., 2022b). Most importantly, the virulence reduction test demonstrated the stability of the attenuated vaccine by returning five consecutive groups of pigs. Hence, ASFV-G-ΔI177L is a safe and feasible vaccine candidate. To date, the live attenuated vaccine (ASFV-G-ΔI177L) developed in Vietnam is the first commercially available African swine fever vaccine in the world (Tran et al., 2022a).

5.2.3.1.5. Malawi Lil-20/1, Georgia 2007, Pretoriuskop/96/4 (Pret4)/9GL gene

Back in 2000, Lewis et al. injected the retrovirus 9GL-R at 10^2 50% tissue culture infectious dose ($TCID_{50}$) or mutant Δ9GL at 10^2, 10^4, and 10^6 $TCID_{50}$ into Yorkshire pigs, and when attacked with parental virulence Malawi Lil-20/1, all Δ9GL-infected animals were protected (Lewis et al., 2000). Thus, ASFV-Δ9GL may prove useful as live-attenuated ASF vaccines. The ASFV Georgia 2007 strain was identified in the Caucasus and Eastern Europe by O'Donnell et al. ASFV lacking the 9GL gene was constructed and then named ASFV-G-Δ9GL. Vaccinated pigs were able to resist challenges with the virulent strain after intramuscular injection of low doses of 10^2 to 10^3 HAD_{50} of ASFV-G-Δ9GL or ASFV-G in commercial pigs (O'Donnell et al., 2015b). Additionally, deletion of the 9GL gene from the ASFV isolates Pretoriuskop/96/4 (Pret4) produced similar attenuation results (Carlson et al., 2016).

5.2.3.1.6. Georgia 2010/E184L

Ramirez-Medina et al. evaluated the effect of removing the E184L gene from the ASFV-G genome on porcine virulence by injecting pigs with 10^2 50% of the HAD_{50} of ASFV-G-Δ184L or ASFV-G and compared them with animals infected with parentally acquired virulent ASFV-G (Ramirez-Medina et al., 2022b). The results showed that the deletion of attenuated strain E184L could distinguish between infected and inoculated animal species (DICA), but the deletion of the attenuated strain did not provide complete protection. Importantly, E184L is the first experimental ASFV gene product to function as a DIVA antigenic marker.

5.2.3.1.7. BA71/CD2v gene

Monteagudo et al. reported that the knockdown of the CD2v gene in ASFV significantly reduced the virulence of BA71 strains by inoculating experimental pigs. It was not only protective against the parental strain BA71 but also the heterologous strain E75, whereas induced immune protection was dose-dependent and varied substantially among different individuals (Monteagudo et al., 2017). Bosch-Camós et al. described the immunization of pigs intranasally vaccinated with the BA71ΔCD2 deletion mutant virus, which induced an *in vitro* recall response (Bosch-Camós et al., 2022).

5.2.3.1.8. Georgia/TK gene

The TK gene is associated with ASFV virulence. Based on this, Sanford et al. constructed and characterized ASFV-g/VΔTK by removing the TK gene from a Georgian ASFV strain (Sanford et al., 2016). *In vitro* experiments showed that this strain replicated in Vero cells but with a lower replication capacity than the parental strain. In addition, *in vivo* animal studies suggested that ASFVG/V-ΔTK injected with 10^6 $TCID_{50}$ did not cause disease in pigs but was not resistant to challenge by the parental strain.

5.2.3.1.9. OURT88/3I329L

Another promising study reported the increased safety of OURT88/3 by deleting I329L, a gene that suppresses the safety of the host's innate immune response in swine, and showed that deletion of I329L significantly reduced protection against the virulent OURT88/1 isolate (Reis et al., 2020).

5.2.3.1.10. Benin 97/1/MGF

In fact, not all attenuated strains can be ideal vaccine candidates. A study concluded that naturally attenuated ASFV isolate OURT88/3 and deletion mutant BeninΔMGF were immunized in a single intramuscular dose in domestic swine, respectively, with the latter surviving longer. After 130 days of inoculation, all animals showed typical ASFV symptoms and elevated IL-10 levels. High levels of IL-10 suppressed the immune response to ASFV (Sánchez-Cordón et al., 2020). As already mentioned above, evidence suggests that regulatory components of the immune system inhibit effective protection (Franzoni et al., 2023).

Further, the protection induced by LAVs is related to the replication level of LAVs and the number of immunogenic genes expressed. If the replication of LAVs is severely impaired, the immunogenicity induced by LAVs is also diminished (Gladue et al., 2021; Zhang et al., 2021b; Tran et al., 2022a). Thus, the safety and efficacy of LAVs need to be balanced.

5.2.3.2. Multiple deleted genes LAVs

Safety is the key to attenuated vaccines; therefore, vaccine developers reported a trend in the development of LAVs from single to multiple gene deletions to increase the safety of LAVs (Borca et al., 2020, 2021a,b).

Chinese scholars constructed a completely deleted 7-gene HLJ/18-7GD strain (genes encoding MGF505-1R, MGF505-2R, MGF505-3R, MGF360-12l, MGF360-13l, MGF360-14l, and CD2v) using Chinese ASFV HLJ/18 as the backbone. The results of the safety and protection evaluation showed that all pigs (4/4) inoculated with HLJ/18-7GD at 10^3 and 10^5 $TCID_{50}$ survived and were fully viable in the challenge with the ASFV HLJ/18 strain. Therefore, HLJ/-18-7GD can be used as a vaccine strain against ASFV (Chen et al., 2020).

The team knocked out six genes of the Georgia 2007 strain MGF360/505, containing MGF505-1R, MGF360-12L, MGF360-13L, MGF360-14L, MGF505-2R, and MGF505-3R, namely ASFV-G-MGF. *In vitro* experiments showed that the recombinant virus exhibited the same replication efficiency as the parental virus in porcine macrophages. *In vivo* experiments showed that animals injected with the recombinant virus did not develop disease and survived the challenge with the parental strain, and ASFV-G-MGF is the first experimental vaccine reported to induce protection in pigs infected with the same parental virus (O'Donnell et al., 2015a). Subsequent research suggested that deletion strains lacking the 9GL and UK virulence genes provided homologous protection only 14 days after immunization, but full attenuation was achieved through additional deletion of DP96R (UK; O'Donnell et al., 2016).

In addition, knocking out immunosuppressive genes, virulence genes, or important functional genes of ASFV using molecular biology techniques such as gene editing and reverse genetics reduces ASFV virulence and enhances the immune response (Sánchez-Cordón et al., 2018). Such as the knockdown of the MGF360/505, CD2v, and DP148R genes and so on in the ASFV genome. Further, Gallardo et al. constructed EP153R, A224L, A238L, and A276R deletion strains based on the ASFV/NH/P68 natural weak strain using a reverse genetic approach (Gallardo et al., 2018). In subsequent immunoprotection experiments, these deletion strains were found to help immunize animals against genotype I ASFV/L60 strains but failed to defend against genotype II ASFV/Arm07 strains in immunized animals (Gallardo et al., 2018); To date, the results of ASFV genetic modifications, which may be unpredictable, have been confirmed (Urbano and Ferreira, 2022). For example, the experimental vaccine strains ASFV-GΔ9GL/ΔCD2v (Gladue et al., 2020), ASFV-GΔ9GL/ΔMGF (Zhang J. et al., 2021), and ASFV-GΔ9GL/ΔNL/ΔUK (Ramirez-Medina et al., 2019), all of which had dramatically reduced protective potential compared to experimental strains lacking the individual ORFs.

Some novel recombinant viruses have been reported, including the deletion of the QP509L and QP383R genes (ASFV-ΔQP509L/QP383R) from the highly virulent ASFV CN/GS/2018 strain results in complete viral attenuation in swine (Li D. et al., 2022).The generation of a double gene-deleted ASFV mutant, ASFV-SY18-ΔCD2v/UK, from a highly virulent field strain, ASFV-SY18, isolated in China, caused a loss of hemadsorption properties but did not significantly affect the *in vitro* replication of the virus in primary porcine alveolar macrophages (Teklue et al., 2020b). In the genome of the virulent ASFV isolate Benin 97/1, deletion genes of MGF360 (MGF360-10L, 11L, 12L, 13L, and 14L) and MGF530/505

(MGF530/505-1R, 2R, and 3R) and interrupting genes (MGF360-9L and MGF530/505-4R) suggested significant modulation of the IFN response on virus attenuation and induction of protective immunity (Reis et al., 2016). And the deletion of either EP402R or EP153R genes individually or in combination with BeninΔDP148R genome was shown not to reduce virus replication in macrophages *in vitro* (Petrovan et al., 2022). Furthermore, research first described that Arm/07/CBM/c4 impaired the ability to control the cGAS-STING pathway *in vitro*, similar to the NH/P68 attenuated strain, while Arm/07/CBM/c2 prevented STING and IRF3 activation (Pérez-Núñez et al., 2020).

Overall, LAVs are far from commercialized due to safety concerns. Mass vaccination can increase the risk of virulence in LAVs. Moreover, the lack of cell lines for large-scale production of LAVs is another challenge. Mutations and sequence loss in the genome of ASFV among different genotypes or even different strains of the same genotype may lead to changes in antigenicity and virulence (Bao et al., 2019). Finally, the cross-protective ability of LAVs needs to be further evaluated.

Although the development of attenuated vaccines has been unsuccessful, the Harbin Veterinary Research Institute in China has developed a seven-gene deletion attenuated vaccine strain that has completed laboratory studies, with an initial demonstration of safety and efficacy (Chen et al., 2020). Newly developed, promising LAVs candidates are summarized in Table 3.

5.3. Genetically-engineered vaccines

5.3.1. Subunit vaccines

ASF subunit vaccine, which primarily delivers protective antigens and antigen discovery within the ASFV genome, has recently emerged as a promising strategy against ASF (Lopera-Madrid et al., 2021). The ASFV subunit vaccine, as previously mentioned, is a potential vaccine that can effectively produce specific humoral and cellular immunity after specific gene and protein expression. Subunit vaccines are still in the laboratory phase of research, and their practical application requires further investigation. A few ASFV antigens have been shown to exhibit protective effects (Ruiz-Gonzalvo et al., 1996; Hernáez et al., 2004). For example, p30, p54, and p72 proteins are neutralizing; p72 and p54 inhibit viral adsorption; p72 and p30 activate cytotoxic T lymphocyte (CTL) responses, and p30 inhibits viral internalization (Gómez-Puertas et al., 1996). Other envelope or intramembrane proteins of ASFV, such as CD2v, p12, and D117L, may also induce neutralizing antibodies and inhibit viral invasion and release (Escribano et al., 2013).

Subunit vaccines of p30, p54, and p72 proteins were developed using a baculovirus expression system by Gómez-Puertas et al. (1996). However, after injecting the vaccines into experimental animals, effective immune protection was observed in only some of them. Subsequently, Neilan et al. showed that pigs vaccinated with a mixture of baculovirus-expressing p30, p54, p72, and p22 failed to resist the virulent strain of ASFV Pr4 (Neilan et al., 2004). In addition, recombinant baculoviruses with the ASFV hemagglutinin (HA) gene were constructed and were homologous to the T lymphocyte surface antigen CD2, and pigs immunized with recombinant HA produced hemagglutination inhibitory antibodies and temporary inhibitory antibodies, which recognized the 75-kDa structural protein and protected them from lethal infection (Gómez-Puertas et al., 1996). Based on several similarities between ASFV and HIV and poxviruses (Zhu, 2022), others have successfully prepared two p30-reactive monoclonal antibodies, 2H2 and 5E8, from mice immunized with recombinant p30 protein (Wang L. et al., 2022; Zhou et al., 2022), among the potential of genetically engineered vaccines, providing additional evidence that addresses biological challenges in subunit platform development. CD8 + T cells play an important role in protective immunity, as confirmed by the strong Portuguese ASFV strain OUR/T88/1 (Oura et al., 2005). Fan et al. also speculated that CD8 + T cell-mediated immunity plays a central role in the immune protection underlying the HLJ/18-7GD strain. The role of CD8 + T cells in ASF cellular immunity has been studied gradually (Fan et al., 2022).

In a study of immunized pigs with a fusion of genes encoding p30 and p54 proteins and the virus soluble hemagglutinin (sHA) gene, domestic swine exhibited a strong specific antibody response, which did not protect them from a strong viral attack (Argilaguet et al., 2011). However, the fusion of genes encoding the same antigens with ubiquitin resulted in the protection of 33% of immunized animals from ASFV attack (Imhof et al., 1990). The investigators also constructed an ASFV genomic expression library fused to ubiquitin (excepting for p30, p54, and the ORF for hemagglutinin), and 50 to 60% of immunized domestic swine were protected. The two pigs that survived (2/8) had no detectable virus in their blood or excreta during infection, which suggests the ability of ubiquitin to enhance class I antigen presentation and enhance CTL cell response. The protection provided by the other antigens of ASFV in the genome remains to be elucidated (Lacasta et al., 2014).

Currently, most of the ASFV protective antigens are insufficient to provide complete protection (Ivanov et al., 2011). However, Goatley et al. found that using rAd prime and MVA boosted as a delivery system with the antigens shown as immunogenic ex-ASFV, which combine eight different antigens (B602L, B646L/p72, CP204L/p30, E183L/p54, E199L, EP153R, F317L, and MGF505-5R), can protect pigs from fatal disease after challenge with a virulent genotype I strain of ASFV (Goatley et al., 2020). New strategies to develop disabled infectious single-cycle (DISC) or replication-deficient mutants as potential immunizing agents against the ASFV were proposed (Freitas et al., 2019; Urbano and Ferreira, 2022). Confirmation of the pA104R sequence demonstrates that this protein may have the potential for use in subunit vaccine design. In addition, Huang et al. screened for efficient adjuvants and provided a strategy for subunit vaccine development by constructing *Lactobacillus* p72 protein-expressing adjuvants containing IL-33 and CTA1-DD, respectively, to stimulate specific antibody production in immunized mice (Huang et al., 2022). Unfortunately, additional protective antigens need to be identified in ASFV to enable the induction of effective neutralizing antibodies to improve the immune efficacy of subunit vaccines. In our laboratory, we expressed the p30, p54, and p72 proteins encoded by ASFV *in vitro* using the *Lactobacillus lactis* expression system. Findings suggested that recombinant *Lactobacillus* induced humoral, cellular, and local mucosal immunity via orally administered rabbits at a dose of 10^8 CFU/ml of combined immunization (Zhang et al., 2023).

Notably, Mazloum et al. accelerated the understanding of the effect of proteins with unknown functions on ASF virus replication in the CV-1 cell line by evaluating recombinant plasmids pCI-neo/E248R, pCI-neo/EP402R, and pCI-neo/X69R (Mazloum et al., 2019).

TABLE 3 LAVs candidates.

ASFV strain	p72 genotype	Virulence	Attenuation strategy	Protection	References
Georgia 2010	II	High	Gene deleted (E184L)	Homologous strain (Georgia 2010)	Ramirez-Medina et al. (2022b)
Georgia 2010	II	High	Gene deleted (9GL, CD2v, and EP153R)	Homologous strain (Georgia 2010)	Gladue et al. (2020)
Georgia 2010	II	High	EP402R (CD2v)	Homologous strain (Georgia 2010)	Borca et al. (2020)
Georgia 2010	II	High	Gene deleted (A137R)	Heterologous strain (Georgia 2010)	Gladue et al. (2021)
Georgia 2007/1	II	High	Gene deleted (I177L)	Homologous strain (Georgia 2007/1)	Borca et al. (2021a,b)
Georgia 2007/1	II	High	Gene deleted (I177L)	Homologous strain (Georgia 2007/1)	Borca et al. (2020)
Georgia 2007/1	II	High	Gene deleted [MGF505/360(6)]	Homologous strain (Georgia 2007/1)	O'Donnell et al. (2015a)
Georgia 2007/1	II	High	Gene deleted [DP96R (UK) and B119L (9GL)]	Homologous strain (Georgia 2007/1)	O'Donnell et al. (2016)
Georgia 2007/1	II	High	Gene deleted (B119L, DP71L and DP96R)	Homologous strain (Georgia 2007/1)	Ramirez-Medina et al. (2019)
Georgia 2007/1	II	High	Gene deleted (I177L)	Heterologous strain (Georgia 2007/1)	Borca et al. (2021a,b)
Benin 97	II	High	Gene deleted (MGF505/530/360)	Homologous strain (Benin 97)	Reis et al. (2016)
Benin 97	II	High	Gene deleted (DP148R)	Homologous strain (Benin 97)	Reis et al. (2017)
SY18	II	High	Gene deleted (I226R)	Heterologous strain (Georgia 2007)	Zhang et al. (2021b)
SY18	II	High	Gene deleted (L7L-L11L)	Heterologous strain (ASFV-SY18)	Zhang J et al. (2021)
NH/P68	I	Low	Gene deleted (A276R)	Heterologous strain (virulent Arm07)	Gallardo et al. (2018)
HLJ/18	II	High	Gene deleted (MGF505-1R,MGF360-12L, MGF360-13L,MGF360-14L, MGF505-2R, MGF505-3R, and CD2v)	Homologous strain (ASFV HLJ/18)	Chen et al. (2020)
BA71	II	High	Gene deleted [EP402R(CD2v)]	Heterologous strain (Georgia 2007/1)	Monteagudo et al. (2017)
OUR T88/3	I	Low	A151R, p72, C129R, p30, p54, E146L, I215L, I73R, L8L, M448R, MGF110-4L, and MGF110-5L	Heterologous strain (OUR T88/3, OUR T88/1, Georgia 2007/1)	Netherton et al. (2019)

Thus, Several recombinant MVA vectors were constructed by Lopera-Madrid et al. (2021) to evaluate the efficiency of different promoters and secretion signal sequences on ASFV p30 protein expression and immunogenicity. These results indicate that promoter selection may be as vital as the antigen used to develop ASFV subunit vaccines. The satisfactory results of which were evaluated for humoral and cellular immunity in mice by two recombinant fusion proteins, OPM (OprI-p30-modified p54) and OPMT (OprI-p30-modified p54-T cell epitope), suggested that OPMT might be an ideal candidate to elicit immune responses in swine (Zhang G. et al., 2022).

5.3.2. DNA vaccines

Although DNA vaccines can induce high levels of specific T-cell responses in the host (Argilaguet et al., 2012; Bosch-Camós et al., 2020), immunized animals are still not fully resistant to strong strain attacks. Argilaguet et al. confirmed the poor immunogenicity of DNA vaccines in large animals (Argilaguet et al., 2011). The immunized pigs with plasmid DNA encoding two ASFV gene frames (pCMV-PQ), failed to elicit an immune response in pigs. They were, however, successful in mice. Subsequently, a new recombinant plasmid, pCMV-APCH1PQ, was constructed to improve immunization in pigs. The

results hinted that the DNA vaccine did not protect against lethal viral attack, but targeting the antigen to antigen-specific cells significantly enhanced the immune response in pigs. A similar study used a vaccine prepared from an ASFV genomic expression library to immunize breeding pigs, which provided 60% protection against attack by the highly virulent E75 strain (Ivanov et al., 2011). An important strategy investigated the ability of class I molecular antigen presentation and enhancement of the immune response after CTL induction and the construction of a recombinant plasmid PCMV-UbsPQ, confirming the potential of T-cell responses in the prevention of ASF and the development of effective recombinant vaccines in the future (Argilaguet et al., 2012).

The ASF DNA vaccine made using p54/p30 as the target antigen does not produce neutralizing antibodies in pigs or generate cellular immunity (Jancovich et al., 2018). There are some unsatisfactory results, such as the DNA vaccine developed by p54/p30/sHA fusion (Chen et al., 2021), plasmid DNA (CD2v + p72 + p32 and +/−p17), and recombinant proteins (p15 + p35 + p54 and +/−p17) in a cocktail immunization strategy (Sunwoo et al., 2019), the co-immunization using recombinant protein pCD2-E and recombinant plasmid pcDNA312R (Pérez-Núñez et al., 2019; Sunwoo et al., 2019), and a gene fragment encoding the extracellular region HA of ASFV using p54 and p30, all results of above mentioned had no protective capacity against ASFV of pigs (Chen et al., 2021). While the DNA-protein vaccination strategy tested was not effective, it also triggered an earlier onset of clinical signs, viremia, and death after a virulent ASFV challenge compared to non-immunized pigs (Sunwoo et al., 2019). However, a strong CD8 + T cell response was induced by co-immunizing pigs with the ubiquitin gene and the p30 and p54 genes, providing partial protection even in the absence of specific antibodies, suggesting that DNA vaccines enhance cellular immune responses by modifying the antigens (Jancovich et al., 2018; Goatley et al., 2020).

Interestingly, the authors used the concordant sequences of ASFV antigens p12, p17, p22, p54, p72 and CD2v genotypes to predict B-cell, helper T-cell, and cytotoxic T-cell epitopes and conjugated them with adjuvants and linkers to form ASF vaccines (Buan et al., 2022). Immunostimulation experiments showed that the designed ASF vaccine stimulated immune cell effects and cytokine production. Here, Bosch-Camós et al. used data from the SLAI-peptide repertoire presented by a single set of ASFV-infected porcine alveolar macrophages to create a complex DNA vaccine against the Georgia2007/1 lethal challenge, composed of 15 plasmids encoding the individual peptide-bearing ORFs (Bosch-Camós et al., 2021). The result confirmed that two proteins, DNA plasmids encoding M488R and MGF505-7R, a CD8 + T-cell antigen previously described, have T-cell antigens with protective potential. Freitas et Al. described a feasible approach to generating safe and efficient DISC vaccine candidates of ASFV by homologous recombination, in which the A104R gene was replaced by a selection marker (GUS gene; Freitas et al., 2019). In brief, the results suggest that the designed multi-epitope and multi-antigen ASF vaccine requires further exploration.

5.3.3. Vector vaccines

Viral vectors are an emerging type of vaccine in which the internal genome of the viral particle is genetically engineered to carry one or more antigenic genes of the target virus, which can inhibit virus replication. A review described that proteins of p30, pp62, p54, p72, and CD2v were designed as approachable viral vectors because of their strong immunogenicity and the ability to induce the body to produce neutralizing antibodies in the course of the virus cycle (Ravilov et al., 2022). Furthermore, viral vectors can distinguish between infected and vaccinated animals, i.e., the immunogen encoded by the viral vector can be used as a vaccine marker (Gaudreault and Richt, 2019).

Significant discoveries in recent years addressed partly the limitations of traditional inactivated and attenuated virus vaccines. Some authors have based their studies on vectors for gene transfer into mammalian cells, such as by constructing a baculovirus-based gene transfer vector, BacMam-sHAPQ, which is a potential tool for future vaccine development (Argilaguet et al., 2013). Another promising study evaluated two different adjuvants and two immunometric formulations of adenoviral vector (Ad-ASFV) multi-antigens for safety and immunogenicity, which demonstrated for the first time that the Ad-ASFV multi-antigens can be used to induce ASFV anti-specific CTL responses (Lokhandwala et al., 2016). Subsequently, the team also evaluated the protective effect of the adjuvant by intranasal injection of ASFV-Georgia 2007/1 in pigs based on a previous study, which did not result in significant protection (Lokhandwala et al., 2019). Moreover, the immunogenicity of seven adenoviral vectors of ASFV neoantigens (A104R, A151R, B602L, B438L, B119L, EP402RΔPRR, and K205R) was evaluated. Another strategy followed to induce local and systemic immunity via a cocktail of recombinant adenoviruses formulated with adjuvants in pigs was also described (Lokhandwala et al., 2017).

Currently, the antigens for primary and booster immunization are mostly used in subunit vaccines, DNA vaccines, and viral vector vaccines via cross-immunization strategies. For example, p72, p30, p54, E183L, E199L, EP153R, F317, and MGF505-5R recombinant viruses were constructed using poxvirus and adenovirus vectors. Pigs immunized and exposed to Benin97/1 using recombinant poxvirus for primary immunization and recombinant adenovirus for booster immunization represent the best combination of viral vector antigens for immunization to date (Freitas et al., 2019). Chen et al. assessed the immunoassay of piglets and mice using the recombinant virus rBartha-K61-pASFV (Chen et al., 2022). Murgia et al. used an alphavirus vector platform to deliver replicon particles (RPs) expressing ASFV antigens to swine (Murgia et al., 2019). Feng et al. evaluated the effectiveness and safety of recombinant pseudorabies virus [PRV; PRV-ΔgE/ΔgI/ΔTK-(CD2v)] in mice (Feng et al., 2020). Fang et al. established a Semliki Forest virus (SFV) vector expressing ASFV p32 (SFV-p32) and p54 (SFV-p54; Fang et al., 2022). These results highlighted the possibility of developing ASF vaccines using a rational viral vector.

The CRISPR/Cas9-based gene editing technology proposed by Hübner et al. (2018) provides a new direction for screening potential immunoprotective antigens and for developing effective ASFV vector vaccines. Chen et al. constructed and expressed recombinant ASFV p72 protein by reverse genetics using the Newcastle disease virus and evaluated its humoral and cellular immunogenicity in a mouse model but the protective effect of this vaccine in pigs needs further study (Chen et al., 2016). Interestingly, immunization of wild boars with various antigens (p32, p54, p72, and pp62) expressed in adenovirus

induced strong IgGs, IFN-γ, and CTL responses but did not protect against intranasal attack by the ASFV-Georgia 2007/1 strain (Cadenas-Fernández et al., 2020). A strategy incorporating priming with a vector-expressed antigen followed by boosting with an attenuated live virus may broaden the recognition of ASFV epitopes (Murgia et al., 2019). The protective effect of the vector vaccine constructed by Lopera-Madrid et al. remains to be validated. Results of above mentioned showed that limited success in this field attained in previous studies, and protection of vaccines for pigs remains a focus of future research (Lopera-Madrid et al., 2017).

In the future, the design of recombinant vector vaccines will use emerging biological technologies such as gene recombination, reverse genetics, and CRISPR/Cas9 gene editing. Meanwhile, the identification of ASFV virulence genes, functional genes for viral replication, and key genes regulating the host immune response should be encouraged. We expect to combine different viral vectors and multiple efficient protective antigens or genes to construct safe and effective recombinant vector vaccines or DNA vaccines. Newly developed, promising genetically engineered vaccines are summarized in Tables 4, 5.

6. Conclusion

Since January 2020, ASF has been reported in 5 different regions involving 45 countries, resulting in more than 1,931,000 animal losses. The global outbreak of ASF has led to a sharp decline in the global swine production capacity, and the pig industry has been devastated. Due to the insidious and complex nature of ASFV infection, the current epidemic is still unclear. In the long run, coordinating the development of all countries and regions worldwide is critical to relieving the pressure from the ASF epidemic. To commercialize a satisfactory ASF vaccine, however, a variety of challenges must be addressed as a matter of priority. Regarding the authors' published studies, several current problems and future directions of ASF vaccines were summarized as follows:

6.1. Current problems of ASF vaccines

The genome of ASFV is very large, ranging from 170 to 193 kb and encoding 150 to 167 genes with virulence and immune-related functions which is one of the reasons why ASF vaccines are difficult to commerce. Previously, Burmakina et al. proved that ASFV serotype-specific proteins CD2v (EP402R) and/or c-type lectin (EP153R) are important for protection against homologous ASF infection (Burmakina et al., 2019), but the complexities of synergistic interactions among multiple genes are poorly understood (Rowlands et al., 2009; Sánchez-Vizcaíno et al., 2015b; Dixon et al., 2019; Simões et al., 2019). According to the VP72 protein gene B646L, the strains that have lately been common in China, Southeast Asia, and Europe include natural mutations or disappearance mutations, which increase the uncertainty of genome stability (Faburay, 2022). Prior studies have noted the importance of ASFV growing stably and rapidly *in vitro*. Thus, in-depth research on ASF genomics and the function of different genes, including those related to the immune response, is vital to developing an ASF vaccine.

Due of the quick demise of sensitive animals when exposed to virulent strains, previous investigations have been unable to establish a connection between viruses and hosts. Most of the experiments have confirmed that inactivated vaccines led to further expansion of the epidemic and live attenuated vaccines caused a persistent infection, detoxification, and side effects in immunized pigs, while there was still controversy over whether ASFV infection produced neutralizing antibodies. In addition, the low cross-protection between various strains makes screening vaccine candidates challenging (Muñoz-Pérez et al., 2021). According to Qu and colleagues' explanation, this may help pinpoint the virus's origin in an outbreak and may aid in the development of an ASF vaccine (Qu et al., 2022). Up to this point, pigs and biosafety level-3 (BSL-3) laboratories restrict the vaccine's wide development that why it is difficult to obtain reliable animal models for evaluating the immunological effects of vaccines. A numuber of studies sum up the procedures used to ensure the safety of the vaccination and assess the viability of using animals in experiments (Sánchez et al., 2019; Dixon et al., 2020; Sang et al., 2020; Wu et al., 2020). Unfortunately, recent instances of attenuated strains on Chinese farms have led to chronic illnesses, clinical side effects in pig herds, and industrial threats (FAO, 2021). Live virulence vaccines' safety is questioned due to unregistered, illegally attenuated strains.

6.2. Future directions of ASF vaccines

Biosecurity may be the most crucial method to resist the spread of ASF until an effective vaccine is developed. Based on underlying ASF risk factors, it was possible to group the present pandemic's risk factors into the following categories: ASFV, biosecurity, disease control, environment, livestock, sports, network, pig, society, and surveillance (Bergmann et al., 2021). Advancing studies on the potential contribution of mechanical vectors, such as human activity, arthropods, birds, and carnivores, to ASF transmission, are critical (Wu et al., 2020). Besides, it may be worthwhile to investigate the involvement of environmental factors in the development of ASFV. Recently, a successful disease dynamics model was described to explain how ASFV spreads in Vietnamese pig herds and to prevent outbreaks in the future (Mai et al., 2022). Penrith et al. analyzed certain porcine-associated viruses of genotype II, which tended to widen their geographic distribution; meanwhile, the role of ASF survivors as virus carriers, as well as the duration of immunity, still has to be further investigated (Penrith and Kivaria, 2022).

Now, designing some promising methods for distinguishing between infected and vaccinated animals using the distinction between infected and vaccinated animals (DIVA) strategy is necessary for ASFV vaccination campaigns. One of those is a three-independent real-time polymerase chain reaction (qPCR) method to support vaccination campaigns associated with ASFV-ΔMGF, ASFV-G-Δ9GL/ΔUK, and ASFV-ΔI177L or ASFV-ΔI177LΔLVR cell culture live attenuated vaccines (Velazquez-Salinas et al., 2021), and the other is a double indirect ELISA based on p54 and CD2v (Wang Z. et al., 2022). Beyond that, the ASFV E248R gene was selected to be the target for establishing a real-time PCR method, which is used for the efficient detection of infected ASFV and PRRSV live vector viruses expressing ASFV

TABLE 4 ASF subunit and DNA vaccines.

Vaccine type	Sequence source	Gene/protein	Specific antibodies	Neutralizing antibodies	References
Subunit vaccines	E75CV	HA (CD2v)	Yes	No	Ruiz-Gonzalvo et al. (1996)
	Krasnodar 07/17 ASF/ ARRIAH/CV-1	CD2v, pE248R and pX69R	Yes	Yes	Mazloum et al. (2019)
	SY18	p30 and p54	Yes	Yes	Zhang G. et al. (2022)
	Pr4	p54, p30, p72 and p22	Yes	Yes	Neilan et al. (2004)
	E70	Group1: p158, p327, p14 and p220; Group3: p30 and p72	No	/	Ivanov et al. (2011)
	Georgia 2007/1	p30	Yes	No	Lopera-Madrid et al. (2021)
		ASFV-pA104R	/	/	Freitas et al. (2019)
		p14.5, p14.5-IL-33-Mus f and CTA1-p14.5-D-D	Yes	/	Huang et al. (2022)
DNA vaccines	E75	SLA-II/p54/p30 fusion	Yes	No	Argilaguet et al. (2011)
		sHA/p54/p30 fusion	Yes	No	Argilaguet et al. (2012)
		Ub/sHA/p54/p30 fusion	/	/	Argilaguet et al. (2012)
		p54, p30, and the hemagglutinin extracellular domain/ sHA	No	/	Ivanov et al. (2011)
	Georgia2007/1	M448R and MGF505-7R	Yes	Yes	Bosch-Camós et al. (2021)
		p30-Fcc and p54-Fca	Yes	/	Chen et al. (2021)
		47 antigens	Yes	No	Jancovich et al. (2018)
	Ba71V	80 ORFs fragments fused with Ub	Yes	NA	Lacasta et al. (2014)
	Armenia 2007	DNA: CD2v, p72, p30, +/−p17; Proteins: p15, p35, p54, +/−p17	Yes	No	Sunwoo et al. (2019)
	OUR T88/3Benin 97/1	p72, p30, p54, E183L, E199L, EP153R, F317L and MGF505-5R	Yes	Yes	Goatley et al. (2020)
	E70; Ba71V	DNA:CD2v, p30, p72, CP312R; Proteins: p15, p35, p54, p72 and CD2v-E (sHA)	Yes	Yes	Pérez-Núñez et al. (2019)
	NCBI virus database	p12, p17, p22, p54, p72 and CD2v	/	/	Buan et al. (2022)

antigen protein (Li L. et al., 2022). Wu et al. (2022) developed a real-time recombinase-aid amplification (RAA) assay to rapidly detect the different genotypes of ASFV, including the E70 strain (Spanish), the Anhui XCGQ strain, and the Georgia 2007/1 strain and contributed to the development of a control strategy for ASF (Wu et al., 2022). These details could additionally shed light on potential protocols to prevent and control ASF.

Here, we reviewed the preliminary evidence that a safe and effective attenuated vaccine strain with seven gene deletions and Lv17/WB/Rie1 protection against challenge with a virulent ASF virus isolate exists (Barasona et al., 2019). To date, the antigenic and protective properties of two attenuated ASFV strains, MK200 and FK-32/135 (Sereda et al., 2022), evaluated pig samples immunized with a single dose of 10^6 $TCID_{50}$ HLJ/18-7GD (Fan et al., 2022), described the immunization of pigs intranasally inoculated with a BA71ΔCD2 deletion mutant virus, induced *in vitro* recall responses (Bosch-Camós et al., 2022), and found that ASFV-ΔA137R induced higher production of type I interferon (IFN) in PAMs (Sun et al., 2022). Moreover, the design of vaccines intended for wild boars and oral administration is desirable, although these vaccine candidates are still in the preliminary phase and further field experiments need to be carried out. As mentioned earlier, in addition to using numerous ASFV antigens or

TABLE 5 ASF vector vaccines.

Vaccine type	Sequence source	Gene/protein	Specific antibodies	Neutralizing antibodies	References
Vector vaccines	E75	sHA/p54/p30 fusion	No	No	Argilaguet et al. (2013)
	Georgia 2007/1	p30, p54, pp62, and p72	Yes	No	Lokhandwala et al. (2016)
		A151R + B119L + B602L + EP402RΔPRR + B438L + K205R + A104R	Yes	No	Lokhandwala et al. (2017)
		Ad-ASFV-I: A151R, B119L, B602L, EP402RΔPRR, B438L, K205R, A104R, pp62 and p72 Ad-ASFV-II: p30, p54, pp62, p72 and pp220 (p37-34-14, p150-I and p150-II)	Yes	/	Lokhandwala et al. (2017)
		pE199L	/	/	Hübner et al. (2018)
		p72	Yes	/	Chen et al. (2016)
		35 antigens	Yes	/	Cadenas-Fernández et al. (2020)
		p72, p54, p12 and p72, type Lectin (EP153R), CD2v and p72, C-type Lectin (EP153R) and CD2v	Yes No /	No / /	Lopera-Madrid et al. (2017)
	NCBI Virus Database	p30, pp62, p54, p72 and CD2v	Yes	/	Chen et al. (2022)
		p30, p54 and p72	Yes	Yes	Murgia et al. (2019)
		p32 and p54	Yes	/	Fang et al. (2022)
	HLJ/2018	CD2v	Yes	/	Feng et al. (2020)

antigen fragments and optimizing the choice of adjuvants and chemical formulations, attention should be paid to the protective antigens of existing strains and their ideal immunological mechanisms.

A vaccine is, and always will be, the essential strategy, and the best vehicle for preventing and controlling anti-ASFV. Future research on ASFV's virology and functional genomics will focus on topics like protein structure and function, mechanisms of infection and immunity, identification of additional protective antigens as immunogens, targets for vaccines to boost immune protection, and thorough testing in target animals. Safety and immune effect also should be evaluated in future studies.

Author contributions

HoZ and SZ wrote the first draft of the manuscript and looked up the relevant literature. XC and HS guided manuscript writing. HaZ and ZQ performed writing-review and editing. All authors contributed to the article and approved the submitted version.

Funding

This work is based upon research funded by the Shandong Provincial Key Research and Development Program (Major Scientific and Technological Innovation Project; No. 2020CXGC010801-02), the Shandong Province Agricultural Major Application Technology Innovation Project (No. SD2019XM003), the Project of Shandong Province Science and Technology Achievement Transfer Transformation Subsidy (No. 2021 LYXZ020), the Shandong Provincial Major Project of the New-Old Kinetic Energy Conversion [No. (2020)1220], and the Shandong Province Natural Science Foundation (No. ZR201910250090).

Conflict of interest

HZ was employed by the company Qingdao Haihua Biological Group Co., Ltd, Qingdao, China.

The remaining authors declare that the research was conducted in the absence of any commercial or financial relationships that could be construed as a potential conflict of interest.

Publisher's note

All claims expressed in this article are solely those of the authors and do not necessarily represent those of their affiliated organizations, or those of the publisher, the editors and the reviewers. Any product that may be evaluated in this article, or claim that may be made by its manufacturer, is not guaranteed or endorsed by the publisher.

Supplementary material

The Supplementary material for this article can be found online at: https://www.frontiersin.org/articles/10.3389/fmicb.2023.1139494/full#supplementary-material

References

Acharya, K. P., and Wilson, R. T. (2020). Pig production is at risk from African swine fever (ASF) in Nepal. *Transbound. Emerg. Dis.* 67, 2269–2270. doi: 10.1111/tbed.13720

Achenbach, J. E., Gallardo, C., Nieto-Pelegrín, E., Rivera-Arroyo, B., Degefa-Negi, T., Arias, M., et al. (2017). Identification of a new genotype of African swine fever virus in domestic pigs from Ethiopia. *Transbound. Emerg. Dis.* 64, 1393–1404. doi: 10.1111/tbed.12511

Argilaguet, J. M., Pérez-Martín, E., Gallardo, C., Salguero, F. J., Borrego, B., Lacasta, A., et al. (2011). Enhancing DNA immunization by targeting ASFV antigens to SLA-II bearing cells. *Vaccine* 29, 5379–5385. doi: 10.1016/j.vaccine.2011.05.084

Argilaguet, J. M., Pérez-Martín, E., López, S., Goethe, M., Escribano, J. M., Giesow, K., et al. (2013). BacMam immunization partially protects pigs against sublethal challenge with African swine fever virus. *Antivir. Res.* 98, 61–65. doi: 10.1016/j.antiviral.2013.02.005

Argilaguet, J. M., Pérez-Martín, E., Nofrarías, M., Gallardo, C., Accensi, F., Lacasta, A., et al. (2012). DNA vaccination partially protects against African swine fever virus lethal challenge in the absence of antibodies. *PLoS One* 7:e40942. doi: 10.1371/journal.pone.0040942

Arias, M., de la Torre, A., Dixon, L., Gallardo, C., Jori, F., Laddomada, A., et al. (2017). Approaches and perspectives for development of African swine fever virus vaccines. *Vaccines* 5:35. doi: 10.3390/vaccines5040035

Baños, J. V., Boklund, A., Gogin, A., Gortázar, C., Guberti, V., Helyes, G., et al. (2022). Epidemiological analyses of African swine fever in the European Union: (September 2020 to august 2021). *EFSA J.* 20:e07290. doi: 10.2903/j.efsa.2022.7290

Bao, J., Wang, Q., Lin, P., Liu, C., Li, L., Wu, X., et al. (2019). Genome comparison of African swine fever virus China/2018/AnhuiXCGQ strain and related European p72 genotype II strains. *Transbound. Emerg. Dis.* 66, 1167–1176. doi: 10.1111/tbed.13124

Barasona, J. A., Cadenas-Fernández, E., Kosowska, A., Barroso-Arévalo, S., Rivera, B., Sánchez, R., et al. (2021). Safety of African swine fever vaccine candidate Lv17/WB/Rie1 in wild boar: overdose and repeated doses. *Front. Immunol.* 12:761753. doi: 10.3389/fimmu.2021.761753

Barasona, J. A., Gallardo, C., Cadenas-Fernández, E., Jurado, C., Rivera, B., Rodríguez-Bertos, A., et al. (2019). First Oral vaccination of Eurasian wild boar against African swine fever virus genotype II. *Front. Vet. Sci.* 6:137. doi: 10.3389/fvets.2019.00137

Bastos, A. D. S., Penrith, M.-L., Crucière, C., Edrich, J. L., Hutchings, G., Roger, F., et al. (2003). Genotyping field strains of African swine fever virus by partial p72 gene characterisation. *Arch. Virol.* 148, 693–706. doi: 10.1007/s00705-002-0946-8

Beato, M. S., D'Errico, F., Iscaro, C., Petrini, S., Giammarioli, M., and Feliziani, F. (2022). Disinfectants against African swine fever: an updated review. *Viruses* 14:1384. doi: 10.3390/v14071384

Berends, J., Bendita da Costa Jong, J., Cooper, T. L., Dizyee, K., Morais, O., Pereira, A., et al. (2021). Investigating the socio-economic and livelihoods impacts of African swine fever in Timor-Leste: an application of spatial group model building. *Front. Vet. Sci.* 8:687708. doi: 10.3389/fvets.2021.687708

Bergmann, H., Schulz, K., Conraths, F. J., and Sauter-Louis, C. (2021). A review of environmental risk factors for African swine fever in European wild boar. *Animals* 11:2692. doi: 10.3390/ani11092692

Blome, S., Gabriel, C., and Beer, M. (2014). Modern adjuvants do not enhance the efficacy of an inactivated African swine fever virus vaccine preparation. *Vaccine* 32, 3879–3882. doi: 10.1016/j.vaccine.2014.05.051

Blome, S., Gabriel, C., Dietze, K., Breithaupt, A., and Beer, M. (2012). High virulence of African swine fever virus caucasus isolate in European wild boars of all ages. *Emerg. Infect. Dis.* 18:708. doi: 10.3201/eid1804.111813

Boinas, F. S., Hutchings, G. H., Dixon, L. K., and Wilkinson, P. J. (2004). Characterization of pathogenic and non-pathogenic African swine fever virus isolates from *Ornithodoros erraticus* inhabiting pig premises in Portugal. *J. Gen. Virol.* 85, 2177–2187. doi: 10.1099/vir.0.80058-0

Bonnet, S. I., Bouhsira, E., de Regge, N., Fite, J., Etoré, F., Garigliany, M., et al. (2020). Putative role of arthropod vectors in African swine fever virus transmission in relation to their bio-ecological properties. *Viruses* 12:778. doi: 10.3390/v12070778

Borca, M. V., Holinka, L. G., Berggren, K. A., and Gladue, D. P. (2018). CRISPR-Cas9, a tool to efficiently increase the development of recombinant African swine fever viruses. *Sci. Rep.* 8:3154. doi: 10.1038/s41598-018-21575-8

Borca, M. V., Rai, A., Ramirez-Medina, E., Silva, E., Velazquez-Salinas, L., Vuono, E., et al. (2021a). A cell culture-adapted vaccine virus against the current African swine fever virus pandemic strain. *J. Virol.* 95:e0012321. doi: 10.1128/JVI.00123-21

Borca, M. V., Ramirez-Medina, E., Silva, E., Vuono, E., Rai, A., Pruitt, S., et al. (2021b). ASFV-G-ΔI177L as an effective oral nasal vaccine against the Eurasia strain of Africa swine fever. *Viruses* 13:765. doi: 10.3390/v13050765

Borca, M. V., Ramirez-Medina, E., Silva, E., Vuono, E., Rai, A., Pruitt, S., et al. (2020). Development of a highly effective African swine fever virus vaccine by deletion of the I177L gene results in sterile immunity against the current epidemic Eurasia strain. *J. Virol.* 94, e02017–e02019. doi: 10.1128/JVI.02017-19

Bosch-Camós, L., Alonso, U., Esteve-Codina, A., Chang, C. Y., Martín-Mur, B., Accensi, F., et al. (2022). Cross-protection against African swine fever virus upon intranasal vaccination is associated with an adaptive-innate immune crosstalk. *PLoS Pathog.* 18:e1010931. doi: 10.1371/journal.ppat.1010931

Bosch-Camós, L., López, E., Collado, J., Navas, M. J., Blanco-Fuertes, M., Pina-Pedrero, S., et al. (2021). M448R and MGF505-7R: two African swine fever virus antigens commonly recognized by ASFV-specific T-cells and with protective potential. *Vaccine* 9:508. doi: 10.3390/vaccines9050508

Bosch-Camós, L., López, E., and Rodriguez, F. (2020). African swine fever vaccines: a promising work still in progress. *Porcine Health Manag.* 6:17. doi: 10.1186/s40813-020-00154-2

Boshoff, C. I., Bastos, A. D., Gerber, L. J., and Vosloo, W. (2007). Genetic characterisation of African swine fever viruses from outbreaks in southern Africa (1973-1999). *Vet. Microbiol.* 121, 45–55. doi: 10.1016/j.vetmic.2006.11.007

Bourry, O., Hutet, E., le Dimna, M., Lucas, P., Blanchard, Y., Chastagner, A., et al. (2022). Oronasal or intramuscular immunization with a thermo-attenuated ASFV strain provides full clinical protection against Georgia 2007/1 challenge. *Viruses* 14:2777. doi: 10.3390/v14122777

Brown, V. R., and Bevins, S. N. (2018). A review of African swine fever and the potential for introduction into the United States and the possibility of subsequent establishment in feral swine and native ticks. *Front. Vet. Sci.* 5:11. doi: 10.3389/fvets.2018.00011

Buan, A. K. G., Reyes, N. A. L., Pineda, R. N. B., and Medina, P. M. B. (2022). In silico design and evaluation of a multi-epitope and multi-antigenic African swine fever vaccine. *ImmunoInformatics* 8:100019. doi: 10.1016/j.immuno.2022.100019

Burmakina, G., Malogolovkin, A., Tulman, E. R., Xu, W., Delhon, G., Kolbasov, D., et al. (2019). Identification of T-cell epitopes in African swine fever virus CD2v and C-type lectin proteins. *J. Gen. Virol.* 100, 259–265. doi: 10.1099/jgv.0.001195

Cadenas-Fernández, E., Sánchez-Vizcaíno, J. M., Kosowska, A., Rivera, B., Mayoral-Alegre, F., Rodríguez-Bertos, A., et al. (2020). Adenovirus-vectored African swine fever virus antigens cocktail is not protective against virulent Arm07 isolate in Eurasian wild boar. *Pathogens* 9:171. doi: 10.3390/pathogens9030171

Cadenas-Fernández, E., Sánchez-Vizcaíno, J. M., van den Born, E., Kosowska, A., van Kilsdonk, E., Fernández-Pacheco, P., et al. (2021). High doses of inactivated African swine fever virus are safe, but do not confer protection against a virulent challenge. *Vaccine* 9:242. doi: 10.3390/vaccines9030242

Carlson, J., O'Donnell, V., Alfano, M., Velazquez Salinas, L., Holinka, L. G., Krug, P. W., et al. (2016). Association of the host immune response with protection using a live attenuated African swine fever virus model. *Viruses* 8:291. doi: 10.3390/v8100291

Chen, C., Hua, D., Shi, J., Tan, Z., Zhu, M., Tan, K., et al. (2021). Porcine immunoglobulin fc fused P30/P54 protein of African swine fever virus displaying on surface of *S. cerevisiae* elicit strong antibody production in swine. *Virol. Sin.* 36, 207–219. doi: 10.1007/s12250-020-00278-3

Chen, X., Yang, J., Ji, Y., Okoth, E., Liu, B., Li, X., et al. (2016). Recombinant Newcastle disease virus expressing African swine fever virus protein 72 is safe and immunogenic in mice. *Virol. Sin.* 31, 150–159. doi: 10.1007/s12250-015-3692-2

Chen, L., Zhang, X., Shao, G., Shao, Y., Hu, Z., Feng, K., et al. (2022). Construction and evaluation of recombinant pseudorabies virus expressing African swine fever virus antigen genes. *Front. Vet. Sci.* 9:832255. doi: 10.3389/fvets.2022.832255

Chen, W., Zhao, D., He, X., Liu, R., Wang, Z., Zhang, X., et al. (2020). A seven-gene-deleted African swine fever virus is safe and effective as a live attenuated vaccine in pigs. *Sci. China Life Sci.* 63, 623–634. doi: 10.1007/s11427-020-1657-9

Costard, S., Mur, L., Lubroth, J., Sanchez-Vizcaino, J. M., and Pfeiffer, D. U. (2013). Epidemiology of African swine fever virus. *Virusres* 173, 191–197. doi: 10.1016/j.virusres.2012.10.030

Costard, S., Wieland, B., de Glanville, W., Jori, F., Rowlands, R., Vosloo, W., et al. (2009). African swine fever: how can global spread be prevented? *Philos. Trans. R. Soc. Lond., B, Biol. Sci.* 364, 2683–2696. doi: 10.1098/rstb.2009.0098

Davies, K., Goatley, L. C., Guinat, C., Netherton, C. L., Gubbins, S., Dixon, L. K., et al. (2017). Survival of African swine fever virus in excretions from pigs experimentally infected with the Georgia 2007/1 isolate. *Transbound. Emerg. Dis.* 64, 425–431. doi: 10.1111/tbed.12381

Dee, S. A., Bauermann, F. V., Niederwerder, M. C., Singrey, A., Clement, T., de Lima, M., et al. (2019). Correction: survival of viral pathogens in animal feed ingredients under transboundary shipping models. *PLoS One* 14:e0214529. doi: 10.1371/journal.pone.0214529

Dharmayanti, N. I., Sendow, I., Ratnawati, A., Settypalli, T. B. K., Saepulloh, M., Dundon, W. G., et al. (2021). African swine fever in North Sumatra and West Java provinces in 2019 and 2020, Indonesia. *Transbound. Emerg. Dis.* 68, 2890–2896. doi: 10.1111/tbed.14070

Dixon, L. K., Stahl, K., Jori, F., Vial, L., and Pfeiffer, D. U. (2020). African swine fever epidemiology and control. *Annu. Rev. Anim. Biosci.* 8, 221–246. doi: 10.1146/annurev-animal-021419-083741

Dixon, L. K., Sun, H., and Roberts, H. (2019). African swine fever. *Antivir. Res.* 165, 34–41. doi: 10.1016/j.antiviral.2019.02.018

Dodantenna, N., Ranathunga, L., Chathuranga, W. A. G., Weerawardhana, A., Cha, J. W., Subasinghe, A., et al. (2022). African swine fever virus EP364R and C129R target cyclic GMP-AMP to inhibit the cGAS-STING signaling pathway. *J. Virol.* 96:e0102222. doi: 10.1128/jvi.01022-22

Escribano, J. M., Galindo, I., and Alonso, C. (2013). Antibody-mediated neutralization of African swine fever virus: myths and facts. *Virus Res.* 173, 101–109. doi: 10.1016/j.virusres.2012.10.012

Faburay, B. (2022). Genome plasticity of African swine fever virus: implications for diagnostics and live-attenuated vaccines. *Pathogens* 11:145. doi: 10.3390/pathogens11020145

Fan, Y., Chen, W., Jiang, C., Zhang, X., Sun, Y., Liu, R., et al. (2022). Host responses to live-attenuated ASFV (HLJ/18-7GD). *Viruses* 14:2003. doi: 10.3390/v14092003

Fang, N., Yang, B., Xu, T., Li, Y., Li, H., Zheng, H., et al. (2022). Expression and immunogenicity of recombinant African swine fever virus proteins using the Semliki Forest virus. *Front. Vet. Sci.* 9:870009. doi: 10.3389/fvets.2022.870009

FAO (2021). ASF situation in Asia & Pacific update. FAO ASF situation update - African swine fever (ASF) - FAO emergency prevention system for animal health (EMPRES-AH). Available at: https://www.fao.org/ag/againfo/programmes/en/empres/ASF/situation_update.html (Accessed November 4, 2022).

Feng, Z., Chen, J., Liang, W., Chen, W., Li, Z., Chen, Q., et al. (2020). The recombinant pseudorabies virus expressing African swine fever virus CD2v protein is safe and effective in mice. *J. Virol.* 17:180. doi: 10.1186/s12985-020-01450-7

Forth, J. H., Calvelage, S., Fischer, M., Hellert, J., Sehl-Ewert, J., Roszyk, H., et al. (2023). African swine fever virus - variants on the rise. *Emerg. Microbes Infect.* 12:2146537. doi: 10.1080/22221751.2022.2146537

Franzoni, G., Dei Giudici, S., Loi, F., Sanna, D., Floris, M., Fiori, M., et al. (2020). African swine fever circulation among free-ranging pigs in Sardinia: data from the eradication program. *Vaccines* 8:549. doi: 10.3390/vaccines8030549

Franzoni, G., Pedrera, M., and Sánchez-Cordón, P. J. (2023). African swine fever virus infection and cytokine response *in vivo*: an update. *Viruses* 15:233. doi: 10.3390/v15010233

Freitas, F. B., Simões, M., Frouco, G., Martins, C., and Ferreira, F. (2019). Towards the generation of an ASFV-pA104R DISC mutant and a complementary cell line-a potential methodology for the production of a vaccine candidate. *Vaccine* 7:68. doi: 10.3390/vaccines7030068

Galindo, I., and Alonso, C. (2017). African swine fever virus: a review. *Viruses* 9:103. doi: 10.3390/v9050103

Gallardo, C., Fernández-Pinero, J., Pelayo, V., Gazaev, I., Markowska-Daniel, I., Pridotkas, G., et al. (2014). Genetic variation among African swine fever genotype II viruses, eastern and Central Europe. *Emerg. Infect. Dis.* 20, 1544–1547. doi: 10.3201/eid2009.140554

Gallardo, C., Sánchez, E. G., Pérez-Núñez, D., Nogal, M., de León, P., Carrascosa, Á. L., et al. (2018). African swine fever virus (ASFV) protection mediated by NH/P68 and NH/P68 recombinant live-attenuated viruses. *Vaccine* 36, 2694–2704. doi: 10.1016/j.vaccine.2018.03.040

Gallardo, C., Soler, A., Nurmoja, I., Cano-Gómez, C., Cvetkova, S., Frant, M., et al. (2021). Dynamics of African swine fever virus (ASFV) infection in domestic pigs infected with virulent, moderate virulent and attenuated genotype II ASFV European isolates. *Transbound. Emerg. Dis.* 68, 2826–2841. doi: 10.1111/tbed.14222

Gallardo, C., Soler, A., Rodze, I., Nieto, R., Cano-Gómez, C., Fernandez-Pinero, J., et al. (2019). Attenuated and non-haemadsorbing (non-HAD) genotype II African swine fever virus (ASFV) isolated in Europe, Latvia 2017. *Transbound. Emerg. Dis.* 66, 1399–1404. doi: 10.1111/tbed.13132

Gaudreault, N. N., Madden, D. W., Wilson, W. C., Trujillo, J. D., and Richt, J. A. (2020). African swine fever virus: An emerging DNA arbovirus. *Front. Vet. Sci.* 7:215. doi: 10.3389/fvets.2020.00215

Gaudreault, N. N., and Richt, J. A. (2019). Subunit vaccine approaches for African swine fever virus. *Vaccine* 7:56. doi: 10.3390/vaccines7020056

Ge, S., Li, J., Fan, X., Liu, F., Li, L., Wang, Q., et al. (2018). Molecular characterization of African swine fever virus, China, 2018. *Emerg. Infect. Dis.* 24, 2131–2133. doi: 10.3201/eid2411.181274

Ge, S., Liu, Y., Li, L., Wang, Q., Li, J., Ren, W., et al. (2019). An extra insertion of tandem repeat sequence in African swine fever virus, China, 2019. *Virus Genes* 55, 843–847. doi: 10.1007/s11262-019-01704-9

Gil, S., Sepúlveda, N., Albina, E., Leitão, A., and Martins, C. (2008). The low-virulent African swine fever virus (ASFV/NH/P68) induces enhanced expression and production of relevant regulatory cytokines (IFNalpha, TNFalpha and IL12p40) on porcine macrophages in comparison to the highly virulent ASFV/L60. *Arch. Virol.* 153, 1845–1854. doi: 10.1007/s00705-008-0196-5

Gladue, D. P., O'Donnell, V., Ramirez-Medina, E., Rai, A., Pruitt, S., Vuono, E. A., et al. (2020). Deletion of CD2-like (CD2v) and C-type lectin-like (EP153R) genes from African swine fever virus Georgia-Δ9GL abrogates its effectiveness as an experimental vaccine. *Viruses* 12:1185. doi: 10.3390/v12101185

Gladue, D. P., Ramirez-Medina, E., Vuono, E., Silva, E., Rai, A., Pruitt, S., et al. (2021). Deletion of the A137R gene from the pandemic strain of African swine fever virus attenuates the strain and offers protection against the virulent pandemic virus. *J. Virol.* 95:e0113921. doi: 10.1128/JVI.01139-21

Goatley, L. C., Reis, A. L., Portugal, R., Goldswain, H., Shimmon, G. L., Hargreaves, Z., et al. (2020). A Pool of eight virally vectored African swine fever antigens protect pigs against fatal disease. *Vaccine* 8:234. doi: 10.3390/vaccines8020234

Gogin, A., Gerasimov, V., Malogolovkin, A., and Kolbasov, D. (2013). African swine fever in the North Caucasus region and the Russian Federation in years 2007-2012. *Virus Res.* 173, 198–203. doi: 10.1016/j.virusres.2012.12.007

Gómez-Puertas, P., Oviedo, J. M., Rodríguez, F., Coll, J., and Escribano, J. M. (1997). Neutralization susceptibility of African swine fever virus is dependent on the phospholipid composition of viral particles. *Virology* 228, 180–189. doi: 10.1006/viro.1996.8391

Gómez-Puertas, P., Rodríguez, F., Oviedo, J. M., Ramiro-Ibáñez, F., Ruiz-Gonzalvo, F., Alonso, C., et al. (1996). Neutralizing antibodies to different proteins of African swine fever virus inhibit both virus attachment and internalization. *J. Virol.* 70, 5689–5694. doi: 10.1128/JVI.70.8.5689-5694.1996

Gonzague, M., Roger, F., Bastos, A., Burger, C., Randriamparany, T., Smondack, S., et al. (2001). Isolation of a non-haemadsorbing, non-cytopathic strain of African swine fever virus in Madagascar. *Epidemiol. Infect.* 126, 453–459. doi: 10.1017/s0950268801005465

Guinat, C., Gogin, A., Blome, S., Keil, G., Pollin, R., Pfeiffer, D. U., et al. (2016). Transmission routes of African swine fever virus to domestic pigs: current knowledge and future research directions. *Vet. Rec.* 178, 262–267. doi: 10.1136/vr.103593

Hernáez, B., Díaz-Gil, G., García-Gallo, M., Ignacio Quetglas, J., Rodríguez-Crespo, I., Dixon, L., et al. (2004). The African swine fever virus dynein-binding protein p54 induces infected cell apoptosis. *FEBS Lett.* 569, 224–228. doi: 10.1016/j.febslet.2004.06.001

Huang, Q., Niu, T., Zou, B., Wang, J., Xin, J., Niu, H., et al. (2022). *Lactobacillus* plantarum surface-displayed ASFV (p14.5) can stimulate immune responses in mice. *Vaccine* 10:355. doi: 10.3390/vaccines10030355

Hübner, A., Keil, G. M., Kabuuka, T., Mettenleiter, T. C., and Fuchs, W. (2018). Efficient transgene insertion in a pseudorabies virus vector by CRISPR/Cas9 and marker rescue-enforced recombination. *J. Virol. Methods* 262, 38–47. doi: 10.1016/j.jviromet.2018.09.009

Imhof, R. E., Whitters, C. J., and Birch, D. J. (1990). Opto-thermal in vivo monitoring of sunscreens on skin. *Phys. Med. Biol.* 35, 95–102. doi: 10.1088/0031-9155/35/1/009

Iscaro, C., Dondo, A., Ruocco, L., Masoero, L., Giammarioli, M., Zoppi, S., et al. (2022). January 2022: index case of new African swine fever incursion in mainland Italy. *Transbound. Emerg. Dis.* 69, 1707–1711. doi: 10.1111/tbed.14584

Ivanov, V., Efremov, E. E., Novikov, B. V., Balyshev, V. M., Tsibanov SZh, , Kalinovsky, T., et al. (2011). Vaccination with viral protein-mimicking peptides postpones mortality in domestic pigs infected by African swine fever virus. *Mol. Med. Rep.* 4, 395–401. doi: 10.3892/mmr.2011.454

Jancovich, J. K., Chapman, D., Hansen, D. T., Robida, M. D., Loskutov, A., Craciunescu, F., et al. (2018). Immunization of pigs by DNA prime and recombinant vaccinia virus boost to identify and rank African swine fever virus immunogenic and protective proteins. *J. Virol.* 92, e02219–e02217. doi: 10.1128/JVI.02219-17

Jean-Pierre, R. P., Hagerman, A. D., and Rich, K. M. (2022). An analysis of African swine fever consequences on rural economies and smallholder swine producers in Haiti. *Front. Vet. Sci.* 9:960344. doi: 10.3389/fvets.2022.960344

Karalyan, Z., Avetisyan, A., Avagyan, H., Ghazaryan, H., Vardanyan, T., Manukyan, A., et al. (2019). Presence and survival of African swine fever virus in leeches. *Vet. Microbiol.* 237:108421. doi: 10.1016/j.vetmic.2019.108421

Karger, A., Pérez-Núñez, D., Urquiza, J., Hinojar, P., Alonso, C., Freitas, F. B., et al. (2019). An update on African swine fever virology. *Viruses* 11:864. doi: 10.3390/v11090864

Khoo, C. K., Norlina, D., Roshaslinda, D., Iti Suraya Hani, M., Zunaida, B., Mohd Hasrul, A. H., et al. (2021). African swine fever in backyard pigs of Sabah state, East Malaysia, 2021. *Trop. Biomed.* 38, 499–504. doi: 10.47665/tb.38.4.095

Kim, S. H., Lee, S. I., Jeong, H. G., Yoo, J., Jeong, H., Choi, Y., et al. (2021). Rapid emergence of African swine fever virus variants with different numbers of a tandem repeat sequence in South Korea. *Transbound. Emerg. Dis.* 68, 1726–1730. doi: 10.1111/tbed.13867

King, K., Chapman, D., Argilaguet, J. M., Fishbourne, E., Hutet, E., Cariolet, R., et al. (2011). Protection of European domestic pigs from virulent African isolates of African swine fever virus by experimental immunisation. *Vaccine* 29, 4593–4600. doi: 10.1016/j.vaccine.2011.04.052

Krug, P. W., Holinka, L. G., O'Donnell, V., Reese, B., Sanford, B., Fernandez-Sainz, I., et al. (2015). The progressive adaptation of a georgian isolate of African swine fever virus to vero cells leads to a gradual attenuation of virulence in swine corresponding to major modifications of the viral genome. *J. Virol.* 89, 2324–2332. doi: 10.1128/JVI.03250-14

Lacasta, A., Ballester, M., Monteagudo, P. L., Rodríguez, J. M., Salas, M. L., Accensi, F., et al. (2014). Expression library immunization can confer protection against lethal challenge with African swine fever virus. *J. Virol.* 88, 13322–13332. doi: 10.1128/JVI.01893-14

Lacasta, A., Monteagudo, P. L., Jiménez-Marín, Á., Accensi, F., Ballester, M., Argilaguet, J., et al. (2015). Live attenuated African swine fever viruses as ideal tools to dissect the mechanisms involved in viral pathogenesis and immune protection. *Vet. Res.* 46:135. doi: 10.1186/s13567-015-0275-z

Leitão, A., Cartaxeiro, C., Coelho, R., Cruz, B., Parkhouse, R. M. E., Portugal, F. C., et al. (2001). The non-haemadsorbing African swine fever virus isolate ASFV/NH/P68 provides a model for defining the protective anti-virus immune response. *J. Gen. Virol.* 82, 513–523. doi: 10.1099/0022-1317-82-3-513

Lewis, T., Zsak, L., Burrage, T. G., Lu, Z., Kutish, G. F., Neilan, J. G., et al. (2000). An African swine fever virus ERV1-ALR homologue, 9GL, affects virion maturation and viral growth in macrophages and viral virulence in swine. *J. Virol.* 74, 1275–1285. doi: 10.1128/jvi.74.3.1275-1285.2000

Li, L., du, N., Chen, J., Zhang, K., Tong, W., Zheng, H., et al. (2022). Establishment and application of a quantitative PCR method for E248R gene of African. Swine fever virus. *Vet. Sci.* 9:417. doi: 10.3390/vetsci9080417

Li, D., Liu, Y., Qi, X., Wen, Y., Li, P., Ma, Z., et al. (2021a). African swine fever virus MGF-110-9L-deficient mutant has attenuated virulence in pigs. *Virol. Sin.* 36, 187–195. doi: 10.1007/s12250-021-00350-6

Li, D., Wu, P., Liu, H., Feng, T., Yang, W., Ru, Y., et al. (2022). A QP509L/QP383R-deleted African swine fever virus is highly attenuated in swine but does not confer protection against parental virus challenge. *J. Virol.* 96:e0150021. doi: 10.1128/JVI.01500-21

Li, D., Yang, W., Li, L., Li, P., Ma, Z., Zhang, J., et al. (2021b). African swine fever virus MGF-505-7R negatively regulates cGAS-STING-mediated signaling pathway. *J. Immunol.* 206, 1844–1857. doi: 10.4049/jimmunol.2001110

Liu, L., Wang, X., Mao, R., Zhou, Y., Yin, J., Sun, Y., et al. (2021). Research progress on live attenuated vaccine against African swine fever virus. *Microb. Pathog.* 158:105024. doi: 10.1016/j.micpath.2021.105024

Liu, Y., Zhang, X., Qi, W., Yang, Y., Liu, Z., An, T., et al. (2021). Prevention and control strategies of African swine fever and Progress on pig farm repopulation in China. *Viruses* 13:2552. doi: 10.3390/v13122552

Lokhandwala, S., Petrovan, V., Popescu, L., Sangewar, N., Elijah, C., Stoian, A., et al. (2019). Adenovirus-vectored African swine fever virus antigen cocktails are immunogenic but not protective against intranasal challenge with Georgia 2007/1 isolate. *Vet. Microbiol.* 235, 10–20. doi: 10.1016/j.vetmic.2019.06.006

Lokhandwala, S., Waghela, S. D., Bray, J., Martin, C. L., Sangewar, N., Charendoff, C., et al. (2016). Induction of robust immune responses in swine by using a cocktail of adenovirus-vectored African swine fever virus antigens. *Clin. Vaccine Immunol.* 23, 888–900. doi: 10.1128/CVI.00395-16

Lokhandwala, S., Waghela, S. D., Bray, J., Sangewar, N., Charendoff, C., Martin, C. L., et al. (2017). Adenovirus-vectored novel African swine fever virus antigens elicit robust immune responses in swine. *PLoS One* 12:e0177007. doi: 10.1371/journal.pone.0177007

Lopera-Madrid, J., Medina-Magües, L. G., Gladue, D. P., Borca, M. V., and Osorio, J. E. (2021). Optimization in the expression of ASFV proteins for the development of subunit vaccines using poxviruses as delivery vectors. *Sci. Rep.* 11:23476. doi: 10.1038/s41598-021-02949-x

Lopera-Madrid, J., Osorio, J. E., He, Y., Xiang, Z., Adams, L. G., Laughlin, R. C., et al. (2017). Safety and immunogenicity of mammalian cell derived and modified vaccinia Ankara vectored African swine fever subunit antigens in swine. *Vet. Immunol. Immunopathol.* 185, 20–33. doi: 10.1016/j.vetimm.2017.01.004

Lopez, E., van Heerden, J., Bosch-Camós, L., Accensi, F., Navas, M. J., López-Monteagudo, P., et al. (2020). Live attenuated African swine fever viruses as ideal tools to dissect the mechanisms involved in cross-protection. *Viruses* 12:1474. doi: 10.3390/v12121474

Lubisi, B. A., Bastos, A. D., Dwarka, R. M., and Vosloo, W. (2005). Molecular epidemiology of African swine fever in East Africa. *Arch. Virol.* 150, 2439–2452. doi: 10.1007/s00705-005-0602-1

Mai, T. N., Sekiguchi, S., Huynh, T. M. L., Cao, T. B. P., le, V. P., Dong, V. H., et al. (2022). Dynamic models of within-herd transmission and recommendation for vaccination coverage requirement in the case of African swine fever in Vietnam. *Vet. Sci.* 9:292. doi: 10.3390/vetsci9060292

Malogolovkin, A., Burmakina, G., Titov, I., Sereda, A., Gogin, A., Baryshnikova, E., et al. (2015). Comparative analysis of African swine fever virus genotypes and serogroups. *Emerg. Infect. Dis.* 21, 312–315. doi: 10.3201/eid2102.140649

Martínez-Avilés, M., Iglesias, I., and De La Torre, A. (2020). Evolution of the ASF infection stage in wild boar within the EU (2014-2018). *Front. Vet. Sci.* 7:155. doi: 10.3389/fvets.2020.00155

Mazloum, A., Zhukov, I. U., Aronova, E. B., Igolkin, A. S., and Vlasova, N. N. (2019). ASF virus replication features in the presence of recombinant proteins CD2v, pX69R and pE248R. *Vopr. Virusol.* 64, 193–200. doi: 10.36233/0507-4088-2019-64-4-193-200

Mazur-Panasiuk, N., Walczak, M., Juszkiewicz, M., and Woźniakowski, G. (2020). The spillover of African swine fever in Western Poland revealed its estimated origin on the basis of O174L, K145R, MGF 505-5R and IGR I73R/I329L genomic sequences. *Viruses* 12:1094. doi: 10.3390/v12101094

Mazur-Panasiuk, N., Żmudzki, J., and Woźniakowski, G. (2019). African swine fever virus - persistence in different environmental conditions and the possibility of its indirect transmission. *J. Vet. Res.* 63, 303–310. doi: 10.2478/jvetres-2019-0058

Mighell, E., and Ward, M. P. (2021, 2021). African swine fever spread across Asia, 2018-2019. *Transbound. Emerg. Dis.* 68, 2722–2732. doi: 10.1111/tbed.14039

Monteagudo, P. L., Lacasta, A., López, E., Bosch, L., Collado, J., Pina-Pedrero, S., et al. (2017). BA71ΔCD2: a new recombinant live attenuated African swine fever virus with cross-protective capabilities. *J. Virol.* 91, e01058–e01017. doi: 10.1128/JVI.01058-17

Mulumba-Mfumu, L. K., Goatley, L. C., Saegerman, C., Takamatsu, H. H., and Dixon, L. K. (2016). Immunization of African indigenous pigs with attenuated genotype I African swine fever virus OURT88/3 induces protection against challenge with virulent strains of genotype I. *Transbound. Emerg. Dis.* 63, e323–e327. doi: 10.1111/tbed.12303

Mulumba-Mfumu, L. K., Saegerman, C., Dixon, L. K., Madimba, K. C., Kazadi, E., Mukalakata, N. T., et al. (2019). African swine fever: update on eastern, central and southern Africa. *Transbound. Emerg. Dis.* 66, 1462–1480. doi: 10.1111/tbed.13187

Muñoz-Pérez, C., Jurado, C., and Sánchez-Vizcaíno, J. M. (2021). African swine fever vaccine: turning a dream into reality. *Transbound. Emerg. Dis.* 68, 2657–2668. doi: 10.1111/tbed.14191

Murgia, M. V., Mogler, M., Certoma, A., Green, D., Monaghan, P., Williams, D. T., et al. (2019). Evaluation of an African swine fever (ASF) vaccine strategy incorporating priming with an alphavirus-expressed antigen followed by boosting with attenuated ASF virus. *Arch. Virol.* 164, 359–370. doi: 10.1007/s00705-018-4071-8

Neilan, J. G., Zsak, L., Lu, Z., Burrage, T. G., Kutish, G. F., and Rock, D. L. (2004). Neutralizing antibodies to African swine fever virus proteins p30, p54, and p72 are not sufficient for antibody-mediated protection. *Virology* 319, 337–342. doi: 10.1016/j.virol.2003.11.011

Netherton, C. L., Goatley, L. C., Reis, A. L., Portugal, R., Nash, R. H., Morgan, S. B., et al. (2019). Identification and immunogenicity of African swine fever virus antigens. *Front. Immunol.* 10:1318. doi: 10.3389/fimmu.2019.01318

Nguyen, V. T., Cho, K. H., Mai, N. T. A., Park, J. Y., Trinh, T. B. N., Jang, M. K., et al. (2022). Multiple variants of African swine fever virus circulating in Vietnam. *Arch. Virol.* 167, 1137–1140. doi: 10.1007/s00705-022-05363-4

O'Donnell, V., Holinka, L. G., Gladue, D. P., Sanford, B., Krug, P. W., Lu, X., et al. (2015a). African swine fever virus Georgia isolate harboring deletions of MGF360 and MGF505 genes is attenuated in swine and confers protection against challenge with virulent parental virus. *J. Virol.* 89, 6048–6056. doi: 10.1128/JVI.00554-15

O'Donnell, V., Holinka, L. G., Krug, P. W., Gladue, D. P., Carlson, J., Sanford, B., et al. (2015b). African swine fever virus Georgia 2007 with a deletion of virulence-associated gene 9GL (B119L), when administered at low doses, leads to virus attenuation in swine and induces an effective protection against homologous challenge. *J. Virol.* 89, 8556–8566. doi: 10.1128/JVI.00969-15

O'Donnell, V., Risatti, G. R., Holinka, L. G., Krug, P. W., Carlson, J., Velazquez-Salinas, L., et al. (2016). Simultaneous deletion of the 9GL and UK genes from the African swine fever virus Georgia 2007 isolate offers increased safety and protection against homologous challenge. *J. Virol.* 91, e01760–e01716. doi: 10.1128/JVI.01760-16

O'Hara, K. C., Beltrán-Alcrudo, D., Hovari, M., Tabakovski, B., and Martínez-López, B. (2021). Descriptive and multivariate analysis of the pig sector in North Macedonia and its implications for African swine fever transmission. *Front. Vet. Sci.* 8:733157. doi: 10.3389/fvets.2021.733157

Olesen, A. S., Lohse, L., Hansen, M. F., Boklund, A., Halasa, T., Belsham, G. J., et al. (2018). Infection of pigs with African swine fever virus via ingestion of stable flies (*Stomoxys calcitrans*). *Transbound. Emerg. Dis.* 65, 1152–1157. doi: 10.1111/tbed.12918

Oura, C. A. L., Denyer, M. S., Takamatsu, H., and Parkhouse, R. M. E. (2005). In vivo depletion of CD8+ T lymphocytes abrogates protective immunity to African swine fever virus. *J. Gen. Virol.* 86, 2445–2450. doi: 10.1099/vir.0.81038-0

Penrith, M. L., and Kivaria, F. M. (2022). One hundred years of African swine fever in Africa: where have we been, where are we now, where are we going? *Transbound. Emerg. Dis.* 69, e1179–e1200. doi: 10.1111/tbed.14466

Pérez-Núñez, D., Castillo-Rosa, E., Vigara-Astillero, G., García-Belmonte, R., Gallardo, C., and Revilla, Y. (2020). Identification and isolation of two different subpopulations within African swine fever virus arm/07 stock. *Vaccine* 8:625. doi: 10.3390/vaccines8040625

Pérez-Núñez, D., Sunwoo, S. Y., Sánchez, E. G., Haley, N., García-Belmonte, R., Nogal, M., et al. (2019). Evaluation of a viral DNA-protein immunization strategy against African swine fever in domestic pigs. *Vet. Immunol. Immunopathol.* 208, 34–43. doi: 10.1016/j.vetimm.2018.11.018

Petrini, S., Feliziani, F., Casciari, C., Giammarioli, M., Torresi, C., and De Mia, G. M. (2019). Survival of African swine fever virus (ASFV) in various traditional Italian dry-cured meat products. *Prev. Vet. Med.* 162, 126–130. doi: 10.1016/j.prevetmed.2018.11.013

Petrovan, V., Rathakrishnan, A., Islam, M., Goatley, L. C., Moffat, K., Sanchez-Cordon, P. J., et al. (2022). Role of African swine fever virus proteins EP153R and EP402R in reducing viral persistence in blood and virulence in pigs infected with BeninΔDP148R. *J. Virol.* 96:e0134021. doi: 10.1128/JVI.01340-21

Phillips, D. E., Mee, P. T., Lynch, S. E., da Conceição, F., da Costa, B., Jong, J., et al. (2021). Use of field based loop mediated isothermal amplification (LAMP) technology for a prevalence survey and proof of freedom survey for African swine fever in Timor-Leste in 2019. *Front. Vet. Sci.* 8:672048. doi: 10.3389/fvets.2021.672048

Pietschmann, J., Guinat, C., Beer, M., Pronin, V., Tauscher, K., Petrov, A., et al. (2015). Course and transmission characteristics of oral low-dose infection of domestic pigs and

European wild boar with a Caucasian African swine fever virus isolate. *Arch. Virol.* 160, 1657–1667. doi: 10.1007/s00705-015-2430-2

Pikalo, J., Porfiri, L., Akimkin, V., Roszyk, H., Pannhorst, K., Kangethe, R. T., et al. (2022). Vaccination with a gamma irradiation-inactivated African swine fever virus is safe but does not protect against a challenge. *Front. Immunol.* 13:832264. doi: 10.3389/fimmu.2022.832264

Portugal, R., Coelho, J., Höper, D., Little, N. S., Smithson, C., Upton, C., et al. (2015). Related strains of African swine fever virus with different virulence: genome comparison and analysis. *J. Gen. Virol.* 96, 408–419. doi: 10.1099/vir.0.070508-0

Portugal, R., Goatley, L. C., Husmann, R., Zuckermann, F. A., and Dixon, L. K. (2020). A porcine macrophage cell line that supports high levels of replication of OURT88/3, an attenuated strain of African swine fever virus. *Emerg. Microbes. Infect.* 9, 1245–1253. doi: 10.1080/22221751.2020.1772675

Probst, C., Globig, A., Knoll, B., Conraths, F. J., and Depner, K. (2017). Behaviour of free ranging wild boar towards their dead fellows: potential implications for the transmission of African swine fever. *R. Soc. Open Sci.* 4:170054. doi: 10.1098/rsos.170054

Qu, H., Ge, S., Zhang, Y., Wu, X., and Wang, Z. (2022). A systematic review of genotypes and serogroups of African swine fever virus. *Virus Genes* 58, 77–87. doi: 10.1007/s11262-021-01879-0

Quembo, C. J., Jori, F., Vosloo, W., and Heath, L. (2018). Genetic characterization of African swine fever virus isolates from soft ticks at the wildlife/domestic interface in Mozambique and identification of a novel genotype. *Transbound. Emerg. Dis.* 65, 420–431. doi: 10.1111/tbed.12700

Rajukumar, K., Senthilkumar, D., Venkatesh, G., Singh, F., Patil, V. P., Kombiah, S., et al. (2021). Genetic characterization of African swine fever virus from domestic pigs in India. *Transbound. Emerg. Dis.* 68, 2687–2692. doi: 10.1111/tbed.13986

Ramirez-Medina, E., Vuono, E., O'Donnell, V., Holinka, L. G., Silva, E., Rai, A., et al. (2019). Differential effect of the deletion of African swine fever virus virulence-associated genes in the induction of attenuation of the highly virulent Georgia strain. *Viruses* 11:599. doi: 10.3390/v11070599

Ramirez-Medina, E., Vuono, E., Rai, A., Pruitt, S., Espinoza, N., Velazquez-Salinas, L., et al. (2022b). Deletion of E184L, a putative DIVA target from the pandemic strain of African swine fever virus, produces a reduction in virulence and protection against virulent challenge. *J. Virol.* 96:e0141921. doi: 10.1128/JVI.01419-21

Ramirez-Medina, E., Vuono, E., Silva, E., Rai, A., Valladares, A., Pruitt, S., et al. (2022a). Evaluation of the deletion of MGF110-5L-6L on swine virulence from the pandemic strain of African swine fever virus and use as a DIVA marker in vaccine candidate ASFV-G-ΔI177L. *Virol. J.* 96:e0059722. doi: 10.1128/jvi.00597-22

Ran, Y., Li, D., Xiong, M. G., Liu, H. N., Feng, T., Shi, Z. W., et al. (2022). African swine fever virus I267L acts as an important virulence factor by inhibiting RNA polymerase III-RIG-I-mediated innate immunity. *PLoS Pathog.* 18:e1010270. doi: 10.1371/journal.ppat.1010270

Ravilov, R. K., Rizvanov, A. A., Mingaleev, D. N., Galeeva, A. G., Zakirova, E. Y., Shuralev, E. A., et al. (2022). Viral vector vaccines against ASF: problems and Prospectives. *Front. Vet. Sci.* 9:830244. doi: 10.3389/fvets.2022.830244

Reis, A. L., Abrams, C. C., Goatley, L. C., Netherton, C., Chapman, D. G., Sanchez-Cordon, P., et al. (2016). Deletion of African swine fever virus interferon inhibitors from the genome of a virulent isolate reduces virulence in domestic pigs and induces a protective response. *Vaccine* 34, 4698–4705. doi: 10.1016/j.vaccine.2016.08.011

Reis, A. L., Goatley, L. C., Jabbar, T., Lopez, E., Rathakrishnan, A., and Dixon, L. K. (2020). Deletion of the gene for the type I interferon inhibitor I329L from the attenuated African swine fever virus OURT88/3 strain reduces protection induced in pigs. *Vaccine* 8:262. doi: 10.3390/vaccines8020262

Reis, A. L., Goatley, L. C., Jabbar, T., Sanchez-Cordon, P. J., Netherton, C. L., Chapman, D. A. G., et al. (2017). Deletion of the African swine fever virus gene DP148R does not reduce virus replication in culture but reduces virus virulence in pigs and induces high levels of protection against challenge. *J. Virol.* 91, e01428–e01417. doi: 10.1128/JVI.01428-17

Revilla, Y., Pérez-Núñez, D., and Richt, J. A. (2018). African swine fever virus biology and vaccine approaches. *Adv. Virus Res.* 100, 41–74. doi: 10.1016/bs.aivir.2017.10.002

Rock, D. L. (2017). Challenges for African swine fever vaccine development-"… perhaps the end of the beginning.". *Vet. Microbiol.* 206, 52–58. doi: 10.1016/j.vetmic.2016.10.003

Rowlands, R. J., Duarte, M. M., Boinas, F., Hutchings, G., and Dixon, L. K. (2009). The CD2v protein enhances African swine fever virus replication in the tick vector, *Ornithodoros erraticus*. *Virology* 393, 319–328. doi: 10.1016/j.virol.2009.07.040

Rowlands, R. J., Michaud, V., Heath, L., Hutchings, G., Oura, C., Vosloo, W., et al. (2008). African swine fever virus isolate, Georgia, 2007. *Emerg. Infect. Dis.* 14, 1870–1874. doi: 10.3201/eid1412.080591

Ruiz-Gonzalvo, F., Rodríguez, F., and Escribano, J. M. (1996). Functional and immunological properties of the baculovirus-expressed hemagglutinin of African swine fever virus. *Virology* 218, 285–289. doi: 10.1006/viro.1996.0193

Sánchez, E. G., Pérez-Núñez, D., and Revilla, Y. (2019). Development of vaccines against African swine fever virus. *Virus Res.* 265, 150–155. doi: 10.1016/j.virusres.2019.03.022

Sánchez-Cordón, P. J., Chapman, D., Jabbar, T., Reis, A. L., Goatley, L., Netherton, C. L., et al. (2017). Different routes and doses influence protection in pigs immunised with the naturally attenuated African swine fever virus isolate OURT88/3. *Antivir. Res.* 138, 1–8. doi: 10.1016/j.antiviral.2016.11.021

Sánchez-Cordón, P. J., Jabbar, T., Berrezaie, M., Chapman, D., Reis, A., Sastre, P., et al. (2018). Evaluation of protection induced by immunisation of domestic pigs with deletion mutant African swine fever virus BeninΔMGF by different doses and routes. *Vaccine* 36, 707–715. doi: 10.1016/j.vaccine.2017.12.030

Sánchez-Cordón, P. J., Jabbar, T., Chapman, D., Dixon, L. K., and Montoya, M. (2020). Absence of Long-term protection in domestic pigs immunized with attenuated African swine fever virus isolate OURT88/3 or BeninΔMGF correlates with increased levels of regulatory T cells and Interleukin-10. *J. Virol.* 94, e00350–e00320. doi: 10.1128/JVI.00350-20

Sánchez-Vizcaíno, J. M., Mur, L., Bastos, A. D., and Penrith, M. L. (2015a). New insights into the role of ticks in African swine fever epidemiology. *Rev. Sci. Tech.* 34, 503–511. doi: 10.20506/rst.34.2.2375

Sánchez-Vizcaíno, J. M., Mur, L., Gomez-Villamandos, J. C., and Carrasco, L. (2015b). An update on the epidemiology and pathology of African swine fever. *J. Comp. Pathol.* 152, 9–21. doi: 10.1016/j.jcpa.2014.09.003

Sanford, B., Holinka, L. G., O'Donnell, V., Krug, P. W., Carlson, J., Alfano, M., et al. (2016). Deletion of the thymidine kinase gene induces complete attenuation of the Georgia isolate of African swine fever virus. *Virus Res.* 213, 165–171. doi: 10.1016/j.virusres.2015.12.002

Sang, H., Miller, G., Lokhandwala, S., Sangewar, N., Waghela, S. D., Bishop, R. P., et al. (2020). Progress toward development of effective and safe African swine fever virus vaccines. *Front. Vet. Sci.* 7:84. doi: 10.3389/fvets.2020.00084

Schulz, K., Staubach, C., and Blome, S. (2017). African and classical swine fever: similarities, differences and epidemiological consequences. *Vet. Res.* 48:84. doi: 10.1186/s13567-017-0490-x

Senthilkumar, D., Rajukumar, K., Venkatesh, G., Singh, F., Tosh, C., Kombiah, S., et al. (2022). Complete genome analysis of African swine fever virus isolated from domestic pigs during the first ASF outbreaks in India. *Transbound. Emerg. Dis.* 69, e2020–e2027. doi: 10.1111/tbed.14536

Sereda, A. D., Balyshev, V. M., Kazakova, A. S., Imatdinov, A. R., and Kolbasov, D. V. (2020). Protective properties of attenuated strains of African swine fever virus belonging to Seroimmunotypes I-VIII. *Pathogens* 9:274. doi: 10.3390/pathogens9040274

Sereda, A. D., Kazakova, A. S., Namsrayn, S. G., Vlasov, M. E., and Kolbasov, D. V. (2022). The attenuated ASFV strains MK-200 and FK-32/135 as possible models for investigation of protective immunity by ASFV infection. *PLoS One* 17:e0270641. doi: 10.1371/journal.pone.0270641

Simões, M., Freitas, F. B., Leitão, A., Martins, C., and Ferreira, F. (2019). African swine fever virus replication events and cell nucleus: new insights and perspectives. *Virus Res.* 270:197667. doi: 10.1016/j.virusres.2019.197667

Śmietanka, K., Woźniakowski, G., Kozak, E., Niemczuk, K., Frączyk, M., Bocian, Ł., et al. (2016). African swine fever epidemic, Poland, 2014-2015. *Emerg. Infect. Dis.* 22, 1201–1207. doi: 10.3201/eid2207.151708

Stoian, A. M. M., Zimmerman, J., Ji, J., Hefley, T. J., Dee, S., Diel, D. G., et al. (2019). Half-life of African swine fever virus in shipped feed. *Emerg. Infect. Dis.* 25, 2261–2263. doi: 10.3201/eid2512.191002

Sun, E., Huang, L., Zhang, X., Zhang, J., Shen, D., Zhang, Z., et al. (2021). Genotype I African swine fever viruses emerged in domestic pigs in China and caused chronic infection. *Emerg. Microbes Infect.* 10, 2183–2193. doi: 10.1080/22221751.2021.1999779

Sun, M., Yu, S., Ge, H., Wang, T., Li, Y., Zhou, P., et al. (2022). The A137R protein of African swine fever virus inhibits type I interferon production via the autophagy-mediated lysosomal degradation of TBK1. *J. Virol.* 96:e0195721. doi: 10.1128/jvi.01957-21

Sunwoo, S., Pérez-Núñez, D., Morozov, I., Sánchez, E. G., Gaudreault, N. N., Trujillo, J. D., et al. (2019). DNA-protein vaccination strategy does not protect from challenge with African swine fever virus Armenia 2007 strain. *Vaccine* 7:12. doi: 10.3390/vaccines7010012

Teklue, T., Sun, Y., Abid, M., Luo, Y., and Qiu, H. J. (2020a). Current status and evolving approaches to African swine fever vaccine development. *Transbound. Emerg. Dis.* 67, 529–542. doi: 10.1111/tbed.13364

Teklue, T., Wang, T., Luo, Y., Hu, R., Sun, Y., and Qiu, H. J. (2020b). Generation and evaluation of an African swine fever virus mutant with deletion of the CD2v and UK genes. *Vaccine* 8:763. doi: 10.3390/vaccines8040763

Thanapongtharm, W., Wongphruksasoong, V., Sangrat, W., Thongsrimoung, K., Ratanavanichrojn, N., Kasemsuwan, S., et al. (2022). Application of spatial risk assessment integrated with a mobile app in fighting against the introduction of African swine fever in pig farms in Thailand: development study. *JMIR Form. Res.* 6:e34279. doi: 10.2196/34279

Tlaxca, J. L., Ellis, S., and Remmele, R. L. (2015). Live attenuated and inactivated viral vaccine formulation and nasal delivery: potential and challenges. *Adv. Drug Deliv. Rev.* 93, 56–78. doi: 10.1016/j.addr.2014.10.002

Tran, X. H., le, T. T. P., Nguyen, Q. H., do, T. T., Nguyen, V. D., Gay, C. G., et al. (2022a). African swine fever virus vaccine candidate ASFV-G-ΔI177L efficiently protects European and native pig breeds against circulating Vietnamese field strain. *Transbound. Emerg. Dis.* 69, e497–e504. doi: 10.1111/tbed.14329

Tran, X. H., Phuong, L. T. T., Huy, N. Q., Thuy, D. T., Nguyen, V. D., Quang, P. H., et al. (2022b). Evaluation of the safety profile of the ASFV vaccine candidate ASFV-G-ΔI177L. *Viruses* 14:896. doi: 10.3390/v14050896

Turlewicz-Podbielska, H., Kuriga, A., Niemyjski, R., Tarasiuk, G., and Pomorska-Mól, M. (2021). African swine fever virus as a difficult opponent in the fight for a vaccine-current data. *Viruses* 13:1212. doi: 10.3390/v13071212

Urbano, A. C., and Ferreira, F. (2022). African swine fever control and prevention: an update on vaccine development. *Emerg. Microbes. Infect.* 11, 2021–2033. doi: 10.1080/22221751.2022.2108342

Van Etten, J. (2009). Lesser known large dsDNA viruses. Preface. *Curr. Top. Microbiol. Immunol.* 328, v–vii.

Velazquez-Salinas, L., Ramirez-Medina, E., Rai, A., Pruitt, S., Vuono, E. A., Espinoza, N., et al. (2021). Development real-time PCR assays to genetically differentiate vaccinated pigs from infected pigs with the Eurasian strain of African swine fever virus. *Front. Vet. Sci.* 8:768869. doi: 10.3389/fvets.2021.768869

Walczak, M., Juszkiewicz, M., Szymankiewicz, K., Szczotka-Bochniarz, A., and Woźniakowski, G. (2022). ASF -survivors' sera do not inhibit African swine fever virus replication in vitro. *J. Vet. Res.* 66, 21–27. doi: 10.2478/jvetres-2022-0016

Wang, Z., Ai, Q., Huang, S., Ou, Y., Gao, Y., Tong, T., et al. (2022). Immune escape mechanism and vaccine research Progress of African swine fever virus. *Vaccine* 10:344. doi: 10.3390/vaccines10030344

Wang, L., Fu, D., Tesfagaber, W., Li, F., Chen, W., Zhu, Y., et al. (2022). Development of an ELISA method to differentiate animals infected with wild-type African swine fever viruses and attenuated HLJ/18-7GD vaccine candidate. *Viruses* 14:1731. doi: 10.3390/v14081731

Wang, T., Wang, L., Han, Y., Pan, L., Yang, J., Sun, M., et al. (2021). Adaptation of African swine fever virus to HEK293T cells. *Transbound. Emerg. Dis.* 68, 2853–2866. doi: 10.1111/tbed.14242

Wang, N., Zhao, D., Wang, J., Zhang, Y., Wang, M., Gao, Y., et al. (2019). Architecture of African swine fever virus and implications for viral assembly. *Science (New York, N.Y.)* 366, 640–644. doi: 10.1126/science.aaz1439. aaz 1439

Wen, X., He, X., Zhang, X., Zhang, X., Liu, L., Guan, Y., et al. (2019). Genome sequences derived from pig and dried blood pig feed samples provide important insights into the transmission of African swine fever virus in China in 2018. *Emerg. Microbes. Infect.* 8, 303–306. doi: 10.1080/22221751.2019.1565915

Wu, K., Liu, J., Wang, L., Fan, S., Li, Z., Li, Y., et al. (2020). Current state of global African swine fever vaccine development under the prevalence and transmission of ASF in China. *Vaccine* 8:531. doi: 10.3390/vaccines8030531

Wu, Y., Yang, Y., Ru, Y., Qin, X., Li, M., Zhang, Z., et al. (2022). The development of a real-time recombinase-aid amplification assay for rapid detection of African swine fever virus. *Front. Microbiol.* 13:846770. doi: 10.3389/fmicb.2022.846770

Yang, J., Li, S., Feng, T., Zhang, X., Yang, F., Cao, W., et al. (2021). African swine fever virus F317L protein inhibits NF-κB activation to evade host immune response and promote viral replication. *mSphere* 6:e0065821. doi: 10.1128/mSphere.00658-21

Zani, L., Masiulis, M., Bušauskas, P., Dietze, K., Pridotkas, G., Globig, A., et al. (2020). African swine fever virus survival in buried wild boar carcasses. *Transbound. Emerg. Dis.* 67, 2086–2092. doi: 10.1111/tbed.13554

Zhang, Y., Ke, J., Zhang, J., Yang, J., Yue, H., Zhou, X., et al. (2021b). African swine fever virus bearing an I226R gene deletion elicits robust immunity in pigs to African swine fever. *J. Virol.* 95:e0119921. doi: 10.1128/JVI.01199-21

Zhang, Y., Ke, J., Zhang, J., Yue, H., Chen, T., Li, Q., et al. (2021a). I267L is neither the virulence- nor the replication-related gene of African swine fever virus and its deletant is an ideal fluorescent-tagged virulence strain. *Viruses* 14:53. doi: 10.3390/v14010053

Zhang, G., Liu, W., Gao, Z., Chang, Y., Yang, S., Peng, Q., et al. (2022). Antigenic and immunogenic properties of recombinant proteins consisting of two immunodominant African swine fever virus proteins fused with bacterial lipoprotein. OprI. *Virol. J.* 19:16. doi: 10.1186/s12985-022-01747-9

Zhang, K., Yang, B., Shen, C., Zhang, T., Hao, Y., Zhang, D., et al. (2022). MGF360-9L is a major virulence factor associated with the African swine fever virus by antagonizing the JAK/STAT signaling pathway. *MBio* 13:e0233021. doi: 10.1128/mbio.02330-21

Zhang, J., Zhang, Y., Chen, T., Yang, J., Yue, H., Wang, L., et al. (2021). Deletion of the L7L-L11L genes attenuates ASFV and induces protection against homologous challenge. *Viruses* 13:255. doi: 10.3390/v13020255

Zhang, H., Zhao, S., Zhang, H., Shen, Y., Zhang, P., Shan, H., et al. (2023). Orally administered recombinant Lactobacillus expressing African swine fever virus antigens that induced immunity responses. *Front. Microbiol.* 13:1103327. doi: 10.3389/fmicb.2022.1103327

Zhao, D., Liu, R., Zhang, X., Li, F., Wang, J., Zhang, J., et al. (2019). Replication and virulence in pigs of the first African swine fever virus isolated in China. *Emerg. Microbes. Infect.* 8, 438–447. doi: 10.1080/22221751.2019.1590128

Zhou, G., Shi, Z., Luo, J., Cao, L., Yang, B., Wan, Y., et al. (2022). Preparation and epitope mapping of monoclonal antibodies against African swine fever virus P30 protein. *Appl. Microbiol. Biotechnol.* 106, 1199–1210. doi: 10.1007/s00253-022-11784-7

Zhu, J. J. (2022). African swine fever vaccinology: the biological challenges from immunological perspectives. *Viruses* 14:2021. doi: 10.3390/v14092021

frontiers | Frontiers in Microbiology

TYPE Original Research
PUBLISHED 05 May 2023
DOI 10.3389/fmicb.2023.1164170

OPEN ACCESS

EDITED BY
Zhenyu Zhang,
University of Wisconsin-Madison, United States

REVIEWED BY
Sidang Liu,
Shandong Agricultural University, China
Hualei Wang,
Jilin University, China

*CORRESPONDENCE
Ruihua Zhang
✉ zhangruihua1012@163.com
Xiulei Cai
✉ xlcai_99@163.com
Hu Shan
✉ shanhu67@163.com

RECEIVED 12 February 2023
ACCEPTED 04 April 2023
PUBLISHED 05 May 2023

CITATION
Zhang H, Duan X, Liu G, Li Y, Dong S, Lin J, Zhang R, Cai X and Shan H (2023) Comparative transcriptomic analysis of PK15 cells infected with a PRV variant and the Bartha-K/61 vaccine strain. *Front. Microbiol.* 14:1164170. doi: 10.3389/fmicb.2023.1164170

Comparative transcriptomic analysis of PK15 cells infected with a PRV variant and the Bartha-K/61 vaccine strain

Hongliang Zhang[1], Xiaoxiao Duan[2], Gang Liu[1], Yingguang Li[1], Shaoming Dong[1], Jiaxu Lin[1], Ruihua Zhang[3]*, Xiulei Cai[1]* and Hu Shan[1]*

[1]Shandong Collaborative Innovation Center for Development of Veterinary Pharmaceuticals, College of Veterinary Medicine, Qingdao Agricultural University, Qingdao, China, [2]Qingdao Animal Disease Prevention and Control Center, Qingdao, China, [3]Key Laboratory of Preventive Veterinary Medicine, Department of Veterinary Medicine, Animal Science College, Hebei North University, Zhangjiakou, China

Introduction: Pseudorabies virus (PRV) is a herpesvirus that can infect domestic animals, such as pigs, cattle and sheep, and cause fever, itching (except pigs), and encephalomyelitis. In particular, the emergence of PRV variants in 2011 have resulted in serious economic losses to the Chinese pig industry. However, the signaling pathways mediated by PRV variants and their related mechanisms are not fully understood.

Methods: Here, we performed RNA-seq to compare the gene expression profiling between PRV virulent SD2017-infected PK15 cells and Bartha-K/61-infected PK15 cells.

Results: The results showed that 5,030 genes had significantly different expression levels, with 2,239 upregulated and 2,791 downregulated. GO enrichment analysis showed that SD2017 significantly up-regulated differentially expressed genes (DEGs) were mainly enriched in the binding of cell cycle, protein and chromatin, while down-regulated DEGs were mainly enriched in ribosomes. KEGG enrichment analysis revealed that the pathways most enriched for upregulated DEGs were pathways in cancer, cell cycle, microRNAs in cancer, mTOR signaling pathway and autophagy-animal. The most down-regulated pathways of DEGs enrichment were ribosome, oxidative phosphorylation, and thermogenesis. These KEGG pathways were involved in cell cycle, signal transduction, autophagy, and virus-host cell interactions.

Discussion: Our study provides a general overview of host cell responses to PRV virulent infection and lays a foundation for further study of the infection mechanism of PRV variant strain.

KEYWORDS

pseudorabies virus, mutant, Bartha-K/61, PK15 cells, RNA-seq, transcriptomic

Introduction

Pseudorabies (PR), also known as Aujeszky's disease (AD), is an acute and severe infectious disease caused by Pseudorabies virus (PRV) (Wozniakowski and Samorek-Salamonowicz, 2015). PRV can infect a variety of mammals, including humans, pigs, dogs, and rodents (Müller et al., 2011; Holt et al., 2014; Yang et al., 2019). Pigs are the natural host of PRV, and PRV infection in pigs can cause nervous system disorders, respiratory diseases, abortion of pregnant sows, and piglet death, causing huge economic losses to the pig industry (Cui et al., 2018; He et al., 2019). Until 2011, the Bartha-K6 strain vaccine was widely used in China to control PR. PRV variants began to circulate in China at the end of 2011, and

new features emerged after the virus-infected pigs (Yu et al., 2014; Wu et al., 2017). Many large-scale pig farms immunized with the Bartha-K/61 strain vaccine showed the epidemic of PRV (Cui et al., 2018; Sun et al., 2018). Phylogenetic analysis classified the mutants into PRV II type (Ye et al., 2015). To prevent and control the epidemic of PRV scientifically, it is necessary to understand the pathogenic mechanism of PRV mutants and analyze the changes in various biological signal pathways in host cells after PRV infection.

With the development of high-throughput sequencing technology, it is possible to transfer the study of virus–host cell interaction from the detailed decomposition to the whole system. By integrating bioinformatic data, a comprehensive understanding of viral infections can be achieved. Among these, transcriptomics, as a useful tool for the systematic study of the physiological and chemical states of cells, has emerged as an important tool for the study of the cellular mechanisms and molecular functions of viral infection (Zhang et al., 2017; Chen et al., 2022). The bioinformatics analysis of differentially expressed genes (DEGs) extracted from transcripts after virus infection is helpful for a comprehensive understanding of the host response (Ai et al., 2021). For example, the changes in various biological processes and related molecules in the core pathway provide an important basis for the analysis of viral pathogenesis (Zhang et al., 2017; Liu et al., 2018; Reyes et al., 2018). At present, there are few reports about the transcriptomic differences of PK15 cells infected by PRV with different virulence. The Bartha-K/61 vaccine appeared to provide only suboptimal protection against these variants (Wu et al., 2013; Sun et al., 2018), although other studies do show adequate protection against such variants (An et al., 2013; Wang and Zhang, 2019). Because of this controversy, we attempted to analyze the differences between the PRV variant and conventional vaccine strain on infected host cells by transcriptomic techniques. In this study, the transcripts of PK15 cells infected with the PRV SD2017 variant strain and Bartha-K/61 strain were analyzed. The results provide a reference for understanding the mechanism of pathogenicity and immune evasion of the PRV mutants.

Materials and methods

Virus and cell lines

The wild-type PRV mutant SD2017 strain was isolated from the brain of a PRV-infected piglet in December 2017 in Linyi, Shandong province. Sequence analysis showed that both the 48th and 497th amino acid sequences of gE protein had L-Aspartic Acid insertion (D), which was consistent with the mutation characteristics of PRV type II mutants prevalent in China. The SD2017 strain was preserved in the Chinese General Microbiological Culture Collection Center (No. 22047). The main genomic information of the SD2017 strain has been published in GenBank (Acc. No. MW535259-MW535265). The PRV Bartha-K/61 vaccine strain was obtained from Shandong Huahong Biological Engineering Co., Ltd. PK15 (Sus scrofa epithelial kidney) cells used for PRV culture were obtained from the American Type Culture Collection (Manassas, VA, USA).

Cell culture and virus infection

PK15 porcine kidney cells were cultured in DMEM (Gibco, Grand Island, NY, USA) containing 10% fetal bovine serum (Gibco, Grand Island, NY, USA) at 37°C in 5% CO_2 in a humidified incubator. Confluent PK15 cell monolayers were dispersed with 0.25% trypsin and 0.02% EDTA, seeded in 6 cm cell culture flasks, cultured for 24 h to 70% confluency, and washed two times with PBS before virus infection. PRV SD2017 and PRV Bartha-K/61 were added at an MOI of 0.1 for 1 h, and the cells were then washed followed by the addition of 2% FBS/DMEM. PBS was used for mock-infected control. Cells were harvested at 24 h post-infection (hpi) in three independent biological replicates. A porcine pseudorabies virus (gB gene) Real-time PCR Detection Kit (Biotephy, Qingdao, China) was used for the quantitative detection of PRV.

Total RNA from PRV SD2017 strain-infected, Bartha-K/61 strain-infected, and non-infected PK15 cells was extracted using TRIzol reagent (Invitrogen, Shanghai, China), and the concentration and purity of RNA samples were determined using a NanoDrop ND-1000 spectrophotometer (Nano Drop Inc., Wilmington, DE, USA). The integrity of total RNA samples was determined using an Agilent 2100 Bioanalyzer system (Agilent Technologies, Santa Clara, CA, USA).

Library construction and transcriptome sequencing

A total amount of 1 μg RNA per sample was used as input material for the RNA sample preparations. Sequencing libraries were generated using a NEBNext® UltraTM RNA Library Prep Kit for Illumina® (NEB, USA), following the manufacturer's recommendations, and index codes were added to attribute sequences to each sample.

To preferentially select cDNA fragments of 250–300 bp in length, the library fragments were purified with the AMPure XP system (Beckman Coulter, Beverly, USA). Then, 3 μl of USER Enzyme (NEB, USA) was used with size-selected, adaptor-ligated cDNA at 37°C for 15 min, followed by 5 min at 95°C before PCR. Then, PCR was performed with Phusion High-Fidelity DNA polymerase, Universal PCR primers, and Index (X) Primer. At last, PCR products were purified (AMPure XP system), and library quality was assessed on an Agilent Bioanalyzer 2100 system. The clustering of the index-coded samples was performed on a cBot Cluster Generation System using a TruSeq PE Cluster Kit v3-cBot-HS (Illumina), according to the manufacturer's instructions. After cluster generation, the library preparations were sequenced on an Illumina NovaSeq platform, and 150 bp paired-end reads were generated.

Data analysis

Raw data (raw reads) of FASTQ format were first processed through in-house Perl scripts. Reference genome and gene model annotation files Sus scrofa 11.1 were downloaded from

Ensembl (ftp://ftp.ensembl.org/pub/release-91/fasta/sus_scrofa/dna) directly. The index of the reference genome was built using Hisat2 v2.0.5, and paired-end clean reads were aligned to the reference genome using Hisat2 v2.0.5. Feature Counts v1.5.0-p3 was used to count the read numbers mapped to each gene, and then, FPKM of each gene was calculated based on the length of the gene and reads count mapped to this gene. Differential expression analysis of two groups was performed using the DESeq2 R package (1.16.1). DESeq2 provides statistical routines for determining differential expression in digital gene expression data using a model based on the negative binomial distribution. The resulting *P*-values were adjusted using Benjamini and Hochberg's approach for controlling the false discovery rate. Genes with an adjusted *P*-value of <0.05 found by DESeq2 were assigned as differentially expressed. Gene Ontology (GO) enrichment analysis of DEGs was implemented by the cluster Profiler R package, in which gene length bias was corrected. GO terms with a corrected *P*-value of <0.05 were considered to be significantly enriched by differentially expressed genes. KEGG (http://www.genome.jp/kegg/) is a database resource for understanding high-level functions and utilities of the biological system. We used the cluster Profiler R package to test the statistical enrichment of differentially expressed genes in KEGG pathways.

RT-qPCR validation of differentially transcribed genes

A total of nine genes with increased or decreased transcription levels were randomly selected according to the sequencing results, and glyceraldehyde-3-phosphate dehydrogenase (GAPDH) was used as the internal reference gene to validate the high-throughput sequencing results. Primers were designed using Premier 6.0 (Table 1). The total RNA of samples was reverse-transcribed into cDNA using HiScript® II Q RT SuperMix for qPCR (Vazyme, Nanjing, China) as a template for qPCR. The relative transcription levels of each gene were calculated using the $2^{-\Delta\Delta Ct}$ method, and the *t*-test was performed using GraphPad Prism 5.0.

TABLE 1 Primers for real-time PCR.

Gene name	Primer	Primer sequence (5′ → 3′)	Product size (bp)
FKBP5	F	AGTCTCCCCAAAATTCCCTCG	148
	R	TCGCTCCTTCGTTGGGATTTG	
ARHGAP2	F	CTGCCCAACGGCTATGTGAC	73
	R	TGTTGTGCTGGCCCGACTCTC	
DUSP6	F	CAGCGACTGGAACGAGAATAC	123
	R	AACTCGGCTTGGAACTTACTG	
TCF19	F	GTTGGCAGAACTGGACGATGAG	132
	R	CGAGGACGCCCACGACGATT	
AIMP1	F	AAGTGCTGACTCAAAGCCTGTT	256
	R	CATTACCATTGCCTGAGATACTACT	
NPM1	F	GAAAAAACTCCTAAAACACCG	176
	R	CACTGCCAGAGATCTTGAAT	
VAPB	F	AACCCGACAGACCGGAATGTG	138
	R	ATCATAATCGAAAGGCTGTAACATC	
SLC25A40	F	ACGTTTCCAGGGAACGCTG	97
	R	TGCCATCACTAAGGTAGGAGG	
SLC37A4	F	GGACTCCGCAACCTGGACCCT	145
	R	AGCACGTCTTTACGCCAAATACC	

Results

Kinetics of PRV propagation in PK15 cells

PK15 cells were infected with the PRV SD2017 strain and Bartha-K/61 strain at 0.1 MOI, respectively. Quantitative analysis of PRV at 24 hpi was performed using a fluorescence quantitative PCR assay. CT values (23.8 and 24.2) showed that viral replication remained at a high level in both PRV-infected groups (Figure 1). Therefore, PK15 cells can be sampled for transcriptome sequencing at 24 hpi.

Quality control of sequencing data

RNA was extracted from PRV SD2017-infected PK15 cells and Bartha-K/61-infected PK15 cells (three replicates per group). RNA integrity was assessed using an Agilent 2100 bioanalyzer (Figure 2).

The library was constructed according to the instructions of the NEBNext® Ultra™ RNA Library Prep Kit and sequenced using an Illumina high-throughput sequencing platform (Hi Seq/Mi Seq). The mean original readings for samples from the SD2017 (SD) group were 55,275,026 and 63,529,356 for samples from the Bartha-K/61 (BK) group. After filtering out low-quality reads, we obtained an average of 53,796,261 clean reads from the SD2017 group and 61,989,240 clean reads from the Bartha-K/61 group. Percentage values of Q20 and Q30 were higher than 97.71 and 94.03%, respectively (Table 2), which met data quality requirements and could be used for subsequent analysis.

Analysis of DEGs

To screen the DEGs of PRV SD2017 and Bartha-K/61-infected PK15 cells, DEG analysis was performed by DESeq2, as biological replicas were available in this study. Compared with Bartha-K/61 samples in $|\log2(\text{FoldChange})| > 0$ & padj < 0.05. A total of 2,239 significantly upregulated genes and 2,791 significantly downregulated genes were screened under the 0.05 criterion (Figure 3A; Supplementary Table S1). We used mainstream hierarchical clustering to perform cluster analysis on FPKM (fragments per kilobase million) values of genes and conducted Z-score for row homogenization. As shown in Figure 3B, different gene expression trends were observed in SD2017 and Bartha-K/61 samples, indicating that infection with

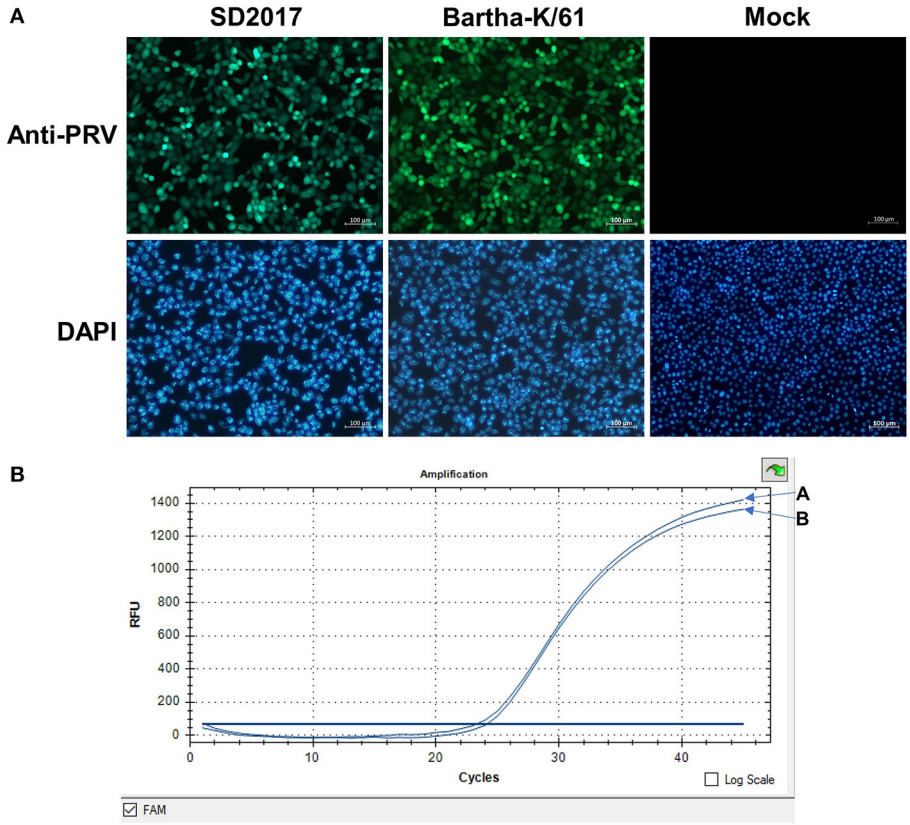

FIGURE 1
Detection of PRV in PK15 cells by fluorescence quantitative PCR. **(A)** PRV SD2017-infected PK15 cells. **(B)** PRV Bartha-K/61-infected PK15 cells.

these two strains induced significant gene expression changes in PK15 cells.

GO Analysis of DEGs

Gene Ontology (GO) is a comprehensive database describing gene function, which can be divided into three parts as follows: biological process, cellular component, and molecular function. Taking padj <0.05 as the threshold for significant GO enrichment, enrichment analysis results of DEGs GO in PRV SD2017 and Bartha-K/61-infected PK15 cells were obtained from Supplementary Table S2. The 30 terms with the most significant upregulation and downregulation were selected to draw bar charts for display (Figure 3). Among GO terms with significant enrichment of upregulated genes (Figure 4A), mitotic cell cycle process (GO:1903047), cell cycle phase transition (GO:0044770), cell cycle G1/S phase transition (GO:0044843), and mitotic cell cycle phase transition (GO:0044772) were the four most prominent in the BP category. In addition, protein domain-specific binding (GO:0019904) and chromatin binding (GO:0003682) were the most prominent GO terms in the MF category. In terms of the significantly enriched GO of downregulated genes (Figure 4B), ribosome (0042254), cytosolic ribosome (GO:0022626), and ribosomal subunit (GO:0044391) were the three most prominent GO terms in the CC category. Moreover, the structural constituent of ribosome (GO:0003735) was the most prominent GO term in the MF category. GO results showed that compared with Bartha-K/61 infection, SD2017 infection significantly upregulated DEGs enrichment mainly in the cell cycle, protein, and chromatin binding while downregulated DEGs were mainly enriched in ribosomes.

KEGG analysis of DEGs

From the KEGG enrichment results (Supplementary Table S3), the most significant 20 KEGG pathways were selected to draw scatter plots for presentation, as shown in Figure 5. The KEGG enrichment analysis showed that pathways with the most upregulated DEGs enrichment (Figure 5A) were pathways in cancer (KEGG: ssc05200), cell cycle (KEGG: ssc04110), microRNAs in cancer (KEGG: ssc05206), mTOR signaling pathway (KEGG: ssc04150), and autophagy-animal (KEGG: ssc04140). The pathways with the most downregulated DEG enrichment (Figure 5B) were ribosome (KEGG: ssc03010), oxidative phosphorylation (KEGG: ssc00190), thermogenesis (KEGG: KEGG: ssc04714), Parkinson's disease (KEGG: ssc05012), and Alzheimer's disease (KEGG: ssc05010). These KEGG pathways were mainly related to cell cycle, signal transduction, and autophagy and were involved in virus–host cell interactions.

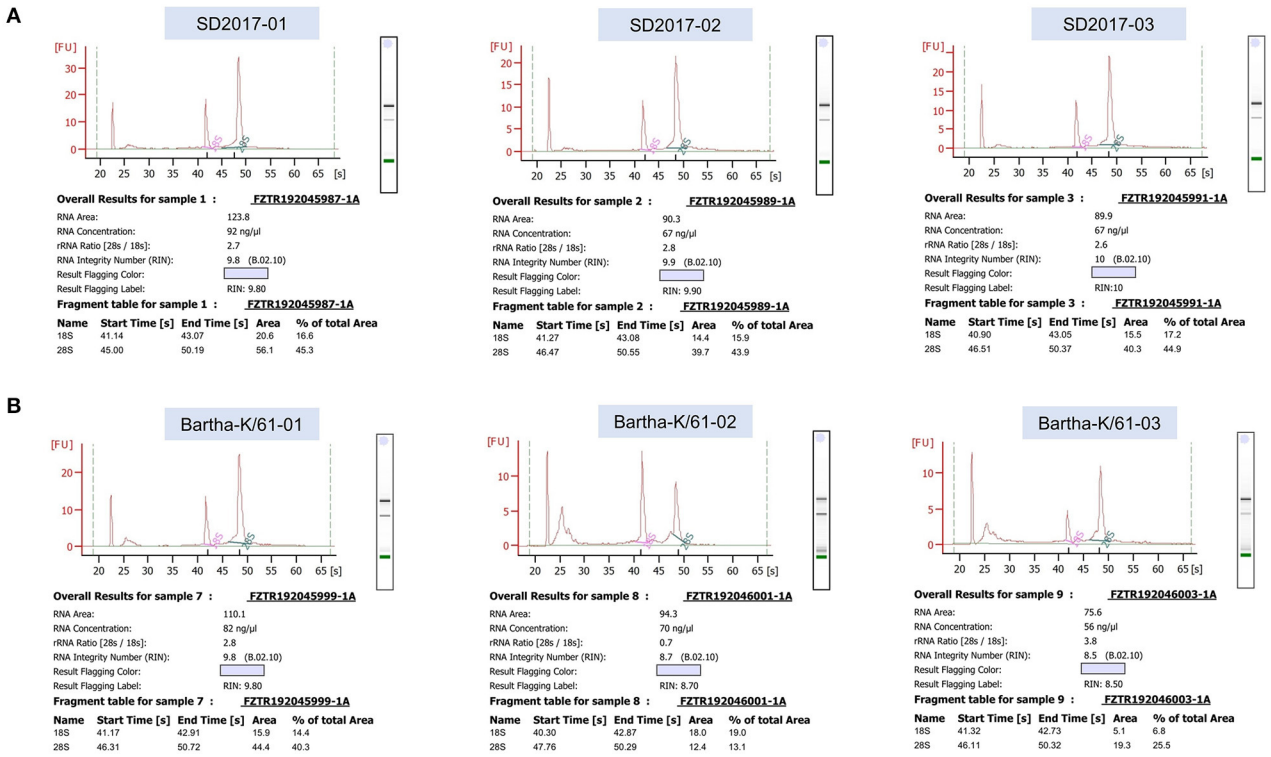

FIGURE 2
Results of RNA integrity testing of transcriptome sequencing samples. **(A)** PRV SD2017-infected PK15 cell samples. **(B)** PRV Bartha-K/61-infected PK15 cell samples.

TABLE 2 Analysis of RNA-seq sequencing data quality assessment.

Sample	Raw_reads	Clean_reads	Clean_bases	Error_rate	Q20 (%)	Q30 (%)	GC (%)
SD01	54,592,364	52,915,068	7.94G	0.02	98.12	94.60	56.20
SD02	53,995,846	52,509,870	7.88G	0.02	98.01	94.35	56.06
SD03	57,236,868	55,963,846	8.39G	0.03	97.90	94.03	56.03
BK01	63,211,510	61,728,968	9.26G	0.03	97.71	94.07	69.69
BK02	62,468,336	60,805,442	9.12G	0.02	97.87	94.38	68.95
BK03	64,908,222	63,433,310	9.51G	0.03	97.78	94.16	70.75

Validation of the expression of DEGs by qRT-PCR

To further validate the transcriptome analysis results, we performed a qPCR analysis to determine the reproducibility of the differential gene expression. GAPDH mRNA was amplified as the endogenous control. A total of four upregulated genes (*FKBP5*, *ARHGAP24*, *DUSP6*, and *TCF19*) and five downregulated genes (*AIMP1*, *NPM1*, *VAPB*, *SLC25A40*, and *SLC37A4*) were analyzed. As shown in Figure 6 and Supplementary Table S4, the qRT-PCR results corresponded with transcriptome analysis results. Interestingly, many DEG expressed proteins are important regulators of host immune responses. For example, the upregulation of dual-specificity phosphatase 6 (DUSP6) impairs infectious bronchitis virus replication by negatively regulating the ERK pathway and promoting apoptosis (Ma C. et al., 2022). Aminoacyl tRNA synthetase complex interacting multifunctional protein 1 (AIMP1) regulates TCR signaling and induces differentiation of regulatory T cells by interfering with lipid raft binding (Chen et al., 2021). AIMp1 enhances Th1 polarization and is essential for effective antitumor and antiviral immunity (Liang et al., 2017). The absence of vesicle-associated membrane protein-associated protein B (VAPB) regulates autophagy in a Beclin 1-dependent manner (Escande-Beillard et al., 2020).

Discussion

In recent years, high-throughput sequencing has been widely used in the study of differential transcriptomes caused by a viral infection, providing basic data for the analysis of viral infection

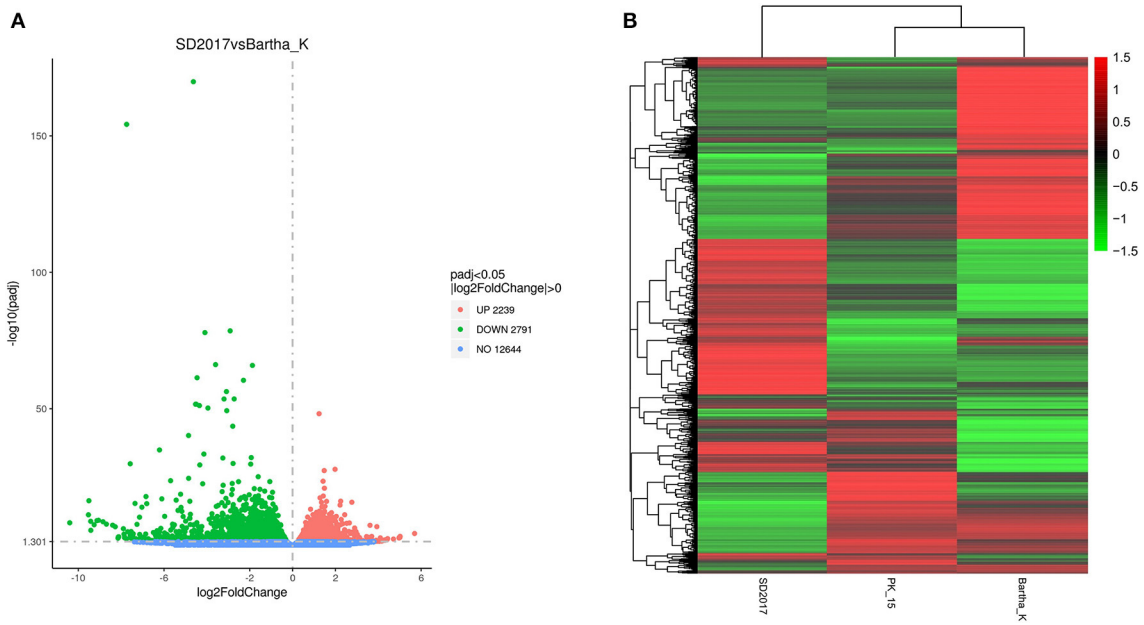

FIGURE 3
Quantitative analysis of DEGs. **(A)** Volcano plots of the distribution of DEGs. The *x*-axis is the log2FoldChange value, the *y*-axis is −log10padj, and the blue dotted line represents the threshold line of the differential gene screening criteria. **(B)** Cluster map of DEGs. The *x*-axis is the sample name, and the *y*-axis is the normalized value of the differential gene FPKM. The redder the color, the higher the expression, and the greener the color, the lower the expression.

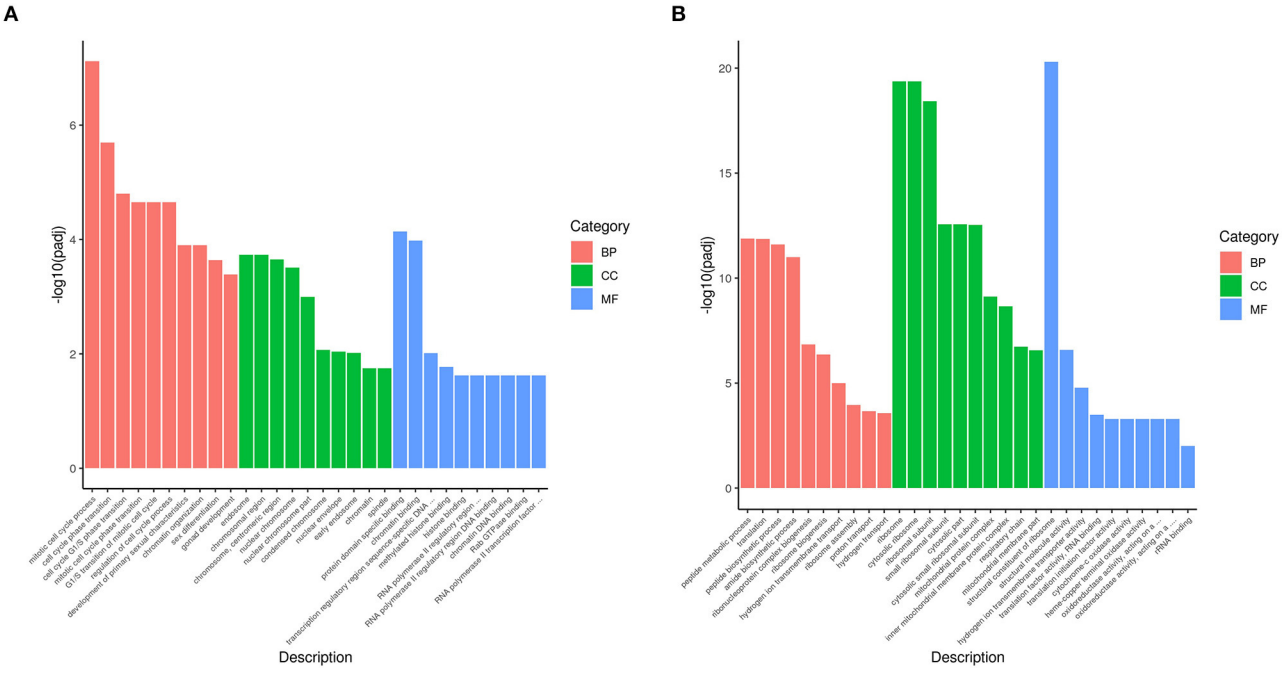

FIGURE 4
GO annotation of analysis of DEGs. **(A)** GO functional classification of the upregulated DEGs. **(B)** GO functional classification of the downregulated DEGs. The *x*-axis is GO Term. The *y*-axis is the significance level of GO term enrichment. The higher the value, the higher the significance. The different colors represent the three GO subclasses of BP, CC, and MF.

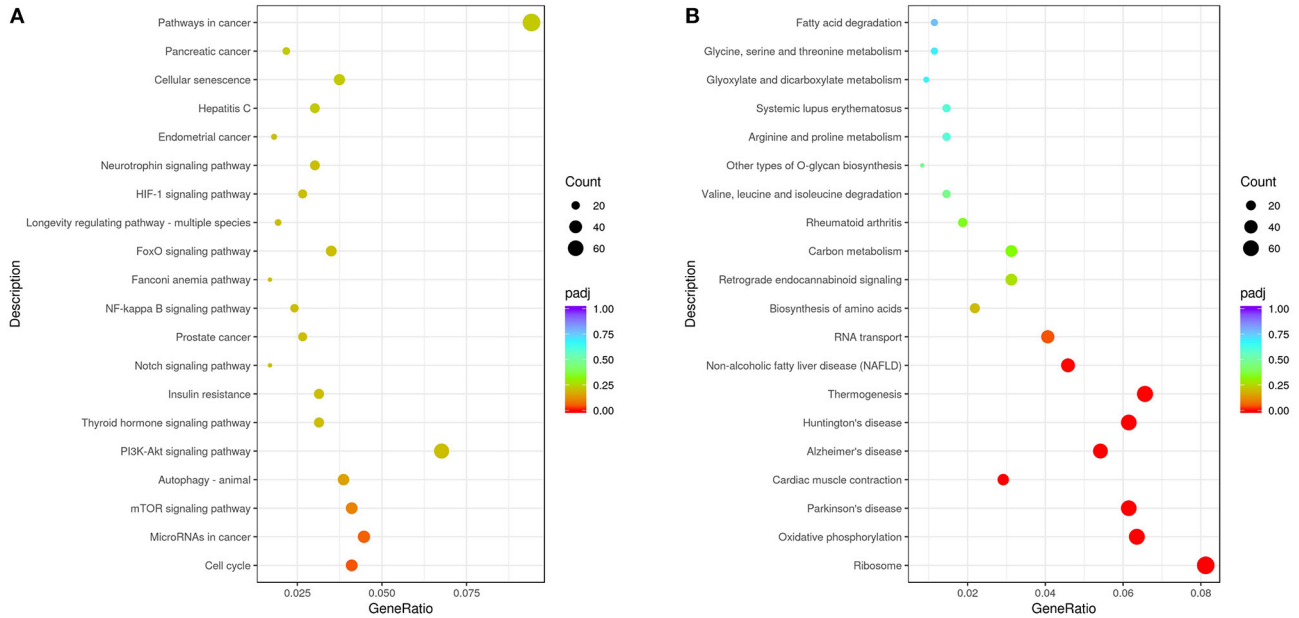

FIGURE 5
Analysis of KEGG enrichment. **(A)** Analysis of KEGG enrichment of the upregulated DEGs. **(B)** Analysis of KEGG enrichment of the downregulated DEGs. The *x*-axis is the ratio of the number of differential genes annotated to the KEGG pathway to the total number of differential genes. The *y*-axis is the KEGG pathway. The size of the dots represents the number of genes annotated to the KEGG pathway, and the color from red to purple represents the significance of the enrichment.

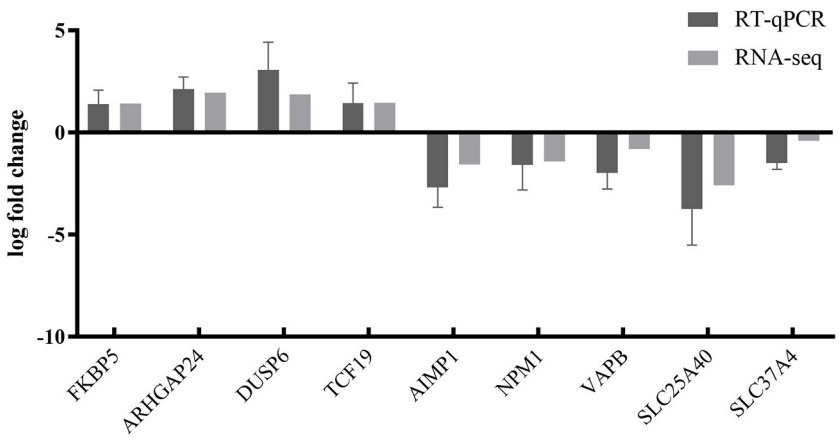

FIGURE 6
Comparison of fold changes of DEGs between RNA-seq and qRT-PCR. PK15 cells were infected with PRV SD2017 and Bartha-K/61 for 24 h; then, qRT-PCR was performed to detect the relative expression of selected DEGs. The horizontal axis represents the name, and the vertical axis indicates log2 fold changes of DEGs.

mechanisms (Wang et al., 2019a; Ai et al., 2021). Recent reports have shown that functional lncRNAs and differential circRNA in PRV type II infected cells (Thomas et al., 2012; Rodríguez-Galán et al., 2021). However, there are few reports on the transcriptomic differences of PK15 cells infected by PRV with different virulence. Liu et al. analyzed the differential expression of miRNA induced by the PRV Fa ΔgE/gI strain and Fa wild strain in PK15 cells. GO analysis showed that the differentially expressed miRNA target genes in PK15 cells infected by PRV Faδge/gI and Fa wild strains were mainly involved in biological regulation and metabolic processes. STRING analysis showed that immune-related target genes of differentially expressed miRNAs in the toll-like receptor, B-cell receptor, T-cell receptor, nuclear factor-κB, and transforming growth factor-β signaling pathways were correlated (Wang et al., 2017). To comprehensively understand the changes in the total transcription level of cells infected with PRV type II mutant wild strain and traditional vaccine strain, the DEGs of PRV SD2017-infected PK15 cells and Bartha-K/61-infected PK15 cells were analyzed in this study. A total of 2,239 genes were upregulated. The expression of 2,791 genes was downregulated. These DEGs widely exist in cellular components, such as cell membranes and cytoplasm, and are involved in

various intracellular processes. The results showed that the SD2017 infection caused a violent cell response. To identify the signaling pathways involved in DEGs, GO, and KEGG databases were used for enrichment analysis. GO functional annotation of differential genes showed that they were mainly enriched in cell cycle, protein and chromatin binding, and ribosome (Figure 4). A total of 13 KEGG pathways were significantly enriched, including cell cycle, mTOR signaling pathway, autophagy-animal, ribosome, oxidative phosphorylation, thermogenesis, Parkinson's disease, and Alzheimer's disease (Figure 5). These results suggest that PRV type II mutant wild strain infection has extensive effects on host cells. This is the first report of differential transcriptome infecting pig cell lines with PRV mutant wild strain and Bartha-K/61 vaccine strain.

Previous studies have shown that PRV infection can lead to changes in cellular immunity, metabolism, nucleic acid degradation, biosynthesis, MAPK, and many other biological processes and pathways. For example, PRV-encoded UL13 protein kinase acts as an antagonist of innate immunity by targeting IRF3 signaling pathways (Lv et al., 2020). PRV mediates apoptosis and DNA degradation by inducing oxidative stress and MAPK pathways (Yeh et al., 2008; Lai et al., 2019). Heat shock protein 27 (Hsp27) attenuates cGAS-mediated IFN-β signaling through ubiquitination of cGAS and promotes PRV infection (Li et al., 2022). PRV infection can induce the degradation of interferon type I receptors and lead to the upregulation of interferon-stimulated gene 15 (ISG15) expression (Zhang et al., 2017; Liu et al., 2018). The latency-associated transcript (LAT) gene is the only transcriptional region during latent infection of PRV that plays the key role in regulating viral latent infection and inhibiting apoptosis (Deng et al., 2022). The GO and KEGG enrichment results of DEGs in this study are consistent with the above conclusions. Compared with Bartha-K/61, PRV SD2017-infected PK15 cells, aminoacyl tRNA synthetase complex interacting multifunctional protein 1 (AIMP1), transforming growth factor beta induced (TGFBI), and tetraspanin CD9 were downregulated. In particular, CD9 is a key regulator of cell adhesion in the immune system (Reyes et al., 2018). These results suggest that the immune response of host cells to PRV SD2017 infection may be mediated by the above immune-related pathways. In addition, the peptide metabolic process, amide biosynthetic process, ribonucleoprotein complex biogenesis, ribosome assembly, mitochondrial protein complex, and other metabolism-related pathways have been enriched. This has suggested that PRV SD2017 infection may break the original material metabolism and biosynthesis process of PK15 cells, which is significantly different from Bartha-K/61-infected cells. In conclusion, the differential transcriptome data caused by infection of PRV variants in this study are the basis for analyzing the interaction between virus and host cells at the molecular level and also the premise for further exploring the pathogenic mechanism and immune response of PRV variants.

Viruses use a variety of strategies and molecular targets to influence host cell processes. These include cell cycle regulation, cytokine-mediated signaling, and immune response. Moreover, viruses often manipulate the host cell cycle to create a favorable environment for replication (Fan et al., 2018). It has been reported that RIPK3-dependent necroptosis limits PRV replication in PK15 cells (Gou et al., 2021). Although there have been many reports on the pathogenesis of PRV and its interaction with the host in recent years, the changes in the target cells of PRV after infection remain unclear (Li et al., 2019; Wang et al., 2019b). Our results showed that infection of PRV SD2017 significantly upregulated the cell cycle pathway of PK15 cells compared with Bartha-K/61. The related DEGs in the cell cycle pathway include ORC1, CDKN1B, SMAD3, CDC25C, MCM7, FZR1, CDC23, CDC25B, and CDC14B. The expression of these DEGs affects the cell cycle and thus the replication of the virus. Especially, short protein-binding motifs in ORC1 and CDC6 control the initiation of DNA replication (Hossain et al., 2021). Cyclin-dependent kinase inhibitor 1B (CDKN1B) mediates apoptosis of neuronal cells and inflammation induced by oxyhemoglobin via miR-502-5p (Chen et al., 2020). As an important cell cycle regulatory protein, cell division cycle 25C (CDC25C) activates the cyclin B1/CDK1 complex in cells for entering mitosis and regulates G2/M progression (Liu et al., 2020). Fizzy-related 1 (FZR1) is an activator of the anaphase-promoting complex/cyclosome (APC/C) and an important regulator of the mitotic cell division cycle (Holt et al., 2014). Cell division cycle 25 B (CDC25B) is a member of the CDC25 phosphatase family. It can dephosphorylate cyclin-dependent kinases and regulate the cell division cycle. Moreover, siRNA knockdown of CDC25B impairs influenza A virus (IAV) replication (Cui et al., 2018). Cell division cycle 14B (CDC14B) regulates mammalian RNA polymerase II and represses cell cycle transcription (Guillamot et al., 2011). The findings of these DEGs help us to understand the mechanism of PRV variant strain infection affecting host cells and provide new ideas for the development of targeted drugs.

At present, there have been many studies on the interaction between PRV and host natural immune signaling pathways. For example, after PRV infects cells, TNF-α can induce autophagy by activating p38 MAPK and JNK/SAPK signaling pathways (Yeh et al., 2008). In addition, PRV can degrade JAK through the proteasome pathway and inhibit the expression of interferon-stimulating genes (Yin et al., 2021). Compared with Bartha-K/61-infected cells, it was also found that PRV SD2017-infected PK15 cells showed DEGs in multiple innate immune pathways, such as the mTOR signaling pathway, autophagy-animal, the NF-κB signaling pathway, the TNF signaling pathway, and the NOD-like receptor signaling pathway. Autophagy plays a crucial role in maintaining cellular homeostasis and is closely related to the occurrence of a variety of diseases. Many studies have shown that a number of signal transduction pathways are involved in the regulation of autophagy (Jung et al., 2010; Yu et al., 2010; Wang and Zhang, 2019). Previous research has shown that the tegument protein UL21 (unique long region 21) in PRV dampens type I interferon signaling by triggering the degradation of CGAS (cyclic GMP–AMP synthase) through the macroautophagy/autophagy–lysosome pathway (Ma Z. et al., 2022). PRV induced autophagy via the classical Beclin-1-Atg7-Atg5 pathway to enhance viral replication in N2a cells *in vitro* (Xu et al., 2018). PRV infection triggers persistent NF-κB activation in an unorthodox way and dramatically modulates the NF-κB signaling axis, preventing typical proinflammatory gene expression and the responsiveness of cells to canonical NF-κB signaling, which may aid the virus in modulating early proinflammatory responses in the infected host (Romero et al., 2020). These results are helpful to further

explore the molecular mechanism of the PRV variant escaping host immunity.

In conclusion, in this study, differential transcriptome data of PRV SD2017 and Bartha-K/61 strains-infected PK15 cells were obtained by high-throughput sequencing and bioinformatic analysis. We also enriched DEGs into various biological processes, such as metabolism, immunity, biosynthesis, cell cycle, autophagy, and NF-κB signaling pathways. It provided basic data for further study on the molecular mechanism of PRV variant infection.

Data availability statement

The original contributions presented in the study are included in the article/Supplementary material, further inquiries can be directed to the corresponding authors.

Author contributions

HZ and RZ designed the experiments, wrote the manuscript, and analyzed the data analysis. HZ, XD, SD, YL, and JL carried out the experiments. GL and XC performed writing—review and editing. XC and HS checked the manuscript. All authors read and approved the final version. All authors agree to be accountable for the content of the study.

Funding

This research was funded by the China Science and Technology Innovation 2030 Major Project (No. 2021 ZD0113802), the Project of Shandong Province Science and Technology Achievement Transfer Transformation Subsidy (No. 2021 LYXZ020), and the China Agriculture Research System of MOF and MARA.

Acknowledgments

We thank Professor Yongjun Wen for technical support.

Conflict of interest

The authors declare that the research was conducted in the absence of any commercial or financial relationships that could be construed as a potential conflict of interest.

Publisher's note

All claims expressed in this article are solely those of the authors and do not necessarily represent those of their affiliated organizations, or those of the publisher, the editors and the reviewers. Any product that may be evaluated in this article, or claim that may be made by its manufacturer, is not guaranteed or endorsed by the publisher.

Supplementary material

The Supplementary Material for this article can be found online at: https://www.frontiersin.org/articles/10.3389/fmicb.2023.1164170/full#supplementary-material

References

Ai, Q., Lin, X., Xie, H., Li, B., Liao, M., Fan, H., et al. (2021). Proteome analysis in PAM cells reveals that african swine fever virus can regulate the level of intracellular polyamines to facilitate its own replication through ARG113. *Viruses* 13, 1236. doi: 10.3390./v13071236

An, T. Q., Peng, J. M., Tian, Z. J., Zhao, H. Y., Li, N., Liu, Y. M., et al. (2013). Pseudorabies virus variant in Bartha-K61-vaccinated pigs, China, 2012. *Emerg. Infect. Dis.* 19, 1749–55. doi: 10.3201/eid1911.130177

Chen, D., Wang, X., Huang, J., Cui, S., and Zhang, L. (2020). CDKN1B mediates apoptosis of neuronal cells and inflammation induced by oxyhemoglobin via miR-502-5p after subarachnoid hemorrhage. *J. Mol. Neurosci.* 70, 1073–1080. doi: 10.1007/s12031-020-01512-z

Chen, S., Zhang, X., Nie, Y., Li, H., Chen, W., Lin, W., et al. (2021). African swine fever virus protein E199L promotes cell autophagy through the interaction of PYCR2. *Virol. Spin*. 36, 196–206. doi: 10.1007/s12250-021-00375-x

Chen, Y., Cai, Q., Pan, C., Liu, W., Li, L., Liu, J., et al. (2022). CDK2 inhibition enhances antitumor immunity by increasing IFN response to endogenous retroviruses. *Cancer Immunol. Res*. 10, 525–539. doi: 10.1158/2326-6066.CIR-21-0806

Cui, L., Mahesutihan, M., Zheng, W., Meng, L., Fan, W., Li, J., et al. (2018). CDC25B promotes influenza A virus replication by regulating the phosphorylation of nucleoprotein. *Virology* (2018) 525, 40–7. doi: 10.1016/j.virol.09, 005.

Deng, J., Wu, Z., Liu, J., Ji, Q., and Ju, C. (2022). The role of latency-associated transcripts in the latent infection of pseudorabies virus. *Viruses* 14, 1379. doi: 10.3390/v14071379

Escande-Beillard, N., Loh, A., Saleem, S. N., Kanata, K., Hashimoto, Y., Altunoglu, U., et al. (2020). Loss of PYCR2 causes neurodegeneration by increasing cerebral glycine levels via SHMT2. *Neuron* (2020) 107, 82–94.e6. doi: 10.1016/j.neuron.03, 028.

Fan, Y., Sanyal, S., and Bruzzone, R. (2018). Breaking bad: how viruses subvert the cell cycle. *Front. Cell. Infect. Microbiol.* 8, 396. doi: 10.3389/fcimb.2018.00396

Gou, H., Bian, Z., Cai, R., Chu, P., Song, S., Li, Y., et al. (2021). RIPK3-dependent necroptosis limits PRV replication in PK-15 cells. *Front. Microbiol.* 12, 664353. doi: 10.3389/fmicb.2021.664353

Guillamot, M., Manchado, E., Chiesa, M., Gómez-López, G., Pisano, D. G., Sacristán, M. P., et al. (2011). Cdc14b regulates mammalian RNA polymerase II and represses cell cycle transcription. *Sci. Rep.* 1, 189. doi: 10.1038/srep00189

He, W., Auclert, L. Z., Zhai, X., Wong, G., Zhang, C., Zhu, H., et al. (2019). Interspecies transmission, genetic diversity, and evolutionary dynamics of pseudorabies virus. *J. Infect. Dis.* 219, 1705–1715. doi: 10.1093/infdis/jiy731

Holt, J. E., Pye, V., Boon, E., Stewart, J. L., García-Higuera, I., Moreno, S., et al. (2014). The APC/C activator FZR1 is essential for meiotic prophase I in mice. *Development* 141, 1354–1365. doi: 10.1242/dev.104828

Hossain, M., Bhalla, K., and Stillman, B. (2021). Multiple, short protein binding motifs in ORC1 and CDC6 control the initiation of DNA replication. *Mol. Cell.* (2021) 81, 1951–69.e6. doi: 10.1016/j.molcel.03, 003.

Jung, C. H., Ro, S. H., Cao, J., Otto, N. M., and Kim, H. D. (2010). mTOR regulation of autophagy. *FEBS Lett.* 584, 1287–1295. doi: 10.1016/j.febslet.01, 017.

Lai, I. H., Chang, C. D., and Shih, L. W. (2019). Apoptosis induction by pseudorabies virus via oxidative stress and subsequent DNA damage signaling. *Intervirology* 62, 116–123. doi: 10.1159/000502047

Li, X., Xie, J., Li, D., Li, H., Niu, Y., Wu, B., et al. (2022). HSP27 attenuates cGAS-mediated IFN-β signaling through ubiquitination of cGAS and promotes PRV infection. *Viruses* 14, 1851. doi: 10.3390/v14091851

Li, X., Zhang, W., Liu, Y., Xie, J., Hu, C., Wang, X., et al. (2019). Role of p53 in pseudorabies virus replication, pathogenicity, and host immune responses. *Vet. Res.* 50, 9. doi: 10.1186/s13567-019-0627-1

Liang, D., Tian, L., You, R., Halpert, M. M., Konduri, V., Baig, Y. C., et al. (2017). AIMp1 potentiates T(H)1 polarization and is critical for effective antitumor and antiviral immunity. *Front. Immunol.* 8, 1801. doi: 10.3389/fimmu.2017.01801

Liu, H., Li, S., Yang, X., Wang, X., Li, Y., Wang, C., et al. (2018). Porcine ISG15 modulates the antiviral response during pseudorabies virus replication. *Gene* (2018) 679, 212–8. doi: 10.1016/j.gene.09, 007.

Liu, K., Zheng, M., Lu, R., Du, J., Zhao, Q., Li, Z., et al. (2020). The role of CDC25C in cell cycle regulation and clinical cancer therapy: a systematic review. *Cancer Cell Int.* 20, 213. doi: 10.1186/s12935-020-01304-w

Lv, L., Cao, M., Bai, J., Jin, L., Wang, X., Gao, Y., et al. (2020). PRV-encoded UL13 protein kinase acts as an antagonist of innate immunity by targeting IRF3-signaling pathways. *Vet. Microbiol.* 250, 108860. doi: 10.1016/j.vetmic.2020.108860

Ma, C., Gao, B., Wang, Z., You, W., Yu, Z., Shen, H., et al. (2022). GrpEL1 regulates mitochondrial unfolded protein response after experimental subarachnoid hemorrhage *in vivo* and *in vitro*. *Brain Res. Bull.* (2022) 181, 97–108. doi: 10.1016/j.brainresbull.01, 014.

Ma, Z., Bai, J., Jiang, C., Zhu, H., Liu, D., Pan, M., et al. (2022). Tegument protein UL21 of alpha-herpesvirus inhibits the innate immunity by triggering CGAS degradation through TOLLIP-mediated selective autophagy. *Autophagy* (2022). 1–21. doi: 10.1080./15548627.2022.2139921

Müller, T., Hahn, E. C., Tottewitz, F., Kramer, M., Klupp, B. G., Mettenleiter, T. C., et al. (2011). Pseudorabies virus in wild swine: a global perspective. *Arch. Virol.* 156, 1691–1705. doi: 10.1007/s00705-011-1080-2

Reyes, R., Cardeñes, B., Machado-Pineda, Y., and Cabañas, C. (2018). Tetraspanin CD9: a key regulator of cell adhesion in the immune system. *Front. Immunol.* 9, 863. doi: 10.3389/fimmu.2018.00863

Rodríguez-Galán, A., Dosil, S. G., Gómez, M. J., Fernández-Delgado, I., Fernández-Messina, L., Sánchez-Cabo, F., et al. (2021). MiRNA post-transcriptional modification dynamics in T cell activation. *iScience* 24, 102530. doi: 10.1016/j.isci.2021.102530

Romero, N., Van Waesberghe, C., and Favoreel, W. H. (2020). Pseudorabies virus infection of epithelial cells leads to persistent but aberrant activation of the NF-κB pathway, inhibiting hallmark NF-κB-induced proinflammatory gene expression. *J. Virol.* 94, e00196–e00120. doi: 10.1128/JVI.00196-20

Sun, Y., Liang, W., Liu, Q., Zhao, T., Zhu, H., Hua, L., et al. (2018). Epidemiological and genetic characteristics of swine pseudorabies virus in mainland China between 2012 and 2017. *PeerJ* 6, e5785. doi: 10.7717/peerj.5785

Thomas, M. F., Abdul-Wajid, S., Panduro, M., Babiarz, J. E., Rajaram, M., Woodruff, P., et al. (2012). Eri1 regulates microRNA homeostasis and mouse lymphocyte development and antiviral function. *Blood* 120, 130–142. doi: 10.1182/blood-2011-11-394072

Wang, C., Li, D., Zhang, L., Jiang, S., Liang, J., Narita, Y., et al. (2019a). Sequencing analyses of gene expression during epstein-barr virus infection of primary B lymphocytes. *J. Virol.* 93, JVI.00226–19. doi: 10.1128./JVI.00226-19

Wang, J., Kang, L., Song, D., Liu, L., Yang, S., Ma, L., et al. (2017). Ku70 senses HTLV-1 DNA and modulates HTLV-1 replication. *J. Immunol.* 199, 2475–2482. doi: 10.4049/jimmunol.1700111

Wang, J., Wang, C. F., Ming, S. L., Li, G. L., Zeng, L., Wang, M. D., et al. (2019b). Porcine IFITM1 is a host restriction factor that inhibits pseudorabies virus infection. *Int. J. Biol. Macromol.* (2020) 151:1181–93. doi: 10.1016/j.ijbiomac.10, 162.

Wang, Y., and Zhang, H. (2019). Regulation of autophagy by mTOR signaling pathway. *Adv. Exp. Med. Biol.* 1206, 67–83. doi: 10.1007/978-981-15-0602-4_3

Wozniakowski, G., and Samorek-Salamonowicz, E. (2015). Animal herpesviruses and their zoonotic potential for cross-species infection. *Ann. Agric. Environ. Med.* 22, 191–194. doi: 10.5604/12321966.1152063

Wu, R., Bai, C., Sun, J., Chang, S., and Zhang, X. (2013). Emergence of virulent pseudorabies virus infection in northern China. *J. Vet. Sci.* 14, 363–365. doi: 10.4142/jvs.14, 3.363

Wu, X. M., Chen, Q. Y., Chen, R. J., Che, Y. L., Wang, L. B., Wang, C. Y., et al. (2017). Pathogenicity and whole genome sequence analysis of a pseudorabies virus strain FJ-2012 isolated from Fujian, Southern China. *Can. J. Infect. Dis. Med. Microbiol.* 2017, 9073172. doi: 10.1155/2017/9073172

Xu, C., Wang, M., Song, Z., Wang, Z., Liu, Q., Jiang, P., et al. (2018). Pseudorabies virus induces autophagy to enhance viral replication in mouse neuro-2a cells *in vitro*. *Virus Res.* (2018) 248, 44–52. doi: 10.1016/j.virusres.02, 004.

Yang, H., Han, H., Wang, H., Cui, Y., Liu, H., Ding, S., et al. (2019). Case of human viral encephalitis caused by pseudorabies virus infection in China. *Front. Neurol.* 10, 534. doi: 10.3389/fneur.2019.00534

Ye, C., Zhang, Q. Z., Tian, Z. J., Zheng, H., Zhao, K., Liu, F., et al. (2015). Genomic characterization of emergent pseudorabies virus in China reveals marked sequence divergence: evidence for the existence of two major genotypes. *Virology* 483, 32–43. doi: 10.1016/j.virol.04, 013.

Yeh, C. J., Lin, P. Y., Liao, M. H., Liu, H. J., Lee, J. W., Chiu, S. J., et al. (2008). TNF-alpha mediates pseudorabies virus-induced apoptosis via the activation of p38 MAPK and JNK/SAPK signaling. *Virology* (2008) 381, 55–66. doi: 10.1016/j.virol.08,023.

Yin, Y., Romero, N., and Favoreel, W. H. (2021). Pseudorabies virus inhibits Type I and Type III interferon-induced signaling via proteasomal degradation of Janus Kinases. *J. Virol.* 95, e0079321. doi: 10.1128/JVI.00793-21

Yu, L., McPhee, C. K., Zheng, L., Mardones, G. A., Rong, Y., Peng, J., et al. (2010). Termination of autophagy and reformation of lysosomes regulated by mTOR. *Nature* 465, 942–946. doi: 10.1038/nature09076

Yu, X., Zhou, Z., Hu, D., Zhang, Q., Han, T., Li, X., et al. (2014). Pathogenic pseudorabies virus, China, 2012. *Emerg. Infect. Dis.* 20, 102–104. doi: 10.3201/eid2001.130531

Zhang, R., Xu, A., Qin, C., Zhang, Q., Chen, S., Lang, Y., et al. (2017). Pseudorabies virus dUTPase UL50 induces lysosomal degradation of type i interferon receptor 1 and antagonizes the alpha interferon response. *J. Virol.* (2017) 91, JVI.01148–17. doi: 10.1128./JVI.01148-17

frontiers | Frontiers in Microbiology

TYPE Original Research
PUBLISHED 11 May 2023
DOI 10.3389/fmicb.2023.1120305

OPEN ACCESS

EDITED BY
Qing Pan,
Qingdao Agricultural University, China

REVIEWED BY
Marthie Magdaleen Ehlers,
University of Pretoria, South Africa
Ján Matiašovic,
Veterinary Research Institute (VRI), Czechia

*CORRESPONDENCE
Paola Cremonesi
✉ paola.cremonesi@ibba.cnr.it

†These authors have contributed equally to this work

RECEIVED 11 December 2022
ACCEPTED 24 April 2023
PUBLISHED 11 May 2023

CITATION
Locatelli C, Gattolin S, Monistero V, Castiglioni B, Moroni P, Addis MF and Cremonesi P (2023) *Staphylococcus aureus coa* gene sequence analysis can prevent misidentification of coagulase-negative strains and contribute to their control in dairy cow herds.
Front. Microbiol. 14:1120305.
doi: 10.3389/fmicb.2023.1120305

Staphylococcus aureus coa gene sequence analysis can prevent misidentification of coagulase-negative strains and contribute to their control in dairy cow herds

Clara Locatelli[1,2†], Stefano Gattolin[3†], Valentina Monistero[1,2], Bianca Castiglioni[3], Paolo Moroni[1,2,4], Maria Filippa Addis[1,2] and Paola Cremonesi[3*]

[1]Department of Veterinary Medicine and Animal Sciences, Università degli Studi di Milano, Lodi, Italy, [2]Laboratorio di Malattie Infettive degli Animali, Università degli Studi di Milano, Lodi, Italy, [3]Italian National Research Council, Institute of Agricultural Biology and Biotechnology, Lodi, Italy, [4]Quality Milk Production Services, Animal Health Diagnostic Center, Cornell University, Ithaca, NY, United States

Accurate and precise differentiation of staphylococci isolated from milk is of importance for udder health management. In particular, the rapid and specific identification of *Staphylococcus aureus* plays an essential role in the prevention and treatment programs for bovine mastitis. Plasma gelatinization in coagulase assays is routinely used to discriminate *S. aureus* from other species by detecting the presence of extracellular free staphylocoagulase. However, rarely occurring coagulase-deficient *S. aureus* strains can be responsible for clinical and subclinical mastitis cases. By investigating *S. aureus* isolates from a single herd over a 10-year period we identified the persistence of a phenotypically coagulase-negative *S. aureus* strain and pinpointed the possible cause to a single base pair deletion in the *coa* gene sequence. Our results support the need to integrate primary biochemical tests with molecular/sequence analysis approaches for correctly identifying and discriminating atypical *S. aureus* in bovine herds, as the coagulase test alone may fail to detect persistent mastitis-causing strains.

KEYWORDS

coagulase gene, dairy cow, genotyping, sequencing, *Staphylococcus aureus*

1. Introduction

The family *Staphylococcaceae* comprises the genus *Staphylococcus*, a diverse group of gram-positive bacteria globally recognized as commensal colonizers of humans and warm-blooded animals (Founou et al., 2018). In food-producing animals, their principal reservoirs are the skin and mucosa of pigs, chickens, sheep, goats, and cows (Huber et al., 2011). Among them, the majority of species shares the inability to clot rabbit plasma and are referred to as coagulase-negative staphylococci (CoNS). Though CoNS are frequently detected in

dairy cattle (De Buck et al., 2021), they are considered "minor pathogens" (Hamel et al., 2020; Ryman et al., 2021). On the other hand, coagulase-positive staphylococci (CoPS) including *Staphylococcus aureus*, *S. intermedius* and *S. hyicus*, are ubiquitous and highly versatile microorganisms implicated in a large variety of infections, ranging from dermatitis to septicemia, with *S. aureus* being the best-known of these pathogens.

In dairy cows, *S. aureus* is predominantly classified as a contagious mastitis causative agent whose presence is more frequently associated with subclinical than clinical cases, although staphylococcal infections may also occur in clinical forms (Schroeder, 2012). This microorganism is characterized by lower recovery rates than the other staphylococci, despite the efforts in controlling its presence and spread in dairy herds (Exel et al., 2022). The accurate and precise differentiation of staphylococci isolated from milk samples has therefore a major impact on udder health management. In particular, the rapid and specific identification of *S. aureus* plays an essential role in bovine mastitis prevention and treatment programs, at the point that CoNS are currently referred as Non-*aureus* Staphylococci (NAS), stressing this dichotomy. As this species differs from other staphylococcal species for being generally β-hemolytic, the hemolysis detection can also represent a fast and cost-effective method for testing the presumptive *S. aureus* presence in primary cultures, despite the low sensitivity and specificity (Ryman et al., 2021). However, previous studies demonstrated that almost 20–25% of *S. aureus* isolates from bovine intramammary infections (IMIs) show no visible β-hemolysis on blood agar plates (Ryman et al., 2021). On the other hand, as several NAS species also show β-hemolysis, selective media like Baird-Parker + RPF (Rabbit Plasma Fibrinogen) Agar or Mannitol Salt Agar (MSA) can be alternatively used for the differential growth of staphylococci (Pumipuntu et al., 2017). Nevertheless, the former works through the same principle of coagulase activity and the latter yields positive reaction also with some NAS.

Therefore, in diagnostic laboratories using primary and secondary biochemical tests for bacterial species identification, the coagulase assay is most frequently used to differentiate *S. aureus* from NAS (Peetermans et al., 2015). The bound form or clumping factor can be detected by a slide test, while extracellular free *S. aureus* coagulase (staphylocoagulase) can be detected by plasma gelatinization in a standard coagulase test tube (CTT), normally prepared from rabbit or horse whole blood (Peetermans et al., 2015). This enzyme can prime the non-proteolytic activation of prothrombin and cleavage of fibrinogen to promote coagulation (McAdow et al., 2012). Nevertheless, some *S. aureus* strains may not express this major characteristic, producing false negative results (Akineden et al., 2011). These CTT-negative *S. aureus* could therefore be erroneously classified as NAS and managed as such, with a potential for a spread within the herd (Akineden et al., 2011; Sunagar et al., 2013).

Although Matrix-Assisted Laser Desorption/Ionization Time-of-Flight Mass Spectrometry (MALDI-TOF MS) technique is being increasingly applied in veterinary microbiology, many laboratories still carry out bacterial identification with primary biochemical tests as they are easy to set up and cost-effective. In these settings, coagulase deficiencies in *S. aureus* due to transcriptional or post-transcriptional alterations in the *coa* gene (McAdow et al., 2012) may therefore lead to an erroneous species identification, with adverse effects on udder health control programs.

In our laboratory work, we repeatedly isolated coagulase-deficient *S. aureus* from clinical and subclinical mastitis cases occurring in a single herd over a 10-year period. In this study, we present the detailed characterization of the *coa* gene of the coagulase-negative *S. aureus* strain isolated from this dairy farm with the aim of understanding the molecular basis for this phenotypic behavior and suggesting mitigation measures to possible identification bias.

2. Materials and methods

2.1. Sample collection and *S. aureus* identification

During the daily diagnostic activity at the Laboratorio di Malattie Infettive degli Animali (MiLab, Università degli Studi di Milano, Italy), from December 2013 to August 2022, a total of 31 staphylococcal isolates were obtained from as many milk samples from a single Italian dairy farm and presumptively identified as *S. aureus*. The samples (15 quarter clinical mastitis, 14 composite and 2 quarter milk samples with high somatic cell count, **Table 1**) were cultured and evaluated according to National Mastitis Council procedures (National Mastitis Council, 2017), including CTT (Pumipuntu et al., 2017). The typical colony morphology and the beta-hemolysis on blood agar suggested to subculture the isolates onto Mannitol Salt Agar (MSA, Oxoid, Basingstoke, United Kingdom) and Baird Parker with Rabbit Plasma (BP + RPF, Microbiol, Cagliari, Italy) for further characterization. All the isolates were frozen in Nutrient Broth (Microbiol, Cagliari, Italy) added with 15% glycerol (Carlo Erba Reagents, Milan, Italy) until further analyses.

2.2. DNA extraction and molecular identification

DNA was extracted using the DNA isolation system kit (Clonit, Medical System, Genova, Italy) according to the protocol described by Cremonesi et al. (2006), starting from step 2. DNA quality and quantity were measured using a NanoDrop ND-1000 spectrophotometer (Nano-Drop Technologies, Wilmington, DE); the samples were stored at −20°C until further use.

To check the specificity of the isolates, the DNA extracted was amplified with *nuc* (thermonuclease coding gene) and *coa* (coagulase coding gene) primers, as previously described (Cremonesi et al., 2005). As positive controls, *S. aureus* reference strains (ATCC 19040, ATCC 19041, ATCC 19048, ATCC 700699) were used in each PCR assay. All amplified PCR fragments were separated by 2% agarose gel electrophoresis (GellyPhor, Euroclone, Milan, Italy), stained with ethidium bromide (0.05 mg/mL; Sigma-Aldrich), and visualized under UV transilluminator (BioView Ltd., Nes Ziona, Israel). A 100-bp DNA ladder (Finnzymes, Espoo, Finland) was included in each gel.

TABLE 1 *Staphylococcus aureus* isolates collected from a single herd analyzed in this study.

No.	Isolates	Type of sample	Isolation date	Cow	Coagulase test	MALDI-TOF MS log score	Genotype
1	2948	Composite	10/12/2013	169	Negative	2.43	GTBN
2	2949	Clinical mastitis	10/12/2013	259 RR	Negative	2.28	GTBN
3	2937	Composite	28/10/2013	274	Negative	2.19	GTBN
4	2936	Composite	28/10/2013	169	Negative	2.39	GTBN
5	2947	Composite	10/12/2013	286	Negative	2.15	GTBN
6	2976	Composite	17/04/2014	297	Negative	2.32	GTBN
7	2977	Composite	17/04/2014	55	Negative	2.24	GTBN
8	2978	Composite	17/04/2014	213	Negative	2.37	GTBN
9	2979	Clinical mastitis	17/04/2014	169 FR	Negative	2.22	GTBN
10	2980	Clinical mastitis	17/04/2014	213 RR	Negative	2.21	GTBN
11	3023	Clinical mastitis	24/09/2014	354	Negative	2.47	GTBN
12	3119	Clinical mastitis	09/12/2015	161 FR	Negative	2.56	GTBN
13	3209	Composite	31/01/2017	316	Negative	2.33	GTBN
14	3245	Clinical mastitis	20/06/2017	245 FL	Negative	2.27	GTBN
15	3254	Clinical mastitis	10/10/2017	223	Negative	2.45	GTBN
16	3259	Quarter milk	15/01/2018	223	Negative	2.15	GTBN
17	3260	Quarter milk	15/01/2018	223	Negative	2.36	GTBN
18	3263	Clinical mastitis	05/06/2018	139 FL	Negative	2.25	GTBN
19	3264	Clinical mastitis	05/06/2018	312 RL	Negative	2.32	GTBN
20	3265	Composite	05/06/2018	223	Negative	2.54	GTBN
21	3277	Clinical mastitis	07/05/2019	156	Positive	2.50	GTA^{I}
22	3282	Composite	16/07/2019	26	Positive	2.42	GTA^{I}
23	3283	Composite	16/07/2019	61	Negative	2.31	GTBN
24	3473	Clinical mastitis	28/06/2022	21	Positive	2.19	GTA^{I}
25	3474	Clinical mastitis	28/06/2022	23	Positive	2.11	GTA^{I}
26	3482	Composite	22/08/2022	409	Negative	2.20	GTBN
27	3483	Clinical mastitis	22/08/2022	409	Negative	2.14	GTBN
28	56	Composite	22/08/2022	321	Positive	2.34	GTA
29	88	Composite	22/08/2022	299	Positive	2.30	GTA
30	117	Clinical mastitis	08/08/2022	37 FL	Positive	2.30	GTA
31	125	Clinical mastitis	08/08/2022	270 FR	Positive	2.36	GTA

2.3. Confirmation through MALDI-TOF MS

MALDI-TOF MS (Bruker Daltonik GmbH, Bremen, Germany) has been introduced in routine mastitis diagnostics at MiLab since January 2021. All the isolates were analyzed following the protocol described in Monistero et al. (2021) and Rosa et al. (2022).

2.4. RS-PCR typing

All the 31 isolates were also genotyped by RS-PCR as previously described with a detailed working protocol (Fournier et al., 2008; Graber, 2016). The method is based on the amplification of the 16S–23S rRNA intergenic spacer region. The PCR products were analyzed using the miniaturized electrophoresis system DNA 7500 LabChip (Agilent Technologies, Santa Clara, CA). Genotypes were inferred from the electrophoresis profile using the Mahal software, which is freely available online (Graber, 2016).[1]

2.5. Library preparation, sequencing, bioinformatics analysis

The DNA was amplified for the entire coagulase gene by using the following primers designed by the Primer3 programme[2]: FORWARD = GCCGCTTTAATACCAGCAAC;

1 https://mahal.vitech.dev/#/

2 https://primer3.ut.ee/

REVERSE = CTTCCGATTGTTCGATGCTT (amplicon size = 2268 bp). The PCR amplifications were performed in 25 μl volumes per sample. A total of 12.5 μl of GoTaq® Long PCR Master Mix, 2X (Promega Corporation, Madison, USA) and 0.2 μl of each primer (100 μM) were added to 2 μl of genomic DNA (5 ng/μl). A first amplification step was performed in an Applied Biosystem 2700 thermal cycler (ThermoFisher Scientific). Samples were denatured at 95°C for 2 min, followed by 30 cycles with a denaturing step at 94°C for 30 s, annealing at 55°C for 30 s and extension at 68°C for 2 min, with a final extension at 72°C for 10 min. The amplicons were then cleaned with Agencourt AMPure XP (Beckman, Coulter Brea, CA, USA) and libraries were prepared following the Nextera XT DNA library Prep Kit Protocol (Illumina, San Diego, CA, USA), using a tagmentation of 15 min with *Pdm*I enzyme. The libraries obtained were quantified by Real Time PCR with KAPA Library Quantification Kits (Kapa Biosystems, Inc., MA, USA), pooled in equimolar proportion and sequenced in one MiSeq (Illumina) run with 2 × 300-base paired-end reads. FASTQ files were mapped with BWA-MEM2 against staphylocoagulase GenBank locus sequence LOCUS JN861807 (strain MSSA_129) on the Galaxy Platform (Afgan et al., 2018) and reads coverage was visualized using IGV (Robinson et al., 2011).

2.6. Molecular phylogenetic analysis by the neighbor-joining method

CDS DNA sequences used for phylogenetic analysis from different *S. aureus* strains and subspecies were obtained from the NCBI database.[3] Phylogenetic relationships were estimated in MEGAX (Kumar et al., 2018). DNA sequences (**Supplementary material**) were aligned by MUSCLE with default settings. Where a frameshift mutation was present, the whole sequence was used to allow for a full length alignment. Evolutionary relationships among coagulase sequences were inferred by using the Neighbor-Joining method and evolutionary distances were computed using the Maximum Composite Likelihood method and are in the units of the number of base substitutions per site. The rate variation among sites was modeled with a gamma distribution. The reliability of the phylogenetic tree was estimated by setting 1000 bootstrap replicates.

2.7. Sanger sequencing

All the samples were also analyzed by conventional sanger sequencing. The DNA was amplified for the coagulase gene by using the following primers designed in conserved regions: FORWARD = ATGGGATAACAAAGCAGATG; REVERSE = GGTTCTTCAACTTTCTTCTC (amplicon size = 900 bp). The PCR amplifications were performed in 25 μl volumes per sample. A total of 12.5 μl of PCR Master Mix, 2X (Thermofisher Scientific) and 0.2 μl of each primer (100 μM) were added to 2 μl of genomic DNA (5 ng/μl). The amplification step was performed in an Applied Biosystem 2700 thermal cycler (ThermoFisher Scientific). Samples were denatured at 95°C for 2 min, followed by 30 cycles with a denaturing step at 95°C for 1 min, annealing at 54°C for 1 min and extension at 72°C for 1 min, with a final extension at 72°C for 10 min. The amplicons were then cleaned with Wizard® SV Gel and PCR Clean-Up System (Promega Italia, Milan, Italy) and the cleaned products were sequenced by Eurofins Genomics (Ebersberg, Germany), following the instructions of the manufacturer.

3. Results and discussion

3.1. Bacteriological analysis and coagulase test

As previously described (Akineden et al., 2011), the discrimination between CoPS and CoNS catalase-positive cocci represents one of the most important routine procedures for identifying the etiological agents of contagious mastitis within a dairy herd. Coagulase is considered a virulence factor and staphylococci that are not able to produce this protein are reported to be less pathogenic. This is why the CTT for *S. aureus* coagulase activity remains the reference and the most used method in the laboratory routine. Although rare, some atypical *S. aureus* strains may occur (Akineden et al., 2011; Sunagar et al., 2013) and coagulase test specificity should be considered to avoid misclassification. From bacteriological analysis, 23 isolates (10 quarter clinical mastitis, 11 composite and 2 quarter high somatic cell samples, **Table 1**) resulted unexpectedly negative at the coagulase test after both 4 and 24 h of incubation at 37°C. The 23 CTT-negative isolates found in this study demonstrated the importance of applying appropriate screening testing to avoid *S. aureus* misclassification and to prevent staphylococcal infection spread within farms. The remaining 8 *S. aureus* analyzed were CTT-positive isolates producing a typical coagulase halo around the colonies on BP-RPF demonstrating lecithinase activity, whereas this was weak to absent for the 23 CTT-negative isolates. Aside from CTT results, all 31 *S. aureus* isolates evaluated in this study showed a positive reaction on MSA, proving the higher sensitivity of this selective medium compared to BP-RPF. As an initial screening method and compared to CTT, using MSA represents a low cost good choice for a more sensitive and still acceptably rapid *S. aureus* identification. However, due to the limited specificity, *S. aureus* identified through MSA positive results should be confirmed by further molecular methods (Pumipuntu et al., 2017).

3.2. Molecular characterization: amplification of *nuc* and *coa* genes and RS-PCR analysis

The identification as *S. aureus* was also confirmed by MALDI-TOF results, with scores >2.00 for all the isolates (**Table 1**). A misidentified *S. aureus* due to a negative CTT could drive to severe consequences as the other virulence factors activity (i.e., enterotoxins) could be conserved. The MALDI-TOF identification was further supported by PCR on the thermonuclease (*nuc*)

3 https://www.ncbi.nlm.nih.gov/

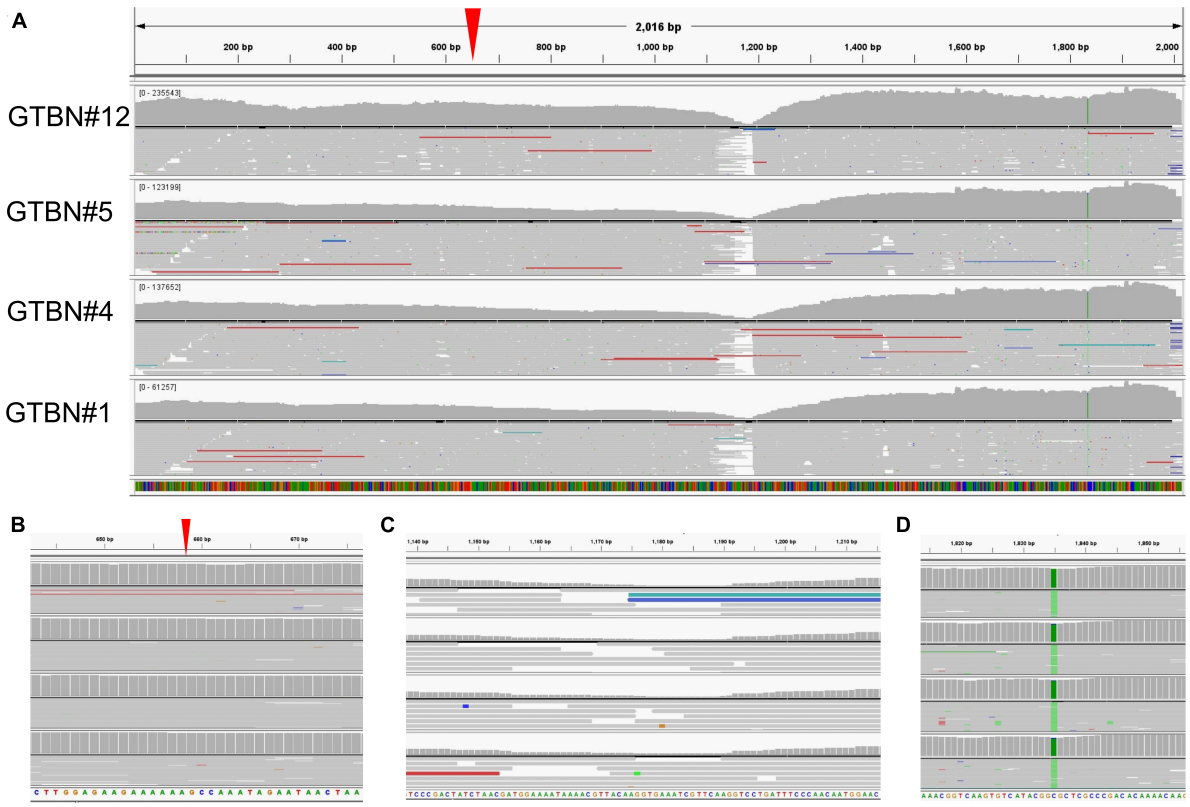

FIGURE 1
Molecular analysis of sequence variants observed in the GTBN coagulase genes. **(A)** Sequencing reads obtained from isolates GTBN#1, 4, 5, and 12 were mapped using MSSA_129 as reference sequence. Gray signals correspond to sequence identity with MSSA_129. The boxes show in more detail **(B)** the position of the single A deletion at position 653 bp in both the reference and the four samples (red arrowhead), **(C)** an area with drop in read coverage at around 1,165–1,190 and **(D)** a SNP (C to A) at position 1,835 common to all sequenced samples.

and coagulase (*coa*) genes for all the 31 isolates evaluated in this study. Moreover, the RS-PCR carried out for verification of the genotypes circulating in the herd in the time frame evaluated in this study revealed that all the 23 coagulase-negative *S. aureus* belonged to genotype GTBN (**Table 1**), while the 8 coagulase-positive *S. aureus* belonged to genotypes GTA (N = 6 in 2022) and GTA^{I} (n = 2 in 2019). Previous studies (Cremonesi et al., 2015; Cosandey et al., 2016) using the RS-PCR technique, however, demonstrated that *S. aureus* isolated from bovine IMIs are genetically heterogeneous, with some *S. aureus* genotypes showing a limited tendency to spread in the herd, as for GTBN, GTA and GTA^{I}. The knowledge of the characteristics of *S. aureus* circulating in the herd might help to formulate strategies for focused treatment and control of disease (Monistero et al., 2018).

3.3. Sequencing of the *coa* gene

Out of the 23 isolates with the same GTBN genotype, 4 (isolates number 1, 4, 5, 12) were randomly chosen and analyzed in one Miseq run in order to determine the nucleotide sequence of the *coa* gene. As previously described (Watanabe et al., 2005, 2009; Johler et al., 2012), this gene is known to be divided into six regions: the signal sequence, the D1 and D2 regions enabling contact with prothrombin, the central region, a repeat region, and the C-terminal sequence.

In order to choose a suitable reference for mapping, preliminary BLAST searches using individual reads from the FASTQ sequencing files were carried out against *S. aureus* from the GenBank database. Since all the reads used aligned to strain MSSA_129 (sequence JN861807, Johler et al., 2012), this strain was used as reference. The *coa* gene from the methicillin-susceptible *S. aureus* MSSA_129 strain was previously reported to harbor a single base deletion at position 653 within the D2 region of the gene, leading to a frameshift and premature termination of the resulting protein (Johler et al., 2012). The four GTBN *S. aureus* strains revealed the same sequence (**Figure 1A**), and complete identity to MSSA_129 around position 653 in the D2 region of the gene (**Figure 1B** and **Supplementary material 2A**). This was further confirmed in all the 23 GTBN isolates by Sanger sequencing, by using primers chosen in conserved regions between the sequences from GTBN of interest (isolates 1, 4, 5, 12) and sequences from non-GTBN genotypes (NCTC7485, ATCC6538, SA1428). Conversely, the deletion at position 653 was not observed in the GTA and GTA^{I} coagulase sequences. As the MSSA_129 strain (Johler et al., 2012), also all our GTBN samples would therefore be characterized by a premature stop codon resulting in a predicted 223 aa peptide that is most likely not functional. By inspecting the rest of the sequence, no differences to the reference used were found

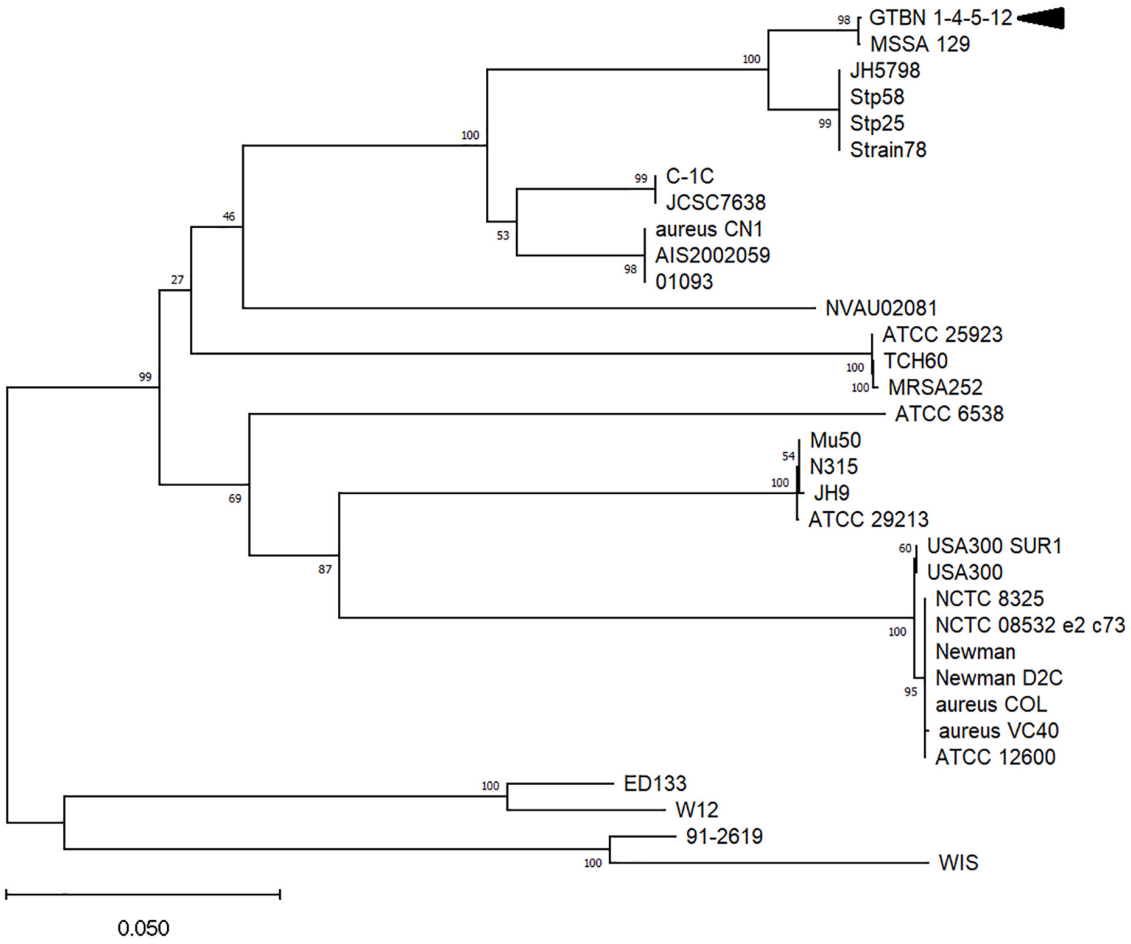

FIGURE 2
Evolutionary relationships among coagulase genes in different *Staphylococcus aureus* strains and subspecies. Only bootstrap values >50 are shown. The arrowhead indicates the sequence corresponding to the four isolates (GTBN#1, 4, 5, and 12).

in the central portion of the gene, not even at around 1,165–1,190 bp where fewer reads were available to ensure coverage (**Figure 1C**). Finally, sequence comparison revealed that the four GTBN strains could be genetically differentiated from the reference used (MSSA_129) by the presence of a SNP, (C to A) at position 1,835 (**Figure 1D**).

To gain insights into the variability of *coa* genes from different *S. aureus* strains and subspecies, the sequence from the GTBN isolates and that of MSSA_129 were aligned to 21 *coa* CDS obtained from GenBank (listed in **Supplementary material**), and their relationships were inferred by using the Neighbor-Joining method (**Figure 2**). This analysis showed that the sequences were separated in different clusters, and that those of GTBN isolates and MSSA_129 clustered closely, among others, with the two sequences Stp58 and Stp25 (Watanabe et al., 2009). These two were CTT-positive MSSA isolated in Japan (Watanabe et al., 2009). The Stp58 *coa* sequence was identical to the Stp25 *coa* sequence; their alignment revealed the lack of the single base deletion at position 653 bp observed in the 4 GTBN samples from this study (**Supplementary material 2B**), resulting in a predicted full length peptide in these two strains (**Supplementary material 2C**). Since Stp58 and Stp25 were reported as CTT-positive, this is further evidence that the base deletion is responsible for the lack of coagulase activity in GTBN 1, 4, 5, and 12.

The collection of samples over a 10-years period suggested the persistence of the low diffusive GTBN in the same herd; all these coagulase negative strains were characterized by an indel-mutation in *coa* gene. This study has potential limitations as analysis by using whole genome sequencing (WGS), cheaper today than few years ago, would provide deeper information on the atypical *S. aureus* circulating in bovine herds and allow to inspect the sequences of genes other than coagulase. However, the use of gene sequence analysis is nowadays still far from being a routine method, and in this specific case study this approach was enough to provide an answer to the issue encountered. As no single phenotypic test can guarantee reliable results in *S. aureus* detection, our work emphasizes the usefulness of MALDI-TOF or molecular methods in routine analyses to identify and discriminate atypical staphylococci from bovine mastitis cases. Where such advanced identification techniques are not yet available, combining the results of more than one test is crucial to avoid misidentification due to atypical strains. The knowledge about the epidemiology of coagulase–negative *S. aureus* genotypes might support control measures directed to reduce the spread of a contagious pathogen within dairy herds.

Data availability statement

The datasets presented in this study can be found in online repositories. The names of the repository/repositories and accession number(s) can be found below: NCBI SRA – SAMN32298094.

Author contributions

CL and PC designed and performed the experiments. SG helped with the data analysis. BC, PM, and MA gave advices to the researchers. VM, CL, SG, MA, and PC wrote the manuscript. All authors critically reviewed the manuscript and approved the final version.

Funding

This research was supported by the EU funding within the NextGenerationEU-MUR PNRR Extended Partnership initiative on Emerging Infectious Diseases (project no. PE00000007, INF-ACT).

Conflict of interest

The authors declare that the research was conducted in the absence of any commercial or financial relationships that could be construed as a potential conflict of interest.

Publisher's note

Supplementary material

The Supplementary Material for this article can be found online at: https://www.frontiersin.org/articles/10.3389/fmicb.2023.1120305/full#supplementary-material

References

Afgan, E., Baker, D., Batut, B., van den Beek, M., Bouvier, D., Cech, M., et al. (2018). The Galaxy platform for accessible, reproducible and collaborative biomedical analyses: 2018 update. *Nucl. Acids Res.* 46, W537–W544. doi: 10.1093/nar/gky379

Akineden, O., Hassan, A. A., Schneider, E., and Usleber, E. (2011). A coagulase-negative variant of *Staphylococcus aureus* from bovine mastitis milk. *J. Dairy Res.* 78, 38–42. doi: 10.1017/S0022029910000774

Cosandey, A., Boss, R., Luini, M., Artursson, K., Bardiau, M., Breitenwieser, F., et al. (2016). *Staphylococcus aureus* genotype B and other genotypes isolated from cow milk in European countries. *J. Dairy Sci.* 99, 529–540. doi: 10.3168/jds.2015-9587

Cremonesi, P., Castiglioni, B., Malferrari, G., Biunno, I., Vimercati, C., Moroni, P., et al. (2006). Technical note: Improved method for rapid DNA extraction of mastitis pathogens directly from milk. *J. Dairy Sci.* 89, 163–169. doi: 10.3168/jds.S0022-0302(06)72080-X

Cremonesi, P., Luzzana, M., Brasca, M., Morandi, S., Lodi, R., Vimercati, C., et al. (2005). Development of a multiplex PCR assay for the identification of *Staphylococcus aureus* enterotoxigenic strains isolated from milk and dairy products. *Mol. Cell Probes* 19, 299–305. doi: 10.1016/j.mcp.2005.03.002

Cremonesi, P., Pozzi, F., Raschetti, M., Bignoli, G., Capra, E., Graber, H. U., et al. (2015). Genomic characteristics of *Staphylococcus aureus* strains associated with high within-herd prevalence of intramammary infections in dairy cows. *J. Dairy Sci.* 98, 6828–6838. doi: 10.3168/jds.2014-9074

De Buck, J., Ha, V., Naushad, S., Nobrega, D. B., Luby, C., Middleton, J. R., et al. (2021). Non-aureus *Staphylococci* and bovine health: Current understanding and knowledge gaps. *Front. Vet. Sci.* 8:658031. doi: 10.3389/fvets.2021.658031

Exel, C. E., Halasa, T., Koop, G., Steeneveld, W., Lam, T. J. G. M., Benedictus, L., et al. (2022). A stochastic modelling approach to determine the effect of diverse *Staphylococcus aureus* strains on the economic and epidemiological outcomes of mastitis intervention strategies in dairy cattle. *Prev. Vet. Med.* 199:105566. doi: 10.1016/j.prevetmed.2021.105566

Founou, L. L., Founou, R. C., Essack, S. Y., and Djoko, C. F. (2018). Mannitol-fermenting methicillin-resistant staphylococci (MRS) in pig abattoirs in Cameroon and South Africa: A serious food safety threat. *Int. J. Food Microbiol.* 285, 50–60. doi: 10.1016/j.ijfoodmicro.2018.07.006

Fournier, C., Kuhnert, P., Frey, J., Miserez, R., Kirchhofer, M., Kaufmann, T., et al. (2008). Bovine *Staphylococcus aureus*: Association of virulence genes, genotypes and clinical outcome. *Res. Vet. Sci.* 85, 439–448. doi: 10.1016/j.rvsc.2008.01.010

Graber, H. U. (2016). Genotyping of *Staphylococcus aureus* by ribosomal spacer PCR (RS-PCR). *J. Vis. Exp.* 117:54623. doi: 10.3791/54623

Hamel, J., Zhang, Y., Wente, N., and Krömker, V. (2020). Non-*S. aureus* staphylococci (NAS) in milk samples: Infection or contamination? *Vet. Microbiol.* 242:108594. doi: 10.1016/j.vetmic.2020.108594

Huber, H., Ziegler, D., Pflüger, V., Vogel, G., Zweifel, C., and Stephan, R. (2011). Prevalence and characteristics of methicillin-resistant coagulase-negative staphylococci from livestock, chicken carcasses, bulk tank milk, minced meat, and contact persons. *BMC Vet. Res.* 7:6. doi: 10.1186/1746-6148-7-6

Johler, S., Moser, M., Engl, C., Tasara, T., Corti, S., Chen, J., et al. (2012). A coagulase- and α-glucosidase-negative variant of *Staphylococcus aureus*: A challenge for routine microbiological diagnostics. *J. Clin. Microbiol.* 50, 1827–1828. doi: 10.1128/JCM.06345-11

Kumar, S., Stecher, G., Li, M., Knyaz, C., and Tamura, K. (2018). MEGA X: Molecular evolutionary genetics analysis across computing platforms. *Mol. Biol. Evol.* 35, 1547–1549. doi: 10.1093/molbev/msy096

McAdow, M., Missiakas, D. M., and Schneewind, O. (2012). *Staphylococcus aureus* secretes coagulase and von Willebrand factor binding protein to modify the coagulation cascade and establish host infections. *J. Innate Immun.* 4, 141–148. doi: 10.1159/000333447

Monistero, V., Barberio, A., Cremonesi, P., Castiglioni, B., Morandi, S., Lassen, D. C. K., et al. (2021). Genotyping and antimicrobial susceptibility profiling of *Streptococcus uberis* isolated from a clinical bovine mastitis outbreak in a dairy farm. *Antibiotics (Basel)* 10:644. doi: 10.3390/antibiotics10060644

Monistero, V., Graber, H. U., Pollera, C., Cremonesi, P., Castiglioni, B., Bottini, E., et al. (2018). *Staphylococcus aureus* isolates from bovine mastitis in eight countries: Genotypes, detection of genes encoding different toxins and other virulence genes. *Toxins (Basel)* 10:247. doi: 10.3390/toxins10060247

National Mastitis Council (2017). *Laboratory handbook on bovine mastitis*, 3rd Edn. Verona, WI: National Mastitis Council.

Peetermans, M., Verhamme, P., and Vanassche, T. (2015). Coagulase activity by *Staphylococcus aureus*: A potential target for therapy? *Semin. Thromb. Hemost.* 41, 433–444. doi: 10.1055/s-0035-1549849

Pumipuntu, N., Kulpeanprasit, S., Santajit, S., Tunyong, W., Kong-Ngoen, T., Hinthong, W., et al. (2017). Screening method for *Staphylococcus aureus* identification in subclinical bovine mastitis from dairy farms. *Vet. World* 10, 721–726. doi: 10.14202/vetworld.2017.721-726

Robinson, J. T., Thorvaldsdóttir, H., Winckler, W., Guttman, M., Lander, E. S., Getz, G., et al. (2011). Integrative genomics viewer. *Nat. Biotechnol.* 29, 24–26. doi: 10.1038/nbt.1754

Rosa, N. M., Penati, M., Fusar-Poli, S., Addis, M. F., and Tola, S. (2022). Species identification by MALDI-TOF MS and gap PCR-RFLP of non-aureus *Staphylococcus*, *Mammaliicoccus*, and *Streptococcus* spp. associated with sheep and goat mastitis. *Vet. Res.* 53:84. doi: 10.1186/s13567-022-01102-4

Ryman, V. E., Kautz, F. M., and Nickerson, S. C. (2021). Case study: Misdiagnosis of nonhemolytic *Staphylococcus aureus* isolates from cases of bovine mastitis as coagulase-negative staphylococci. *Animals (Basel)* 11:252. doi: 10.3390/ani11020252

Schroeder, J. W. (2012). *Mastitis control programs: Bovine mastitis and milking management. AS1129 (Revised)*. Fargo, ND: NDSU Extension Circular, North Dakota State University, 1–15.

Sunagar, R., Deore, S. N., Deshpande, P. V., Rizwan, A., Sannejal, A. D., Sundareshan, S., et al. (2013). Differentiation of *Staphylococcus aureus* and *Staphylococcus epidermidis* by PCR for the fibrinogen binding protein gene. *J. Dairy Sci.* 96, 2857–2865. doi: 10.3168/jds.2012-5862

Watanabe, S., Ito, T., Sasaki, T., Li, S., Uchiyama, I., Kishii, K., et al. (2009). Genetic diversity of staphylocoagulase genes (*coa*): Insight into the evolution of variable chromosomal virulence factors in *Staphylococcus aureus*. *PLoS One* 4:e5714. doi: 10.1371/journal.pone.0005714

Watanabe, S., Ito, T., Takeuchi, F., Endo, M., Okuno, E., and Hiramatsu, K. (2005). Structural comparison of ten serotypes of staphylocoagulases in *Staphylococcus aureus*. *J. Bacteriol.* 187, 3698–3707. doi: 10.1128/JB.187.11.3698-3707.2005

frontiers | Frontiers in Microbiology

TYPE Review
PUBLISHED 17 July 2023
DOI 10.3389/fmicb.2023.1167085

OPEN ACCESS

EDITED BY
Qing Pan,
Qingdao Agricultural University, China

REVIEWED BY
Glenn Marsh,
Commonwealth Scientific and Industrial Research Organisation (CSIRO), Australia
Cameron Stewart,
Commonwealth Scientific and Industrial Research Organisation (CSIRO), Australia

*CORRESPONDENCE
Bradley S. Pickering
✉ bradley.pickering@inspection.gc.ca

RECEIVED 15 February 2023
ACCEPTED 26 June 2023
PUBLISHED 17 July 2023

CITATION
Li H, Kim J-YV and Pickering BS (2023) Henipavirus zoonosis: outbreaks, animal hosts and potential new emergence.
Front. Microbiol. 14:1167085.
doi: 10.3389/fmicb.2023.1167085

Henipavirus zoonosis: outbreaks, animal hosts and potential new emergence

Hongzhao Li[1], Ji-Young V. Kim[1] and Bradley S. Pickering[1,2,3]*

[1]National Centre for Foreign Animal Disease, Canadian Food Inspection Agency, Winnipeg, MB, Canada, [2]Department of Medical Microbiology and Infectious Diseases, College of Medicine, Faculty of Health Sciences, University of Manitoba, Winnipeg, MB, Canada, [3]Department of Veterinary Microbiology and Preventive Medicine, College of Veterinary Medicine, Iowa State University, Ames, IA, United States

Hendra virus (HeV) and Nipah virus (NiV) are biosafety level 4 zoonotic pathogens causing severe and often fatal neurological and respiratory disease. These agents have been recognized by the World Health Organization as top priority pathogens expected to result in severe future outbreaks. HeV has caused sporadic infections in horses and a small number of human cases in Australia since 1994. The NiV Malaysia genotype (NiV-M) was responsible for the 1998–1999 epizootic outbreak in pigs with spillover to humans in Malaysia and Singapore. Since 2001, the NiV Bangladesh genotype (NiV-B) has been the predominant strain leading to outbreaks almost every year in Bangladesh and India, with hundreds of infections in humans. The natural reservoir hosts of HeV and NiV are fruit bats, which carry the viruses without clinical manifestation. The transmission pathways of henipaviruses from bats to humans remain poorly understood. Transmissions are often bridged by an intermediate animal host, which amplifies and spreads the viruses to humans. Horses and pigs are known intermediate hosts for the HeV outbreaks in Australia and NiV-M epidemic in Malaysia and Singapore, respectively. During the NiV-B outbreaks in Bangladesh, following initial spillover thought to be through the consumption of date palm sap, the spread of infection was largely human-to-human transmission. Spillover of NiV-B in recent outbreaks in India is less understood, with the primary route of transmission from bat reservoir to the initial human infection case(s) unknown and no intermediate host established. This review aims to provide a concise update on the epidemiology of henipaviruses covering their previous and current outbreaks with emphasis on the known and potential role of livestock as intermediate hosts in disease transmission. Also included is an up-to-date summary of newly emerging henipa-like viruses and animal hosts. In these contexts we discuss knowledge gaps and new challenges in the field and propose potential future directions.

KEYWORDS

henipavirus, Hendra virus, Nipah virus, epidemiology, transmission, animal host, livestock, henipa-like virus

Introduction

Hendra virus (HeV) and Nipah virus (NiV) are highly virulent, prototypic members of the *henipavirus* genus in the *Paramyxoviridae* family (Chua et al., 1999; Nordin, 1999; Chua et al., 2000; ICTV, 2023). The viruses were named after outbreak locations where they were first isolated, the suburban town of Hendra in Australia (Murray et al., 1995; nsw.gov.au, 2023) and the village of Kampung Sungai Nipah in Malaysia (Mohd Nor et al., 2000), respectively. For the

purpose of this review, the term "henipaviruses" is used as traditionally represented for both HeV and NiV. A number of newly emerging viruses closely related to HeV and NiV are collectively referred to as "henipa-like viruses" here, including those that have been officially classified into the *henipavirus* genus (ICTV, 2023) and those whose potential classification into the genus remains to be confirmed. For the time being, these henipa-like viruses have largely uncertain zoonotic and pathogenic potential and are not (yet) established as major public health threats. However, despite the infancy of their research, signs of potentially far-reaching impact are emerging. Therefore, while the prototypic henipaviruses constitute the core of this review, we also summarize and provide perspectives on the new henipa-like viruses in terms of both challenges and opportunities.

The virions of henipaviruses are enveloped and pleomorphic with variable sizes from 120 to 500 nm and have an unsegmented single-stranded RNA genome of negative polarity (Chua et al., 2000). The henipaviral genome contains six protein-coding genes, nucleoprotein (N), phosphoprotein (P), matrix protein (M), fusion protein (F), glycoprotein (G) and large protein/polymerase (L), organized in the order of 3'-N-P-M-F-G-L-5'. The G protein was recently renamed as the receptor binding protein (Rima et al., 2019). However, we keep the traditional name for simplicity in the context of this review. The P gene also allows for the expression of three accessory proteins, V, W and C, through mRNA editing or alternative open reading frames. The genome lengths of henipaviruses (~ 18.2 kilobases) are longer (by ~15%) than those of other paramyxoviruses (~ 15.5 kilobases), largely due to the long 3′ untranslated regions of the N, P, F and G mRNAs (Eaton et al., 2006; Madera et al., 2022; Bruno et al., 2023).

In humans and several animal species, the major pathological consequence of henipaviral infection is a severe acute systemic vasculitis in many major organs, prominently in the brain and lung. This often leads to fatal neurological or/and respiratory disease, which also includes long-term relapsing encephalitis (from several months to over a decade following infection) (Playford et al., 2010; Wong and Ong, 2011; Wong and Tan, 2012; Broder et al., 2013; Abdullah and Tan, 2014; nsw.gov.au, 2023). Henipaviruses are classified as biosafety level 4 pathogens due to extremely high case fatality rates (CFR), up to 70–100% in some of the recent outbreaks, and the absence of licensed vaccines or therapeutics for human use (Skowron et al., 2021; Quarleri et al., 2022; Bruno et al., 2023). It should be noted that Equivac® HeV, a subunit vaccine based on a recombinant soluble and oligomeric form of the HeV G glycoprotein, was released in 2012 for immunization of horses in Australia. It is the first licensed (veterinary) vaccine against a biosafety level 4 agent (Broder et al., 2013). However, a human vaccine currently remains unavailable. The World Health Organization has listed henipaviruses as priority pathogens of epidemic and pandemic potential in urgent need for research and development (Sweileh, 2017; Mehand et al., 2018; WHO, 2023a,b,c).

HeV outbreaks: Australia

Since its emergence in 1994 in Australia, HeV has been causing sporadic infections in horses in most of the subsequent years, and on an annual basis since 2006, with the most recent case reported in July 2022 (Murray et al., 1995; Halpin and Rota, 2014; Wang et al., 2021; nsw.gov.au, 2023; qld.gov.au, 2023). Human infections have been linked to close contact with sick horses. To date, there have been 88 confirmed cases and 20 suspected cases of HeV infection in horses and seven confirmed cases in humans (nsw.gov.au, 2023; qld.gov.au, 2023). Although the case numbers have so far been small, HeV infection shows a concerning pattern of continued and frequent occurrences as mentioned above and a strikingly high pathogenesis. The disease in horses is typically characterized by acute central neurological symptoms and sudden death. Elevated heart rate and respiratory rate have been frequently observed (qld.gov.au, 2023). Based on available data the CFR in horses was estimated to be 80% (Yuen et al., 2021). The precise CFR was not possible to determine as horses with a positive diagnosis of HeV while remaining alive had to be euthanized according to the regulatory policy (Yuen et al., 2021). The human cases demonstrated a CFR of 57% (4/7), mostly underlain by fatal encephalitis (nsw.gov.au, 2023).

Apart from the established HeV prototype, or genotype 1 (HeV-g1), a novel variant, or genotype 2 (HeV-g2), was detected in Australia in horses that suffered acute illness with signs of HeV infection as well as in fruit bats (Wang et al., 2021; Annand et al., 2022; Peel et al., 2022; Taylor et al., 2022). The two genotypes share a 84% or 83.5% nucleotide identity in genomic sequences (Wang et al., 2021; Annand et al., 2022). The sequence divergence accounted for the previous failure to detect HeV-g2 by traditional PCR targeting HeV-g1 (Wang et al., 2021; Annand et al., 2022). At the protein level, HeV-g2 exhibits an 82.3–95.7% (mean 92.5%) amino acid identity to HeV-g1 (Annand et al., 2022). Consistent with the higher degree of conservation in protein sequences, the G proteins of the two genotypes share a conserved receptor tropism, and broadly neutralizing monoclonal antibodies to the F and G proteins were found to potently neutralize both HeV-g1 and HeV-g2 (Wang et al., 2022). These data suggest that the antibody post-exposure prophylaxis and equine vaccine against HeV-g1 should be effective against HeV-g2 (Annand et al., 2022; Wang et al., 2022).

NiV outbreaks: Malaysia-Singapore (NiV-M) and Bangladesh-India (NiV-B)

NiV, initially known as Hendra-like virus, was discovered during the 1998–1999 outbreak in farmed pigs and humans in Malaysia (Chua et al., 1999; Paton et al., 1999; CDC, 1999a,b; Chua et al., 2000; Mohd Nor et al., 2000; Lam and Chua, 2002; Chua, 2003; Kummer and Kranz, 2022). The spread via transport of infected pigs also led to a small number of human cases in Singapore More than a million Malaysian pigs were culled to control the epidemic, a huge loss to the agriculture industry. Infected pigs largely lacked clinical disease while some showed neurological and respiratory symptoms (Mohd Nor et al., 2000). The mortality was low (less than 1–5%) except in piglets (approximately 40%) (Mohd Nor et al., 2000). Human infections, apparently through direct contact with contaminated tissues/body fluids of infected pigs, were characterized by severe febrile encephalitis with a CFR of 38% (106/276) (Chua et al., 2000; Goh et al., 2000; Chong et al., 2002; Lewis and Pickering, 2022).

Since 2001, in Bangladesh and its neighboring regions of India, NiV outbreaks or isolated transmission events have been reported almost every year, mainly during the winter months, and have resulted in hundreds of infections in humans (Hsu et al., 2004; Chadha et al., 2006; Halpin and Rota, 2014). A current NiV outbreak in Bangladesh, according to media reports, has been announced by health authorities on January 29, 2023 (risingbd.com, 2023), and eight people have died

out of 11 identified cases by February 13, 2023 (bdnews24.com, 2023; outbreaknewstoday.com, 2023; thedailystar.net, 2023). With the winter season ongoing at this moment, more cases may occur from this outbreak. The winter seasonality of NiV (and HeV) cases remains to be understood, which might be multi-factorial (Martin et al., 2018; McKee et al., 2021). Variations in NiV spillover were shown to correlate with winter temperatures, which may affect the physiology and viral dynamics in bats and the behaviors of bats and humans (Cortes et al., 2018; McKee et al., 2021). The secretion pulses of HeV were found to be higher in winter (Field et al., 2015). We speculate that this may also be the case for NiV, and in addition NiV shed into the environment may be more stable with infectious activity lasting longer under the lower temperatures in winter. These would increase the chance of infection in exposed hosts.

The latest NiV case in India to our knowledge was documented in a report by the World Health Organization (WHO, 2021) and in a research publication (Yadav et al., 2022). The infections in Bangladesh and India differed in several aspects from the original 1998–1999 Malaysia outbreak: No animal host susceptible to clinical disease was identified with role of viral transmission to humans; The CFRs were significantly higher, ranging from approximately 70% to above 90%, up to 100% (Skowron et al., 2021); A majority of cases resulted from human-to-human transmissions (absent in the Malaysia outbreak), which raises serious concern of potential larger-scale outbreaks or even pandemic in humans; And severe respiratory disease, infrequently seen in the Malaysia outbreak, was found in over 60% of these infections, and might be a contributing factor to the transmission and mortality patterns (Luby et al., 2009b; Halpin and Rota, 2014; Kasloff et al., 2019). Consistent with their distinct epidemiological and clinical features, phylogenetic analysis showed that NiV strains from Malaysia and those from Bangladesh and India represent two separate genetic lineages, defined as NiV-M and NiV-B, respectively (Lo et al., 2012). The NiV-M genotype also includes a Cambodia isolate from bat urine (Reynes et al., 2005; Lo et al., 2012).

NiV-like virus outbreak: Philippines

A possibly new type of NiV or NiV-like virus was reported from a 2014 outbreak in the Philippines (Ching et al., 2015). The outbreak involved 17 human cases, with neurological and influenza-like symptoms and a CFR of 53% (9/17), and 10 fatal cases of horses, characterized by sudden death and neurological symptoms (CFR in horses unavailable with total infection number unknown). It should be noted that there was no clear diagnosis made regarding the cause of death in horses, presumably it was NiV but this was not firmly established. Epidemiological evidence suggested possible horse-to-human and human-to-human transmissions. Serological and molecular data supported that the virus causing this outbreak was a henipa-like virus antigenically and genetically. A sequence read (71 bp) of the viral genome corresponding to the P gene of NiV had 99%, 94–96 and 80% identity with NiV-M, NiV-B and HeV strains, respectively. Further attempts to amplify/sequence additional genomic sequences and isolate the virus were unfortunately unsuccessful (Ching et al., 2015). It is unknown if the same or similar NiV-like viruses are still circulating in their natural reservoir host(s) in the Philippines (or elsewhere). To date there has been no new report of subsequent detection of such viruses or any follow-up investigation into their presence. Molecular and serological surveillance studies of henipaviral infection in wildlife and livestock are encouraged to be carried out in endemic regions, such as in bats and horses in the area of the Philippine outbreak.

Natural hosts for the transmission of henipaviruses

HeV and NiV, like several other major pathogens threatening global public health, are emerging RNA viruses from bats (Tian et al., 2022). Several species of Old World fruit bats (also known as flying foxes) from the genus *Pteropus*, family *Pteropodidae* are the major known reservoir hosts of henipaviruses (Drexler et al., 2009; Halpin et al., 2011; Geisbert et al., 2012; Middleton and Weingartl, 2012; Kessler et al., 2018; Tian et al., 2022). Of interest, most filoviruses, including Ebola and Marburg-related viruses, were identified in other genera of the same bat family, *Pteropodidae* (Tian et al., 2022), while SARS-CoV-2-like coronaviruses were recently found in bats of another family, *Rhinolophidae* (Temmam et al., 2022; Tian et al., 2022). The Pteropus bats have a geographic distribution involving eastern Africa (Madagascar island), Asia, Australia and the Pacific islands (Iehlé et al., 2007; Gurley et al., 2017; Kessler et al., 2018), illustrating a broad area at potential risk for henipavirus disease.

Henipaviruses can be transmitted both among bats and in spillover events to other animals and humans (Quarleri et al., 2022). The Pteropus hosts do not exhibit any evident disease with natural or experimental infection by henipaviruses (Middleton and Weingartl, 2012; Halpin and Rota, 2014; Quarleri et al., 2022). The long-term coexistence in harmony between the viruses and their reservoir hosts may represent a relative equilibrium reached during co-evolution (Halpin and Rota, 2014). Transmission of henipaviruses to humans is often bridged by an intermediate animal host, which amplifies and spreads the viruses to humans. Candidate intermediate hosts can be livestock that interact with both the reservoir hosts and humans (Kummer and Kranz, 2022). Horses and pigs are clearly established intermediate hosts for the HeV outbreaks in Australia and NiV-M epidemic in Malaysia and Singapore, respectively (Halpin and Rota, 2014; Kummer and Kranz, 2022). It is unknown whether other livestock, such as domestic ruminants (goats, sheep and cattle), can serve as intermediate hosts (Skowron et al., 2021; Kummer and Kranz, 2022).

During the NiV-B outbreaks in Bangladesh and India, although the spread of infection was largely through human-to-human transmission, the primary transmission route linking the bat reservoir to the initial human infection case(s) was not known, and no intermediate host was established. Outbreaks in pigs, which had previously contributed to human infections in Malaysia and Singapore, were not seen here (Luby et al., 2009a). In a recent experimental infection study conducted in our lab, NiV-B did not lead to any clinical signs in infected pigs and viremia was not detectable at any sampling time point from short-term and long-term time series. However, infectious viruses were isolated from several pig tissues and nasal washes (Kasloff et al., 2019). A "silent" infection without clinical signs could pose significant risk of viral transmission. In addition, comparing across the past henipavirus outbreaks, the data together suggest that genetic divergence in henipaviruses can shift their

biological behaviors concerning host tropism, pathogenicity, amplification and transmission with epidemiological impact.

Human consumption of date palm sap suspected of henipaviral contamination from bats was found to correlate with risk of NiV-B infection and has been proposed as the most common pathway of NiV-B transmission from bats to humans (Luby et al., 2009a; Luby and Gurley, 2012; Rahman et al., 2012). Infrared wildlife photography showed that Pteropus bats frequently visit date palm trees, lick the sap stream and urinate near the sap collection pot (Luby and Gurley, 2012; Rahman et al., 2012). Skirt barriers of bamboo (or other materials) were tested and found effective to impede bat access to date palm sap (Khan et al., 2012; Nahar et al., 2014). The hypothesis was further supported in a laboratory setting where NiV was transmitted from artificial palm sap to Syrian hamsters (de Wit et al., 2014). To date no NiV has been isolated directly from date palm sap (Rahman et al., 2012). It should be noted that viral isolation attempts have only been made on sap samples collected weeks after an outbreak and the timing may not be suitable for the purpose since Pteropus shedding of NiV is intermittent (Luby and Gurley, 2012). In addition, so far there has been no report whether the prevention of sap contamination by bats using skirt barriers leads to reduced outbreak cases. Additional studies are needed to confirm the role of sap consumption in viral transmission. While no direct evidence has proved the correlation between sap consumption and NiV-B outbreak to be causal in the natural transmission setting, it is an open possibility that alternative mode(s) of transmission may exist and unidentified intermediate host(s) could serve as the transmission route or an additional transmission route between bats and humans (Skowron et al., 2021).

A diversity of undetermined transmission mechanisms

Henipaviral transmissions concerning human infections can occur from bats to intermediate hosts, from intermediate hosts to humans, potentially from bats to humans without intermediate hosts or from humans to humans. These events are commonly featured by close/direct contact with infected hosts or the proximity to bat presence, which has been well supported by scientific observations. However, specific details of the transmission mechanisms remain to be determined while a number of potential modes and vehicles of transmission have been proposed (Luby et al., 2009a; Gazal et al., 2022; Bruno et al., 2023).

Body fluids and excretions from henipavirus-infected bat, horse, pig or human hosts, such as saliva, urine and feces, or materials with these contaminants such as fruits partially eaten by bats and date palm saps in contact with bats have been believed to be vehicles of viral transmission. This applies to the handling or consumption of meat from infected pigs or horses as well (Luby et al., 2009a; Gazal et al., 2022; Bruno et al., 2023). It was also mentioned that direct shedding to receptive animals or inhalation of aerosol NiV virions could be possible modes of transmission from bats to animals (Bruno et al., 2023), which however have not yet been scientifically tested. As respiratory symptoms were indicators of NiV-B infectivity (Nikolay et al., 2019), droplets from coughing and sneezing could be a vehicle of transmission (Hsu et al., 2004; Gurley et al., 2007; Bruno et al., 2022). Finally, semen samples from a survivor of NiV infection in India were tested positive for NiV RNA on days 16 and 26 post onset of illness (Arunkumar et al., 2019). It will be interesting to test the possibility of NiV persistence in semen and transmission through the sexual route, which is true for Ebola and Zika viruses (Arunkumar et al., 2019). Part of the test should be the isolation of infectious NiV virus from semen.

These hypotheses warrant further research as they are both theoretically feasible and have been suggested or supported to some extent by outbreak observations. Their determination will require in-depth epidemiological investigations and controlled laboratory studies.

A wider range of potential hosts for henipaviruses than the known

The host receptors for henipaviruses, ephrin-B2 and ephrin-B3, are highly conserved among mammalian species, which in theory allow the viruses to infect a broad range of hosts. Consistent with this, apart from the known natural hosts bats, horses and pigs, many small animals were able to be experimentally infected by henipaviruses supporting viral replication (Weingartl et al., 2009; Geisbert et al., 2012; Tian et al., 2022). These include guinea pigs, golden hamsters, cats, ferrets and African green monkeys. However, the levels of viral amplification and clinical features vary greatly among these animals, although their viral receptors share similar efficiency in mediating viral entry (Tian et al., 2022). In addition, mice were resistant to henipaviral infection despite having similar functional viral receptors. These suggest that host factors other than the receptors also contribute to the outcomes of henipavirus-host interactions (Tian et al., 2022). Nevertheless, the current data point to the possibility that henipaviruses have the capacity to infect a diverse range of animal hosts. Therefore, it is an open possibility that additional, as-yet-unidentified animal hosts other than the known natural hosts could transmit henipaviruses.

Domestic ruminants as potential intermediate hosts

Domestic ruminants including goats, sheep and cattle constitute significant part of agriculture. They have worldwide distributions in large population numbers, which also involve areas overlapping with habitats of henipaviral reservoir hosts. Particularly, for example, the estimated numbers of goats, sheep and cattle are 14.8 million, 1.9 million and 25.7 million, respectively, in Bangladesh (Banglapedia, 2023), and 148.89 million, 74.26 million and 193.46 million, respectively, in India (pib.gov.in, 2023). Many of them are constantly exposed at the interface between a farming area and bat territory and may well be in a position to bridge henipaviral transmission to humans. Little has so far been studied, however, concerning the potential role of these animals in zoonotic spillover of henipaviruses, especially NiV-B, for which no intermediate hosts have been identified yet. The lack of attention is likely due to the absence of disease outbreaks in ruminants at large scales as seen in pigs during the Malaysia and Singapore NiV-M epidemic. This may possibly reflect difference between NiV-B and NiV-M in host tropism, pathogenicity or/and transmissibility. Another conceivable hypothesis is based on the difference between the ways of raising livestock in the Malaysian

and Bangladesh outbreak areas (Bruno et al., 2023). In the Malaysian case, the rapid and widespread NiV transmission was underlain by dense pig farming. In contrast, in Bangladesh livestock are managed in small groups sparsely populated, which could have limited the scale of possible transmissions.

Several signs suggest potential exposure of ruminants to henipaviruses and their possible involvement in viral transmission to humans. It was reported that in 2004 two goats owned by a Bangladesh family became ill with symptoms including "fever, difficulty walking, walking in circles, and frothing at the mouth" and both died. Within 2 weeks following the goats' death, a boy from the family, who had played with the goats developed encephalitis and tested positive for NiV antibodies (Luby et al., 2009a). This raises the possibility that goats may play a role in transmitting NiV-B, and disease can develop in infected goats. The goat disease is probably a small-scale, low-frequency event, which may often be overlooked or neglected. However, due to human-to-human transmission of NiV-B, a single spillover case from goats could kindle an outbreak in humans. Whether infection events with similar characteristics could also occur in other animals such as cattle and sheep is an open question. In addition, antibodies to NiV glycoprotein were detected in both goats and cattle in a Luminex-based serological assay where sheep were not tested (Chowdhury et al., 2014). Finally, outbreak surveys identified a correlation between NiV-B cases and contact with sick cows (Hsu et al., 2004; Luby et al., 2009a).

These possibilities need to be observed further in epidemiological investigations and tested in controlled experiments. Knowledge on the potential role of ruminants as amplifying hosts for henipavirus transmission, which is currently lacking, is of great veterinary and public health importance, considering the vast quantity of potential interactions between humans and henipavirus reservoir hosts connected through ruminants at the ecological interface. New research findings on whether or not ruminants do play such a role will clearly provide guidance for governments to prioritize targets for prevention, surveillance, diagnosis and further research.

Newly emerging henipa-like viruses and animal hosts

The genus *Henipavirus* was initially created in the family *Paramyxoviridae* following the identification of the two prototype viruses, HeV and NiV (Chua et al., 2000). With the continued discovery of new henipa-like viruses, the genus has currently included three more members, Cedar virus (CedV), Ghana virus (also called Kumasi virus or Ghanaian bat virus) and Mòjiāng virus (MojV) (Amarasinghe et al., 2017), and further expansion is expected to include additional henipa-like viruses that have recently been reported.

CedV was isolated from urine samples collected in a Pteropus bat colony and named after the sampling location, Cedar Grove in Australia (Marsh et al., 2012). The virus shares key features with prototypic henipaviruses including nearly identical genomic size, at 18,162 nucleotides (nt), and coding structure, in the order of 3'-N-P-M-F-G-L-5', as well as antigenic cross-reactivity, and was thus classified into the *henipavirus* genus (Marsh et al., 2012). However, it has several distinct characteristics. CedV is currently considered non-pathogenic (Marsh et al., 2012; Lieu et al., 2015; Laing et al., 2018; Schountz et al., 2019). No outbreaks in humans or livestock have been reported. Experimental CedV infection in ferrets, guinea pigs or hamsters, small animal models known to be susceptible to henipavirus disease, does not cause clinical disease despite viral replication and production of neutralizing antibodies (Marsh et al., 2012; Schountz et al., 2019). The isolation of a non-pathogenic (or less-pathogenic) virus closely related to the highly pathogenic henipaviruses offers a powerful tool for targeted comparative studies into the determinants of differences among these viruses. Such studies will bring valuable insights into the biology of henipaviruses and identify novel targets for the development of vaccines and antivirals. CedV was originally isolated in a containment level 4 laboratory and the live infectious virus is unavailable for use in a lower containment setting since any material to be removed from containment level 4 has to be fully inactivated. For that reason, recombinant CedVs were generated outside containment level 4 using reverse genetics approach, including those expressing a green fluorescent protein or luciferase reporter or G and F proteins of HeV or NiV. These are contributing to basic research and the development of compound and monoclonal antibody antivirals (Laing et al., 2018; Amaya et al., 2021; Doyle et al., 2021). On the genetic level, a major difference between CedV and prototypic henipaviruses lies in the coding strategy of the P gene. In CedV, the P gene does not encode V or W proteins, which are both antagonists used by henipaviruses against host innate antiviral responses. Additionally, for host cell entry CedV uses ephrin-B2, ephrin-B1, ephrin-A2 and ephrin-A5 but not ephrin-B3, while both ephrin-B2 and ephrin-B3 are used by the pathogenic henipaviruses. The failures of CedV to produce V and W proteins and to use the ephrin-B3 receptor have been suggested to be contributing factors to its nonpathogenic phenotype in the animal infection models (Marsh et al., 2012; Lieu et al., 2015; Laing et al., 2018; Schountz et al., 2019). Whether these proposed mechanisms are essential or sufficient for the determination of pathogenicity phenotypes will need to be further addressed by extended revere genetics studies (with mutagenesis or recombination between CedV and prototypic henipaviruses that may cause changes in pathogenicity). Experiments with potential to generate infectious viral mutants of undetermined pathogenicity such as viral rescue or propagation in cell culture would need to be performed in containment level 4 and gain duel use institutional approval.

Ghana virus has been named after the location (Kumasi city, Ghana) where the sequence of its RNA genome was first identified (Drexler et al., 2009; Drexler et al., 2012). Although henipavirus disease outbreaks have so far only been attributed to reservoir bats from the *Pteropus* genus and reported from endemic areas within Australia and Southeast/South Asia, serological and molecular evidences suggest the existence of henipa-like viruses beyond these boundaries. African fruit bats of the *Eidolon* genus (also in the *Pteropodidae* family) may be an additional host type. These bats are found in continental Africa, which has no Pteropus bats, as well as Madagascar. Antibodies to henipaviruses were detected in both Pteropus and Eidolon bats in Madagascar (Iehlé et al., 2007), Eidolon bats in Ghana (Hayman et al., 2008) and Eidolon bats and humans in Cameroon (Pernet et al., 2014b). In all these serological studies, the antibodies displayed neutralization activity against henipaviruses. Genetic sequences corresponding to potential new virus species in close phylogenetic relationship to henipaviruses were identified in African bats (Drexler et al., 2009, 2012). These are currently known to involve five bat genera from the *Pteropodidae* family (*Eidolon,*

Epomophorus, Hypsignathus, Myonycteris and Rousettus) and five central/west African countries (Democratic Republic of the Congo, Republic of the Congo, Gabon, Central African Republic and Ghana) (Drexler et al., 2009, 2012). The full genome sequence of a representative virus (the prototype Ghana virus: originally called GH-M74a, 18,530 nt, GenBank accession number HQ660129) of these confirmed formal classification into the *henipavirus* genus (Drexler et al., 2012). Furthermore, henipa-like sequences were also found in New World bats in central and south America including Costa Rica. These bats belong to genera in other families than *Pteropodidae*, which are genus *Carollia* in family *Phyllostomidae* and genus *Pteronotus* in family *Mormoopidae* (Drexler et al., 2012). These findings were further supported by the detection of antibodies to henipaviruses in Brazilian bats (de Araujo et al., 2017).

MojV, a rodent-borne virus, is the first established member of the *henipavirus* genus that has been reported in a non-bat reservoir host, shifting the paradigm of henipavirus reservoir host range. The virus was named after the Mòjiāng County, Yunnan Province, China, where an outbreak of pneumonia disease with unknown etiology in 2012 resulted in the death of three miners who had been working in a mine cave (CFR 100%). Following the incidence, a virome survey was conducted on anal swab samples of bats, rats and musk shrews collected from the cave, leading to the identification of MojV sequence in rats (*Rattus flavipectus*) (Wu et al., 2014). MojV (GenBank accession no. KF278639) demonstrates typical genomic features of henipaviruses in size (18,404 nt) and organization (3'-N-P-M-F-G-L-5′) and in phylogenetic analysis clusters with the other four members of the *henipavirus* genus, confirming its classification into the genus (Wu et al., 2014). However, the glycoprotein of MojV lacks the ephrin binding motif, which mediates receptor recognition in prototypic henipaviruses, and does not bind ephrin-B2 or ephrin-B3 *in vitro*, suggesting a distinct, ephrin-independent host cell entry mechanism (Rissanen et al., 2017). In addition, antibodies to well-established henipaviruses were not found to cross-react with the glycoprotein of MojV. This implies that serological screening studies based on reagents derived from typical henipaviures may have missed the detection of MojV, leading to a potential underestimation of their prevalence (Rissanen et al., 2017).

Apart from the five members that have so far been formally classified into the *henipavirus* genus (ICTV, 2023), new henipa-like viruses continue to be discovered in the recent years. One of these, the Angavokely virus (AngV), was identified from a urine sample of Eidolon bats in Madagascar (Madera et al., 2022). This is consistent with the previous detection of antibodies to henipaviruses in those bats (Iehlé et al., 2007). The sequence of a nearly complete 16,740-nt genome of this virus was recovered. It displays a structural organization characteristic of the *henipavirus* genus. Protein structure modeling predicted that the glycoprotein of AngV lacks ephrin binding residues, similarly to MojV.

Following MojV, more henipa-like species have been identified in potential reservoir hosts other than bats. A molecular screening study in African rodents and shrews in Zambia identified henipa-like RNA sequences using RT-PCR primers targeting the L gene. In phylogenetic analysis one rodent sequence and seven shrew sequences clustered in close relation to the *henipavirus* genus, pointing to the potential existence of henipa-like viruses not only in rodents but also in shrews (Sasaki et al., 2014). Indeed, shrew-borne henipa-like viruses were later identified in Asia (Korea and China), Africa (Guinea) and Europe (Belgium). Among these are the Gamak virus (GAKV) and Daeryong virus (DARV), named after the locations of their origin in the Republic of Korea (Gamak and Daeryong Mountains, respectively) (Lee et al., 2021). The viruses were detected from kidney tissues of shrews belonging to the *Crocidura* genus in the *Soricidae* family and virus isolation was successful for GAKV (Lee et al., 2021). The nearly complete genomes of GAKV and DARV are approximately 18,460 nt and 19,471 nt in size, respectively. Both present a coding structure typical of henipaviruses, 3'-N-P-M-F-G-L-5′. The P gene sequence appears to encode the P, C,V and W proteins with a putative RNA editing site. Phylogenetic analysis demonstrated that GAKV and DARV are closely related to the *henipavirus* genus (the most closely related to MojV among the genus members) and share a common ancestor with MojV (Lee et al., 2021). In a more recent study, two henipa-like viruses, the Melian virus (MeliV) and Denwin virus (DewV), were detected in Crocidura shrews from Guinea and Belgium, respectively (Vanmechelen et al., 2022). Both viruses have a genomic organization characteristic of henipaviruses in the order of 3'-N-P-M-F-G-L-5′. It should be noted, however, that the sizes of both genomes are noticeably larger than the average size of prototypic henipaviruses, which are 19,944 nt in MeliV and 19,746 nt in DewV (Vanmechelen et al., 2022). This is also observed at least in DARV, while the sequencing of the GAKV and DARV genomes was described as nearly complete (Lee et al., 2021). Phylogenetic analysis indicated that MeliV and DewV are closely related to the *henipavirus* genus and cluster together with MojV, GAKV and DARV (Vanmechelen et al., 2022).

Langya virus (LayV) is the most recently reported shrew-borne henipa-like virus (Mallapaty, 2022; Zhang et al., 2022). A hospital surveillance of febrile patients with a recent history of animal exposure was conducted in the eastern Chinese provinces of Shandong and Henan. As a result, LayV was isolated from a throat swab sample of a patient from the town of Langya in Shandong. The LayV genome exhibits features typical of henipaviruses: 18,402 nt in length and organized as 3'-N-P(also encoding V/W/C)-M-F-G-L-5′. Phylogenetically, the virus clusters with *henipavirus* genus and related henipa-like viruses, with the closest relation to MojV (Zhang et al., 2022). A subsequent investigation identified 35 patients with acute infections involving LayV, of which 26 patients were infected with LayV only. The 26 patients presented a variety of symptoms with variable severities including respiratory symptoms, but there were no fatalities (Mallapaty, 2022; Zhang et al., 2022). To identify potential animal hosts, molecular survey in 25 wild small animals detected LayV RNA predominantly in shrews, supporting their potential role as a reservoir host for LayV. Serological survey in domestic animals detected antibodies to LayV in goats and dogs, suggesting that goats and dogs may be susceptible to LayV infection and could serve as potential intermediate hosts (Zhang et al., 2022).

The rodent-borne and shrew-borne henipa-like viruses appear to cluster together with one another, more closely than they do with the bat-borne viruses, and vice versa (Sasaki et al., 2014; Lee et al., 2021; Hernández et al., 2022; Vanmechelen et al., 2022). Thus, two closely related but distinct viral clades, a rodent/shrew-borne clade and a bat-borne clade, should be considered to constitute the *henipavirus* genus. The rodent/shrew-borne clade seems to be characterized by a conserved putative protein coding region (for a small transmembrane protein) between the M and F genes, which is not found in other paramyxoviruses (Vanmechelen et al., 2022).

Beyond bats, rodents and shrews, a new study pointed to the possibility that henipa-like viruses could be carried by other natural reservoir hosts. In Brazilian opossums (*Marmosa demerarae*) a henipa-like virus was detected, named Peixe-Boi virus (PBV) based on the location of sampling, the municipality of Peixe-Boi, Pará State, Brazil (Hernández et al., 2022). A partial genomic sequence of PBV (2,377 nt), corresponding to part of NiV L gene, was available and deposited into GenBank with accession number MZ615319. In phylogenetic analysis, the PBV sequence shared a common ancestry with the *henipavirus* genus and related henipa-like viruses and clustered with these viruses as a close sister branch but further away from other genera of *Paramyxoviridae* (Hernández et al., 2022).

Finally, it should be noted that among the henipa-like viruses discussed above, CedV, GAKV, LayV are virus isolates whereas the others are viral sequences and remain to be isolated as whole viruses.

As a summary, a table is provided showing the geographic locations, case numbers and CFRs of henipavirus and henipa-like virus infections in humans and animals, based on major or representative outbreak events (Supplementary Table S1). Also provided are three figures illustrating the global locations of henipa and henipa-like viruses (Figure 1), outbreaks in humans causing diseases/fatalities (Figure 2) and hosts of these viruses (Figure 3), respectively.

Discussion

The emergence of henipa-like viruses in new hosts outside the traditionally known endemic regions suggests a tremendous extension of the reservoir diversity and geographic range of the *henipavirus* genus. These new data reinforced the possibility that a much wider range of animal hosts than previously identified may harbor or/and transmit henipa-like viruses. Considering the distinct taxonomic classifications of the currently known hosts, the discovery of additional new hosts would not be surprising, which could further expand the areas under potential threats.

While HeV and NiV, the prototype zoonotic henipaviruses, are among the deadliest pathogens known to humans, the zoonotic and pathogenic potential of the newly detected henipa-like viruses remains largely undetermined. However, their close relation to these inherently deadly zoonotic viruses itself deserves serious attention. Several lines of observations, furthermore, have pointed to the possibility of spillover events of concern. In the Cameroon study mentioned above, antibodies to henipaviruses were detected in 48% and 3–4% of the sampled African Eidolon bats (n = 44) and humans (n = 497), respectively. Human seropositivity was almost exclusively found in those who had butchered bats for meat (Pernet et al., 2014b). This provides evidence suggesting human infections by African henipa-like viruses following spillovers from bats. It is unclear whether these viruses result in disease in infected humans. However, it has been proposed that they might be involved in unrecognized human disease and contribute to the prevalence of unresolved encephalitis cases (Mathers et al., 2007; Hayman et al., 2008; Drexler et al., 2012; Pernet et al., 2014b; Rissanen et al., 2017). Moreover, MojV has a suspected link to fatal pneumonia (Wu et al., 2014). Finally, the correlation between LayV and acute febrile cases has largely been established as causal based on the association of the viral presence, host antibody response, viremia and magnitude of viral load with the disease occurrence, progression and severity (Zhang et al., 2022). An additional note on LayV is that domestic animals such as goats seem to be susceptible to LayV infection, with a conceivable potential to serve as amplification hosts for viral transmission, although it is unknown if they are susceptible to LayV disease (Zhang et al., 2022). These lurking threats deserve urgent further investigation. It should also be stressed that emerging viruses even apparently harmless could rapidly become devastating pathogens, as well exemplified by the Brazilian epidemic of Zika virus, which had been historically thought to be of little or no pathogenicity (Rissanen et al., 2017).

Reservoir hosts of henipaviruses and emerging henipa-like viruses now have an overwhelmingly broad distribution on the planet. Climate change is expected to further increase the emergence of favorable ecological environment leading to the extension of their habitats into new locations (Latinne and Morand, 2022). This will put new areas under the risk of henipavirus disease. Meanwhile, the ever-growing human activities of expansion including unlimited urbanization and excessive farming have been encroaching into wildlife territories. Resulting from these factors, more domestic

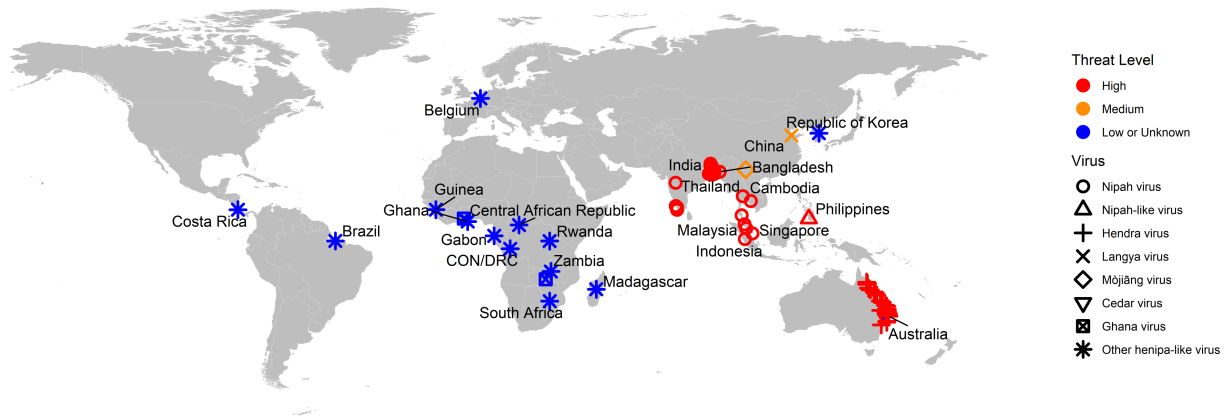

FIGURE 1
Global locations of henipaviruses and henipa-like viruses. The virus type is indicated by shape. The threat level is based on the degree of fatality in humans. CON and DRC=Republic of the Congo and Democratic Republic of the Congo, respectively.

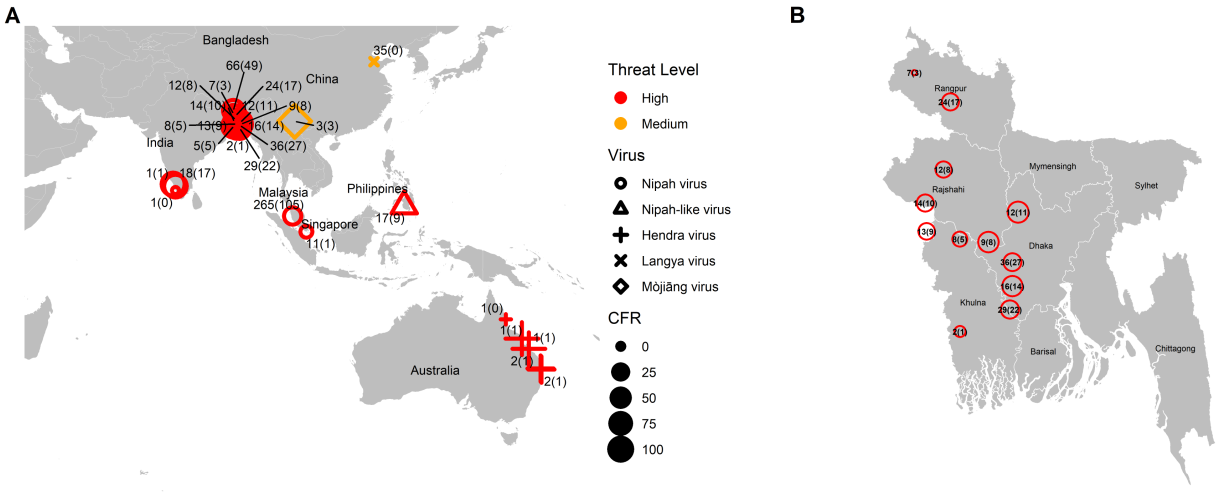

FIGURE 2
Global locations of henipavirus and henipa-like virus outbreaks in humans causing diseases/fatalities. **(A)** Global map. The shape of the symbol represents the virus type, while the size represents the case fatality rate (CFR). The number pair indicates the total number of infected with fatal cases in parentheses. The threat level is determined based on the degree of fatality in humans. **(B)** Enlarged illustration of outbreak cases in Bangladesh.

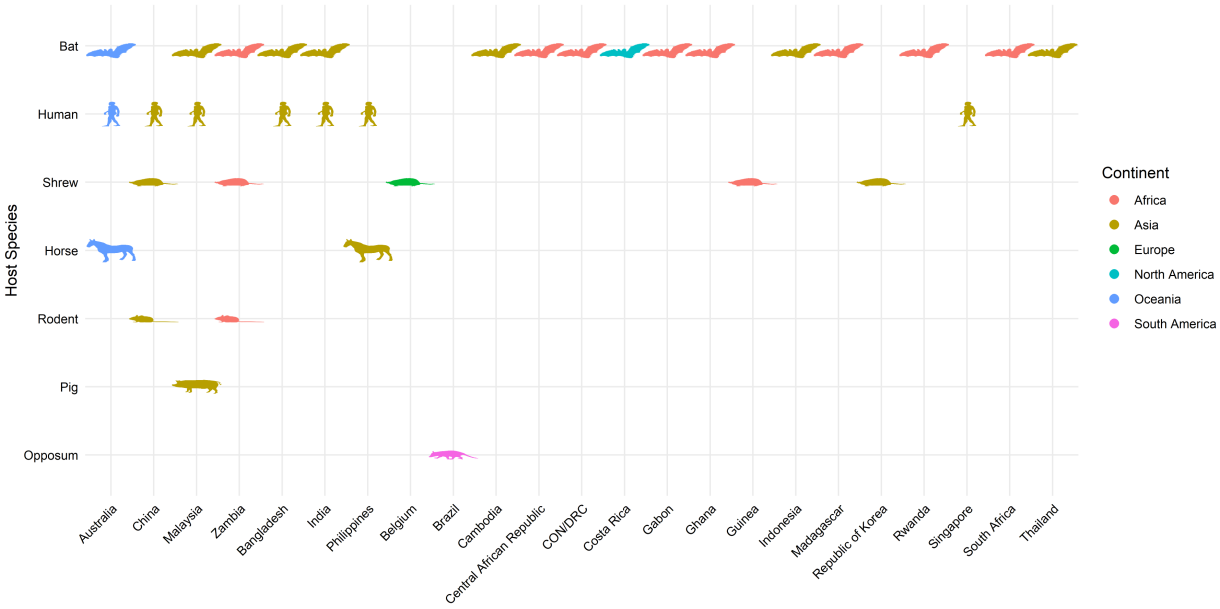

FIGURE 3
Global locations of henipavirus and henipa-like virus hosts. Map indicates organisms with previously reported infection by henipaviruses and henipa-like viruses.

animals such as the ruminants as well as people live in closer contact with the henipavirus reservoirs, resulting in more zoonotic spillover events (Field, 2009; Kessler et al., 2018; Yuen et al., 2021; Latinne and Morand, 2022; Eby et al., 2023). These are occurring repeatedly almost every year, and right now (bdnews24.com, 2023; outbreaknewstoday.com, 2023; risingbd.com, 2023). With each spillover event, the likelihood of mutation in a henipavirus (RNA virus like SARS-CoV-2) increases (Li et al., 2022), and the virus is in an environment that selects for better adaptation in the new host. As a result, a new mutant strain could arise at any time with more efficient and sustained transmission in livestock and/or humans, which could spark a pandemic with devastating impact on the economy and public health. NiV-B possesses the highest potential to become such a mutant virus among currently known henipaviruses and henipa-like viruses due to a combination of seriously concerning characteristics: highest CFR, human-to-human transmission, respiratory disease and possible respiratory transmission, continuing and frequent outbreaks (in regions with high population densities) and unknown intermediate hosts. Since NiV-B causes a CFR of 70–100% in humans, a mutant strain with a similar CFR and high

human-to-human transmissibility would be catastrophic. A highly transmissible henipavirus outbreak will respect no borders in the increasingly globalized and interconnected world and its spread can be facilitated by international travel, transportation and trade. The prevention of such outbreaks at the source undoubtedly requires a thorough understanding of the viral transmission pathways in order to establish targets for minimizing, blocking or eliminating spillover events. Furthermore, during the spread of an epidemic or pandemic following an unfortunate onset, the development of effective, targeted response plans to contain the spread or further to prevent resurgence of infections would be challenging with poor knowledge on the transmission routes involving unidentified animal hosts. Proactive spillover prevention and outbreak preparedness will depend on continued serological and molecular surveillance in wildlife and domestic animals in areas at risk as well as controlled experimental investigation to determine the role of these animals in viral transmission, particularly for example the role of domestic ruminants in NiV-B transmission as proposed above. Experimental inoculation studies in ruminants or other animals should complete a comprehensive and in-depth characterization of the biological and clinical features of henipaviral infection. Concerning the potential role of an animal host in amplifying and transmitting the virus, such studies may reach one of the following findings: Noticeable or severe disease accompanied by high-level viral amplification and shedding, no obvious signs of disease but substantial-level viral amplification and shedding, resistance to infection and disease without viral amplification or shedding, or transitional or mixed phenotypes of these. Notably, a cryptic infection in livestock with high level viral amplification and shedding but no prominent signs of illness, if occurring unrecognized, will pose great risk to farmers, slaughterhouse workers and even household consumers who come into contact with infected animals or contaminated meat products.

The resulting knowledge from these efforts will guide the development of targeted strategies to prevent and contain future henipavirus outbreaks. An extreme idea might be to remove the identified viral reservoirs, which would be practically impossible and disastrous given the large numbers and broad distribution of the reservoir hosts and the importance of these animals to the ecosystem and biodiversity. It should be noted that loss of biodiversity often leads to increased disease transmission (Keesing et al., 2010; Drexler et al., 2012). Under the One Health approach, ecological communities harboring the natural reservoir hosts should be treated with conservation and respect rather than interference or destruction. Alternatively, human activities such as urban constructions and agricultural developments should follow optimized design strategies to avoid or minimize human and livestock contact with reservoir hosts. Furthermore, vaccination of livestock populations at risk is a conceivably feasible and effective solution, expected to prevent both disease in livestock and further transmission from intermediate hosts to humans. Vaccination of humans is also anticipated to provide protection against transmission from infected reservoir hosts, intermediate hosts, or humans.

On a final, encouraging note, although the emergence of new henipa-like viruses signifies new challenges, it also provides new opportunities. Different characteristics among closely related viruses can be utilized in comparative functional investigations to understand aspects of henipavirus biology such as evolution, host tropism, cross-species transmission and pathogenicity. So far CedV (Marsh et al., 2012; Lieu et al., 2015; Laing et al., 2018, 2019; Schountz et al., 2019; Yeo et al., 2021), KV (Pernet et al., 2014a; Lee et al., 2015) and MojV (Rissanen et al., 2017; Cheliout Da Silva et al., 2021) have been involved in a number of such studies. Non-pathogenic henipa-like viruses such as CedV could also be used as immunogen vectors in vaccines against pathogenic henipavirus disease, since antigenic overlap could induce cross-reactivity between closely related viruses. Following this idea, we found reports of vaccine development based on recombinant measles virus and recombinant Newcastle disease virus expressing NiV G protein (Kong et al., 2012; Yoneda et al., 2013). Note that these two viruses belong to the same family (*Paramyxoviridae*) as but different genera (*Morbillivirus* and *Avulavirus*, respectively) from henipaviruses. In comparison, a vaccine vector derived from CedV is expected to elicit better cross-protection due to higher extent of antigenic overlap within the *henipavirus* genus. Our previous study suggested that the soluble G protein vaccine was not effective in inducing cellular immunity (Pickering et al., 2016). We propose that CedV as a viral vector could possibly enhance the vaccine efficacy by strengthening the cellular arm of immune protection. Recombinant CedVs displaying G and F proteins of HeV or NiV (Doyle et al., 2021) are anticipated to be exceptional candidate vaccines for testing in livestock and humans.

Author contributions

HL and BP contributed to the conception and design of the review. HL wrote the first draft of the manuscript. J-YK generated Figures 1–3 and Supplementary Table S1. BP reviewed and edited the manuscript, acquired funding, and supervised the work. All authors contributed to the manuscript revision, read, and approved the submitted version.

Funding

This work was supported by funding from Canadian Food Inspection Agency.

Conflict of interest

The authors declare that the research was conducted in the absence of any commercial or financial relationships that could be construed as a potential conflict of interest.

Publisher's note

Supplementary material

The Supplementary material for this article can be found online at: https://www.frontiersin.org/articles/10.3389/fmicb.2023.1167085/full#supplementary-material

References

Abdullah, S., and Tan, C. T. (2014). Henipavirus encephalitis. *Handb. Clin. Neurol.* 123, 663–670. doi: 10.1016/B978-0-444-53488-0.00032-8

Amarasinghe, G. K., Bào, Y., Basler, C. F., Bavari, S., Beer, M., Bejerman, N., et al. (2017). Taxonomy of the order Mononegavirales: update 2017. *Arch. Virol.* 162, 2493–2504. doi: 10.1007/s00705-017-3311-7

Amaya, M., Cheng, H., Borisevich, V., Navaratnarajah, C. K., Cattaneo, R., Cooper, L., et al. (2021). A recombinant cedar virus based high-throughput screening assay for henipavirus antiviral discovery. *Antivir. Res.* 193:105084. doi: 10.1016/j.antiviral.2021.105084

Annand, E. J., Horsburgh, B. A., Xu, K., Reid, P. A., Poole, B., de Kantzow, M. C., et al. (2022). Novel Hendra virus variant detected by sentinel surveillance of horses in Australia. *Emerg. Infect. Dis.* 28, 693–704. doi: 10.3201/eid2803.211245

Arunkumar, G., Abdulmajeed, J., Santhosha, D., Aswathyraj, S., Robin, S., Jayaram, A., et al. (2019). Persistence of Nipah virus RNA in semen of survivor. *Clin. Infect. Dis.* 69, 377–378. doi: 10.1093/cid/ciy1092

Banglapedia (2023). *Livestock*. Available at: https://en.banglapedia.org/index.php/Livestock (Accessed February 10, 2023).

bdnews24.com (2023). *Bangladesh reports two new Nipah virus deaths*. Available at: https://bdnews24.com/health/03lrm6ebbo (Accessed February 10, 2023).

Broder, C. C., Xu, K., Nikolov, D. B., Zhu, Z., Dimitrov, D. S., Middleton, D., et al. (2013). A treatment for and vaccine against the deadly Hendra and Nipah viruses. *Antivir. Res.* 100, 8–13. doi: 10.1016/j.antiviral.2013.06.012

Bruno, L., Nappo, M. A., Ferrari, L., di Lecce, R., Guarnieri, C., Cantoni, A. M., et al. (2023). Nipah virus disease: epidemiological, clinical, diagnostic and legislative aspects of this unpredictable emerging zoonosis. *Animals (Basel)* 13:159. doi: 10.3390/ani13010159

CDC (1999a). Outbreak of Hendra-like virus--Malaysia and Singapore, 1998-1999. *MMWR Morb. Mortal. Wkly Rep.* 48, 265–269.

CDC (1999b). Update: outbreak of Nipah virus--Malaysia and Singapore, 1999. *MMWR Morb. Mortal. Wkly Rep.* 48, 335–337.

Chadha, M. S., Comer, J. A., Lowe, L., Rota, P. A., Rollin, P. E., Bellini, W. J., et al. (2006). Nipah virus-associated encephalitis outbreak, Siliguri, India. *Int. Conf. Emerg. Infect. Dis.* 12, 235–240. doi: 10.3201/eid1202.051247

Cheliout Da Silva, S., Yan, L., Dang, H. V., Xu, K., Epstein, J. H., Veesler, D., et al. (2021). Functional analysis of the fusion and attachment glycoproteins of Mojiang Henipavirus. *Viruses* 13:517. doi: 10.3390/v13030517

Ching, P. K., de los Reyes, V. C., Sucaldito, M. N., Tayag, E., Columna-Vingno, A. B., Malbas, F. F. Jr., et al. (2015). Outbreak of henipavirus infection, Philippines, 2014. *Emerg. Infect. Dis.* 21, 328–331. doi: 10.3201/eid2102.141433

Chong, H. T., Kunjapan, S. R., Thayaparan, T., Geok Tong, J. M., Petharunam, V., Jusoh, M. R., et al. (2002). Nipah encephalitis outbreak in Malaysia, clinical features in patients from Seremban. *Can. J. Neurol. Sci.* 29, 83–87. doi: 10.1017/s0317167100001785

Chowdhury, S., Khan, S. U., Crameri, G., Epstein, J. H., Broder, C. C., Islam, A., et al. (2014). Serological evidence of henipavirus exposure in cattle, goats and pigs in Bangladesh. *PLoS Negl. Trop. Dis.* 8:e3302. doi: 10.1371/journal.pntd.0003302

Chua, K. B. (2003). Nipah virus outbreak in Malaysia. *J. Clin. Virol.* 26, 265–275. doi: 10.1016/s1386-6532(02)00268-8

Chua, K. B., Bellini, W. J., Rota, P. A., Harcourt, B. H., Tamin, A., Lam, S. K., et al. (2000). Nipah virus: a recently emergent deadly paramyxovirus. *Science* 288, 1432–1435. doi: 10.1126/science.288.5470.1432

Chua, K. B., Goh, K. J., Wong, K. T., Kamarulzaman, A., Tan, P. S., Ksiazek, T. G., et al. (1999). Fatal encephalitis due to Nipah virus among pig-farmers in Malaysia. *Lancet* 354, 1257–1259. doi: 10.1016/S0140-6736(99)04299-3

Cortes, M. C., Cauchemez, S., Lefrancq, N., Luby, S. P., Jahangir Hossain, M., Sazzad, H. M. S., et al. (2018). Characterization of the spatial and temporal distribution of Nipah virus spillover events in Bangladesh, 2007–2013. *J. Infect. Dis.* 217, 1390–1394. doi: 10.1093/infdis/jiy015

de Araujo, J., Lo, M. K., Tamin, A., Ometto, T. L., Thomazelli, L. M., Nardi, M. S., et al. (2017). Antibodies Against Henipa-Like Viruses in Brazilian Bats. *Vector Borne Zoonotic Dis.* 17, 271–274. doi: 10.1089/vbz.2016.2051

de Wit, E., Prescott, J., Falzarano, D., Bushmaker, T., Scott, D., Feldmann, H., et al. (2014). Foodborne transmission of nipah virus in Syrian hamsters. *PLoS Pathog.* 10:e1004001. doi: 10.1371/journal.ppat.1004001

Doyle, M. P., Kose, N., Borisevich, V., Binshtein, E., Amaya, M., Nagel, M., et al. (2021). Cooperativity mediated by rationally selected combinations of human monoclonal antibodies targeting the henipavirus receptor binding protein. *Cell Rep.* 36:109628. doi: 10.1016/j.celrep.2021.109628

Drexler, J. F., Corman, V. M., Gloza-Rausch, F., Seebens, A., Annan, A., Ipsen, A., et al. (2009). Henipavirus RNA in African bats. *PLoS One* 4:e6367. doi: 10.1371/journal.pone.0006367

Drexler, J. F., Corman, V. M., Müller, M. A., Maganga, G. D., Vallo, P., Binger, T., et al. (2012). Bats host major mammalian paramyxoviruses. *Nat. Commun.* 3:796. doi: 10.1038/ncomms1796

Eaton, B. T., Broder, C. C., Middleton, D., and Wang, L. F. (2006). Hendra and Nipah viruses: different and dangerous. *Nat. Rev. Microbiol.* 4, 23–35. doi: 10.1038/nrmicro1323

Eby, P., Peel, A. J., Hoegh, A., Madden, W., Giles, J. R., Hudson, P. J., et al. (2023). Pathogen spillover driven by rapid changes in bat ecology. *Nature* 613, 340–344. doi: 10.1038/s41586-022-05506-2

Field, H. E. (2009). Bats and emerging zoonoses: henipaviruses and SARS. *Zoonoses Public Health* 56, 278–284. doi: 10.1111/j.1863-2378.2008.01218.xJVB1218 [pii]

Field, H., Jordan, D., Edson, D., Morris, S., Melville, D., Parry-Jones, K., et al. (2015). Spatiotemporal aspects of Hendra virus infection in pteropid bats (flying-foxes) in eastern Australia. *PLoS One* 10:e0144055. doi: 10.1371/journal.pone.0144055

Gazal, S., Sharma, N., Gazal, S., Tikoo, M., Shikha, D., Badroo, G. A., et al. (2022). Nipah and Hendra viruses: deadly zoonotic paramyxoviruses with the potential to cause the next pandemic. *Pathogens* 11:1419. doi: 10.3390/pathogens11121419

Geisbert, T. W., Feldmann, H., and Broder, C. C. (2012). Animal challenge models of henipavirus infection and pathogenesis. *Curr. Top. Microbiol. Immunol.* 359, 153–177. doi: 10.1007/82_2012_208

Goh, K. J., Tan, C. T., Chew, N. K., Tan, P. S., Kamarulzaman, A., Sarji, S. A., et al. (2000). Clinical features of Nipah virus encephalitis among pig farmers in Malaysia. *N. Engl. J. Med.* 342, 1229–1235. doi: 10.1056/NEJM200004273421701

Gurley, E. S., Hegde, S. T., Hossain, K., Sazzad, H. M. S., Hossain, M. J., Rahman, M., et al. (2017). Convergence of humans, bats, trees, and culture in Nipah virus transmission, Bangladesh. *Int. Conf. Emerg. Infect. Dis.* 23, 1446–1453. doi: 10.3201/eid2309.161922

Gurley, E. S., Montgomery, J. M., Hossain, M. J., Bell, M., Azad, A. K., Islam, M. R., et al. (2007). Person-to-person transmission of Nipah virus in a Bangladeshi community. *Emerg. Infect. Dis.* 13, 1031–1037. doi: 10.3201/eid1307.061128

Halpin, K., Hyatt, A. D., Fogarty, R., Middleton, D., Bingham, J., Epstein, J. H., et al. (2011). Pteropid bats are confirmed as the reservoir hosts of henipaviruses: a comprehensive experimental study of virus transmission. *Am. J. Trop. Med. Hyg.* 85, 946–951. doi: 10.4269/ajtmh.2011.10-0567

Halpin, K., and Rota, P. (2014). A review of Hendra virus and Nipah virus infections in man and other animals. *Zoonoses* 997–1012. doi: 10.1007/978-94-017-9457-2_40

Hayman, D. T., Suu-Ire, R., Breed, A. C., McEachern, J. A., Wang, L., Wood, J. L., et al. (2008). Evidence of henipavirus infection in West African fruit bats. *PLoS One* 3:e2739. doi: 10.1371/journal.pone.0002739

Hernández, L. H. A., da Paz, T. Y. B., Silva, S. P. D., Silva, F. S. D., Barros, B. C. V., Nunes, B. T. D., et al. (2022). First genomic evidence of a Henipa-like virus in Brazil. *Viruses* 14:2167. doi: 10.3390/v14102167

Hsu, V. P., Hossain, M. J., Parashar, U. D., Ali, M. M., Ksiazek, T. G., Kuzmin, I., et al. (2004). Nipah virus encephalitis reemergence, Bangladesh. *Int. Conf. Emerg. Infect. Dis.* 10, 2082–2087. doi: 10.3201/eid1012.040701

ICTV (2023). *Genus: Henipavirus*. Available at: https://ictv.global/report/chapter/paramyxoviridae/paramyxoviridae/henipavirus (Accessed February 11, 2023).

Iehlé, C., Razafitrimo, G., Razainirina, J., Andriaholinirina, N., Goodman, S. M., Faure, C., et al. (2007). Henipavirus and Tioman virus antibodies in Pteropodid bats, Madagascar. *Int. Conf. Emerg. Infect. Dis.* 13, 159–161. doi: 10.3201/eid1301.060791

Kasloff, S. B., Leung, A., Pickering, B. S., Smith, G., Moffat, E., Collignon, B., et al. (2019). Pathogenicity of Nipah henipavirus Bangladesh in a swine host. *Sci. Rep.* 9:5230. doi: 10.1038/s41598-019-40476-y

Keesing, F., Belden, L. K., Daszak, P., Dobson, A., Harvell, C. D., Holt, R. D., et al. (2010). Impacts of biodiversity on the emergence and transmission of infectious diseases. *Nature* 468, 647–652. doi: 10.1038/nature09575

Kessler, M. K., Becker, D. J., Peel, A. J., Justice, N. V., Lunn, T., Crowley, D. E., et al. (2018). Changing resource landscapes and spillover of henipaviruses. *Ann. N. Y. Acad. Sci.* 1429, 78–99. doi: 10.1111/nyas.13910

Khan, S. U., Gurley, E. S., Hossain, M. J., Nahar, N., Sharker, M. A., and Luby, S. P. (2012). A randomized controlled trial of interventions to impede date palm sap contamination by bats to prevent nipah virus transmission in Bangladesh. *PLoS One* 7:e42689. doi: 10.1371/journal.pone.0042689

Kong, D., Wen, Z., Su, H., Ge, J., Chen, W., Wang, X., et al. (2012). Newcastle disease virus-vectored Nipah encephalitis vaccines induce B and T cell responses in mice and long-lasting neutralizing antibodies in pigs. *Virology* 432, 327–335. doi: 10.1016/j.virol.2012.06.001

Kummer, S., and Kranz, D. C. (2022). Henipaviruses-a constant threat to livestock and humans. *PLoS Negl. Trop. Dis.* 16:e0010157. doi: 10.1371/journal.pntd.0010157 PNTD-D-21-00815 [pii]

Laing, E. D., Amaya, M., Navaratnarajah, C. K., Feng, Y. R., Cattaneo, R., Wang, L. F., et al. (2018). Rescue and characterization of recombinant cedar virus, a non-pathogenic Henipavirus species. *Virol. J.* 15:56. doi: 10.1186/s12985-018-0964-0

Laing, E. D., Navaratnarajah, C. K., Cheliout da Silva, S., Petzing, S. R., Xu, Y., Sterling, S. L., et al. (2019). Structural and functional analyses reveal promiscuous and species specific use of ephrin receptors by cedar virus. *Proc. Natl. Acad. Sci. U. S. A.* 116, 20707–20715. doi: 10.1073/pnas.1911773116

Lam, S. K., and Chua, K. B. (2002). Nipah virus encephalitis outbreak in Malaysia. *Clin. Infect. Dis.* 34, S48–S51. doi: 10.1086/338818

Latinne, A., and Morand, S. (2022). Climate anomalies and spillover of bat-borne viral diseases in the Asia-Pacific region and the Arabian peninsula. *Viruses* 14:1100. doi: 10.3390/v14051100

Lee, S. H., Kim, K., Kim, J., No, J. S., Park, K., Budhathoki, S., et al. (2021). Discovery and genetic characterization of novel paramyxoviruses related to the genus Henipavirus in Crocidura species in the Republic of Korea. *Viruses* 13:2020. doi: 10.3390/v13102020

Lee, B., Pernet, O., Ahmed, A. A., Zeltina, A., Beaty, S. M., and Bowden, T. A. (2015). Molecular recognition of human ephrinB2 cell surface receptor by an emergent African henipavirus. *Proc. Natl. Acad. Sci. U. S. A.* 112, E2156–E2165. doi: 10.1073/pnas.1501690112

Lewis, C. E., and Pickering, B. (2022). Livestock and risk group 4 pathogens: researching zoonotic threats to public health and agriculture in maximum containment. *ILAR J.* 61, 86–102. doi: 10.1093/ilar/ilab029

Li, H., Bello, A., Smith, G., Kielich, D. M. S., Strong, J. E., and Pickering, B. S. (2022). Degenerate sequence-based CRISPR diagnostic for Crimean-Congo hemorrhagic fever virus. *PLoS Negl. Trop. Dis.* 16:e0010285. doi: 10.1371/journal.pntd.0010285 PNTD-D-21-00739 [pii]

Lieu, K. G., Marsh, G. A., Wang, L. F., and Netter, H. J. (2015). The non-pathogenic Henipavirus cedar paramyxovirus phosphoprotein has a compromised ability to target STAT1 and STAT2. *Antivir. Res.* 124, 69–76. doi: 10.1016/j.antiviral.2015.09.017

Lo, M. K., Lowe, L., Hummel, K. B., Sazzad, H. M., Gurley, E. S., Hossain, M. J., et al. (2012). Characterization of Nipah virus from outbreaks in Bangladesh, 2008–2010. *Emerg. Infect. Dis.* 18, 248–255. doi: 10.3201/eid1802.111492

Luby, S. P., and Gurley, E. S. (2012). Epidemiology of henipavirus disease in humans. *Curr. Top. Microbiol. Immunol.* 359, 25–40. doi: 10.1007/82_2012_207

Luby, S. P., Gurley, E. S., and Hossain, M. J. (2009a). Transmission of human infection with Nipah virus. *Clin. Infect. Dis.* 49, 1743–1748. doi: 10.1086/647951

Luby, S. P., Hossain, M. J., Gurley, E. S., Ahmed, B. N., Banu, S., Khan, S. U., et al. (2009b). Recurrent zoonotic transmission of Nipah virus into humans, Bangladesh, 2001-2007. *Emerg. Infect. Dis.* 15, 1229–1235. doi: 10.3201/eid1508.081237

Madera, S., Kistler, A., Ranaivoson, H. C., Ahyong, V., Andrianiaina, A., Andry, S., et al. (2022). Discovery and genomic characterization of a novel Henipavirus, Angavokely virus, from fruit bats in Madagascar. *J. Virol.* 96:e0092122. doi: 10.1128/jvi.00921-22

Mallapaty, S. (2022). New 'Langya' virus identified in China: what scientists know so far. *Nature* 608, 656–657. doi: 10.1038/d41586-022-02175-z

Marsh, G. A., de Jong, C., Barr, J. A., Tachedjian, M., Smith, C., Middleton, D., et al. (2012). Cedar virus: a novel Henipavirus isolated from Australian bats. *PLoS Pathog.* 8:e1002836. doi: 10.1371/journal.ppat.1002836

Martin, G., Yanez-Arenas, C., Plowright, R. K., Chen, C., Roberts, B., and Skerratt, L. F. (2018). Hendra virus spillover is a bimodal system driven by climatic factors. *EcoHealth* 15, 526–542. doi: 10.1007/s10393-017-1309-y

Mathers, C. D., Ezzati, M., and Lopez, A. D. (2007). Measuring the burden of neglected tropical diseases: the global burden of disease framework. *PLoS Negl. Trop. Dis.* 1:e114. doi: 10.1371/journal.pntd.0000114

McKee, C. D., Islam, A., Luby, S. P., Salje, H., Hudson, P. J., Plowright, R. K., et al. (2021). The ecology of Nipah virus in Bangladesh: a Nexus of land-use change and opportunistic feeding behavior in bats. *Viruses* 13:169. doi: 10.3390/v13020169

Mehand, M. S., Millett, P., Al-Shorbaji, F., Roth, C., Kieny, M. P., and Murgue, B. (2018). World health organization methodology to prioritize emerging infectious diseases in need of research and development. *Emerg. Infect. Dis.* 24:e171427. doi: 10.3201/eid2409.171427

Middleton, D. J., and Weingartl, H. M. (2012). Henipaviruses in their natural animal hosts. *Curr. Top. Microbiol. Immunol.* 359, 105–121. doi: 10.1007/82_2012_210

Mohd Nor, M. N., Gan, C. H., and Ong, B. L. (2000). Nipah virus infection of pigs in peninsular Malaysia. *Rev. Sci. Tech.* 19, 160–165. doi: 10.20506/rst.19.1.1202

Murray, K., Selleck, P., Hooper, P., Hyatt, A., Gould, A., Gleeson, L., et al. (1995). A morbillivirus that caused fatal fisease in horses and humans. *Science* 268, 94–97. doi: 10.1126/science.7701348

Nahar, N., Mondal, U. K., Hossain, M. J., Khan, M. S., Sultana, R., Gurley, E. S., et al. (2014). Piloting the promotion of bamboo skirt barriers to prevent Nipah virus transmission through date palm sap in Bangladesh. *Glob. Health Promot.* 21, 7–15. doi: 10.1177/1757975914528249

Nikolay, B., Salje, H., Hossain, M. J., Khan, A., Sazzad, H. M. S., Rahman, M., et al. (2019). Transmission of Nipah virus - 14 years of investigations in Bangladesh. *N. Engl. J. Med.* 380, 1804–1814. doi: 10.1056/NEJMoa1805376

Nordin, M. N. (1999). Nipah DIsease in Maysia. *OIE Dis. Inf.* 12:20.

nsw.gov.au (2023). *Summary of human cases of Hendra virus infection*. Available at: https://www.health.nsw.gov.au/Infectious/controlguideline/Pages/hendra-case-summary.aspx (Accessed February 10, 2023).

outbreaknewstoday.com (2023). *Bangladesh Nipah virus update: 10 cases and 7 deaths in 2023*. Available at: http://outbreaknewstoday.com/bangladesh-nipah-virus-update-10-cases-and-7-deaths-in-2023/ (Accessed February 11, 2023).

Paton, N. I., Leo, Y. S., Zaki, S. R., Auchus, A. P., Lee, K. E., Ling, A. E., et al. (1999). Outbreak of Nipah-virus infection among abattoir workers in Singapore. *Lancet* 354, 1253–1256. doi: 10.1016/S0140-6736(99)04379-2

Peel, A. J., Yinda, C. K., Annand, E. J., Dale, A. S., Eby, P., Eden, J. S., et al. (2022). Novel Hendra virus variant circulating in black flying foxes and grey-headed flying foxes, Australia. *Int. Conf. Emerg. Infect. Dis.* 28, 1043–1047. doi: 10.3201/eid2805.212338

Pernet, O., Beaty, S., and Lee, B. (2014a). Functional rectification of the newly described African henipavirus fusion glycoprotein (Gh-M74a). *J. Virol.* 88, 5171–5176. doi: 10.1128/JVI.03655-13

Pernet, O., Schneider, B. S., Beaty, S. M., LeBreton, M., Yun, T. E., Park, A., et al. (2014b). Evidence for henipavirus spillover into human populations in Africa. *Nat. Commun.* 5:5342. doi: 10.1038/ncomms6342

pib.gov.in (2023). *Livestock census*. Available at: https://pib.gov.in/PressReleaseIframePage.aspx?PRID=1813802 (Accessed February 10, 2023).

Pickering, B. S., Hardham, J. M., Smith, G., Weingartl, E. T., Dominowski, P. J., Foss, D. L., et al. (2016). Protection against henipaviruses in swine requires both, cell-mediated and humoral immune response. *Vaccine* 34, 4777–4786. doi: 10.1016/j.vaccine.2016.08.028

Playford, E. G., McCall, B., Smith, G., Slinko, V., Allen, G., Smith, I., et al. (2010). Human Hendra virus encephalitis associated with equine outbreak, Australia, 2008. *Emerg. Infect. Dis.* 16, 219–223. doi: 10.3201/eid1602.090552

qld.gov.au (2023). *Summary of Hendra virus incidents in horses*. Available from: https://www.business.qld.gov.au/industries/service-industries-professionals/service-industries/veterinary-surgeons/guidelines-hendra/incident-summary (Accessed February 10, 2023).

Quarleri, J., Galvan, V., and Delpino, M. V. (2022). Henipaviruses: an expanding global public health concern? *Geroscience*. 44, 2447–2459. doi: 10.1007/s11357-022-00670-9

Rahman, M. A., Hossain, M. J., Sultana, S., Homaira, N., Khan, S. U., Rahman, M., et al. (2012). Date palm sap linked to Nipah virus outbreak in Bangladesh, 2008. *Vector Borne Zoonotic Dis.* 12, 65–72. doi: 10.1089/vbz.2011.0656

Reynes, J. M., Counor, D., Ong, S., Faure, C., Seng, V., Molia, S., et al. (2005). Nipah virus in Lyle's flying foxes, Cambodia. *Int. Conf. Emerg. Infect. Dis.* 11, 1042–1047. doi: 10.3201/eid1107.041350

Rima, B., Balkema-Buschmann, A., Dundon, W. G., Duprex, P., Easton, A., Fouchier, R., et al. (2019). ICTV virus taxonomy profile: Paramyxoviridae. *J. Gen. Virol.* 100, 1593–1594. doi: 10.1099/jgv.0.001328

risingbd.com (2023). *Nipah virus claims 5 lives this year: home minister*. Available at: https://www.risingbd.com/english/national/news/93117 (Accessed February 11, 2023).

Rissanen, I., Ahmed, A. A., Azarm, K., Beaty, S., Hong, P., Nambulli, S., et al. (2017). Idiosyncratic Mòjiāng virus attachment glycoprotein directs a host-cell entry pathway distinct from genetically related henipaviruses. *Nat. Commun.* 8:16060. doi: 10.1038/ncomms16060

Sasaki, M., Muleya, W., Ishii, A., Orba, Y., Hang'ombe, B. M., Mweene, A. S., et al. (2014). Molecular epidemiology of paramyxoviruses in Zambian wild rodents and shrews. *J. Gen. Virol.* 95, 325–330. doi: 10.1099/vir.0.058404-0

Schountz, T., Campbell, C., Wagner, K., Rovnak, J., Martellaro, C., DeBuysscher, B. L., et al. (2019). Differential innate immune responses elicited by Nipah virus and cedar virus correlate with disparate in vivo pathogenesis in hamsters. *Viruses* 11:219. doi: 10.3390/v11030291

Skowron, K., Bauza-Kaszewska, J., Grudlewska-Buda, K., Wiktorczyk-Kapischke, N., Zacharski, M., Bernaciak, Z., et al. (2021). Nipah virus-another threat from the world of zoonotic viruses. *Front. Microbiol.* 12:811157. doi: 10.3389/fmicb.2021.811157

Sweileh, W. M. (2017). Global research trends of World Health Organization's top eight emerging pathogens. *Glob. Health* 13:9. doi: 10.1186/s12992-017-0233-9 10.1186/s12992-017-0233-9 [pii]

Taylor, J., Thompson, K., Annand, E. J., Massey, P. D., Bennett, J., Eden, J. S., et al. (2022). Novel variant Hendra virus genotype 2 infection in a horse in the greater Newcastle region, New South Wales, Australia. *One Health* 15:100423. doi: 10.1016/j.onehlt.2022.100423

Temmam, S., Vongphayloth, K., Baquero, E., Munier, S., Bonomi, M., Regnault, B., et al. (2022). Bat coronaviruses related to SARS-CoV-2 and infectious for human cells. *Nature* 604, 330–336. doi: 10.1038/s41586-022-04532-4

thedailystar.net (2023). *One dies of Nipah virus at DMCH*. Available at: https://www.thedailystar.net/health/disease/coronavirus/events-who/deaths-infections/news/1-covid-19-death-24-hours-positivity-rate-045-3246631 (Accessed February 15, 2023)

Tian, J., Sun, J., Li, D., Wang, N., Wang, L., Zhang, C., et al. (2022). Emerging viruses: Cross-species transmission of coronaviruses, filoviruses, henipaviruses, and rotaviruses from bats. *Cell Rep.* 39:110969. doi: 10.1016/j.celrep.2022.110969

Vanmechelen, B., Meurs, S., Horemans, M., Loosen, A., Joly Maes, T., Laenen, L., et al. (2022). The characterization of multiple novel paramyxoviruses highlights the diverse nature of the subfamily *Orthoparamyxovirinae*. *Virus Evol.* 8:veac061. doi: 10.1093/ve/veac061

Wang, J., Anderson, D. E., Halpin, K., Hong, X., Chen, H., Walker, S., et al. (2021). A new Hendra virus genotype found in Australian flying foxes. *Virol. J.* 18:197. doi: 10.1186/s12985-021-01652-7

Wang, Z., Dang, H. V., Amaya, M., Xu, Y., Yin, R., Yan, L., et al. (2022). Potent monoclonal antibody-mediated neutralization of a divergent Hendra virus variant. *Proc. Natl. Acad. Sci. U. S. A.* 119:e2122769119. doi: 10.1073/pnas.2122769119

Weingartl, H. M., Berhane, Y., and Czub, M. (2009). Animal models of henipavirus infection: a review. *Vet. J.* 181, 211–220. doi: 10.1016/j.tvjl.2008.10.016 S1090-0233(08)00376-6 [pii]

WHO (2021). *Nipah virus disease - India*. Available at: https://www.who.int/emergencies/disease-outbreak-news/item/nipah-virus-disease---india (Accessed February 10, 2023).

WHO (2023a). *Prioritizing diseases for research and development in emergency contexts*. Available at: https://www.who.int/activities/prioritizing-diseases-for-research-and-development-in-emergency-contexts (Accessed February 11, 2023)

WHO (2023b). *R&D Blueprint*. Available at: https://www.who.int/teams/blueprint (Accessed February 11, 2023).

WHO (2023c). *WHO to identify pathogens that could cause future outbreaks and pandemics*. Geneva World Health Organization

Wong, K. T., and Ong, K. C. (2011). Pathology of acute henipavirus infection in humans and animals. *Pathol. Res. Int.* 2011:567248. doi: 10.4061/2011/567248

Wong, K. T., and Tan, C. T. (2012). Clinical and pathological manifestations of human henipavirus infection. *Curr. Top. Microbiol. Immunol.* 359, 95–104. doi: 10.1007/82_2012_205

Wu, Z., Yang, L., Yang, F., Ren, X., Jiang, J., Dong, J., et al. (2014). Novel Henipa-like virus, Mojiang Paramyxovirus, in rats, China, 2012. *Emerg. Infect. Dis.* 20, 1064–1066. doi: 10.3201/eid2006.131022

Yadav, P. D., Sahay, R. R., Balakrishnan, A., Mohandas, S., Radhakrishnan, C., Gokhale, M. D., et al. (2022). Nipah virus outbreak in Kerala state, India amidst of COVID-19 pandemic. *Front. Public Health* 10:818545. doi: 10.3389/fpubh.2022.818545

Yeo, Y. Y., Buchholz, D. W., Gamble, A., Jager, M., and Aguilar, H. C. (2021). Headless Henipaviral receptor binding glycoproteins reveal fusion modulation by the head/stalk Interface and post-receptor binding contributions of the head domain. *J. Virol.* 95:e0066621. doi: 10.1128/JVI.00666-21

Yoneda, M., Georges-Courbot, M. C., Ikeda, F., Ishii, M., Nagata, N., Jacquot, F., et al. (2013). Recombinant measles virus vaccine expressing the Nipah virus glycoprotein protects against lethal Nipah virus challenge. *PLoS One* 8:e58414. doi: 10.1371/journal.pone.0058414

Yuen, K. Y., Fraser, N. S., Henning, J., Halpin, K., Gibson, J. S., Betzien, L., et al. (2021). Hendra virus: epidemiology dynamics in relation to climate change, diagnostic tests and control measures. *One Health* 12:100207. doi: 10.1016/j.onehlt.2020.100207

Zhang, X. A., Li, H., Jiang, F. C., Zhu, F., Zhang, Y. F., Chen, J. J., et al. (2022). A zoonotic Henipavirus in febrile patients in China. *N. Engl. J. Med.* 387, 470–472. doi: 10.1056/NEJMc2202705

Frontiers in Microbiology

Explores the habitable world and the potential of microbial life

The largest and most cited microbiology journal which advances our understanding of the role microbes play in addressing global challenges such as healthcare, food security, and climate change.

Discover the latest Research Topics

See more →

Frontiers

Avenue du Tribunal-Fédéral 34
1005 Lausanne, Switzerland
frontiersin.org

Contact us

+41 (0)21 510 17 00
frontiersin.org/about/contact